UCLA
UCLA Electronic Theses and Dissertations

Title

Amides and Cyclic 1,2,3-Trienes as Synthetic Building Blocks

Permalink

https://escholarship.org/uc/item/3fb0h514

Author

Bulger, Ana Sydelle

Publication Date

2024

Peer reviewed|Thesis/dissertation

eScholarship.org Powered by the California Digital Library
University of California

UNIVERSITY OF CALIFORNIA

Los Angeles

Amides and Cyclic 1,2,3-Trienes as Synthetic Building Blocks

A dissertation submitted in partial satisfaction of the

requirements for the degree Doctor of Philosophy

in Chemistry

by

Ana Sydelle Bulger

2024

© Copyright by

Ana Sydelle Bulger

2024

ABSTRACT OF THE DISSERTATION

Studies Pertaining to Amides and Cyclic 1,2,3-Trienes as Synthetic Building Blocks

by

Ana Sydelle Bulger

Doctor of Philosophy in Chemistry

University of California, Los Angeles, 2024

Professor Neil K. Garg, Chair

This dissertation describes the development of reaction methodologies that utilize unconventional building blocks in chemical synthesis. One major effort involves the net hydrolysis of amides to give carboxylic acids via the nickel-catalyzed cleavage of traditionally inert amide C–N bonds. Additionally, the development of the first enantioselective reaction of amide electrophiles proceeding with the usage of a chiral catalyst through C–N bond activation is disclosed. At the other end of the reactivity spectrum, studies of minimally explored strained intermediates including cyclic 1,2,3-trienes and azacyclic 1,2,3-trienes are reported. These efforts

expand on fundamental structure and reactivity of the cyclic trienes, give rise to new mechanistic understanding, and allow access to polycyclic products.

Chapter one outlines the current state of the art in nickel and iron-catalyzed cross-couplings of traditionally inert electrophiles. Specifically, recent advances in base-metal-catalyzed reactions of phenol, aniline, ester, and amide derivatives that proceed via aryl or acyl C–O/C–N bond activation are described. This brief review chapter should provide context for some of the subsequent studies presented in this dissertation. Furthermore, summarizing recent efforts in this field is expected to highlight the utility of base-metal-catalyzed cross-couplings of traditionally-inert electrophiles in organic synthesis.

Chapter two describes the development of a nickel-catalyzed net hydrolysis of amides. The methodology strategically employs a nickel-catalyzed esterification using 2-(trimethylsilyl)-ethanol, followed by a fluoride-mediated deprotection in a single-pot operation. The selectivity and mildness of this transformation are demonstrated through competition experiments and the net-hydrolysis of a complex valine-derived substrate. This strategy addresses a limitation in the field with regard to functional groups accessible from amides using transition metal-catalyzed C–N bond activation.

Chapter three describes an enantioselective Mizoroki–Heck cyclization of amide electrophiles. In recent years, numerous cross-coupling reactions of amide electrophiles have been disclosed, however, this study constitutes the first known enantioselective variant proceeding through amide C–N bond activation using a chiral metal catalyst. Ligand design and reaction optimization are discussed, as well as a brief scope of the reaction. Additionally, the synthetic utility of the method is demonstrated through synthetic elaborations to enantioenriched,

medicinally-relevant heterocycles and products bearing multiple stereocenters. This study establishes a proof-of-concept for using amide electrophiles in asymmetric catalysis.

Chapter four describes the development of strained 1,2,3-cyclohexatrienes, which have remained underexplored historically, as synthetic building blocks. Studies of the reactivity of the unsubstituted 1,2,3-cyclohexatriene, as well as its mono- and disubstituted derivatives are reported, thus expanding the scope of reactions known for such intermediates. Combined computational and experimental studies elucidate the factors controlling regioselectivity in reactions of an unsymmetrical strained triene. Furthermore, the potential utility of strained trienes in rapidly generating complex scaffolds is demonstrated through the integration of triene trapping reactions into multistep synthetic sequences to access polycyclic products. These studies highlight the potential of these traditionally avoided species in synthetic chemistry.

Chapter five describes the mechanistic study of a C–C bond fragmentation that was observed in Chapter four studies. Experimental deuterium-labeling studies are combined with computational transition-state analysis to suggest that a carbonyl-retro-ene mechanism is operative. These studies demonstrate the synergy between experimental and theoretical chemistry and should promote the usage of both to better understand complex reaction mechanisms.

Chapter six illustrates the development of the reactivity of strained azacyclic 1,2,3-trienes. Experiments show the precursor to the pyridone triene can be generated on gram-scale and that it can be trapped efficiently in (4+2) cycloadditions. Current and future efforts are focused on discovering the modes of reactivity available to these trienes, examining the regioselectivity of unsubstituted and substituted variants, and performing intramolecular trappings. These studies should provide predictive understanding for the reactivity and selectivity of a previously

unexplored class of strained cyclic intermediate and should give access to diversely substituted pyridone products.

The dissertation of Ana Sydelle Bulger is approved.

Kendall N. Houk

Ellen M. Sletten

Yi Tang

Neil K. Garg, Committee Chair

University of California, Los Angeles

2024

"People help the people."

– Birdy

For my grandmother, Marilyn

For my parents, James and Mary

For Elisa and Darrin

For my husband, Nathaniel, and our precious cat, Bella

TABLE OF CONTENTS

ABSTRACT OF THE DISSERTATION ii

COMMITTEE PAGE vi

DEDICATION PAGE vii

TABLE OF CONTENTS viii

LIST OF FIGURES xv

LIST OF TABLES xxix

LIST OF ABBREVIATIONS xxxi

ACKNOWLEDGEMENTS xxxvi

BIOGRAPHICAL SKETCH xlviii

CHAPTER ONE: Activation of C–O and C–N Bonds Using Non-Precious-Metal Catalysis 1

1.1 Introduction 1

1.2 Activation of Aryl C–O Bonds 4

1.3 Activation of Aryl C–N Bonds 9

1.4 Activation of Acyl C–O Bonds 10

1.5 Activation of Acyl C–N Bonds 14

1.6 Outlook and Future Directions 24

1.7 Notes and References 25

CHAPTER TWO: Nickel-Catalyzed Conversion of Amides to Carboxylic Acids 58

2.1 Abstract 58

2.2 Introduction 58

2.3 Reaction Discovery and Optimization 59

2.4 Scope of Methodology 61

2.5 Selectivity Studies 63

2.6 Conclusion 65

2.7 Experimental Section 66

2.7.1 Materials and Methods 66

2.7.2 Experimental Procedures 67

2.7.2.1 Initial Experiments for Amide Hydrolysis 67

2.7.2.2 Optimization and Relevant Control Experiments 68

2.8.2.3 Scope of Methodology 70

2.8.2.4 1.0 mmol-Scale Reaction 74

2.8.2.5 Competition Experiments 75

2.8.2.6 Selective Cleavage of Aryl Amide in the Presence of an Ester 77

2.8 Spectra Relevant to Chapter Two 78

2.9 SFC Traces 82

2.10 Notes and References 84

CHAPTER THREE: Nickel-Catalyzed Conversion of Amides to Carboxylic Acids 90

3.1 Abstract 90

3.2 Introduction 90

3.3 Reaction Design 92

3.4 Reaction Discovery and Optimization 93

3.5 Scope of Methodology 100

3.6 Synthetic Elaboration of Indanone **3.9** 101

3.7 Conclusion 104

3.8 Experimental Section 106

3.8.1 Materials and Methods 106

3.8.2 Experimental Procedures 109

3.8.2.1 Ligand Syntheses 109

3.8.2.2 Reaction Discovery 116

3.8.2.2.1 Ligand Optimization 116

3.8.2.2.2 Reaction Optimization 119

3.8.2.3 Syntheses of Heck Cyclization Substrates 127

3.8.2.3.1 Syntheses of Carbonate Reductive Coupling Partners. 127

3.8.2.3.2 Reductive Cross-Coupling of Imides and Carbonates . 130

3.8.2.4 Syntheses of Racemic Indanones **(±)-3.25** and **(±)-3.27** 132

3.8.2.5 Scope of Methodology 133

3.8.2.6 Synthetic Elaboration of Mizoroki–Heck Cyclization Product **(+)-3.9** 136

3.8.2.7 Assignment of Absolute Stereochemical Configuration of Indanone **(+)-3.9** 146

3.9 SFC Traces 150

3.10 Spectra Relevant to Chapter Three 164

3.11 Notes and References 198

CHAPTER FOUR: Strain-Promoted Reactions of 1,2,3-Cyclohexatriene and Its Derivatives 210

4.1 Abstract 210

4.2 Introduction 211

4.3 Computational Structural Analysis 215

4.4 Reactivity of 1,2,3-Cyclohexatriene (**4.5**) 216

4.5 Reactivity of a Substituted 1,2,3-Cyclohexatriene Derivative 219

4.6 Regioselective Reactions of a Silyl-Substituted Triene 223

4.7 Leveraging Cyclic Trienes to Access Complex Scaffolds 226

4.8 Conclusion 228

4.9 Experimental Section 229

4.9.1 Method for Literature Searches for Strained Intermediate Studies 229

4.9.2 Materials and Methods 229

4.9.3 Experimental Procedures 232

4.9.3.1 Optimization of Trapping Reactions of 1,2,3-Cyclohexatriene (**4.5**) 232

4.9.3.2 Scope of Trapping Reactions of 1,2,3-Cyclohexatriene (**4.5**) 234

4.9.3.3 Synthesis of Silyl Triflate **4.42** 239

4.9.3.4 Scope of Trapping Reactions of Triene **4.43** 242

4.9.3.5 Synthesis of Silyl Triflate **4.76** 253

4.9.3.6 Trapping Reactions of Silyl Triene **4.75**.....256

4.9.3.7 Synthetic Elaboration of Triene Trapping Products 258

4.9.3.8 Competition Experiment with 1,2,3-Cyclohexatriene (**4.5**) and Benzyne (**4.20**).....275

4.9.4 Computational Section..... 275

4.9.4.1 Computational Methods.....275

4.9.4.2 Calculated Energies of Selected C_6H_6 Isomers.....276

4.9.4.3 Structure of 1,2,3-Cyclohexatriene (**4.5**) 276

4.9.4.4 Transition State Analysis for Reaction of Triene **4.80** with Phenoxide **4.34**.....277

4.9.4.5 Relative Stereochemical Assignment of Thietanes **4.69** and **4.93** 279

4.9.4.6 Cartesian Coordinates of Optimized Geometries 281

4.10 Spectra Relevant to Chapter Four 282

4.11 Notes and References 336

CHAPTER FIVE: Evaluation of Retro-Aldol vs Retro-Carbonyl-Ene Mechanistic Pathways in a Complexity Generating C–C Bond Fragmentation 348

5.1 Abstract 348

5.2 Introduction 348

5.3 Plausible Mechanistic Pathways 351

5.4 Computational Studies 352

5.5 Experimental Results 355

5.6 Conclusion 356

5.7 Experimental Section 357

5.7.1 Materials and Methods 357

5.7.2 Experimental Procedures 358

5.7.2.1 Deuterium Labeling Trapping Experiment 358

5.7.2.2 Grignard Addition 360

5.7.2.3 Formation of Compound **5.8-*d*** 361

5.7.3 Computational Section 362

5.7.3.1 Computational Methods 362

5.7.3.2 Transition State Analysis for the Potential Retro-Carbonyl-Ene and Retro Aldol Mechanistic Pathways 363

5.7.3.3 Cartesian Coordinates 365

5.8 Spectra Relevant to Chapter Five 366

5.9 Notes and References 371

CHAPTER SIX: Generation and Trapping of an Azacyclic 1,2,3-Hexatriene.....378

6.1 Abstract.....378

6.2 Introduction.....378

6.3 Synthesis of Azacyclic Triene Precursor.....380

6.4 Key Validation of Azacyclic Triene.....381

6.5 Future Directions.....381

6.6 Conclusion.....384

6.7 Experimental Section.....386

6.7.1 Materials and Methods.....386

6.7.2 Experimental Procedures.....388

6.7.2.1 Synthesis of azacyclic triene precursor **6.14**.....388

6.7.2.2 Azacyclic 1,2,3-triene trapping experiments.....392

6.8 Spectra Relevant to Chapter Six.....394

6.9 Notes and References.....403

LIST OF FIGURES

CHAPTER ONE

Figure 1.1 (A) Classical building blocks and those historically considered inert under traditional cross-coupling conditions. (B) Overview of recently explored electrophiles in cross-coupling reactions 2

Figure 1.2 The scope of this review, which focuses on the activation of phenol, amide, and ester electrophiles 3

Figure 1.3 Overview of our laboratory's studies on using phenol derivatives as cross-coupling electrophiles in base-metal-catalyzed C–C and C–N bond-forming reactions 4

Figure 1.4 Select examples of Ni- and Fe-catalyzed cross-couplings of pivalates, carbonates, and carbamates reported by our laboratory 6

Figure 1.5 Select examples of nickel- and iron-catalyzed cross-couplings of sulfamates reported by our laboratory 8

Figure 1.6 Benchtop aminations of aryl sulfamates and carbamates and gram-scale coupling of **1.27** in a green solvent 9

Figure 1.7 Overview of aniline derivatives employed in metal-catalyzed cross-coupling reactions 10

Figure 1.8 Historical approaches to metal-catalyzed ester acyl C–O bond activation and advantages of alkyl esters as substrates 11

Figure 1.9 Recent advances in the nickel-catalyzed amidation of methyl esters 13

Figure 1.10 Nickel-catalyzed domino Heck and decarbonylative cross-couplings of methyl esters 14

Figure 1.11 The resonance stabilization and potential synthetic utility of amide C–N bond activations 15

Figure 1.12 Recent advances in the nickel-catalyzed activation of aryl amide C–N bonds by our laboratory.....18

Figure 1.13 Asymmetric reactions of aryl amides developed by our laboratory 19

Figure 1.14 Recent advances in the nickel-catalyzed activation of aliphatic amide C–N bonds by our laboratory 21

Figure 1.15 Practical advances in nickel-catalyzed activations of amides disclosed by our laboratory.....22

Figure 1.16 *N*-substituent variation, alternative reaction modes, and decarbonylative reactions of amides utilizing nickel catalysis.....23

CHAPTER TWO

Figure 2.1 Select examples of recent advances in the nickel-catalyzed activation of amides 59

Figure 2.2 Initial studies and control experiments for the nickel-catalyzed hydrolysis of amides..... 60

Figure 2.3 Scope of the amide substrate..... 62

Figure 2.4 Competition experiments demonstrate substrate selectivity..... 64

Figure 2.5 Cleavage of a valine-derived amide in the presence of an ester 65

Figure 2.6 ^{1}H NMR (500 MHz, DMSO-d_6) of compound **2.6**.....79

Figure 2.7 ^{1}H NMR (300 MHz, $CDCl_3$) of compound **2.2** 79

Figure 2.8 ^{1}H NMR (600 MHz, $CDCl_3$) of compound **2.10** 80

Figure 2.9 ^{1}H NMR (500 MHz, DMSO-d_6) of compound **2.11** 80

Figure 2.10 ^{1}H NMR (600 MHz, DMSO-d_6) of compound **2.12** 81

Figure 2.11 ^{1}H NMR (600 MHz, DMSO-d_6) of compound **2.13** 81

Figure 2.12 ^{1}H NMR (300 MHz, $CDCl_3$) of compound **2.18** 82

Figure 2.13 SFC trace of **rac-2.18** 83

Figure 2.14 SFC trace of **2.18** 83

CHAPTER THREE

Figure 3.1 (A) Asymmetric metal-catalyzed reactions of acyl electrophiles and current limitations. (B) Current state-of-the-art of amide cross-coupling reactions 92

Figure 3.2 Overview of the reaction design and proposed mechanism..... 93

Figure 3.3 Survey of Chiral NHC salts with in situ free-basing 95

Figure 3.4 Results using select chiral NHC ligand salts with amide **3.6** 96

Figure 3.5 Generation of free carbene **3.10**..... 97

Figure 3.6 Survey of alcohol and amine additives in the transformation..... 99

Figure 3.7 Examples of methodology 101

Figure 3.8 Determination of the absolute stereochemistry of **3.9** 102

Figure 3.9 Synthetic elaboration of indanone **3.9** to skeletal editing derivatives **3.29**–**3.31**.....103

Figure 3.10 Synthetic elaboration of indanone **3.9** to complex products **3.35** and **3.36** 104

Figure 3.11 NHC salts evaluated during asymmetric reaction development. 118

Figure 3.12 ORTEP representation of X-ray crystallographic structure of **(–)-3.28** ..148
Figure 3.13 SFC trace for **(±)-3.9** ..153
Figure 3.14 SFC trace for **(+)-3.9** ..153
Figure 3.15 SFC trace for **(±)-3.23** ..154
Figure 3.16 SFC trace for **(+)-3.23** ..154
Figure 3.17 SFC trace for **(±)-3.25** ..155
Figure 3.18 SFC trace for **(+)-3.25** ..155
Figure 3.19 SFC trace for **(±)-3.27** ..156
Figure 3.20 SFC trace for **(+)-3.27** ..156
Figure 3.21 SFC trace for **(±)-3.12** ..157
Figure 3.22 SFC trace for **(+)-3.12** ..157
Figure 3.23 SFC trace for **(±)-3.30** ..158
Figure 3.24 SFC trace for **(+)-3.30** ..158
Figure 3.25 SFC trace for **(±)-3.31** ..159
Figure 3.26 SFC trace for **(+)-3.31** ..159
Figure 3.27 SFC trace for **(±)-3.35** ..160
Figure 3.28 SFC trace for **(–)-3.35** ..160
Figure 3.29 SFC trace for **(±)-3.71** ..161
Figure 3.30 SFC trace for **(–)-3.71** ..161
Figure 3.31 SFC trace for **(±)-3.36** ..162
Figure 3.32 SFC trace for **(–)-3.36** ..162
Figure 3.33 SFC trace for **(±)-3.72** ..163
Figure 3.34 SFC trace for **(–)-3.72** ..163

Figure 3.35 ^{1}H NMR (500 MHz, $CDCl_3$) of compound **L3.19**.....165

Figure 3.36 ^{13}C NMR (125 MHz, $CDCl_3$) of compound **L3.19**.....165

Figure 3.37 ^{1}H NMR (500 MHz, $CDCl_3$) of compound **L3.8**.....166

Figure 3.38 ^{13}C NMR (125 MHz, $CDCl_3$) of compound **L3.8**.....166

Figure 3.39 ^{1}H NMR (500 MHz, $CDCl_3$) of compound **L3.16**.....167

Figure 3.40 ^{13}C NMR (125 MHz, $CDCl_3$) of compound **L3.16**.....167

Figure 3.41 ^{1}H NMR (500 MHz, $CDCl_3$) of compound **L3.17**.....168

Figure 3.42 ^{13}C NMR (125 MHz, $CDCl_3$) of compound **L3.17**.....168

Figure 3.43 ^{19}F NMR (282 MHz, $CDCl_3$) of compound **L3.17** 169

Figure 3.44 ^{1}H NMR (500 MHz, $CDCl_3$) of compound **L3.18**.....170

Figure 3.45 ^{13}C NMR (125 MHz, $CDCl_3$) of compound **L3.18**.....170

Figure 3.46 ^{1}H NMR (500 MHz, $CDCl_3$) of compound **L3.14**.....171

Figure 3.47 ^{13}C NMR (125 MHz, $CDCl_3$) of compound **L3.14**.....171

Figure 3.48 ^{1}H NMR (500 MHz, $CDCl_3$) of compound **3.61** 172

Figure 3.49 ^{13}C NMR (125 MHz, $CDCl_3$) of compound **3.61** 172

Figure 3.50 ^{1}H NMR (500 MHz, $CDCl_3$) of compound **L3.15**.....173

Figure 3.51 ^{13}C NMR (125 MHz, $CDCl_3$) of compound **L3.15**.....173

Figure 3.52 ^{1}H NMR (500 MHz, toluene-D8) of compound **3.10** 174

Figure 3.53 ^{13}C NMR (125 MHz, toluene-D8) of compound **3.10** 174

Figure 3.54 ^{1}H NMR (600 MHz, $CDCl_3$) of compound **3.64** 175

Figure 3.55 ^{13}C NMR (125 MHz, $CDCl_3$) of compound **3.64** 175

Figure 3.56 ^{1}H NMR (500 MHz, $CDCl_3$) of compound **3.66** 176

Figure 3.57 ^{13}C NMR (125 MHz, $CDCl_3$) of compound **3.66** 176

Figure 3.58 ^{1}H NMR (600 MHz, $CDCl_3$) of compound **3.26** 177

Figure 3.59 ^{13}C NMR (150 MHz, $CDCl_3$) of compound **3.26** 177

Figure 3.60 ^{1}H NMR (500 MHz, $CDCl_3$) of compound **3.24** 178

Figure 3.61 ^{13}C NMR (125 MHz, $CDCl_3$) of compound **3.24** 178

Figure 3.62 ^{1}H NMR (500 MHz, $CDCl_3$) of compound **3.25** 179

Figure 3.63 ^{13}C NMR (150 MHz, $CDCl_3$) of compound **3.25** 179

Figure 3.64 ^{1}H NMR (600 MHz, $CDCl_3$) of compound **3.27** 180

Figure 3.65 ^{13}C NMR (150 MHz, $CDCl_3$) of compound **3.27** 180

Figure 3.66 ^{1}H NMR (600 MHz, $CDCl_3$) of compound **3.9** 181

Figure 3.67 ^{1}H NMR (500 MHz, $CDCl_3$) of compound **3.23** 181

Figure 3.68 ^{1}H NMR (600 MHz, $CDCl_3$) of compound **3.12** 182

Figure 3.69 ^{1}H NMR (600 MHz, $CDCl_3$) of compound **3.69** 183

Figure 3.70 ^{13}C NMR (150 MHz, $CDCl_3$) of compound **3.69** 183

Figure 3.71 ^{1}H NMR (600 MHz, $CDCl_3$) of compound **3.29** 184

Figure 3.72 ^{13}C NMR (125 MHz, $CDCl_3$) of compound **3.29** 184

Figure 3.73 ^{1}H NMR (600 MHz, $CDCl_3$) of compound **3.70** 185

Figure 3.74 ^{13}C NMR (125 MHz, $CDCl_3$) of compound **3.70** 185

Figure 3.75 ^{1}H NMR (600 MHz, $CDCl_3$) of compound **3.30** 186

Figure 3.76 ^{13}C NMR (150 MHz, $CDCl_3$) of compound **3.30** 186

Figure 3.77 ^{1}H NMR (600 MHz, $CDCl_3$) of compound **3.31** 187

Figure 3.78 ^{13}C NMR (125 MHz, $CDCl_3$) of compound **3.31** 187

Figure 3.79 ^{1}H NMR (600 MHz, $CDCl_3$) of compound **3.32** 188

Figure 3.80 ^{13}C NMR (125 MHz, $CDCl_3$) of compound **3.32** 188

Figure 3.81 ^{1}H NMR (600 MHz, $CDCl_3$) of compound **3.34** 189

Figure 3.82 ^{13}C NMR (150 MHz, $CDCl_3$) of compound **3.34** 189

Figure 3.83 NOESY (600 MHz, $CDCl_3$) of compound **3.34** 190

Figure 3.84 ^{1}H NMR (600 MHz, DMSO-D_6) of compound **3.35** 191

Figure 3.85 ^{13}C NMR (150 MHz, DMSO-D_6) of compound **3.35** 191

Figure 3.86 NOESY (600 MHz, DMSO-D_6) of compound **3.35** 192

Figure 3.87 ^{1}H NMR (500 MHz, DMSO-D_6) of compound **3.71** 193

Figure 3.88 ^{13}C NMR (125 MHz, DMSO-D_6) of compound **3.71** 193

Figure 3.89 ^{1}H NMR (600 MHz, $CDCl_3$) of compound **3.36** 194

Figure 3.90 ^{13}C NMR (150 MHz, $CDCl_3$) of compound **3.36** 194

Figure 3.91 NOESY (600 MHz, $CDCl_3$) of compound **3.36** 195

Figure 3.92 ^{1}H NMR (600 MHz, $CDCl_3$) of compound **3.72** 196

Figure 3.93 ^{13}C NMR (150 MHz, $CDCl_3$) of compound **3.72** 196

Figure 3.94 ^{1}H NMR (300 MHz, $CDCl_3$) of compound **3.28** 197

Figure 3.95 ^{13}C NMR (125 MHz, $CDCl_3$) of compound **3.28** 197

CHAPTER FOUR

Figure 4.1 Selected strained isomers of benzene (**4.1**) and comparison of reaction coordinate diagrams 212

Figure 4.2 Strained cyclic intermediates and overview of current study 214

Figure 4.3A Geometry-optimized structures and frontier molecular orbitals 216

Figure 4.3B Scope of reactions of triene **4.5** 218

Figure 4.4A Synthesis of silyl triflate **4.42** 220

Figure 4.4B Scope of reactions of triene **4.43** 222

Figure 4.5 Structure and regioselective reactions of a monosubstituted cyclic triene 225

Figure 4.6 Strained 1,2,3-cyclohexatrienes in multistep synthesis 227

Figure 4.7 ORTEP representation of X-ray crystallographic structure **4.81** 261

Figure 4.8 ORTEP representation of X-ray crystallographic structure **4.84** 267

Figure 4.9 SFC trace for **(±)-4.78** 273

Figure 4.10 SFC trace for **(+)-4.78** 273

Figure 4.11 SFC trace for **(±)-4.19** 274

Figure 4.12 SFC trace for **(+)-4.19** 274

Figure 4.13 Geometry of 1,2,3-cyclohexatriene (**4.5**) 276

Figure 4.14 DIAS strain analysis along a relaxed scan of the forming C–O bond 278

Figure 4.15 Transition state structures for the attack of **4.34** (Na^+ omitted) onto **4.80** 279

Figure 4.16 Atom numbers used in Table 4.8 and Table 4.9 281

Figure 4.17 ^{1}H NMR (600 MHz, C_6D_6) of compound **4.27** 283

Figure 4.18 ^{1}H NMR (600 MHz, C_6D_6) of compound **4.28** 284

Figure 4.19 ^{13}C NMR (150 MHz, C_6D_6) of compound **4.28** 284

Figure 4.20 ^{1}H NMR (600 MHz, C_6D_6) of compound **4.29** 285

Figure 4.21 ^{13}C NMR (150 MHz, C_6D_6) of compound **4.29** 285

Figure 4.22 ^{1}H NMR (500 MHz, CD_2Cl_2) of compound **4.30** 286

Figure 4.23 ^{13}C NMR (125 MHz, CD_2Cl_2) of compound **4.30** 286

Figure 4.24 ^{1}H NMR (500 MHz, C_6D_6) of compound **4.35** 287

Figure 4.25 ^{13}C NMR (100 MHz, C_6D_6) of compound **4.35**.....287
Figure 4.26 ^{1}H NMR (500 MHz, C_6D_6) of compound **4.36**.....288
Figure 4.27 ^{13}C NMR (125 MHz, C_6D_6) of compound **4.36**.....288
Figure 4.28 ^{1}H NMR (600 MHz, C_6D_6) of compound **4.37**.....289
Figure 4.29 ^{13}C NMR (150 MHz, C_6D_6) of compound **4.37**.....289
Figure 4.30 ^{1}H NMR (500 MHz, C_6D_6) of compound **4.38**.....290
Figure 4.31 ^{13}C NMR (125 MHz, C_6D_6) of compound **4.38**.....290
Figure 4.32 ^{1}H NMR (500 MHz, $CDCl_3$) of compound **4.40** 291
Figure 4.33 ^{13}C NMR (150 MHz, $CDCl_3$) of compound **4.40** 291
Figure 4.34 ^{1}H NMR (400 MHz, $CDCl_3$) of compound **4.41** 292
Figure 4.35 ^{13}C NMR (100 MHz, $CDCl_3$) of compound **4.41** 292
Figure 4.36 ^{1}H NMR (600 MHz, $CDCl_3$) of compound **4.42** 293
Figure 4.37 ^{13}C NMR (150 MHz, $CDCl_3$) of compound **4.42** 293
Figure 4.38 ^{19}F NMR (376 MHz, $CDCl_3$) of compound **4.42**.....294
Figure 4.39 ^{1}H NMR (600 MHz, C_6D_6) of compound **4.50**.....295
Figure 4.40 ^{13}C NMR (150 MHz, C_6D_6) of compound **4.50**.....295
Figure 4.41 ^{1}H NMR (500 MHz, $CDCl_3$) of compound **4.51** 296
Figure 4.42 ^{13}C NMR (125 MHz, $CDCl_3$) of compound **4.51** 296
Figure 4.43 ^{1}H NMR (600 MHz, $CDCl_3$) of compound **4.52** 297
Figure 4.44 ^{13}C NMR (150 MHz, $CDCl_3$) of compound **4.52** 297
Figure 4.45 ^{1}H NMR (500 MHz, $CDCl_3$) of compound **4.53** 298
Figure 4.46 ^{13}C NMR (125 MHz, $CDCl_3$) of compound **4.53** 298
Figure 4.47 ^{1}H NMR (500 MHz, C_6D_6) of compound **4.54**.....299

Figure 4.48 ^{13}C NMR (125 MHz, C_6D_6) of compound **4.54**.....299

Figure 4.49 ^{1}H NMR (500 MHz, CD_3CN) of compound **4.55**.....300

Figure 4.50 ^{13}C NMR (150 MHz, C_6D_6) of compound **4.55**.....300

Figure 4.51 ^{1}H NMR (500 MHz, C_6D_6) of compound **4.56**.....301

Figure 4.52 ^{13}C NMR (125 MHz, C_6D_6) of compound **4.56**.....301

Figure 4.53 ^{1}H NMR (500 MHz, C_6D_6) of compound **4.57**.....302

Figure 4.54 ^{13}C NMR (150 MHz, CD_2Cl_2) of compound **4.57**.....302

Figure 4.55 ^{1}H NMR (600 MHz, $CDCl_3$) of compound **4.58**.....303

Figure 4.56 ^{13}C NMR (150 MHz, $CDCl_3$) of compound **4.58**.....303

Figure 4.57 ^{1}H NMR (600 MHz, $CDCl_3$) of compound **4.66**.....304

Figure 4.58 ^{13}C NMR (150 MHz, CD_3CN) of compound **4.66**.....304

Figure 4.59 ^{1}H NMR (500 MHz, C_6D_6) of compound **4.67**.....305

Figure 4.60 ^{13}C NMR (125 MHz, $CDCl_3$) of compound **4.67**.....305

Figure 4.61 ^{1}H NMR (500 MHz, C_6D_6) of compound **4.68**.....306

Figure 4.62 ^{13}C NMR (125 MHz, C_6D_6) of compound **4.68**.....306

Figure 4.63 ^{1}H NMR (600 MHz, C_6D_6) of compound **4.69**.....307

Figure 4.64 ^{13}C NMR (150 MHz, C_6D_6) of compound **4.69**.....307

Figure 4.65 ^{13}C NMR (125 MHz, C_6D_6) of compound **4.69** and **4.93**.....308

Figure 4.66 ^{1}H NMR (500 MHz, C_6D_6) of compound **4.70**.....309

Figure 4.67 ^{13}C NMR (125 MHz, C_6D_6) of compound **4.70**.....309

Figure 4.68 ^{1}H NMR (500 MHz, C_6D_6) of compound **4.71**.....310

Figure 4.69 ^{13}C NMR (150 MHz, $CDCl_3$) of compound **4.71**.....310

Figure 4.70 ^{1}H NMR (600 MHz, CD_2Cl_2) of compound **4.72**.....311

Figure 4.71 ^{13}C NMR (150 MHz, CD_2Cl_2) of compound **4.72** 311
Figure 4.72 ^{1}H NMR (500 MHz, $CDCl_3$) of compound **4.73** 312
Figure 4.73 ^{13}C NMR (150 MHz, $CDCl_3$) of compound **4.73** 312
Figure 4.74 ^{1}H NMR (500 MHz, C_6D_6) of compound **4.74** 313
Figure 4.75 ^{13}C NMR (125 MHz, C_6D_6) of compound **4.74** 313
Figure 4.76 ^{1}H NMR (600 MHz, $CDCl_3$) of compound **4.94** 314
Figure 4.77 ^{13}C NMR (150 MHz, $CDCl_3$) of compound **4.94** 314
Figure 4.78 ^{1}H NMR (600 MHz, $CDCl_3$) of compound **4.96** 315
Figure 4.79 ^{13}C NMR (150 MHz, $CDCl_3$) of compound **4.96** 315
Figure 4.80 ^{1}H NMR (600 MHz, C_6D_6) of compound **4.76** 316
Figure 4.81 ^{13}C NMR (150 MHz, C_6D_6) of compound **4.76** 316
Figure 4.82 ^{19}F NMR (376 MHz, C_6D_6) of compound **4.76** 317
Figure 4.83 ^{1}H NMR (600 MHz, $CDCl_3$) of compound **4.78** 318
Figure 4.84 ^{13}C NMR (150 MHz, $CDCl_3$) of compound **4.78** 318
Figure 4.85 ^{1}H NMR (600 MHz, C_6D_6) of compound **4.79** 319
Figure 4.86 ^{13}C NMR (150 MHz, C_6D_6) of compound **4.79** 319
Figure 4.87 ^{1}H NMR (500 MHz, C_6D_6) of compound **4.81** 320
Figure 4.88 ^{13}C NMR (125 MHz, C_6D_6) of compound **4.81** 320
Figure 4.89 NOESY (600 MHz, acetone-d_6) of compound **4.81** 321
Figure 4.90 ^{1}H NMR (600 MHz, acetone-d_6) of compound **4.97** 322
Figure 4.91 ^{13}C NMR (125 MHz, acetone-d_6) of compound **4.97** 322
Figure 4.92 NOESY (600 MHz, acetone-d_6) of compound **4.97** 323
Figure 4.93 ^{1}H NMR (600 MHz, C_6D_6) of compound **4.82** 324

Figure 4.94 ^{13}C NMR (150 MHz, C_6D_6) of compound **4.82**.....324

Figure 4.95 NOESY (600 MHz, C_6D_6) of compound **4.82**.....325

Figure 4.96 ^{1}H NMR (600 MHz, C_6D_6) of compound **4.98**.....326

Figure 4.97 ^{13}C NMR (125 MHz, C_6D_6) of compound **4.98**.....326

Figure 4.98 NOESY (600 MHz, C_6D_6) of compound **4.98**.....327

Figure 4.99 ^{1}H NMR (600 MHz, C_6D_6) of compounds **4.83** and **4.99**.....328

Figure 4.100 ^{13}C NMR (125 MHz, C_6D_6) of compounds **4.83** and **4.99**.....328

Figure 4.101 NOESY (600 MHz, C_6D_6) of compounds **4.83** and **4.99**.....329

Figure 4.102 ^{1}H NMR (500 MHz, C_6D_6) of compound **4.84**.....330

Figure 4.103 ^{13}C NMR (150 MHz, CD_3OD) of compound **4.84**.....330

Figure 4.104 ^{1}H NMR (600 MHz, $CDCl_3$) of compound (–)-**4.87**.....331

Figure 4.105 ^{13}C NMR (150 MHz, $CDCl_3$) of compound (–)-**4.87**.....331

Figure 4.106 ^{1}H NMR (400 MHz, $CDCl_3$) of compound (–)-**4.100**.....332

Figure 4.107 ^{13}C NMR (100 MHz, $CDCl_3$) of compound (–)-**4.100**.....332

Figure 4.108 NOESY (400 MHz, $CDCl_3$) of compound (–)-**4.100**.....333

Figure 4.109 ^{1}H NMR (600 MHz, $CDCl_3$) of compound (+)-**4.19**.....334

Figure 4.110 ^{13}C NMR (150 MHz, $CDCl_3$) of compound (+)-**4.19**.....334

Figure 4.111 NOESY (800 MHz, $CDCl_3$) of compound (+)-**4.19**.....335

CHAPTER FIVE

Figure 5.1 A) Prior studies of strained intermediates. B) Reactivity of 1,2,3-cyclohexatrienes. C) Elaboration of triene **5.6** to adduct **5.8**.....349

Figure 5.2 Trapping of 1,2,3-triene **5.6** and elaboration to **5.8** via retro-carbonyl-ene reaction or retro-aldol reaction.....351

Figure 5.3 Details of plausible mechanistic pathways 352

Figure 5.4 Computational study of reaction pathways predicts the retro-carbonyl-ene pathway is favorable 354

Figure 5.5 Synthesis of **5.8-*d*** and results of Diels–Alder/rearrangement cascade indicating a retro-carbonyl-ene pathway 356

Figure 5.6 Distances of two partially formed bonds in **TS-5.1** along the IRC 363

Figure 5.7 Relax scan of the C–C bond length from **5.12**, corresponding to the retro-aldol pathway.....364

Figure 5.8 Computed energy diagram for the formation of **5.8** in DMSO.....365

Figure 5.9 ^{1}H NMR (500 MHz, C_6D_6) of compound **5.10-*d***.....367

Figure 5.10 ^{2}H NMR (77 MHz, C_6H_6) of compound **5.10-*d***.....367

Figure 5.11 ^{1}H NMR (600 MHz, C_6D_6) of compound **5.11-*d***.....368

Figure 5.12 ^{2}H NMR (77 MHz, C_6H_6) of compound **5.11-*d***.....368

Figure 5.13 ^{1}H NMR (600 MHz, C_6D_6) of compound **5.7-*d***.....369

Figure 5.14 ^{2}H NMR (77 MHz, C_6H_6) of compound **5.7-*d***.....369

Figure 5.15 ^{1}H NMR (600 MHz, C_6D_6) of compound **5.8-*d***.....370

Figure 5.16 ^{2}H NMR (77 MHz, C_6H_6) of compound **5.8-*d***.....370

CHAPTER SIX

Figure 6.1 Overview of strained intermediates 379

Figure 6.2 Route to azacyclic triene precursor **6.14**.....380

Figure 6.3 (4+2) Cycloadditions using precursor **6.14**.....381

Figure 6.4 Outline for future studies 384

Figure 6.5 ^{1}H NMR (500 MHz, $CDCl_3$) of compound **6.11** 395

Figure 6.6 ^{1}H NMR (600 MHz, C_6D_6) of compound **6.12**.....396

Figure 6.7 ^{13}C NMR (150 MHz, C_6D_6) of compound **6.12**.....396

Figure 6.8 ^{1}H NMR (600 MHz, $CDCl_3$) of compound **6.13** 397

Figure 6.9 ^{13}C NMR (125 MHz, $CDCl_3$) of compound **6.13** 397

Figure 6.10 ^{19}F NMR (565 MHz, $CDCl_3$) of compound **6.13**.....398

Figure 6.11 ^{1}H NMR (600 MHz, $CDCl_3$) of compound **6.14** 399

Figure 6.12 ^{13}C NMR (150 MHz, $CDCl_3$) of compound **6.14** 399

Figure 6.13 ^{19}F NMR (565 MHz, $CDCl_3$) of compound **6.14**.....400

Figure 6.14 ^{1}H NMR (500 MHz, $CDCl_3$) of compound **6.15** 401

Figure 6.15 ^{13}C NMR (125 MHz, $CDCl_3$) of compounds **6.15**.....401

Figure 6.16 ^{1}H NMR (500 MHz, $CDCl_3$) of compounds **6.18**.....402

Figure 6.17 ^{13}C NMR (125 MHz, $CDCl_3$) of compound **6.18** 402

LIST OF TABLES

CHAPTER TWO

Table 2.1 Optimization of Reaction Conditions 61

Table 2.2 Variation of the *N*-Substituents.....63

Table 2.3 Relevant Control Experiments.....69

CHAPTER THREE

Table 3.1 Ligand evaluation results 119

Table 3.2 Evaluation of stoichiometric loading of NaO*t*-Bu with **3.6** and **L3.15** ...121

Table 3.3 Variation of base employed with **3.6** and **L3.15**.....121

Table 3.4 Solvent variation with **3.6** and **3.10** 124

Table 3.5 Temperature variation with **3.6** and **3.10**.....124

Table 3.6 Variation of catalyst stoichiometry with **3.6**.....124

Table 3.7 Evaluation of alcohol additives with **3.6** and **3.10**.....125

Table 3.8 Evaluation of acyclic amine additives with **3.6** and **3.10** 125

Table 3.9 Evaluation of cyclic amine additives with **3.6** and **3.10** 126

Table 3.10 Crystal data and structure refinement for compound **(–)-3.28**.....149

Table 3.11 SFC conditions and data 150

CHAPTER FOUR

Table 4.1 Selected Optimization Screening Results 233

Table 4.2 Crystal Data and Structure Refinement for Compound **4.81**.....261

Table 4.3 Crystal Data and Structure Refinement for Compound **4.84**.....267

Table 4.4 SFC Conditions and Data 272

Table 4.5 Computed Energies of Selected C_6H_6 Isomers 276

Table 4.6 Computed Energies for the Reaction of Triene **4.80** with Phenoxide **4.34** 277

Table 4.7 Distortion/Interaction-Activation Strain Analysis 277

Table 4.8 Comparison of Experimental and Computed NMR Chemical Shifts for Structure **4.69** 280

Table 4.9 Comparison of Experimental and Computed NMR Chemical Shifts for Structure **4.93** 281

LIST OF ABBREVIATIONS

α	alpha
β	beta
γ	gamma
λ	wavelength
μ	micro
π	pi
δ	chemical shift
Δ	heat or difference
(Het)	hetero
app.	apparent
aq.	aqueous
Ar	aryl
B3LYP	Becke, 3-parameter, Lee–Yang–Parr (functional)
Bn	benzyl
Boc	*tert*-butyloxy carbonyl
BOX	bis(oxazoline)
br	broad
BRSM	based on recovered starting material
Bu	butyl
n-Bu	butyl (linear)
t-Bu	*tert*-butyl
c	concentration for specific rotation measurements
°C	degrees Celsius
calcd	calculated
Cbz	carboxybenzyl
CCDC	Cambridge Crystallographic Data Centre
cm	centimeter
cod	1,5-cyclooctadiene
conc.	concentration
Cp	cyclopentadienyl
CREST	conformer-rotamer ensemble sampling tool
Cy	cyclohexyl
DABCO	1,4-diazabicyclo[2.2.2]octane

DART-MS	Direct Analysis in Real Time – Mass Spectroscopy
dba	dibenzylideneacetone
d	doublet
dd	doublet of doublets
ddd	doublet of doublet of doublets
dddd	doublet of doublet of doublet of doublets
ddt	doublet of doublet of triplets
dq	doublet of quartets
dr	diastereomeric ratio
dt	doublet of triplets
δ	chemical shift
DFT	density functional theorem
dist	distortion
DMAP	4-dimethylaminopyridine
dmdba	3,5,3',5'-dimethoxydibenzylideneacetone
DME	1,2-dimethoxyethane
DMF	*N*,*N*-dimethylformamide
DMSO	dimethyl sulfoxide
ε	dielectric constant
E_a	activation energy
EDC	1-ethyl-3-(3-dimethylaminopropyl)carbodiimide
ee	enantiomeric excess
equiv	equivalent
er	enantiomeric ratio
ESI	electrospray ionization
Et	ethyl
EtOAc	ethyl acetate
η	eta
Fe	iron
FT	Fourier transform
g	gram(s)
G	Gibb's free energy
h	hour(s)
HCl	hydrochloric acid

HF	Hartree Fock
Het	heterocycle
HMPA	hexamethylphosphoramide
HOMO	highest occupied molecular orbital
HRMS	high resolution mass spectroscopy
Hz	hertz
int	interaction
IR	infrared (spectroscopy)
i-Pr	iso-propyl
J	coupling constant
kcal/mol	kilocalories to mole ratio
KHMDS	Potassium hexamethyldisilazide
LANL2DZ	Los Alamos National Laboratory 2 double-zeta basis set
Leu	leucine
L	liter or ligand
LDA	lithium diisopropylamide
LiHMDS	Lithium hexamethyldisilazide
LUMO	lowest unoccupied molecular orbital
m	multiplet or milli
m	meta
M	molar
m/z	mass to charge ratio
Me	methyl
MeCN	acetonitrile
MeOH	methanol
MHz	megahertz
min	minute(s)
mm	millimeter
mol	mole(s)
mp	melting point
N_2	nitrogen gas
NaHMDS	Sodium hexamethyldisilazide
NaO*t*-Bu	Sodium *tert*-butoxide
Nf	nonafluorobutanesulfonyl

NMR	nuclear magnetic resonance
NO_3	nitrate
NOESY	Nuclear Overhauser Enhancement Spectroscopy
o	ortho
ORTEP	Oak Ridge Thermal-Ellipsoid Plot Program
p	para
Ph	phenyl
PHOX	phosphinooxazoline
PMP	para-methoxy phenyl
ppm	parts per million
q	quartet
quant	quantitative
quint	quintet
rac	racemic
rt	room temperature
R_f	retention factor
s	singlet
sat.	saturated
SDD	Stuttgart/Dresden pseudopotential
SFC	supercritical fluid chromatography
SMD	solvation model based on density
SSA	shield-solvation analysis
t	triplet
temp	temperature
TBAF	tetrabutylammonium fluoride
TES	triethylsilyl
TESCl	triethylsilyl chloride
Tf	trifluoromethanesulfonyl
THF	tetrahydrofuran
TLC	thin layer chromatography
TMSCl	trimethylsilyl chloride
tol	tolyl
Ts	*p*-toluenesulfonyl (tosyl)
TS	transition state

UV	ultraviolet
val	valine
w/w	weight by weight
wt%	percentage by mass
ZPVE	zero-point vibrational energy

ACKNOWLEDGEMENTS

Before my graduate career began, there were several people who inspired me in the decision to pursue a career in chemistry. Without their support I would almost certainly not be here today. My interest in chemistry was first sparked in my junior year of high school during chemistry class, by my teacher, Mr. Hoffman. His witty jokes and enthusiasm for the subject inspired me to learn more, and he was the first person to actually encourage me to study chemistry. Although I initially evaded his advice and tried to major in biology once I made my way to Westmont College in 2015, I soon switched to the chemistry major and never looked back. This was heavily influenced by my decision to take the honors general chemistry course taught by professor Kristi Lazar Cantrell, who tackled a variety of concepts with impressive depth. She served as an incredibly intelligent and kind mentor throughout my undergraduate studies. I am also so grateful to the other professors that supported me in the chemistry department at Westmont, including professors Carrie Hill, Michael Everest, Brandon Haines, Stephen Contakes, and Amanda Silberstein. Professor Carrie Hill was the first to allow me an opportunity to explore teaching as an undergraduate lab teaching assistant. Dr. Everest taught me important concepts in quantum mechanics and thermodynamics in our senior year seminar class. Dr. Haines entered Westmont during the last year of my undergraduate studies, and I was very privileged to gain an introduction to computational chemistry under his mentorship. I took many classes taught by Dr. Contakes, who was the first to expose me to excellent scientific writing, and who was also not afraid to ask tough questions that helped shape me into a better scientist and person. Dr. Amanda Silberstein provided me with my first opportunity to research and I am so grateful to have had the opportunity to work in her lab during my last year at Westmont. She is an incredibly bright person with a quick-

witted sense of humor, and she was really the person who inspired and supported in my decision to pursue graduate studies in organic chemistry. As a prior Garg lab alumna, she also introduced me to the idea of attending UCLA. Most of all, I am so grateful to have had her as a friend.

At my first exposure to the Garg lab during my orientation visit to UCLA, I was immediately impressed by Neil's management of the lab to make it simultaneously an efficient and fun place to do chemistry. I want to sincerely thank Neil for his mentorship, advice, and guidance over the years. I really admire his unwavering dedication to everyone who joins the lab and his commitment to helping them be the best chemist they can be. During my time at UCLA, Neil served as the department chair every year but my last year and led the department through a global pandemic, while still staying individually engaged and committed to our group of 15+ people, which is not an easy task. Neil is always thoughtful about how to help his students grow and puts an enormous amount of effort into helping them succeed. Coming into the lab, I experienced a lot of social anxiety, and Neil helped me to gain confidence by encouraging me to speak up and ask questions when I had something to say. Neil is also really good at questioning traditional thinking and asking those "what if?" questions that have continued the lab's excellent research program, and has inspired me to think differently about chemistry and what is possible. I am so grateful for all of his support for both me and Nat during our time at UCLA.

I would next like to thank my committee members, Professors Yi Tang, Ellen Sletten, and Ken Houk. Their advice, mentorship, and support were very important for my development as a scientist throughout my graduate school studies.

I would also like to thank TC Ong, Bob Taylor, Robert Peterson, and Greg Khitrov for their support in the MIC and their maintenance of the instruments that make chemistry research at UCLA even possible.

I am so grateful to all of the members of the Garg lab that I have overlapped with and wish to acknowledge them now. These people are some of the most truly exceptional, extraordinarily intelligent, quality humans I have ever met. Although I am very excited for the next chapter in my life, I will never forget the people who supported me and helped me grow into the chemist and person that I am today. Having moved from the east coast, far away from family, the people in the lab have been the people I have leaned on, and they have really been there for me. The words in this section will not do justice to them and what they all mean to me, but I will try my best.

During my time in the lab, I have had the privilege of working with five generations of bright and talented postdocs. The first was at the tail end of Dr. Evan Darzi's postdoc when I first joined the lab in 2019. I began my time in the Garg lab working directly next to Evan, and even in our short time working alongside each other, I appreciated his wisdom and advice, as well as his 90s musical jam sessions.

The next generation was comprised of Dr. Veronica Tona and Dr. Logan Bachman, two very hardworking and intelligent postdocs. Although we mostly overlapped during COVID, I still was able to get to know Veronica during our overlapping shifts, and appreciated her drive and great sense of humor. Logan was always a calm force in the lab. I really appreciated his down-to-earth nature and also his creativity.

During the beginning of my second year, we were joined by the next generation of postdocs, Dr. Nathan Adamson and Dr. Daniel Nasrallah. I got to know Nathan better when I moved to 5229 in my 3rd year, and came to value his positivity and support (and even some of his dad jokes) during this time. I had the absolute privilege of working on a project with Dan. Although chemistry could be tough, I admired the drive and responsibility that Dan took as a project leader. Dan is also such a good-natured person, and is always thinking of others and how he can help.

During his time here I witnessed numerous times where he jumped in to help in the lab or to teach a younger student (myself included). Dan is a natural born teacher, and I am really excited to see his career grow as a professor.

The next group of postdocs were Dr. Lukas Wein and Dr. Jacob Sorrentino. I overlapped with Lukas during my 4th year in the lab in 5229. Lukas is incredibly smart and also hilarious, and I always felt comfortable going to him for chemistry advice. In my 5th year, I moved to 5235 and was lucky to sit directly behind Jacob. Jacob is not only a very bright and thoughtful person, but he is also very kind. Whenever I or any other student was feeling discouraged, he was always there to lend positivity, solutions, and encouragement, which inspired me as an older student to be more supportive of younger students in this way.

The last class of postdocs is Dr. Jiaming Ding and Dr. Sarah French. Jiaming entered the lab in the middle of my 5th year as an extremely bright and motivated scientist. He has an impressive grasp on chemistry, and I have really appreciated being able to ask him questions and to gain his insight. From the moment I met Sarah, she became my friend. I have met few people so driven and dedicated as her, and she is truly inspiring. She is incredibly smart and I admire her integrity. I also appreciate her adventurous spirit and openness to try new things, qualities which I have been motivated to adopt myself.

While here, I also overlapped briefly with a visiting student from Germany, Lisa Kamecke. I really enjoyed getting to know Lisa, who fit in with the group immediately, and I really admired her ability to speak up and voice her opinion in group meetings and to contribute her scientific advice and ideas. She was also always ready for an adventure and to try new things. I also had the chance to overlap with an undergraduate student, Lauren Van Auken. I am really glad she has joined the lab and am excited she is exploring chemistry as a path for her future.

During my first year as a graduate student, Dr. Michael Yamano, Dr. Rob Susick, Dr. Jordan Dotson, and Dr. Jacob Dander were the 5th year class of students. Michael is a talented scientist who brought a lively energy to the lab with his witty jokes. Although we worked in different rooms and did not overlap as much, I always appreciated Rob's encouragement of younger students to ask questions. Even in our short time of overlap, I learned a lot from Jordan in group meetings about how to think about physical organic chemistry concepts in chemical reactions. I had the privilege of sitting next to Jacob during my first year of graduate school. Jacob is a natural story-teller and also has an incredible skill for writing, amongst many of his other skills. Even though graduate school was a tough transition for me, Jacob was very encouraging and often lent me advice and shared experience, which made me feel like I was not alone. I will never forget our chats in 5234 that first year and the laughter we all shared.

The next class, the class of 2021, was Dr. Sarah Anthony, Dr. Melissa Ramirez, and Dr. Timothy Boit. Sarah was a strong mentor to all in the lab, and I really appreciated her unwavering willingness to help and support during my first two years in the lab. Melissa is a very talented computational and synthetic chemist, and was always a kind and uniting presence in the lab. Since her graduation, I have appreciated getting to know Melissa even more as she has come back to visit and get to know new lab members. I am so excited to see her future career as she starts her independent research at the University of Minnesota. I was lucky to work alongside Tim in 5234, and we spent many shifts working together in the lab during COVID. Tim is super smart and hardworking, and inspired me to work hard myself, while also giving me important advice about mentorship and how to lead a project.

The next class was Dr. Francesca Ippoliti, Dr. Jason Chari, and Dr. Rachel Knapp. Francesca was always such a positive source of support for me and other younger students during

my time in the lab. I have always been inspired by her integrity and the ability to look at any situation with a positive outlook. I am very grateful for our friendship, and really miss our game nights with Nat and Josh! I worked alongside Jason during his last year in 5229 and my 3rd year in the lab. Jason has the unique ability to see the best qualities in everyone around him. He was a great listener and really made me feel seen as a person. I also really admired his creativity and excellent writing skills, and enjoyed listening to our favorite musical artists together. Then there is Rachel. Rachel was my mentor and guide in the Garg lab, beginning in my first year of graduate school. She taught me the ropes of graduate school, and I always felt I could go to her for sound advice. Rachel is an incredibly level-headed and pragmatic person, which made her an excellent mentor, as well as a friend. Her commitment to learning about and tackling research projects in various different areas made her an extremely well-rounded chemist, and really inspired me to try to diversify my own skills during my graduate school career.

The class above me was Dr. Katie Spence, Dr. Andrew Kelleghan, and Dr. Milauni Mehta. Katie was in 5234 when I joined the Garg lab in 2019, and quickly became a friend. Katie is very smart and also embodied to me what it looks like to be a strong woman in science and a self-advocate. I always admired how Katie could set a goal for herself and achieve whatever she set her mind to. Andrew and I became friends during a completely random trip that we were not meant to even be on, to an abysmal wasteland called Bombay Beach (down by the Salton Sea) during a Labor Day weekend back in 2021. Since then, the rest was history and Andrew has become a close friend and I have been grateful to learn so much from him, both in and outside of the lab. Andrew is also a very kind and caring friend. He was a big source of support for me and Nat during some very challenging life experiences and I will always appreciate that. The last member of the class of 2023 is Milauni Mehta. Milauni and I were placed together by fate at the start of my 3rd year.

Milauni is a wonderful scientist and has been a very close friend. She has taken me in during hard times, and has also stood with me during the happy ones, including my wedding. She is also someone who I feel I can talk with about virtually anything, which is a rarity for me, and became my home away from home. She really helped me to find my self-confidence, to be more secure in my feelings, and to also be more open and honest, and leads by example. I am immensely grateful for our friendship and am glad we get to be close by in this next chapter of life!

In my current class is soon-to-be Dr. Matthew McVeigh and Dr. Laura Wonilowicz. Words cannot express how grateful I am to have shared the journey with these two wonderful people, and to be Lauranamatt together. Matt is an incredibly creative and hardworking chemist, and a true team player. He is a stabilizing presence in the lab, and truly has a heart of gold. He is a natural born leader and will no doubt be an excellent medicinal chemist and addition to any team he joins. I met Laura during orientation at UCLA, and as fate would have it, we were roommates that weekend. Since then, Laura has been a constant friend and support to me, something I have cherished. Laura is one of the kindest, most understanding people I have ever met, and she is committed to doing what is right. She holds herself to a very high standard and it is something I have always admired about her. I will always remember our wine nights, seeing the Barbie movie, and going to Taylor Swift together. Thank you both for being amazing friends to Nat and I, and I am selfishly glad that you will be close by so we can visit you in San Diego!

The class of students below me, Dominick Witkowski, Arismel Tena Meza, and Luca McDermott Catena, has proven to be incredibly adaptable despite starting in the middle of the pandemic. Dominick is a fellow New Englander and cat-person. We worked together on the triene projects and I have admired his incredibly strong work ethic, ambition, and confidence as a chemist. I am excited to see his continued growth in his future career. I had the distinct pleasure

of working with Ari and serving as a mentor to her in my second year, and also learned a lot from her in turn. I have admired her ability to simultaneously tackle both research as well as all of her efforts outside of the lab in OCDS and making chemistry more accessible to others, and I have been inspired by her strong values. I am really excited to see her continue as a leader to others in the lab and beyond. I moved to the same lab as Luca in 5229 during my 3rd year in the Garg lab, and have had the privilege of working in the same room as him for the last three years of my PhD. Luca has a unique and inspiring enthusiasm for chemistry, that is contagious to those around him. He is always excited to be in the lab, to look at a TLC or cool new reaction, and to know what everyone in the lab is working on. It has made being in lab with him so fun, and I have also really appreciated how he takes time to teach and learn with the younger students. He will no doubt make an excellent professor one day.

The next class is Jordan Gonzalez and Georgia Scherer. I was fortunate to be in the same room as Jordan when he joined the lab in the summer of 2021. Jordan is a dedicated organic chemist and a superb human being. He is a steadfast and caring labmate and has already become an excellent mentor to the younger students. We sat next to each other in 5229, and I could always tell if I had successfully told a good joke from Jordan's quiet chuckles. He has also taught me and others the Gen Z lingo (Jordan you're the goat). In my 5th year, I was honored to work in the same room as Georgia Scherer. Georgia is truly a wonderful person and a joy to be around. I have learned a lot from her, and I have loved having discussions with her and growing more in our chemistry journeys together. She is a person who truly seeks to be the best version of herself and also has a great deal of compassion and thus seeks the best for others. This has been infectious for me, and I really feel I have become a better and more positive version of myself because of her.

The next class of rising 3rd years is Allison Hands, Zach Walters, and Dani Turner. Allison is another fellow New Englander and I have really enjoyed getting to know her more. She is a very responsible and motivated chemist and sets a high bar for herself. It is always fun to chat and laugh with her, and she has the kind of personality that makes anyone in her presence feel welcome. I got to work next to Zach during my 4th year in the lab in 5229. Zach is very intelligent and very quickly picks up on any skill he sets his mind to, and has even become part computational chemist in his second year. I have also really enjoyed getting to know Zach as well as his awesome wife Hannah outside of the lab, especially at yarn night, and really appreciate how down-to-earth, caring, and fun they are. I have had the privilege to also serve as a mentor to Dani during my 4th year, and he very quickly became my friend. Dani is a great chemist and I have learned a lot from him. When Dani walks into the room, my day immediately brightens. Dani is committed to his fashion and is so true to himself, and he inspires me to be myself as well. He is the type of person who makes you understand what it looks like to be a truly good friend to others. I have really enjoyed working on projects together, through the laughter and the harder days, going for walks, and crocheting together. I look forward to having many more fun adventures together!

The final class is Ben Janda, Allison Clark, Christina Rivera, and Giulianna Miseo. I have really enjoyed getting to know this class more and it is clear that they are a group of eager-to-learn scientists. Ben Janda and Allison Clark have both overlapped with me in 5235 and I have really enjoyed listening to their stories, laughing together, learning from them (especially more of the Gen Z lingo from Ben), and eating hard chips together. I am really grateful to say my last year in 5235, even when times were stressful, that I truly looked forward to going into our room each day and talking with you both, and I really believe it helped me through some challenging times. This

class is no doubt an exceptional group of people, I am really glad you all joined the lab, and I look forward to seeing all of your careers in chemistry flourish.

I would like to thank and acknowledge my family for all of their support for me. They have always provided a safe haven for me, and have loved me through every challenge I have faced. I am especially grateful to my grandmother, Marilyn, aka Mema. She is the strongest person I know and is a role model for me. Next, I would like to thank my parents. They have always made me feel loved and cherished. Being musicians themselves, they have always encouraged me to pursue any career path that brings me joy, and I have always appreciated their support. Ever since I left home almost 10 years ago, both of them have flown out numerous times to support me for celebrations, or during hard times, just to take me out to dinner or cheer me up. My dad has always had a way of making me feel special, and has always believed in me when I did not believe in myself. My mom has always been the person I can talk to about everything, and who knows everything about me and loves me. I love you both. To my sister Elisa, I am so glad we became closer over the last few years, and I feel like you have become one of my best friends. It is so special to me that we share so many memories and experiences from our childhood and understand each other on another level. I have also really been grateful to get to know Darrin and am so glad that you, Darrin, Nat, and I can share such a strong bond together. It never matters where we are when we are together, we always have a good time and share lots of laughter.

Finally, I would like to thank my husband and life-partner, Nathaniel. Nat and I met our second year of college at Westmont, and I was immediately drawn to his intelligence and his sense of calm that was a huge complement to my restless nature. I mean this when I say: I could not have done any of this without you. Thank you for all your support, for doing so many of the household chores, cooking meals, planning dates, being there for me to talk to and cry to, and so much more.

I know it has not been the most straightforward or easy chapter of our lives, but you have never wavered in your support and love for me, and that means the world to me. Thank you for being patient with me, and for being the ultimate companion. We have already had so many great adventures together, and I am excited to begin the next chapter with you (and Bella). I love you.

Chapter 1 is a version of Boit, T. B.; Dander, J. E.; Bulger, A. S.; Garg, N. K. *ACS Catal*. **2020**, *10,* 12109–12129. Boit, Dander, Bulger, and Garg were responsible for preparing the manuscript.

Chapter 2 is a version of Knapp, R. R.; Bulger, A. S.; Garg, N. K. *Org*. *Lett*. **2020**, *22,* 2833–2837. Knapp and Bulger were responsible for experimental work.

Chapter 3 is a version of Bulger, A. S.; Nasrallah, D. J.; Tena Meza, A.; Garg, N. K. *Chem*. *Sci*. **2024**, *15*, 2593–2600. Bulger, Nasrallah, and Tena Meza were responsible for experimental work.

Chapter 4 is a version of Kelleghan, A. V.; Bulger, A. S.; Witkowski, D. C.; Garg, N. K. *Nature* **2023,** *618*, 748–754. Kelleghan, Bulger, and Witkowski were responsible for experimental work. Kelleghan and Witkowski were responsible for computational work.

Chapter 5 is a version of Bulger, A. S.; Turner, D. W.; Zhou, Q.; Houk, K. N.; Garg, N. K. *Org*. *Lett*. **2024**, *26*, 3602–3606. Bulger and Turner were responsible for experimental work. Zhou was responsible for computational work.

Chapter 6 is unpublished material. Bulger, Witkowski, and Turner were responsible for experimental work.

BIOGRAPHICAL SKETCH

Education:

University of California, Los Angeles, CA

- Ph.D. in Organic Chemistry, anticipated Spring 2024
- Current GPA: 4.00/4.00
- NSF Graduate Research Fellow, 2021–2024

Westmont College, Santa Barbara, CA

- B.S. in Chemistry with Honors (GPA 4.00/4.00)

Professional and Academic Experience:

Graduate Research Assistant: University of California, Los Angeles, CA

- August 2019 – present; Advisor: Prof. Neil K. Garg
  - Optimized reaction conditions and developed scope of unsubstituted and dimethyl substituted 1,2,3-cyclohexatrienes in (4+2), (3+2), and (2+2) cycloadditions, nucleophilic addition reactions, and σ-bond insertion reactions
  - Designed and performed a mechanistic deuterium-incorporation study on the trapping reaction of a TES-substituted cyclic triene and use deuterium labeling to determine the mechanism of a carbonyl-retro-ene reaction
  - Designed, synthesized, and investigated chiral *N*-heterocyclic carbene ligands and achieved the first asymmetric Mizoroki–Heck cyclization of amides
  - Developed the nickel-catalyzed net-hydrolysis of benzamides to carboxylic acids, performed scope studies, and demonstrated scale-up capability
  - Mentored two graduate student researchers on proper laboratory techniques

Undergraduate Course Instructor: University of California, Los Angeles, CA

- Summer 2022 & 2023; Undergraduate chemistry course elective
  - Taught students about concepts pertaining to the drug discovery processes, as well as career paths in medicinal and process chemistry

Graduate Teaching Assistant: University of California, Los Angeles, CA

- Sept. 2019 – Dec. 2020; Undergraduate organic chemistry laboratory sections
  - Taught students safe laboratory practice, fundamental organic chemistry lab techniques and the underlying chemical concepts

Undergraduate Research Assistant: Westmont College, Santa Barbara, CA

- Jan. 2018 – May 2019; Advisor: Prof. Amanda Silberstein
  - Explored the reaction scope of a nickel-catalyzed borylation of aryl sulfamates
  - Prepared honors thesis and gave a senior seminar on undergraduate research

Undergraduate Teaching Assistant: Westmont College, Santa Barbara, CA

- Aug. 2017 – May 2019
  - Taught undergraduate students organic chemistry, led discussion sections, and graded homework assignments

Honors and Awards:

- Donald J. Cram Dissertation Award, 2024
- Theodore A. Geissman Excellence in Research Award, 2023
- Jim and Barbara Tsay Excellence in Second Year Research and Academics, UCLA, 2022

- Senior Christopher S. Foote Fellowship, UCLA, 2022–2023
- Michael E. Jung Excellence in Teaching Award, UCLA, 2021
- National Science Foundation Graduate Research Fellowship, 2021–2024
- Christopher S. Foote Fellowship, UCLA, 2019 – 2020
- Summa cum laude, Westmont College, 2019
- Faculty Scholarship Award, Westmont College, 2019
- Chemistry Department Senior Award, Westmont College, 2019
- John Stauffer Memorial Scholarship, Westmont College, 2018
- John Stauffer Summer Research Fellowship, Westmont College, 2018
- Phi Kappa Phi induction, Westmont College, 2018
- John Stauffer Memorial Scholarship, Westmont College, 2017
- Presidential Scholarship, Westmont College, 2015

Publications:

1. **Evaluation of Retro-Aldol vs Retro-Carbonyl-Ene Mechanistic Pathways in a Complexity Generating C–C Bond Fragmentation.** Ana S. Bulger, Daniel W. Turner, Qingyang Zhou, K. N. Houk, and Neil K. Garg. *Org. Lett.* **2024**, *26*, 3602–3606.
2. **Enantioselective Nickel-Catalyzed Mizoroki–Heck Cyclizations of Amide Electrophiles.** Ana S. Bulger,† Daniel J. Nasrallah,† Arismel Tena Meza,† and Neil K. Garg. *Chem. Sci.* **2024**, *15*, 2593–2600.
3. **Strain-Promoted Reactions of 1,2,3-Cyclohexatriene and its Derivatives.** Andrew V. Kelleghan,† Ana S. Bulger,† Dominick C. Witkowski, and Neil K. Garg. *Nature* **2023**, *618*, 748–754.
4. **Synthesis of Carboxylic Acids from Benzamide Precursors Using Nickel Catalysis.** Ana S. Bulger, Dominick C. Witkowski, and Neil K. Garg. *Org. Synth.* **2022**, *99*, 305–325.
5. **Activation of Strong Bonds Using Non-Precious Metal Catalysis.** Timothy B. Boit,† Ana S. Bulger,† Jacob E. Dander,† and Neil K. Garg. *ACS Catal*. **2020**, *10*, 12109–12126.
6. **Nickel-Catalyzed Conversion of Amides to Carboxylic Acids.** Rachel R. Knapp, Ana S. Bulger, and Neil K. Garg. *Org. Lett.* **2020**, *22*, 2833 – 2837.

†These authors contributed equally

Outreach:

- Served as UCLA representative for Empowering Women in Organic Chemistry (EWOC). Responsibilities entail organizing meetups, planning networking events, and moderating panels to bridge the gap between women in academia and industry (February 2023–May 2024).
- Participated in the Exploring Your Universe (EYU) event at UCLA which involved teaching chemistry concepts to students in elementary school and middle school by teaching them about molecules responsible for smells like vanilla and orange (November 2023).
- Judged for LA County Science Fair for the senior chemistry division and nominated winners to be advanced to the state science fair (March 2022).

CHAPTER ONE

Activation of C–O and C–N Bonds Using Non-Precious-Metal Catalysis

Timothy B. Boit,[†] Ana S. Bulger,[†] Jacob E. Dander,[†] and Neil K. Garg.

ACS Catal. **2020**, *10*, 12109–12126.

1.1 Introduction

Metal-catalyzed cross-couplings represent one of the most important reaction platforms in modern synthetic chemistry (Figure 1.1A).[1] Although the field enjoys a rich history, there remains fervent interest in expanding the frontiers of cross-coupling chemistry. Some areas of current exploration include the development of new modes of reactivity (dual catalysis,[2] photoredox catalysis,[3] cross-electrophile couplings,[4] chemoenzymatic transformations,[5] etc.), stereoselective couplings,[6] and the utilization of new classes of electrophiles. With respect to the latter, non-precious-metal catalysis has been particularly enabling.

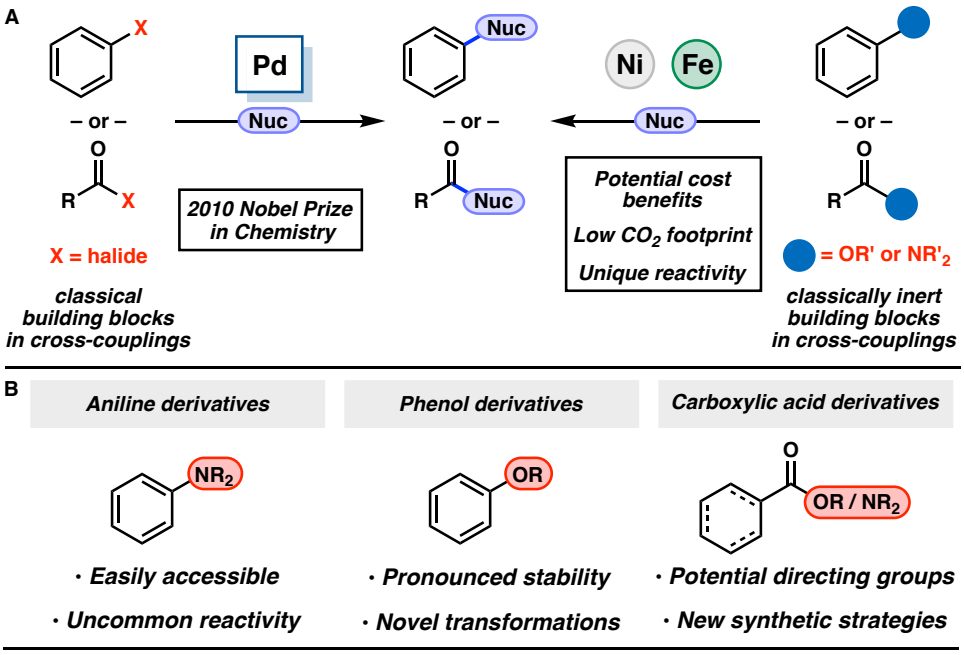


Figure 1.1. (A) Classical building blocks and those historically considered inert under traditional cross-coupling conditions. (B) Overview of recently explored electrophiles in cross-coupling reactions.

In addition to potential cost, toxicity, and environmental benefits relative to precious metal alternatives, non-precious-metal catalysts can effect unique and challenging transformations (Figure 1.1A).[7] In particular, iron[7a–f,j] and nickel[7f–j] catalysis have become focal points in this arena. At the time our laboratory began in 2007, nickel-catalyzed cross-couplings were known, but significantly underexplored compared to palladium-catalyzed variants. Since 2007, more than 1200 manuscripts involving nickel-catalyzed cross-couplings have been published.[8] Moreover, several reviews covering advances in nickel catalysis have been published over the past decade, highlighting the rapid growth of the field.[7] This expansion has largely been driven by recognition of nickel's ability to participate in single-electron processes[9] and to activate strong bonds[10] historically considered inert in cross-coupling reactions.[7e,f,11] Notably, the use of non-traditional building blocks (e.g., aniline-, phenol-, and carboxylic acid-derivatives) in cross-couplings offers several advantages owing to their abundance, bench stability, utility as directing groups, and

orthogonal reactivity to more common aryl and acyl halide electrophiles (Figure 1.1B). As a result, these methodologies can enable novel disconnections and improvements in synthetic strategy.

In the context of strong bond activation,[12] our laboratory has been particularly interested in the activation and cross-coupling of phenol, amide, and ester electrophiles, using nickel or iron catalysis. Herein, we highlight our laboratory's contributions in this area, which are summarized in Figure 1.2. First, we consider cross-couplings of phenol-derived pivalates, carbonates, carbamates, and sulfamates to form C–N and C–C bonds (Figure 1.2A). Additionally, we discuss our efforts to develop nickel-catalyzed activations of esters and amides (Figures 1.2B and 1.2C, respectively). Where illustrative, we also outline some of the many contributions from others in the field. Lastly, we provide insight into potential future directions in these areas.

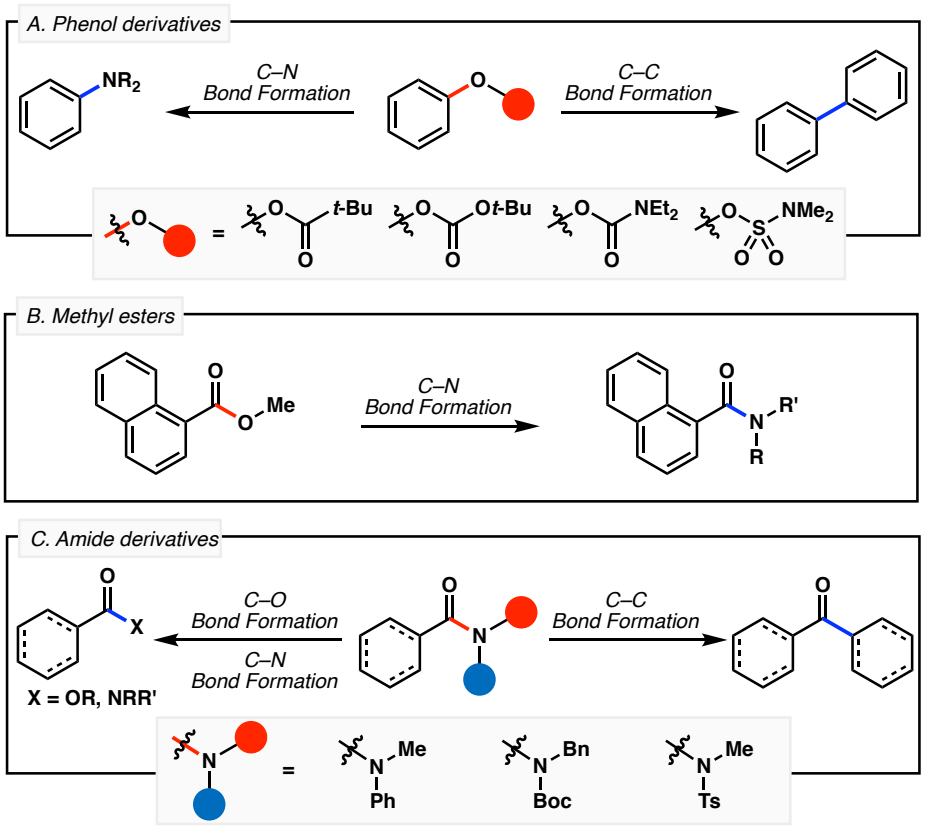


Figure 1.2. The scope of this review, which focuses on the activation of phenol, amide, and ester electrophiles.

1.2 Activation of Aryl C–O Bonds

The use of phenol-derivatives in cross-couplings is particularly attractive due to their broad availability, stability, and utility as directing groups in aromatic ring functionalization (Figure 1.3).[13] Although cross-couplings of aryl sulfonates are common,[14] methodologies that employ inexpensive phenol derivatives that are unreactive under Pd-catalysis and can serve as directing groups offer practical and conceptual advantages.[15,16,17,18] For example, phenolic electrophiles could be leveraged in conjunction with orthogonal cross-coupling handles to allow for the facile construction of privileged polyfunctionalized aromatics.[19] Although couplings of aryl and vinyl methyl ethers had been described by Wenkert and Chatani, respectively,[20,21,22,23,24] when our laboratory opened in 2007, cross-couplings of simple *O*-acylated phenols were unknown.

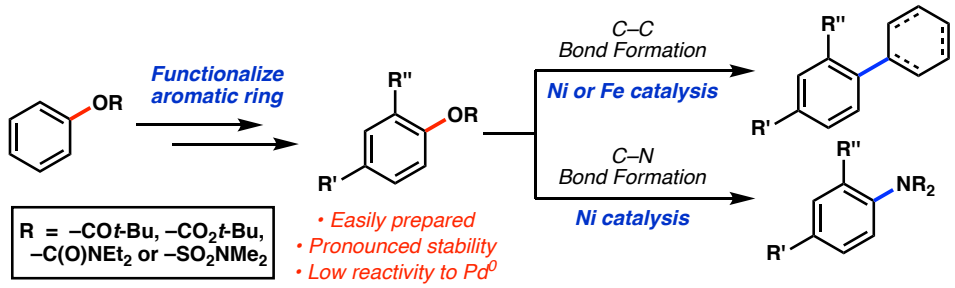


Figure 1.3. Overview of our laboratory's studies on using phenol derivatives as cross-coupling electrophiles in base-metal-catalyzed C–C and C–N bond-forming reactions.

Our initial efforts in this area focused on nickel-catalyzed C–C and C–N bond-forming reactions of pivalates, carbonates, and carbamates (Figure 1.4).[25] We first developed the nickel-catalyzed Suzuki–Miyaura coupling of aryl pivalates. Of note, this reaction avoids competitive activation of the acyl C–O bond, which has been observed in related cross-couplings of aryl ethers.[26,27] An example of the pivalate cross-coupling methodology is shown in Figure 1.4 involving the synthesis of disubstituted naphthalene derivative **1.4**. First, regioselective bromination of naphthyl-1-pivalate at C4 gave naphthyl bromide **1.1**, which underwent Suzuki–

Miyaura coupling with indolylboronic ester **1.2** to deliver indole **1.3**. Subsequently, nickel-catalyzed cross-coupling of aryl pivalate **1.3** with phenylboronic acid gave **1.4** in 88% yield.[28] This concise route to **1.4** underscores the value of *O*-acylated phenols as orthogonal cross-coupling electrophiles in the synthesis of polyaromatic molecules.[19] In a subsequent study, we found that aryl *tert*-butylcarbonates could serve as cross-coupling electrophiles, as illustrated by the nickel-catalyzed coupling of carbonate **1.5** to forge biaryl **1.6** in 65% yield.[29]

Aryl carbamates also proved to be versatile electrophiles in C–C and C–N bond-forming cross-coupling reactions, as demonstrated by the examples shown in Figure 1.4.[29] Importantly, this substrate class can be used to functionalize the ortho position on aromatic rings via directed lithiation.[30] Using $NiCl_2(PCy_3)_2$, naphthyl carbamate **1.7** smoothly underwent nickel-catalyzed cross-coupling to furnish biaryl product **1.8** in 86% yield.[29] The corresponding amination of aryl carbamates was enabled by the use of *N*-heterocyclic carbene ligand, SIPr, and could be used to generate naphthylmorpholine **1.11** in excellent yield.[31] Developing methodologies to construct sp^2–sp^3 C–C bonds represents another frontier in cross-couplings.[32] Toward this end, we turned to iron catalysis to achieve the Kumada coupling of aryl carbamates,[33,34] which allowed for the formation of sterically-hindered sp^2–sp^3 C–C bonds, such as that found in **1.12**.[35] Finally, a catalytic reduction of aryl carbamates (**1.7** → **1.14**, Figure 1.4) was achieved using inexpensive 1,1,3,3-tetramethyldisiloxane (TMDSO) as the reductant,[36] thereby providing a means to achieve the deoxygenation of aromatic rings. In addition, one can perform net cine substitution processes using directed ortho-metallation/functionalization, followed by reductive removal of the carbamate. Since our initial studies in this area, there have been a number of other contributions from other groups toward expanding the scope and mechanistic understanding of cross-couplings of *O*-acylated phenol-derivatives.[37]

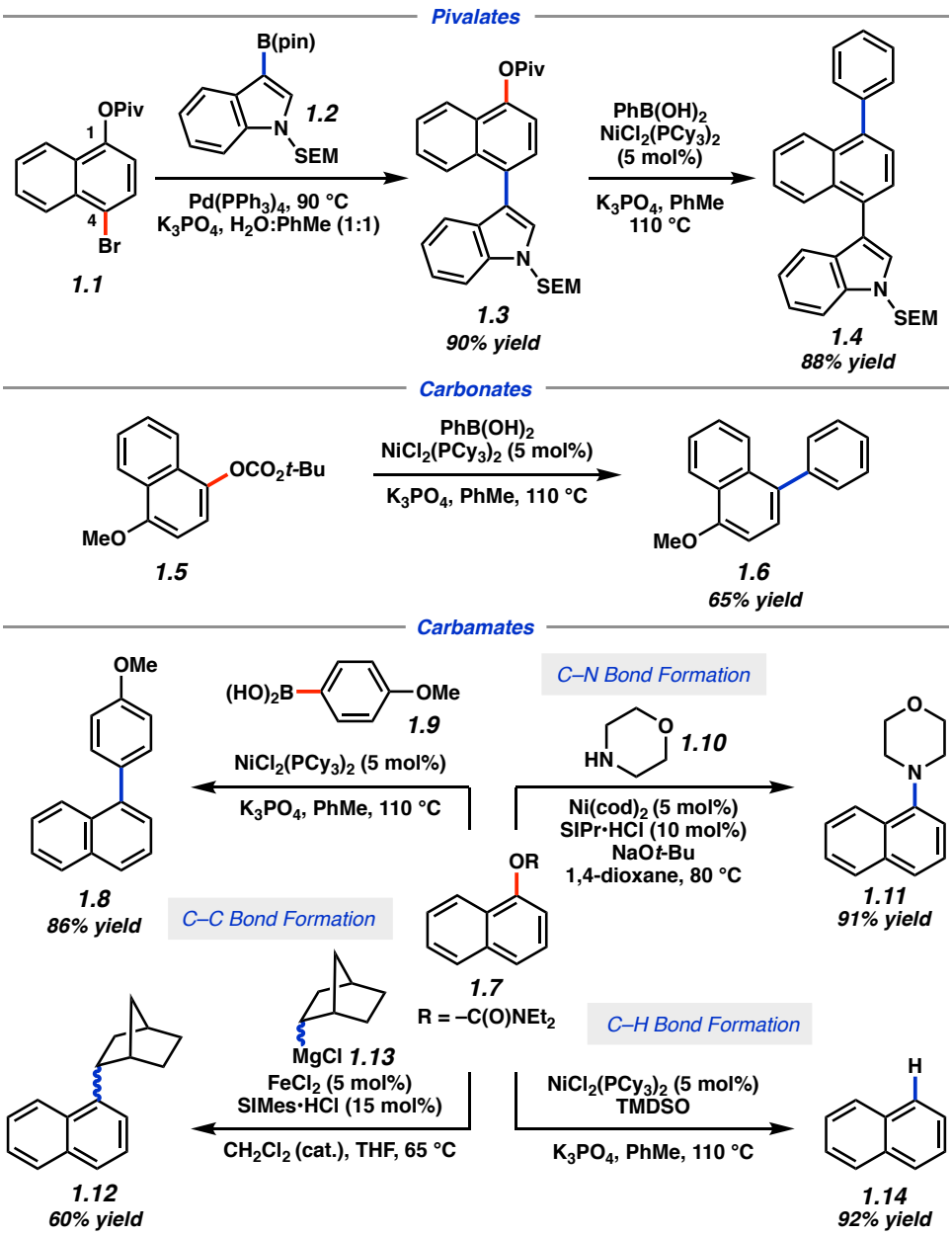


Figure 1.4. Select examples of Ni- and Fe-catalyzed cross-couplings of pivalates, carbonates, and carbamates reported by our laboratory.

The cross-coupling of sulfamate electrophiles presented another attractive opportunity, as they are also common directing groups in ortho-metalation reactions as established by Snieckus.[30] Nickel-catalyzed Kumada couplings of aryl sulfamates had been reported,[18] but milder C–C and C–N bond-forming cross-couplings of these substrates were unknown. With regard to the former

challenge, sulfamates proved to be viable substrates in nickel-catalyzed Suzuki–Miyaura cross-couplings. In fact, subsequent experimental and computational studies carried out in collaboration with the Houk group revealed aryl sulfamates to be more reactive electrophiles in comparison to aryl carbamates.[38] Importantly, this transformation avoids the use of highly basic and nucleophilic organometallic reagents, allowing for coupling of vinyl sulfamate **1.15** to give substituted cyclohexenone **1.17** in 78% yield (Figure 1.5).[29] Sulfamates were also competent electrophiles in iron-catalyzed Kumada couplings, as shown by the formation of tricyclic product **1.19** in 82% yield.[35] Additionally, the use of aryl sulfamates in catalytic amination reactions highlights their versatility as cross-coupling handles, and allowed for the rapid synthesis of linezolid (**1.22**) from fluorosulfamate **1.20**. Following sulfamate-directed ortho-functionalization,[29] aryl sulfamate **1.20** underwent a nickel-catalyzed cross-coupling with morpholine (**1.10**) to deliver arylated amine **1.21** in 84% yield.[39] As previously mentioned, subsequent computational and experimental efforts from others in the field have greatly contributed to the rapid growth in understanding and scope of base-metal-catalyzed cross-couplings of non-traditional phenol-derived electrophiles.[37k,40]

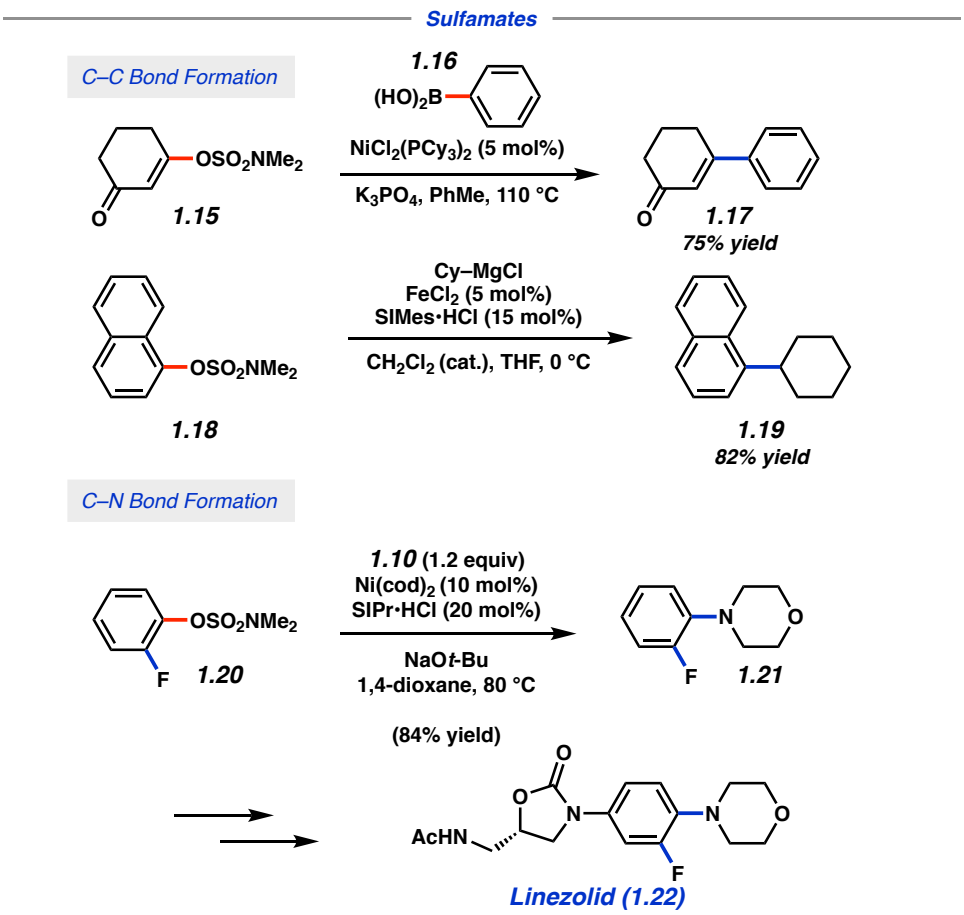


Figure 1.5. Select examples of nickel- and iron-catalyzed cross-couplings of sulfamates reported by our laboratory.

A common limitation of nickel-catalyzed methodologies, including those developed by our own laboratory, is the air- and moisture-sensitivity of the precatalysts and/or ligands employed. To avoid the need for glovebox manipulations in the nickel-catalyzed amination of carbamates and sulfamates, we investigated the use of a variety of air-stable Ni(II) complexes.[41] $NiCl_2$(DME) (**1.23**) and PhB(pin) were identified as a suitable precatalyst and mild reductant, respectively, to achieve a range of nickel-catalyzed aminations on the benchtop. For example, the methodology tolerated electron-deficient and heterocyclic substrates as well as a variety of amine nucleophiles, giving rise to **1.21** and **1.24**–**1.26** in 50–98% yields (Figure 1.6).[42] Recognizing that the use of industrially-friendly solvents could further enhance the practicality of this methodology through a

collaboration with the ACS Green Chemistry Institute's Pharmaceutical Roundtable, we evaluated the coupling of (hetero)aryl sulfamates with amine nucleophiles in 2-methyl-THF using nickel-catalysis.[43] The robustness of this method was evidenced by the gram-scale coupling of trifluoromethyl aryl sulfamate **1.27** with morpholine (**1.10**) to give arylated amine **1.28** in 97% yield using only 3 mol% $NiCl_2$(DME).

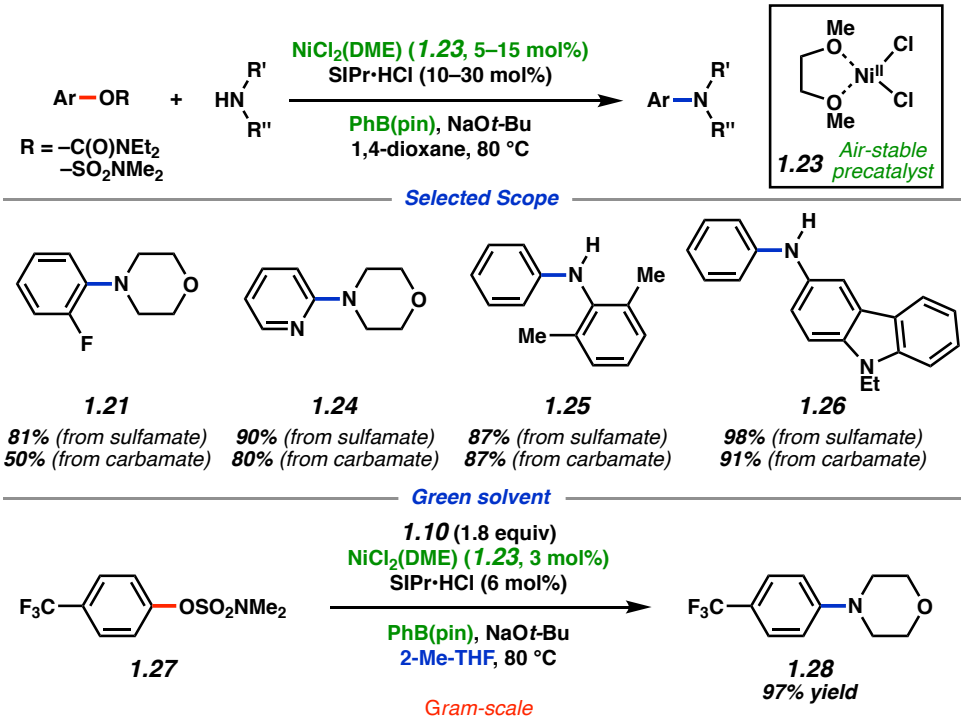


Figure 1.6. Benchtop aminations of aryl sulfamates and carbamates and gram-scale coupling of **1.27** in a green solvent.

1.3 Activation of Aryl C–N Bonds

Although not a focus of our laboratory's research, base-metal-catalyzed cross-couplings of aniline derivatives also represent an active field of inquiry (Figure 1.7). Historically, aniline-derived diazonium salts have been extensively employed in palladium-catalyzed cross-couplings.[44,45] However, the use of safer and more robust aniline-derivatives in coupling reactions has recently garnered significant attention.[46] MacMillan and coworkers reported a nickel-catalyzed Suzuki–Miyaura coupling of aryltrimethylammonium triflates in 2003,[47] building upon the

foundational report by Wenkert on Kumada couplings of these species.[48] More recently, Shi described a directing group-free nickel-catalyzed Suzuki–Miyaura coupling of *N*,*N*-dimethylaryl amines, overcoming a key limitation in comparable Ru-catalyzed reactions.[49,50] Moreover, a nickel-catalyzed Suzuki–Miyaura coupling of azoles was published by Robins,[51] which allowed for the synthesis of important arylated purine nucleoside analogs **1.29** and **1.30** in good yields.[52] Finally, the Nakao group and others have investigated transition-metal-catalyzed cross-couplings of nitroarenes and this strategy has been applied toward the syntheses of polycyclic aromatic hydrocarbons.[53] We are optimistic that base-metal-catalyzed aryl C–N bond activation will continue to see use in complex molecule synthesis.

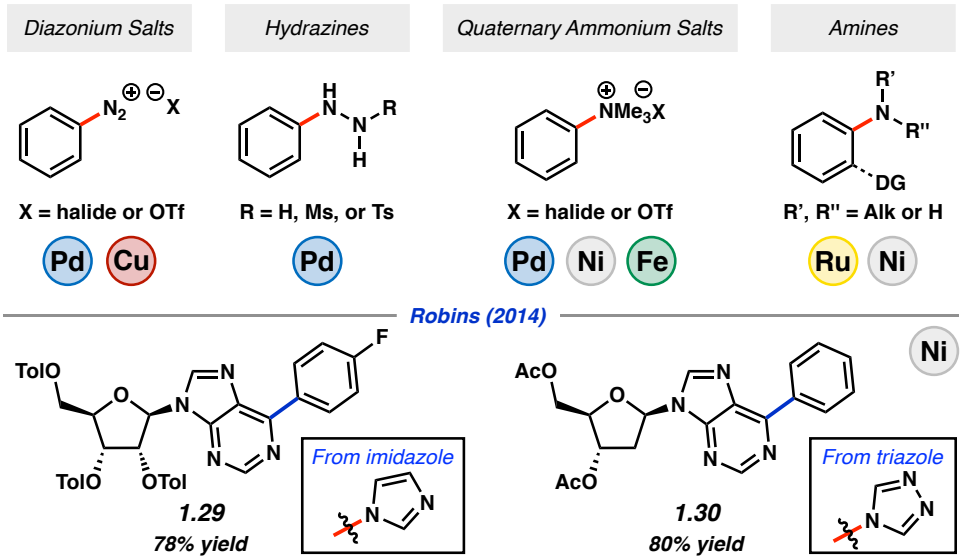


Figure 1.7. Overview of aniline derivatives employed in metal-catalyzed cross-coupling reactions.

1.4 Activation of Acyl C–O Bonds

Interest in the metal-catalyzed cleavage of the acyl C–O bonds of esters dates back to Yamamoto's seminal 1976 report utilizing stoichiometric nickel complexes.[54] Although cross-couplings of esters, including decarboxylative variants pioneered by Itami[55] and Gooßen,[56] have since established the feasibility of metal-catalyzed acyl C–O bond activation for subsequent

functional group interconversion, these reports were limited to the coupling of structurally or electronically activated substrates. Specifically, aryl esters employed in these couplings featured metal-chelating[57] or electron-withdrawing[58] *O*-substituents to facilitate oxidative addition (Figure 1.8).[59] These substrates are often synthesized from carboxylic acid precursors and are generally more reactive than alkyl esters. In contrast, simple methyl esters are naturally abundant, commercially available, and unreactive under Pd-catalysis. As a result, chemists could consider sequential cross-coupling strategies that take advantage of this orthogonal reactivity.

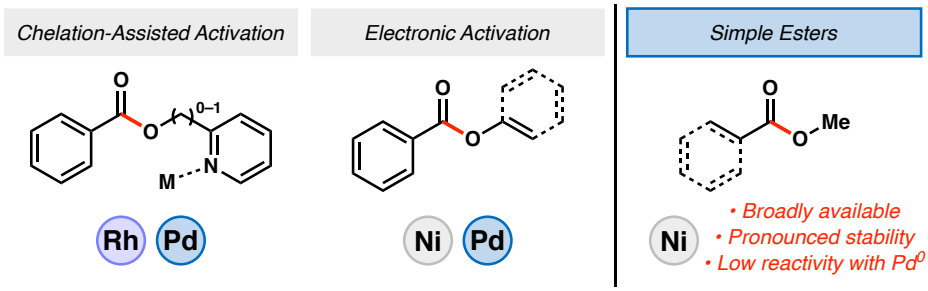


Figure 1.8. Historical approaches to metal-catalyzed ester acyl C–O bond activation and advantages of alkyl esters as substrates.

At the time our laboratory entered this field,[60] cross-couplings of methyl esters were unknown. Notably, these transformations feature high kinetic barriers to oxidative additions due to resonance stabilization of the acyl C–O bond.[61] However, we hypothesized that the unique reactivity of nickel(0) in the activation of strong bonds[7e,f.10,11] may allow for catalytic cross-couplings of methyl esters. Noting the importance of amide bond formations in industry,[62] we first pursued a nickel-catalyzed amidation of methyl esters.[60] Ultimately, the combined use of a Ni/NHC catalyst and Al(O*t*-Bu)$_3$ additive was found to effect the desired transformation. Computations performed by the Houk group[60] indicated that the Al(O*t*-Bu)$_3$ additive facilitates the rate-limiting oxidative addition step and drives product formation through the generation of a favorable Lewis acid-base complex with the amide product. Although this methodology was limited to the activation of naphthyl-derived substrates, its utility was illustrated in the synthesis

of complex anilide **1.33** (Figure 1.9). Treatment of **1.31**, which was prepared via sequential Buchwald–Hartwig and DCC couplings of a suitable methyl naphthoate precursor, with optimized amidation conditions generated anilide **1.33** in 60% yield without observable epimerization. This sequence highlights the mildness of the methodology and illustrates the utility of late-stage methyl ester activations in complex molecule synthesis.

Further studies have improved the efficiency and scope of nickel-catalyzed amidations of methyl esters. Newman and coworkers have described an additive-free variant of this methodology utilizing elevated temperatures.[63] In doing so, they were able to achieve amidations of enantioenriched aliphatic methyl esters to access products like furanylamide **1.34** in high yields (Figure 1.9). A range of aromatic substrates could also be coupled utilizing these conditions, allowing for the improved synthesis of α-amino-3-hydroxy-5-methyl-4-isoxazolepropionic acid receptors (AMPAR) positive modulator **1.35**. In a subsequent survey of NHC ligands in this transformation,[64] the same group reported the selective amidation of an alkyl methyl ester in the presence of an aryl methyl ester to form **1.36** in 65% yield. A reductive cross-coupling of nitroarenes and methyl esters has also been described.[65] Notably, nitroarenes are widely used in industry as inexpensive precursors to aryl amines. In an impressive application of this methodology, Hu and coworkers treated known ester **1.37** with their optimized Ni/Zn conditions to generate (–)-rhazinilam **1.38** in 59% yield.[65,66] As a result, the synthesis of the natural product was completed with improved step economy and comparable efficiency.

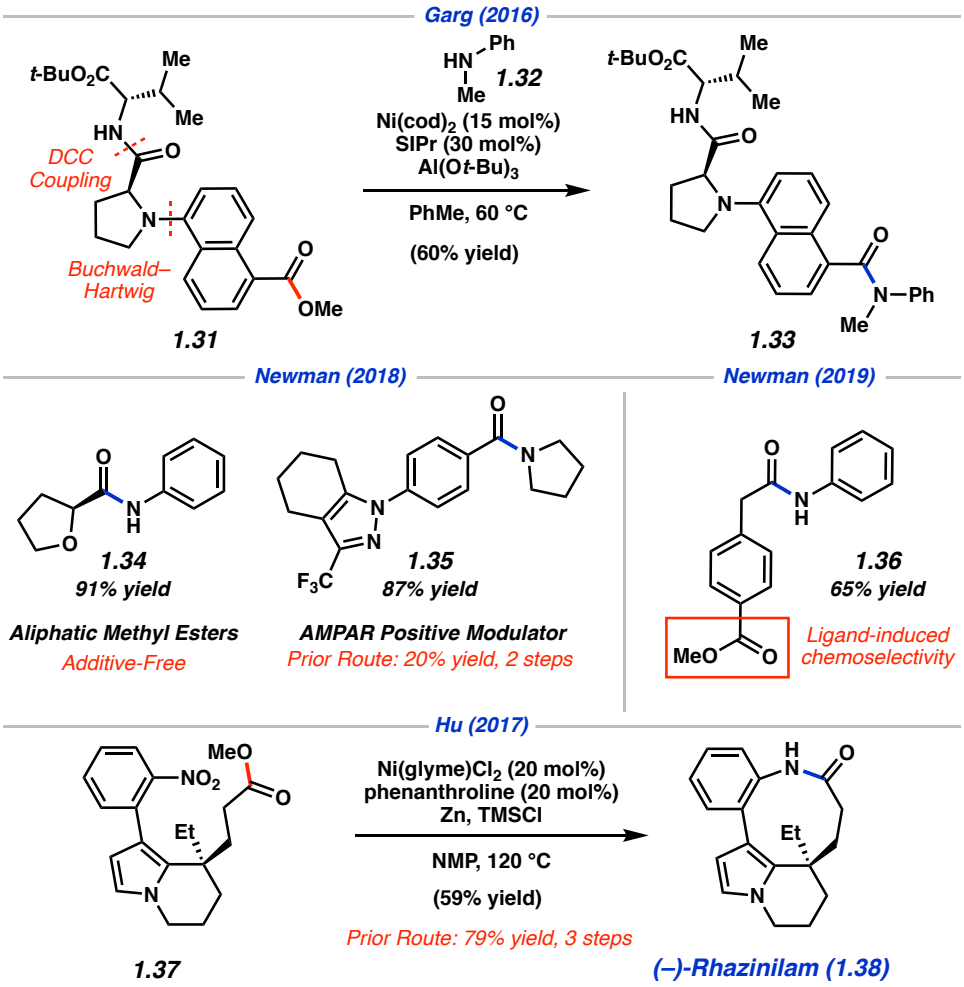


Figure 1.9. Recent advances in the nickel-catalyzed amidation of methyl esters.

Additional advances have broadened the scope of bond formations possible using nickel-catalyzed activations of methyl esters (Figure 1.10). Similar to Heck-type reactions of amides developed in our lab (vida infra),[67] Newman recently reported domino Heck reactions of methyl esters that form a C–C bond intramolecularly as well as a terminating C–C or C–H bond in a single catalytic transformation.[68] The generation of indanones **1.40** and **1.41** in 51% and 79% yields, respectively, from methyl ester substrate **1.39** highlights the potential utility of this methodology in divergent synthesis. Furthermore, nickel-catalyzed activations of methyl esters that proceed with decarbonylation have been reported. Specifically, the Rueping laboratory has utilized methyl esters to generate a variety of aryl stannanes, such as substituted pyridine **1.44**.[69] A decarbonylative

methylation of aryl methyl esters was reported by Yamaguchi and coworkers, and was utilized to access 2-methylindole **1.45** in 48% yield.[70] We anticipate that the exploration of new bond formations and modes of reactivities will continue to be an important driver of innovation in this field.

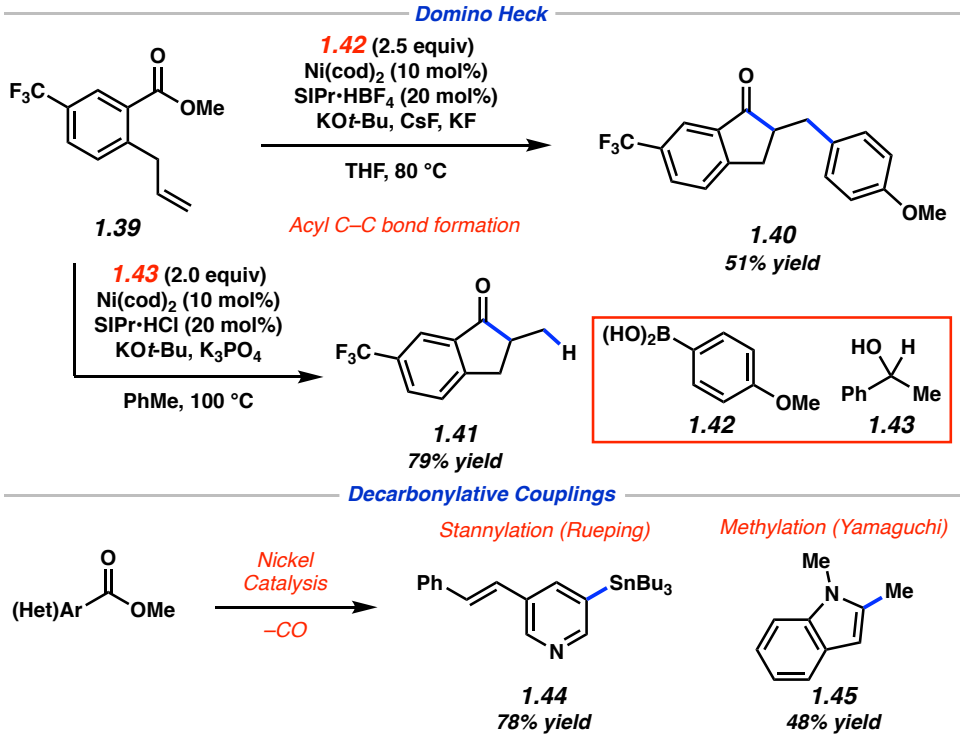


Figure 1.10. Nickel-catalyzed domino Heck and decarbonylative cross-couplings of methyl esters.

1.5 Activation of Acyl C–N Bonds

Although amide C–N bond cleavage is common in Nature, synthetic methods for activation of the amide C–N bond remain challenging due to well-understood resonance effects (Figure 1.11).[71] The pronounced stability of amides, however, renders them ideal functional handles to be carried through multi-step synthetic sequences. Moreover, as they are also common directing groups in C–H activations,[72] strategies to merge amide-directed C–H functionalization with subsequent late-stage C–N bond activation could allow for the rapid assembly of molecular architectures.

Recognizing the potential utility of amides as useful synthetic handles, a number of strategies for the functional group interconversion of amides have been reported.[73] For example, the use of amides featuring chelating *N*-substituents such as *N*-methoxy-*N*-methylamides or "Weinreb amides,"[71a,74] has enabled the single addition of organometallic nucleophiles to amides to access ketone products. Additionally, single-electron reduction of imides can generate reactive radical anion intermediates for subsequent functionalizations.[75] Notably, electrophilic activation of amides to generate versatile imidate intermediates has a rich history, with many elegant examples of this strategy being showcased by the Maulide group in recent years.[76] Another strategy for amide activation involves hydrosilylation using Vaska's complex ($IrCl(CO)(PPH_3)_2$), which has been leveraged by the Dixon group[77] and others[78] for a variety of reductive functionalizations of tertiary amides. Finally, our group and others have been interested in amide activation through direct oxidative addition by a transition-metal catalyst into the amide C–N bond for subsequent cross-coupling reactions. Although unknown at the time our lab entered the field in 2015, we envisioned that this latter approach could provide an alternative synthetic tool for the activation of amides that avoids the use of either highly nucleophilic or electrophilic reagents.[7g,79]

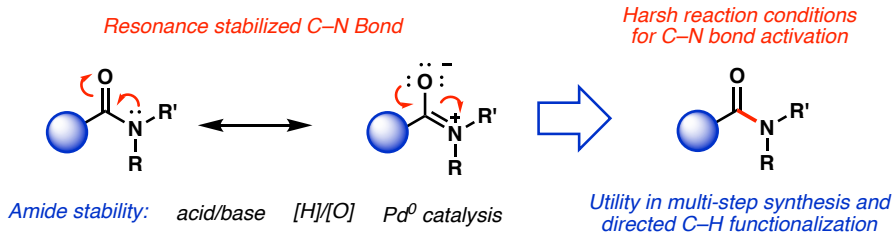


Figure 1.11. The resonance stabilization and potential synthetic utility of amide C–N bond activations.

Beginning with our first disclosure in 2015,[80] our laboratory has reported several nickel-catalyzed transformations that proceed with amide C–N bond activation. Our early investigations focused on the use of amide substrates derived from aromatic carboxylic acids (which are often

referred to as "aryl amides" and are distinct from *N*-aryl amides mentioned below), with select examples shown in Figure 1.12. We identified the conversion of amides to esters, a historically challenging transformation that often proceeds under harshly acidic or basic conditions,[71a] as an exciting starting point for our studies.[80]

In collaboration with the Houk lab, we first computationally and experimentally investigated the effect of amide *N*-substituents in the nickel-catalyzed conversion of benzamides to methyl benzoate. These studies revealed two salient features of this transformation. First, *N*-substituents had a profound influence on the change in Gibbs free energy values for the overall reactions (ΔG). Although esterifications of *N,N*-dialkyl benzamides were calculated to be largely thermodynamically unfavorable or thermoneutral, esterifications of *N*-aryl amides were found to be thermodynamically favorable, with a calculated ΔG of –6.8 kcal/mol for the conversion of *N*-phenyl-*N*-methyl benzamide to methyl benzoate. The effect of amide *N*-substituents on the oxidative addition barrier using nickel catalysis with commercially available NHC ligand SIPr[81] was also evaluated computationally. In comparison to the calculated barriers for *N*-dialkyl amides, those for *N*-aryl amides were estimated to be more reasonable, with the oxidative addition barrier for *N*-phenyl-*N*-methyl benzamide calculated to be 26 kcal/mol. Overall, the computational predictions were supported by experiments as we observed quantitative yield in the nickel-catalyzed conversion of *N*-phenyl-*N*-methyl benzamide to methyl benzoate. These initial collaborative studies with the Houk lab greatly informed our understanding of the impact of *N*-substituents on the performance of amides in various nickel-catalyzed transformations. Moreover, the Szostak group has bolstered the field by provided valuable insight into the physical properties and reactivity of non-planar, or "twisted", amides (in particular, glutaramides).[79a,82]

Using *N*-alkyl-*N*-phenyl benzamides, we found the use of nickel precatalyst / ligand combination of $Ni(cod)_2$ / SIPr allowed for the mild coupling of with a range of alcohol nucleophiles to furnish ester products, such as menthyl ester **1.46**, in high yields (Figure 1.12).[80] We then explored additional C–heteroatoms bond-forming reactions of *N,N*-alkyl, phenyl benzamides using nickel catalysis. Although water could not be directly employed as a nucleophile to access carboxylic acids from amides,[83] we designed a one-pot, two-step net-hydrolysis reaction. Specifically, in situ-generation of a silyl ester, followed by subsequent deprotection provided carboxylic acids, such as **1.47**, in good yields using mild reaction conditions.[84] We were also interested in overcoming the longstanding challenge of secondary amide transamidation utilizing our nickel catalysis platform.[85] Toward this end, a two-step, Boc-activation/nickel catalysis approach enabled the catalytic transamidation of secondary amides, notably providing ready access to amino-acid derived amide **1.48** on gram-scale.[86] Reasoning that these reactions could proceed through a Ni(0)/Ni(II) catalytic cycle, a hypothesis supported by DFT calculations performed by the Houk group, we became interested in leveraging well-established M(0)/M(II) cross-coupling platforms to form C–C bonds.[80] Indeed, we found that and aryl amides could smoothly undergo nickel-catalyzed Suzuki–Miyaura (*N*-alkyl-*N*-Boc amides) and Negishi (*N*-Me-*N*-tosyl and *N*-benzyl-*N*-Boc amides) couplings to form biaryl and aryl–alkyl ketones, respectively.[87,88] Notably, both of these methodologies proved to be scalable, providing gram-scale access to ketones **1.49**, an antiproliferative tubulin-binding agent,[89] and **1.50**, a key intermediate in Pfizer's synthesis of a glucagon receptor modulator,[90] respectively.

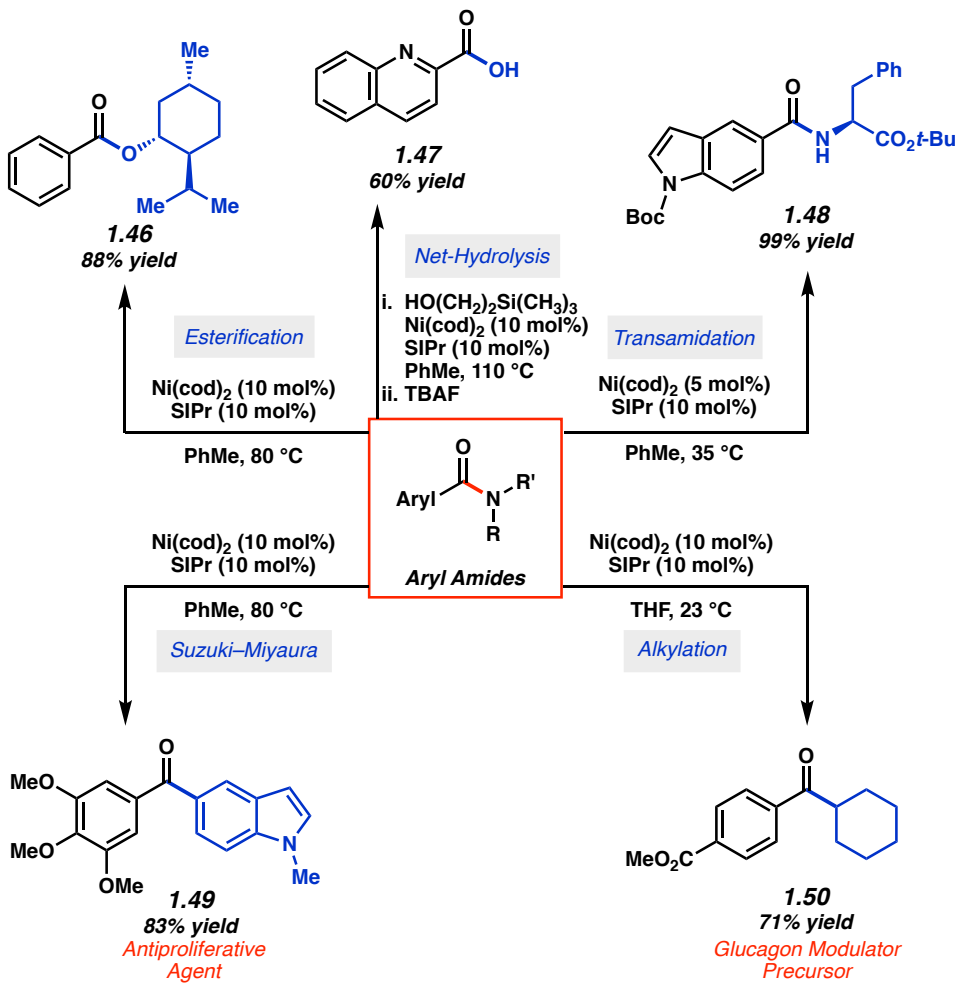


Figure 1.12. Recent advances in the nickel-catalyzed activation of aryl amide C–N bonds by our laboratory.

Nickel-catalyzed cross-couplings of amides that build stereocomplexity represent an important frontier of the field. Through the development of intramolecular Mizoroki–Heck cyclizations, we achieved the synthesis of indanones bearing α-quaternary stereocenters from *N*-benzyl-*N*-Boc amides (Figure 1.13).[67] Notably, this methodology provided diastereoselective access to indanone **1.52**, establishing vicinal stereocenters, one of which is quaternary, in a single transformation. Stanley and coworkers have extended this strategy to include domino-Heck reactions incorporating boron nucleophiles.[91] We were also interested in pursuing methodologies that generate stereocenters at the originating amide carbonyl carbon through the net addition of

two nucleophiles. Ultimately, a one-pot chemoenzymatic synthesis of enantioenriched alcohols was achieved through the combined use of nickel- and biocatalysis in a collaboration with Codexis.[92] For example, enantioenriched diarylmethanol **1.54** was accessed in 72% yield and 97% ee utilizing the methodology, which combined a Suzuki–Miyaura cross-coupling and ketoreductase (KRED)-mediated reduction in a one-pot, sequential process. These studies validated the utility of amide C–N bond activation in stereocomplexity-generating transformations. We view the development of asymmetric methods as a fruitful area for further exploration in this field.

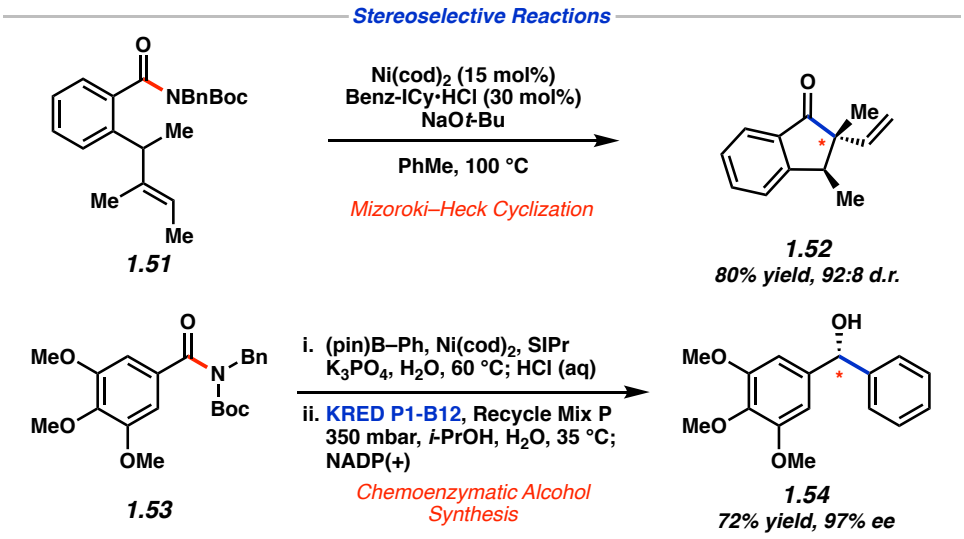


Figure 1.13. Asymmetric reactions of aryl amides developed by our laboratory.

Notably, the aforementioned methodologies were limited to the activation of aryl amide substrates. The activation of amides derived from aliphatic carboxylic acids (often referred to as "aliphatic amides") presents an even greater challenge as a result of increased steric requirements and a presumed lack of catalyst–substrate pre-complexation.[93] In considering esterifications of aliphatic amides, the use of terpyridine as the ligand proved effective in a collaborative study with Boehringer–Ingelheim (Figure 1.14).[94] This methodology provided efficient access to steroidal ester **1.55**, and could be used in a macrocyclic ring-opening to form ester **1.56**. Subsequently, we

evaluated C–C and C–N bond-forming reactions of alkyl amides through the use of the electron-rich NHC ligand precursor, Benz-Icy•HCl.[81,95,96,97] Specifically, we developed a Suzuki–Miyaura coupling of aliphatic amides, which provided access to ketone **1.57** from an enantioenriched amide with minimal racemization. Importantly, this methodology affords enolizable ketone products, which can then be further elaborated. For example, a Suzuki–Miyaura cross-coupling of a tetrahydropyranyl amide and concatenate Fischer indolization provided spiroindolenine **1.58** in rapid fashion. Transamidation of aliphatic secondary amides was also possible using this catalytic system, following C–N bond activation via *N*-functionalization. Of note, the stereoretentive transamidation of a prolinamide to provide secondary amide **1.59** in 60% yield and 99% ee was possible utilizing the methodology.[95] With the development of these protocols, our laboratory established the viability of aliphatic amides in C–O, C–C, and C–N bond-forming reactions using nickel catalysis.

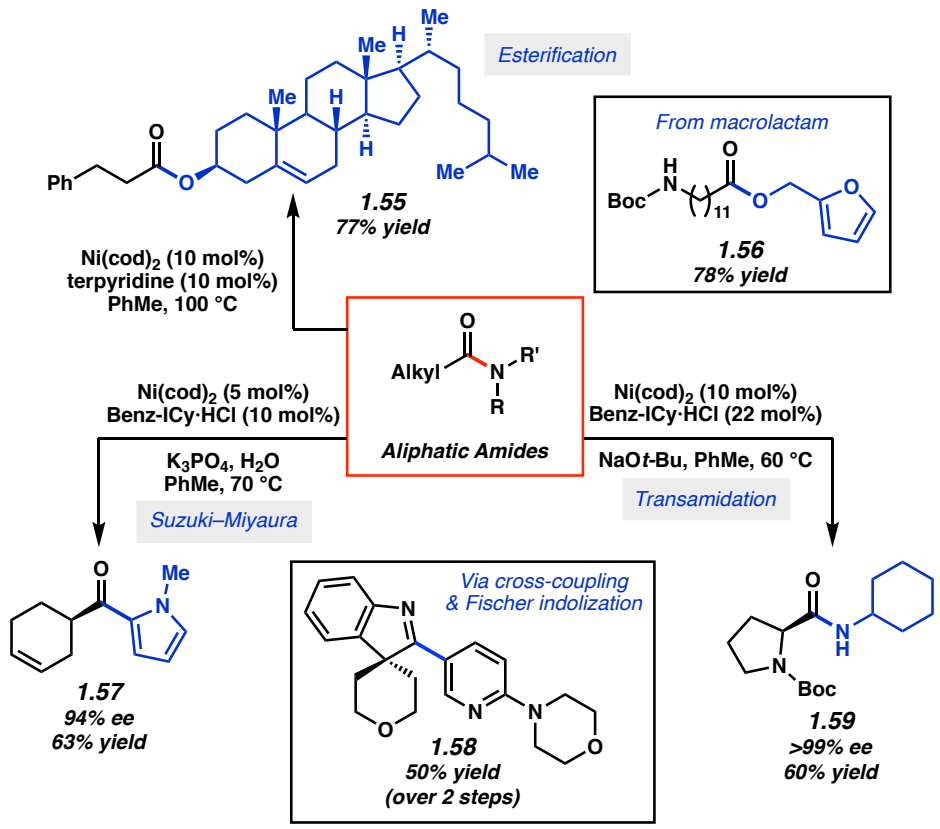


Figure 1.14. Recent advances in the nickel-catalyzed activation of aliphatic amide C–N bonds by our laboratory.

As previously noted, our laboratory has an interest in improving the practicality of nickel-catalyzed methods. Toward this end, we sought to optimize the catalytic efficiency of the esterification of amides reported by our laboratory.[98] A highlight of this collaborative effort with AbbVie, which combined experimentation and kinetic modeling,[99] was the realization of a 5 gram-scale coupling of aryl amide **1.60** and menthol (**1.61**) at a reduced temperature (45 °C vs. 80 °C) using <1 mol% $Ni(cod)_2$ to give ester **1.46** in 97% yield (Figure 1.15). Another key challenge in the area of nickel catalysis lies in the development of glovebox-free cross-couplings.[100] Encapsulating air- and moisture-sensitive reagents in paraffin wax has been an effective means to carry out transition-metal-catalyzed reactions on the benchtop,[101,102] including in undergraduate instructional laboratories.[103] In this regard, we successfully employed paraffin–$Ni(cod)_2$/Benzy-

ICy•HCl capsules in the benchtop Suzuki–Miyaura coupling of piperidinyl amide **1.62** to give polyheterocyclic ketone **1.64** in 73% yield on gram-scale. We are hopeful that future advances in these areas will promote greater use of base-metal catalysis in academia and industry.

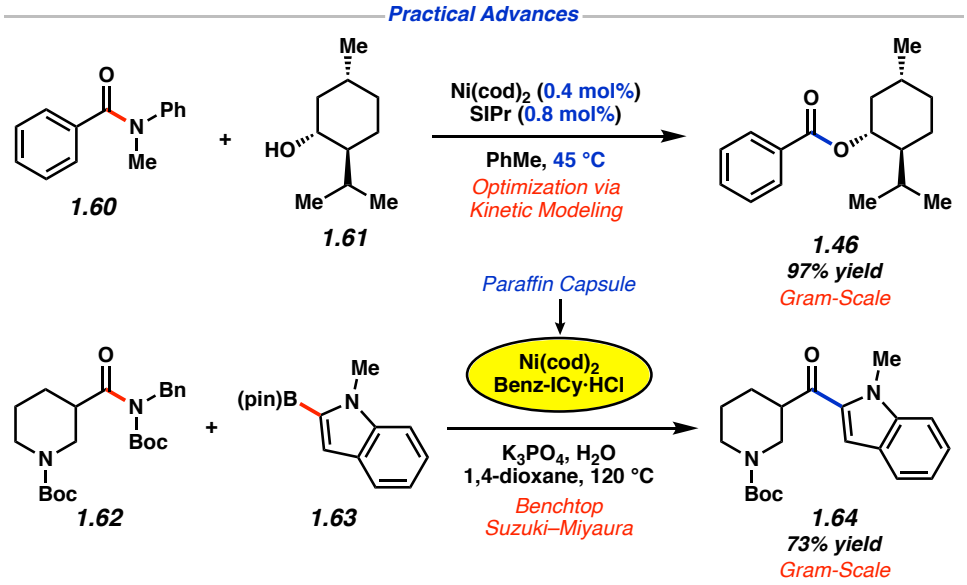


Figure 1.15. Practical advances in nickel-catalyzed activations of amides disclosed by our laboratory.

The field of amide C–N bond activation using transition metal catalysis, including breakthroughs with palladium catalysis led by Szostak,[104] has flourished in recent years, particularly when considering the introduction of alternative amide electrophiles and novel modes of reactivity. More than 85 studies involving transition-metal-catalyzed amide C–N bond activation have been reported since our initial study in 2015.[105] Select examples of amide derivatives that have been employed successfully by other groups in nickel-catalyzed cross-couplings are shown in Figure 1.16.[106] Amides have also seen use as acyl synthons in emerging cross-coupling manifolds, testifying to the rapid growth of this field. For instance, Hu and coworkers demonstrated a nickel-catalyzed reductive transamidation of *N,N*-Bn,Boc benzamides using nitroarenes.[66,107] Notably, this methodology was tolerant of a range of functional groups, including aryl bromides, allowing for the formation of aryl amide **1.67** in 69% yield. Additionally,

Molander and coworkers reported a Ni/Ir dual-catalytic photoredox approach to access alkyl–alkyl ketones such as 1,4-dicarbonyl **1.70**.[108] Finally, a number of Ni-catalyzed decarbonylative reactions of amides have been reported, expanding the scope of functional groups directly accessible from amides, as illustrated by the synthesis of compounds **1.71**–**1.73**.[109,110,111] The continued exploration of new modes of reactivity and bond-forming reactions is critical to advancing amides as useful building blocks in complex molecule synthesis.

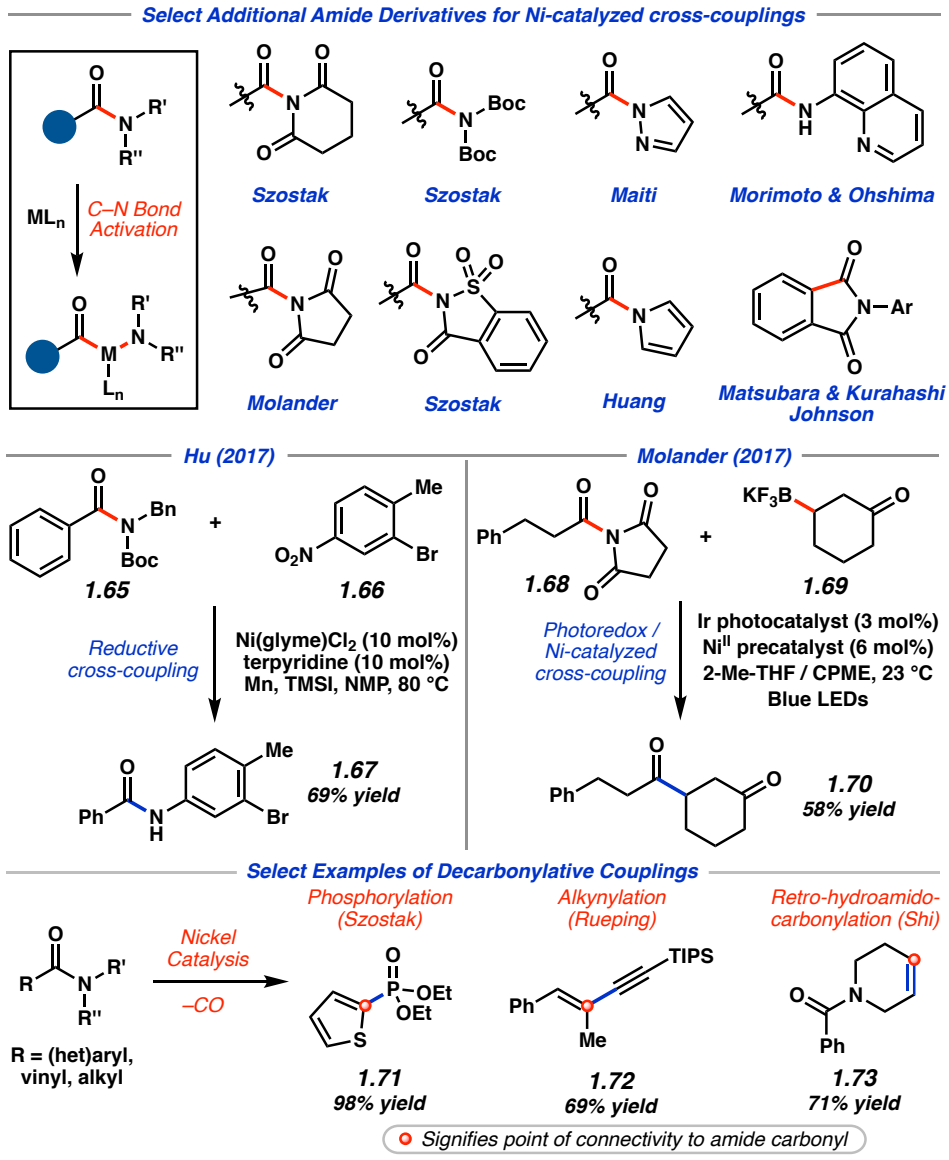


Figure 1.16. *N*-substituent variation, alternative reaction modes, and decarbonylative reactions of amides utilizing nickel catalysis.

1.6 Outlook and Future Directions

Although the field of base-metal-catalyzed activation of strong bonds has grown rapidly in recent years, there remains tremendous opportunity for future discovery. For example, expanding the scope of substrates that can undergo activation to include (sp^3)C–O/N electrophiles[112,113] and developing catalytic systems to activate amides, phenols, and anilines without the need for electron-withdrawing or chelating substituents[114] could allow chemists to directly manipulate common moieties in commodity chemicals and natural products. Another frontier for this field lies in the application of cross-couplings involving the activation of strong bonds to the synthesis of complex molecules. In this regard, the development of both chemo- and stereoselective reactions is expected to be highly enabling. Additionally, collaborations between academia and industry as well as amongst academic research groups would help achieve the future directions outlined above and expedite the adoption of novel methodologies in industrial settings.[115] Finally, computational investigations into reaction mechanisms and selectivities will undoubtedly lead to improvements in existing methodologies, inspire the development of others, and lead to the disclosure of tools to predict selectivities and outcomes in these transformations. Of note, although nickel catalysis has seen widespread use in the activation of strong bonds, there remains significant interest in exploring the utility of alternative non-precious metal catalysts in this arena and more broadly in cases where it could lower the cost of drug manufacturing.[115,116] We also envision that the optimization of reaction conditions and catalyst loadings, the discovery of new inexpensive ligand frameworks,[117] and the disclosure of well-defined, air-stable pre-catalysts[118] will promote the use of base-metal catalysis in academia and industry. We hope and anticipate that strong bond activation using base-metal catalysts will continue to thrive as a field and be viewed as an increasingly valuable strategy in organic synthesis.

1.7 Notes and References

(1) (a) Suzuki, A.; Cross-coupling reactions of organoboranes: an easy way to construct C–C bonds. *Angew. Chem., Int. Ed.* **2011**, *50*, 6723–6737. (b) Negishi, E.-I.. Magical power of transition metals: past, present, and future. *Angew. Chem., Int. Ed.* **2011**, *50*, 6738–6764. (c) Seechurn, C. C. C. J.; Kitching, M. O.; Colacot, T. J.; Snieckus, V. Palladium-catalyzed cross-coupling: a historical contextual perspective to the 2010 Nobel Prize. *Angew. Chem., Int. Ed.* **2012**, *51*, 5062–5085.

(2) For representative reviews, see: (a) Duschek, A.; Kirsch, S. F. Combining the concepts: dual catalysis with carbophilic Lewis acids. *Angew. Chem., Int. Ed.* **2008**, *47*, 5703–5705. (b) Hirner, J. J.; Shi, Y.; Blum, S. A. Organogold reactivity with palladium, nickel, and rhodium: transmetalation, cross-coupling and dual catalysis. *Acc. Chem. Res.* **2011**, *44*, 603–613. (c) Hanna, L. E.; Jarvo, E. R. Selective cross-electrophile coupling by dual catalysis. *Angew. Chem., Int. Ed.* **2015**, *54*, 15618–15620. (d) Afewerki, S.; Córdova, A. Combinations of aminocatalysts and metal catalysts: a powerful cooperative approach in selective organic synthesis. *Chem. Rev.* **2016**, *116*, 13512–13570. (e) Krautwald, S.; Carreira, E. M. Stereodivergence in asymmetric catalysis. *J. Am. Chem. Soc.* **2017**, *139,* 5627–5639. (f) Romiti, F.; del Pozo, J.; Paioti, P. H. S.; Gonsales, S. A.; Li, X.; Hartrampf, F. W. W.; Hoveyda, A. H. Different strategies for designing dual-catalytic enantioselective processes: from fully cooperative to non-cooperative systems. *J. Am. Chem. Soc.* **2019**, *141*, 17952–17961.

(3) For representative reviews, see: (a) Zhiwei, Z.; Ahnemna, D. T.; Chu, L.; Terrett, J. A.; Doyle, A. G.; MacMillan, D. W. C. Merging photoredox with nickel catalysis: coupling of α-

carboxyl sp^3-carbons with aryl halides. *Science* **2014**, *345*, 437–440. (b) Twilton, J.; Le, C.; Zhang, P.; Shaw, M. H.; Evans, R. W.; MacMillan D. W. C. The merger of transition metal and photocatalysis. *Nat. Rev. Chem.* **2017**, *1*, 0052. (c) Hopkinson, M. N.; Tlahuext-Aca, A.; Glorius, F. Merging visible light photoredox and gold catalysis. *Acc. Chem. Res.* **2016**, *49*, 2261–2272. (d) Douglas, J. J.; Sevrin, M. J.; Stephenson, C. R. J. Visible light photocatalysis: applications and new disconnections in the synthesis of pharmaceutical agents. *Org. Process. Res. Dev.* **2016**, *20*, 1134–1147.

(4) For representative reviews, see: (a) Lucas, E. L.; Jarvo, E. R. Stereospecific and stereoconvergent cross-couplings between alkyl electrophiles. *Nat. Rev. Chem.* **2017**, *1*, 65. (b) Weix, D. J. Methods and mechanisms for cross-electrophile coupling of Csp^2 halides with alkyl electrophiles. *Acc. Chem. Res.* **2015**, *48*, 1767–1775. (c) Hanna, L. E.; Jarvo, E. R. Selective cross-electrophile coupling by dual catalysis. *Angew. Chem., Int. Ed.* **2015**, *54*, 15618–15620. (d) Everson, D. A.; Weix, D. J. Cross-electrophile coupling: principles of reactivity and selectivity. *J. Org. Chem.* **2014**, *79*, 4793–4798.

(5) For representative publications on combining chemo- and biocatalysis, see: (a) Rudroff, F.; Mihovilovic, M. D.; Gröger, H.; Snajdrova, R.; Iding, H.; Bornscheuer, W. T. Opportunities and challenges for combining chemo- and biocatalysis. *Nat. Catal.* **2018**, *1*, 12–22. (b) Denard, C. A.; Hartwig, J. F.; Zhao, H. Multistep one-pot reactions combining biocatalysis and chemical catalysts for asymmetric synthesis. *ACS Catal.* **2013**, *3*, 2856–2864. (c) Gröger, H.; Hummel, W. Combining the 'two worlds' of chemocatalysis and biocatalysis towards multi-step one-pot processes in aqueous media. *Curr. Opin. Chem. Biol.* **2014**, *19*, 171–179. (d) Ríos-Lombardía, N.; García-Álvarez, J.; González-Sabín, J. One-pot combination of

metal- and biocatalysis in water for the synthesis of chiral molecules. *Catalysts* **2018**, *8*, 75. (e) Sirasani, G.; Tong, L.; Balskus, E. P. A biocompatible alkene hydrogenation merges organic synthesis with microbial metabolism. *Angew. Chem., Int. Ed.* **2014**, *53*, 7785–7788. (f) Wallace, S.; Balskus, E. P. Interfacing microbial styrene production with a biocompatible cyclopropanation reaction. *Angew. Chem., Int. Ed.* **2015**, *54*, 7106–7109.

(6) For representative publications, see: (a) Lucas, E. L.; Jarvo, E. R. Keeping track of the electrons. *Acc. Chem. Res.* **2018**, *51*, 567–572. (b) Brozek, L. A.; Ardolino, M. J.; Morken, J. P. Diasterocontrol in asymmetric allyl–allyl cross-coupling: stereocontrolled reaction of prochiral allylboronates with prochiral allyl chlorides. *J. Am. Chem. Soc.* **2011**, *133*, 16778–16781. (c) Kainz, Q. M.; Matier, C. D.; Bartoszewicz, A.; Zultanski, S. L.; Peters, J. C.; Fu, G. C. Asymmetric copper-catalyzed C–N cross-couplings induced by visible light. *Science* **2016**, *351*, 681–684. (d) Wang, Z.; Yin, H.; Fu, G. C. Catalytic enantioconvergent coupling of secondary and tertiary electrophiles with olefins. *Nature* **2018**, *563*, 379–383. (e) Huo, H.; Gorsline, B. J.; Fu, G. C. Catalyst-controlled doubly enantioconvergent coupling of racemic alkyl nucleophiles and electrophiles. *Science* **2020**, *367*, 559–564.

(7) (a) Bolm, C.; Legros, J.; Le Paih, J.; Zani, L. Iron-catalyzed reactions in organic synthesis. *Chem. Rev.* **2004**, *104*, 6217−6254. (b) Enthaler, S.; Junge, K.; Beller, M. Sustainable metal catalysis with iron: from rust to rising star? *Angew. Chem., Int. Ed.* **2008**, *47*, 3317−3321. (c) Bauer, E. B. Recent advances in iron catalysis in organic synthesis. *Curr. Org. Chem*. **2008**, *12*, 1341−1369. (d) Fürstner, A.; Iron catalysis in organic synthesis: A critical assessment of what is takes to make this base metal a multitasking champion. *ACS Central Sci.* **2016**, *2*, 778–789. (e) Fürstner, A.; Leitner A.; Méndez, M.; Krause, H. Iron-catalyzed cross-coupling

reactions. *J. Am. Chem. Soc.* **2002**, *124*, 13856–13863. (f) Mesganaw, T.; Garg, N. K. Ni- and Fe-catalyzed cross-coupling reactions of phenol derivatives. *Org. Process Res. Dev*. **2013**, *17*, 29−39. (g) Tasker, S. Z.; Standley, E. A.; Jamison, T. F. Recent advances in homogeneous nickel catalysis. *Nature* **2014**, *509*, 299−309. (h) Ananikov, V. P. Nickel: the "Spirited Horse" of transition metal catalysis. *ACS Catal.* **2015**, *5*, 1964–1971. (i) Dander, J. E.; Garg, N. K. Breaking amides using nickel catalysis. *ACS Catal.* **2017**, *7*, 1413–1423. (j) Su, B.; Cao, Z.-C.; Shi, Z.-J. Exploration of earth-abundant transition metals (Fe, Co, and Ni) as catalysts in unreactive chemical bond activations. *Acc. Chem. Res.* **2015**, *48*, 886–896.

(8) On the basis of a SciFinder search for the research topic "nickel cross-coupling" and narrowing the search to only journal articles (i.e. excluding review articles) published between 2008 and 2020 (accessed July 30, 2020).

(9) Nickel readily participates in radical pathways due to the relatively stability of open-shell nickel-complexes. For theoretical and experimental studies, see: (a) Poli, R.; Cacelli, I. Orbital splitting and pairing energy in open-shell organometallics: A study of two families of 16-electron complexes [Cp_2M] (M = Cr, Mo, W) and [$CpM(PH_3)$] (M = Co, Rh, Ir). *Eur. J. Inorg. Chem.* **2005**, 2324–2331. (b) Tsou, T. T.; Kochi, J. Mechanism of oxidative addition. Reaction of nickel(0) complexes with aromatic halides. *J. Am. Chem. Soc.* **1979**, *101*, 6319–6332. (c) Schley, N. D.; Fu, G. C. Nickel-catalyzed Negishi arylations of propargylic bromides: A mechanistic investigation. *J. Am. Chem. Soc.* **2014**, *136*, 16588–16593.

(10) In comparison to palladium, nickel has a smaller atomic radius, is less electronegative, and is more easily oxidized. In turn, oxidative addition is more facile to Ni(0) relative to Pd(0). For theoretical and experimental studies, see: (a) Mann, J. B.; Meek, T. L.; Knight, E. T.; Capitani,

J. F.; Allen, L. C. Configuration energies of the d-block elements. *J. Am. Chem. Soc.* **2000**, *122*, 5132–5317. (b) Lide, D. R. CRC handbook of chemistry and physics, 87th ed.; CRC Press: 2008. Chapter 4 p. 1 (c) Batsanov, S. S. Van der Waals radii of elements. *Inorg. Mater*. **2001**, *37*, 871−885. (d) Hartwig, J. F. *Organotransition Metal Chemistry: From Bonding to Catalysis*; Murdzek, J., Eds.; University Science Books: Mill Valley, CA, 2010; p 8.

(11) (a) Diccianni, J.; Lin, W.; Diao, T. Mechanisms of nickel-catalyzed coupling reactions and applications in alkene functionalization. *Acc. Chem. Res.* **2020**, *53*, 906–919. (b) Diccianni, J. B.; Diao, T. Mechanisms of nickel-catalyzed cross-coupling reactions. *Trends. Chem.* **2019**, *1*, 830–844.

(12) In the context of this Viewpoint, we consider a "strong bond" as one that has been traditionally inert to oxidative addition using palladium catalysis.

(13) (a) Rosen, B. M.; Quasdorf, K. W.; Wilson, D. A.; Zhang, N.; Resmerita, A.-M.; Garg, N. K.; Percec, V. Nickel-catalyzed cross-couplings involving carbon–oxygen bonds. *Chem. Rev.* **2011**, *111*, 1346–1416. (b) Yu, D.-G.; Li, B.-J.; Shi, Z.-J. Exploration of new C–O electrophiles in cross-coupling reactions. *Acc. Chem. Res.* **2010**, *43*, 1486−1495. (c) Li, B.-J.; Yu, D.-G.; Sun, C.-L.; Shi, Z.-J. Activation of "inert" alkenyl/aryl C–O bond and its applications in cross-coupling reactions. *Chem. Eur. J.* **2011**, *17*, 1728−1759. (d) Gooßen, L. J.; Gooßen, K.; Stanciu, C. C(aryl)–O activation of aryl carboxylates in nickel-catalyzed biaryl syntheses. *Angew. Chem., Int. Ed.* **2009**, *48*, 3569–3571.

(14) For reviews, see: (a) Miyaura, N.; Suzuki, A. Palladium-catalyzed cross-coupling reactions of organoboron compounds. *Chem. Rev*. **1995**, *95*, 2457–2483. (b) Suzuki, A. Recent advances in the cross-coupling reactions of organoboron derivatives with organic

electrophiles. *Organomet. Chem.* **1999**, *576*, 147–168. (c) Miyaura, N. In *Advances in Metal-Organic Chemistry*; Liebeskind, L. S., Ed.; JAI: London, 1998; Vol. 6, p. 187–243. (d) Suzuki, A. In *Metal-Catalyzed Cross-Coupling Reactions*; Diederich, F., Stang, P. J., Eds.; Wiley-VCH: New York, 1998; p. 761–813. (e) Stanforth, S. P. Catalytic cross-coupling reactions in biaryl synthesis. *Tetrahedron* **1998**, *54*, 263–303.

(15) Approximate reagent costs by Aldrich Chemical Co., Inc. are: (a) Triflic anhydride = $280 per mol. (b) Methanesulfonyl chloride = $12 per mol. (c) Trimethylacetyl chloride (pivaloyl chloride) = $15 per mol. (d) Iodomethane = $68 per mol.

(16) Although aryl sulfonates have been established as viable cross-coupling partners, their utility in ortho-lithiation reactions is limited. For examples of alkyl benzenesulfonates as directing groups in ortho-metalation reactions, see: (a) Bonfiglio, J. N. Directed ortho-lithiation of alkyl arene sulfonates. *J. Org. Chem.* **1986**, *51*, 2833–2835. (b) Spangler, L. A. A novel method for the preparation of 2,6-disubstituted benzenesulfonates and benzenesulfonyl chlorides utilizing the powerful alkyl sulfonate ortho directing group. *Tetrahedron Lett.* **1996**, *37*, 3639–3642.

(17) For examples of aryl mesylates and tosylates in cross-coupling reactions, see: (a) Zim, D.; Lando, V. R.; Dupont, J.; Monteiro, A. L. $NiCl_2(PCy_3)_2$: A simple and efficient catalyst precursor for the Suzuki cross-coupling of aryl tosylates and arylboronic acids. *Org. Lett.* **2001**, *3*, 3049–3051. (b) Tang, Z.-Y; Hu, Q.-S. Room-temperature Ni(0)-catalyzed cross-coupling reactions of aryl arenesulfonates with arylboronic acids. *J. Am. Chem. Soc.* **2004**, *126*, 3058–3059. (c) Percec, V.; Golding, G. M.; Smidrkal, J.; Weichold, O. $NiCl_2$(dppe)-catalyzed cross-coupling of aryl mesylates, arenesulfonates, and halides with arylboronic

acids. *J. Org. Chem.* **2004**, *69*, 3447–3452. (d) Zhang, L.; Meng, T.; Wu, J. Palladium-catalyzed Suzuki−Miyaura cross-couplings of aryl tosylates with potassium aryltrifluoroborates. *J. Org. Chem.* **2007**, *72*, 9346–9349. (e) Munday, R. H.; Martinelli, J. R.; Buchwald, S. L. Palladium-catalyzed carbonylation of aryl tosylates and mesylates. *J. Am. Chem. Soc.* **2008**, *130*, 2754–2755.

(18) Macklin, T. K.; Snieckus, V. Directed ortho metalation methodology. The *N,N*-dialkyl aryl *O*-sulfamate as a new directed metalation group and cross-coupling partner for Grignard reagents. *Org. Lett.* **2005**, *7*, 2519–2522.

(19) Polyfunctionalized aromatics are important scaffolds in medicines, ligands for catalysis, and materials chemistry. For examples, see: (a) Kotha, S.; Lahiri, K.; Kashinath, D. Recent applications of the Suzuki–Miyaura cross-coupling reaction in organic synthesis. *Tetrahedron* **2002**, *58*, 9633–9695. (b) Kertesz, M.; Choi, C. H.; Yang, S. Conjugated polymers and aromaticity. *Chem. Rev.* **2005**, *105*, 3448–3481. (c) Martin, R.; Buchwald, S. L. Palladium-catalyzed Suzuki–Miyaura cross-coupling reactions employing dialkylbiaryl phosphine ligands. *Acc. Chem. Res.* **2008**, *41*, 1461–1473. (d) Surry, D. S.; Buchwald, S. L. Biaryl phosphane ligands in palladium-catalyzed amination. *Angew. Chem., Int. Ed.* **2008**, *47*, 6338–6361.

(20) (a) Wenkert, E.; Michelotti, E. L.; Swindell, C. S. Nickel-induced conversion of carbon-oxygen into carbon-carbon bonds. One-step transformations of enol ethers into olefins and aryl ethers into biaryls. *J. Am. Chem. Soc*. **1979**, *101*, 2246–2247. (b) Wenkert, E.; Michelotti, E. L.; Swingdell, C. S.; Tingoli, M. Transformation of carbon-oxygen into carbon-carbon bonds mediated by low-valent nickel species. *J. Org. Chem.* **1984**, *49*, 4894–4899.

(21) Dankwardt, J. W. Nickel-catalyzed cross-coupling of aryl Grignard reagents with aromatic alkyl ethers: an efficient synthesis of unsymmetrical biaryls. *Angew. Chem., Int. Ed.* **2004**, *43*, 2428–2432.

(22) Guan, B.-T.; Xiang, S.-K.; Wu, T.; Sun, Z.-P.; Wang, B.-Q.; Zhao, K.-Q.; Shi, Z.-J. Methylation of arenes via Ni-catalyzed aryl C–O/F activation. *Chem. Commun.* **2008**, 1437–1439.

(23) Tobisu, M.; Shimasaki, T.; Chatani, N. Nickel-catalyzed cross-coupling of aryl methyl ethers with aryl boronic esters. *Angew. Chem., Int. Ed.* **2008**, *47*, 4866–4869.

(24) More recently, Sergeev and Hartwig disclosed the nickel-catalyzed hydrogenolysis of diaryl ethers: Sergeev, A. G.; Hartwig, J. F. Selective, nickel-catalyzed hydrogenolysis of aryl ethers. *Science* **2011**, *322*, 439–443.

(25) The Suzuki–Miyaura coupling of aryl pivalates was simultaneously reported by our laboratory and the laboratory of Shi: Guan, B.-T.; Wang, Y.; Li, B.-J.; Yu, D.-G.; Shi, Z.-J. Biaryl construction via Ni-catalyzed C−O activation of phenolic carboxylates. *J. Am. Chem. Soc.* **2008**, *130*, 14468–14470.

(26) (a) Ishizu, J.; Yamamoto, T.; Yamamoto, A. Selective cleavage of C–O bonds in esters through oxidative addition to Ni(0) complexes. *Chem. Lett.* **1976**, *5*, 1091–1094. (b) Yamamoto, T.; Ishizu, J.; Kohara, T.; Komiya, S.; Yamamoto, A. Oxidative addition of aryl carboxylates to nickel(0) complexes involving cleavage of the acyl-oxygen bond. *J. Am. Chem. Soc.* **1980**, *102*, 3758–3764.

(27) In general, while evaluating the feasibility of new methodologies, we often employ naphthyl substrates as oxidative addition to these substrates tends to be more facile.

(28) Quasdorf, K. W.; Tian. X.; Garg, N. K. Cross-coupling reactions of aryl pivalates with boronic acids. *J. Am. Chem. Soc.* **2008**, *130*, 14422–14423.

(29) Quasdorf, K. W.; Riener, M.; Petrova, K. V.; Garg, N. K. Suzuki–Miyaura coupling of aryl carbamates, carbonates, and sulfamates. *J. Am. Chem. Soc.* **2009**, *131*, 17748–17749.

(30) Snieckus, V. Directed ortho metalation. Tertiary amide and O-carbamate directors in synthetic strategies for polysubstituted aromatics. *Chem. Rev.* **1990**, *90*, 879–933.

(31) Mesganaw, T.; Silberstein, A. L.; Ramgren, S. D.; Fine Nathel, N. F.; Hong, X.; Liu, P.; Garg, N. K. Nickel-catalyzed amination of aryl carbamates and sequential site-selective cross-couplings. *Chem. Sci.* **2011***, 2*, 1766–1771.

(32) For reviews in the area of sp^2–sp^3 C–C cross-couplings, see: (a) Tellis, J. C.; Kelley, C. B.; Primer, D. N.; Jouffroy, M.; Patel, N. R.; Molander, G. A. Single-electron transmetalation via photoredox/nickel dual catalysis: unlocking a new paradigm for sp^3−sp^2 cross-coupling. *Acc. Chem. Res.* **2016**, *49*, 1429–1439. (b) Iwasake, T.; Kambe, N. Ni-catalyzed C–C couplings using alkyl electrophiles. *Top. Curr. Chem.* **2016**, *374*, 1–36. (c) Miyaura, N.; Suzuki, A. Palladium-catalyzed cross-coupling reactions of organoboron compounds. *Chem. Rev.* **1995**, *95*, 2457–2483.

(33) For examples of iron-catalyzed alkylations of aryl halides, triflates, and sulfonates, see: (a) Fürstner, A.; Leitner, A. Iron-catalyzed cross-coupling reactions of alkyl-Grignard reagents with aryl chlorides, tosylates, and triflates. *Angew. Chem., Int. Ed.* **2002**, *41*, 609–612. (b) Fürstner, A.; Leitner, A.; Méndez, M.; Krause, H. Iron-catalyzed cross-coupling reactions. *J. Am. Chem. Soc.* **2002**, *124*, 13856–13863. (c) Fürstner, A.; Martin, R.; Krause, H.; Günter, S.; Goddard, R.; Lehmann, C. W. Preparation, structure, and reactivity of nonstabilized

organoiron compounds. Implications for iron-catalyzed cross coupling reactions. *J. Am. Chem. Soc.* **2008**, *130*, 8773–8787.

(34) For the iron-catalyzed alkylation of heteroaromatic sulfonates and phosphates, see: (a) Gøgsig, T. M.; Lindhardt, A. T.; Skrydstrup, T. Heteroaromatic sulfonates and phosphates and electrophiles in iron-catalyzed cross-couplings. *Org. Lett.* **2009**, *11*, 4886–4888. (b) Kleimark, J.; Larsson, P.-F.; Emamy, P.; Hedström, A.; Norrby, P.-O. Low temperature studies of iron-catalyzed cross-coupling of alkyl Grignard reagents with aryl electrophiles. *Adv. Synth. Catal.* **2012**, *354*, 448–456.

(35) Silberstein, A. L.; Ramgren, S. D.; Garg, N. K. Iron-catalyzed alkylations of aryl sulfamates and carbamates. *Org. Lett.* **2012**, *14*, 3796–3799.

(36) Mesganaw, T.; Fine Nathel, N. F.; Garg, N. K. Cine substitution of arenes using the aryl carbamate as a removable directing group. *Org. Lett*. **2012**, *14*, 2918–2921.

(37) (a) Yoshikai, N.; Matsuda, H.; Nakamura, E. Hydroxyphosphine ligand for nickel-catalyzed cross-coupling through nickel/magnesium bimetallic cooperation. *J. Am. Chem. Soc.* **2009**, *131*, 9590–9599. (b) Li, B.-J.; Wu, Z.-H.; Guan, B.-T.; Sun, C.-L.; Wang, B.-Q.; Shi, Z.-J. Cross-coupling of alkenyl/aryl carboxylates with Grignard reagent via Fe-catalyzed C–O bond activation. *J. Am. Chem. Soc.* **2009**, *131*, 14656–14657. (c) Xu, L.; Li, B.-J.; Wu, Z.-H.; Lu, X.-Y.; Guan, B.-T.; Wang, B.-Q.; Zhao, K.-Q.; Shi, Z.-J.; Nickel catalyzed efficient and practical Suzuki–Miyaura coupling of alkenyl and aryl carbamates with aryl boroxines. *Org. Lett.* **2010**, *12*, 884–887. (d) Shimasaki, T.; Tobisu, M.; Chatani, N. Nickel-catalyzed amination of aryl pivalates by the cleavage of aryl C–O bonds. *Angew. Chem., Int. Ed.* **2010**, *49*, 2929–2932. (e) Tobisu, M.; Yamakawa, K.; Shimasaki, T.; Chatani, N. Nickel-catalyzed

reductive cleavage of aryl–oxygen bonds in alkoxy- and pivaloxyarenes using hydrosilanes as a mild reducing agent. *Chem. Commun.* **2011**, *47*, 2946–2948. (f) Zhao, F.; Yu, D.-G.; Zhu, R.-Y.; Xi, Z.; Shi, Z.-J. Cross-coupling of aryl/alkenyl silyl ethers with Grignard reagents through nickel-catalyzed C–O bond activation. *Chem. Lett.* **2011**, *40*, 1001–1003. (g) Yu, D. G.; Shi, Z.-J. Mutual activation: Suzuki–Miyaura coupling through direct cleavage of the sp^2 C–O bond of naphtholate. *Angew. Chem., Int. Ed.* **2011**, *50*, 7097–7100. (h) Huang, K.; Yu, D.-G.; Zheng, S.-F.; Wu, Z.-H.; Shi, Z.-J. Borylation of aryl and alkenyl carbamates through Ni-catalyzed C–O activation. *Chem. Eur. J.* **2011**, *17*, 786–791. (i) Zhao, F.; Zhang, Y.-F.; Wen, J.; Yu, D.-G.; Wei, J.-B.; Xi, Z.; Shi, Z.-J. Programmed selective sp^2 C–O bond activation toward multiarylated benzenes. *Org. Lett.* **2013**, *15*, 3230–3233. (j) Hong, X.; Liang, Y.; Houk, K. N. Mechanisms and origins of switchable chemoselectivity of Ni-catalyzed C(aryl)–O and C(acyl)–O activation of aryl esters with phosphine ligands. *J. Am. Chem. Soc.* **2014**, *136*, 2017–2025. (k) Yue, H.; Guo, L.; Liu, X.; Rueping, M. Nickel-catalyzed synthesis of primary aryl and heteroaryl amines via C–O bond cleavage. *Org. Lett.* **2017**, *19*, 1788–1791.

(38) Quasdorf, K. W.; Antoft-Finch, A.; Liu, P.; Silberstein, A. L.; Komaromi, A.; Blackburn, T.; Ramgren, S. D.; Houk, K. N.; Snieckus, V.; Garg, N. K. Suzuki–Miyaura cross-coupling of aryl carbamates and sulfamates: experimental and computational studies. *J. Am. Chem. Soc*. **2011**, *133*, 6352–6363.

(39) Ramgren, S. D.; Silberstein, A. L.; Yang, Y.; Garg, N. K. Nickel-catalyzed amination of aryl sulfamates. *Angew. Chem., Int. Ed.* **2011**, *50*, 2171–2173.

(40) (a) Jezorek, R. L.; Zhang, N.; Leowanawat, P.; Bunner, M. H.; Gutsche, N.; Pesti, A. K. R.; Olsen, J. T.; Percec, V. Air-stable nickel precatalysts for fast and quantitative cross-coupling of aryl sulfamates with aryl neopentylglycolboronates at room temperature. *Org. Lett.* **2014**, *16*, 6326–6239. (b) Beromi, M. M.; Nova, A.; Balcells, D.; Brasacchio, A. M.; Brudvig, G. W.; Guard, L. M.; Hazari, N.; Vinyard, D. J. Mechanistic study of an improved Ni precatalyst for Suzuki–Miyaura reactions of aryl sulfamates: Understanding the role of Ni(I) species. *J. Am. Chem. Soc.* **2017**, *139*, 922–936. (c) Zhang, N.; Hoffman, D. J.; Gutsche, N.; Gupta, J.; Percec, V. Comparison of arylboron-based nucleophiles in Ni-catalyzed Suzuki–Miyaura cross-coupling with aryl mesylates and sulfamates. *J. Org. Chem.* **2012**, *77*, 5956–5964. (d) Muto, K.; Yamaguchi, J.; Lei, A.; Itami, K. Isolation, structure, and reactivity of an arylnickel(II) pivalate complex in catalytic C–H/C–O biaryl coupling. *J. Am. Chem. Soc.* **2013**, *135*, 16384–16387. (e) Leowanawat, P.; Zhang, N.; Safi, M.; Hoffman, D. J.; Fryberger, M. C.; George, A.; Percec, V. *trans*-Chloro(1-naphthyl)bis(triphenylphosphine)nickel(II)/PCy_3 catalyzed cross-coupling of aryl and heteroaryl neopentylglycolboronates with aryl and heteroaryl mesylates and sulfamates at room temperature. *J. Org. Chem.* **2012**, *77*, 2885–2982. (f) Leowanawat, P.; Zhang, N.; Percec, V. Nickel catalyzed cross-coupling of aryl C–O based electrophiles with aryl neopentylglycolboronates. *J. Org. Chem.* **2012**, *77*, 1018–1025. (g) Leowanawat, P.; Zhang, N.; Resmerita, A.-M.; Rosen, B. M.; Percec, V. $Ni(COD)_2/PCy_3$ Catalyzed cross-coupling of aryl and heteroaryl neopentylglycolboronates with aryl and heteroaryl mesylates and sulfamates in THF at room temperature. *J. Org. Chem.* **2011**, *76*, 9946–9955.

(41) For representative publications on the development of air-stable Ni(II) precatalysts, see: (a) Standley, E. A. and Jamison, T. F. Simplifying nickel(0) catalysis: an air-stable nickel precatalyst for the internally selective benzylation of terminal alkenes. *J. Am. Chem. Soc.* **2013**, *135*, 1585–1592. (b) Strieth-Kalthoff, F.; Longstreet, A. R.; Weber, J. M.; Jamison, T. F. Bench-stable *N*-heterocyclic carbene nickel precatalysts for C–C and C–N bond-forming reactions. *ChemCatChem* **2018**, *10*, 1–6. (c) Weber, J. M.; Longstreet, A. R.; Jamison, T. F. Bench-stable nickel precatalysts with Heck-type activation. *Organometallics* **2018**, *37*, 2716–2722. (d) Shields, J. D.; Gray, E. E.; Doyle, A. G. A modular, air-stable nickel precatalyst. *Org. Lett.* **2015**, *17,* 2166−2169.

(42) Hie, L.; Ramgren, S.D.; Mesganaw, T.; Garg, N.K. Nickel-catalyzed amination of aryl sulfamates and carbamates using an air-stable precatalyst. *Org. Lett.* **2012**, *14*, 4182–4185.

(43) Nathel, N. F. N.; Kim, J.; Hie, L.; Jiang, X.; Garg, N.K. Nickel-catalyzed amination of aryl chlorides and sulfamates in 2-methyl THF. *ACS Catal.* **2014**, *4*, 3289–3293.

(44) Roglans, A.; Pla-Quintana, A.; Moreno-Mañas, M. Diazonium salts as substrates in palladium-catalyzed cross-coupling reactions. *Chem. Rev.* **2006**, *106*, 4622−4643.

(45) Though Cu(I) catalyzed reactions of aryl diazononium salts are well-established, these transformations typically proceed via single-electron-transfer and aryl radical reactivity rather than through traditional M(0)/M(II) cross-coupling catalytic cycles.

(46) For a comprehensive review, see: Ouyang, K.; Hao, W.; Zhang, W.-X.; Xi, Z. Transition-metal-catalyzed cleavage of C–N single bonds. *Chem. Rev.* **2015**, *115*, 12045–12090.

(47) Blakey, S. B.; MacMillan, D. W. C. The first Suzuki cross-couplings of aryltrimethylammonium salts. *J. Am. Chem. Soc.* **2003**, *125*, 6046−6047.

(48) Wenkert, E.; Han, A.-L.; Jenny, C.-J. Nickel-induced conversion of carbon−nitrogen into carbon−carbon bonds. one-step transformations of aryl, quaternary ammonium salts into alkylarenes and biaryls. *J. Chem. Soc., Chem. Commun.* **1988**, 975−976.

(49) Cao, Z.-C.; Xie, S.-J.; Fang, H.; Shi, Z.-J. Ni-catalyzed cross-coupling of dimethyl aryl amines with arylboronic esters under reductive conditions. *J. Am. Chem. Soc.* **2018**, *140*, 13575−13579.

(50) For examples, see: (a) Ueno, S.; Chatani, N.; Kakiuchi, F. Ruthenium-catalyzed carbon−carbon bond formation via the cleavage of an unreactive aryl carbon−nitrogen bond in aniline derivatives with organoboronates. *J. Am. Chem. Soc.* **2007**, *129*, 6098–6099. (b) Koreeda, T.; Kochi, T.; Kakiuchi, F. Cleavage of C−N bonds in aniline derivatives on a ruthenium center and its relevance to catalytic C−C bond formation. *J. Am. Chem. Soc.* **2009**, *131*, 7238–7239. (c) Koreeda, T.; Kochi, T.; Kakiuichi, F. Substituent effects on stoichiometric and catalytic cleavage of carbon–nitrogen bonds in aniline derivatives by ruthenium–phosphine complexes. *Organometallics* **2013**, *32*, 682–690. (d) Koreeda, T.; Kochi, T.; Kakuichi, F. Ruthenium-catalyzed reductive deamination and tandem alkylation of aniline derivatives. *J. Organomet. Chem.* **2013**, *741−742*, 148−152. (e) Zhao, Y.; Snieckus, V. Beyond directed ortho metalation: ruthenium-catalyzed amide-directed C_{Ar}−N activation/C−C coupling reaction of anthranilamides with organoboronates. *Org. Lett*. **2014**, *16*, 3200−3203.

(51) Liu, J.; Robins, M. J. Azoles as Suzuki cross-coupling leaving groups: syntheses of 6-arylpurine 2′-deoxynucleosides and nucleo- sides from 6-(imidazol-1-yl)- and 6-(1,2,4-triazol-4-yl)purine derivatives. *Org. Lett.* **2004**, *6*, 3421−3423.

(52) For reports on the application of nucleoside analogs as potential therapeutics or chemical probes, see: (a) Hocek, M.; Holy, A.; Votruba, I.; Dvořáková, H. Synthesis and cytostatic activity of substituted 6-phenylpurine bases and nucleosides: application of the Suzuki–Miyaura cross-coupling reactions of 6-chloropurine derivatives with phenylboronic acids. *J. Med. Chem.* **2000**, *43*, 1817–1825. (b) Perez, O. D.; Chang, Y.-T.; Rosania, G.; Sutherlin, D.; Schultz, P. G. Inhibition and reversal of myogenic differentiation by purine-based microtubule assembly inhibitors. *Chem. Biol.* **2002**, *9*, 475–483.

(53) Notably, Pd-catalyzed cross-couplings of nitroarenes have been reported by Nakao and coworkers. (a) Ramu Yadav, M.; Nagaoka, M.; Kashihara, M.; Zhong, R.-L.; Miyazaki, T.; Sakaki, S.; Nakao, Y. The Suzuki–Miyaura coupling of nitroarenes. *J. Am. Chem. Soc.* **2017**, *139*, 9423–9426. (b) Inoue, F.; Kashihara, M.; Ramu Yadav, M; Nakao, Y. Buchwald–Hartwig amination of nitroarenes. *Angew. Chem., Int. Ed.* **2017**, *56*, 13307–13309. (c) Rocard, L.; Hatych, D.; Chartier, T.; Cauchy, T.; Hudhomme, P. Original Suzuki−Miyaura coupling using nitro derivatives for the synthesis of perylenediimide-based multimers. *Eur. J. Org. Chem.* **2019**, 7635−7643. (d) Zhou, F.; Zhou, F.; Su, R.; Yang, Y.; You, J. Build-up of double carbohelicenes using nitroarenes: Dual role of the nitro Functionality as an activating and leaving group. *Chem. Sci.* **2020**, *11*, 7424−7428. (e) Muto, K.; Okita, T.; Yamaguchi, J. Transition-metal-catalyzed denitrative coupling of nitroarenes. *ACS Catal.* **2020**, *10*, 9856–9871.

(54) Yamamoto, T.; Ishizu, J.; Kohara, T.; Komiya, S.; Yamamoto, A. Oxidative addition of aryl carboxylates to nickel (0) complexes involving cleavage of the acyl–oxygen bond. *J. Am. Chem. Soc.* **1980**, *102*, 3758–3764.

(55) (a) Amaike, K.; Muto, K.; Yamaguchi, J.; Itami, K. Decarbonylative C–H coupling of azoles and aryl esters: unprecedented nickel catalysis and applications to the synthesis of Muscoride A. *J. Am. Chem. Soc.* **2012**, *134*, 13573–13576. (b) Meng, L.; Kamada, Y.; Muto, K.; Yamaguchi, J.; Itami, K. C–H alkenylation of azoles with enols and esters by nickel catalysis. *Angew. Chem., Int. Ed.* **2013**, *52*, 10048–10051. (c) Muto, K.; Yamaguchi, J.; Musaev, D. G.; Itami, K. Decarbonylative organoboron cross-coupling of esters by nickel catalysis. *Nat. Commun.* **2015**, *6*, 7508. (d) Muto, K. Hatakeyama, R.; Itami, K.; Yamaguchi, J. Palladium-catalyzed decarbonylative cross-coupling of azinecarboxylates with arylboronic acids. *Org. Lett.* **2016**, *18*, 5106–5109.

(56) (a) Gooßen, L. J.; Paetzold, J. Pd-catalyzed decarbonylative olefination of aryl esters: towards a waste-free Heck reaction. *Angew. Chem., Int. Ed.* **2002**, *41*, 1237–1241. (b) Gooßen, L. J.; Paetzold, J. Decarbonylative Heck olefination of enol esters: salt-fre e and environmentally friendly access to vinyl arenes. *Angew. Chem., Int. Ed.* **2004**, *43*, 1095–1098.

(57) For the chelation-assisted transition-metal-catalyzed activation of esters, see (a) Chatani, N.; Tatamidani, H.; Ie, Y.; Kakiuchi, F.; Murai, S. The ruthenium-catalyzed reductive decarboxylation of esters: catalytic reactions involving the cleavage of acyl–oxygen bonds of esters. *J. Am. Chem. Soc.* **2001**, *123*, 4849–4850. (b) Tatamidani, H.; Yokota, K.; Kakiuchi, F.; Chatani, N. Catalytic cross-coupling reaction of esters with organoboron compounds and decarbonylative reduction of esters with $HCOONH_4$: A new route to acyl transition metal complexes through the cleavage of acyl–oxygen bonds in esters. *J. Org. Chem.* **2004**, *69*, 5615–5621. (c) Tatamidani, H.; Kakiuchi, F.; Chatani, N. A new ketone synthesis by

palladium-catalyzed cross-coupling reactions of esters with organoboron compounds. *Org. Lett.* **2004**, *6*, 3597–3599.

(58) For the use of electronically-activated esters in transition-metal-catalyzed couplings, see: (a) Refs. 55 and 56. (b) LaBerge, N. A.; Love, J. A. Nickel-catalyzed decarbonylative coupling of aryl esters and arylboronic acids. *Eur. J. Org. Chem.* **2015**, 5546–5553. (c) Halima, T. B.; Vandavasi, J. K.; Shkoor, M.; Newman, S. G. A cross-coupling approach to amide bond formation from esters. *ACS Catal.* **2017**, *7*, 2176–2180. (d) Kruckenberg, A.; Wadepohl, H.; Gade, L. H. Bis(diisospropylphosphinomethyl)amine nickel(II) and nickel(0) complexes: coordination chemistry, reactivity, and catalytic decarbonylative C–H arylation of benzoxazole. *Organometallics* **2013**, *32*, 5153–5170. (e) Yue, H.; Guo, L.; Liao, H.-H.; Cai, Y.; Zhu, C.; Rueping, M. Catalytic ester and amide to amine interconversion: nickel-catalyzed decarbonylative amination of esters and amides by C–O and C–C bond activation. *Angew. Chem., Int. Ed.* **2017**, *56*, 4282–4285. (f) Yu, H.; Guo, L.; Lee, S.-C.; Liu, X.; Rueping, M. Selective reductive removal of ester and amide groups from arenes and heteroarenes through nickel-catalyzed C–O and C–N bond activation. *Angew. Chem., Int. Ed.* **2017**, *56*, 3972–3976. (g) Halima, T. B.; Zhang, W.; Yalaoui, I.; Hong, X.; Yang, Y.; Houk, K. N.; Newman, S. G. Palladium-catalyzed Suzuki–Miyaura coupling of aryl esters. *J. Am. Chem. Soc.* **2017**, *139*, 1311–1318.

(59) For transition-metal-catalyzed cross-couplings of acid anhydrides, see: (a) Wang, D.; Zhang, Z. Palladium-catalyzed cross-coupling reactions of carboxylic anhydrides with organozinc reagents. *Org. Lett.* **2003**, *5*, 4645−4648. (b) Cook, M. J.; Rovis, T. Enantioselective rhodium-catalyzed alkylative desymmetrization of 3,5-dimethylglutaric anhydride. *Synthesis* **2009**, *2*,

335−338. (c) Bercot, E. A.; Rovis, T. A mild and efficient catalytic alkylative monofunctionalization of cyclic anhydrides. *J. Am. Chem. Soc.* **2002**, *124*, 174−175. (d) Bercot, E. A.; Rovis, T. Highly efficient nickel-catalyzed cross-coupling of succinic and glutaric anhydrides with organozinc reagents. *J. Am. Chem. Soc.* **2005**, *127*, 247−254. (e) Johnson, J. B.; Cook, M. J.; Rovis, T. Ligand differentiated complementary Rh-catalyst systems for the enantioselective desymmetrization of meso-cyclic anhydrides. *Tetrahedron* **2009**, *65*, 3202−3210. (f) Rogers, R. L.; Moore, J. L.; Rovis, T. Alkene-directed regioselective nickel-catalyzed cross-coupling of cyclic anhydrides with diorganozinc reagents. *Angew. Chem., Int. Ed.* **2007**, *46*, 9301−9304. (g) Bercot, E. A.; Rovis, T. A palladium-catalyzed enantioselective alkylative desymmetrization of meso-succinic anhydrides. *J. Am. Chem. Soc.* **2004**, *126*, 10248−10249. (h) Johnson, J. B.; Yu, R. T.; Fink, P.; Bercot, E. A.; Rovis, T. Selective substituent transfer from mixed zinc reagents in Ni-catalyzed anhydride alkylation. *Org. Lett.* **2006**, *8*, 4307−4310. (i) Johnson, J. B.; Bercot, E. A.; Rowley, J. M.; Coates, G. W.; Rovis, T. Ligand-dependent catalytic cycle and role of styrene in nickel-catalyzed anhydride cross-coupling: evidence for turnover-limiting reductive elimination. *J. Am. Chem. Soc.* **2007**, *129*, 2718−2725. (j) Cook, M. J.; Rovis, T. Rhodium-catalyzed enantioselective desymmetrization of meso-3,5-dimethyl glutaric anhydride: A general strategy to *syn*-deoxypolypropionate synthons. *J. Am. Chem. Soc.* **2007**, *129*, 9302−9303. (k) Stephan, M. S.; Teunissen, A. J. J. M.; Verzijl, G. K. M.; de Vries, J. G. Heck reactions without salt formation: aromatic carboxylic anhydrides as arylating agents. *Angew. Chem., Int. Ed.* **1998**, *37*, 662–664. (l) Gooßen, L. J.; Ghosh, K. Palladium-catalyzed synthesis of aryl ketones from boronic acids and carboxylic acids or anhydrides. *Angew. Chem., Int. Ed.* **2001**, *40*, 3458–

3460. (m) Kajita, Y.; Kurahashi, T.; Matsubara, S. Nickel-catalyzed decarbonylative addition of anhydrides to alkynes. *J. Am. Chem. Soc.* **2008**, *130*, 17226–17227.

(60) Hie, L.; Nathel, N. F. N.; Hong, X.; Yang, Y.-F.; Houk, K. N.; Garg, N. K. Nickel-catalyzed activation of acyl C–O bonds of methyl esters. *Angew. Chem., Int. Ed.* **2016**, *55*, 2810–2814.

(61) Carey, F. A.; Sundberg, R. J. *Advanced Organic Chemistry Part A: Structure and Mechanisms.* Springer: New York, 2000; p. 9–11.

(62) Brown, D. G.; Boström, J. Analysis of past and present synthetic methodologies on medicinal chemistry: where have all the new reactions gone? *J. Med. Chem.* **2016**, *59*, 4443–4458.

(63) Halima, T. B. Masson-Makdissi, J.; Newman, S. G. Nickel-catalyzed amide bond formation from methyl esters. *Angew. Chem., Int. Ed.* **2018**, *57*, 12925–12929.

(64) Zheng, Y.-L.; Newman, S. G. Methyl esters as cross-coupling electrophiles: direct synthesis of amide bonds. *ACS Catal.* **2019**, *9*, 4426–4433.

(65) Cheung, C. W.; Leendert, P.; Hu, X. Direct amination of esters with nitroarenes. *Nat. Commun.* **2017**, *8*, 14878.

(66) Hu and coworkers note that, rather than proceeding via nickel-catalyzed oxidative addition to the acyl C–O bond, this transformation likely proceeds through a nickel nitrene intermediate, which could undergo insertion into the acyl C–O bond to generate a Ni(II) amido species. See ref. 65 for further discussion of the mechanism.

(67) Medina, J. M.; Moreno, J.; Racine, S.; Du, S.; Garg, N. K. Mizoroki–Heck cyclizations of amide derivatives for the introduction of quaternary centers. *Angew. Chem., Int. Ed.* **2017**, *56*, 6567–6571.

(68) Zheng, Y.-L.; Newman, S. G. Nickel-catalyzed domino Heck-type reactions using methyl esters as cross-coupling electrophiles. *Angew. Chem., Int. Ed.* **2019**, *58*, 18159–18164.

(69) Yue, H.; Zhu, C.; Rueping, M. Catalytic ester to stannane functional group interconversion via decarbonylative cross-coupling of methyl esters. *Org. Lett.* **2018**, *20*, 385–388.

(70) Okita, T.; Muto, K.; Yamaguchi, J. Decarbonylative methylation of aromatic esters by a nickel catalyst. *Org. Lett.* **2018**, *20*, 3132–3135.

(71) (a) *The Amide Linkage: Structural Significance in Chemistry, Biochemistry, and Materials Science*; Greenberg, A., Breneman, C. M., Liebman, J. F., Eds.; Wiley: Hoboken, NJ, 2003; p. 33–43. (b) Pauling, L.; Corey, R. B.; Branson, H. R. The structure of proteins: two hydrogen-bonded helical configurations of the polypeptide chain. *Proc. Natl. Acad. Sci. USA* **1951**, *37*, 205−211.

(72) For select examples of amide-directed C−H functionalization, see: Rouquet, G.; Chatani, N. Catalytic functionalization of $C(sp^2)$–H and $C(sp^3)$–H bonds by using bidentate directing groups. *Angew. Chem., Int. Ed.* **2013**, *52*, 11726−11743 and references therein.

(73) Kaiser, D.; Bauer, A.; Lemmerer, M.; Maulide, N. Amide activation: An emerging tool for chemoselective synthesis. *Chem. Soc. Rev.* **2018**, *47*, 7899–7925.

(74) (a) Nahm, S.; Weinreb, S. M. N-methoxy-N-methylamides as effective acylating agents. *Tetrahedron Lett.* **1981**, *22*, 3815–3818.

(75) (a) Jensen, C. M.; Lindsay, K. B.; Taaning, R. H.; Karaffa, J.; Hansen, A. M.; Skrydstrup, T. Can decarbonylation of acyl radicals be overcome in radical addition reactions? En route to a solution employing *N*-acyl oxazolidinones and SmI_2/H_2O. *J. Am. Chem. Soc.* **2005**, *127*, 6544–6545. (b) Shi, S.; Lalancette, R.; Szostak, R.; Szostak, M. Highly chemoselective

synthesis of indolizidine lactams by SmI_2-induced umpolung of the amide bond via aminoketyl radicals: Efficient entry to alkaloid scaffolds. *Chem. Eur. J.* **2016**, *22*, 11949–11953. (c) Huang, H.-M.; Procter, D. J. Radical-radical cyclization cascades of barbiturates triggered by electron-transfer reduction of amide-type carbonyls. *J. Am. Chem. Soc.* **2016**, *138*, 7770–7775. (d) Huang, H.-M.; Procter, D. J. Dearomatizing radical cyclizations and cyclization cascades triggered by electron-transfer reduction of amide-type carbonyls. *J. Am. Chem. Soc.* **2017**, *139*, 1661–1667. (e) Huang, H.-M; Bonilla, P.; Procter, D. J. Selective construction of quaternary stereocentres in radical cyclisation cascades triggered by electron-transfer reduction of amide-type carbonyls. *Org. Biomol. Chem.* **2017**, *15*, 4159–4164.

(76) For select examples, see: (a) Madelaine, C.; Valerio, V.; Maulide, N. Unexpected electrophilic rearrangements of amides: A stereoselective entry to challenging substituted lactones. *Angew. Chem., Int. Ed.* **2010**, *49*, 1583–1586. (b) Peng, B.; Geerdrink D.; Maulide, N. Electrophilic rearrangements of chiral amides: A traceless asymmetric α-allylation. *J. Am. Chem. Soc.* **2013**, *135*, 14968–14971. (c) Tona, V.; Maryasin, B.; de la Torre, A.; Sprachmann, J.; González, L.; Maulide, N. Direct regioselective synthesis of tetrazolium salts by activation of secondary amides under mild conditions. *Org. Lett.* **2017**, *19*, 2662–2665.

(77) (a) Gregory, A. W.; Chambers, A.; Hawkins, A.; Jakubec, P.; Dixon, D. J. Iridium-catalyzed reductive nitro-Mannich cyclization. *Chem. Eur. J.* **2015**, *21*, 111−114. (b) Fuentes de Arriba, Á . L.; Lenci, E.; Sonawane, M.; Formery, O.; Dixon, D. J. Iridium-catalyzed reductive Strecker reaction for late-stage amide and lactam cyanation. *Angew. Chem., Int. Ed.* **2017**, *56*, 3655−3659. (c) Xie, L.-G.; Dixon, D. J. Tertiary amine synthesis via reductive coupling of amides with Grignard reagents. *Chem. Sci.* **2017**, *8*, 7492−7497. (d) Gabriel, P.; Xie, L.-G.;

Dixon, D. J. Iridium-catalyzed reductive coupling of Grignard reagents and tertiary amides. *Org. Synth.* **2019**, *96*, 511−527. (e) Xie, L. G.; Dixon, D. J. Iridium-catalyzed reductive Ugi-type reactions of tertiary amides. *Nat. Commun.* **2018**, *9*, 2841. (f) Gabriel, P.; Gregory, A. W.; Dixon, D. J. Iridium-catalyzed aza-spirocyclization of indole-tethered amides: An interrupted Pictet−Spengler reaction. *Org. Lett.* **2019**, *21*, 6658−6662. (g) For a review, see: Mathea-Raven, D.; Gabriel, P.; Leitch, J. A.; Almehmadi, Y. A.; Yamazaki, K.; Dixon, D. J. Catalytic reductive functionalization of tertiary amides using Vaska's complex: Synthesis of complex tertiary amine building blocks and natural products. *ACS Catal.* **2020**, *10*, 8880–8897.

(78) (a) Nakajima, M.; Sato, T.; Chida, N. Iridium-catalyzed chemoselectivu-Ravene reductive nucleophilic addition to *N*-Methoxyamides. *Org. Lett.* **2015**, *17*, 1696−1699. (b) Huang, P.-Q.; Ou, W.; Han, F. Chemoselective reductive alkynylation of tertiary amides by Ir and Cu(I) bis-metal sequential catalysis. *Chem. Commun*. **2016**, *52*, 11967−11970. (c) Hu, X.-N.; Shen, T.-L.; Cai, D.-C.; Zheng, J.-F.; Huang, P.-Q. The iridium-catalysed reductive coupling reaction of tertiary lactams/amides with isocyanoacetates. *Org. Chem. Front.* **2018**, *5*, 2051−2056. (d) Takahashi, Y.; Sato, T.; Chida, N. Iridium-catalyzed reductive nucleophilic addition to tertiary amides. *Chem. Lett.* **2019**, *48*, 1138−1141.

(79) For recent reviews, see: (a) Meng, G.; Shi, S.; Szostak, M. Cross-coupling of amides by N−C bond activation. *Synlett* **2016**, *27*, 2530−2540. (b) Takise, R.; Muto, K.; Yamaguchi, J. Cross-coupling of aromatic esters and amides. *Chem. Soc. Rev.* **2017**, *46*, 5864−5888. (c) Kaiser, D.; Bauer, A.; Lemmerer, M.; Maulide, N. Amide activation: an emerging tool for chemoselective synthesis. *Chem. Soc. Rev.* **2018**, *47*, 7899−7925.

(80) Hie, L.; Fine Nathel, N. F.; Shah, T. K.; Baker, E. L.; Hong, X.; Yang, Y.; Liu, P.; Houk, K. N.; Garg, N. K. Conversion of amides to esters by nickel-catalysed activation of amide C–N bonds. *Nature* **2015**, *524*, 79–83.

(81) (a) Huynh, H. V. Electronic properties of *N*-heterocyclic carbenes and their experimental determination. *Chem. Rev.* **2018**, *118*, 9457–9492. (b) Dröge, T.; Glorius, F. The measure of all rings–*N*-heterocyclic carbenes. *Angew. Chem., Int. Ed.* **2010**, *49*, 6940–6952. (c) Kelly III, R. A; Clavier, H.; Guidice, S.; Scott, N. M.; Stevens, E. D.; Bordner, J.; Samardjiev, I.; Hoff, C. D.; Cavallo, L.; Nolan, S. P. Determination of *N*-heterocyclic carbene (NHC) steric and electronic parameters using the [(NHC)Ir(CO)$_2$Cl] system. *Organometallics* **2008**, *27*, 202–210. (d) Gómez-Suárez, A.; Nelson, D. J.; Nolan, S. P. Quantifying and understanding the steric properties of *N*-heterocyclic carbenes. *Chem. Commun.* **2017**, *53*, 2650–2660.

(82) Liu, C.; Szostak, M. Twisted amides: From obscurity to broadly useful transition-metal-catalyzed reactions by N–C amide bond activation. *Chem. Eur. J.* **2017**, *23*, 7157–7173.

(83) Using our previously established conditions for the nickel-catalyzed esterification of amides, the use of H_2O as a nucleophile delivered no product. Moreover, in the presence of benzoic acid, the nickel-catalyzed esterification of *N*-Ph,Me benzamide failed to deliver product, indicating catalyst poisoning.

(84) Knapp, R. R.; Bulger, A. S.; Garg, N. K. Nickel-catalyzed conversion of amides to carboxylic acids. *Org. Lett.* **2020**, *22*, 2833–2837.

(85) Transamidation of secondary amides has been historically difficult due to the resonance stability of amides and the often thermoneutral nature of this conversion. For further reading on this topic, see: (a) Lanigan, R. M.; Sheppard, T. D. Recent developments in amide

synthesis: direct amidation of carboxylic acids and transamidation reactions. *Eur. J. Org. Chem.* **2013**, 7453–7465. (b) Musci, Z.; Chass, G. A.; Csizmadia, I. G. Amidicity change as a significant driving force and thermodynamic selection rule of transamidation reactions. A synergy between experiment and theory. *J. Phys. Chem. B* **2008**, *112*, 7885–7893.

(86) Baker, E. L.; Yamano, M. M.; Zhou, Y.; Anthony, S. M.; Garg, N. K. A two-step approach to achieve secondary amide transamidation enabled by nickel catalysis. *Nat. Commun.* **2016**, *7*, 1–5.

(87) Weires, N. A.; Baker, E. L.; Garg, N. K. Nickel-catalyzed Suzuki–Miyaura coupling of amides. *Nat. Chem.* **2016**, *8*, 75–79.

(88) Simmons, B. J.; Weires, N. A.; Dander, J. E.; Garg, N. K. Nickel-catalyzed alkylation of amide derivatives. *ACS Catal*. **2016**, *6*, 3176–3179.

(89) Hu, L.; Jiang, J.; Qu, J.; Li, Y.; Jin, J.; Li, Z.; Boykin, D. W. Novel potent antimitotic heterocyclic ketones: synthesis, antiproliferative activity, and structure–activity relationships. *Bioorg. Med. Chem. Lett.* **2007**, *17*, 3613–3617.

(90) Apnes, G. E.; Didluk, M. T.; Filipski, K. J.; Guzman-Perez, A.; Lee, E. C. Y.; Pfefferkorn, J. A.; Stevens, B. D.; Tu, M. M. Glucagon Receptor Modulators. U.S. Patent 20120202834, Aug. 9, 2012.

(91) Walker, Jr., J. A.; Vickerman, K. L.; Humke, J. N.; Stanley, L. M. Ni-catalyzed alkene carboacylation via amide C–N bond activation. *J. Am. Chem. Soc.* **2017**, *139*, 10228–10231.

(92) Dander, J. E.; Giroud, M.; Racine, S.; Darzi, E. R.; Alvizo, O.; Entwistle, D.; Garg, N. K. Chemoenzymatic conversion of amides to enantioenriched alcohols in aqueous medium. *Communications Chemistry* **2019**, *2*, 82.

(93) Computations suggest that the active Ni–NHC catalyst coordinates to aryl substrates prior to amide C–N bond activation, thereby lowering the entropic cost associated with the barrier to oxidative addition (see ref. 80).

(94) Hie, L.; Baker, E. L.; Anthony, S. M.; Desrosiers, J.; Senanayake, C.; Garg, N. K. Nickel-catalyzed esterification of aliphatic amides. *Angew. Chem., Int. Ed.* **2016**, *55*, 15129–15132.

(95) Dander, J. E.; Baker, E. L.; Garg, N. K. Nickel-catalyzed transamidation of aliphatic amide derivatives. *Chem. Sci.* **2017**, *8*, 6433–6438.

(96) Boit, T. B.; Weires, N. A.; Kim, J.; Garg, N. K. Nickel-catalyzed Suzuki–Miyaura coupling of aliphatic amides. *ACS Catal.* **2018**, *8*, 1003–1008.

(97) The NHC ligand, Benz-ICy, is formed from the precursor salt, Benz-ICy•HCl, via deprotonation in situ: Arduengo III, A. J.; Harlow, R. L.; Kline M. A stable crystalline carbene. *J. Am. Chem. Soc.* **1991**, *113*, 361–363.

(98) Weires, N. A.; Caspi, D. D.; Garg, N. K. Kinetic modeling of the nickel-catalyzed esterification of amides. *ACS Catal.* **2017**, *7*, 4381–4385.

(99) Our collaborator, Dan Caspi, employed *DynoChem* software to model the kinetics of the transformation and perform *in silico* simulations to calculate ideal reaction conditions.

(100) For air-stable Ni(0)–olefin precatalysts recently reported by the Cornellaand Engle labs, see: (a) Tran, V. T.; Li, Z.-Q.; Apolinar, O.; Derosa, J.; Joannou, M. V.; Wisniewski, S. R.; Eastgate, M. D.; Engle, K. M. Ni(COD)(DQ): an air-stable 18-electron Ni(0)-olefin precatalyst. *Angew. Chem., Int. Ed.* **2020**, *59*, 7409–7413. (b) Nattmann, L; Saeb, R.; Nöthling, N.; Cornella, J. An air-stable binary Ni(0)-olefin catalyst. *Nat. Catal.* **2020**, *3*, 6–13.

(101) (a) Sather, A. C.; Lee, H. G.; Colombe, J. R.; Zhang, A.; Buchwald, S. L. Dosage delivery of sensitive reagents enables glove- box free synthesis. *Nature* **2015**, *524*, 208−211. (b) Fang, Y.; Liu, Y.; Ke, Y.; Guo, C.; Zhu, N.; Mi, X.; Ma, Z.; Hu, Y. A new chromium-based catalyst coated with paraffin for ethylene oligomerization and the effect of chromium state on oligomerization selectivity. *Appl. Catal., A* **2002**, *235*, 33−38. (c) Taber, D. F.; Frankowski, K. J. Grubbs' catalyst in paraffin: an air-stable preparation for alkene metathesis. *J. Org. Chem.* **2003**, *68*, 6047−6048.

(102) Mehta, M. M.; Boit, T. B.; Dander, J. E.; Garg, N. K. Ni-catalyzed Suzuki–Miyaura cross-coupling of aliphatic amides on the benchtop. *Org. Lett.* **2020**, *22*, 1–5.

(103) For additional examples of using a paraffin-encapsulation strategy from our laboratory, see: (a) Dander, J. E.; Weires, N. A.; Garg, N. K. Benchtop delivery of $Ni(cod)_2$ using paraffin capsules. *Org. Lett.* **2016**, *18*, 3934–3936. (b) Dander, J. E.; Morill, L. A.; Nguyen, M. M.; Chen, S.; Garg, N. K. Breaking amide C–N bonds in an undergraduate organic chemistry laboratory. *J. Chem. Ed.* **2019**, *96*, 776–780.

(104) For Pd-catalyzed amide C−N bond activations, see: (a) Li, X.; Zou, G. Acylative Suzuki coupling of amides: acyl-nitrogen activation via synergy of independently modifiable activating groups. *Chem. Commun.* **2015**, *51*, 5089−5092. (b) Yada, A.; Okajima, S.; Murakami, M. Palladium-catalyzed intramolecular insertion of alkenes into the carbon−nitrogen bond of β-lactams. *J. Am. Chem. Soc.* **2015**, *137*, 8708−8711. (c) Meng, G.; Szostak, M. Palladium-catalyzed Suzuki−Miyaura coupling of amides by carbon−nitrogen cleavage: general strategy for amide N−C bond activation. *Org. Biomol. Chem.* **2016**, *14*, 5690−5705. (d) Meng, G.; Szostak, M. General olefin synthesis by the palladium-catalyzed

Heck reaction of amides: sterically-controlled chemoselective N−C activation. *Angew. Chem., Int. Ed.* **2015**, *54*, 14518−14522. (e) Meng, G.; Szostak, M. Sterically controlled Pd-catalyzed chemoselective ketone synthesis via N−C cleavage in twisted amides. *Org. Lett.* **2015**, *17*, 4364−4367. (f) Liu, C.; Meng, G.; Liu, Y.; Liu, R.; Lalancette, R.; Szostak, R.; Szostak, M. *N*-Acylsaccharins: stable electrophilic amide-based acyl transfer reagents in Pd-catalyzed Suzuki−Miyaura coupling via N−C cleavage. *Org. Lett.* **2016**, *18*, 4194−4197. (g) Lei, P.; Meng, G.; Szostak, M. General method for the Suzuki−Miyaura cross-coupling of amides using commercially available, air- and moisture-stable palladium/ NHC (NHC = *N*-heterocyclic carbene) complexes. *ACS Catal.* **2017**, *7*, 1960−1965. (h) Liu, C.; Liu, Y.; Liu, R.; Lalancette, R.; Szostak, R.; Szostak, M. Palladium-catalyzed Suzuki−Miyaura cross-coupling of *N*-mesylamides by N−C cleavage: electronic effect of the mesyl group. *Org. Lett.* **2017**, *19*, 1434−1437. (i) Liu, C.; Meng, G.; Szostak, M. *N*- Acylsaccharins as amide-based arylating reagents via chemoselective N−C cleavage: Pd-catalyzed decarbonylative Heck reaction. *J. Org. Chem.* **2016**, *81*, 12023−12030. (j) Meng, G.; Shi, S.; Szostak, M. Palladium-catalyzed Suzuki−Miyaura cross-coupling of amides via site-selective N−C bond cleavage by cooperative catalysis. *ACS Catal.* **2016**, *6*, 7335−7339. (k) Cui, M.; Wu, H.; Jian, J.; Wang, H.; Liu, C.; Stelck, D.; Zeng, Z. Palladium-catalyzed Sonogashira coupling of amides: access to ynones via C−N bond cleavage. *Chem. Commun.* **2016**, *52*, 12076−12079. (l) Wu, H.; Li, Y.; Cui, M.; Jian, J.; Zeng, Z. Suzuki coupling of amides via palladium-catalyzed C−N cleavage of *N*-acylsaccharins. *Adv. Synth. Catal.* **2016**, *358*, 3876−3880. (m) Shi, S.; Szostak, M. Decarbonylative cyanation of amides by palladium catalysis. *Org. Lett.* **2017**, *19*, 3095−3098. (n) Lei, P.; Meng, G.; Ling, Y.; An, J.; Szostak, M. Pd-PEPPSI: Pd-NHC

precatalyst for Suzuki−Miyaura cross-coupling reactions of amides. *J. Org. Chem.* **2017**, *82*, 6638−6646. (o) Meng, G.; Szostak, R.; Szostak, M. Suzuki−Miyaura cross-coupling of *N*-acylpyrroles and pyrazoles: planar, electronically activated amides in catalytic N−C cleavage. *Org. Lett.* **2017**, *19*, 3596−3599. (p) Meng, G.; Lalancette, R.; Szostak, R.; Szostak, M. N-Methylamino pyrimidyl amides (MAPA): highly reactive, electronically-activated amides in catalytic N−C(O) cleavage. *Org. Lett.* **2017**, *19*, 4656−4659. (q) Osumi, Y.; Liu, C.; Szostak, M. *N*-Acylsuccinimides: twist-controlled, acyl transfer reagents in Suzuki− Miyaura cross-coupling by N−C amide bond activation. *Org. Biomol. Chem.* **2017**, *15*, 8867−8871. (r) Lei, P.; Meng, G.; Ling, Y.; An, J.; Nolan, S. P.; Szostak, M. General method for the Suzuki−Miyaura cross-coupling of primary amide-derived electrophiles enabled by [Pd(NHC)(cin)−Cl] at room temperature. *Org. Lett.* **2017**, *19*, 6510−6513. (s) Li, X.; Zou, G. Palladium-catalyzed acylative cross-coupling of amides with diarylboronic acids and sodium tetraarylborates. *J. Organomet. Chem.* **2015**, *794*, 136−145. (t) Liu, C.; Li, G.; Shi, S.; Meng, G.; Lalancette, R.; Szostak, R.; Szostak, M. Acyl and decarbonylative Suzuki coupling of *N*-acetyl amides: electronic tuning of twisted, acyclic amides in catalytic carbon−nitrogen bond cleavage. *ACS Catal.* **2018**, *8*, 9131−9139. (u) Meng, G.; Szostak, M. Palladium/NHC (NHC = *N*-heterocyclic carbene)-catalyzed β-alkyl Suzuki cross-coupling of amides by selective N−C bond cleavage. *Org. Lett.* **2018**, *20*, 6789−6793. (v) Shi, S.; Szostak, M. Decarbonylative borylation of amides by palladium catalysis. *ACS Omega* **2019**, *4*, 4901−4907. (w) Zhou, T.; Li, G.; Nolan, S. P.; Szostak, M. [Pd(NHC)(acac)Cl]: well-defined, air-stable, and readily available precatalysts for Suzuki and Buchwald−Hartwig cross-coupling (transamidation) of amides and esters by N−C/O−C activation. *Org. Lett.* **2019**, *21*, 3304−3309. (x) Rahman, M.

M.; Buchspies, J.; Szostak, M. *N*-Acylphthalimides: efficient acyl coupling reagents in Suzuki−Miyaura cross-coupling by N−C cleavage catalyzed by Pd-PEPPSI precatalysts. *Catalysts* **2019**, *9*, 129. (y) Liu, C.; Lalancette, R.; Szostak, R.; Szostak, M. Sterically hindered ketones via palladium-catalyzed Suzuki−Miyaura cross-coupling of amides by N−C(O) activation. *Org. Lett.* **2019**, *21*, 7976−7981. (z) Li, G.; Zhou, T.; Poater, A.; Cavallo, L.; Nolan, S. P.; Szostak, M. Buchwald−Hartwig cross-coupling by air-and moisture-stable [Pd(NHC)(allyl)Cl] pre-catalysts: catalyst evaluation and mechanism. *Catal. Sci. Technol.* **2020**, *10*, 710–716.

(105) Conservatively estimated on the basis of SciFinder search results (accessed July 30, 2020).

(106) (a) Shi, S.; Szostak, M. Nickel-catalyzed diaryl ketone synthesis by N−C bond cleavage: direct Negishi cross-coupling of primary amides by site-selective *N,N*-di-Boc activation. *Org. Lett.* **2016**, *18*, 5872−5875. (b) Shi, S.; Szostak, M. Efficient synthesis of diaryl ketones by nickel-catalyzed Negishi cross-coupling of amides via carbon−nitrogen bond cleavage at room temperature accelerated by solvent effect. *Chem. Eur. J.* **2016**, *22*, 10420−10424. (c) Dey, A.; Sasmal, S.; Seth, K.; Lahiri, G. K.; Maiti, D. Nickel-catalyzed deamidative step-down reduction of amides to aromatic hydrocarbons. *ACS Catal.* **2017**, *7*, 433−437. (d) Ni, S.; Zhang, W.; Mei, H.; Han, J.; Pan, Y. Ni-catalyzed reductive cross-coupling of amides with aryl iodide electrophiles via C−N bond activation. *Org. Lett.* **2017**, *19*, 2536−2539. (e) Shi, S.; Szostak, M. Nickel-catalyzed Negishi cross-coupling of *N*-acylsuccinimides: stable, amide-based, twist-controlled acyl transfer reagents via N−C activation. *Synthesis* **2017**, *49*, 3602−3608. (f) Huang, P.-Q.; Chen, H. Ni-catalyzed cross-coupling reactions of *N*-acylpyrrole-type amides with organoboron reagents. *Chem. Commun.* **2017**, *53*,

12584−12587. (g) Deguchi, T.; Xin, H.-L.; Morimoto, H.; Ohshima, T. Direct catalytic alcoholysis of unactivated 8-aminoquinoline amides. *ACS Catal.* **2017**, *7*, 3157−3161.

(107) Cheung, C. W.; Ploeger, M. L.; Hu, X. Nickel-catalyzed reductive transamidation of secondary amides with nitroarenes. *ACS Catal.* **2017**, *7*, 7092–7096.

(108) Amani, J.; Alam, R.; Badir, S.; Molander, G. A. synergistic visible-light photoredox/nickel-catalyzed synthesis of aliphatic ketones via N–C cleavage of imides. *Org. Lett.* **2017**, *19*, 2426−2429.

(109) Srimontree, W.; Chatupheeraphat, A.; Liao, H.-H.; Rueping, M. Amide to alkyne interconversion via a nickel/copper-catalyzed deamidative cross-coupling of aryl and alkenyl amides. *Org. Lett.* **2017**, *19*, 3901–3094.

(110) (c) Hu, J.; Wang, M.; Pu, X.; Shi, Z. Nickel-catalysed retro-hydroamidocarbonylation of aliphatic amides to olefins. *Nat. Commun.* **2017**, *8*, 14993.

(111) Liu, C.; Szostak, M. Decarbonylative phosphorylation of amides by palladium and nickel catalysis: The Hirao cross-coupling of amide derivatives. *Angew. Chem., Int. Ed.* **2017**, *56*, 12718–12722.

(112) For cross-couplings of acyclic alkyl C–O electrophiles, see: (a) Robbins, W. R.; Hartwig, J. F.; Sterically controlled alkylation of arenes through iridium-catalyzed C–H borylation. *Angew. Chem., Int. Ed.* **2013**, *52*, 933–937. (b) Lucas, E. L.; Jarvo, E. R. Stereospecific and stereoconvergent cross-couplings between alkyl electrophiles. *Nat. Rev. Chem.* **2017**, *1*, 0065. (c) Zhang, S.; Taylor, B. L. H.; Ji, C.; Gao, Y.; Harris, M. R.; Hanna, L. E.; Jarvo, E. R.; Houk, K. N.; Hong, X. Mechanism and origins of ligand-controlled stereoselectivity of Ni-catalyzed Suzuki–Miyaura coupling with benzylic esters: A computational study. *J. Am.*

Chem. Soc. **2017**, *139*, 12994–13005. (d) Shugrue, C. R.; Sculimbrene, B. R.; Jarvo, E. R.; Mercado, B. Q.; Miller, S. J. Outer-sphere control for divergent multicatalysis with common catalytic moieties. *J. Org. Chem.* **2019**, *84*, 1664–1672. (e) Sanford, A. B.; Tollefson, E. J.; Jarvo, E. R. Stereospecific cross-coupling reactions provide conformationally-biased arylalkanes with anti-leukemia activity. *Isr. J. Chem.* **2020**, *60*, 402–405. (f) Sanford, A. B.; Thane, T. A.; McGinnis, T. M.; Chen, P.-P.; Hong, X.; Jarvo, E. R. Nickel-catalyzed alkyl–alkyl cross-electrophile coupling reaction of 1,3-dimesylates for the synthesis of alkylcyclopropanes. *J. Am. Chem. Soc.* **2020**, *142*, 5017–5023. (g) Zhou, Q.; Srinivas, H. D.; Dasgupta, S.; Watson, M. P. Nickel-catalyzed cross-couplings of benzylic pivalates with arylboroxines: Stereospecific formation of diarylalkanes and triarylmethanes. *J. Am. Chem. Soc.* **2013**, *135*, 3307–3310.

(113) For cross-couplings of alkyl C–N electrophiles, see: (h) Calet, S.; Urso, F.; Alper, H. Enantiospecific and stereospecific rhodium(I)-catalyzed carbonylation and ring expansion of aziridines. Asymmetric synthesis of β-lactams and the kinetic resolution of aziridines. *J. Am. Chem. Soc*. **1989**, *111*, 931−934. (i) Ney, J. E.; Wolfe, J. P. Synthesis and reactivity of azapalladacyclobutanes. *J. Am. Chem. Soc.* **2006***, 128*, 15415−15422. (j) Lin, B. L.; Clough, C. R.; Hillhouse, G. L. Interactions of aziridines with nickel complexes: Oxidative-addition and reductive-elimination reactions that break and make C−N bonds. *J. Am. Chem. Soc.* **2002**, *124*, 2890−2891. (k) Huang, C.-Y.; Doyle, A. G. Nickel-catalyzed Negishi alkylations of styrenyl aziridines. *J. Am. Chem. Soc.* **2012**, *134*, 9541−9544. (l) Nielsen, D. K.; Huang, C.-Y.; Doyle, A. G. Directed nickel-catalyzed Negishi cross-Coupling of alkyl aziridines. *J. Am. Chem. Soc*. **2013**, *135*, 13605−13609. (m) Huang, C.-Y.; Doyle, A. G. Electron-deficient

olefin ligands enable generation of quaternary carbons by Ni-catalyzed cross-coupling. *J. Am. Chem. Soc.* **2015**, *137*, 5638−5641.

(114) (a) Liu, C.; Li, G.; Shi, S.; Meng, G.; Lalancette, R.; Szostak, R.; Szostak, M. Acyl and decarbonylative Suzuki coupling of N-acetyl amides: electronic tuning of twisted, acyclic amides in catalytic carbon–nitrogen bond cleavage. *ACS Catal.* **2018**, *8*, 9131–9139. (b) Iranpoor, N.; Panahi, F.; Jamedi, F. Nickel-catalyzed one-pot synthesis of biaryls from phenols and arylboronic acids via C–O activation using TCT reagent. *J. Organomet. Chem.* **2015**, *781*, 6–10. (c) Chen, L.; Lang, H.; Fang, L.; Zhu, M.; Liu, J.; Yu, J.; Wang, L. Nickel-catalyzed one-pot Suzuki–Miyaura cross-coupling of phenols and arylboronic acids mediated by *N*,*N*-ditosylaniline. *Eur. J. Org. Chem.* **2014**, 4953–4957. (d) Chen, G.; Huang, J.; Gao, L.; Han, F. Nickel-catalyzed cross-coupling of phenols and arylboronic acids through an in situ phenol activation mediated by PyBroP. *Chem. Eur. J.* **2011**, *17*, 4038–4042. (e) Oger, N.; d'Halluin, M.; Grognec, E.L.; Felpin, F. Using aryl diazonium salts in palladium-catalyzed reactions under safer conditions. *Org. Process. Res. Dev.* **2014**, *18*, 1786–1801.

(115) Hardy, M. A.; Wright, B. A.; Bachman, J. L.; Boit, T. B.; Haley, H. M. S.; Knapp, R. R.; Lusi, R. F.; Okada, T.; Tona, V.; Garg, N. K.; Sarpong, R. Treating a global health crisis with a dose of synthetic chemistry. *ACS Cent. Sci.* **2020**, *6*, 1017–1030.

(116) For reviews on cross-couplings catalyzed by base-metals, see: (a) Thapa, S.; Shrestha, B.; Gurung, S. K.; Giri, R. Copper-catalysed cross-coupling: an untapped potential. *Org. Biomol. Chem.* **2015**, *13*, 4816–4827. (b) Cahiez, G.; Moyeux, A. Cobalt-catalyzed cross-coupling reactions. *Chem. Rev.* **2010**, *110*, 1435–1462. (c) Mako, T. L.; Byers, J. A. Recent advances

in iron-catalysed cross-coupling reactions and their mechanistic underpinning. *Inorg. Chem. Front.* **2016**, *3*, 766–790.

(117) Expensive NHC ligands are often required for nickel-catalyzed activations of strong bonds.

(118) Hazari, N.; Melvin, P. R.; Beromi, M. M. Well-defined nickel and palladium precatalysts for cross-coupling. *Nat. Rev. Chem.* **2017**, *1*, 25.

CHAPTER TWO

Nickel-Catalyzed Conversion of Amides to Carboxylic Acids

Rachel R. Knapp, Ana S. Bulger, and Neil K. Garg.

Org. Lett. **2020**, *22*, 2833–2837.

2.1 Abstract

We report the conversion of amides to carboxylic acids using non-precious metal catalysis. The methodology strategically employs a nickel-catalyzed esterification using 2-(trimethylsilyl)ethanol, followed by a fluoride-mediated deprotection in a single-pot operation. This approach circumvents catalyst poisoning observed in attempts to directly hydrolyze amides using nickel catalysis. The selectivity and mildness of this transformation is shown through competition experiments and the net-hydrolysis of a complex valine-derived substrate. This strategy addresses a limitation in the field with regard to functional groups accessible from amides using transition-metal catalysis and should prove useful in synthetic applications.

2.2 Introduction

Despite being well known for their pronounced stability, amides have recently become valuable synthetic building blocks in transition-metal-catalyzed reactions.[1] An array of carbon–carbon and carbon–heteroatom bond-forming reactions using amides have now been disclosed using palladium,[2] rhodium,[3] or nickel[4] catalysis. Figure 2.1 highlights several functional group conversions beginning from amides that can now be achieved using non-precious metal catalysis.[4a–c,4g,4l,4n,4s] Although several methodologies have been reported in recent years, one of the most fundamental transformations, namely the conversion of amides to carboxylic acids,[5] has

not yet been disclosed using transition-metal catalysis. We report a means to achieve this transformation using nickel catalysis.

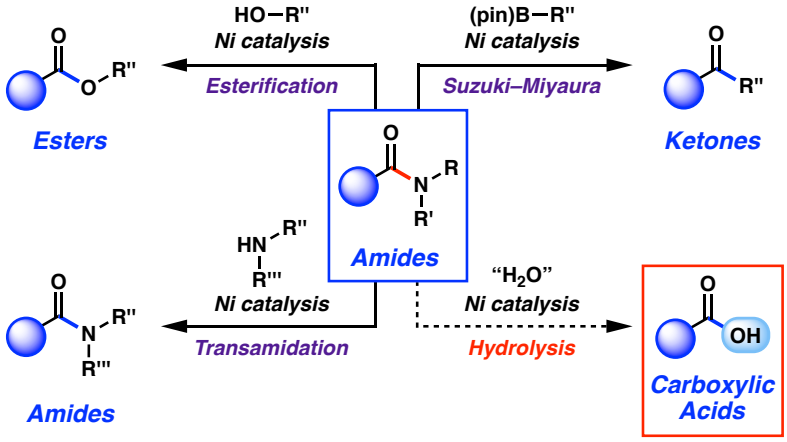
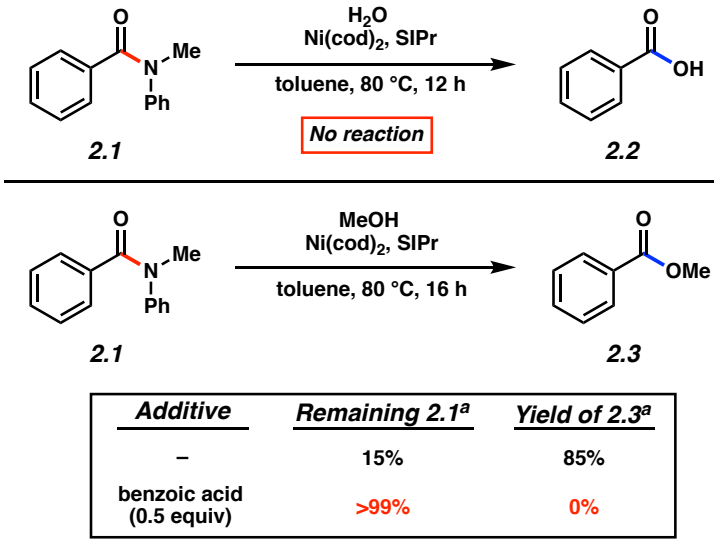


Figure 2.1. Select examples of recent advances in the nickel-catalyzed activation of amides.

2.3 Reaction Discovery and Optimization

Our studies commenced with attempts to modify our previously established protocol for the conversion of amides to esters.[4a,4l] Specifically, we evaluated the activation of amide **2.1** using $Ni(cod)_2$ and the *N*-heterocyclic carbene ligand SIPr, with water as a nucleophile (Figure 2.2). Unfortunately, we did not observe formation of the desired product, benzoic acid (**2.2**). This was surprising, given that many oxygen nucleophiles have been used in nickel-catalyzed amide esterification reactions. To further assess if the direct conversion to the carboxylic acid was possible, additional experiments were performed involving the nickel-catalyzed esterification of amide **2.1** using MeOH as the nucleophile. In the absence of any additive, the reaction proceeded as expected to give ester **2.3** in 85% yield. However, when the reaction was carried out with 0.5 equivalents of benzoic acid (**2.2**) as an additive, the esterification failed, indicative of catalyst poisoning. Recognizing the incompatibility of the carboxylic acid functional group with the catalyst system, we sought to develop an alternative strategy to effect the conversion of amides to carboxylic acids using nickel catalysis.

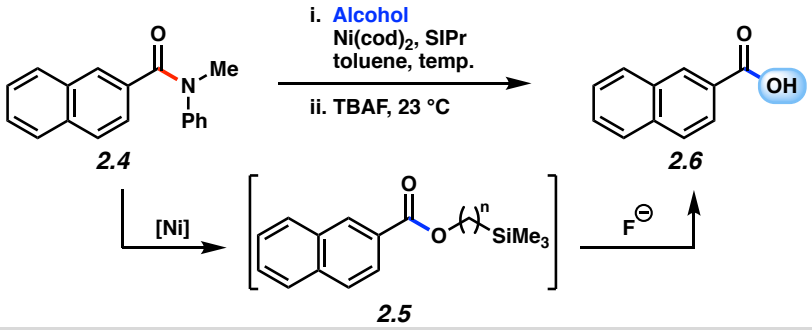


Additive	Remaining 2.1[a]	Yield of 2.3[a]
–	15%	85%
benzoic acid (0.5 equiv)	>99%	0%

Figure 2.2. Initial studies and control experiments for the nickel-catalyzed hydrolysis of amides. Conditions: amide **2.1** (1.0 equiv), $Ni(cod)_2$ (10 mol%), SIPr (10 mol%), methanol or water (1.2 equiv), and toluene (1.0 M) heated at 80 °C for 12 or 16 h in a sealed vial under an atmosphere of N_2. [a]Yields were determined by ^1H NMR analysis using 1,3,5-trimethoxybenzene as an external standard.

An alternative one-pot approach to achieve the amide to carboxylic acid conversion was conceived, as depicted using amide substrate **2.4** (Table 2.1). Strategically, this was designed to proceed by nickel-catalyzed esterification to give protected carboxylic acid **2.5** which would then be deprotected in the same reaction vessel through the addition of a mild fluoride source. Table 2.1 shows select key results using two types of nucleophiles, each bearing a silyl group. Although the use of trimethylsilanol (TMS–OH) as a nucleophile failed to generate the desired ester intermediate **2.5** (entry 1), the use of 2-(trimethylsilyl)ethanol (TMS-ethanol, **2.7**) proved more fruitful (entries 2 and 3). For example, using standard reaction conditions at a temperature of 80 °C, the conversion of amide **2.4** to carboxylic acid **2.6** could be achieved in 83% yield using a straightforward esterification / TBAF-mediated deprotection protocol (entry 2).[6] Increasing the temperature to 110 °C gave naphthyl carboxylic acid **2.6** in a slightly improved yield of 87% (entry 3).

Table 2.1. Optimization of Reaction Conditions



entry	*alcohol*	*temp. (°C)*	*yield of 2.5*[a]	*yield of 2.6*[a]
1	TMS-OH	80	0%	–
2	TMS-ethanol (***2.7***)	80	0%	83%
3	TMS-ethanol (***2.7***)	110	0%	87%

Conditions: amide **2.4** (1.0 equiv), $Ni(cod)_2$ (10 mol%), SIPr (10 mol%), alcohol (1.25 equiv), and toluene (1.0 M) heated at 80–110 °C for 24 h in a sealed vial under an atmosphere of N_2; TBAF (2.5 equiv) at 23 °C for 2 h. [a]Yields were determined by ^1H NMR analysis using 1,3,5-trimethoxybenzene as an external standard.

2.4 Scope of Methodology

Having identified an operationally-simple means to achieve the nickel-catalyzed conversion of amides to carboxylic acids, we evaluated several benzamide derivatives[7] in the methodology (Figure 2.3). The use of the parent naphthyl substrate **2.4** (Table 2.1) furnished 2-naphthoic acid (**2.6**) in 90% isolated yield. Benzoic acids **2.2**[8] and **2.10**–**2.12** could also be accessed through this transformation. The formation of carboxylic acids **2.11** and **2.12**, in 84% and 79% yield, respectively, highlights the tolerance of electron-withdrawing and electron-donating groups. Additionally, use of a quinoline substrate gave rise to **2.13** in 60% yield, thus demonstrating the tolerance of the methodology toward an important nitrogen-containing heterocycle.

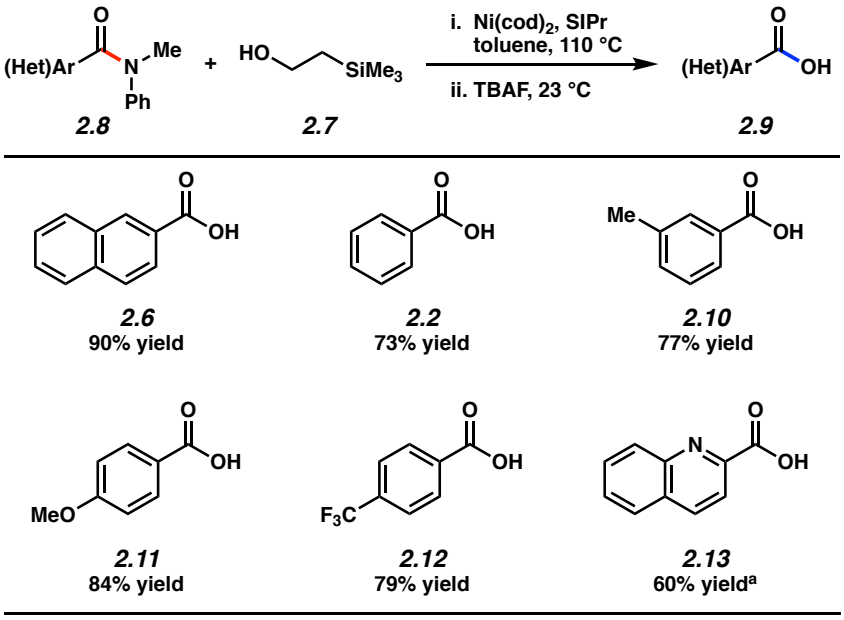
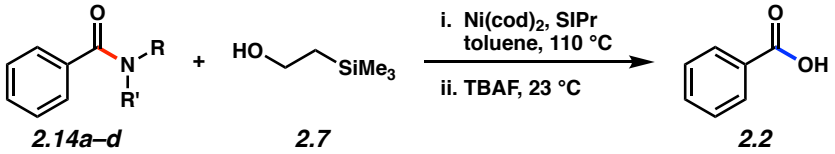


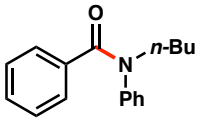
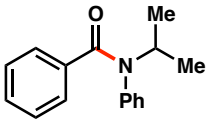
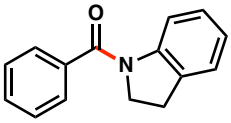
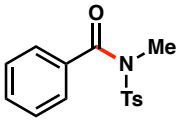
Figure 2.3. Scope of the amide substrate**.** Conditions: amide **2.8** (1.0 equiv), $Ni(cod)_2$ (10 mol%), SIPr (10 mol%), **2.7** (1.25 equiv), and toluene (1.0 M) heated at 110 °C for 24 h in a sealed vial under an atmosphere of N_2; TBAF (2.5 equiv) at 23 °C for 2 h. Yields reflect the average of two isolation experiments. [a]Yield was determined by ^1H NMR analysis using 1,3,5-trimethoxybenzene as an external standard.

As shown in Table 2.2, variation of the amide *N*-substituents was also possible. The use of benzamide **2.14a**, bearing an *n*-butyl group in place of a methyl group, afforded benzoic acid (**2.2**) in 77% yield (entry 1). Additionally, the more sterically encumbered *N*-isopropyl benzamide seen in **2.14b** (entry 2) and the indoline present in **2.14c** (entry 3) were tolerated. Moreover, tosyl derivative **2.14d** could be employed in the methodology to provide **2.2** in 71% yield (entry 4).

Table 2.2. Variation of the *N*-Substituents.



2.14a–d *2.7* *2.2*

entry	*substrate*	*yield*
1	 *2.14a*	77%
2	 *2.14b*	60%
3	 *2.14c*	56%
4	 *2.14d*	71%

Conditions: amide **2.14a**–**d** (1.0 equiv), Ni(cod)$_2$ (10 mol%), SIPr (10 mol%), **2.7** (1.25 equiv), and toluene (1.0 M) heated at 110 °C for 24 h in a sealed vial under an atmosphere of N_2; TBAF (2.5 equiv) at 23 °C for 2 h. Yields reflect the average of two isolation experiments.

2.5 Selectivity Studies

Competition experiments were performed to gauge substrate-based selectivity for the nickel-catalyzed conversion of amides to carboxylic acids (Figure 2.4). The first involved benzamide **2.1** and cyclohexyl amide **2.15**, which gave selective reaction of **2.1** to furnish net-hydrolyzed product **2.2** in 86% yield. Aliphatic amide **2.15** was recovered in quantitative yield. We also performed a competition experiment using tertiary amide **2.1** and secondary amide **2.16**.

This led to selective reaction of **2.1** to give benzoic acid (**2.2**), with quantitative recovery of secondary amide **2.16**. The ability to preferentially manipulate subclasses of amides through selective conversion to carboxylic acids should prove useful in synthetic applications.

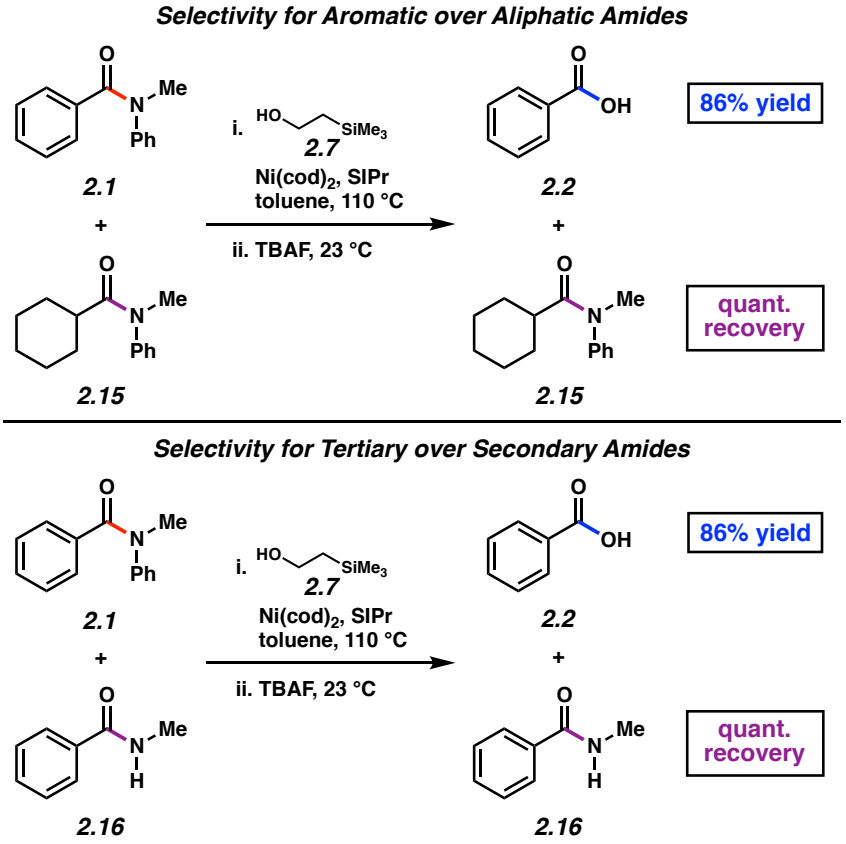


Figure 2.4. Competition experiments demonstrate substrate selectivity. Conditions: amide **2.1** (1.0 equiv), **2.15** or **2.16** (1.0 equiv), $Ni(cod)_2$ (10 mol%), SIPr (10 mol%), **2.7** (1.25 equiv), and toluene (1.0 M) heated at 110 °C for 24 h in a sealed vial under an atmosphere of N_2; TBAF (2.5 equiv) at 23 °C for 2 h. Yields reflect the average of two isolation experiments.

One further evaluation of the methodology to assess mildness and selectivity is shown in Figure 2.5. Substrate **2.17** (derived from L-valine)[4a] bearing an amide, an ester, and an epimerizable stereocenter, was subjected to our typical reaction protocol. This gave benzoic acid (**2.2**) and amine **2.18** in 67% and 72% yield, respectively. Of note, amine **2.18** was recovered in 99% ee and the ester functional group remained intact. As classical hydrolysis conditions are often

incompatible with esters and epimerizable stereocenters,[5] this result underscores the mild nature of our strategy for the conversion of amides to carboxylic acids.

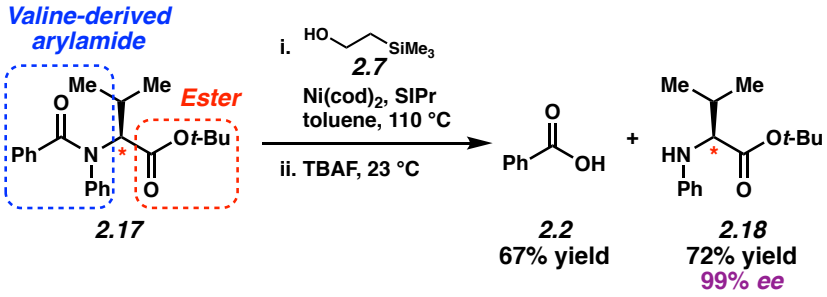


Figure 2.5. Cleavage of a valine-derived amide in the presence of an ester. Conditions: amide **2.17** (1.0 equiv), $Ni(cod)_2$ (20 mol%), SIPr (20 mol%), **2.7** (1.25 equiv), and toluene (1.0 M) heated at 110 °C for 24 h in a sealed vial under an atmosphere of N_2; TBAF (2.5 equiv) at 23 °C for 2 h. Yields reflect the average of two isolation experiments.

2.6 Conclusion

We have developed an operationally-simple procedure to convert amides to carboxylic acids using non-precious metal catalysis. The methodology strategically circumvents catalyst poisoning through the use of a nickel-catalyzed esterification, followed by a fluoride-mediated deprotection in a single-pot operation. We have demonstrated that a variety of amides with aryl groups and *N*-substituents can be employed in this transformation. Additionally, we have shown the process can be utilized to cleave amides in a mild and selective manner. This strategy offers a practical means to convert subclasses of amides to carboxylic acids while addressing a limitation with regard to functional groups accessible using transition-metal-catalyzed reactions of amides.

2.7 Experimental Section

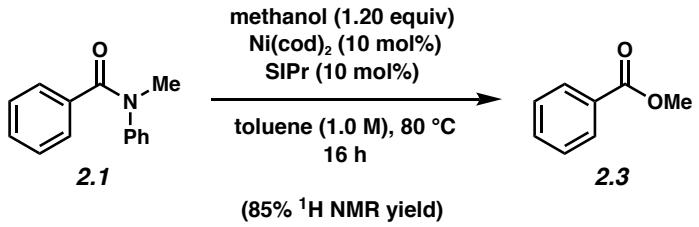
2.7.1 Materials and Methods

Unless stated otherwise, reactions were conducted in flame-dried glassware under an atmosphere of nitrogen and commercially obtained reagents were used as received. (Trimethylsilyl)ethanol (**2.7**) was obtained from Combi-Blocks and distilled and sparged with N_2 for ≥10 min prior to use. Tetrabutylammonium fluoride was obtained from Sigma Aldrich. $Ni(cod)_2$ and SIPr were obtained from Strem Chemicals and degassed by sparging with N_2 for ≥10 min prior to use. Toluene was obtained from Fisher Scientific and purified by distillation over CaH_2 then taken through five freeze-pump-thaw cycles prior to use. 1,3,5-Trimethoxybenzene was obtained from Alfa Aesar and used as received. Reaction temperatures were controlled using an IKAmag temperature modulator, and unless stated otherwise, reactions were performed at room temperature (approximately 23 °C). Thin-layer chromatography (TLC) was conducted with EMD gel 60 F254 pre-coated plates (0.25 mm for analytical chromatography and 0.50 mm for preparative chromatography) and visualized using a combination of UV light, anisaldehyde, iodine, and potassium permanganate staining techniques. Silicycle Siliaflash P60 (particle size 0.040–0.063 mm) was used for flash column chromatography. ^{1}H NMR spectra were recorded on Bruker spectrometers (400, 500, and 600 MHz) and are reported relative to residual solvent signals. Data for ^{1}H NMR spectra are reported as follows: chemical shift (δ ppm), multiplicity, coupling constant (Hz), integration. Determination of enantiopurity was carried out on a Mettler Toledo SFC (supercritical fluid chromatography) using a Daicel ChiralPak IA-3 column. Optical rotations were measured with a Rudolph Autopol III Automatic Polarimeter.

*Note: Supporting information for the syntheses of amides **2.1**, **2.4**, **2.14a–d**, **2.17**, and **2.21–24**[4a] have been published and spectral data match those previously reported.*

2.7.2 Experimental Procedures

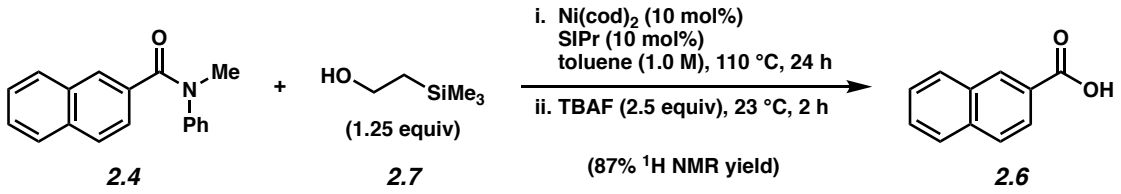
2.7.2.1 Initial Experiments for Amide Hydrolysis



Representative Procedure for Figure 2.2. A 2-dram vial containing amide **2.1** (40.9 mg, 0.194 mmol, 1.00 equiv) and a magnetic stir bar was charged with $Ni(cod)_2$ (5.33 mg, 0.019 mmol, 10.0 mol%) and SIPr (7.56 mg, 0.019 mmol, 10.0 mol%) in a glove box. Subsequently, toluene (0.19 mL, 1.0 M) and then methanol (9.40 μL, 0.232 mmol, 1.20 equiv) were added. The vial was sealed with a Teflon-lined screw cap, removed from the glove box, and stirred at 80 °C in a preheated aluminum block for 16 h. After cooling to 23 °C, the mixture was diluted with hexanes (0.5 mL) and filtered over a plug of silica gel (10 mL of EtOAc eluent). The volatiles were removed under reduced pressure and the yield was determined by ^1H NMR analysis with 1,3,5-trimethoxybenzene as an external standard.

Any modifications of the conditions shown in the representative procedure above are specified in Figure 2.2.

2.7.2.2 Optimization and Relevant Control Experiments



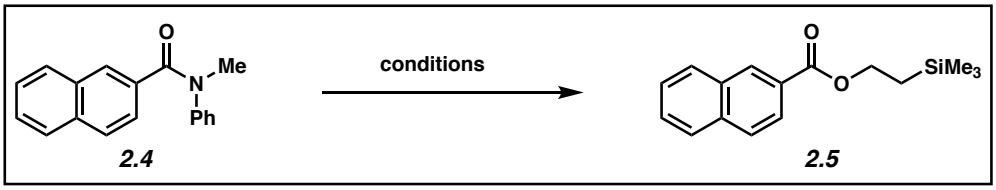
Representative Procedure for the net hydrolysis of amides from Table 2.1. (Entry 3 is used as an example). A 2-dram vial containing amide **2.4** (40.0 mg, 0.153 mmol, 1.00 equiv) and a magnetic stir bar was charged with $Ni(cod)_2$ (4.21 mg, 0.015 mmol, 10 mol%) and SIPr (3.00 mg, 0.015 mmol, 10 mol%) in a glove box. Subsequently, toluene (0.15 mL, 1.0 M) and TMS-ethanol (**2.7**) (27.4 µL, 0.191 mmol, 1.25 equiv) were added. The vial was sealed with a Teflon-lined screw cap, removed from the glove box, and stirred at 110 °C in a preheated aluminum block for 24 h. After cooling to 23 °C, TBAF (0.383 mmol, 2.50 equiv) was added to the reaction mixture. The resulting mixture was stirred for 2 h. The mixture was quenched with 1.0 M HCl (2.0 mL) and diluted with water (5 mL). The layers were then separated and the aqueous layer was extracted with EtOAc (3 x 6 mL). The combined organic layers were then dried over Na_2SO_4, filtered, and concentrated under reduced pressure. The yield was determined by ^1H NMR analysis with 1,3,5-trimethoxybenzene as an external standard.

Any modifications of the conditions shown in the representative procedure above are specified in Table 2.2.

Using the representative procedure, albeit without the addition of TBAF, a series of control experiments were performed to optimize the nickel-catalyzed esterification using TMS-ethanol

(**2.7**). Key results are shown in Table 2.3. The control experiments indicate the desired transformation is nickel-catalyzed, as no desired ester product was generated.

Table 2.3. Relevant Control Experiments

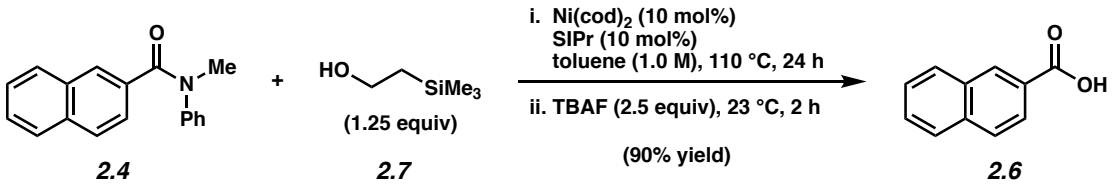


2.4 *2.5*

	Experimental Results	
Reaction Conditions	***2.4***	***2.5***
TMS-ethanol (1.25 equiv), $Ni(cod)_2$ toluene (1.0 M), 110 °C	100%	0%
TMS-ethanol (1.25 equiv), SIPr (10 mol%) toluene (1.0 M), 110 °C	100%	0%
TMS-ethanol (1.25 equiv) toluene (1.0 M), 110 °C	100%	0%

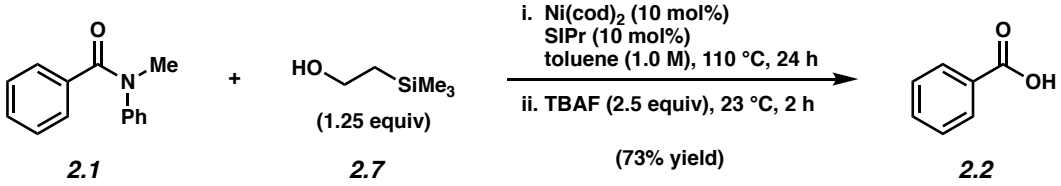
Yields were determined by ^1H NMR analysis using 1,3,5-trimethoxybenzene as an external standard.

2.7.2.3 Scope of Methodology

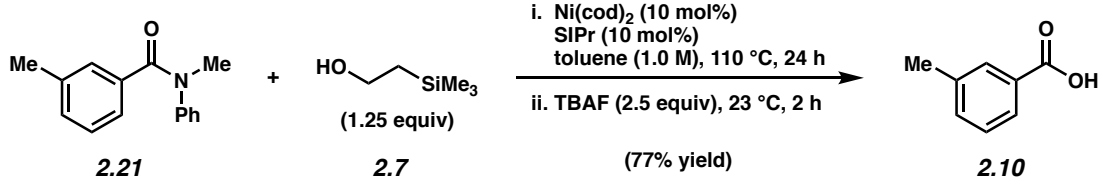


Representative Procedure (net-hydrolysis of amide 2.4 is used as an example).

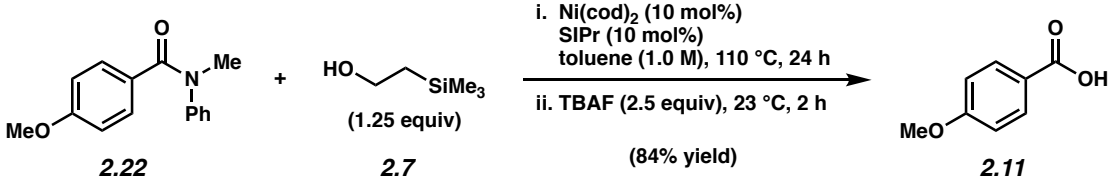
Carboxylic Acid 2.6. A 2-dram vial containing amide **2.4** (50.6 mg, 0.194 mmol, 1.0 equiv) and a magnetic stir bar was charged with $Ni(cod)_2$ (5.33 mg, 0.0194 mmol, 10 mol%) and SIPr (7.56 mg, 0.0194 mmol, 10 mol%) in a glove box. Subsequently, toluene (0.20 mL, 1.0 M) and then TMS-ethanol (34.7 μL, 0.242 mmol, 1.25 equiv) were added. The vial was sealed with a Teflon-lined screw cap, removed from the glove box, and stirred at 110 °C in a preheated aluminum block for 24 h. After cooling to 23 °C, TBAF (0.485 mmol, 2.50 equiv) was added to the reaction mixture. The resulting mixture was stirred for 2 h. Once the reaction was complete, the mixture was quenched with 1.0 M HCl (3.0 mL) and diluted with water (5 mL). The layers were separated and the aqueous layer was extracted with EtOAc (3 x 10 mL). The combined organic layers were then dried over Na_2SO_4, filtered, and concentrated under reduced pressure. The crude residue was purified by flash chromatography (5:1 hexanes:EtOAc + 1% acetic acid) to yield carboxylic acid product **2.6** (30.0 mg, 90% yield, average of two experiments) as a white solid. Carboxylic acid **2.6** R_f 0.55 (5:1 hexanes:EtOAc + 1% acetic acid). ^{1}H NMR (500 MHz, DMSO-d_6): δ 8.59 (s, 1H), 8.08 (dd, J = 7.2, 1.4, 1H), 8.02–7.97 (m, 1H), 7.95–7.87 (m, 2H), 7.66–7.60 (m, 1H), 7.60–7.54 (m, 1H). Spectral data match those previously reported.[9]



Carboxylic Acid 2.2. Purification by flash chromatography (5:1 hexanes:EtOAc + 1% acetic acid) generated carboxylic acid **2.2** (21.4 mg, 73% yield, average of two experiments) as a white solid. Carboxylic acid **2.2**: R_f 0.22 (2:1 hexanes:EtOAc + 1% acetic acid). ^{1}H NMR (300 MHz, $CDCl_3$): δ 8.15 (dd, J = 8.3, 1.3, 2H), 7.65–7.61 (m, 1H), 7.49–7.45 (m, 2H). Spectral data match those previously reported.[9]

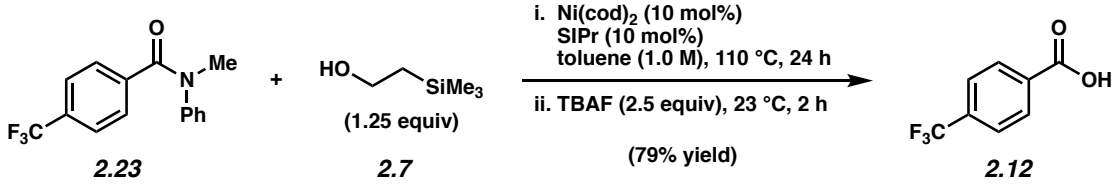


Carboxylic Acid 2.10. Purification by flash chromatography (5:1 hexanes:EtOAc + 1% acetic acid) generated carboxylic acid **2.10** (24.4 mg, 77% yield, average of two experiments) as a white solid. Carboxylic acid **2.10**: R_f 0.54 (5:1 hexanes:EtOAc + 1% acetic acid). ^{1}H NMR (600 MHz, $CDCl_3$): δ 7.96–7.90 (m, 2H), 7.45–7.41 (m, 1H), 7.39–7.35 (m, 1H), 2.43 (s, 3H). Spectral data match those previously reported.[10]

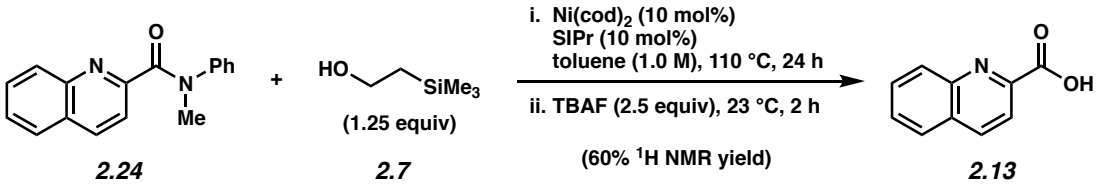


Carboxylic Acid 2.11. Purification by flash chromatography (5:1 hexanes:EtOAc + 1% acetic acid) generated carboxylic acid **2.11** (28.7 mg, 84% yield, average of two experiments) as a white solid. Carboxylic acid **2.11**: R_f 0.33 (5:1 hexanes:EtOAc+ 1% acetic acid). ^{1}H NMR (500 MHz,

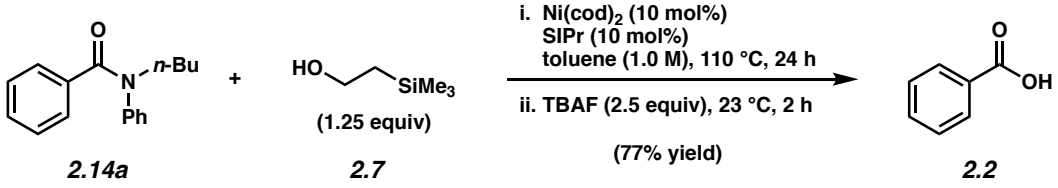
DMSO-d_6): δ 7.85 (d, J = 8.5, 2H), 6.97 (d, J = 8.5, 2H), 3.78 (s, 3H). Spectral data match those previously reported.[9]



Carboxylic Acid 2.12. Purification by flash chromatography (5:1 hexanes:EtOAc + 1% acetic acid) generated carboxylic acid **2.12** (26.9 mg, 79% yield, average of two experiments) as a white solid. Carboxylic acid **2.12**: R_f 0.31 (2:1 hexanes:EtOAc + 1% acetic acid). ^{1}H NMR (600 MHz, DMSO-d_6): δ 8.10 (d, J = 8.1, 2H), 7.84 (d, J = 8.6, 2H). Spectral data match those previously reported.[9]

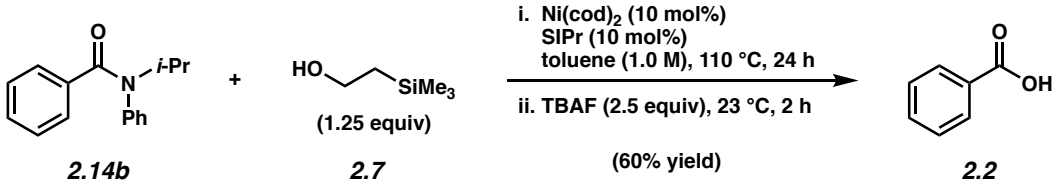


Carboxylic Acid 2.13. ^{1}H NMR (600 MHz, DMSO-d_6) of crude reaction mixture: δ 8.13 (d, J = 8.25, 1H), 7.93 (d, J = 8.25, 1H), 7.85 (d, J = 7.66, 1H), 7.81 (d, J = 8.25, 1H), 7.67–7.63 (m, 1H), 7.75–7.46 (m, 1H). Spectral data of the crude mixture of carboxylic acid **2.13** match those previously reported.[11]

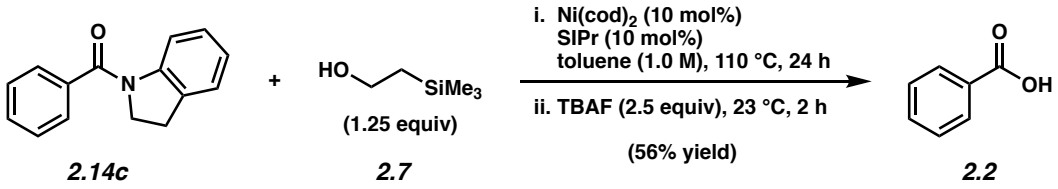


Carboxylic Acid 2.2. Purification by preparative thin-layer chromatography (5:1 benzene:EtOAc + 0.1% acetic acid) generated carboxylic acid **2.2** (21.1 mg, 77% yield, average of two

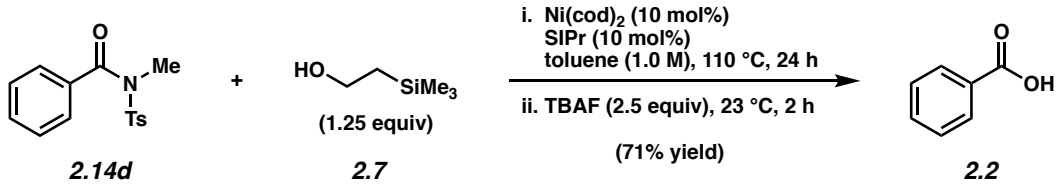
experiments) as a white solid. Carboxylic acid **2.2**: R_f 0.22 (2:1 hexanes:EtOAc + 1% acetic acid). ^{1}H NMR (300 MHz, $CDCl_3$): δ 8.15 (dd, J = 8.3, 1.3, 2H), 7.65–7.61 (m, 1H), 7.49–7.45 (m, 2H). Spectral data match those previously reported.[9]



Carboxylic Acid 2.2. Purification by preparative thin-layer chromatography (5:1 benzene:EtOAc + 0.1% acetic acid) generated carboxylic acid **2.2** (16.6 mg, 60% yield, average of two experiments) as a white solid. Carboxylic acid **2.2**: R_f 0.22 (2:1 hexanes:EtOAc + 1% acetic acid). ^{1}H NMR (300 MHz, $CDCl_3$): δ 8.15 (dd, J = 8.3, 1.3, 2H), 7.65–7.61 (m, 1H), 7.49–7.45 (m, 2H). Spectral data match those previously reported.[9]



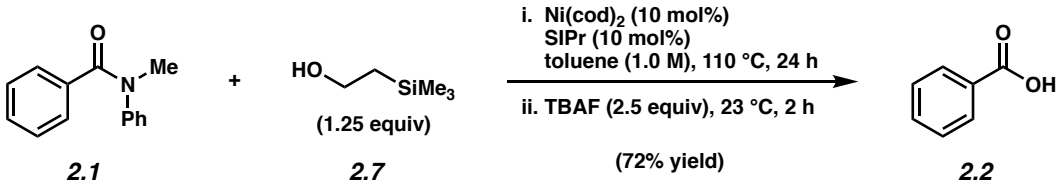
Carboxylic Acid 2.2. Purification by preparative thin-layer chromatography (1:1:3 benzene:EtOAc:DCM) generated carboxylic acid **2.2** (17.2 mg, 56% yield, average of two experiments) as a white solid. Carboxylic acid **2.2**: R_f 0.22 (2:1 hexanes:EtOAc + 1% acetic acid). ^{1}H NMR (300 MHz, $CDCl_3$): δ 8.15 (dd, J = 8.3, 1.3, 2H), 7.65–7.61 (m, 1H), 7.49–7.45 (m, 2H). Spectral data match those previously reported.[9]



2.14d *2.7* *2.2*

Carboxylic Acid 2.2. Purification by preparative thin-layer chromatography (1:1:2 benzene:EtOAc:DCM) generated carboxylic acid **2.2** (16.9 mg, 71% yield, average of two experiments) as a white solid. Carboxylic acid **2.2**: R_f 0.22 (2:1 hexanes:EtOAc + 1% acetic acid). ^{1}H NMR (300 MHz, $CDCl_3$): δ 8.15 (dd, J = 8.3, 1.3, 2H), 7.65–7.61 (m, 1H), 7.49–7.45 (m, 2H). Spectral data match those previously reported.[9]

2.7.2.4 1.0 mmol-Scale Reaction

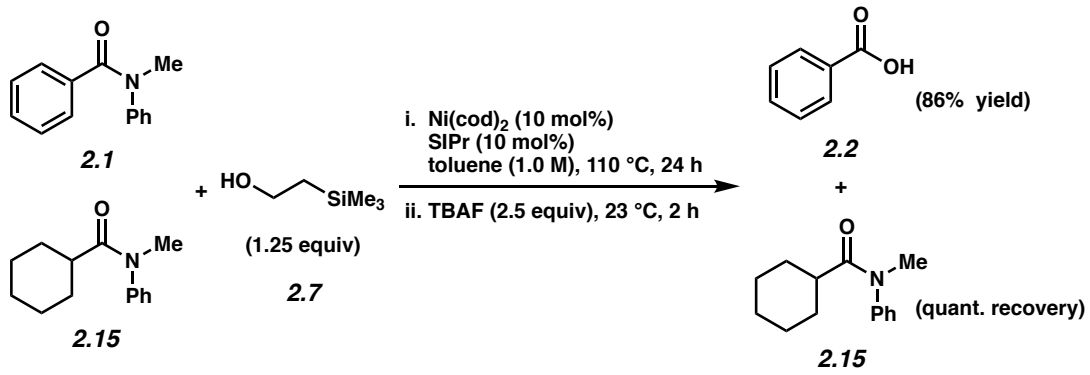


2.1 *2.7* *2.2*

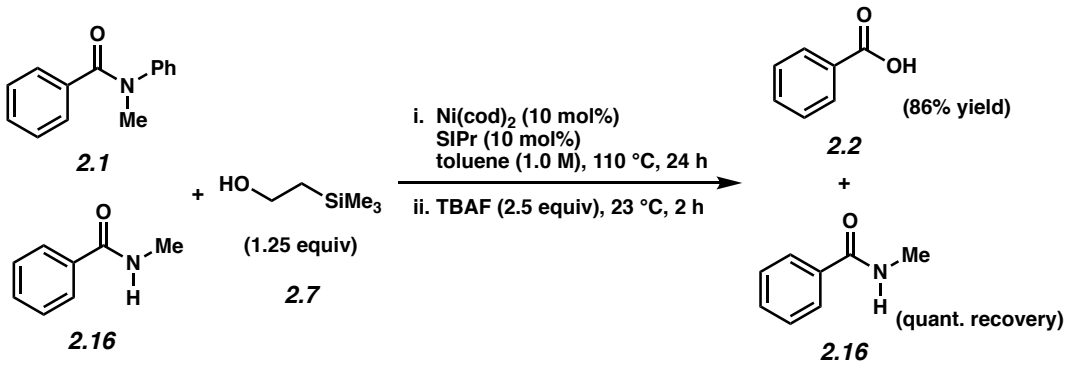
Carboxylic Acid 2.2. A 2-dram vial containing amide **2.1** (220 mg, 1.0 mmol, 1.0 equiv) and a magnetic stir bar was charged with $Ni(cod)_2$ (28.6 mg, 0.10 mmol, 10 mol%) and SIPr (40.7 mg, 0.10 mmol, 10 mol%) in a glove box. Subsequently, toluene (1.0 mL, 1.0 M) and then TMS-ethanol (187 μL, 1.25 mmol, 1.25 equiv) were added. The vial was sealed with a Teflon-lined screw cap, removed from the glove box, and stirred at 110 °C in a preheated aluminum block for 24 h. After cooling to 23 °C, TBAF (2.50 mmol, 2.50 equiv) was added to the reaction mixture. The resulting mixture was stirred for 2 h. Once the reaction was complete, the mixture was quenched with 1.0 M HCl (5.0 mL) and diluted with water (10 mL). The layers were separated and the aqueous layer was extracted with EtOAc (3 x 15 mL). The combined organic layers were then dried over Na_2SO_4, filtered, and concentrated under reduced pressure. The crude residue was purified by flash chromatography (20:1 hexanes:EtOAc + 1% acetic acid) to yield carboxylic acid

product **2.2** (91.0 mg, 72% yield, average of two experiments) as a white solid. Spectral data match those previously reported for carboxylic acid **2.2** (see page 14).

2.7.2.5 Competition Experiments

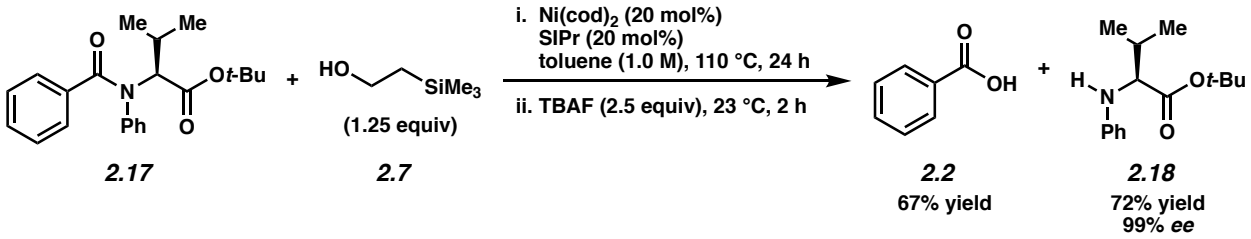


Selectivity for Aromatic over Aliphatic Amides. A 2-dram vial containing amide **2.1** (52.4 mg, 0.248 mmol, 1.0 equiv), amide **2.15** (53.9 mg, 0.248 mmol, 1.0 equiv) and a magnetic stir bar was charged with $Ni(cod)_2$ (6.82 mg, 0.025 mmol, 10 mol%) and SIPr (9.69 mg, 0.025 mmol, 10 mol%) in a glove box. Subsequently, toluene (0.25 mL, 1.0 M) and then TMS-ethanol (44.4 µL, 0.310 mmol, 1.25 equiv) were added. The vial was sealed with a Teflon-lined screw cap, removed from the glove box, and stirred at 110 °C in a preheated aluminum block for 24 h. After cooling to 23 °C, TBAF (0.620 mmol, 2.5 equiv) was added to the reaction mixture. The resulting mixture was stirred for 2 h. The mixture was quenched with 1.0 M HCl (3.0 mL) and diluted with water (5 mL). The layers were separated and the aqueous layer was extracted with EtOAc (3 x 10 mL). The combined organic layers were then dried over Na_2SO_4, filtered, and concentrated under reduced pressure. Spectral data match those previously reported for carboxylic acid **2.2** (see page 14).



Selectivity for Tertiary over Secondary Amides. A 2-dram vial containing amide **2.1** (54.0 mg, 0.256 mmol, 1.0 equiv), amide **2.16** (34.2 mg, 0.253 mmol, 0.99 equiv) and a magnetic stir bar was charged with $Ni(cod)_2$ (7.03 mg, 0.026 mmol, 10 mol%) and SIPr (9.98 mg, 0.026 mmol, 10 mol%) in a glove box. Subsequently, toluene (0.26 mL, 1.0 M) and then TMS-ethanol (45.8 μL, 0.320 mmol, 1.25 equiv) were added. The vial was sealed with a Teflon-lined screw cap, removed from the glove box, and stirred at 110 °C in a preheated aluminum block for 24 h. After cooling to 23 °C, TBAF (0.64 mL, 0.639 mmol, 2.50 equiv) was added to the reaction mixture via syringe. The resulting mixture was stirred at 23 °C for 2 h. Then, the mixture was quenched with 1.0 M HCl (4.0 mL) and diluted with water (3 mL). The layers were separated and the aqueous layer was extracted with EtOAc (3 x 10 mL). The combined organic layers were then washed with saturated NaCl (15 mL), dried over Na_2SO_4, filtered, and concentrated under reduced pressure. Spectral data match those previously reported for carboxylic acid **2.2** (see page 14).

2.7.2.6 Selective Cleavage of Aryl Amide in the Presence of an Ester



Carboxylic Acid 2.2 and Amine 2.18. A 2-dram vial containing amide **2.17** (50.9 mg, 0.144 mmol, 1.0 equiv) and a magnetic stir bar was charged with $Ni(cod)_2$ (7.92 mg, 0.029 mmol, 20 mol%) and SIPr (11.3 mg, 0.029 mmol, 20 mol%) in a glove box. Subsequently, toluene (0.14 mL, 1.0 M) and then TMS-ethanol (25.8 µL, 0.180 mmol, 1.25 equiv) were added. The vial was sealed with a Teflon-lined screw cap, removed from the glove box, and stirred at 110 °C in a preheated aluminum block for 24 h. After cooling to 23 °C, TBAF (0.360 mmol, 2.5 equiv) was added to the reaction mixture. The resulting mixture was stirred for 2 h. Then, the mixture was quenched with water (6.0 mL) and diluted further with water (5 mL). The layers were separated and the aqueous layer was extracted with EtOAc (3 x 10 mL). The combined organic layers were then dried over Na_2SO_4, filtered, and concentrated under reduced pressure. The crude residue was purified by preparative thin-layer chromatography (5:1 hexanes:EtOAc + 1% acetic acid) to yield carboxylic acid product **2.2** (11.8 mg, 67% yield, average of two experiments) as a white solid and amine **2.18** (25.7 mg, 72% yield, 99% *ee*, average of two experiments) as a clear oil. Spectral data matched those previously reported.[4a] Carboxylic acid **2.2**: R_f 0.22 (2:1 hexanes:EtOAc + 1% acetic acid). Amine **2.18**: R_f 0.24 (9:1 hexanes:EtOAc). ^1H NMR (300 MHz, $CDCl_3$): δ 7.16 (m, 2H), 6.71 (m, 1H), 6.63 (m, 2H), 4.14 (br s, 1H), 3.75 (m, 1H), 2.09 (o, J = 5.6, 1.1, 1H), 1.43 (s, 9H), 1.03 (dd, J = 6.7, 4.3, 6H). Spectral data match those previously reported.[4a]

2.8 Spectra Relevant to Chapter Two:

Nickel-Catalyzed Conversion of Amides to Carboxylic Acids

Rachel R. Knapp, Ana S. Bulger, and Neil K. Garg.

Org. Lett. **2020**, *22*, 2833–2837.

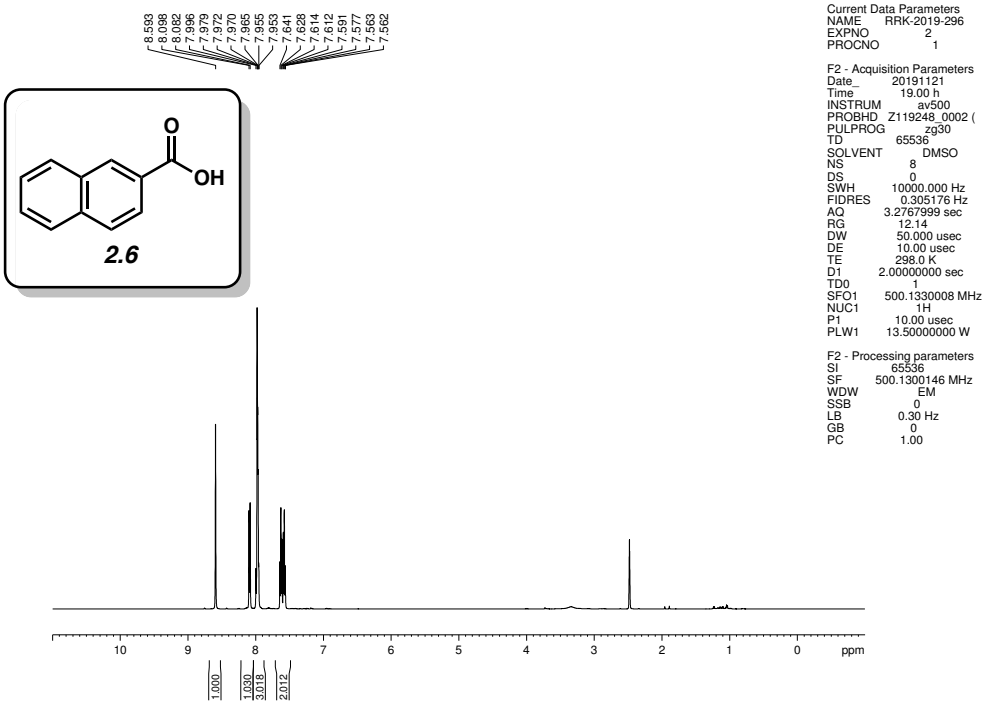


Figure 2.6. ^{1}H NMR (500 MHz, DMSO-d_6) of compound **2.6**.

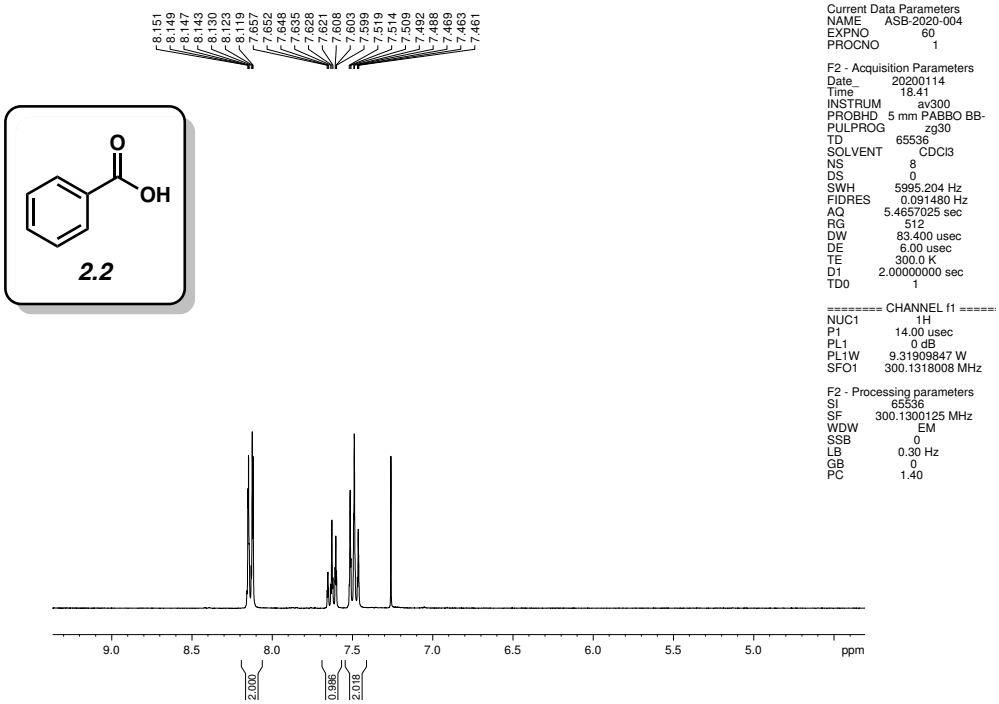


Figure 2.7. ^{1}H NMR (300 MHz, $CDCl_3$) of compound **2.2**.

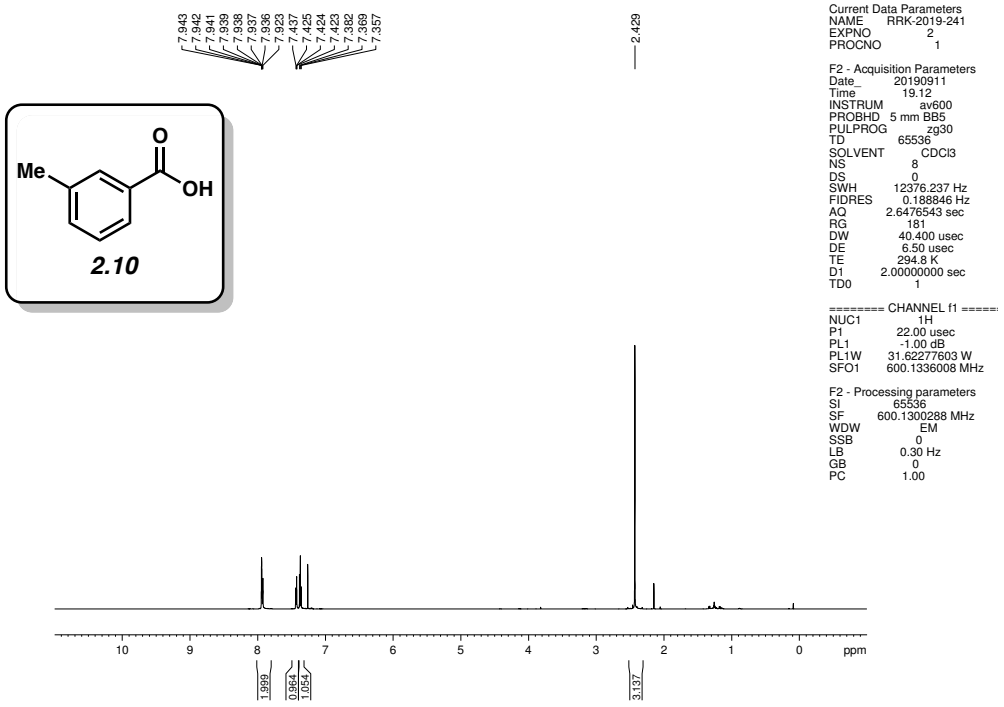


Figure 2.8. ^{1}H NMR (600 MHz, $CDCl_3$) of compound **2.10**.

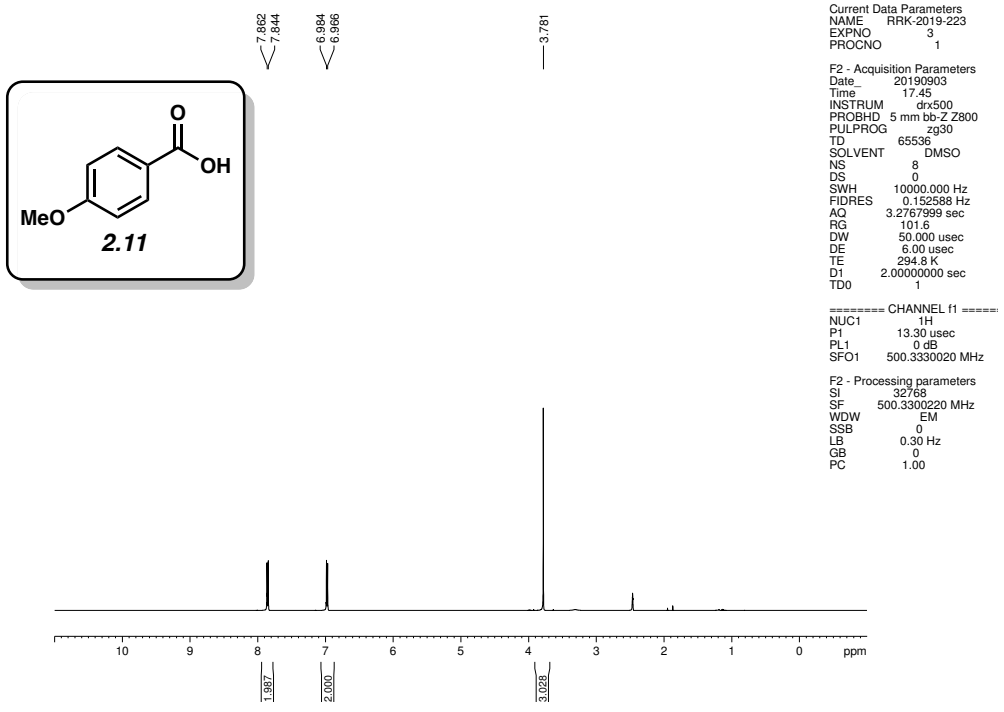


Figure 2.9. ^{1}H NMR (500 MHz, DMSO-d_6) of compound **2.11**.

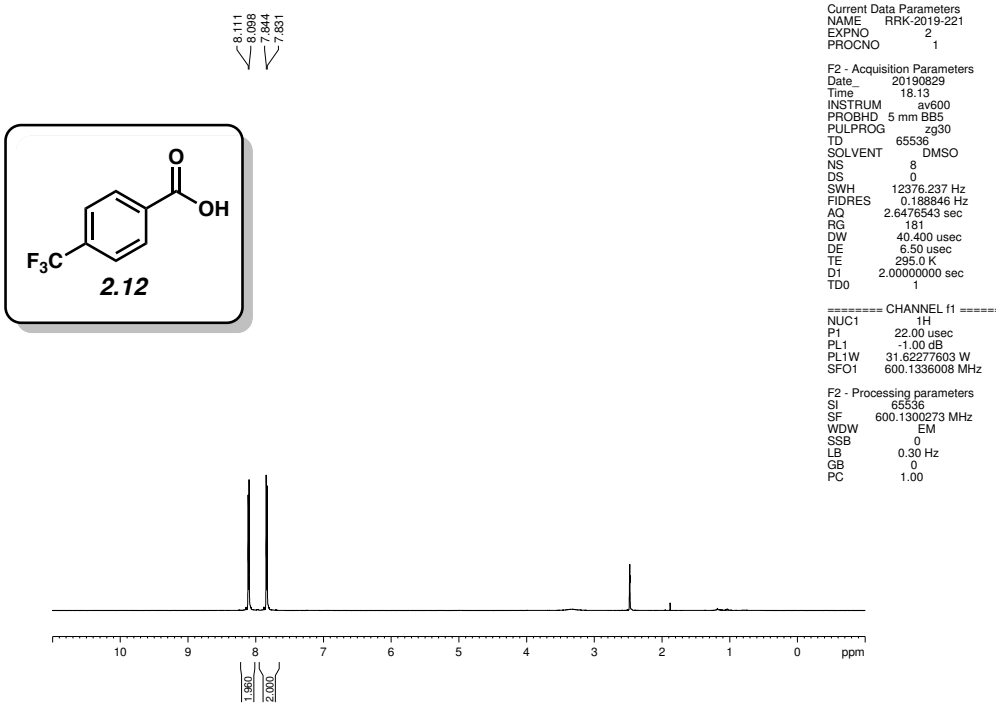


Figure 2.10. ^{1}H NMR (600 MHz, DMSO-d_6) of compound **2.12**.

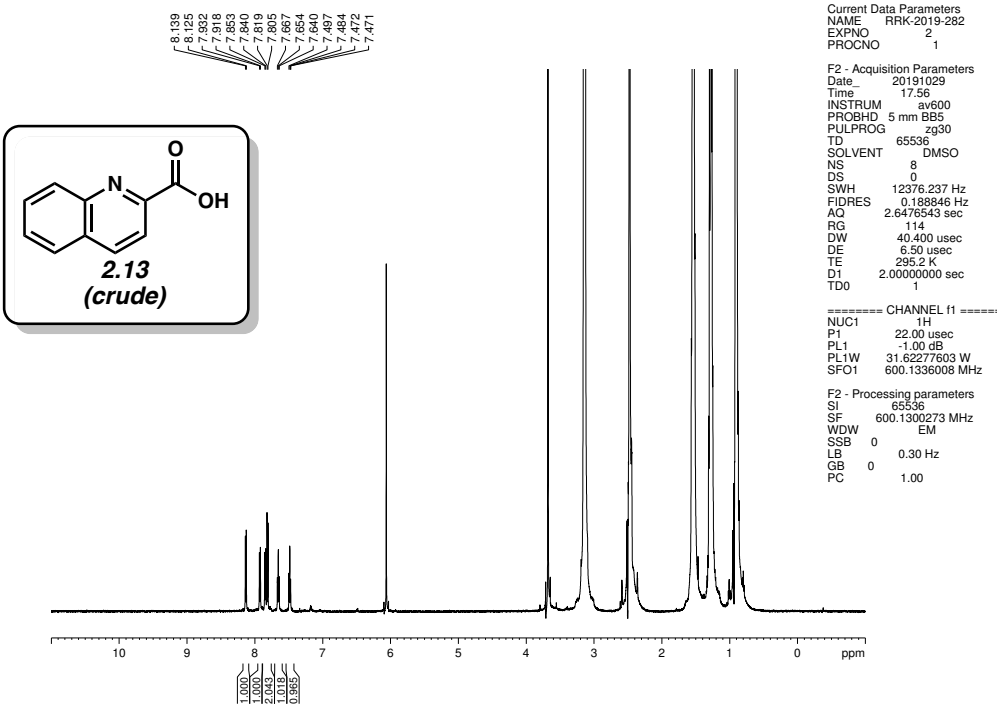


Figure 2.11. ^{1}H NMR (600 MHz, DMSO-d_6) of compound **2.13**.

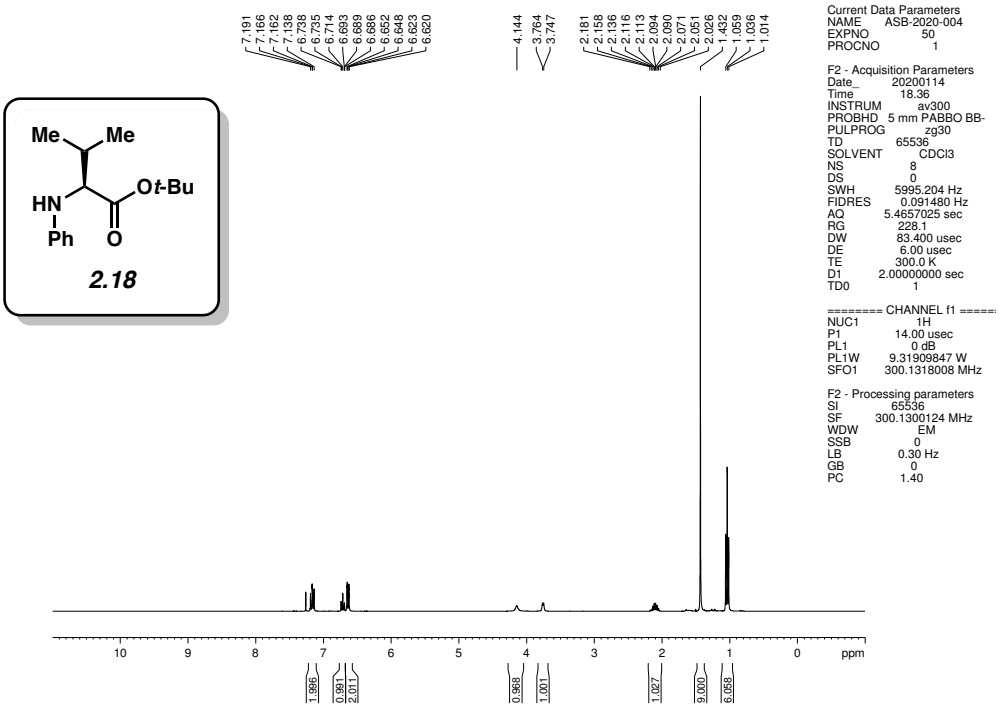
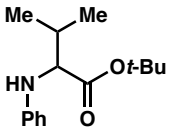
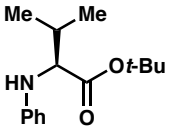
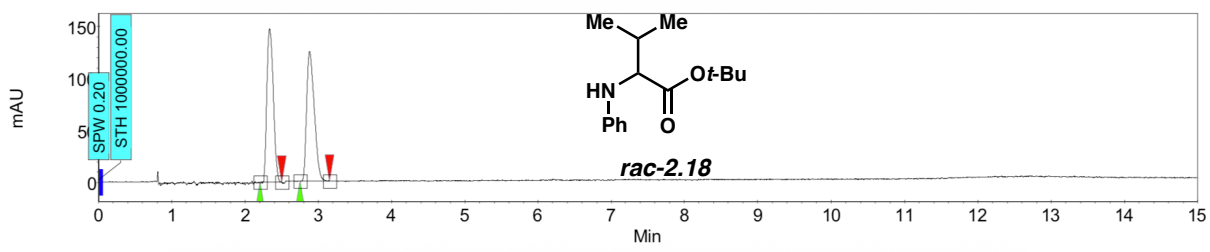


Figure 2.12. ^{1}H NMR (300 MHz, $CDCl_3$) of compound **2.18**.

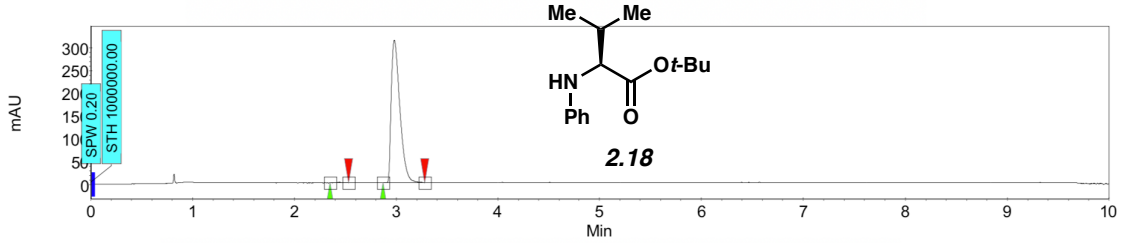
2.9 SFC Traces

Compound	SFC Method Column/Temp. Abs. Wavelength	Sovlent	Method Flow Rate	Retention Times (min)	Enantiomeric Ratio (er)
 ***rac-2.18***	Daicel ChiralPak IA-3/35 °C λabs = 210 nm	2% isopropanol in CO_2	3.5 mL/min	2.20/2.75	50:50
 ***2.18***	Daicel ChiralPak IA-3/35 °C λabs = 210 nm	2% isopropanol in CO_2	3.5 mL/min	2.35/2.87	100:0



Index	Name	Start	Time	End	RT Offset	Quantity	Height	Area	Area
		[Min]	[Min]	[Min]	[Min]	[% Area]	[µV]	[µV.Min]	[%]
2	UNKNOWN	2.20	2.33	2.50	0.00	50.06	147.5	15.1	50.060
1	UNKNOWN	2.75	2.88	3.15	0.00	49.94	124.8	15.0	49.940
Total						100.00	272.3	30.1	100.000

Figure 2.13. SFC trace of **rac-2.18**.



Index	Name	Start	Time	End	RT Offset	Quantity	Height	Area	Area
		[Min]	[Min]	[Min]	[Min]	[% Area]	[µV]	[µV.Min]	[%]
2	UNKNOWN	2.35	2.44	2.53	0.00	0.16	0.9	0.0	0.161
1	UNKNOWN	2.87	2.98	3.28	0.00	99.84	312.3	30.7	99.839
Total						100.00	313.2	30.8	100.000

Figure 2.14. SFC trace of **2.18**.

2.10 Notes and References

(1) For recent reviews, see: (a) Dander, J. E.; Garg, N. K. Breaking amides using nickel catalysis. *ACS Catal.* **2017**, *7*, 1413–1423. (b) Meng, G.; Shi, S.; Szostak, M. Cross-coupling of amides by N–C bond activation. *Synlett* **2016**, *27*, 2530–2540. (c) Takise, R.; Muto, K.; Yamaguchi, J. Cross-coupling of aromatic esters and amides. *Chem. Soc. Rev.* **2017**, *46*, 5864–5888. (d) Kaiser, D.; Bauer, A.; Lemmerer, M.; Maulide, N. Amide activation: an emerging tool for chemoselective synthesis. *Chem. Soc. Rev*. **2018**, *47*, 7899–7925.

(2) For Pd-catalyzed amide C−N bond activations, see: (a) Li, X.; Zou, G. Acylative Suzuki coupling of amides: acyl-nitrogen activation via synergy of independently modifiable activating groups. *Chem. Commun.* **2015**, *51*, 5089−5092. (b) Yada, A.; Okajima, S.; Murakami, M. Palladium-catalyzed intramolecular insertion of alkenes into the carbon−nitrogen bond of β-lactams. *J. Am. Chem. Soc.* **2015**, *137*, 8708−8711. (c) Meng, G.; Szostak, M. Palladium-catalyzed Suzuki−Miyaura coupling of amides by carbon−nitrogen cleavage: general strategy for amide N−C bond activation. *Org. Biomol. Chem.* **2016**, *14*, 5690−5705. (d) Meng, G.; Szostak, M. General olefin synthesis by the palladium-catalyzed Heck reaction of amides: sterically-controlled chemoselective N−C activation. *Angew. Chem., Int. Ed.* **2015**, *54*, 14518−14522. (e) Meng, G.; Szostak, M. Sterically controlled Pd-catalyzed chemoselective ketone synthesis via N−C cleavage in twisted amides. *Org. Lett.* **2015**, *17*, 4364−4367. (f) Liu, C.; Meng, G.; Liu, Y.; Liu, R.; Lalancette, R.; Szostak, R.; Szostak, M. *N*-Acylsaccharins: stable electrophilic amide-based acyl transfer reagents in Pd-catalyzed Suzuki−Miyaura coupling via N−C cleavage. *Org. Lett.* **2016**, *18*, 4194−4197. (g) Lei, P.; Meng, G.; Szostak, M. General method for the Suzuki−Miyaura cross-coupling of amides using commercially available, air- and moisture-stable palladium/NHC (NHC = *N*-

heterocyclic carbene) complexes. *ACS Catal.* **2017**, *7*, 1960−1965. (h) Liu, C.; Liu, Y.; Liu, R.; Lalancette, R.; Szostak, R.; Szostak, M. Palladium-catalyzed Suzuki−Miyaura cross-coupling of *N*-mesylamides by N−C cleavage: electronic effect of the mesyl group. *Org. Lett.* **2017**, *19*, 1434−1437. (i) Liu, C.; Meng, G.; Szostak, M. *N*-Acylsaccharins as amide-based arylating reagents via chemoselective N−C cleavage: Pd-catalyzed decarbonylative Heck reaction. *J. Org. Chem.* **2016**, *81*, 12023−12030. (j) Meng, G.; Shi, S.; Szostak, M. Palladium-catalyzed Suzuki−Miyaura cross-coupling of amides via site-selective N−C bond cleavage by cooperative catalysis. *ACS Catal.* **2016**, *6*, 7335−7339. (k) Cui, M.; Wu, H.; Jian, J.; Wang, H.; Liu, C.; Stelck, D.; Zeng, Z. Palladium-catalyzed Sonogashira coupling of amides: access to ynones via C−N bond cleavage. *Chem. Commun.* **2016**, *52*, 12076−12079. (l) Wu, H.; Li, Y.; Cui, M.; Jian, J.; Zeng, Z. Suzuki coupling of amides via palladium-catalyzed C−N cleavage of *N*-acylsaccharins. *Adv. Synth. Catal.* **2016**, *358*, 3876−3880. (m) Shi, S.; Szostak, M. Decarbonylative cyanation of amides by palladium catalysis. *Org. Lett.* **2017**, *19*, 3095−3098. (n) Lei, P.; Meng, G.; Ling, Y.; An, J.; Szostak, M. Pd-PEPPSI: Pd-NHC precatalyst for Suzuki−Miyaura cross-coupling reactions of amides. *J. Org. Chem.* **2017**, *82*, 6638−6646. (o) Meng, G.; Szostak, R.; Szostak, M. Suzuki−Miyaura cross-coupling of *N*-acylpyrroles and pyrazoles: planar, electronically activated amides in catalytic N−C cleavage. *Org. Lett.* **2017**, *19*, 3596−3599. (p) Meng, G.; Lalancette, R.; Szostak, R.; Szostak, M. *N*-Methylamino pyrimidyl amides (MAPA): highly reactive, electronically-activated amides in catalytic N−C(O) cleavage. *Org. Lett.* **2017**, *19*, 4656−4659. (q) Osumi, Y.; Szostak, M. *N*-Acylsuccinimides: twist-controlled, acyl transfer reagents in Suzuki−Miyaura cross-coupling by N−C amide bond activation. *Org. Biomol. Chem.* **2017**, *15*, 8867−8871. (r) Lei, P.; Meng, G.; Ling, Y.; An, J.; No lan, S. P.; Szostak, M. General method for the Suzuki−Miyaura cross-

coupling of primary amide-derived electrophiles enabled by [Pd(NHC)(cin)–Cl] at room temperature. *Org. Lett.* **2017**, *19*, 6510−6513. (s) Li, X.; Zou, G. Palladium-catalyzed acylative cross-coupling of amides with diarylboronic acids and sodium tetraarylborates. *J. Organomet. Chem.* **2015**, *794*, 136−145. (t) Liu, C.; Li, G.; Shi, S.; Meng, G.; Lalancette, R.; Szostak, R.; Szostak, M. Acyl and decarbonylative Suzuki coupling of *N*-acetyl amides: Electronic tuning of twisted, acyclic amides in catalytic carbon−nitrogen bond cleavage. *ACS Catal.* **2018**, *8*, 9131−9139. (u) Meng, G.; Szostak, M. Palladium/NHC (NHC = *N*-heterocyclic carbene)-catalyzed β-alkyl Suzuki cross-coupling of amides by selective N−C bond cleavage. *Org. Lett.* **2018**, *20*, 6789−6793. (v) Shi, S.; Szostak, M. Decarbonylative borylation of amides by palladium catalysis. *ACS Omega* **2019**, *4*, 4901−4907. (w) Zhou, T.; Li, G.; Nolan, S. P.; Szostak, M. [Pd(NHC)(acac)Cl]: well-defined, air-stable, and readily available precatalysts for Suzuki and Buchwald−Hartwig cross-coupling (transamidation) of amides and esters by N−C/O−C activation. *Org. Lett.* **2019**, *21*, 3304−3309. (x) Rahman, M. M.; Buchspies, J.; Szostak, M. *N*-Acylphthalimides: efficient acyl coupling reagents in Suzuki–Miyaura cross-coupling by N–C cleavage catalyzed by Pd-PEPPSI precatalysts. *Catalysts* **2019**, *9*, 129. (y) Liu, C.; Lalancette, R.; Szostak, R.; Szostak, M. Sterically hindered ketones via palladium-catalyzed Suzuki–Miyaura cross-coupling of amides by N–C(O) activation. *Org. Lett.* **2019**, *21*, 7976–7981. (z) Li, G.; Zhou, T.; Poater, A.; Cavallo, L.; Nolan, S. P.; Szostak, M. Buchwald–Hartwig cross-coupling by air- and moisture-stable [Pd(NHC)(allyl)Cl] pre-catalysts: catalyst evaluation and mechanism. *Catal. Sci. Technol.* **2020**, *10*, 710–716.

(3) Meng, G.; Szostak, M. Rhodium-catalyzed C–H bond functionalization with amides by double C–H/C–N bond activation. *Org. Lett.* **2016**, *18*, 796–799.

(4) For nickel-catalyzed reactions proceeding with cleavage of the amide C−N bond, see: (a) Hie, L.; Fine Nathel, N. F.; Shah, T. K.; Baker, E. L.; Hong, X.; Yang, Y.-F.; Liu, P.; Houk, K. N.; Garg, N. K. Conversion of amides to esters by the nickel-catalysed activation of amide C−N bonds. *Nature* **2015**, *524*, 79−83. (b) Weires, N. A.; Baker, E. L.; Garg, N. K. Nickel-catalysed Suzuki−Miyaura coupling of amides. *Nat. Chem.* **2016**, *8*, 75−79. (c) Baker, E. L.; Yamano, M. M.; Zhou, Y.; Anthony, S. M.; Garg, N. K. A two-step approach to achieve secondary amide transamidation enabled by nickel catalysis. *Nat. Commun.* **2016**, *7*, 11554. (d) Simmons, B. J.; Weires, N. A.; Dander, J. E.; Garg, N. K. Nickel-catalyzed alkylation of amide derivatives. *ACS Catal.* **2016**, *6*, 3176−3179. (e) Shi, S.; Szostak, M. Nickel-catalyzed diaryl ketone synthesis by N−C bond cleavage: direct Negishi cross-coupling of primary amides by site-selective *N*,*N*-di-Boc activation. *Org. Lett.* **2016**, *18*, 5872−5875. (f) Shi, S.; Szostak, M. Efficient synthesis of diaryl ketones by nickel-catalyzed Negishi cross-coupling of amides via carbon−nitrogen bond cleavage at room temperature accelerated by solvent effect. *Chem. Eur. J.* **2016**, *22*, 10420−10424. (g) Hie, L.; Baker, E. L.; Anthony, S. M.; Desrosiers, J.-N.; Senanayake, C.; Garg, N. K. Nickel-catalyzed esterification of aliphatic amides. *Angew. Chem., Int. Ed.* **2016**, *55*, 15129−15132. (h) Dey, A.; Sasmal, S.; Seth, K.; Lahiri, G. K.; Maiti, D. Nickel-catalyzed deamidative step-down reduction of amides to aromatic hydrocarbons. *ACS Catal.* **2017**, *7*, 433−437. (i) Ni, S.; Zhang, W.; Mei, H.; Han, J.; Pan, Y. Ni-catalyzed reductive cross-coupling of amides with aryl iodide electrophiles via C−N bond activation. *Org. Lett.* **2017**, *19*, 2536−2539. (j) Medina, J. M.; Moreno, J.; Racine, S.; Du, S.; Garg, N. K. Mizoroki−Heck cyclizations of amide derivatives for the introduction of quaternary centers. *Angew. Chem., Int. Ed.* **2017**, *56*, 6567−6571. (k) Hu, J.; Wang, M.; Pu, X.; Shi, Z. Nickel-catalysed retro-hydroamidocarbonylation of aliphatic amides to olefins. *Nat. Commun.* **2017**,

8, 14993. (l) Weires, N. A.; Caspi, D. D.; Garg, N. K. Kinetic modeling of the nickel-catalyzed esterification of amides. *ACS Catal.* **2017**, *7*, 4381−4385. (m) Shi, S.; Szostak, M. Nickel-catalyzed Negishi cross-coupling of *N*-acylsuccinimides: stable, amide-based, twist-controlled acyl transfer reagents via N−C activation. *Synthesis* **2017**, 3602−3608. (n) Dander, J. E.; Baker, E. L.; Garg, N. K. Nickel-catalyzed transamidation of aliphatic amide derivatives. *Chem. Sci.* **2017**, *8*, 6433−6438. (o) Huang, P.-Q.; Chen, H. Ni-catalyzed cross-coupling reactions of *N*-acylpyrrole-type amides with organoboron reagents. *Chem. Commun.* **2017**, *53*, 12584−12587. (p) Deguchi, T.; Xin, H.-L.; Morimoto, H.; Ohshima, T. Direct catalytic alcoholysis of unactivated 8-aminoquinoline amides. *ACS Catal.* **2017**, *7*, 3157−3161. (q) Dander, J. E.; Giroud, M.; Racine, S.; Darzi, E. R.; Alvizo, O.; Entwistle, D.; Garg, N. K. Chemoenzymatic conversion of amides to enantioenriched alcohols in aqueous medium. *Commun. Chem.* **2019**, *2*, 82. (r) Wang, H.; Zhang, S.; Hong, X. Computational studies on Ni-catalyzed amide C–N bond activation. *Chem. Commun.* **2019**, *55*, 11330–11341. (s) Mehta, M. M.; Boit, T. B.; Dander, J. E.; Garg, N. K. Ni-catalyzed Suzuki–Miyaura cross-coupling of aliphatic amides on the benchtop. *Org. Lett.* **2020**, *22*, 1–5. (t) Yu, C.; Matsuo, Y. Nickel-catalyzed deaminative acylation of activated aliphatic amines with aromatic amides via C–N bond activation. *Org. Lett.* **2020**, *22*, 950–955.

(5) (a) Steiger, R. E. α-Aminodiethylacetic acid. *Org. Synth.* **1942**, *22*, 13. (b) Brown, R. S.; Bennet, A. J.; Slebocka-Tilk, H. Recent perspectives concerning the mechanism of H_3O+- and OH-promoted amide hydrolysis. *Acc. Chem. Res.* **1992**, *25*, 481–488. (c) Smith, M. B.; March, J. "Aliphatic nucleophilic substitution." *March's Advanced Organic Chemistry*, John Wiley & Sons, Inc. **2001**, 474–477. (d) Slebocka-Tilk, H.; Neverov, A.; Brown, R. S. Proton inventory

study of the base-catalyzed hydrolysis of formamide. Consideration of the nucleophilic and general base mechanisms. *J. Am. Chem. Soc.* **2003**, *125*, 1851–1858.

(6) See section 2.7.2.3 for experimental details.

(7) Consistent with prior studies, this methodology using Ni/SIPr requires the use of benzamide-type substrates. Density functional theory (DFT) calculations suggest the presence of an aromatic ring attached to the carbonyl enables nickel coordination and amide C–N bond cleavage; see reference 4a.

(8) Reaction was also run on a 1.0 mmol scale, affording benzoic acid (**2.2**) in 72% isolated yield.

(9) Bhunia, S. K.; Das, P.; Nandi, S.; Jana, R. Carboxylation of aryl triflates with CO_2 merging palladium and visible-light-photoredox catalysts. *Org. Lett*. **2019**, *21*, 4632–463.

(10) Kobaysashi, K.; Kondo, Y. Transition-metal-free carboxylation of organozinc reagents using CO_2 in DMF solvent. *Org. Lett*. **2009**, *11*, 2035–2037.

(11) Yoshida, M.; Katagiri, Y.; Zhu, W.; Shishido, K. Oxidative carboxylation of arylaldehydes with water by a sulfoxylalkyl-substituted *N*-heterocyclic carbene catalyst. *Org. Biomol. Chem.* **2009**, *7*, 4062–4066.

CHAPTER THREE

Enantioselective Nickel-Catalyzed Mizoroki–Heck Cyclizations of Amide Electrophiles

Ana S. Bulger[†], Daniel J. Nasrallah[†], Arismel Tena Meza[†], and Neil K. Garg.

Chem. Sci. **2024**, *15*, 2593–2600.

3.1 Abstract

Amide cross-couplings that rely on C–N bond activation by transition metal catalysts have emerged as valuable synthetic tools. Despite numerous discoveries in this field, no catalytic asymmetric variants have been disclosed to date. Herein, we demonstrate the first such transformation, which is the Mizoroki Heck cyclization of amide substrates using asymmetric nickel catalysis. This proof-of-concept study provides an entryway to complex enantioenriched polycyclic scaffolds and advances the field of amide C–N bond activation chemistry.

3.2 Introduction

Metal-catalyzed cross-coupling reactions are essential tools for synthetic chemists.[1] Our laboratory and others have been interested in investigating unconventional cross-coupling partners to discover new fundamental reactivity, enable chemoselective reactions, and advance the field by expanding the synthetic toolbox.[2] One class of unconventional cross-coupling handles, acyl electrophiles[3] (Fig. 3.1A, **3.2**) are underexplored compared to traditional electrophiles, such as aryl halides and pseudohalides. Of the known acyl electrophiles, thioesters (**3.2a**) have been investigated the most in conventional asymmetric transition-metal catalyzed cross-couplings (i.e., **3.2a** → **3.1**).[4] Anhydrides (**3.2b**) and acid chlorides (**3.2c**) have also been used in asymmetric catalysis in the context of reductive or photochemical cross-couplings (**3.2b**–**c** → **3.1**).[5] Recently,

the far less reactive acyl electrophiles, esters[6] (**3.2d**) and amides[7] (**3.2e**), have been investigated as electrophiles in C–C and C–heteroatom bond-forming reactions. Of note, no catalytic asymmetric examples have been reported using these species as electrophiles (i.e., **3.2d** or **3.2e** → **3.3**).

Amides (Fig. 3.1B, **3.2e**) are particularly attractive as synthetic building blocks. They are known for their pronounced stability under various reaction conditions, including hydrolysis and redox processes. Amides can also be used as directing groups in other useful processes, such as aryl C–H bond functionalization.[8] Thus, amides have the potential to be employed in synthetic sequences, then activated late-stage to access a variety of other functional groups. The pronounced stability of amides is largely attributed to resonance delocalization of the nitrogen lone pair.[9] This leads to the high kinetic barrier associated with breaking the amide C–N bond and has led to the historical avoidance of amides as versatile synthetic handles.[10] Thus, our laboratory and others[11] have been interested in expanding known reactivity of these historically underutilized functional handles under mild conditions. Our specific interests pertain to cross-coupling reactions of amides using transition-metal catalysis, which led to our first report of an amide cross-coupling, published in 2015.[7a] Subsequently, amides have become versatile electrophiles in Pd- and Ni-catalyzed cross-coupling reactions.

Mechanistically, these reactions are typically thought to proceed by oxidative addition to the amide C–N bond to generate acyl metal species **3.4**.[7a] Subsequent interception by a nucleophile gives rise to products **3.5**. Using this platform, amides can now be readily converted to functional groups such as ketones, carboxylic acids, esters, and other amides, through relatively simple net substitution processes. We questioned if the use of a chiral ligand on the metal could provide an opportunity to access enantioenriched products. Despite there being more than a hundred amide cross-couplings involving C–N bond activation reported since 2015,[12] asymmetric variants that

utilize a chiral metal catalyst have not been discovered. Such processes would provide a new avenue in amide bond activation chemistry to allow access to enantioenriched molecules from simple amide precursors.

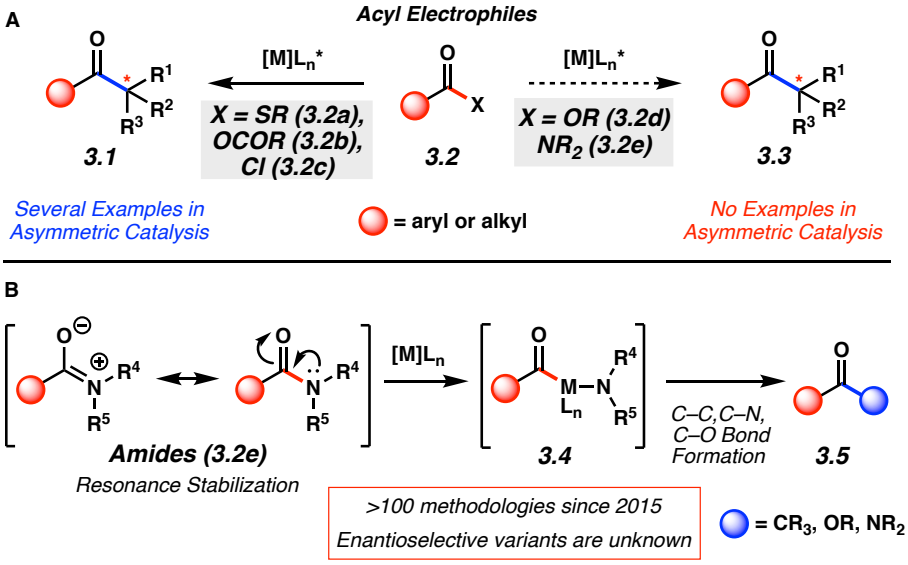


Figure 3.1. (A) Asymmetric metal-catalyzed reactions of acyl electrophiles and current limitations. (B) Current state-of-the-art of amide cross-coupling reactions.

3.3 Reaction Design

We envisioned that an asymmetric Mizoroki–Heck cyclization would be a suitable platform to access enantioenriched products from amide electrophiles.[13] Our reaction design, inspired by prior racemic Heck-type reactions of amide electrophiles discovered by our laboratory[7j] and Stanley's,[7l] and other asymmetric examples involving acyl-metal intermediates[14,15] is shown in Fig. 3.2. Representative amide substrate **3.6** bearing a tethered olefin would undergo oxidative addition using a metal catalyst to form acyl metal species **3.7**. Subsequent olefin coordination and migratory insertion, (the enantiodetermining step) would furnish intermediate **3.8**. β-Hydride elimination would then provide the desired product **3.9**. Importantly, **3.9** would bear a stereodefined quaternary center, which is notable as quaternary stereocenters remain challenging to access and are highly sought-after motifs.[16]

Herein, we demonstrate the success of this approach, which provides the first asymmetric transition-metal-catalyzed reaction involving amide C–N bond cleavage. The transformation is enabled by the design of a new chiral *N*-heterocyclic carbene (NHC)[17] ligand **3.10** (Fig. 3.2) and the use of amine additives, and ultimately delivers select products containing quaternary centers in up to 88% enantiomeric excess (ee). Although currently limited in scope, this proof-of-concept study allows access to several highly complex, enantioenriched scaffolds. Moreover, this study demonstrates the ability to use catalytic amide C–N bond cleavage as an approach to achieve enantioselective synthesis.

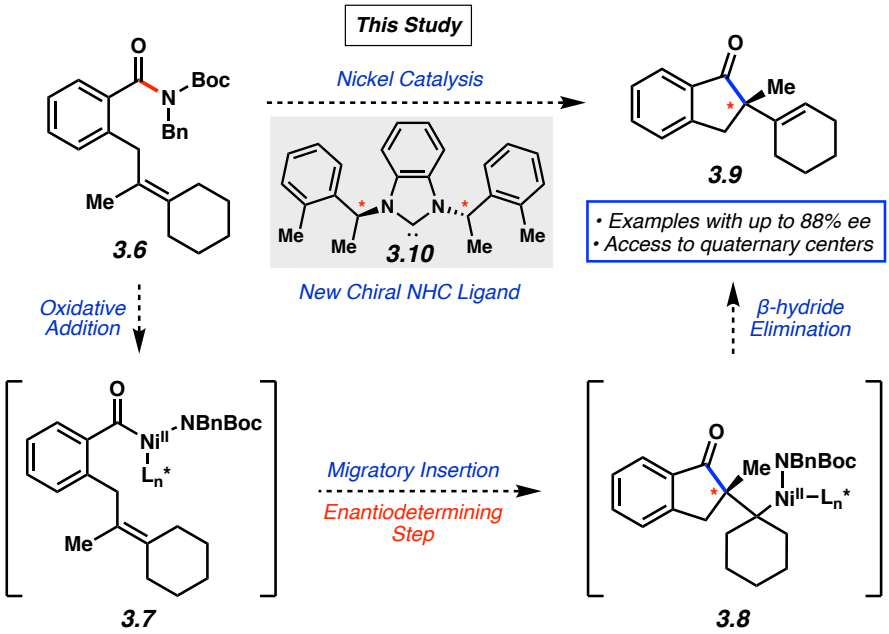


Figure 3.2. Overview of the reaction design and proposed mechanism.

3.4 Reaction Discovery and Optimization

Our studies commenced by attempting the asymmetric Mizoroki–Heck cyclization using nickel catalysis (Fig. 3.3). Prior studies involving amide substrates with tethered olefins (e.g., **3.11**) showed that a highly nucleophilic metal (i.e., nickel[18]), accompanied by strongly electron-donating NHC ligands was required to activate the sterically encumbered and electron-rich amide C–N

bond. A small library of new and known chiral NHC salts was accessible by a combination of acquisition from colleagues in academia (Fig. 3.3 top panel; see Material and Method section 3.8.1) and chemical synthesis (Fig. 3.3 bottom panel). Substrate **3.11** was utilized for initial studies and select results are shown in Fig. 3.3, with further results available in section 3.8.2.2.1.

Known chiral NHC salts **L3.1**–**L3.6** were tested using conditions developed for the racemic transformation[7j] to effect the desired conversion of amide **3.11** to indanone **3.12**. Despite the fact that these ligand salts have been employed in asymmetric reactions such as Ni-catalyzed annulations,[19] Pd-catalyzed C–H activation,[20] Cu-catalyzed allylic alkylations[21] and conjugate borylations,[22] they were found to be ineffective, even at elevated reaction temperatures. We attribute this lack of reactivity to the high degree of steric hindrance and structural rigidity of these chiral NHC ligands, which could render oxidative addition challenging. In order to circumvent this issue, we examined less sterically bulky ligand salts to potentially enable oxidative addition, while still permitting selectivity in the enantiodetermining step. Using **L3.7**–**L3.9** we saw more promising results. Of these, **L3.9**, which has acyclic chiral centers in close proximity to the bound metal, gave the best combination of yield and enantioenrichment of **3.12** (23% yield with 39% ee). Whereas using a ligand salt with ethyl groups in place of methyl groups (i.e., **L3.10**) led to minimal change, more pronounced effects were seen by altering the phenyl ring on **L3.9**. For example, the use of **L3.11**, which contains bulky naphthyl groups, led to no reaction, whereas the use of **L3.12**–**L3.14** gave product **3.12** with higher enantioselectivity. Finally, the use of **L3.15**, the benzimidazolium derivative of **L3.14**, led to the formation of **3.12** in 18% yield with 75% ee. Importantly, the two most promising NHC salts, **L3.14** and **L3.15**, were not known prior to our investigations, and NHC salts **L3.9**, **L3.12**, and **L3.13** had not been used previously in nickel catalysis.

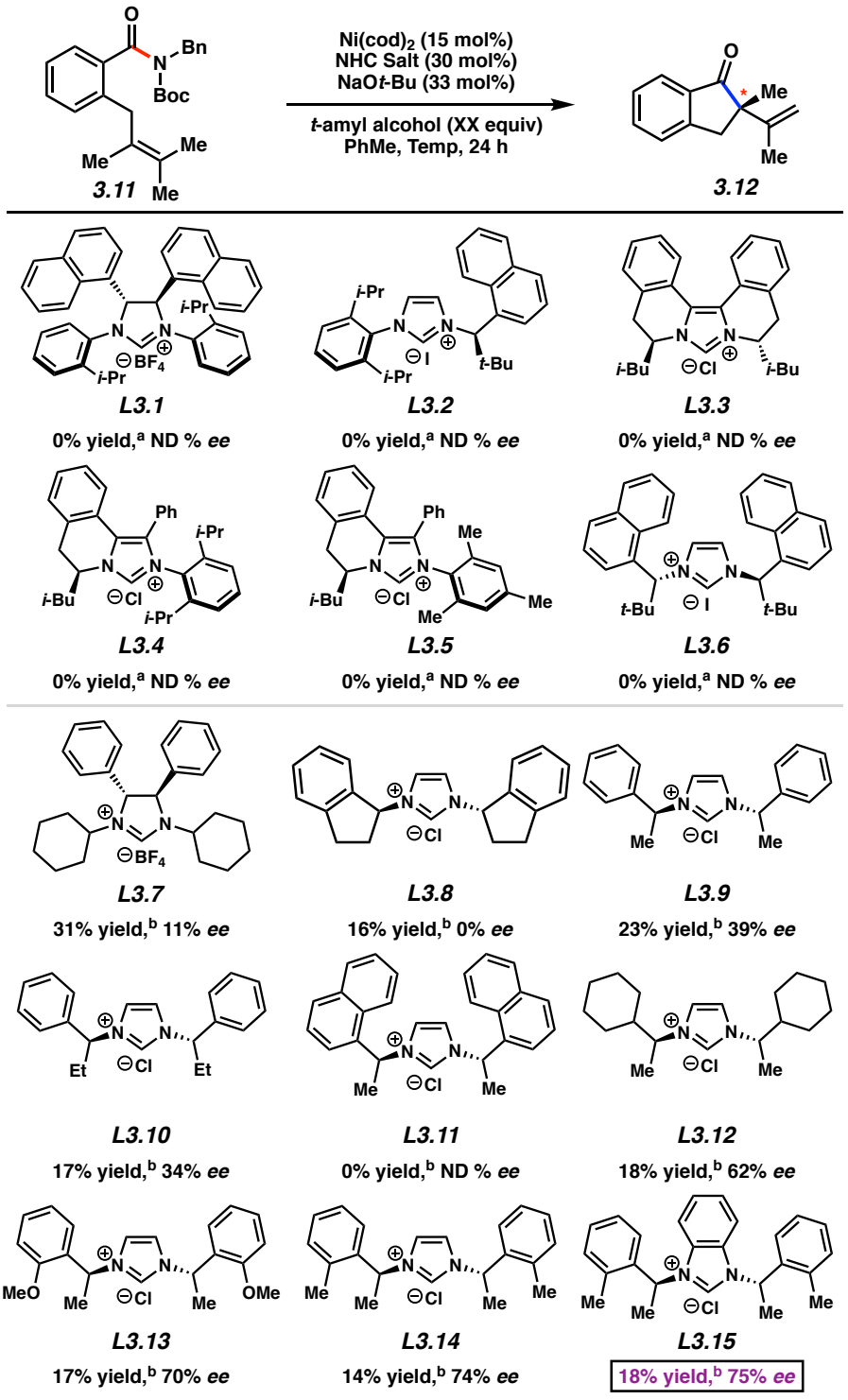


Figure 3.3. Survey of Chiral NHC salts with *in situ* free-basing. [a]Conditions: $Ni(cod)_2$ (15 mol%), NHC Salt (30 mol%), NaO*t*-Bu (33 mol%), PhMe (0.5 M), 100 °C; 24 h in a sealed vial. [b]Conditions: $Ni(cod)_2$ (15 mol%), NHC Salt (30 mol%), NaO*t*-Bu (33 mol%), *t*-amyl alcohol (3.0 equiv), PhMe, (0.5 M), 60 °C; 24 h in a sealed vial. [a,b]Yields determined by ^1H NMR using hexamethylbenzene as an external standard. ND is defined as not determined.

To better understand the influence of different olefin substitution patterns on enantioselectivity, we tested amide substrate **3.6** using the most promising ligands from our aforementioned studies of substrate **3.11** (Fig. 3.4). Specifically, amide **3.6** bears a more sterically congested olefin with the incorporation of an additional ring. Although the use of **L3.7** led to poor enantioselectivity, more promising results were observed using ligand salts **L3.9** and **L3.12**–**L3.15**. The use of **L3.15** produced the best combination of yield and enantiomeric excess, furnishing **3.9** in 32% yield and 88% ee. Although beyond the scope of our present study, these ligands may prove valuable in other applications, such as in the asymmetric reactions of other electrophiles that contain strong bonds.

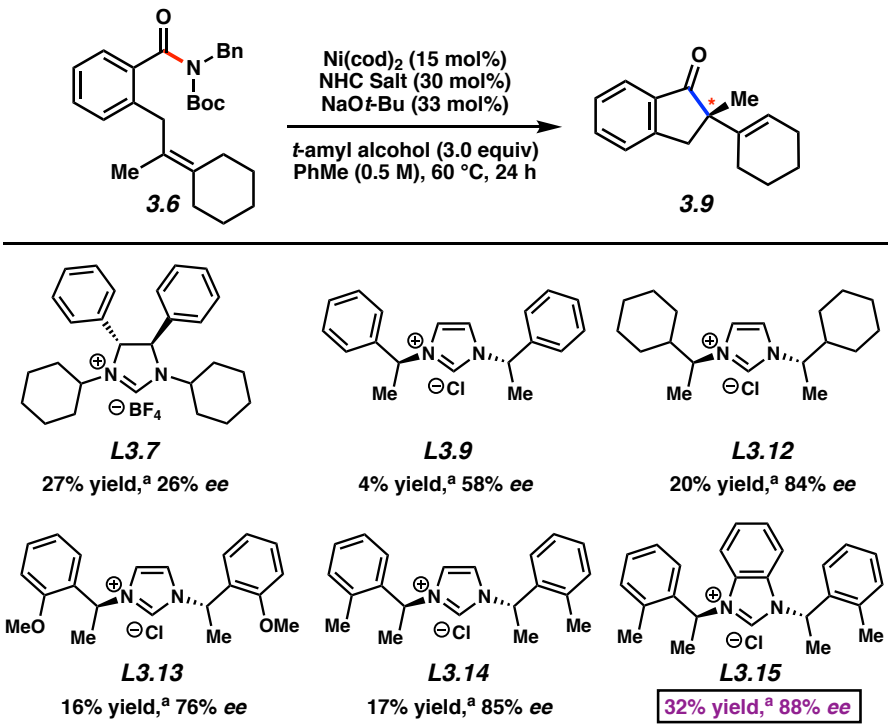


Figure 3.4. Results using select chiral NHC ligand salts with amide **3.6**. [a]Yields determined by ^{1}H NMR using hexamethylbenzene as an external standard.

We attempted an initial optimization, focusing on increasing the yield of the product, using substrate **3.6** with **L3.15**. Gratifyingly, this new chiral NHC salt, **L3.15**, can be readily synthesized from commercially available building blocks on gram-scale and is bench-stable, rendering it an

attractive choice for practical applications. Attempts to optimize the reaction by varying the stoichiometry of NaO*t*-Bu and the identity of the base did not lead to significant increase in yield (see section 3.8.2.2.2 for details). Exhaustive optimization with **L3.15** involving other reaction parameters, such as variation of amide *N*-substituents, solvents, and stoichiometric loading of reagents did not lead to significant catalytic turnover. Thus, in order to reduce variables in the reaction and mitigate potential unwanted base-mediated side pathways (see section 3.8.2.2.2 for details), we sought to generate the free carbene of **L3.15** and subsequently add it as a discrete reagent (Fig. 3.5). Accordingly, this would avoid the use of a base in the catalytic transformation. To our delight, carbene **3.10** could be generated in solution upon treatment of **L3.15** with KO*t*-Bu, analogous to a procedure previously reported by Cramer.[23] The identification of **3.10** was made using ^{13}C NMR, as **3.10** displays a diagnostic signal at 225.0 ppm. Carbene **3.10** was found to be stable under inert conditions in toluene for multiple weeks without any detectable dimerization.

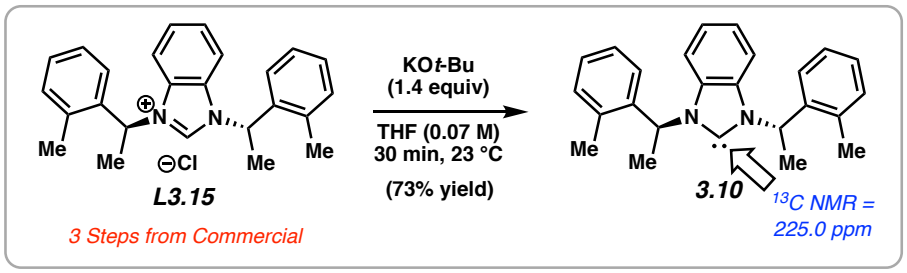
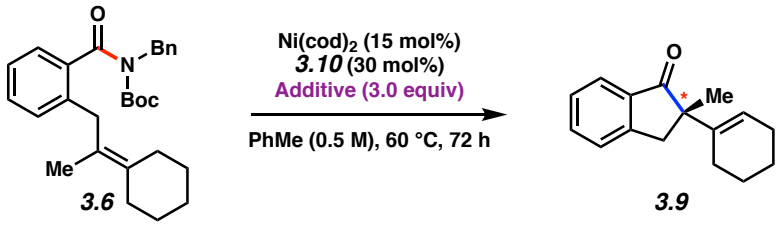


Figure 3.5. Generation of free carbene **3.10**.

Thorough variation of reaction parameters (e.g., variation of *N*-substitution,[24] temperature, solvent, catalyst loading) was performed in the absence of an additive, but did not lead to improved outcomes (see section 3.8.2.2.2 for details). We turned to examining additives, with inspiration from the literature.[25] Additionally, the improvement seen in employing *t*-amyl alcohol (**3.13**) as an additive (Fig. 3.6, entry 2) compared to the lower yield observed in the absence of additive (entry 1) signified that an additive could be important in increasing the conversion of the reaction. A

selection of results are shown in Fig. 3.6, with further results available in section 3.8.2.2.2. Whereas the use of other alcohols (e.g., **3.14**) was ultimately found to give comparable results, amine additives were generally found to be most impactful, with varying results.[26] For example, when primary amines **3.15** and **3.16** were evaluated, α-tertiary amine **3.16** was found to improve the yield of the reaction to 42%, whereas α-primary amine **3.15** inhibited product formation, giving only 4% yield of **3.9**. Moreover, the use of amines **3.17**–**3.19**, which represent acyclic secondary, tertiary, and diamines, respectively, did not lead to superior yields of **3.9**. Cyclic amines were also evaluated. Although the use of piperidine (**3.20**) as an additive was not very promising (entry 9), the employment of morpholine (**3.21**) led to complete consumption of substrate **3.6** and 42% yield of indanone **3.9** (entry 10). The majority of the remaining mass balance was comprised of an undesired morpholine transamidation side-product. As such, the equivalents of morpholine were reduced from three to one. Using these optimized conditions gave indanone **3.9** in 55% yield with 88% ee (entry 11). It is hypothesized that the additive may have an effect on either the rate of β-hydride elimination, potentially due to reduced steric bulk around the metal, or that it could facilitate regeneration of the Ni(0) catalyst. However, future mechanistic studies would be necessary to support either conclusion as to the effect of the amine additive on the turnover-limiting step of this reaction.[27,28] Nonetheless, the findings with regard to ligand optimization and additive evaluation should provide insight into effective reaction conditions for the activation of strong-bond electrophiles in asymmetric catalytic processes.



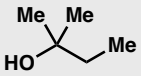
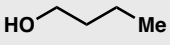
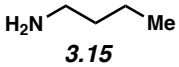
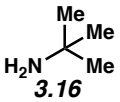
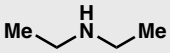
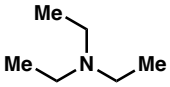
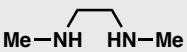
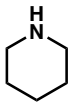
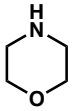
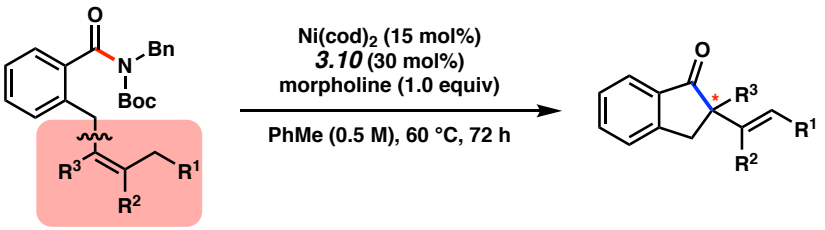
Entry	Additive	Recovered[a] *3.6*	Yield[a] of 3.*9*	% ee
1	-	67%	11%	ND
Alcohols				
2	 *3.13* tertiary	62%	24%	ND
3	 *3.14* primary	34%	27%	ND
Primary amines				
4	 *3.15* α-primary	44%	4%	ND
5	 *3.16* α-tertiary	40%	42%	88%
Secondary amine				
6	 *3.17*	30%	39%	ND
Tertiary amine				
7	 *3.18*	84%	5%	ND
Diamine				
8	 *3.19*	11%	34%	ND
Cyclic amines				
9	 *3.20*	7%	23%	ND
10	 *3.21*	0%	42%	89%
11[b]		0%	55%	88%

Figure 3.6. Survey of alcohol and amine additives in the transformation. [a]Conversions and yields determined by ^{1}H NMR using hexamethylbenzene as an external standard. [b]Morpholine (1.0 equiv).

3.5 Scope of Methodology

Several substrates bearing different olefin substitution patterns were evaluated in the transformation (Fig. 3.7). Cyclohexylidene substrate **3.6** underwent the desired enantioselective transformation to deliver **3.9** in 54% isolated yield and 88% ee. Additionally, we demonstrated the tolerance of heterocycles through the employment of amides **3.22** and **3.24**, which gave rise to products **3.23** and **3.25**, respectively, with good enantioenrichment, albeit in modest yields. Amide **3.26**, bearing a sterically bulky geminal dimethyl moiety, gave rise to spirocycle **3.27** in good yield and moderate enantiomeric excess (80% yield with 54% ee). Additionally, an acyclic olefin (entry 5) could be tolerated in the methodology, giving rise to indanone **3.12** in 41% yield with 78% ee. Although the scope of the transformation is currently limited, these examples demonstrate the potential for amides to serve as acyl electrophiles in enantioselective transformations with tolerance of heterocycles and tri- or tetra-substituted olefins.



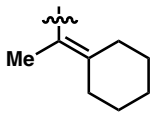
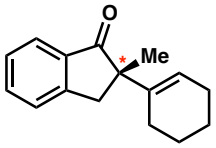
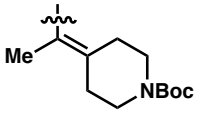
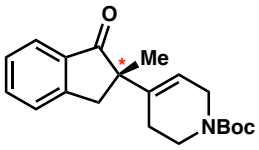
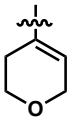
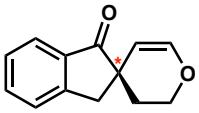
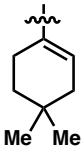
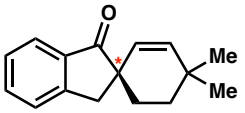
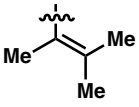
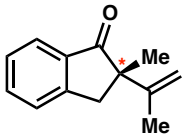
Entry	Alkene		Product		%Yield,% ee
1		*3.6*		*3.9*	54% yield 88% ee
2		*3.22*		*3.23*	36% yield 88% ee
3		*3.24*		*3.25*	36% yield 87% ee
4		*3.26*		*3.27*	80% yield 54% ee
5		*3.11*		*3.12*	41% yield 78% ee

Figure 3.7. Examples of methodology. Yields shown reflect the average of two isolation experiments.

3.6 Synthetic Elaboration of Indanone 3.9

The Mizoroki–Heck cyclization provides access to complex quaternary center-containing products that are well poised to undergo further synthetic elaboration. As shown in Fig. 3.8, we demonstrate this virtue through the elaboration of cyclization product **3.9** to several scaffolds, including stereochemically complex products. One key effort involved condensation of indanone **3.9** with *N*-brosyl hydrazine to give brosyl hydrazone **3.28**. This adduct could be crystallized,

which enabled the assignment of absolute stereochemistry through single crystal X-ray analysis. The absolute configuration at the quaternary stereocenter (in **3.28** and other derivatives of **3.9**) is as depicted throughout Fig. 3.8.

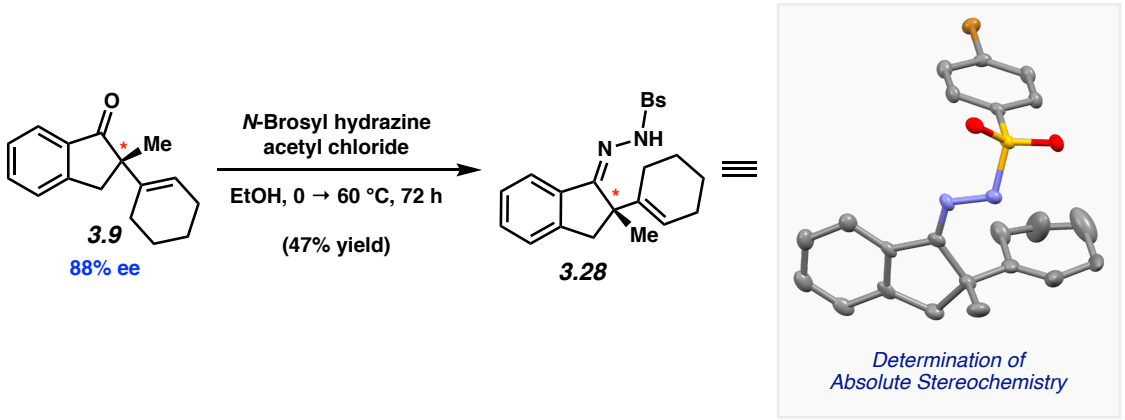


Figure 3.8. Determination of the absolute stereochemistry of **3.9**. See section 3.8.2.7 for experimental details.

Compounds **3.29**–**3.31** are additional derivatives of indanone **3.9** that each bear a defined quaternary stereocenter (Fig. 3.9). Although the scaffolds for these derivatives depart from that of **3.9**, each are readily accessible through the depicted sequence. Lactone **3.29** was obtained by reduction of the olefin using hydrogen-atom transfer (HAT) conditions, followed by Baeyer–Villiger oxidation. Using urea hydrogen peroxide, trifluoroacetic acid (TFA), and boron trifluoride etherate ($BF_3 \cdot OEt_2$), the product arising from the migration of the phenyl group was observed as the major regioisomer. Subsequent reduction of lactone **3.29** using lithium aluminum hydride led to ring cleavage, providing diol **3.30** in quantitative yield. Lastly, diol **3.30** underwent an intramolecular Mitsunobu reaction to form chromane **3.31**, a common motif in bioactive molecules and pharmaceuticals.[29] The elaboration of **3.9** to enantioenriched products **3.29**–**3.31** is reminiscent of the skeletal editing paradigm,[30] which has recently received significant interest from the synthetic community.

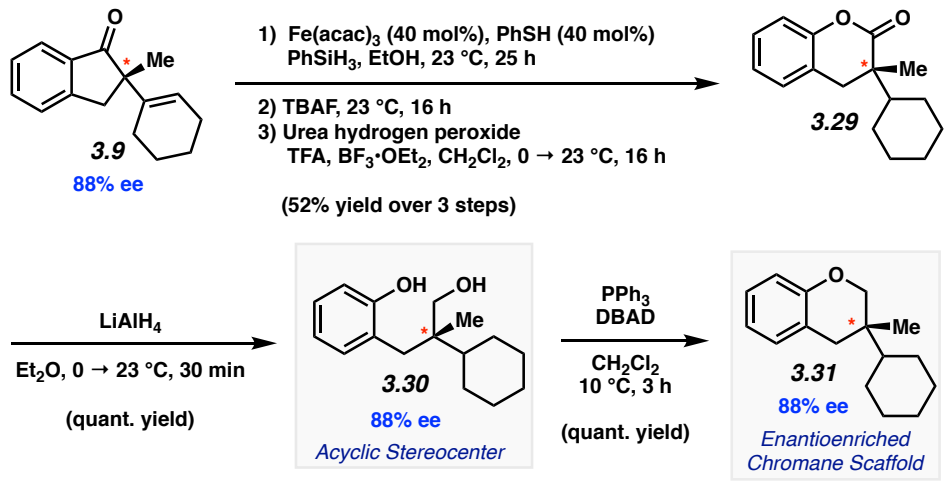


Figure 3.9. Synthetic elaboration of indanone **3.9** to skeletal editing derivatives **3.29**–**3.31.**

As reflected in the remaining sequence shown in Fig. 3.10, we sought to elaborate indanone **3.9** to enantioenriched products that bear additional rings and multiple stereocenters. Wittig homologation of **3.9** provided olefin **3.32** in nearly quantitative yield. A (3 + 2) cycloaddition of **3.32** with in situ-generated nitrile oxide **3.33** delivered spiroheterocycle **3.34**. The reaction proceeds with high chemoselectivity for the more reactive styrenyl olefin in **3.32**. Moreover, the cycloaddition proceeds diastereoselectively (5.3 : 1 dr), with a preference for the isomer shown, presumably by approach of the 1,3-dipole from the less sterically encumbered face of the styrenyl olefin. Finally, spiroheterocycle **3.34** could be elaborated further to isoxazolidine **3.35** and epoxides **3.36**. The former was obtained by 1,2-addition of allyl magnesium chloride, while the latter was accessed by epoxidation of the trisubstituted cyclic olefin. In addition to retaining the quaternary stereocenter generated in the Mizoroki–Heck cyclization, products **3.35** and **3.36** contain multiple stereocenters, as well as multiple heteroatoms, rings, and functional handles for further manipulation. The results shown in Fig. 3.10 underscore the notion that a range of highly complex, enantioenriched scaffolds can now be accessed from amide precursors, ultimately stemming from our methodology involving amide C–N bond activation and asymmetric catalysis.

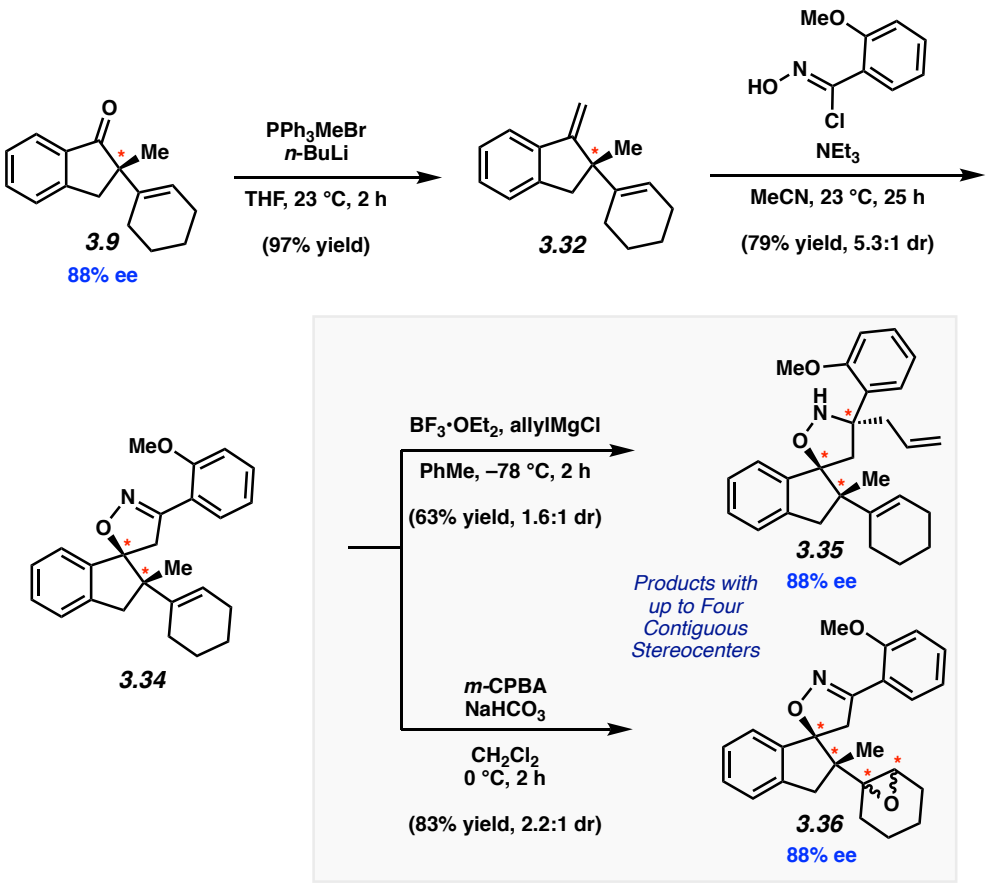


Figure 3.10. Synthetic elaboration of indanone **3.9** to complex products **3.35** and **3.36**.

3.7 Conclusion

We have demonstrated that amides can serve as cross-coupling partners in the asymmetric transition-metal-catalyzed Mizoroki–Heck cyclization. This is notable, as more than a hundred amide cross-couplings involving C–N bond cleavage by a transition metal catalyst have been reported since 2015, but none are asymmetric. Our transformation was enabled by the development of a new NHC ligand **3.10**, as well as extensive reaction optimization. Through cyclization and subsequent synthetic elaborations, we show that a variety of enantioenriched polycyclic products containing difficult-to-access quaternary centers can be made, including complex compounds with up to four stereogenic centers (i.e., **3.36**). Future studies aim to expand the scope of this reaction and develop new methods that rely on the use of amides in C–N bond cleavage reactions using

asymmetric transition metal catalysis. Our studies challenge the conventional understanding of how amides can be used in chemical synthesis and, more broadly, should encourage the study of other non-traditional electrophiles in asymmetric transformations by expanding the library of, and providing knowledge on, the types of ligands that could be employed in such transformations.

3.8 Experimental Section

3.8.1 Materials and Methods

Unless stated otherwise, reactions were conducted in flame-dried glassware under an atmosphere of nitrogen, and commercially obtained reagents were used as received unless otherwise specified. Anhydrous solvents were either freshly distilled or passed through activated alumina columns, unless otherwise stated. Non-commercially available substrates were synthesized according to known preparations or following protocols specified in the Experimental Procedures. Prior to use in carbene generation or nickel-catalyzed reactions, toluene (PhMe) was distilled over CaH_2 and degassed by five freeze pump thaw cycles. Prior to use in carbene generation or nickel-catalyzed reactions, trifluorotoluene ($PhCF_3$), tetrahydrofuran (THF), 1,2-dimethoxyethane (DME), 1,4-dioxane (dioxane), and acetonitrile (MeCN) were passed through an activated alumina column and degassed by five freeze-pump-thaw cycles. Dichloromethane (CH_2Cl_2), diethyl ether (Et_2O), and triethylamine (NEt_3) were passed through an activated alumina column and ethanol (EtOH) was stored over activated 2Å molecular sieves prior to use. *t*-Amyl alcohol (**3.13**) was distilled over K_2CO_3 and stored over activated 2Å molecular sieves for 24 h prior to use. Additives were distilled and degassed prior to use in nickel-catalyzed reactions unless otherwise noted: 1-butanol (**3.14**), *n*-butylamine (**3.15**), *t*-butylamine (**3.16**), *N*,*N*′-dimethylethylenediamine (**3.19**), piperidine (**3.20**), morpholine (**3.21**), aniline (**3.37**), *N*,*N*-dimethylaniline (**3.38**), 4-methylmorpholine (**3.39**), pyrrolidine (**3.40**), 2-methoxyethan-1-amine (**3.41**), diisopropylamine (**3.42**), 1-methylpiperazine (**3.43**), 2,6,6-tetramethyl piperidine (**3.44**), benzylamine (**3.45**), diethylamine (**3.17**), and triethylamine (**3.18**). Diphenylamine (**3.46**) and triphenylamine (**3.47**) were purified by flash chromatography on silica and then recrystallized prior to use. Piperazine (**3.48**) was recrystallized prior to use. Phenol (**3.49**) and potassium carbonate

(K_2CO_3) were obtained from Acros Organics and used as received. Amine **(S)-3.50** was purchased from Enamine Building Blocks and used as received. Ammonium salt **(S)-3.51** was purchased from Ambeed and used as received. Amine **(+)-3.52**, amine **(+)-3.53**, **L3.20**, formaldehyde (37 wt% in H_2O, 1.0 equiv), glyoxal (40 wt% in H_2O, 1.0 equiv), (±)-BINAP, concentrated HCl, potassium *tert*-butoxide (KO*t*-Bu), lithium *tert*-butoxide (LiOt-Bu), sodium *tert*-pentoxide (NaO*t*-amyl), lithium bis(trimethylsilyl)amide (LiHMDS), potassium bis(trimethylsilyl)amide (KHMDS), sodium bis(trimethylsilyl)amide (NaHMDS), potassium phosphate tribasic (K_3PO_4), cesium carbonate (Cs_2CO_3), methyl chloroformate, pyridine, $MgCl_2$, tetrabutylammonium bromide (TBAB), dimethylacetamide (DMA), thiophenol (PhSH), phenylsilane ($PhSiH_3$), tetrabutylammonium fluoride (TBAF) (1.0 M in THF), urea hydrogen peroxide TFA, BF_3•OEt_2, *n*-butyllithium (*n*-BuLi, 2.4 M in hexanes), allylMgCl (2.0 M in THF), *meta*-chloroperoxybenzoic acid (*m*-CPBA), $NaHCO_3$, and 4-bromobenzenesulfonohydrazide were all purchased from Sigma-Aldrich and used as received. Amine **(–)-3.54**, amine **(–)-3.55**, amine **(–)-3.56**, acetic acid (AcOH), 1,2-dibromobenzene, $LiAlH_4$, triethyl orthoformate ($CH(OEt)_3$), triphenylphosphine (PPh_3), and acetyl chloride were obtained from Thermofisher Scientific. $Pd_2(dba)_3$, sodium *tert*-butoxide (NaOt-Bu), bis(1,5-cyclooctadiene)nickel(0) ($Ni(cod)_2$), NiI_2, Zn^0 dust**,** 1,3-dicyclohexylbenzimidazolium chloride (Benz-ICy•HCl), and iron(III) acetylacetonate ($Fe(acac)_3$) were obtained from Strem Chemicals. Di-*tert*-butyl azodicarboxylate (DBAD) and methyltriphenylphosphonium bromide (PPh_3MeBr) were obtained from CombiBlocks. Reaction temperatures at or above 23 °C were controlled using an IKAmag temperature modulator, and unless stated otherwise, performed at room temperature (approximately 23 °C). Thin-layer chromatography (TLC) was conducted with EMD gel 60 F_{254} pre-coated plates (0.25 mm for analytical chromatography and 0.50 mm for preparative chromatography) and visualized using a

combination of UV, anisaldehyde, and potassium permanganate staining techniques. Silicycle Siliaflash P60 (particle size 40–63 μm) or Brockman Grade activated neutral alumina (58Å pore size) were used for flash column chromatography unless otherwise specified. ^{1}H-NMR and 2D-NOESY spectra were recorded on Bruker spectrometers (at 500 and 600 MHz) and are reported relative to the residual solvent signal. Data for ^{1}H-NMR spectra are reported as follows: chemical shift (δ ppm), multiplicity, coupling constant (Hz), and integration. ^{13}C-NMR spectra were recorded on Bruker spectrometers (at 125 and 150 MHz) and are reported relative to the residual solvent signal. Data for ^{13}C-NMR spectra are reported in terms of chemical shift (δ ppm) and, when necessary, multiplicity, and coupling constant (Hz). ^{19}F-NMR spectra were recorded on Bruker spectrometers (at 282 MHz) and are reported in terms of chemical shift (δ ppm), multiplicity, and integration. IR spectra were recorded on a Perkin-Elmer UATR Two FT-IR spectrometer and are reported in terms of frequency absorption (cm^{-1}). ESI-TOF measurements were carried out in positive ionization mode on a Waters LCT-Premier XE Time of Flight Instrument controlled by MassLynx 4.1 software (Waters Corporation, Milford MA). The instrument was equipped with the Multi Mode Ionization source operated in the electrospray mode. A solution of Leucine Enkephalin (Sigma Chemical, L9133) was used in the Lock-Spray to obtain accurate mass measurements. Samples were infused using direct loop injection on a Waters Acquity UPLC system. GC-MS measurements were carried out using an Agilent Model 7693 Autosampler, 7890B Gas Chromatograph, and 7250 Q-TOF Mass Selective Detector in the Electron Ionization mode. Sample injection was carried out in split mode with inlet temperature set to 280 °C. Separation was carried out on an Agilent HP5-MS column with dimensions 30m x 250 µm x 0.25 µm. Ultra High Purity Grade He (Airgas) was used as carrier gas with the flow set to 1.1 mL/min in constant flow mode. The initial oven temperature was set to 70 °C for 1 min

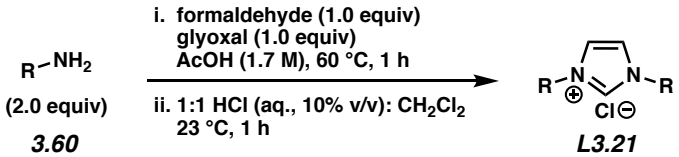
followed by a 20 °C/min ramp to a final temperature of 300 °C which was maintained for 4 min. A 3.0 min solvent delay was used. EI energy was set to 70 eV. The MSD was set to scan the 50–500 m/z range. Data collection and analysis were performed using Mass Hunter Acquisition and Qualitative Analysis software (Agilent). Optical rotations were measured with a Rudolf Autopol III Automatic Polarimeter. Determination of enantiopurity was carried out on a JASCO SFC (supercritical fluid chromatography) and an Agilent 1260 SFC using Daicel ChiralPak IB N-3, IC, and ID columns. Data for SFC chromatograms are reported in enantiomeric excess (ee). Diastereomeric ratios (dr) and regioisomeric ratios (rr) were determined by ^{1}H analysis of crude reaction mixtures.

Ligand salts **L3.1–L3.6** were synthesized by members of the lab of Professor Nicolai Cramer (EPFL) and were kindly donated for our usage. Ligand salts **L3.7**,[31] **L3.9**,[32] **L3.10**,[33] **L3.11**,[33] **L3.12**,[34] **L3.13**[33] and ligand **3.58**[35] were synthesized according to known literature procedures. Amides **3.6**, **3.11**, and **3.22** and indanones **3.9**, **3.12**, and **3.23** are known compounds.[7j] Nitrile oxide precursor **3.59** was synthesized according to a known procedure.[36] Spectral data matched those reported in literature.

3.8.2 Experimental Procedures

3.8.2.1 Ligand Syntheses

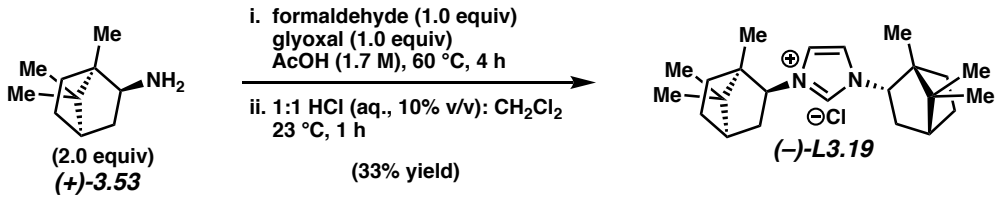
General procedure 3.1 for the syntheses of imidazolium salts:



Imidazoliums L3.21. To a solution of amine **3.60** (2.0 equiv) in AcOH (1.7 M) was added formaldehyde (37 wt% in H_2O, 1.0 equiv) and glyoxal (40 wt% in H_2O, 1.0 equiv). The reaction was heated to 60 °C in a preheated aluminum block and stirred at this temperature for 1 h. The

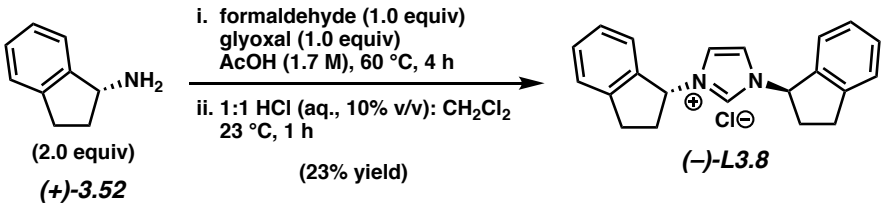
reaction was then cooled to 23 °C and transferred to a round bottom flask containing a stir bar. The mixture was diluted with CH_2Cl_2 (50 mL) and aqueous HCl (10% v/v, 50 mL) was added. The resulting biphasic mixture was stirred vigorously at 23 °C. After 1 h of stirring, the organic and aqueous layers were separated, and the aqueous layer was extracted with CH_2Cl_2 (2 x 30 mL). The combined organic layers were dried with $MgSO_4$, filtered, and concentrated under reduced pressure. The crude material was purified by flash chromatography to provide imidazoliums **L3.21**.

Any modification of the reaction conditions shown in the general procedure above are specified in the following schemes.

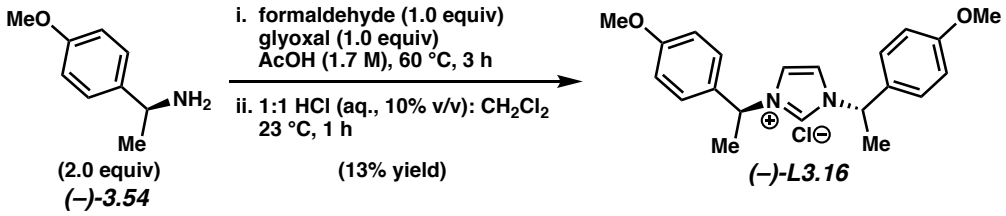


Imidazolium (–)-L3.19. Followed a modified version of General Procedure 3.1 using **(+)-3.53** (320 mg, 2.09 mmol, 2.0 equiv) by altering the reaction time in the first step to 4 h. Purification by flash chromatography on silica (14:1 CH_2Cl_2:MeOH) afforded imidazolium **(–)-L3.19** (110 mg, 0.34 mmol, 33% yield) as an off-white powder. **Imidazolium (–)-L3.19**: Mp: >250 °C; R_f 0.09 (9:1 CH_2Cl_2:MeOH); ^{1}H NMR (500 MHz, $CDCl_3$): δ 11.30 (s, 1H), 7.22 (s, 2H), 5.07 (dd, J = 12.0, 2.8, 2H), 2.54 (ddt, J = 15.0, 11.4, 3.8, 2H), 1.96–1.87 (m, 3H), 1.84 (dd, J = 14.4, 4.8, 2H), 1.81–1.74 (m, 1H), 1.68–1.59 (m, 2H), 1.49–1.38 (m, 2H), 1.14–1.03 (m, 8H), 0.97 (s, 6H), 0.96 (s, 6H); ^{13}C NMR (125 MHz, $CDCl_3$): δ 139.9, 120.7, 66.8, 51.1, 49.8, 44.8, 34.3, 28.3, 27.7, 20.0,

18.7, 13.8; IR (film): 3051, 2951, 2888, 1544, 1392 cm^{-1}; HRMS-ESI (*m/z*) $[M - Cl]^+$ calcd for $C_{23}H_{37}N_2^+$, 341.2947; found 341.2957; $[\alpha]^{24.3}_D$–24.0° (c = 1.00, CH_2Cl_2).

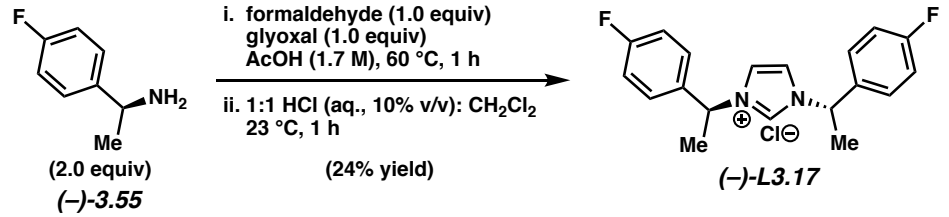


Imidazolium (–)-L3.8. Followed a modified version of General Procedure 3.1 using **(+)-3.52** (300 mg, 2.25 mmol, 2.0 equiv) by altering the reaction time in the first step to 4 h. Purification by flash chromatography on neutral alumina (50:3 EtOAc:*i*-PrOH → 1:1 EtOAc:*i*-PrOH) afforded imidazolium **(–)-L3.8** (89 mg, 0.26 mmol, 23% yield) as an off-white powder. **Imidazolium (–)-L3.8**: Mp: 58 °C; R_f 0.40 (9:1 CH_2Cl_2:MeOH); ^{1}H NMR (500 MHz, $CDCl_3$): δ 11.62–11.57 (m, 1H), 7.39–7.33 (m, 4H), 7.29–7.22 (m, 4H), 6.79 (d, *J* = 1.6, 2H), 6.53 (dd, *J* = 8.0, 5.4, 2H), 3.17 (ddd, *J* = 16.3, 8.7, 5.7, 2H), 3.07 (ddd, *J* = 16.3, 8.6, 5.8, 2H), 2.98 (dtd, *J* = 13.6, 8.7, 5.8, 2H), 2.28 (ddt, *J* = 13.6, 8.6, 5.7, 2H); ^{13}C NMR (125 MHz, $CDCl_3$): δ 144.3, 138.6, 138.2, 130.1, 127.9, 125.7, 125.2, 119.5, 65.2, 34.7, 30.5; IR (film): 3042, 2949, 1630, 1547, 1459 cm^{-1}; HRMS-ESI (*m/z*) $[M - Cl]^+$ calcd for $C_{21}H_{21}N_2^+$, 301.1705; found 301.1710; $[\alpha]^{24.5}_D$–14.0° (c = 1.00, CH_2Cl_2).

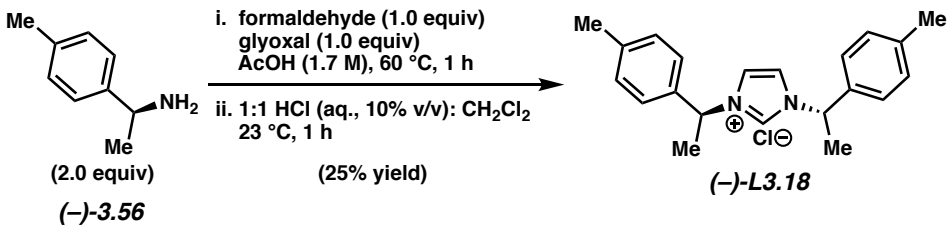


Imidazolium (–)-L3.16. Followed a modified version of General Procedure 3.1 using **(–)-3.54** (500 mg, 3.31 mmol, 2.0 equiv) by altering the reaction time in the first step to 3 h. Purification by flash chromatography on neutral alumina (20:1 EtOAc:*i*-PrOH → 1:1 EtOAc:*i*-PrOH) afforded imidazolium **(–)-L3.16** (80 mg, 0.22 mmol, 13% yield) as a light-yellow solid. **Imidazolium (–)-**

L3.16: Mp: 79 °C; R_f 0.35 (9:1 CH_2Cl_2:MeOH); ^1H NMR (500 MHz, $CDCl_3$): δ 11.61–11.57 (m, 1H), 7.44–7.38 (m, 4H), 6.95–6.88 (m, 6H), 5.98 (q, *J* = 7.0, 2H), 3.80 (s, 6H), 2.01 (d, *J* = 7.0, 6H); ^{13}C NMR (125 MHz, $CDCl_3$): δ 160.3, 137.3, 129.7, 128.6, 119.4, 114.7, 59.5, 55.4, 21.3; IR (film): 3066, 2982, 1515, 1249, 1148 cm^{-1}; HRMS-ESI (*m/z*) $[M - Cl]^+$ calcd for $C_{21}H_{25}N_2O_2^+$, 337.1916; found 337.1923; $[\alpha]^{23.9}_D$–58.0° (c = 1.00, CH_2Cl_2).

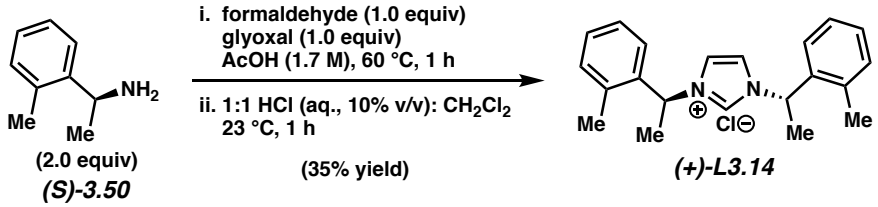


Imidazolium (–)-L3.17. Followed General Procedure 3.1 using **(–)-3.55** (535 mg, 3.84 mmol, 2.0 equiv). Purification by flash chromatography on neutral alumina (15:1 EtOAc:*i*-PrOH → 1:2 EtOAc:*i*-PrOH) afforded imidazolium **(–)-L3.17** (160 mg, 0.46 mmol, 24% yield) as an off-white solid. **Imidazolium (–)-L3.17**: Mp: 177–178 °C; R_f 0.15 (9:1 CH_2Cl_2:MeOH); ^1H NMR (500 MHz, $CDCl_3$): δ 11.75 (s, 1H), 7.55–7.48 (m, 4H), 7.13–7.06 (m, 4H), 7.02–6.96 (m, 2H), 6.07 (q, *J* = 7.0, 2H), 2.03 (d, *J* = 7.1, 6H); ^{13}C NMR (125 MHz, $CDCl_3$): δ 163.3 (d, *J* = 249.1), 137.8, 133.7 (d, *J* = 3.3), 129.3 (d, *J* = 8.5), 119.7, 116.7 (d, *J* = 21.9), 59.4, 21.3; ^{19}F NMR (282 MHz, $CDCl_3$): δ –111.2 (m, 2F); IR (film): 3064, 2987, 1604, 1511, 1226 cm^{-1}; HRMS-ESI (*m/z*) $[M - Cl]^+$ calcd for $C_{19}H_{19}F_2N_2^+$, 313.1516; found 313.1527; $[\alpha]^{24.0}_D$–36.0° (c = 1.00, CH_2Cl_2).



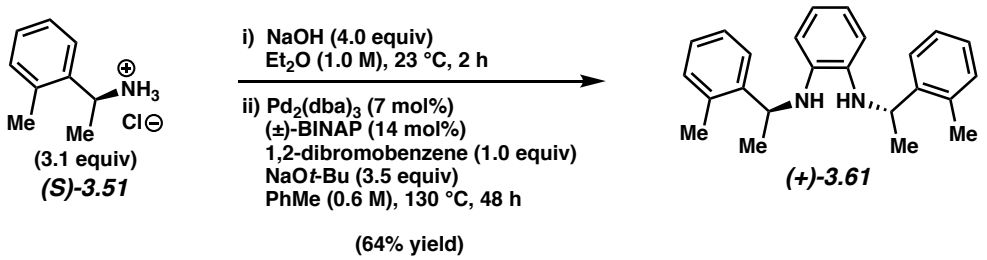
Imidazolium (–)-L3.18. Followed General Procedure 3.1 using **(–)-3.56** (500 mg, 3.70 mmol, 2.0 equiv). Purification by flash chromatography on neutral alumina (15:1 EtOAc:*i*-PrOH → 1:1

EtOAc:*i*-PrOH) afforded imidazolium **(–)-L3.18** (160 mg, 0.46 mmol, 25% yield) as a white solid. **Imidazolium (–)-L3.18**: Mp: 87–89 °C; R_f 0.45 (9:1 CH_2Cl_2:MeOH); ^{1}H NMR (500 MHz, $CDCl_3$): δ 11.61 (s, 1H), 7.33 (d, *J* = 8.0, 4H), 7.20 (d, *J* = 8.0, 4H), 6.96–6.92 (m, 2H), 6.00 (q, *J* = 6.9, 2H), 2.34 (s, 6H), 2.01 (d, J = 6.9, 6H); ^{13}C NMR (125 MHz, $CDCl_3$): δ 139.6, 137.6, 134.9, 130.2, 127.2, 119.7, 59.8, 21.4, 21.3; IR (film): 3060, 2982, 1614, 1546, 1150 cm^{-1}; HRMS-ESI (*m/z*) [M – Cl]$^+$ calcd for $C_{21}H_{25}N_2^+$, 305.2018; found 305.2033; $[\alpha]^{23.7}_D$–44.0° (c = 1.00, CH_2Cl_2).



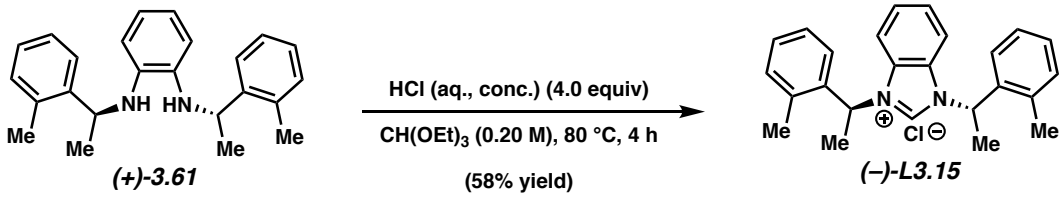
Imidazolium L3.14. Followed General Procedure 3.1 using **(S)-3.50** (590 mg, 4.36 mmol, 2.0 equiv). Purification by flash chromatography on neutral alumina (25:1 EtOAc:*i*-PrOH → 1:1 EtOAc:*i*-PrOH) afforded imidazolium **L3.14** (260 mg, 0.76 mmol, 35% yield) as a beige solid. **Imidazolium L3.14**: Mp: 146–147 °C; R_f 0.10 (9:1 CH_2Cl_2:MeOH); ^{1}H NMR (500 MHz, $CDCl_3$): δ 11.65 (s, 1H), 7.30–7.23 (m, 6H), 7.22–7.18 (m, 2H), 6.90–6.85 (m, 2H), 6.22 (q, *J* = 7.0, 2H), 2.36 (s, 6H), 2.04 (d, *J* = 7.0, 6H); ^{13}C NMR (125 MHz, $CDCl_3$): δ 138.2, 136.7, 135.8, 131.7, 129.5, 127.1, 125.8, 120.1, 56.9, 21.7, 19.5; IR (film): 3064, 2981, 1629, 1544, 1462 cm^{-1}; HRMS-ESI (*m/z*) [M – Cl]$^+$ calcd for $C_{21}H_{25}N_2^+$, 305.2018; found 305.2032; $[\alpha]^{23.3}_D$+8.0° (c = 1.00, CH_2Cl_2).

Synthesis of benzimidazolium salt L3.15:



Diamine (+)-3.61. To a flask containing a stir bar and **(S)-3.51** (4.73 g, 27.6 mmol, 3.1 equiv) in Et_2O (27.6 mL, 1.0 M) was added aqueous 1.0 M NaOH (55 mL, 2.0 equiv). The resulting mixture was stirred vigorously at 23 °C for 2 h. After this time, the organic and aqueous layers were separated and the aqueous layer was extracted with Et_2O (2 x 30 mL). The combined organic layers were dried with Na_2SO_4, filtered, and concentrated under reduced pressure. The resulting amine was immediately transferred to a flame-dried 8-dram vial, secured with a septum cap, and purged with an inlet needle using N_2 and an outlet needle open to air for 5 min. Subsequently, 1,2-dibromobenzene (1.96 g, 8.29 mmol, 1.0 equiv) was added to the vial. A separate 50 mL pressure tube containing a stir bar was fitted with a septum, flame-dried under reduced pressure, and backfilled with N_2. The 8-dram vial and pressure tube were then brought into a glovebox. In the glovebox, $Pd_2(dba)_3$ (529 mg, 0.578 mmol, 7 mol%), (±)-BINAP (720 mg, 1.16 mmol, 14 mol%), and toluene (7 mL) were added to the pressure tube. The tube was sealed and prestirred for 15 minutes at 130 °C in a preheated aluminum block in the glovebox. After this time, the reaction vessel was allowed to cool to 23 °C and the amine and 1,2-dibromobenzene mixture were transferred to the reaction tube using toluene (7 mL, 0.6 M). Then, NaO*t*-Bu (2.78 g, 28.9 mmol, 3.5 equiv) was added to the pressure tube, which was then sealed and brought out of the glovebox. The reaction was then heated to 130 °C in an oil bath and stirred at this temperature for 48 h. After this time, the reaction was allowed to cool to 23 °C and was filtered over a pad of Celite, eluting

with EtOAc (250 mL). The eluate was concentrated under reduced pressure and the crude material was purified by flash chromatography on silica (4:1 hexanes:CH_2Cl_2 → 3:2 hexanes:CH_2Cl_2) to afford diamine **(+)-3.61** (1.83 g, 5.31 mmol, 64% yield) as a white solid. **Diamine (+)-3.61**: Mp: 94–95 °C; R_f 0.35 (4:1 CH_2Cl_2:MeOH); ^{1}H NMR (500 MHz, $CDCl_3$): δ 7.51–7.45 (m, 2H), 7.20–7.11 (m, 6H), 6.56 (dt, *J* = 9.5, 3.8, 2H), 6.30 (dt, *J* = 9.5, 3.8, 2H), 4.69 (q, *J* = 6.5, 2H), 3.72 (s, 2H), 2.46 (s, 6H), 1.54 (d, *J* = 6.5, 6H); ^{13}C NMR (125 MHz, $CDCl_3$): δ 143.0, 136.4, 134.6, 130.7, 126.7, 124.8, 119.2, 113.3, 50.1, 23.5, 19.2 (11 of 12 signals observed); IR (film): 3346, 3022, 2965, 1599, 1508 cm^{-1}; HRMS-ESI (*m/z*) $[M + H]^+$ calcd for $C_{24}H_{29}N_2^+$, 345.2331; found 345.2335; $[\alpha]^{25.9}_D$+308.0° (c = 1.00, CH_2Cl_2).



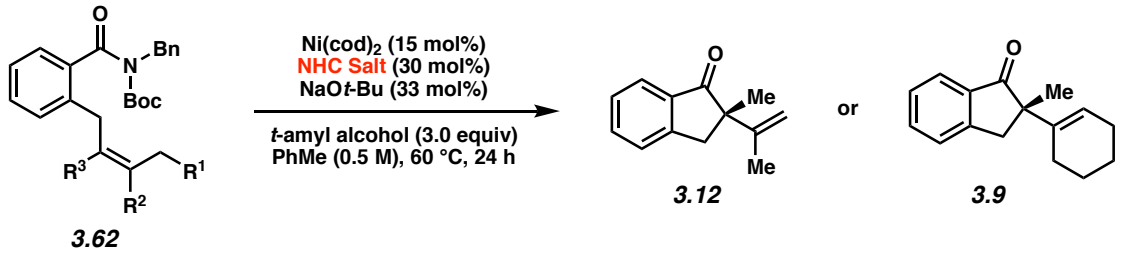
Benzimidazolium (–)-L3.15. To a round bottom flask containing a stir bar was added diamine **(+)-3.61** (1.83 g, 5.31 mmol, 1.0 equiv), followed by $CH(OEt)_3$ (26.6 mL, 0.20 M). Then, concentrated aqueous HCl (12 M, 1.8 mL, 21.2 mmol, 4.0 equiv) was added to the reaction vial. The reaction flask was fitted with an air condenser, which was capped with a septum that was pierced with a needle and left open to air. The resulting reaction was heated to 80 °C in an oil bath and stirred for 4 h. After this time, the reaction was allowed to cool to 23 °C and the reaction mixture was loaded directly onto a column and purification by flash chromatography on silica (EtOAc → 4:1 EtOAc:MeOH) affording an oily residue containing benzimidazolium (–)-**L3.15**. The resulting salt was crystallized by solvent diffusion after transferring the oily residue to a vial and dissolving it in MeOH (2 mL) followed by slow addition of Et_2O (10 mL) down the side of the vial. The resulting salt was allowed to crystallize over 14 h at –20 °C, after which, the mother

liquor was decanted and the crystals were washed with cold Et_2O (10 mL), providing benzimidazolium (–)-**L3.15** (1.20 g, 3.08 mmol, 58% yield) as a white crystalline solid. **Benzimidazolium** (–)-**L3.15**: Mp: 234–235 °C; R_f 0.15 (9:1 CH_2Cl_2:MeOH); ^{1}H NMR (500 MHz, $CDCl_3$): δ 12.37 (s, 1H), 7.39–7.34 (m, 2H), 7.31–7.27 (m, 2H), 7.26–7.24 (m, 4H), 7.22–7.18 (m, 2H), 7.17–7.14 (m, 2H), 6.47 (q, J = 6.9, 2H), 2.43 (s, 6H), 2.31 (d, J = 6.9, 6H); ^{13}C NMR (125 MHz, $CDCl_3$): δ 143.4, 135.8, 135.6, 131.5, 131.2, 129.1, 127.2, 126.6, 125.8, 114.2, 56.6, 20.9, 19.6; IR (film): 3112, 2979, 1552, 1462, 1249 cm^{-1}; HRMS-ESI (*m/z*) [M – Cl]$^+$ calcd for $C_{25}H_{27}N_2^+$, 355.2174; found 355.2184; $[\alpha]^{22.3}_D$–14.0° (c = 1.00, CH_2Cl_2).

3.8.2.2 Reaction Discovery

3.8.2.2.1 Ligand Optimization

General procedure 3.2 for ligand optimization



A flame-dried 1-dram vial containing a stir bar was charged with amide **3.62** (34.3 mg, 0.087 mmol, 1.0 equiv). The vial was brought into a glovebox and charged sequentially with $Ni(cod)_2$ (3.6 mg, 0.013 mmol, 15 mol%), NHC salt (0.026 mmol, 30 mol%), NaO*t*-Bu (2.8 mg, 0.029 mmol, 33 mol%), toluene (0.18 mL, 0.5 M), and *t*-amyl alcohol (29 μL, 0.26 mmol, 3.0 equiv). The vial was then sealed with a Teflon-lined screw cap, removed from the glovebox, the gap between the cap and the vial was sealed with electrical tape, and the vial was stirred at 60 °C for 24 h. After cooling to 23 °C, the mixture was filtered through a plug of silica, eluting with EtOAc (10 mL). The eluate was concentrated and then analyzed by ^{1}H NMR using hexamethylbenzene

as an external standard. Purification by preparative thin layer silica chromatography (3:1 hexanes:EtOAc) afforded analytical samples of indanones **3.12** or **3.9**, which were then subjected to analysis by supercritical fluid chromatography to determine enantiomeric excess.

*The absolute stereochemistry shown for **3.12** and **3.9** is not necessarily representative of the major enantiomer observed for all ligands examined.*

A range of ligands (see Figure 3.11 below for structures) were examined using General Procedure 3.2, and results of these reactions appear below in Table 3.1. Apart from **L3.20**, which is commercially available, all chiral NHC salts in Table 3.1 were synthesized according to the procedures above or using known procedures referenced in the Materials and Methods section 3.8.1.

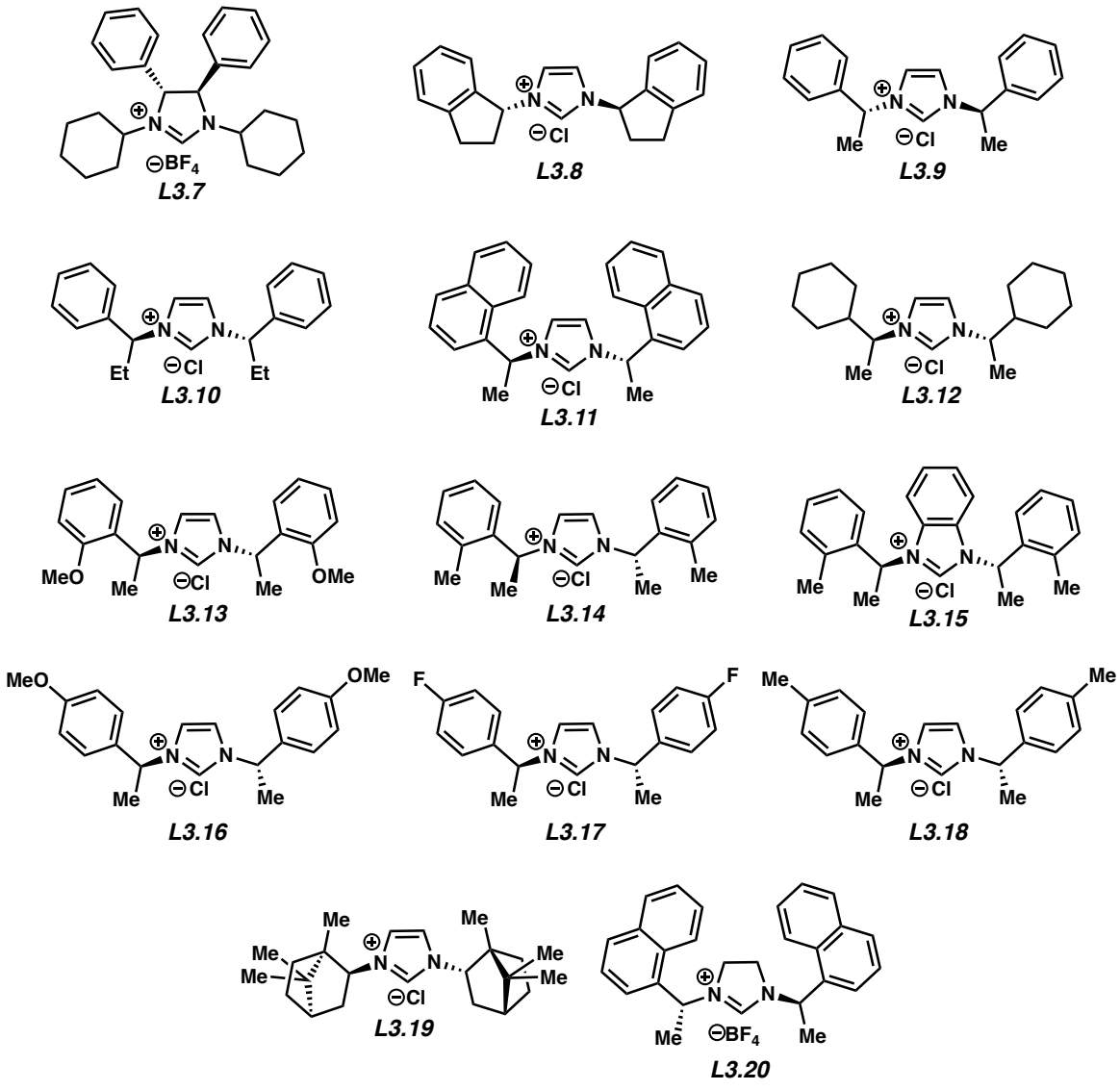
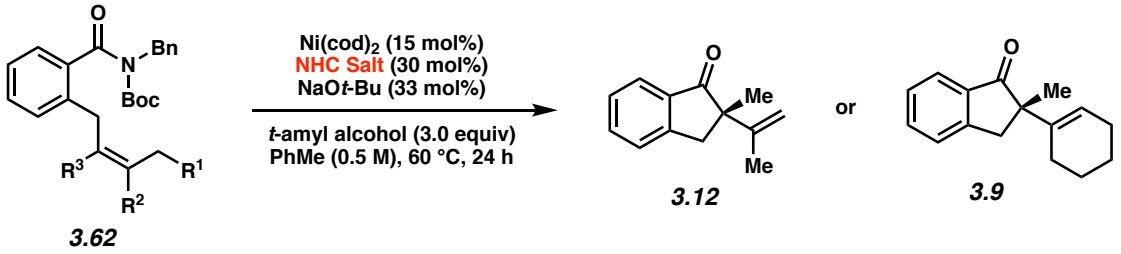


Figure 3.11. NHC salts evaluated during asymmetric reaction development.

Table 3.1. Ligand evaluation results. See Figure 3.11 above for NHC salts.

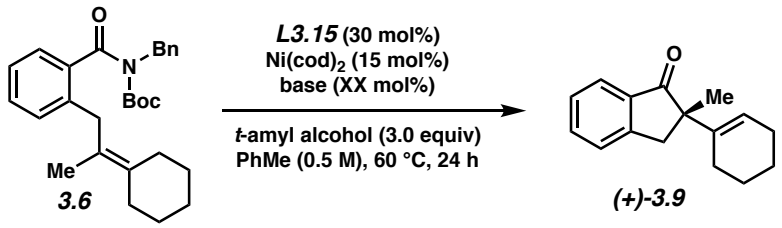


Entry	NHC Salt	Yield of 3.12[a]	% ee of 3.12	Yield of 3.9[a]	% ee of 3.9
1	**L3.7**	31%	11%	27%	26%
2	**L3.8**	16%	0%	N.D.	N.D.
3	**L3.9**	23%	39%	4%	58%
4	**L3.10**	17%	34%	2%	62%
5	**L3.11**	0%	N.D.	N.D.	N.D.
6	**L3.12**	18%	62%	20%	84%
7	**L3.13**	17%	70%	16%	76%
8	**L3.14**	14%	74%	17%	85%
9	**L3.15**	18%	75%	32%	88%
10	**L3.16**	10%	43%	N.D.	N.D.
11	**L3.17**	0%	N.D.	N.D.	N.D.
12	**L3.18**	2%	49%	7%	58%
13	**L3.19**	0%	N.D.	0%	N.D.
14	**L3.20**	0%	N.D.	2%	74%

[a]Yields determined via ^{1}H NMR analysis using hexamethylbenzene as an external standard
Ligand optimization revealed that **L3.15** gave the best combination of yield and enantioselectivity in the formation of products **3.12** and **3.9**.

3.8.2.2.2 Reaction optimization

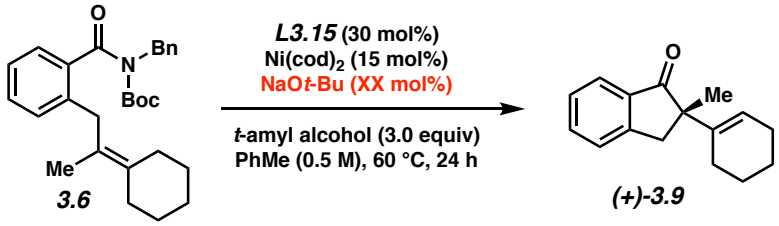
General procedure 3.3 for optimization of reaction conditions with L3.15



A flame-dried 1-dram vial containing a stir bar was brought into a glovebox and charged with **L3.15** (0.030 mmol, 30 mol%) followed by base (0.030–0.040 mmol, 30–65 mol%). Then, $Ni(cod)_2$ (0.015 mmol, 15 mol%) was added followed by **3.6** (0.060 mmol, 1.0 equiv). Subsequently, *t*-amyl alcohol (3 equiv) and toluene (0.5 M with respect to amide **3.6**) were added to the reaction vial. The vial was then sealed with a Teflon-lined screw cap, removed from the glovebox, the gap between the cap and the vial was sealed with electrical tape, and the vial was stirred at the indicated temperature for 24 h. After cooling to 23 °C, the mixture was filtered through a plug of silica, eluting with EtOAc (10 mL). The eluate was concentrated under reduced pressure and hexamethylbenzene was used as an external standard to determine ^{1}H NMR yields.

Any modification of the reaction conditions shown in the general procedure above are specified.

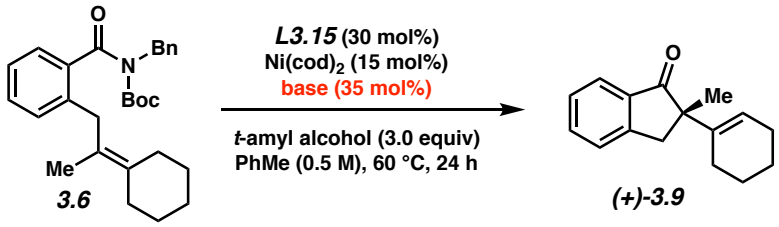
Table 3.2. Evaluation of stoichiometric loading of NaO*t*-Bu with **3.6** and **L3.15**.



Entry	mol%	Yield of (+)-3.9[a]	Recovered 3.6[a]
1	30	3%	88%
2	35	33%	46%
3	40	28%	36%

[a]Yields determined via ^{1}H NMR analysis using hexamethylbenzene as an external standard

Table 3.3. Variation of base employed with **3.6** and **L3.15**.

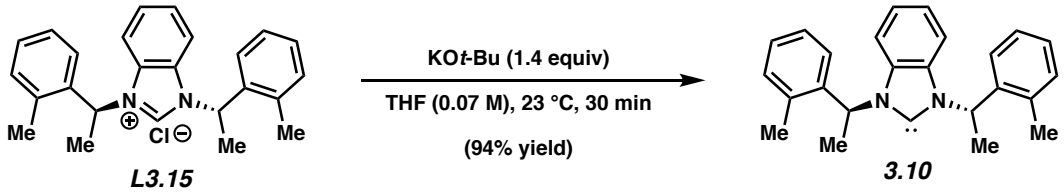


Entry	Base	Yield of (+)-3.9[a]	Recovered 3.6[a]
1	NaO*t*-Bu	33%	46%
2	LiO*t*-Bu	1%	75%
3	KO*t*-Bu	31%	50%
4	NaO*t*-amyl	30%	35%
5	LiHMDS	0%	84%
6	KHMDS	41%	37%
7	NaHMDS	23%	54%
8	K_2CO_3	0%	97%
9	K_3PO_4	0%	98%
10	Cs_2CO_3	0%	100%

[a]Yields determined via ^{1}H NMR analysis using hexamethylbenzene as an external standard

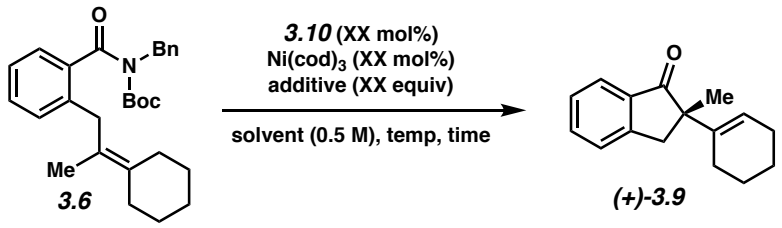
In-situ generation of the free carbene did not lead to significant increase in yield or catalyst turnover. Additionally, during our optimization efforts, we observed varying amounts of removal of the Boc group from the amide starting material which through control reactions we found could occur through the use of base, therefore, we sought to add the free carbene as a discrete reagent and omit the use of base overall.

Generation of Free Carbene 3.10



Carbene 3.10. A flame-dried scintillation vial containing a stir bar was brought into a glovebox and charged with **L3.15** (145.6 mg, 0.37 mmol, 1 equiv) and KO*t*-Bu (58.5 mg, 0.52 mmol, 1.4 equiv). Next, THF (5.3 mL, 0.07 M) was added. The vial was capped with a Teflon-lined screw cap and stirred for 30 mins in the glovebox. The reaction was then eluted through a Celite plug with THF (2 x 0.5 mL) and collected in a flame-dried scintillation vial. The solvent was removed under reduced pressure and a white residue was left on the sides of the vial. The material was then dissolved in toluene, and then eluted through another Celite plug with toluene (2 x 0.5 mL), and collected in a tared flame-dried scintillation vial in the glovebox. The solvent was removed under reduced pressure, providing free carbene **3.10** (123.9 mg, 0.35 mmol, 94% yield) as a white solid that was dissolved and stored in toluene (0.1 mg/μL) for ease of addition to reaction vials. **Carbene 3.10**: ^{1}H NMR (500 MHz, toluene-d_8): δ 7.40–7.34 (m, 2H), 6.96–6.89 (m, 6H), 6.84–6.79 (m, 2H), 6.73–6.68 (m, 2H), 5.66 (q, *J* = 6.9, 2H), 2.26 (s, 6H), 2.09 (d, *J* = 6.9, 6H); ^{13}C NMR (125 MHz, toluene-d_8): δ 225.0, 141.8, 135.9, 134.8, 130.8, 127.3, 126.8, 126.1, 121.4, 110.7, 54.7, 22.7, 19.2.

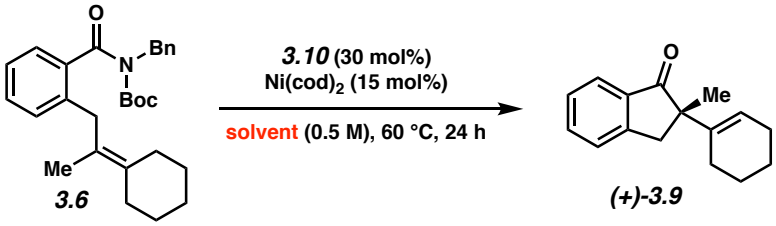
General procedure 3.4 for optimization of reaction conditions with free carbene 3.10



A flame-dried 1-dram vial containing a stir bar was brought into a glovebox and charged with a solution of **3.10** (0.015–0.080 mmol, 15–80 mol%) in solvent (0.5 M with respect to amide **3.6**). Then, the $Ni(cod)_2$ (0.015–0.040 mmol, 15–40 mol%) was added and the reaction was allowed to stir at 23 °C for 30 min. Subsequently, **3.6** (0.060 mmol, 1.0 equiv) and additive (0–3 equiv) were added to the reaction vial. The vial was then sealed with a Teflon-lined screw cap, removed from the glovebox, the gap between the cap and the vial was sealed with electrical tape, and the vial was stirred at the indicated temperature for a given time. After cooling to 23 °C, the mixture was filtered through a plug of silica, eluting with EtOAc (10 mL). The eluate was concentrated under reduced pressure, and hexamethylbenzene was used as an external standard to determine ^1H NMR yields. In cases where SFC data were obtained, purification by preparative thin-layer chromatography (benzene) afforded analytical samples of indanone **3.9**, which were then subjected to analysis by supercritical fluid chromatography to determine enantiomeric excess.

Any modification of the reaction conditions shown in the general procedure above are specified.

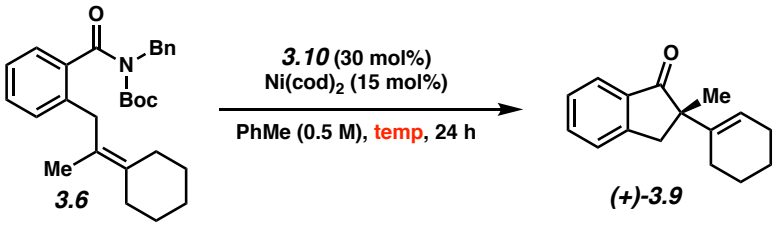
Table 3.4. Solvent variation with **3.6** and **3.10**.



Entry	Solvent	Yield of (+)-3.9[a]	Recovered 3.6[a]
1	PhMe	10%	70%
2	$PhCF_3$	7%	78%
3	THF	6%	83%
4	1,2-Dimethoxyethane	8%	70%
5	1,4-Dioxane	4%	81%
6	Acetonitrile	0%	82%

[a]Yields determined via ^{1}H NMR analysis using hexamethylbenzene as an external standard

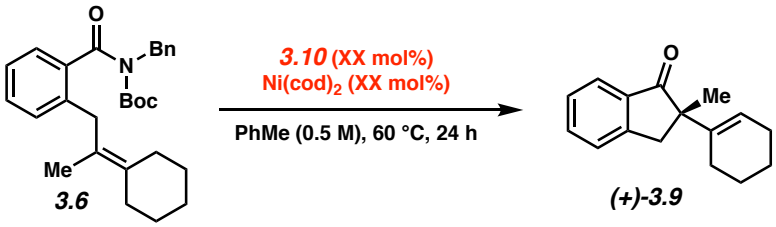
Table 3.5. Temperature variation with **3.6** and **3.10**.



Entry	Temp	Yield of (+)-3.9[a]	Recovered 3.6[a]
1	40 °C	3%	72%
2	60 °C	10%	70%
3	80 °C	0%	79%
4	100 °C	2%	71%
5	120 °C	2%	53%

[a]Yields determined via ^{1}H NMR analysis using hexamethylbenzene as an external standard

Table 3.6. Variation of catalyst stoichiometry with **3.6**.



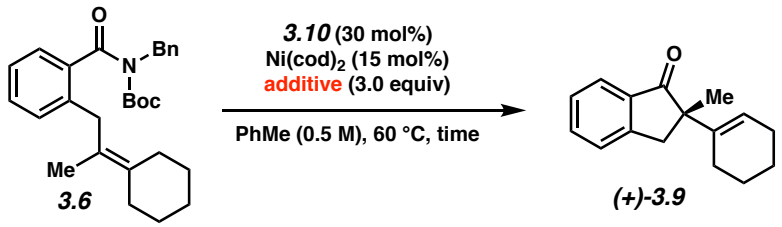
Entry	mol% of 3.10	$Ni(cod)_2$ mol%	Yield of (+)-3.9[a]	Recovered 3.6[a]
1	30	15	10%	70%

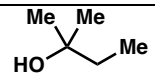
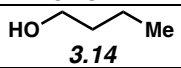
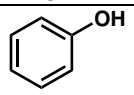
2	15	15	11%	62%
3	60	15	0%	80%
4	80	40	28%	40%

[a]Yields determined via ^{1}H NMR analysis using hexamethylbenzene as an external standard

Optimization attempts varying solvent, temperature, and catalyst loading did not improve the yield of the reaction using the free carbene without any additive. Optimization was investigated using alcohol and amine additives and select examples of these efforts are shown in tables 3.7–3.9 below. Optimized conditions were found using 1.0 equivalent of morpholine as an additive (see Table 3.9, entry 3).

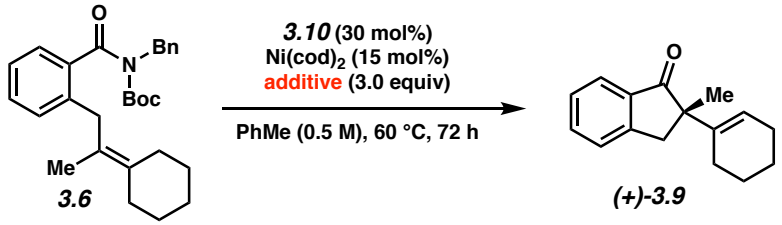
Table 3.7. Evaluation of alcohol additives with **3.6** and **3.10**.

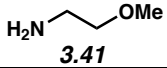


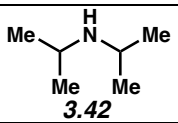
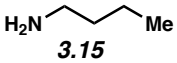
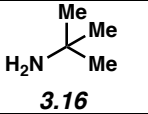
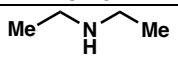
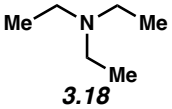
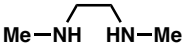
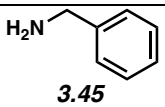
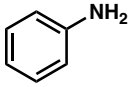
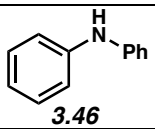
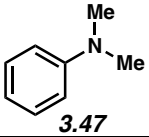
Entry	Additive	Time	Yield of (+)-3.9[a]	Recovered 3.6[a]
1	 3.13	72 h	24%	62%
2	 3.14	72 h	27%	34%
3	 3.49	24 h	0%	82%

[a]Yields determined via ^{1}H NMR analysis using hexamethylbenzene as an external standard

Table 3.8. Evaluation of acyclic amines additives with **3.6** and **3.10**.

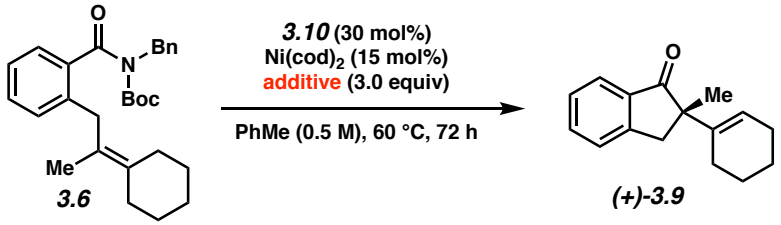


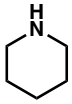
Entry	Additive	Yield of (+)-3.9[a]	% ee of (+)-3.9	Recovered 3.6[a]
1	 3.41	12%	N.D.	0%

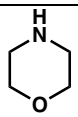
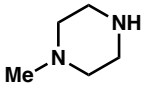
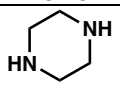
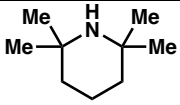
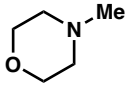
2	 **3.42**	10%	N.D.	70%
3	 **3.15**	4%	N.D.	44%
4	 **3.16**	42%	N.D.	40%
5	 **3.17**	39%	N.D.	30%
6	 **3.18**	5%	N.D.	84%
7	 **3.19**	34%	N.D.	11%
8	 **3.45**	6%	N.D.	31%
9	 **3.37**	40%	89%	59%
10	 **3.46**	15%	N.D.	85%
11	 **3.47**	13%	N.D.	84%

[a]Yields determined via ^{1}H NMR analysis using hexamethylbenzene as an external standard

Table 3.9. Evaluation of cyclic amine additives with **3.6** and **3.10**.



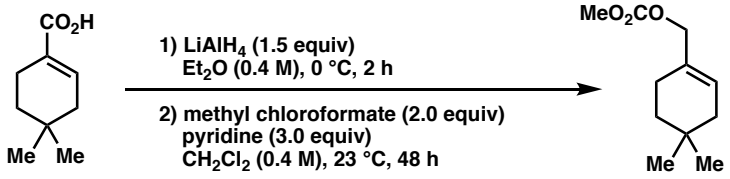
Entry	Additive	Yield of (+)-3.9[a]	% ee of (+)-3.9	Recovered 3.6[a]
1	 **3.20**	23%	N.D.	7%

2 3	 ***3.21***	42% 55%[b]	89% 88%[b]	0% 0%[b]
4	 ***3.40***	13%	N.D.	0%
5	 ***3.43***	36%	N.D.	0%
6	 ***3.48***	22%	N.D.	0%
7	 ***3.44***	30%	87%	80%
8	 ***3.39***	13%	N.D.	75%

[a]Yields determined via ^{1}H NMR analysis using hexamethylbenzene as an external standard
[b]Reaction run with 1 equiv of morpholine

3.8.2.3 Syntheses of Heck Cyclization Substrates

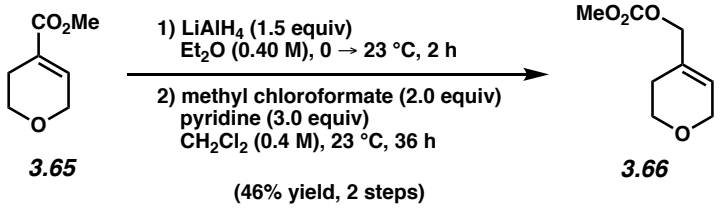
3.8.2.3.1 Syntheses of Carbonate Reductive Coupling Partners



3.63 (71% yield, 2 steps) ***3.64***

Carbonate 3.64. To a solution of carboxylic acid **3.63** (2.5 g, 16.0 mmol, 1.0 equiv) in Et_2O (41 mL, 0.4 M) at 0 °C was added $LiAlH_4$ (12 mL, 2 M in THF, 1.5 equiv) dropwise over 10 min via syringe. After stirring for 2 h, deionized water (20 mL) was added dropwise over 5 min at 0 °C. The resulting heterogeneous mixture was filtered through a plug of Celite, eluting with Et_2O (100 mL), and the filtrate was diluted with deionized water (50 mL). The layers were separated and the aqueous layer was extracted with Et_2O (3 x 50 mL). The organic layers were combined, dried over

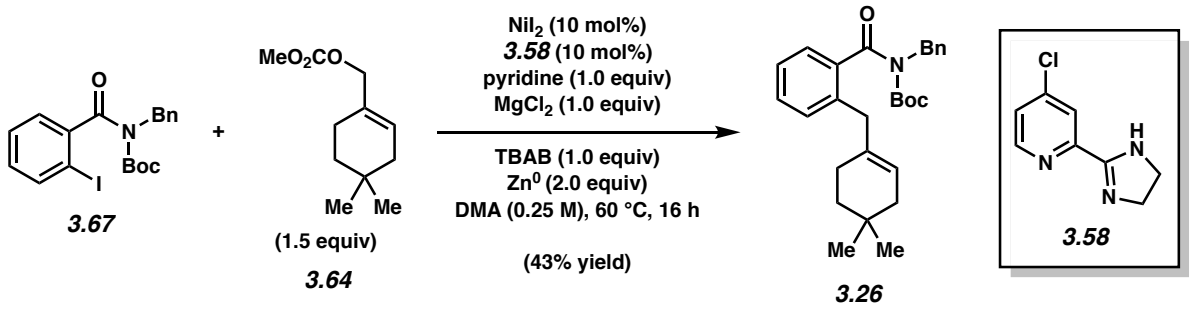
$MgSO_4$, and concentrated under reduced pressure (100 mbar, at 23 °C) to afford the corresponding alcohol, which was used in the subsequent step without further purification. To a solution of the crude alcohol in CH_2Cl_2 (41 mL, 0.4 M) was added pyridine (4.0 mL, 49.0 mmol, 3.0 equiv from **3.63**). The reaction was cooled to 0 °C. After stirring for 5 min, methyl chloroformate (2.5 mL, 33.0 mmol, 2.0 equiv from **3.63**) was added dropwise over 1 min. The reaction was allowed to warm to 23 °C. After stirring for 48 h, the reaction mixture was poured into brine (150 mL) and diluted with CH_2Cl_2 (100 mL). The layers were separated and the aqueous layer was extracted with CH_2Cl_2 (3 x 100 mL). The organic layers were combined, washed with 1 N HCl (50 mL), dried over $MgSO_4$, and concentrated under reduced pressure (100 mbar, at 23 °C). The crude mixture was purified via flash chromatography on silica (95:5 hexanes:EtOAc) to afford carbonate **3.64** (2.3 g, 11.4 mmol, 71% yield, 2 steps) as a colorless oil. **Carbonate 3.64**: R_f 0.55 (9:1 hexanes:EtOAc); ^{1}H NMR (600 MHz, $CDCl_3$): δ 5.72–5.68 (m, 1H), 4.53–4.51 (m, 2H), 3.78 (s, 3H), 2.07–2.00 (m, 2H), 1.85–1.81 (m, 2H), 1.39 (t, J = 6.4, 2H), 0.90 (s, 6H) ^{13}C NMR (125 MHz, $CDCl_3$): δ 155.9, 131.0, 126.3, 72.2, 54.7, 38.9, 35.1, 28.5, 28.1, 23.6; IR (film): 3018, 2958, 2852, 1750, 1266 cm^{-1}; HRMS-ESI (*m/z*) $[M + H]^+$ calcd for $C_{11}H_{19}O_3^+$, 199.1334; found 199.1345.



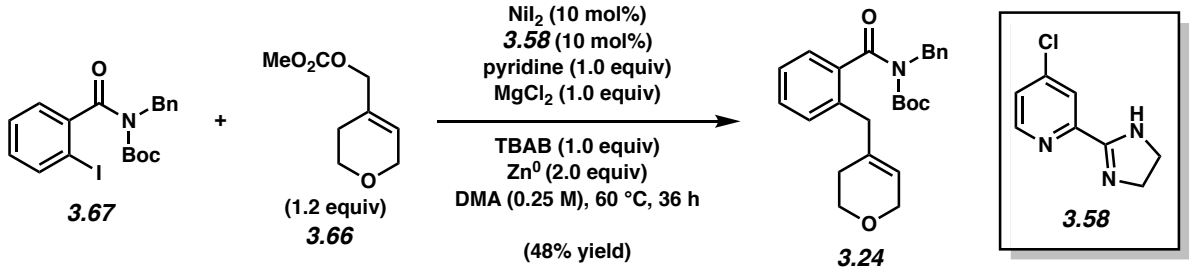
Carbonate 3.66. To a solution of methyl ester **3.65** (4.0 g, 28.0 mmol, 1.0 equiv) in Et_2O (70 mL, 0.4 M) at 0 °C was added $LiAlH_4$ (21.1 mL, 2 M in THF, 1.5 equiv) dropwise over 10 min via syringe. After stirring for 2 h, deionized water (40 mL) was added dropwise over 5 min at 0 °C. The resulting heterogeneous mixture was filtered through a plug of Celite eluting with Et_2O (150 mL) and the filtrate was diluted with deionized water (100 mL). The layers were separated and the

aqueous layer was extracted with Et_2O (3 x 80 mL). The organic layers were combined, dried over $MgSO_4$, and concentrated under reduced pressure (100 mbar, at 23 °C) to afford the corresponding alcohol, which was used in the subsequent step without further purification. To a solution of the crude alcohol (1.0 equiv) in CH_2Cl_2 (55 mL) was added pyridine (5.3 mL, 65.7 mmol, 3.0 equiv from **3.65**). The reaction was cooled to 0 °C. After stirring for 5 min, methyl chloroformate (3.4 mL, 43.8 mmol, 2.0 equiv from **3.65**) was added dropwise over 1 min. The reaction was allowed to warm to 23 °C. After stirring for 36 h, the reaction mixture was poured into brine (150 mL) and diluted with CH_2Cl_2 (100 mL). The layers were separated and the aqueous layer was extracted with CH_2Cl_2 (3 x 100 mL). The organic layers were combined, washed with 1 N HCl (50 mL), dried over $MgSO_4$, and concentrated under reduced pressure (100 mbar, at 23 °C). The crude mixture was purified via flash chromatography on silica (95:5 hexanes:EtOAc) to afford carbonate **3.66** (1.8 g, 12.9 mmol, 46% yield, 2 steps) as a yellow oil. **Carbonate 3.66**: R_f 0.17 (9:1 hexanes:EtOAc); ^{1}H NMR (500 MHz, $CDCl_3$): δ 5.83–5.77 (m, 1H), 4.55 (s, 2H), 4.17–4.13 (m, 2H), 3.83–3.80 (m, 2H), 3.79 (s, 3H), 2.17–2.10 (m, 2H); ^{13}C NMR (125 MHz, $CDCl_3$): δ 155.8, 130.4, 125.2, 70.8, 65.1, 64.1, 55.0, 26.0 ; IR (film): 2962, 2826, 2849, 1749, 1268 cm^{-1}; HRMS-ESI (*m/z*) $[M + Na]^+$ calcd for $C_8H_{12}O_4Na^+$, 195.0633; found 195.0644.

3.8.2.3.2 Reductive Cross-Coupling of Imides and Carbonates

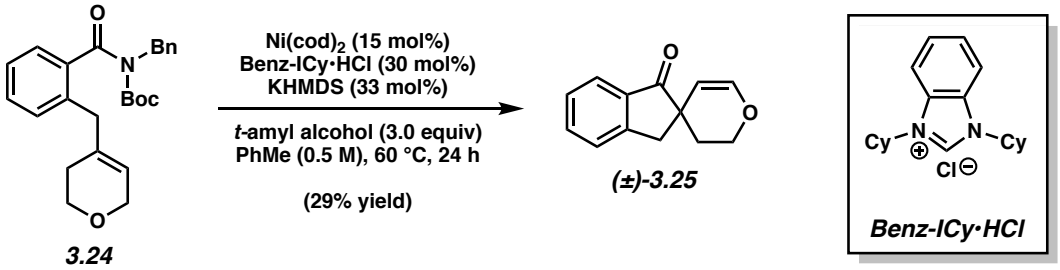


Amide 3.26. A flame-dried 250 mL round bottom flask equipped with a large 3 cm football-shaped stir bar was brought into a glovebox and charged with amide **3.67**[7j] (3.5 g, 8.00 mmol, 1.0 equiv), ligand **3.58** (145 mg, 0.80 mmol, 10 mol%), NiI_2 (250 mg, 0.80 mmol, 10 mol%), $MgCl_2$ (726 mg, 8.00 mmol, 1.0 equiv), TBAB (2.58 g, 8.00 mmol, 1.0 equiv) and Zn^0 (1.1 g, 16.0 mmol, 2.0 equiv). The flask was removed from the glovebox, at which point DMA (32.0 mL, 0.25 M), pyridine (647 μL, 8.0 mmol, 1.0 equiv), and carbonate **3.64** (2.38 g, 12.0 mmol, 1.5 equiv) were added. The flask was quickly sealed with an air condenser and stirred at 60 °C for 16 h. After cooling to 23 °C, the mixture was passed through a plug of silica gel eluting with 5:2 hexanes:EtOAc (150 mL) until TLC indicated the desired product had eluted. The volatiles were removed under reduced pressure and the crude mixture was further purified by flash chromatography on silica (99:1 hexanes:EtOAc) to yield amide **3.26** (1.5 g, 3.50 mmol, 43% yield) as a colorless oil. **Amide 3.26**: R_f 0.55 (9:1 hexanes:EtOAc); ^{1}H NMR (600 MHz, $CDCl_3$): δ 7.43 (d, *J* = 7.3, 2H), 7.35–7.26 (m, 4H), 7.22–7.13 (m, 3H), 5.38–5.34 (m, 1H), 5.01 (s, 2H), 3.31 (s, 2H), 1.85–1.80 (m, 2H), 1.79–1.76 (m, 2H), 1.30 (t, *J* = 6.4, 2H), 1.11 (s, 9H), 0.87 (s, 6H); ^{13}C NMR (150 MHz, $CDCl_3$, 23 of 24 signals observed): δ 172.4, 152.9, 138.4, 138.0, 137.5, 134.8, 129.7, 129.4, 128.5, 128.4, 127.5, 126.4, 125.7, 123.3, 83.3, 48.1, 40.9, 39.5, 35.8, 28.6, 28.4, 27.5, 26.1; IR (film): 2955, 2867, 1730, 1673, 1231 cm^{-1}; HRMS-ESI (*m/z*) $[M + Na]^+$ calcd for $C_{28}H_{35}NO_3Na^+$, 456.2515; found 456.2519.

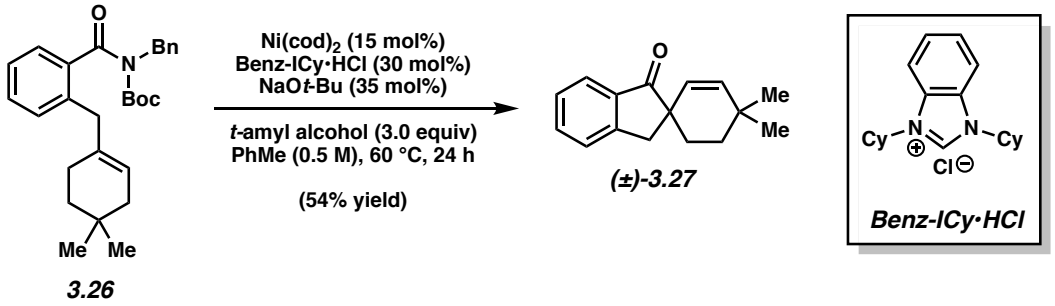


Amide 3.24. A flame-dried 250 mL round bottom flask equipped with a large 3 cm football-shaped stir bar was brought into a glovebox and charged with amide **3.67**[7j] (3.8 g, 8.70 mmol, 1.0 equiv), ligand **3.58** (160 mg, 0.87 mmol, 10 mol%), NiI_2 (270 mg, 0.87 mmol, 10 mol%), $MgCl_2$ (83.0 mg, 8.70 mmol, 1.0 equiv), TBAB (2.80 g, 8.7 mmol, 1.0 equiv) and Zn^0 (1.1 g, 17.4 mmol, 2.0 equiv). The flask was removed from the glovebox, at which point DMA (35.0 mL), pyridine (700 μL, 8.7 mmol, 1.0 equiv), and carbonate **3.66** (1.80 g, 10.0 mmol, 1.2 equiv) were added. The flask was quickly sealed with an air condenser and stirred at 60 °C for 36 h. After cooling to 23 °C, the mixture was passed through a plug of silica gel and eluted with 5:2 hexanes:EtOAc (150 mL) until TLC indicated the desired product had eluted. The volatiles were removed under reduced pressure and the crude mixture was further purified by flash chromatography on silica (99:1 hexanes:EtOAc) to yield amide **3.24** (1.7 g, 4.2 mmol, 48% yield) as a colorless oil. **Amide 3.24**: R_f 0.34 (95:5 benzene: MeCN; ^{1}H NMR (500 MHz, $CDCl_3$): δ 7.43 (d, J = 7.3, 2H), 7.36–7.30 (m, 3H), 7.28 (overlapped with residual solvent peak, 1H), 7.24–7.13 (m, 3H), 5.39 (br s, 1H), 5.02 (s, 2H), 4.09–4.04 (m, 2H), 3.71 (t, J = 5.5, 2H), 3.37 (s, 2H), 2.00–1.91 (m, 2H), 1.12 (s, 9H), ^{13}C NMR (125 MHz, $CDCl_3$): δ 172.3, 152.9, 138.4, 137.9, 136.4, 134.2, 130.2, 129.5, 128.6, 128.4, 127.6, 126.4, 126.0, 122.6, 83.5, 65.6, 64.5, 48.1, 40.4, 28.4, 27.6; IR (film): 3037, 2983, 2849, 1725, 1140 cm^{-1}; HRMS-ESI (*m/z*) [M + Na]$^+$ calcd for $C_{25}H_{29}NO_4Na^+$, 430.1994; found 430.2018.

3.8.2.4 Syntheses of Racemic Indanones (±)-3.25 and (±)-3.27



Indanone (±)-3.25. A flame-dried 1-dram vial containing amide **3.24** (35.0 mg, 0.086 mmol, 1.0 equiv) and a magnetic stir bar was sequentially charged with Benz-ICy•HCl (8.2 mg, 0.026 mmol, 30 mol%), $Ni(cod)_2$ (3.5 mg, 0.013 mmol, 15 mol%), and KHMDS (6.0 mg, 0.030 mmol, 35 mol%) in a glovebox. Subsequently, toluene (172 μL, 0.5 M) and then *t*-amyl alcohol (28.2 μL, 0.26 mmol, 3.0 equiv) were added. The vial was sealed with a Teflon-lined screw cap, removed from the glovebox, the gap between the cap and the vial was sealed with electrical tape, and the vial was stirred at 60 °C for 24 h. After cooling to 23 °C, the mixture was diluted with hexanes (1.0 mL) and filtered through a plug of silica gel (10 mL of EtOAc eluent). Purification by preparative thin-layer chromatography (95:5 benzene: MeCN) afforded indanone **(±)-3.25** (5.0 mg, 0.025 mmol, 29% yield) as a colorless oil. **Indanone (±)-3.25**: R_f 0.53 (95:5 benzene: MeCN); ^{1}H NMR (500 MHz, $CDCl_3$): δ 7.77 (d, *J* = 7.6, 1H), 7.62 (t, *J* = 7.6, 1H), 7.44 (d, *J* = 7.6, 1H), 7.40 (t, *J* = 7.6, 1H), 6.64 (d, *J* = 6.1, 1H), 4.52 (d, *J* = 6.1, 1H), 4.44 (ddd, *J* = 10.9, 7.5, 3.0, 1H), 4.02 (ddd, *J* = 10.9, 7.5, 3.0, 1H), 3.23 (d, *J* = 17.1, 1H), 3.07 (d, *J* = 17.1, 1H), 2.13–2.04 (m, 1H), 1.77 (ddd, *J* = 13.9, 7.4, 3.0, 1H).^{13}C NMR (150 MHz, $CDCl_3$): δ 208.8, 151.8, 146.1, 135.5, 135.3, 127.9, 126.7, 124.8, 102.9, 63.1, 46.5, 43.2, 32.5; IR (film): 2916, 2849, 1712, 1641, 1250 cm^{-1}; HRMS-ESI (*m/z*) $[M + H]^+$ calcd for $C_{13}H_{13}O_2^+$, 201.0916; found 201.0920.

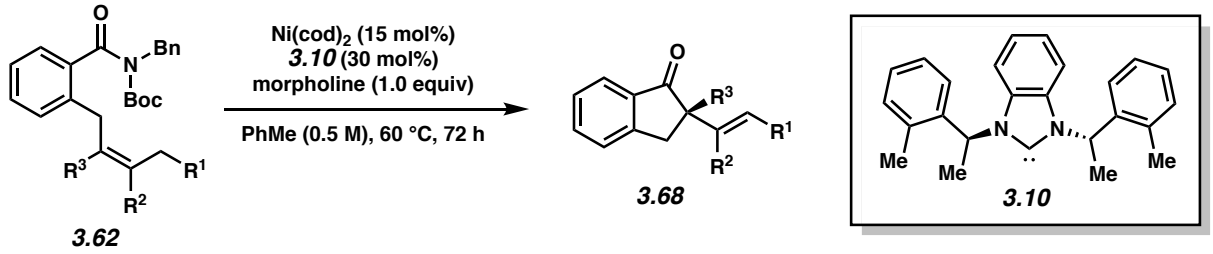


Indanone (±)-3.27. A flame-dried 1-dram vial containing amide **3.26** (40.2 mg, 0.093 mmol, 1.0 equiv) and a magnetic stir bar was sequentially charged with Benz-ICy•HCl (8.9 mg, 0.028 mmol, 30 mol%), $Ni(cod)_2$ (3.8 mg, 0.014 mmol, 15 mol%), and NaO*t*-Bu (3.1 mg, 0.033 mmol, 35 mol%) in a glovebox. Subsequently, toluene (185 μL, 0.5 M) and then *t*-amyl alcohol (31 μL, 0.28 mmol, 3.0 equiv) were added. The vial was sealed with a Teflon-lined screw cap, removed from the glovebox, the gap between the cap and the vial was sealed with electrical tape, and the vial was stirred at 60 °C for 24 h. After cooling to 23 °C, the mixture was diluted with hexanes (1.0 mL) and filtered through a plug of silica gel (10 mL of EtOAc eluent). The volatiles were removed under reduced pressure. Purification by preparative thin-layer chromatography (95:5 benzene:MeCN) afforded indanone **(±)-3.27** (11.3 mg, 0.050 mmol, 54% yield) as a colorless oil.

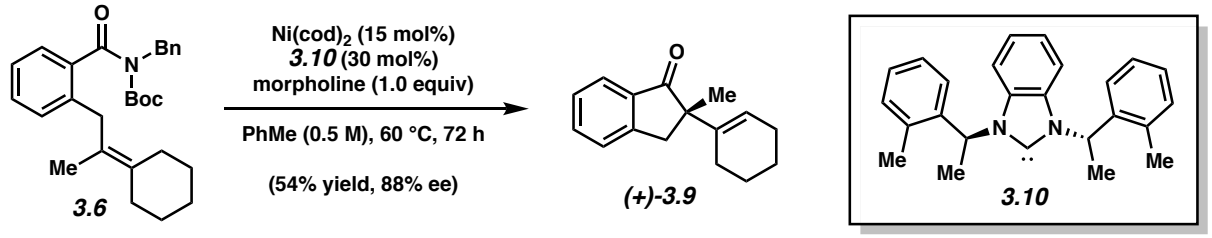
Indanone (±)-3.27: R_f 0.76 (95:5 benzene:MeCN; ^{1}H NMR (600 MHz, $CDCl_3$): δ 7.76 (d, *J* = 7.6, 1H), 7.59 (td, *J* = 7.4, 1.2, 1H), 7.43 (dt, *J* = 7.7, 0.9, 1H), 7.40–7.35 (m, 1H), 5.71 (dd, *J* = 9.9, 1.0, 1H), 5.30 (dd, *J* = 9.9, 1.0, 1H), 3.14–3.05 (m, 2H), 1.98 (ddd, *J* = 13.4, 10.8, 3.1, 1H), 1.81 (dddd, *J* = 13.3, 7.1, 3.2, 0.8, 1H), 1.60–1.53 (m, 1H), 1.52–1.47 (m, 1H), 1.11 (s, 3H), 1.05 (s, 3H); ^{13}C NMR (150 MHz, $CDCl_3$): δ 209.7, 152.6, 140.4, 136.0, 134.9, 127.6, 126.7, 125.9, 124.7, 51.6, 42.2, 34.2, 31.5, 30.3, 30.2, 29.0; IR (film): 2991, 2962, 2852, 1710, 964 cm^{-1}; HRMS-ESI (*m/z*) $[M + H]^+$ calcd for $C_{16}H_{19}O^+$, 227.1436; found 227.1450.

3.8.2.5 Scope of Methodology

General procedure 3.5 for the enantioselective nickel-catalyzed Mizoroki–Heck reaction

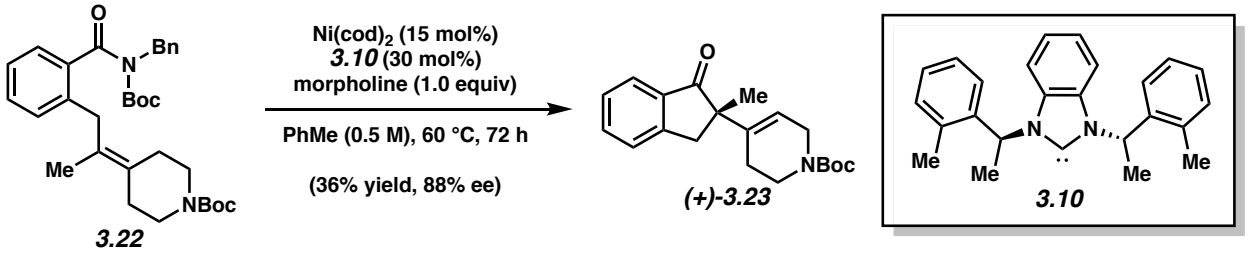


A flame-dried 1-dram vial containing a stir bar was brought into a glovebox and charged sequentially with amide **3.62** (0.1 mmol, 1.0 equiv), $Ni(cod)_2$ (4.1 mg, 0.015 mmol, 15 mol%), and a solution of **3.10** (0.1 mg/μL in PhMe, 106 μL, 10.6 mg, 0.030 mmol, 30 mol%) in toluene (95 μL, 0.5 M total accounting for the volume of the carbene solution). The mixture was then prestirred for 15 minutes in the glovebox at 23 °C. Then, morpholine (8.6 μL, 0.1 mmol, 1.0 equiv) was added to the vial using a micropipette. The vial was then sealed with a Teflon-lined screw cap, removed from the glovebox, the gap between the cap and the vial was sealed with electrical tape, and the vial was stirred at 60 °C for 72 h. After cooling to 23 °C, the mixture was filtered through a plug of silica, eluting with EtOAc (10 mL). The eluate was concentrated under reduced pressure, then purified by flash chromatography on silica to provide products **3.68**.

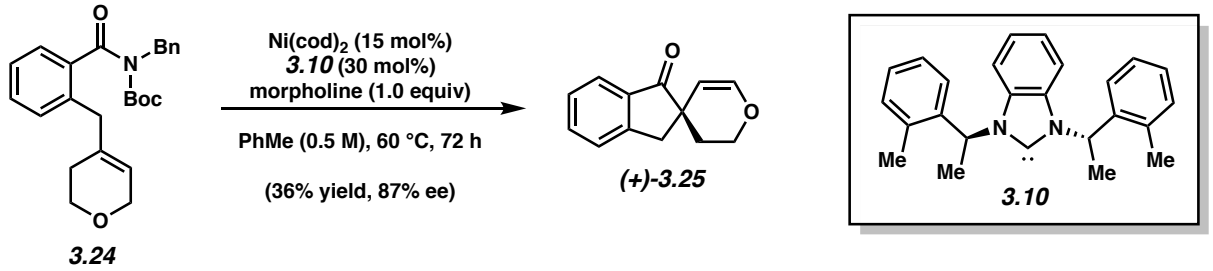


Indanone (+)-3.9. Followed General Procedure 3.5. Purification by preparative thin layer silica chromatography (95:5 benzene:MeCN) afforded indanone product **(+)-3.9** (54% yield, 88% ee,

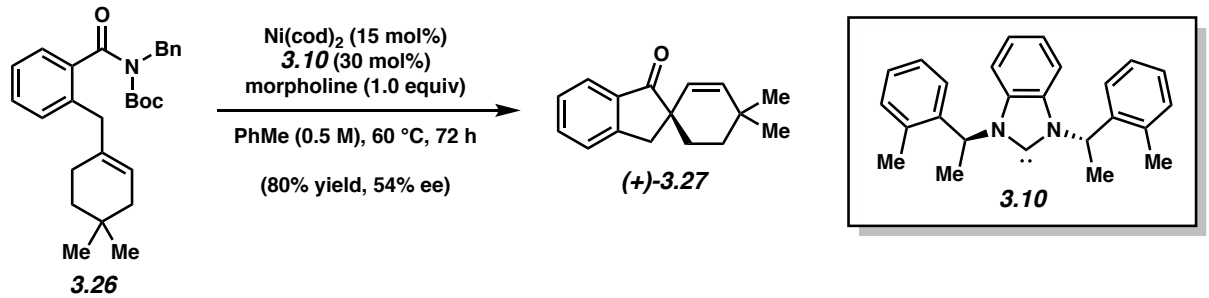
average of two experiments) as a colorless oil. Spectral data match those previously reported.[7j] $[\alpha]^{27.9}_{D}$ +80° (*c* = 1.00, CH_2Cl_2).



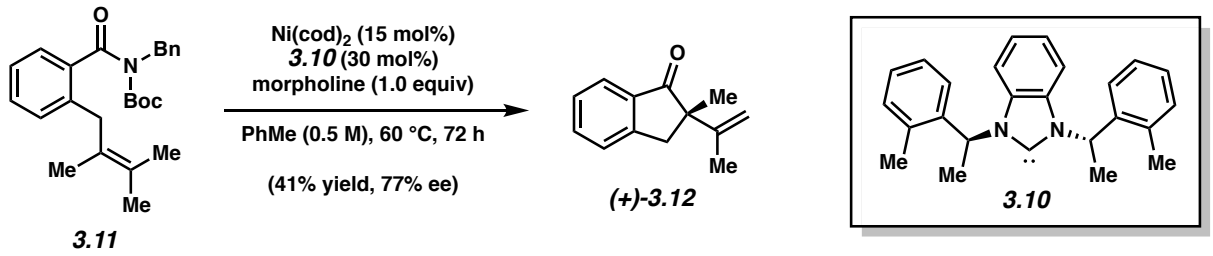
Indanone (+)-3.23. Followed General Procedure 3.5. Purification by preparative thin layer silica chromatography (2:1 hexanes:EtOAc) afforded indanone product **(+)-3.23** (36% yield, 88% ee, average of two experiments) as a colorless oil. Spectral data match those previously reported.[7j] $[\alpha]^{24.0}_{D}$ +14° (*c* = 1.00, CH_2Cl_2).



Indanone (+)-3.25. Followed General Procedure 3.5. Purification by preparative thin layer silica chromatography (95:5 benzene:CH_3CN) afforded indanone product **(+)-3.25** (36% yield, 87% ee, average of two experiments) as a colorless oil. Spectral data match those previously reported in Section D. $[\alpha]^{26.4}_{D}$ +196° (*c* = 1.00, CH_2Cl_2).

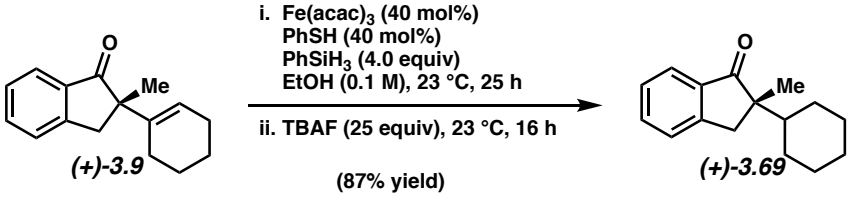


Indanone (+)-3.27. Followed General Procedure 3.5. Purification by preparative thin layer silica chromatography (95:5 benzene:MeCN) afforded indanone product **(+)-3.27** (80% yield, 54% ee, average of two experiments) as a colorless oil. Spectral data match those previously reported in Section D. $[\alpha]^{27.1}_{D}$ +82° (*c* = 1.00, CH_2Cl_2).



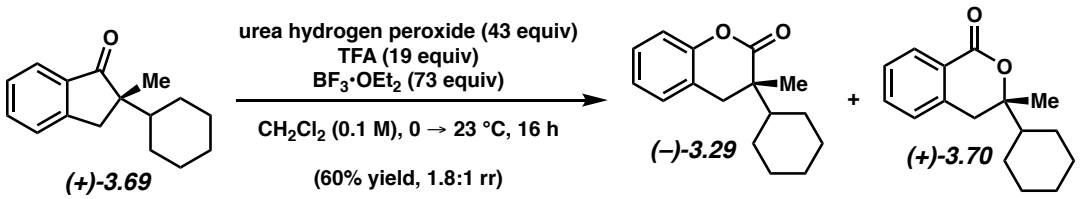
Indanone (+)-3.12. Followed General Procedure 3.5. Purification by preparative thin layer silica chromatography (3:1 hexanes:EtOAc) afforded indanone product **(+)-3.12** (41% yield, 77% ee, average of two experiments) as a colorless oil. Spectral data match those previously reported.[7j] $[\alpha]^{23.6}_{D}$ +18° (*c* = 1.00, CH_2Cl_2).

3.8.2.6 Synthetic Elaboration of Mizoroki–Heck Cyclization Product (+)-3.9



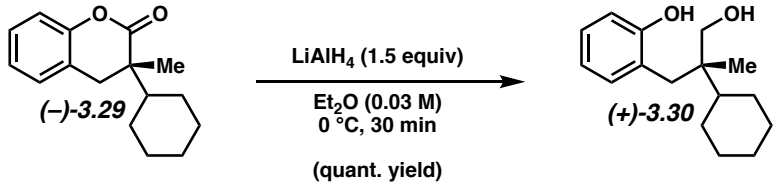
Indanone (+)-3.69. A flame-dried 1-dram vial containing a magnetic stir bar was charged with indanone **(+)-3.9** (30.0 mg, 0.12 mmol, 1.0 equiv) and $Fe(acac)_3$ (17.0 mg, 48 μmol, 40 mol%). The vial was then secured with a septum cap and purged with an inlet needle using N_2 and an outlet needle open to air for 5 min. Then, ethanol (1.2 mL, 0.1 M) was added to the vial and the mixture was stirred for 2 min until homogenous. Subsequently, phenylsilane (59 μL, 0.48 mmol, 4.00 equiv), and thiophenol (0.50 M in *n*-propanol, 95 μL, 48 μmol, 40 mol%) were added sequentially. The reaction was allowed to stir at 23 °C under nitrogen for 25 h. After 25 h, TBAF (1.0 M in

THF, 0.86 mL, 3.0 mmol, 25 equiv) was added to the reaction to eliminate excess phenylsilane and stirred at 23 °C under nitrogen for 16 h. After this time, the crude material was concentrated under reduced pressure. Purification by preparative thin layer silica chromatography (95:5 benzene:MeCN) afforded product **(+)-3.69** (22.9 mg, 0.10 mmol, 87% yield) as a colorless oil. **Indanone (+)-3.69**: R_f 0.33 (benzene); ^{1}H NMR (600 MHz, $CDCl_3$) δ 7.73 (d, *J* = 7.7, 1H), 7.57 (t, *J* = 7.4, 1H), 7.43 (d, *J* = 7.4, 1H), 7.35 (t, *J* = 7.4, 1H), 3.21 (d, *J* = 17.4, 1H), 2.69 (d, *J* = 17.4, 1H), 1.91–1.84 (m, 1H), 1.82–1.76 (m, 1H), 1.72 (tt, *J* = 12.1, 3.2, 1H), 1.67–1.55 (m, 2H), 1.39–1.33 (m, 1H), 1.31–1.17 (m, 5H), 1.09 (tt, *J* = 12.8, 3.1, 1H), 0.98 (qd, *J* = 12.6, 3.6, 1H), 0.86 (qd, *J* = 12.6, 3.6, 1H); ^{13}C NMR (150 MHz, $CDCl_3$): δ 212.5, 153.5, 136.8, 134.8, 127.4, 126.5, 124.0, 52.6, 44.5, 37.6, 28.1, 27.6, 26.8, 26.6, 26.4, 23.0; IR (film): 2960, 2927, 2880, 2852, 1710 cm^{-1}; HRMS-ESI (*m/z*) $[M + H]^+$ calcd for $C_{16}H_{21}O^+$, 229.1587; found 229.1598. $[\alpha]^{26.6}_D$ –60° (*c* = 1.00, CH_2Cl_2).



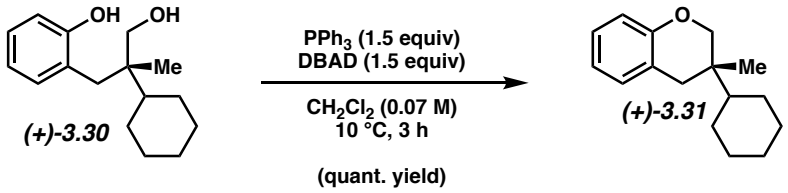
Lactones (–)-3.29 and **(+)-3.70.** To a solution of indanone **(+)-3.69** (17.0 mg, 75 μmol, 1 equiv) and urea hydrogen peroxide (298 mg, 3.16 mmol, 43 equiv) in CH_2Cl_2 (1.1 mL, 0.1 M) at –0 ºC was added TFA (109 μL, 1.41 mmol, 19 equiv). After stirring for 10 min, BF_3•OEt_2 (671 μL, 5.44 mmol, 73 equiv) was added dropwise via syringe. The reaction was allowed to warm to 23 °C over 16 h. After stirring for 16 h, the reaction mixture was poured into deionized water (50 mL) and diluted with CH_2Cl_2 (50 mL). The layers were separated and the aqueous layer was extracted with CH_2Cl_2 (3 x 10 mL). The organic layers were combined, washed with saturated aqueous $NaHCO_3$ (50 mL), dried over $MgSO_4$, and concentrated under reduced pressure (100 mbar, at 23 °C).

Purification by preparative thin layer chromatography (95:5 benzene:MeCN) afforded lactone **(–)-3.29** and lactone **(+)-3.70**, each as a colorless oil (11.0 mg, 45 μmol, 60% combined yield, 1.8:1 rr determined by ^{1}H NMR analysis of the crude reaction mixture). **(–)-3.29**: R_f 0.66 (benzene); ^{1}H NMR (600 MHz, $CDCl_3$): δ 7.26–7.22 (overlapped with residual solvent peak, 1H), 7.13 (d, *J* = 7.3, 1H), 7.07 (t, *J* = 7.3, 1H), 7.00 (d, *J* = 8.2, 1H), 2.99 (d, *J* = 16.1, 1H), 2.78 (d, *J* = 16.1, 1H), 1.80–1.70 (m, 2H), 1.69–1.64 (m, 1H), 1.63–1.59 (m, 2H), 1.57–1.50 (m, 1H), 1.22 (s, 3H), 1.17–0.96 (m, 5H); ^{13}C NMR (125 MHz, $CDCl_3$, 15 of 16 signals observed): δ 173.0, 151.8, 128.4, 128.2, 124.4, 122.0, 116.0, 44.1, 40.3, 33.9, 27.8, 26.7, 26.6, 26.4, 19.6; IR (film): 2929, 2880, 2853, 1762, 1458 cm^{-1}; HRMS-ESI (*m/z*) $[M + H]^+$ calcd for $C_{16}H_{21}O_2^+$, 245.1542; found 245.1553. $[\alpha]^{27.5}_D$ –10° (*c* = 1.00, CH_2Cl_2). **(+)-3.70**: R_f 0.38 (benzene); ^{1}H NMR (600 MHz, $CDCl_3$): δ 8.10–8.07 (m, 1H), 7.52 (td, *J* = 7.6, 1.2, 1H), 7.37 (t, *J* = 7.6, 1H), 7.21 (d, *J* = 7.6 1H), 3.18 (d, *J* = 16.4, 1H), 2.83 (d, *J* = 16.4, 1H), 2.04–1.97 (m, 1H), 1.88–1.77 (m, 3H), 1.71–1.64 (m, 2H), 1.30 (s, 3H), 1.25–1.02 (m, 5H); ^{13}C NMR (125 MHz, $CDCl_3$): 165.3, 138.3, 133.9, 130.1, 128.3, 127.5, 125.3, 85.6, 53.6, 47.1, 35.8, 27.7, 27.0, 26.6, 26.5, 21.9 δ; IR (film): 2928, 2882, 2854, 1715, 1460 cm^{-1}; HRMS-ESI (*m/z*) $[M + H]^+$ calcd for $C_{16}H_{21}O_2^+$, 245.1542; found 245.1553. $[\alpha]^{25.5}_D$ +8° (*c* = 1.00, CH_2Cl_2).



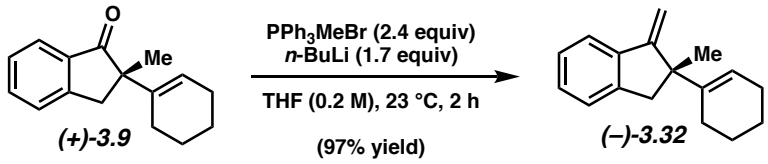
Diol (+)-3.30. To a solution of lactone **(–)-3.29** (2.6 mg, 11 μmol, 1.0 equiv) in Et_2O (0.5 mL, 0.03 M) at 0 °C was added $LiAlH_4$ (8 μL, 2 M in THF, 16 μmol, 1.5 equiv). After stirring for 30 min, deionized water (5 mL) was added dropwise over 5 min at 0 °C. The resulting heterogeneous mixture was filtered through a plug of Celite eluting with Et_2O (10 mL) and the filtrate was diluted

with deionized water (10 mL). The layers were separated and the aqueous layer was extracted with Et_2O (3 x 10 mL). The organic layers were combined, dried over $MgSO_4$, and concentrated under reduced pressure (100 mbar, at 23 °C) to afford the corresponding diol **(+)-3.30**. Purification by preparative thin layer silica chromatography (95:5 benzene:MeCN) afforded diol **(+)-3.30** (2.6 mg, 11 μmol, quant. yield) as a colorless oil. **(+)-3.30**: R_f 0.32 (95:5 benzene:MeCN); ^{1}H NMR (600 MHz, $CDCl_3$): δ 7.16–7.09 (m, 1H), 7.03–6.97 (m, 1H), 6.88 (d, *J* = 7.8, 1H), 6.85–6.79 (m, 1H), 3.45 (d, *J* = 10.9, 1H), 3.16 (d, *J* = 10.9, 1H), 2.77 (d, *J* = 14.2, 1H), 2.59 (d, *J* = 14.2, 1H), 1.99–1.92 (m, 1H), 1.89–1.82 (m, 1H), 1.81–1.75 (m, 1H), 1.74–1.62 (m, 3H), 1.51–1.43 (m, 2H), 1.23–1.02 (m, 5H), 0.75 (s, 3H); ^{13}C NMR (150 MHz, $CDCl_3$): δ 156.1, 133.0, 127.9, 124.6, 120.0, 117.0, 66.3, 42.3, 41.2, 35.2, 29.9, 27.5, 27.23, 27.16, 26.8, 17.1; IR (film): 3208, 3000, 2925, 2882, 2853 cm^{-1}; HRMS-ESI (*m/z*) $[M + H]^+$ calcd for $C_{16}H_{25}O_2^+$, 249.1855; found 249.1869. $[\alpha]^{24.3}_D$ +50° (*c* = 1.00, CH_2Cl_2).



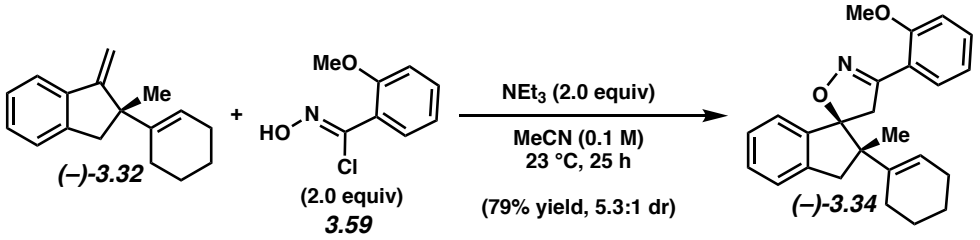
Chromane (+)-3.31. To a flame-dried 1-dram vial containing a stir bar was added diol **(+)-3.30** (2.0 mg, 8.1 μmol, 1 equiv), PPh_3 (3.2 mg, 12 μmol, 1.5 equiv), and DBAD (2.8 mg, 12 μmol, 1.5 equiv). The vial was then secured with a septum cap and purged with an inlet needle using N_2 and an outlet needle open to air for 5 min. Then, CH_2Cl_2 (120 μL, 0.07 M) was added and the vial was sealed with a Teflon-lined cap and cooled to 10 °C. The solution was allowed to stir at 10 °C for 3 h. After this time, the mixture was eluted through a pad of silica using CH_2Cl_2 (10 mL), and the eluate was concentrated under reduced pressure. Purification by flash chromatography on silica (benzene) afforded chromane **(+)-3.31** (1.9 mg, 8.2 μmol, quant. yield) as a volatile, colorless oil.

Chromane (+)-3.31: R_f 0.61 (100% benzene); ^{1}H NMR (600 MHz, $CDCl_3$): δ 7.08 (t, *J* = 7.0, 1H), 7.01 (d, *J* = 7.0, 1H), 6.84 (t, *J* = 7.0, 1H), 6.82–6.76 (m, 1H), 3.85 (s, 2H), 2.71 (d, *J* = 15.9, 1H), 2.45 (d, *J* = 15.9, 1H), 1.83–1.72 (m, 4H), 1.70–1.63 (m, 1H), 1.28–1.03 (m, 6H), 0.89 (s, 3H); ^{13}C NMR (125 MHz, $CDCl_3$): δ 154.2, 130.4, 127.1, 121.9, 120.5, 116.3, 73.7, 43.3, 36.4, 33.7, 27.1, 27.03, 26.96, 26.8, 26.6, 18.0; IR (film): 2968, 2926, 2879, 2853, 1230 cm^{-1}; HRMS-ESI (*m/z*) $[M + Na]^+$ calcd for $C_{16}H_{22}ONa^+$, 253.1568; found 253.1664. $[\alpha]^{24.0}_D$ +200° (*c* = 1.00, CH_2Cl_2).



Olefin (–)-3.32. To a flame-dried 2-dram vial containing a stir bar was added PPh_3MeBr (200 mg, 0.56 mmol, 2.4 equiv). The vial was then secured with a septum cap and purged with an inlet needle using N_2 and an outlet needle open to air for 5 min. Then, THF (610 μL, 0.2 M) was added, followed by the dropwise addition of *n*-BuLi (2.4 M in hexanes, 152 μL, 1.7 equiv) over 1 min at 23 °C, resulting in an orange heterogeneous solution. The solution was allowed to stir at 23 °C for 1 h. Subsequently, indanone **(+)-3.9** (55.6 mg, 0.22 mmol, 1.0 equiv) was dissolved in THF (500 μL) in a separate flame-dried 1-dram vial and was transferred via syringe to the reaction vial and added dropwise over 1 minute. The reaction was allowed to stir at 23 °C for 1 h. After this time, the mixture was eluted through a pad of silica using CH_2Cl_2 (10 mL), and the eluate was concentrated under reduced pressure. Purification by flash chromatography on silica (pentanes) afforded olefin **(–)-3.32** (48.3 mg, 0.22 mmol, 97% yield) as a volatile, colorless oil. **Olefin (–)-3.32**: R_f 0.45 (9:1 hexanes:EtOAc); ^{1}H NMR (600 MHz, $CDCl_3$): δ 7.49 (d, *J* = 7.0, 1H), 7.25–7.17 (m, 3H), 5.72–5.65 (m, 1H), 5.50 (s, 1H), 4.81 (s, 1H), 3.16 (d, *J* = 16.8, 1H), 2.69 (d, *J* =

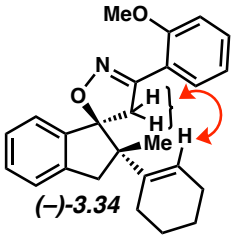
16.8, 1H), 2.14–2.04 (m, 2H), 1.88–1.76 (m, 2H), 1.64–1.55 (m, 2H), 1.54–1.46 (m, 2H), 1.29 (s, 3H); ^{13}C NMR (125 MHz, $CDCl_3$): δ 158.1, 144.3, 142.3, 140.7, 128.6, 126.6, 125.4, 121.1, 120.2, 102.9, 51.4, 44.6, 27.3, 25.70, 25.66, 23.4, 22.8; IR (film): 3075, 2959, 2925, 2854, 1636 cm^{-1}; GCMS-EI (*m/z*) $[M]^+$ calcd for $C_{17}H_{20}^+$, 224.1565; found 224.1559. $[\alpha]^{23.9}_D$ –36° (*c* = 1.00, CH_2Cl_2).

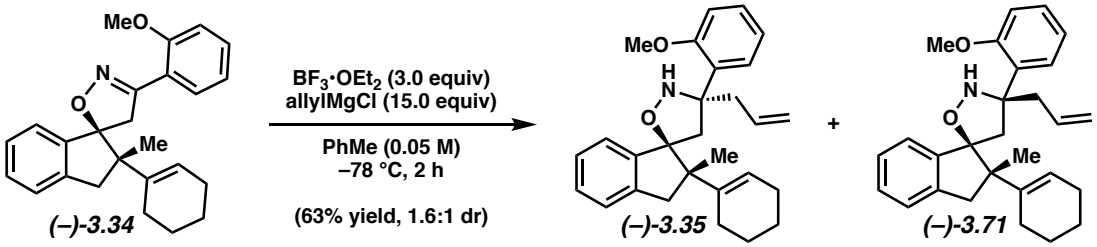


(–)-3.34. To a flame-dried 1-dram vial was added sequentially olefin **(–)-3.32** (21.8 mg, 0.092 mmol, 1.0 equiv), **3.59** (34.3 mg, 0.19 mmol, 2.0 equiv), MeCN (920 μL, 0.1 M), and NEt_3 (25.7 μL, 0.19 mmol, 2.0 equiv). The vial was sealed with a Teflon-lined cap and stirred at 23 °C for 25 h. After this time, the reaction was eluted through a pad of silica with EtOAc (10 mL), and the eluate was concentrated under reduced pressure. Purification by preparative thin layer silica chromatography (4:1 hexanes:EtOAc) afforded **(–)-3.34** (30.4 mg, 0.081 mmol, 79% yield, 5.3:1 dr determined by ^{1}H NMR analysis of the crude reaction mixture) as an off-white foam. **(–)-3.34**: R_f 0.65 (3:1 hexanes:EtOAc); ^{1}H NMR (600 MHz, $CDCl_3$): δ 7.77–7.71 (m, 1H), 7.39–7.34 (m, 1H), 7.32–7.29 (m, 1H), 7.25–7.18 (m, 3H), 6.99 (td, *J* = 7.5, 0.9, 1H), 6.92 (d, *J* = 8.3, 1H), 5.75–5.66 (m, 1H), 3.81 (s, 3H), 3.75 (d, *J* = 18.2, 1H), 3.22–3.12 (m, 2H), 2.69 (d, *J* = 15.2, 1H), 2.16–2.01 (m, 3H), 1.99–1.90 (m, 1H), 1.68–1.42 (m, 4H), 1.27 (s, 3H); ^{13}C NMR (150 MHz, CDCl3, 24 of 25 signals observed): δ 157.7, 156.3, 146.9, 141.9, 139.7, 131.2, 129.6, 128.2, 127.1, 124.9, 122.9, 122.4, 120.9, 119.4, 111.5, 98.0, 56.7, 55.6, 46.1, 42.1, 25.9, 23.4, 22.6, 21.9; IR (film):

3042, 2922, 2854, 1600, 1253 cm^{-1}; HRMS-ESI (*m/z*) $[M + H]^+$ calcd for $C_{25}H_{28}NO_2^+$, 374.2120; found 374.2134. $[\alpha]^{22.2}_D$ –50° (*c* = 1.00, CH_2Cl_2).

The structure of **(–)-3.34** was verified by 2D-NOESY, as the following interactions were observed:

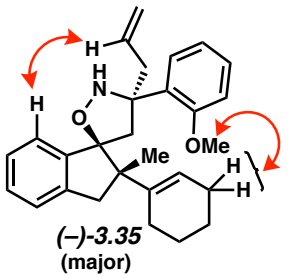




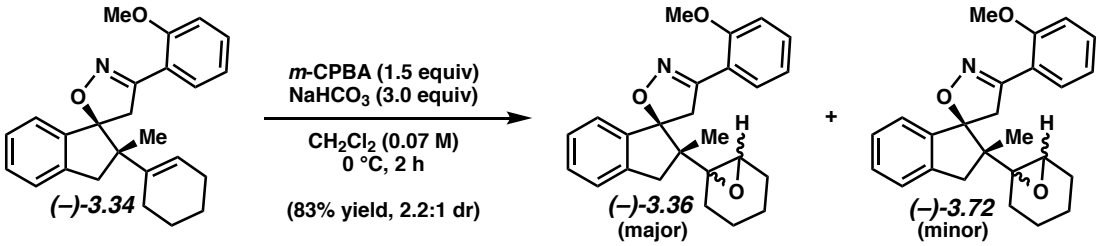
(–)-3.35 and **(–)-3.71.** A flame-dried 1-dram vial was charged with **(–)-3.34** (28.5 mg, 0.068 mmol, 1.0 equiv) and toluene (1.0 mL) and cooled to –78 °C. BF_3OEt_2 (26.0 µL, 0.21 mmol, 3.0 equiv) was then added and the reaction was allowed to stir at –78 °C for 1 h. Subsequently, a solution of allylMgCl (2.0 M in THF, 512 µL, 15.0 equiv) in toluene (0.95 mL) was prepared and added slowly dropwise over 15 min to the reaction vial. The resulting solution was allowed to stir for 1 h and after this time, the reaction was quenched at –78 °C with saturated aqueous $NaHCO_3$ (2 mL) and slowly allowed to warm to 23 °C. The mixture was then diluted with Et_2O (2 mL) and deionized water (2 mL). The organic and aqueous layers were separated, and the aqueous layer was extracted with Et_2O (2 x 2 mL). The combined organic layers were dried with Na_2SO_4, filtered, and concentrated under reduced pressure. Purification by preparative thin layer silica

chromatography (4:1 hexanes:EtOAc) afforded major diastereomer **(–)-3.35** and minor diastereomer **(–)-3.71**, each as colorless oils (19.4 mg, 0.044 mmol, 63% combined yield, 1.6:1 dr determined by ^{1}H NMR analysis of the crude reaction mixture). **(–)-3.35** (major): R_f 0.55 (5:1 hexanes:EtOAc); ^{1}H NMR (600 MHz, $(CD_3)_2SO$): δ 7.65–7.54 (m, 2H), 7.29–7.20 (m, 3H), 7.20–7.15 (m, 1H), 7.04–6.99 (m, 1H), 6.90 (td, *J* = 7.5, 0.9, 1H), 6.18 (br s, 1H), 5.55 (ddt, *J* = 16.9, 10.1, 7.5, 1H), 5.24–5.14 (m, 1H), 4.95–4.83 (m, 2H), 3.79 (s, 3H), 3.00–2.90 (m, 2H), 2.84 (d, *J* = 15.5, 1H), 2.70 (dd, *J* = 14.2, 6.8, 1H), 2.63 (d, *J* = 15.5, 1H), 2.46 (d, *J* = 14.0, 1H), 1.85–1.69 (m, 2H), 1.47–1.37 (m, 1H), 1.34–1.13 (m, 4H), 1.07–0.95 (m, 1H), 0.72 (s, 3H); ^{13}C NMR (150 MHz, $(CD_3)_2SO$): δ 156.5, 147.7, 142.3, 142.0, 134.8, 132.2, 128.00, 127.95, 127.8, 126.6, 124.2, 122.3, 120.6, 119.8, 117.4, 111.7, 97.7, 69.0, 55.3, 53.8, 47.9, 43.5, 40.6, 26.0, 25.0, 22.5, 21.6, 20.0; IR (film): 3359, 3071, 2928, 1601, 1235 cm^{-1}; HRMS-ESI (*/z*) $[M + H]^+$ calcd for $C_{28}H_{34}NO_2^+$, 416.2589; found 416.2595. $[\alpha]^{21.9}_D$ –62° (*c* = 1.00, CH_2Cl_2). **(–)-3.71** (minor): R_f 0.65 (3:1 hexanes:EtOAc); ^{1}H NMR (500 MHz, $(CD_3)_2SO$): δ 7.65–7.48 (m, 1H), 7.34–7.25 (m, 1H), 7.13–6.99 (m, 3H), 6.96–6.85 (m, 1H), 6.84–6.64 (m, 1H), 6.16–5.71 (m, 2H), 5.71–5.60 (m, 1H), 5.59–5.46 (m, 1H), 4.98–4.83 (m, 2H), 3.86–3.79 (m, 3H), 2.97–2.86 (m, 1H), 2.85–2.68 (m, 3H), 2.61–2.57 (m, 1H), 2.56–2.52 (overlapped with residual solvent peak, 1H), 2.12–1.97 (m, 2H), 1.58–1.21 (m, 9H); ^{13}C NMR (125 MHz, $(CD_3)_2SO$, 27 of 28 peaks observed): δ 156.6, 146.0, 142.8, 141.4, 134.4, 131.0, 128.3, 128.2, 128.0, 126.1, 123.8, 122.6, 121.4, 120.1, 117.6, 111.8, 97.4, 69.0, 55.5, 54.9, 47.0, 43.5, 26.3, 25.2, 22.9, 21.7, 19.5; IR (film): 3075, 2928, 1600, 1436, 1236 cm^{-1}; HRMS-APCI (*m/z*) $[M + H]^+$ calcd for $C_{28}H_{34}NO_2^+$, 416.2589; found 416.2585. $[\alpha]^{25.2}_D$ –42° (*c* = 1.00, CH_2Cl_2).

The structure of **(–)-3.35** was verified by 2D-NOESY, as the following interactions were observed:



(–)-3.35
(major)



(–)-3.34

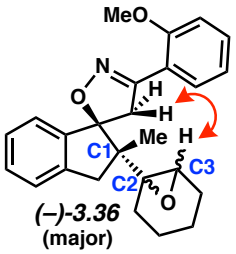
(–)-3.36
(major)

(–)-3.72
(minor)

(–)-3.36 and **(–)-3.72.** A 1-dram vial containing a stir bar was charged with **(–)-3.34** (13.3 mg, 0.033 mmol, 1.0 equiv) and CH_2Cl_2 (490 μL, 0.07 M), and the solution was cooled to 0 °C. Then, $NaHCO_3$ (8.3 mg, 0.098 mmol, 3.0 equiv), and *m*-CPBA (77 wt% purity, 11.0 mg, 0.049 mmol, 1.5 equiv) were added sequentially as solids in singular portions and the reaction was stirred for 2 h at 0 °C. After this time, the reaction was quenched with EtOAc (2 mL) and diluted with saturated aqueous $NaHCO_3$ (2 mL). The organic and aqueous layers were separated, and the aqueous layer was extracted with EtOAc (2 x 2 mL). The combined organic layers were dried with Na_2SO_4, filtered, and concentrated under reduced pressure. Purification by preparative thin layer silica chromatography (4:1 hexanes: EtOAc) afforded unassigned diastereomers **(–)-3.36** and **(–)-3.72**, each as beige foams (11.3 mg, 0.027 mmol, 83% combined yield, 2.2:1 dr determined by ^{1}H NMR analysis of the crude reaction mixture). **(–)-3.36** (major): R_f 0.50 (3:1 hexanes: EtOAc); ^{1}H NMR

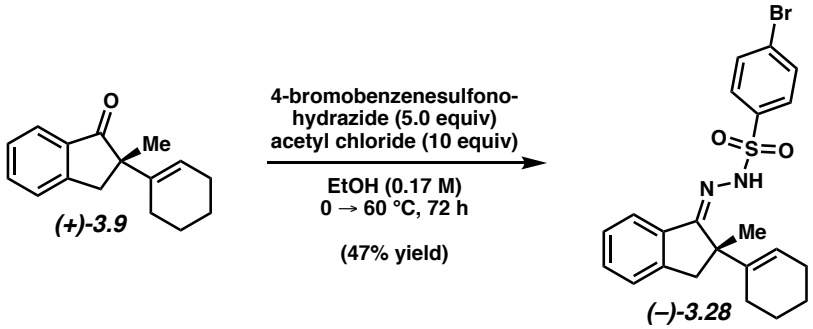
(600 MHz, $CDCl_3$): δ 7.82 (dd, *J* = 7.6, 1.7, 1H), 7.39 (ddd, *J* = 8.3, 7.6, 1.7, 1H), 7.32–7.28 (m, 1H), 7.25–7.19 (m, 2H), 7.18–7.14 (m, 1H), 7.01 (td, *J* = 7.6, 0.9, 1H), 6.94 (d, *J* = 8.3, 1H), 3.98 (d, *J* = 18.2, 1H), 3.83 (s, 3H), 3.51–3.46 (m, 1H), 3.28 (d, *J* = 18.2, 1H), 2.82 (d, *J* = 15.9, 1H), 2.55 (d, *J* = 15.9, 1H), 2.16–2.08 (m, 1H), 1.98 (dt, *J* = 15.6, 5.5, 1H), 1.85 (ddd, 15.6, 9.9, 5.4, 1H), 1.76 (dddd, *J* = 15.2, 8.7, 5.9, 3.0, 1H), 1.48–1.40 (m, 1H), 1.40–1.33 (m, 1H), 1.31 (s, 3H), 1.25–1.17 (m, 1H), 1.04 (dtdd, *J* = 13.7, 9.9, 5.4, 3.0, 1H); ^{13}C NMR (150 MHz, $CDCl_3$): δ 157.6, 155.7, 146.2, 138.9, 131.5, 129.5, 128.6, 127.5, 125.1, 122.9, 121.1, 119.1, 111.6, 97.4, 62.8, 57.1, 55.6, 54.7, 46.0, 39.3, 26.2, 25.7, 21.0, 19.1, 18.9; IR (film): 2994, 2936, 2861, 1600, 1251 cm^{-1}; HRMS-ESI (*m/z*) $[M + H]^+$ calcd for $C_{25}H_{28}NO_3^+$, 390.2069; found 390.2071. $[\alpha]^{23.5}_D$ –72° (*c* = 1.00, CH_2Cl_2). **(–)-3.72** (minor): R_f 0.55 (3:1 hexanes: EtOAc); ^{1}H NMR (600 MHz, $CDCl_3$): δ 7.81–7.75 (m, 1H), 7.40–7.33 (m, 1H), 7.31–7.26 (m, 1H), 7.24–7.18 (m, 2H), 7.18–7.12 (m, 1H), 6.99 (t, *J* = 7.4, 1H), 6.92 (d, *J* = 8.3, 1H), 4.29 (d, *J* = 18.8, 1H), 3.82 (s, 3H), 3.27 (d, *J* = 18.8, 1H), 3.09 (d, *J* = 15.1, 1H), 2.99–2.92 (m, 1H), 2.37–2.28 (m, 2H), 2.05 (dt, *J* = 15.5, 5.2, 1H), 1.86–1.76 (m, 1H), 1.65 (ddd, *J* = 15.5, 9.9, 5.2, 1H), 1.52–1.44 (m, 1H), 1.39–1.29 (m, 2H), 1.27 (s, 3H), 1.20–1.09 (m, 1H); ^{13}C NMR (150 MHz, $CDCl_3$): δ 157.9, 156.2, 147.0. 138.1, 131.3, 129.6, 128.3, 127.4, 125.2, 122.7, 120.9, 119.2, 111.5, 97.1, 63.0, 55.6, 55.5, 54.2, 46.5, 38.0, 25.3, 25.1, 21.34, 21.26, 19.3; IR (film): 3029, 2934, 2854, 1600, 1253 cm^{-1}; HRMS-ESI (*m/z*) $[M + H]^+$ calcd for $C_{25}H_{28}NO_3^+$, 390.2069; found 390.2075. $[\alpha]^{22.4}_D$ –94° (*c* = 1.00, CH_2Cl_2).

The structure of **(–)-3.36** was analyzed by 2D-NOESY, and the following interaction was observed:



Attempts to assign the stereocenters at C2 and C3 were unsuccessful due to the free rotation about the C–C bond between C1 and C2, which resulted in observation of NOESY correlations with the H at C3 in both diastereomers. Efforts at obtaining an X-Ray crystal structure were unsuccessful, therefore, the stereocenters at C2 and C3 remain unassigned. Nonetheless, the ability to access isomers **(–)-3.36** and **(–)-3.72** in enantioenriched form demonstrates that complex structures bearing multiple stereocenters are readily accessible from Mizoroki–Heck cyclization products.

3.8.2.7 Assignment of Absolute Stereochemical Configuration of Indanone (+)-3.9



Brosyl hydrazone (–)-3.28. A flame-dried 1-dram vial containing a stir bar was charged with (+)-**3.9** (29.5 mg, 0.13 mmol, 1.0 equiv) followed by 4-bromobenzene-1-sulfonohydrazide (164 mg, 0.65 mmol, 5.0 equiv). Then, ethanol (1.86 mL, 0.07 M) was added and the vial was cooled to 0 °C. Lastly, acetyl chloride (91.1 µL, 1.30 mmol, 10.0 equiv) was added slowly over 1 minute. The vial was sealed with a Teflon-lined screw cap and then heated to 60 °C and allowed to stir for 72

h. The reaction was allowed to cool to 23 °C and then EtOAc (1.0 mL) was added. The solution was filtered through filter paper using a Buchner funnel and washed with EtOAc (1.0 mL). The solid was discarded and the filtrate was concentrated under reduced pressure. Purification by preparative thin layer silica chromatography (benzene) afforded product **(–)-3.28** (28.3 mg, 0.062 mmol, 47% yield) as a white solid.

Crystals suitable for X-ray diffraction studies were obtained by recrystallization from hot ethanol with the following procedure: **(–)-3.28** (28.3 mg) was added to a scintillation vial along with ethanol (1.2 mL, filtered through a 0.22 μm filter prior to use). The scintillation vial was heated to 75 °C for 5 min until the solid dissolved. The vial was allowed to cool slowly to 23 °C overnight with a septum cap pierced with a vent needle open to air. After 16 h, clear crystals were found on the bottom of the vial. The crystals of **(–)-3.28** that were evaluated by X-ray had the same sign by optical rotation ($[\alpha]^{26.1}_{D}$–294.0° (c = 1.00, CH_2Cl_2)) as the enantioenriched mixture observed after chromatography (i.e., $[\alpha]^{22.5}_{D}$–276.0°). **Brosyl hydrazone (–)-3.28**: Mp: 178–182 °C; R_f 0.65 (8:2 hexanes:EtOAc); ^{1}H NMR (500 MHz, $CDCl_3$): δ 8.55 (s, 1H), 7.88–7.81 (m, 2H), 7.70–7.60 (m, 3H), 7.34 (td, *J* = 7.4, 1.3, 1H), 7.30–7.23 (overlapped with residual solvent peak, 1H), 7.22–7.16 (m, 1H), 5.91–5.82 (m, 1H), 3.09 (d, *J* = 17.3, 1H), 2.77 (d, *J* = 17.3, 1H), 2.22–1.95 (m, 2H), 1.83–1.68 (m, 1H), 1.66–1.15 (m, 8H); ^{13}C NMR (125 MHz, $CDCl_3$): δ 163.0, 146.0, 139.2, 137.5, 137.0, 132.2, 131.2, 129.6, 128.3, 127.5, 125.5, 124.6, 122.5, 51.0, 45.8, 25.6, 25.0, 22.8, 22.2, 20.4; IR (film): 3206, 2928, 2858, 1574, 1355 cm^{-1}; HRMS-ESI (*m/z*) $[M + H]^+$ calcd for $C_{22}H_{24}BrN_2O_2S^+$, 459.0742; found 459.0759; $[\alpha]^{22.5}_{D}$–276.0° (c = 1.00, CH_2Cl_2).

Crystal Structure Analysis for (–)-3.28

Diffraction intensities were collected at 100 K on a Bruker Smart ApexII CCD diffractometer with CuKα radiation, 1.54178 Å. Absorption corrections were applied by SADABS.[37] All calculations

were performed by the SHELXL-2014 packages.[38] Deposition Number 2271421 contains the supplementary crystallographic data for this paper. These data are provided free of charge by the joint Cambridge Crystallographic Data Centre and Fachinformationszentrum Karlsruhe Access Structures service www.ccdc.cam.ac.uk/structures.

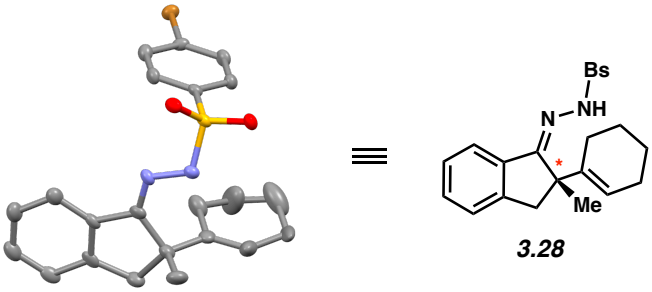


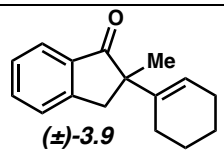
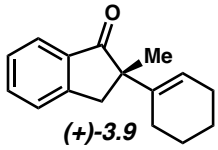
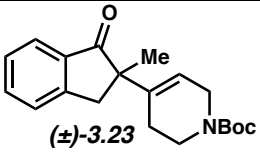
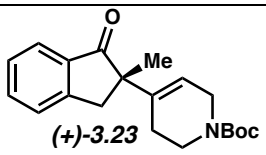
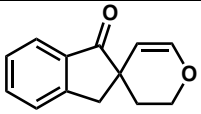
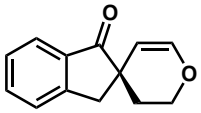
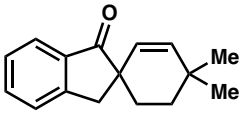
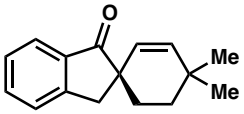
***Figure 3.12*: ORTEP representation of X-ray crystallographic structure of (–)-3.28 (CCDC Registry #2271421).**

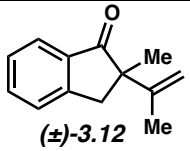
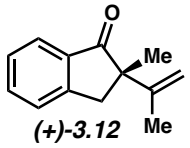
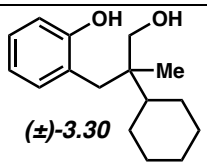
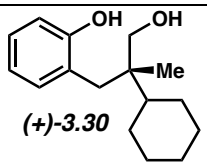
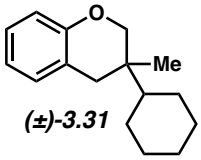
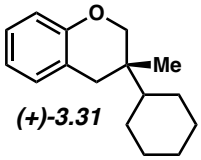
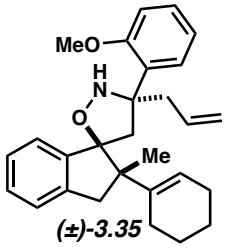
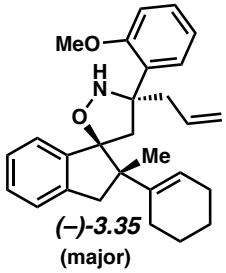
Table 3.10. Crystal data and structure refinement for compound (–)-**3.28**.

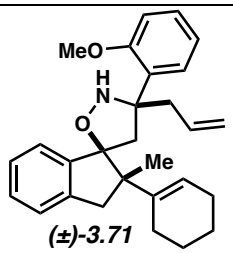
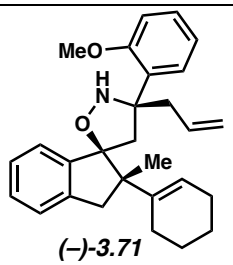
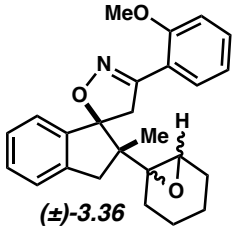
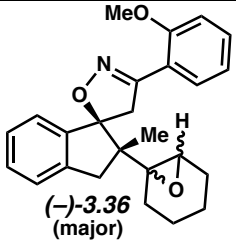
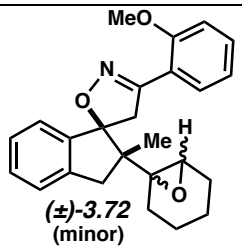
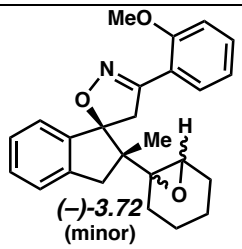
Identification code	cu_garg2304_a	
Empirical formula	C22 H23 Br N2 O2 S	
Formula weight	459.39	
Temperature	100(2) K	
Wavelength	1.54178 Å	
Crystal system	Monoclinic	
Space group	$P2_1$	
Unit cell dimensions	a = 9.5459(2) Å	α = 90°.
	b = 19.1854(5) Å	β = 93.0090(10)°.
	c = 11.5679(3) Å	γ = 90°.
Volume	2115.65(9) $Å^3$	
Z	4	
Density (calculated)	1.442 Mg/m^3	
Absorption coefficient	3.728 mm^{-1}	
F(000)	944	
Crystal size	0.18 x 0.04 x 0.04 mm^3	
Theta range for data collection	3.826 to 69.613°.	
Index ranges	-11<=h<=11, -22<=k<=23, -13<=l<=13	
Reflections collected	26366	
Independent reflections	7768 [R(int) = 0.0457]	
Completeness to theta = 67.679°	99.8	
Absorption correction	Semi-empirical from equivalents	
Max. and min. transmission	0.75 and 0.64	
Refinement method	Full-matrix least-squares on F^2	
Data / restraints / parameters	7768 / 1 / 513	
Goodness-of-fit on F^2	1.040	
Final R indices [I>2sigma(I)]	R1 = 0.0329, wR2 = 0.0700	
R indices (all data)	R1 = 0.0375, wR2 = 0.0712	
Absolute structure parameter	-0.009(8)	
Extinction coefficient	n/a	
Largest diff. peak and hole	0.796 and -0.497 $e.Å^{-3}$	

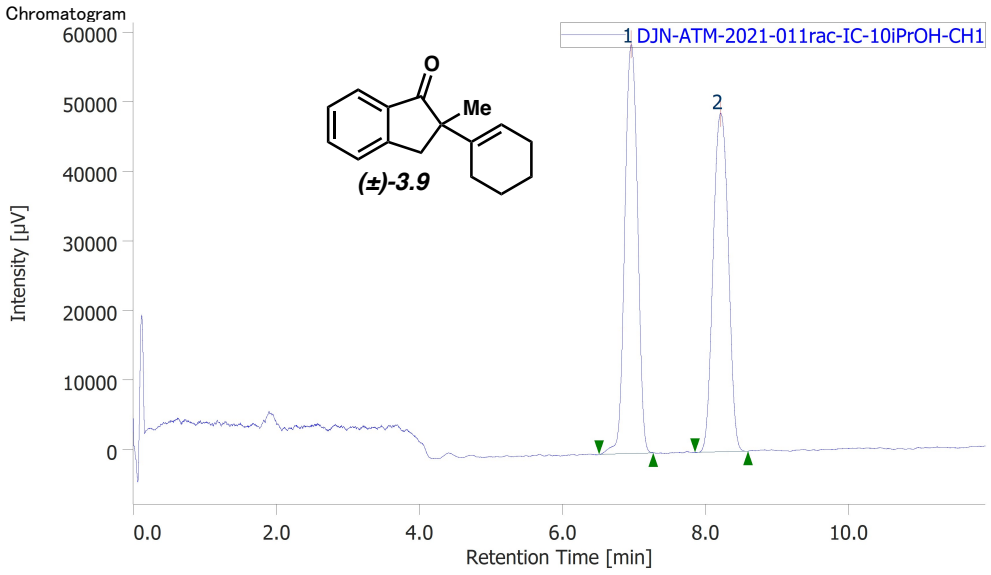
3.9 SFC Traces

Table 3.11. SFC conditions and data.

Compound	Column	Solvent	Flow Rate	Retention Times (min)	Enantiomeric Ratio (er)
 *(±)-3.9*	Daicel ChiralPak IC / 30 °C	10% isopropanol in CO_2	10.0 mL/min	6.96/8.21	50.5 : 49.5
 *(+)-3.9*	Daicel ChiralPak IC / 30 °C	10% isopropanol in CO_2	10.0 mL/min	6.83/7.98	6.2 : 93.8
 *(±)-3.23*	Daicel ChiralPak ID / 30 °C	15% isopropanol in CO_2	4.0 mL/min	4.93/5.66	49.9 : 50.1
 *(+)-3.23*	Daicel ChiralPak ID / 30 °C	15% isopropanol in CO_2	4.0 mL/min	4.67/5.29	6.1 : 93.9
 *(±)-3.25*	Daicel ChiralPak IC / 30 °C	10% isopropanol in CO_2	10.0 mL/min	9.32/11.13	50.0 : 50.0
 *(+)-3.25*	Daicel ChiralPak IC / 30 °C	10% isopropanol in CO_2	10.0 mL/min	9.34/11.18	93.6 : 6.4
 *(±)-3.27*	Daicel ChiralPak IC / 30 °C	10% isopropanol in CO_2	10.0 mL/min	6.05/6.53	50.3 : 49.7
 *(+)-3.27*	Daicel ChiralPak IC / 30 °C	10% isopropanol in CO_2	10.0 mL/min	5.98/6.42	22.9 : 77.1

 ***(±)-3.12***	Daicel ChiralPak IC / 30 °C	10% isopropanol in CO_2	10.0 mL/min	4.25/4.79	49.9 : 50.1
 ***(+)-3.12***	Daicel ChiralPak IC / 30 °C	10% isopropanol in CO_2	10.0 mL/min	4.25/4.78	11.5 : 88.5
 ***(±)-3.30***	Daicel ChiralPak IC / 30 °C	10% isopropanol in CO_2	1.5 mL/min	9.91/14.37	50.1 : 49.9
 ***(+)-3.30***	Daicel ChiralPak IC / 30 °C	10% isopropanol in CO_2	1.5 mL/min	9.89/14.34	5.8 : 94.2
 ***(±)-3.31***	Daicel ChiralPak IB N-3 / 30 °C	10% isopropanol in CO_2	1.5 mL/min	4.41/4.67	50.7 : 49.3
 ***(+)-3.31***	Daicel ChiralPak IB N-3 / 30 °C	10% isopropanol in CO_2	1.5 mL/min	4.51/4.79	94.1 : 5.9
 ***(±)-3.35*** **(major)**	Daicel ChiralPak IC / 30 °C	20% isopropanol in CO_2	1.5 mL/min	6.23/11.11	49.9 : 50.1
 ***(–)-3.35*** **(major)**	Daicel ChiralPak IC / 30 °C	20% isopropanol in CO_2	1.5 mL/min	6.30/11.23	93.9 : 6.1

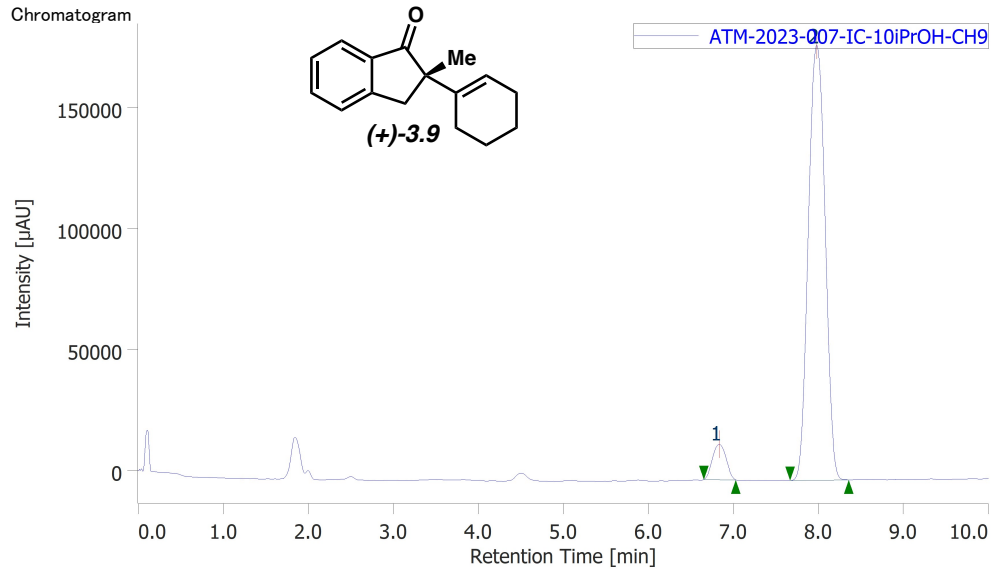
 ***(±)-3.71*** **(minor)**	Daicel ChiralPak IB N-3 / 30 °C	10% isopropanol in CO_2	1.5 mL/min	9.87/18.36	50.2 : 49.8
 ***(–)-3.71*** **(minor)**	Daicel ChiralPak IB N-3 / 30 °C	10% isopropanol in CO_2	1.5 mL/min	9.88/18.52	93.9 : 6.1
 ***(±)-3.36*** **(major)**	Daicel ChiralPak IC / 30 °C	30% isopropanol in CO_2	1.5 mL/min	9.63/11.82	49.8 : 50.2
 ***(–)-3.36*** **(major)**	Daicel ChiralPak IC / 30 °C	30% isopropanol in CO_2	1.5 mL/min	9.61/11.82	93.8 : 6.2
 ***(±)-3.72*** **(minor)**	Daicel ChiralPak IC / 30 °C	20% isopropanol in CO_2	1.5 mL/min	12.82/17.89	50.0 : 50.0
 ***(–)-3.72*** **(minor)**	Daicel ChiralPak IC / 30 °C	20% isopropanol in CO_2	1.5 mL/min	12.77/17.76	93.8 : 6.2



Peak Information

#	Peak Name	CH	tR [min]	Area [μV·sec]	Height [μV]	Area%	Height%	Quantity	NTP	Resolution	Symmetry Factor	Warning
1	Unknown	1	6.955	730939	58833	50.452	54.709	N/A	6753	3.361	1.009	
2	Unknown	1	8.205	717845	48706	49.548	45.291	N/A	6497	N/A	1.026	

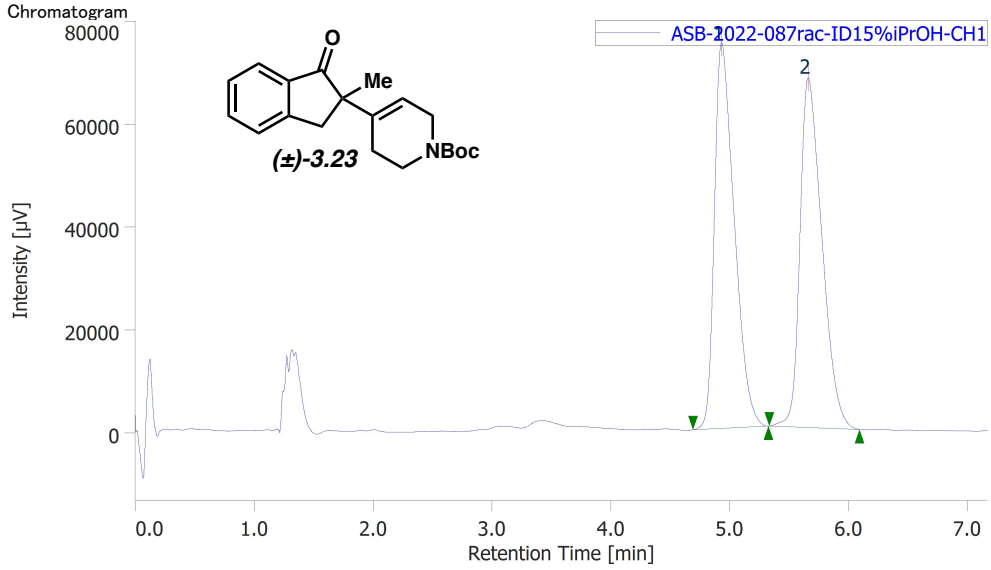
Figure 3.13. SFC trace for **(±)-3.9**.



Peak Information

#	Peak Name	CH	tR [min]	Area [μV·sec]	Height [μV]	Area%	Height%	Quantity	NTP	Resolution	Symmetry Factor	Warning
1	Unknown	9	6.833	162002	14575	6.162	7.500	N/A	7806	3.347	1.020	
2	Unknown	9	7.980	2466920	179762	93.838	92.500	N/A	7141	N/A	1.020	

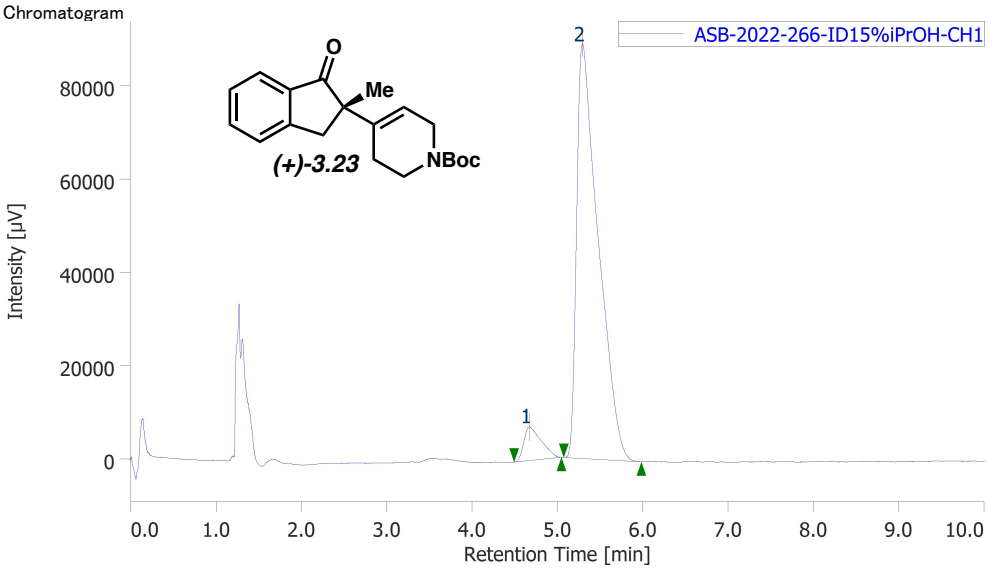
Figure 3.14. SFC trace for **(+)-3.9**.



Peak Information

#	Peak Name	CH	tR [min]	Area [μV·sec]	Height [μV]	Area%	Height%	Quantity	NTP	Resolution	Symmetry Factor	Warning
1	Unknown	1	4.930	867944	74973	49.907	52.456	N/A	4151	2.266	1.508	
2	Unknown	1	5.658	871182	67952	50.093	47.544	N/A	4468	N/A	1.423	

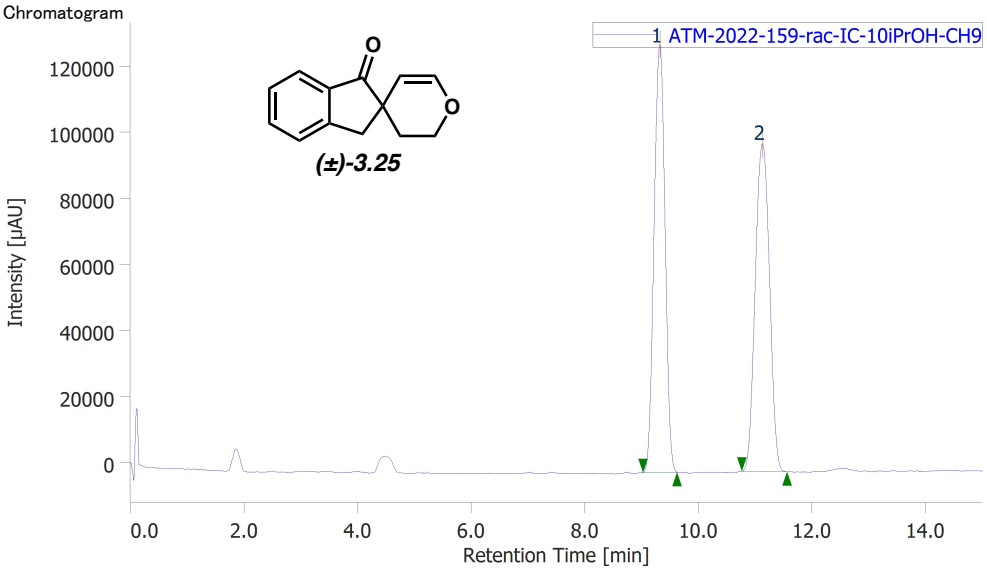
Figure 3.15. SFC trace for **(±)-3.23**.



Peak Information

#	Peak Name	CH	tR [min]	Area [μV·sec]	Height [μV]	Area%	Height%	Quantity	NTP	Resolution	Symmetry Factor	Warning
1	Unknown	1	4.670	101779	7178	6.129	7.464	N/A	2322	1.463	1.686	
2	Unknown	1	5.292	1558738	88987	93.871	92.536	N/A	2079	N/A	2.139	

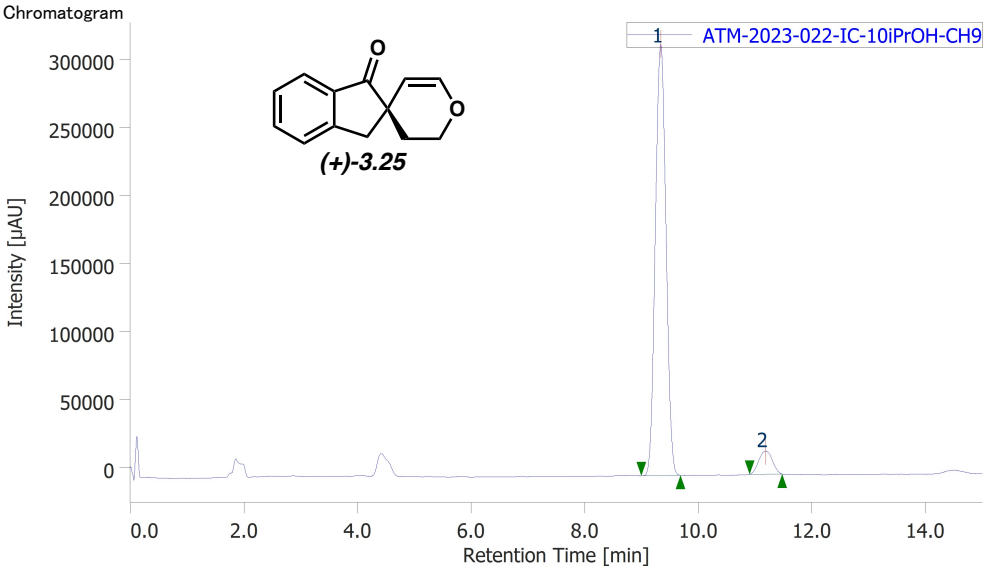
Figure 3.16. SFC trace for **(+)-3.23**.



Peak Information

#	Peak Name	CH	tR [min]	Area [μV·sec]	Height [μV]	Area%	Height%	Quantity	NTP	Resolution	Symmetry Factor	Warning
1	Unknown	9	9.320	1735406	129569	50.000	56.651	N/A	10494	4.292	0.986	
2	Unknown	9	11.127	1735387	99147	50.000	43.349	N/A	8594	N/A	1.016	

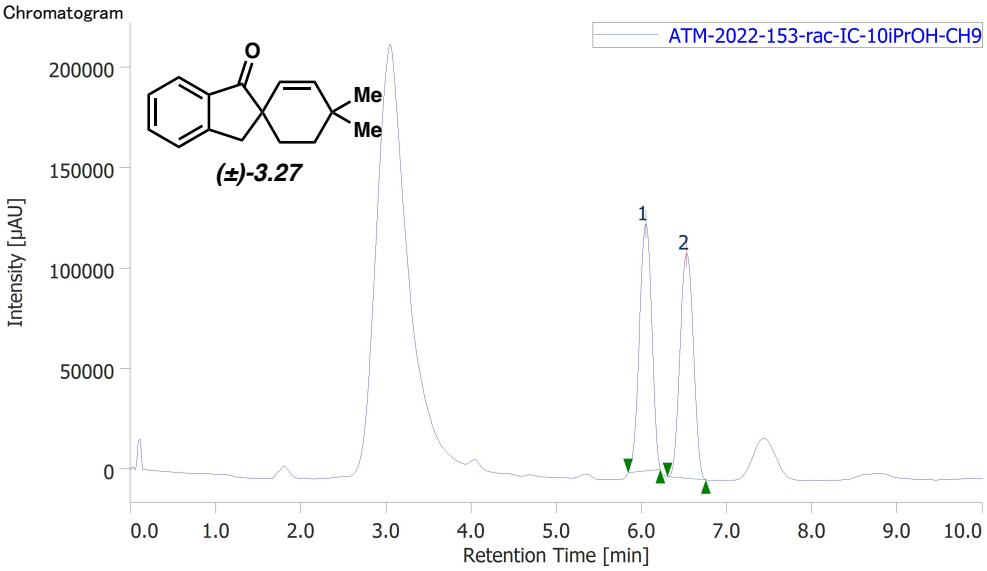
Figure 3.17. SFC trace for **(±)-3.25**.



Peak Information

#	Peak Name	CH	tR [min]	Area [μV·sec]	Height [μV]	Area%	Height%	Quantity	NTP	Resolution	Symmetry Factor	Warning
1	Unknown	9	9.337	4124400	316946	93.554	94.903	N/A	11266	4.548	1.025	
2	Unknown	9	11.177	284158	17022	6.446	5.097	N/A	9466	N/A	1.033	

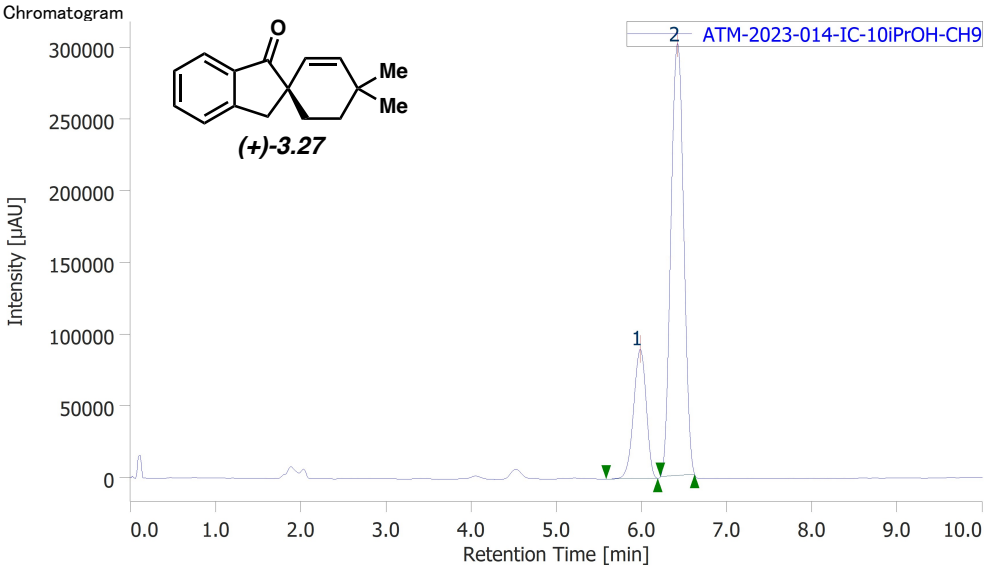
Figure 3.18. SFC trace for **(+)-3.25**.



Peak Information

#	Peak Name	CH	tR [min]	Area [μV·sec]	Height [μV]	Area%	Height%	Quantity	NTP	Resolution	Symmetry Factor	Warning
1	Unknown	9	6.050	1235985	122833	50.324	52.344	N/A	7733	1.673	0.926	
2	Unknown	9	6.530	1220048	111832	49.676	47.656	N/A	7569	N/A	1.007	

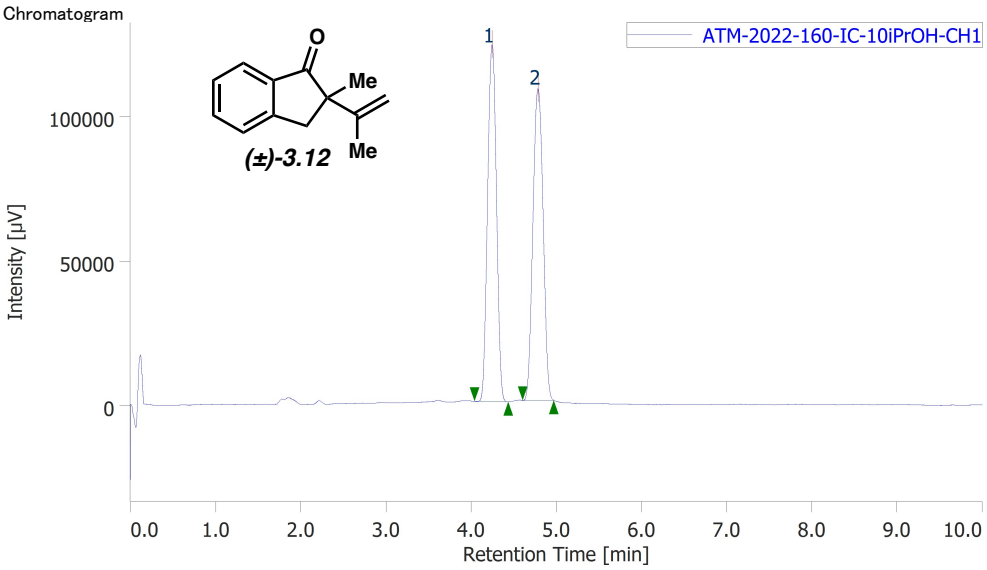
Figure 3.19. SFC trace for **(±)-3.27**.



Peak Information

#	Peak Name	CH	tR [min]	Area [μV·sec]	Height [μV]	Area%	Height%	Quantity	NTP	Resolution	Symmetry Factor	Warning
1	Unknown	9	5.983	933483	90214	22.907	23.052	N/A	7469	1.553	0.918	
2	Unknown	9	6.420	3141658	301141	77.093	76.948	N/A	8021	N/A	1.017	

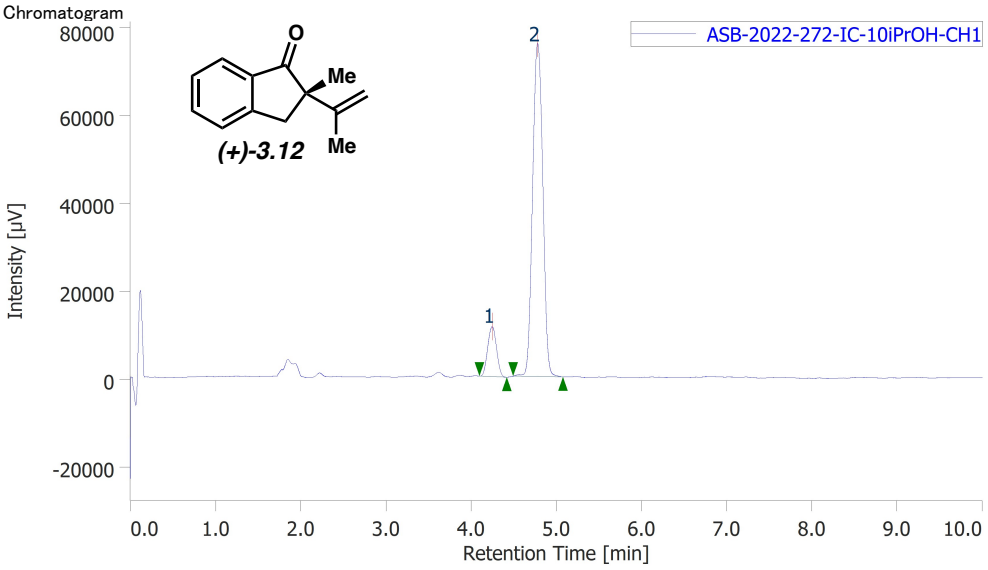
Figure 3.20. SFC trace for **(+)-3.27**.



Peak Information

#	Peak Name	CH	tR [min]	Area [μV·sec]	Height [μV]	Area%	Height%	Quantity	NTP	Resolution	Symmetry Factor	Warning
1	Unknown	1	4.245	891091	123447	49.885	53.408	N/A	7385	2.531	1.008	
2	Unknown	1	4.785	895191	107693	50.115	46.592	N/A	6905	N/A	1.010	

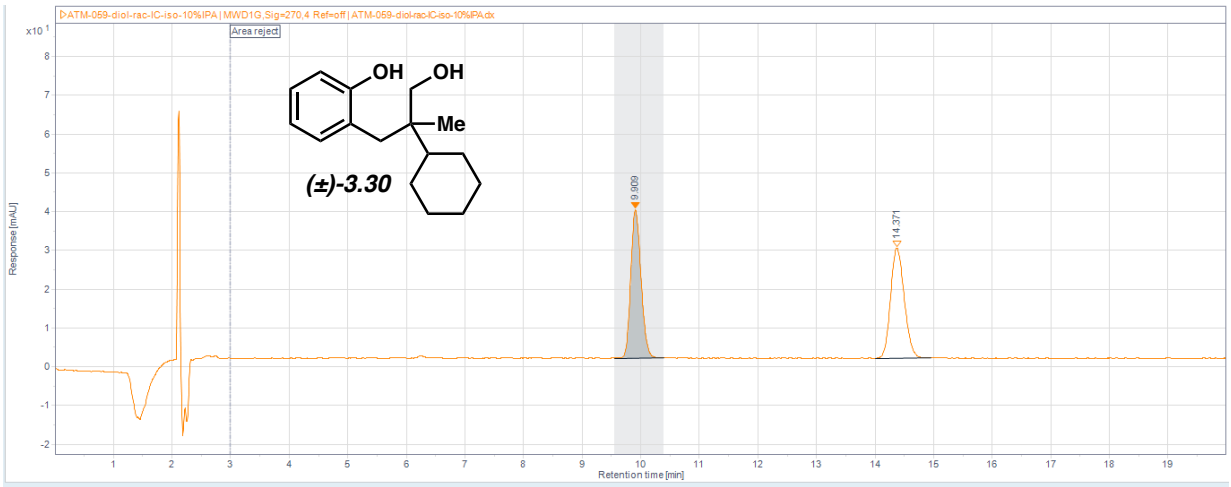
Figure 3.21. SFC trace for **(±)-3.12**.



Peak Information

#	Peak Name	CH	tR [min]	Area [μV·sec]	Height [μV]	Area%	Height%	Quantity	NTP	Resolution	Symmetry Factor	Warning
1	Unknown	1	4.247	81956	11366	11.482	13.034	N/A	7371	2.519	1.009	
2	Unknown	1	4.780	631799	75841	88.518	86.966	N/A	7115	N/A	1.023	

Figure 3.22. SFC trace for **(+)-3.12**.

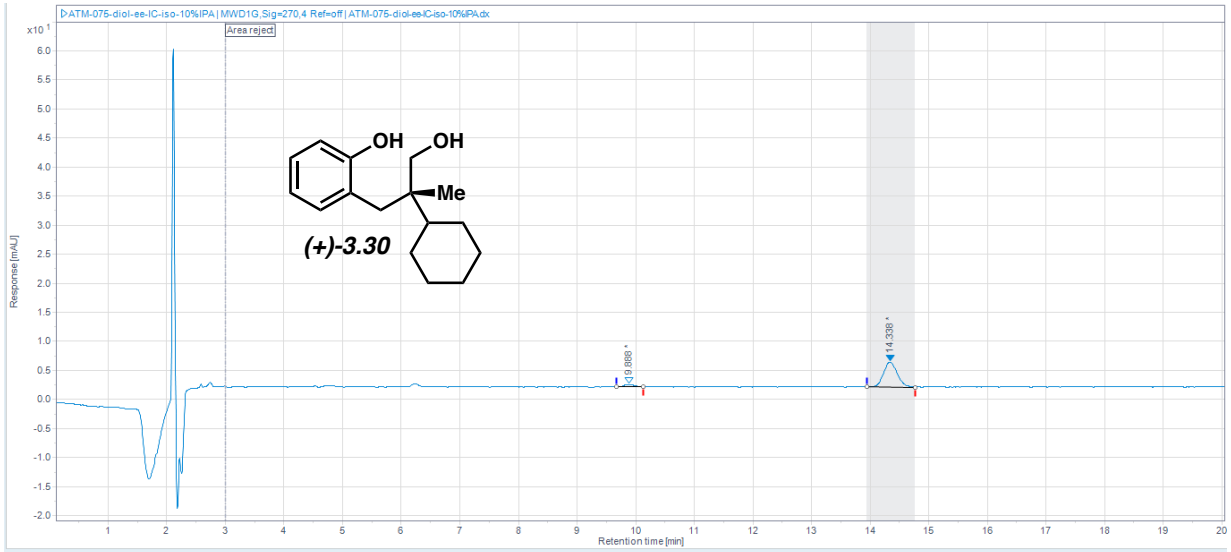


Injection Results

Peaks | Summary

#	Name	Signal description	RT (min)	Area (mAU·s)	Area%	Height (mAU)	Height%	Amount	Concentration	Start time (min)	End time (min)
1		MWD1G,Sig=270,4 Ref=off	9.909	463.312	50.136	38.194	57.34			9.552	10.389
2		MWD1G,Sig=270,4 Ref=off	14.371	460.791	49.864	28.411	42.66			14.002	14.948

Figure 3.23. SFC trace for **(±)-3.30**.

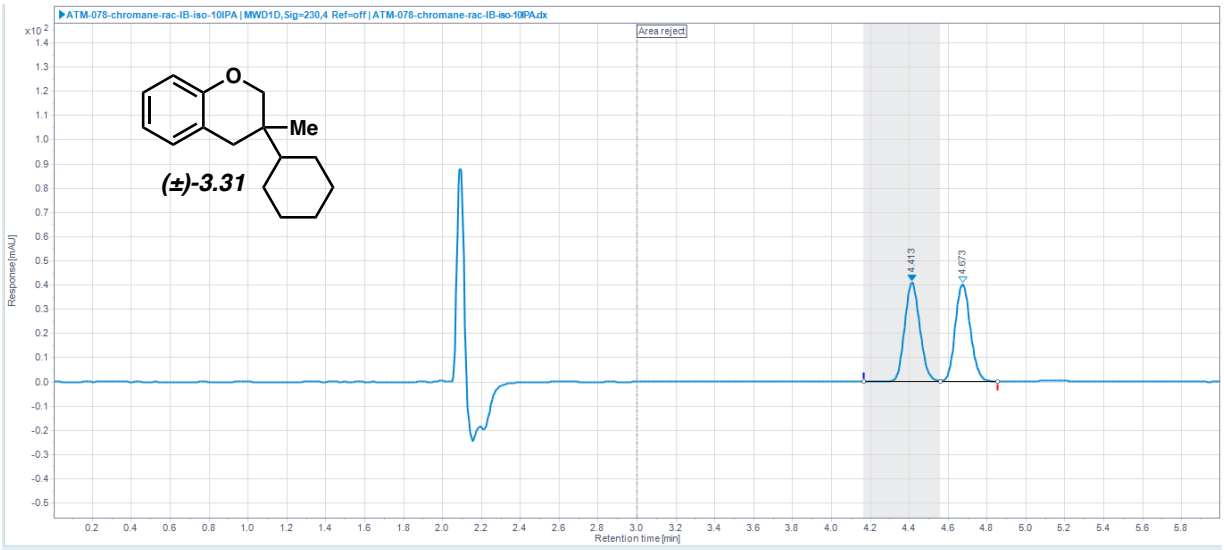


Injection Results

Peaks | Summary

#	Name	Signal description	RT (min)	Area (mAU·s)	Area%	Height (mAU)	Height%	Amount	Concentration	Start time (min)	End time (min)
1		MWD1G,Sig=270,4 Ref=off	9.888	4.292	5.850	0.387	8.35			9.668	10.128
2		MWD1G,Sig=270,4 Ref=off	14.338	69.080	94.150	4.248	91.65			13.940	14.768

Figure 3.24. SFC trace for **(+)-3.30**.

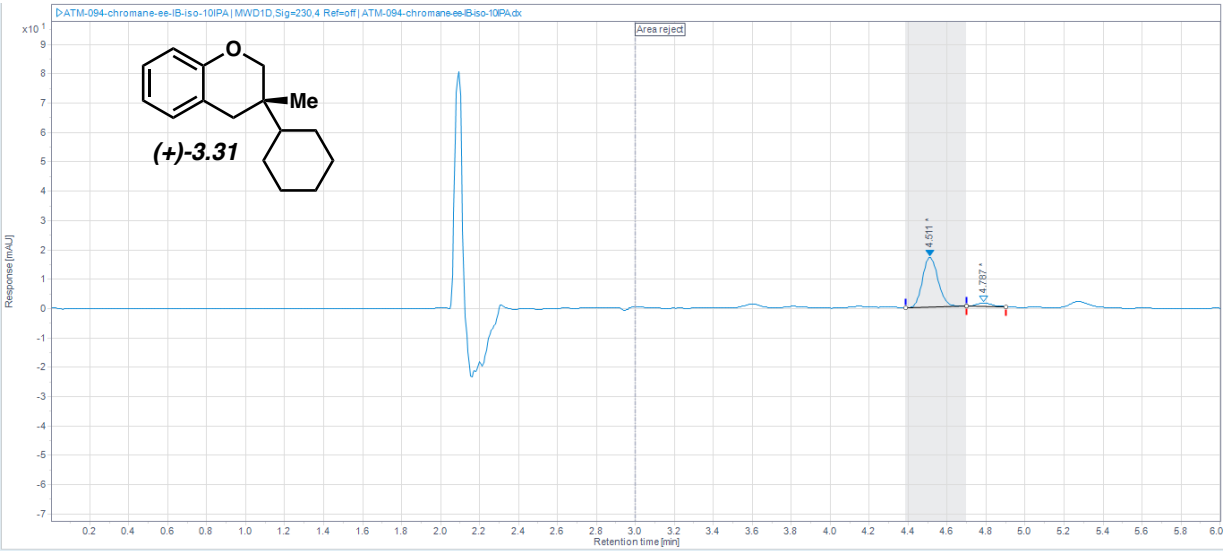


Injection Results

Peaks | Summary

#	Name	Signal description	RT (min)	Area (mAU·s)	Area%	Height (mAU)	Height%	Amount	Concentration	Start time (min)	End time (min)
1		MWD1D,Sig=230,4 Ref=off	4.413	223.789	50.666	40.954	50.46			4.166	4.561
2		MWD1D,Sig=230,4 Ref=off	4.673	217.909	49.334	40.212	49.54			4.561	4.854

Figure 3.25. SFC trace for **(±)-3.31**.



Injection Results

Peaks | Summary

#	Name	Signal description	RT (min)	Area (mAU·s)	Area%	Height (mAU)	Height%	Amount	Concentration	Start time (min)	End time (min)
1		MWD1D,Sig=230,4 Ref=off	4.511	94.408	94.145	16.972	93.97			4.388	4.701
2		MWD1D,Sig=230,4 Ref=off	4.787	5.871	5.855	1.090	6.03			4.701	4.901

Figure 3.26. SFC trace for **(+)-3.31**.

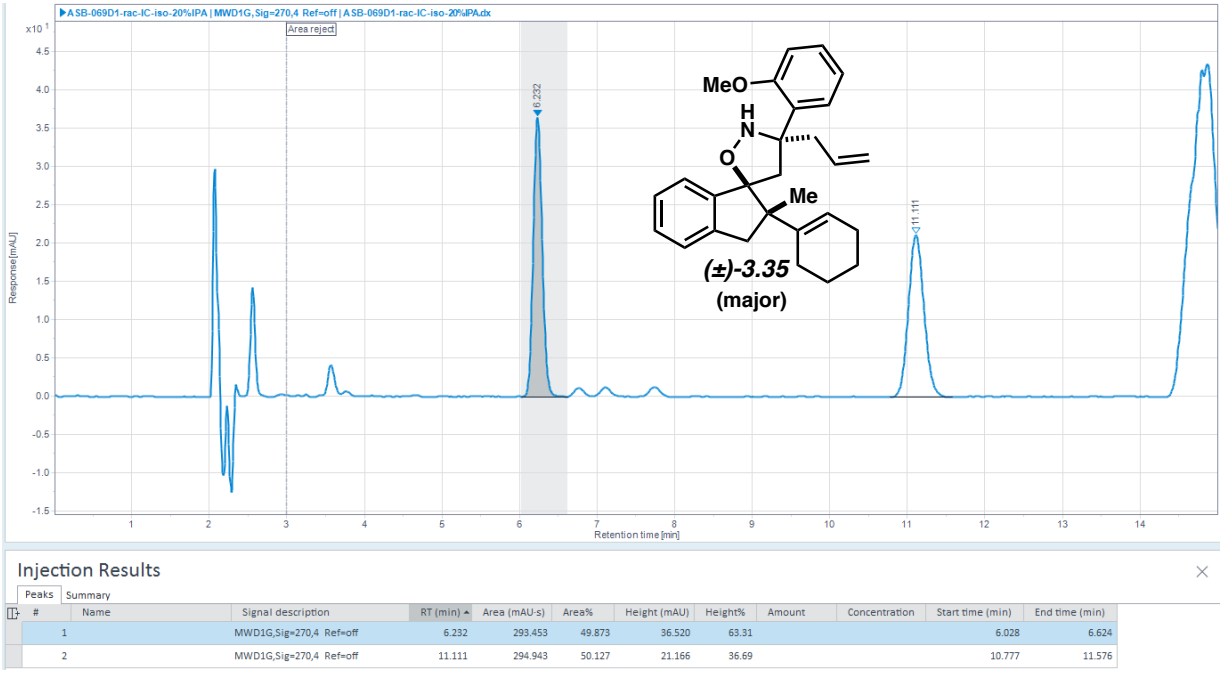


Figure 3.27. SFC trace for **(±)-3.35**.

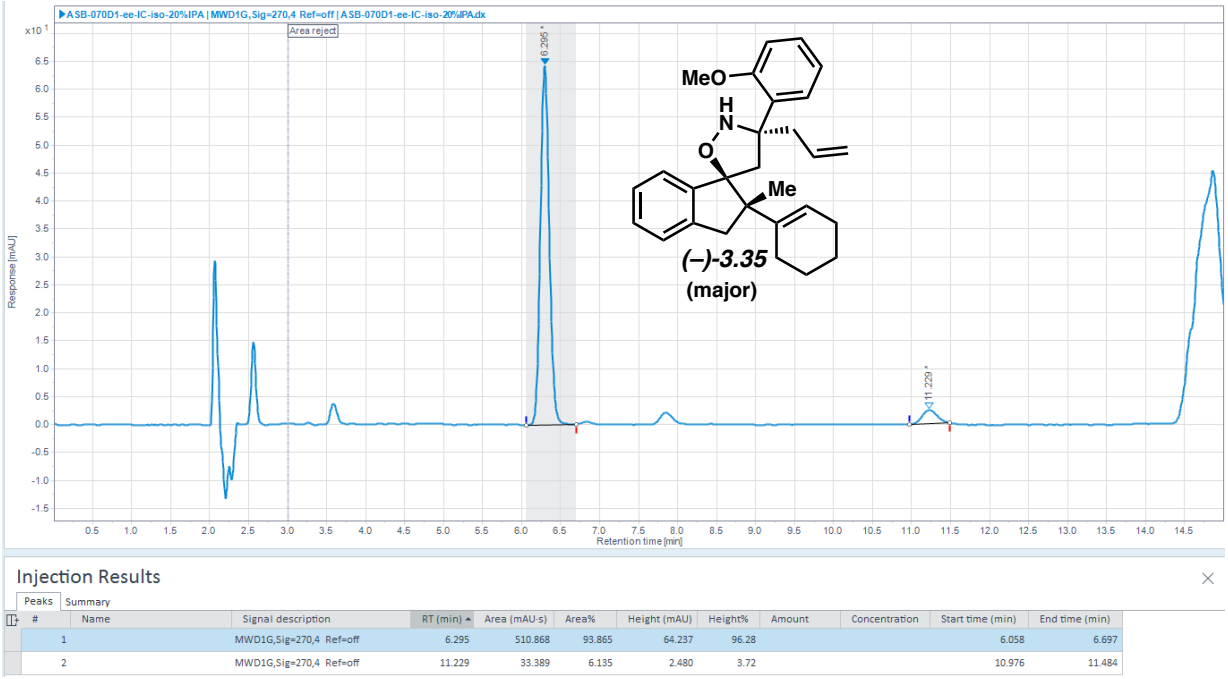
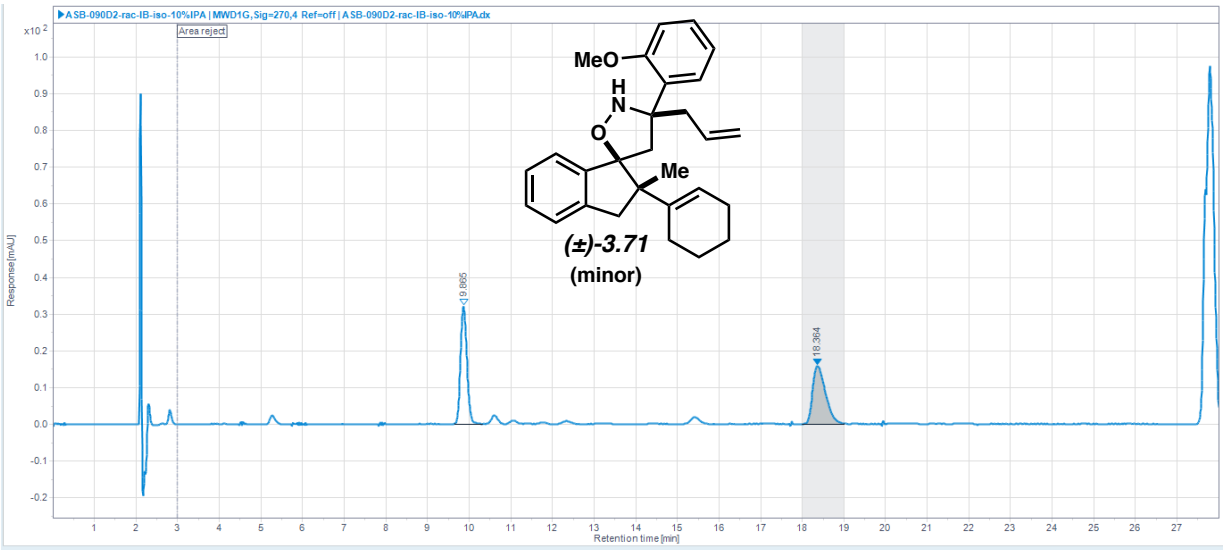


Figure 3.28. SFC trace for **(–)-3.35**.

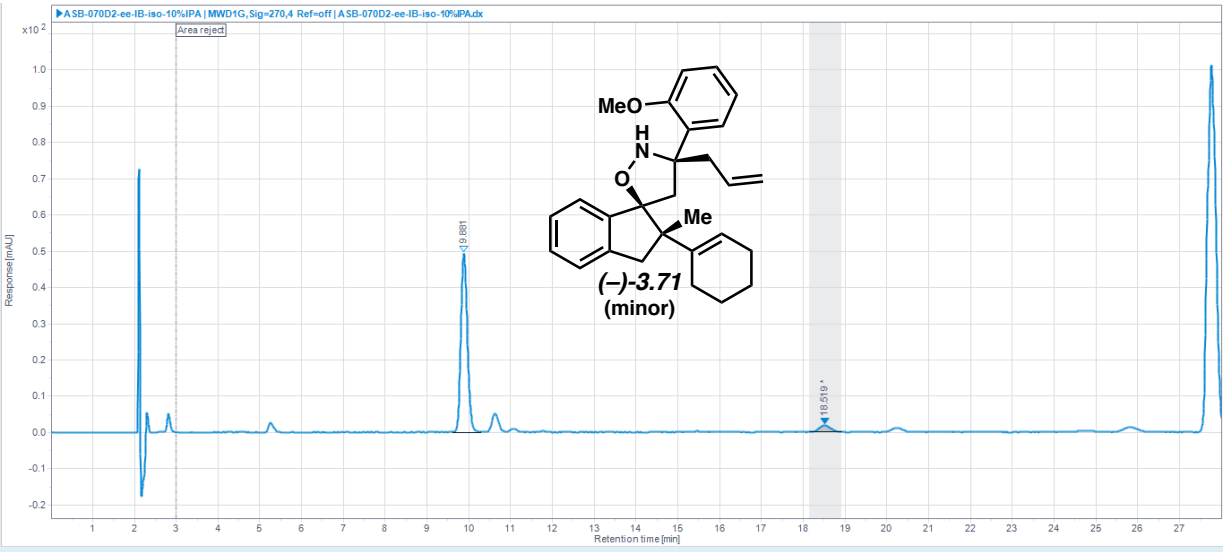


Injection Results

Peaks | Summary

#	Name	Signal description	RT (min)	Area (mAU·s)	Area%	Height (mAU)	Height%	Amount	Concentration	Start time (min)	End time (min)
1		MWD1G,Sig=270,4 Ref=off	9.865	344.021	50.170	32.173	67.00			9.660	10.312
2		MWD1G,Sig=270,4 Ref=off	18.364	341.686	49.830	15.848	33.00			17.995	18.994

Figure 3.29. SFC trace for **(±)-3.71**.



Injection Results

Peaks | Summary

#	Name	Signal description	RT (min)	Area (mAU·s)	Area%	Height (mAU)	Height%	Amount	Concentration	Start time (min)	End time (min)
1		MWD1G,Sig=270,4 Ref=off	9.881	533.540	93.944	49.424	96.44			9.622	10.294
2		MWD1G,Sig=270,4 Ref=off	18.519	34.393	6.056	1.827	3.56			18.148	18.920

Figure 3.30. SFC trace for **(–)-3.71**.

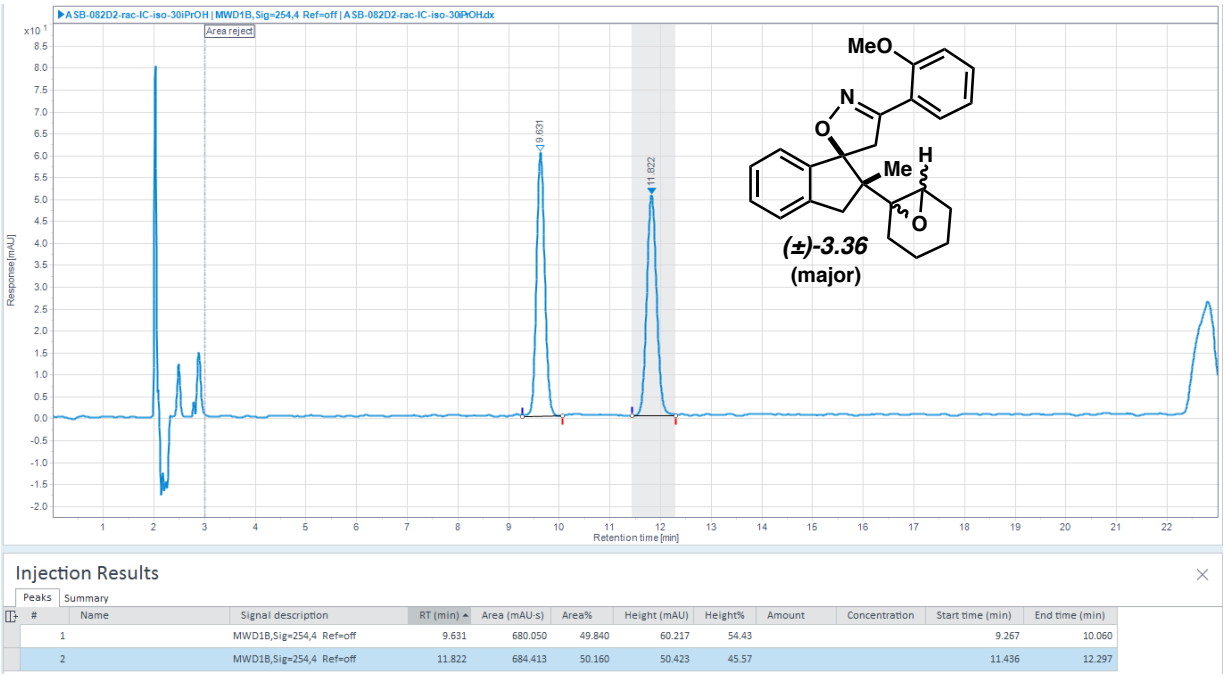


Figure 3.31. SFC trace for **(±)-3.36**.

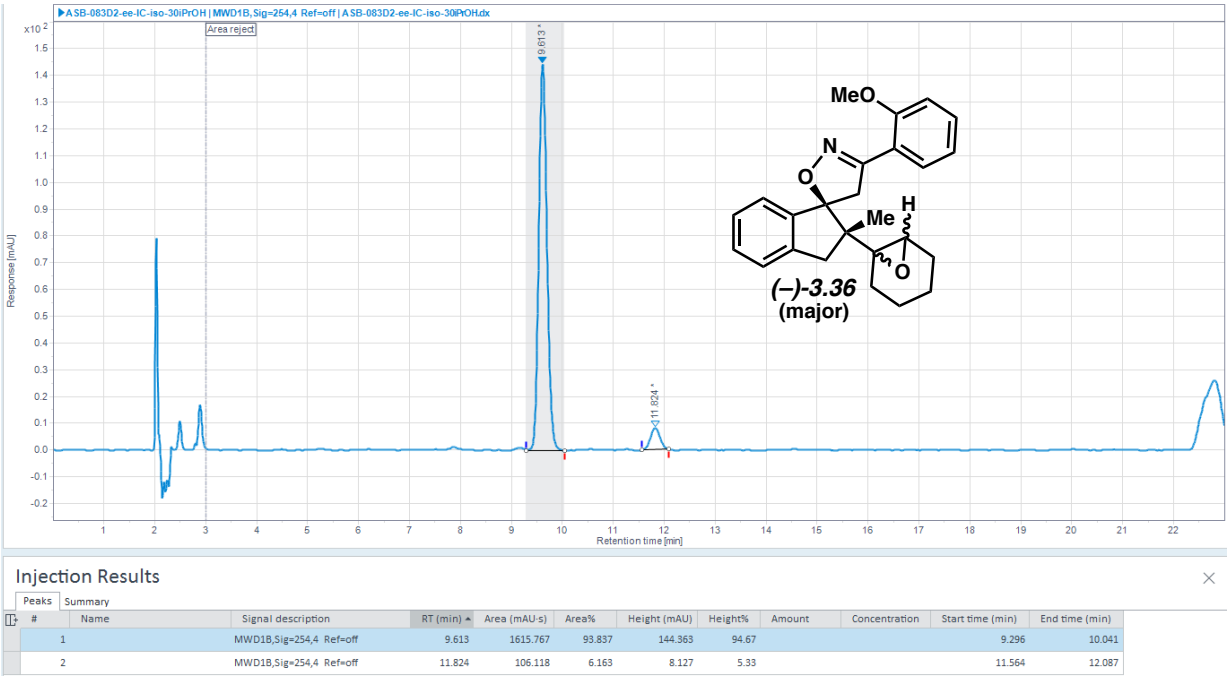


Figure 3.32. SFC trace for **(–)-3.36**.

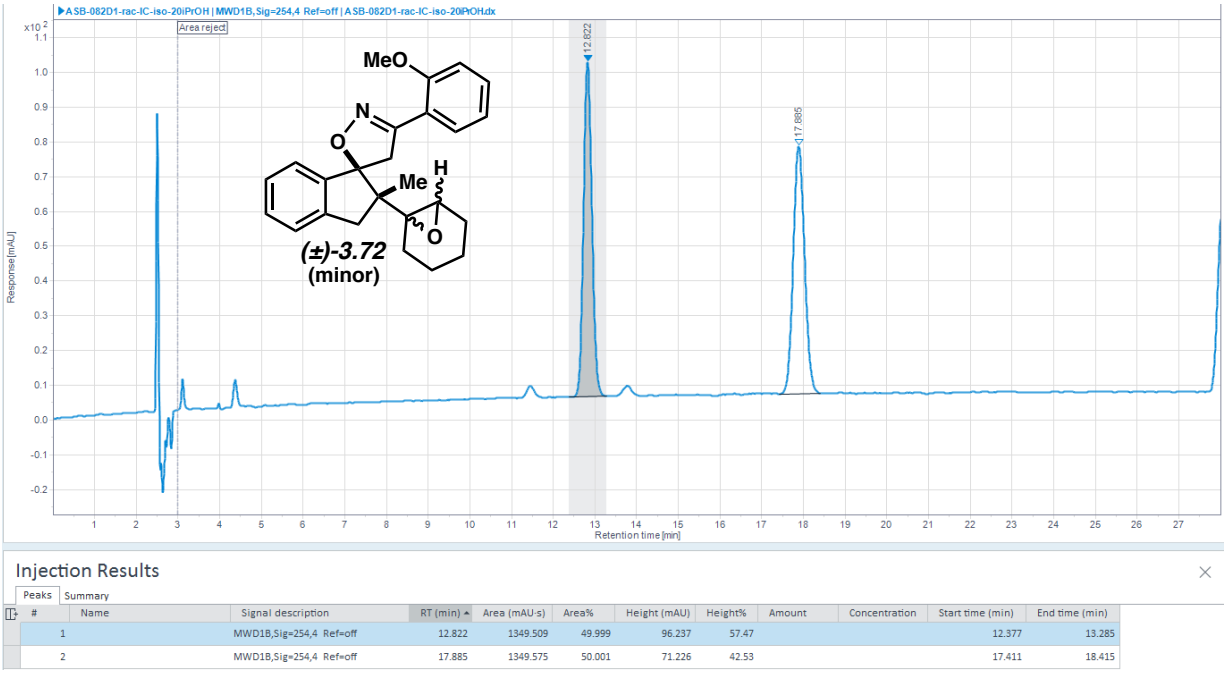


Figure 3.33. SFC trace for **(±)-3.72**.

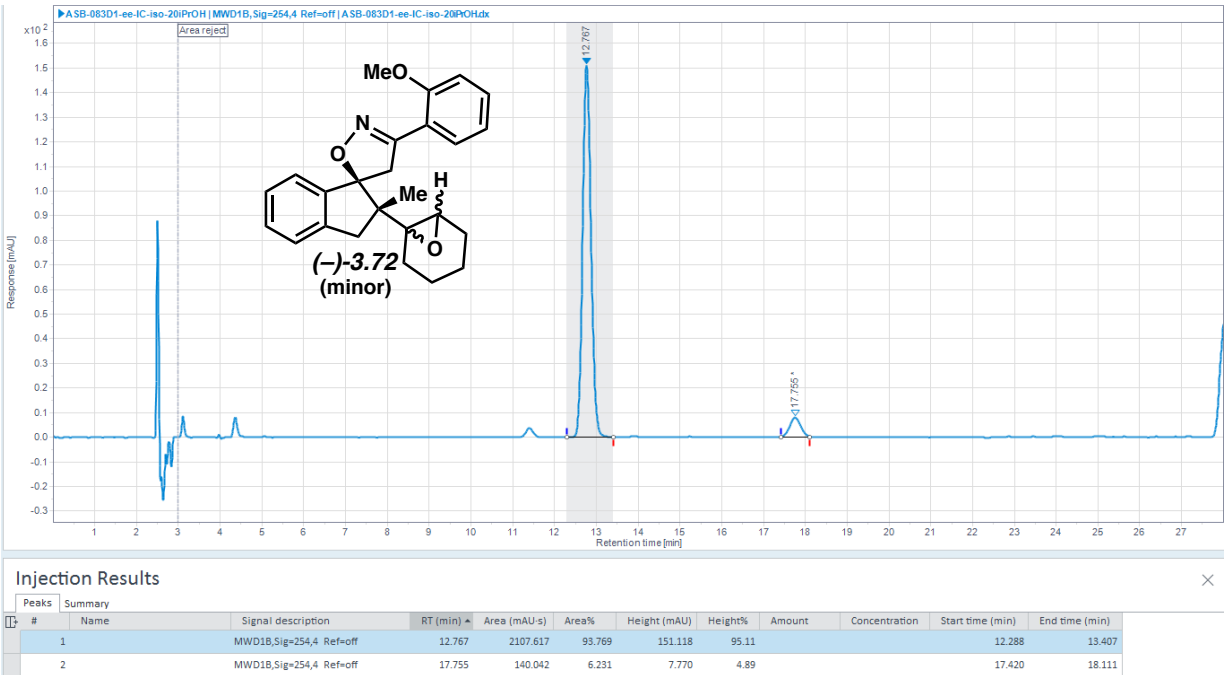


Figure 3.34. SFC trace for **(–)-3.72**.

3.10 Spectra Relevant to Chapter Three:

Enantioselective Nickel-Catalyzed Mizoroki–Heck Cyclizations of Amide Electrophiles

Ana S. Bulger[†], Daniel J. Nasrallah[†], Arismel Tena Meza[†], and Neil K. Garg.

Chem. Sci. **2024**, *15*, 2593–2600.

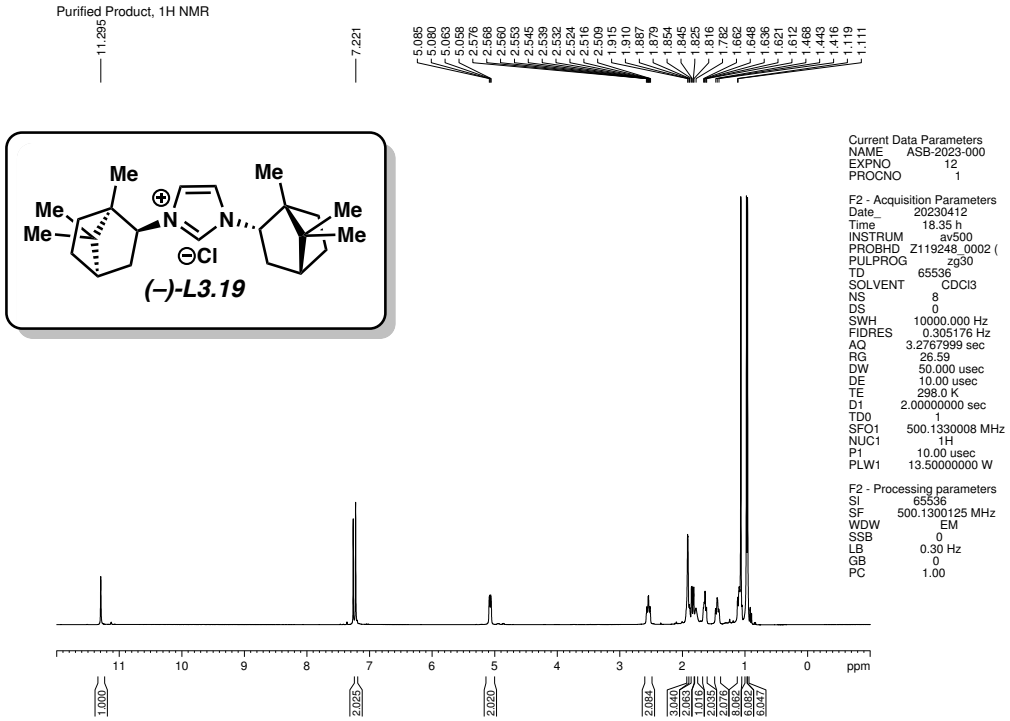


Figure 3.35. ^{1}H NMR (500 MHz, $CDCl_3$) of compound **L3.19**.

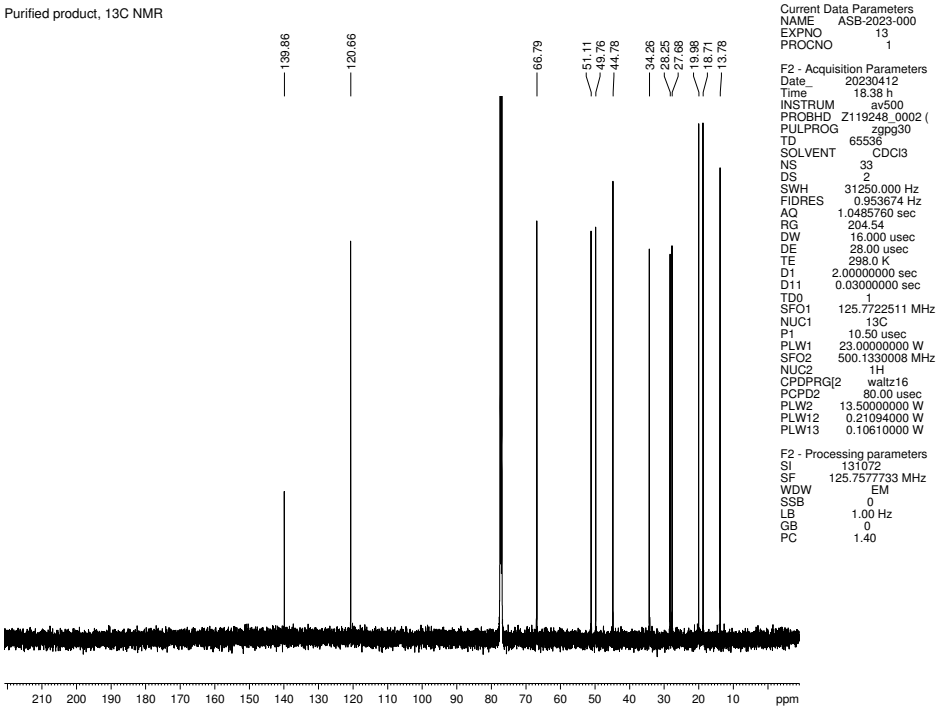


Figure 3.36. ^{13}C NMR (125 MHz, $CDCl_3$) of compound **L3.19**.

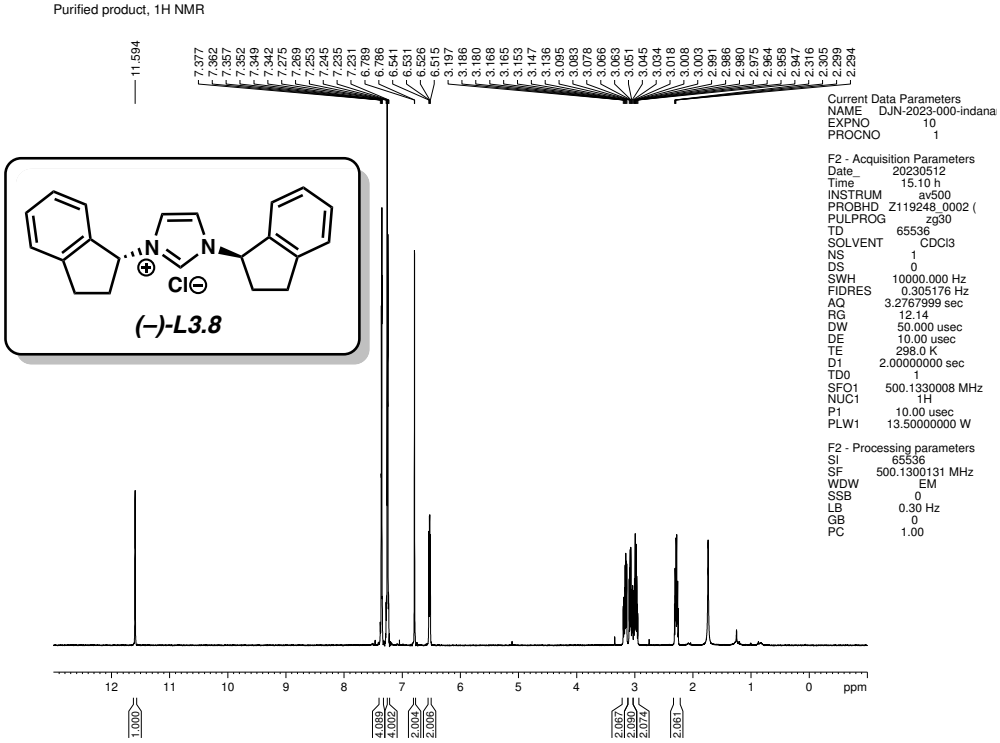


Figure 3.37. ^{1}H NMR (500 MHz, $CDCl_3$) of compound **L3.8**.

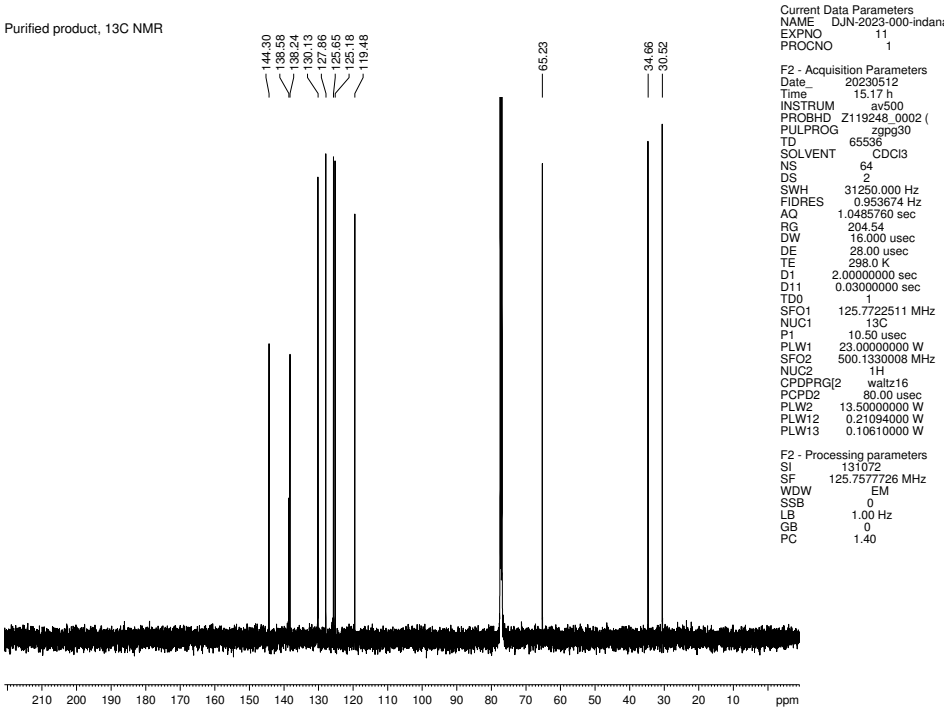


Figure 3.38. ^{13}C NMR (125 MHz, $CDCl_3$) of compound **L3.8**.

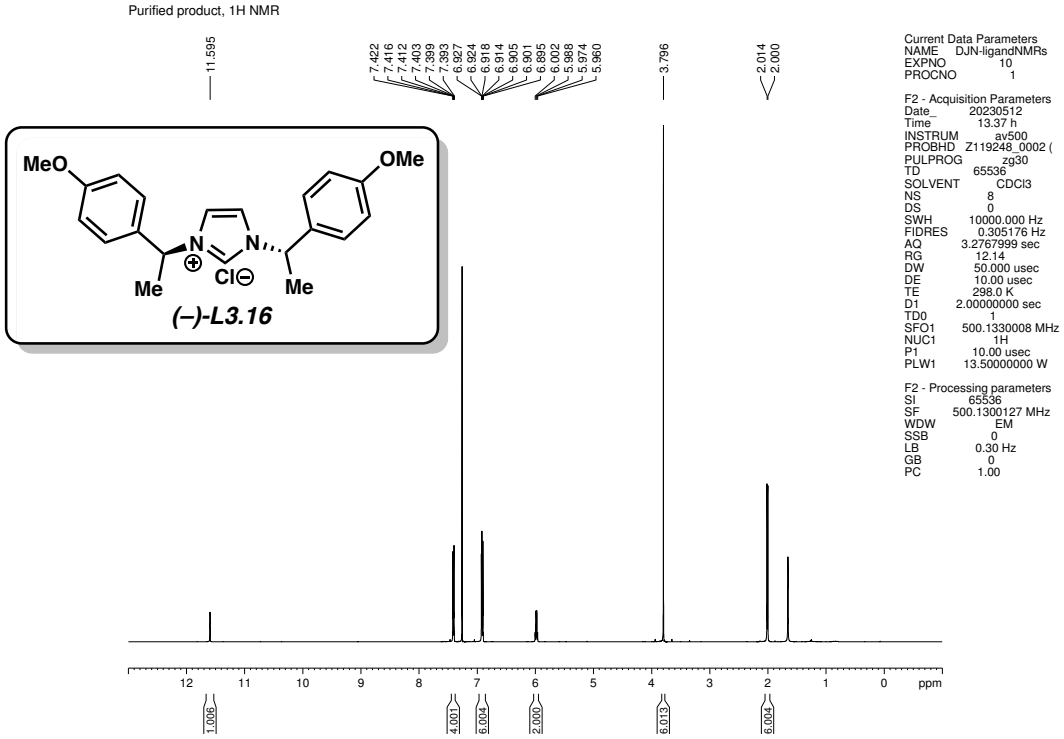


Figure 3.39. ^{1}H NMR (500 MHz, $CDCl_3$) of compound **L3.16**.

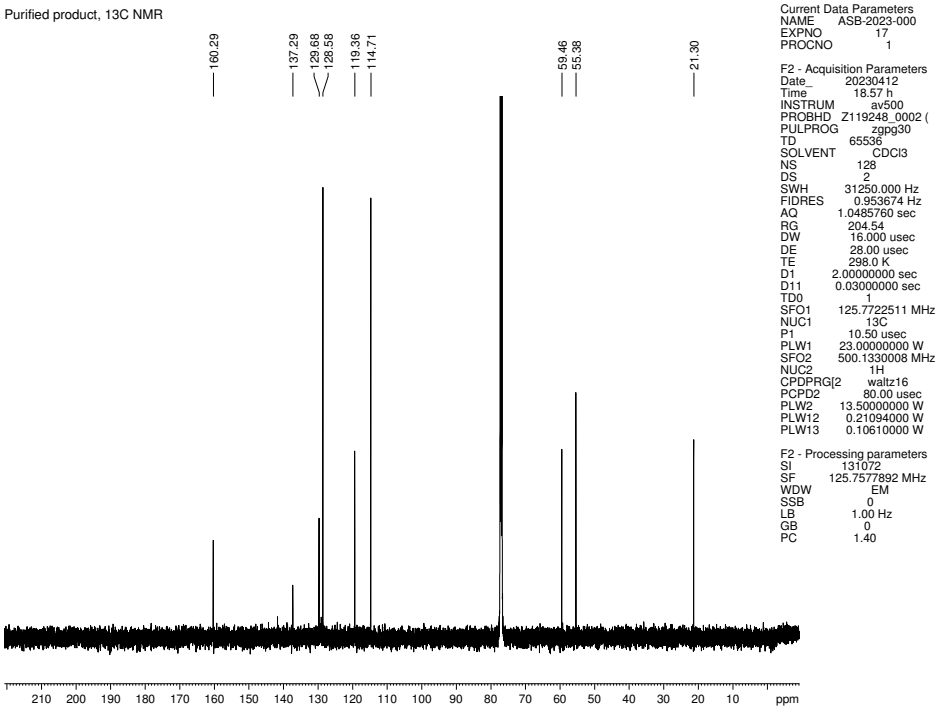


Figure 3.40. ^{13}C NMR (125 MHz, $CDCl_3$) of compound **L3.16**.

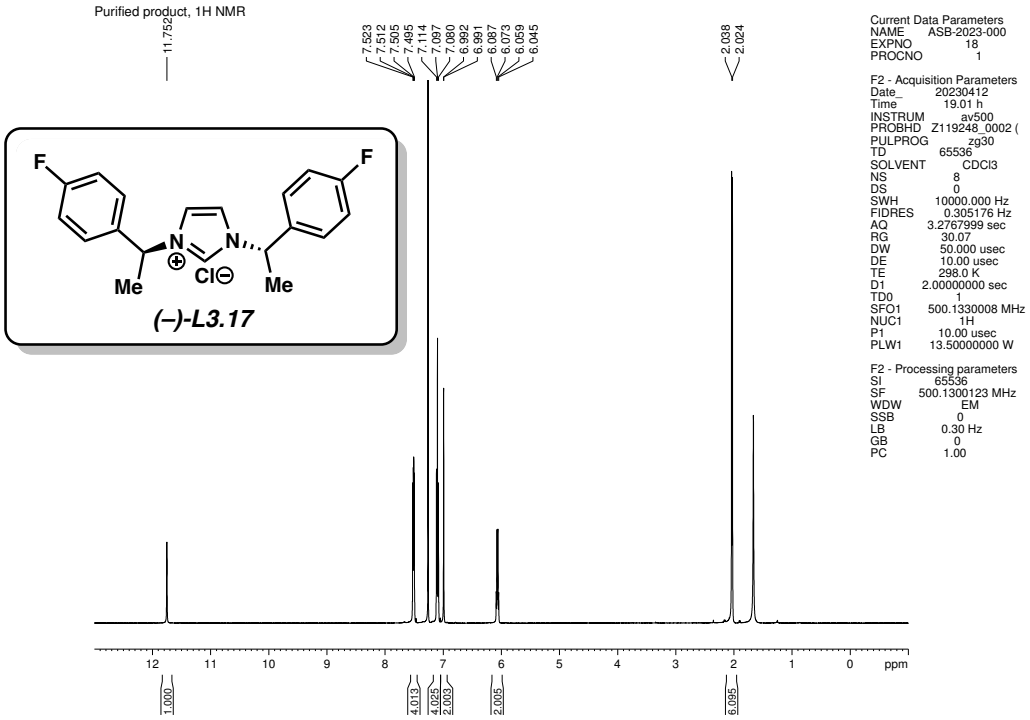


Figure 3.41. ^{1}H NMR (500 MHz, $CDCl_3$) of compound **L3.17**.

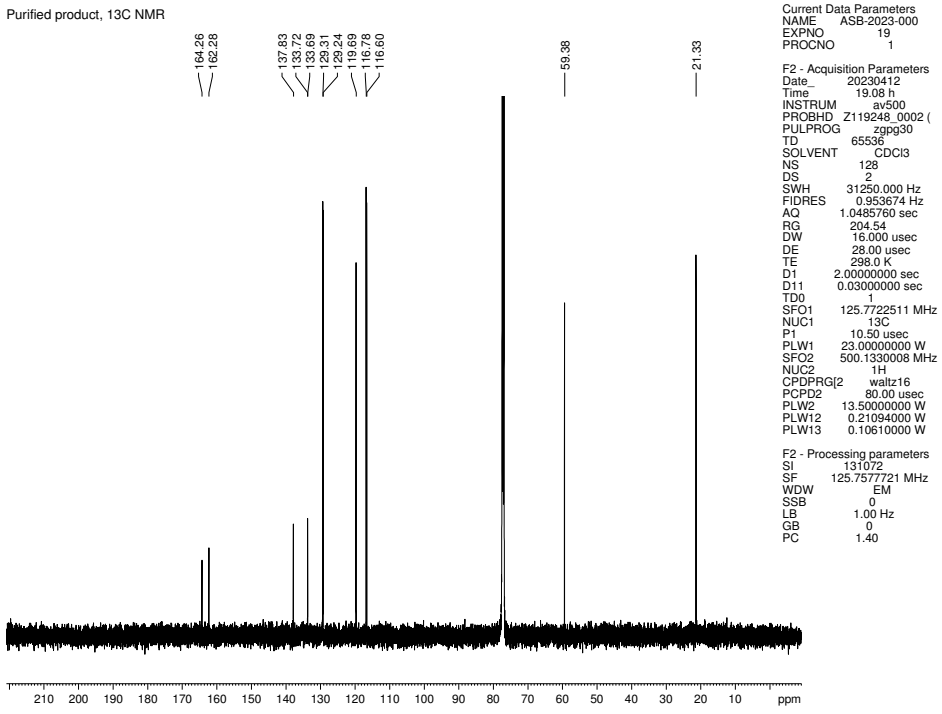


Figure 3.42. ^{13}C NMR (125 MHz, $CDCl_3$) of compound **L3.17**.

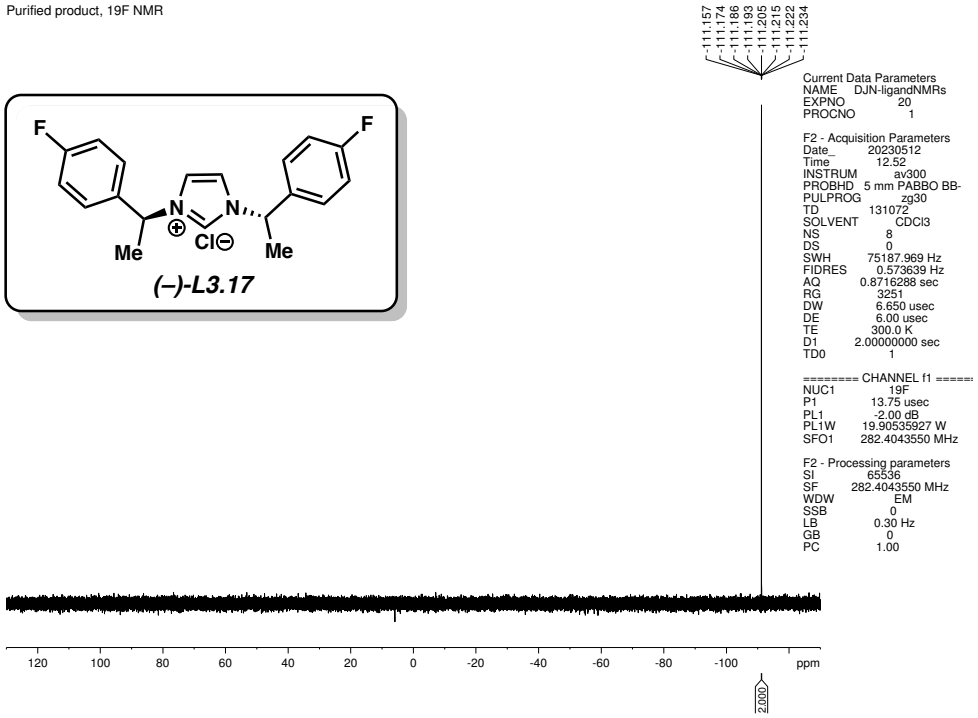


Figure 3.43. ^{19}F NMR (282 MHz, $CDCl_3$) of compound **L3.17**.

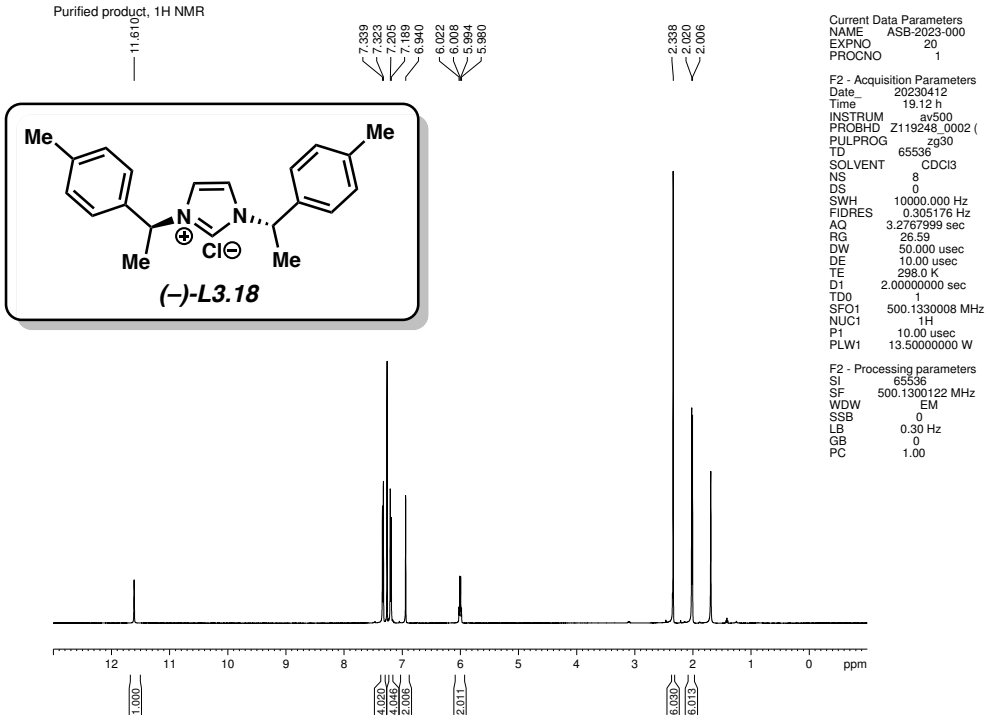


Figure 3.44. ^{1}H NMR (500 MHz, $CDCl_3$) of compound **L3.18**.

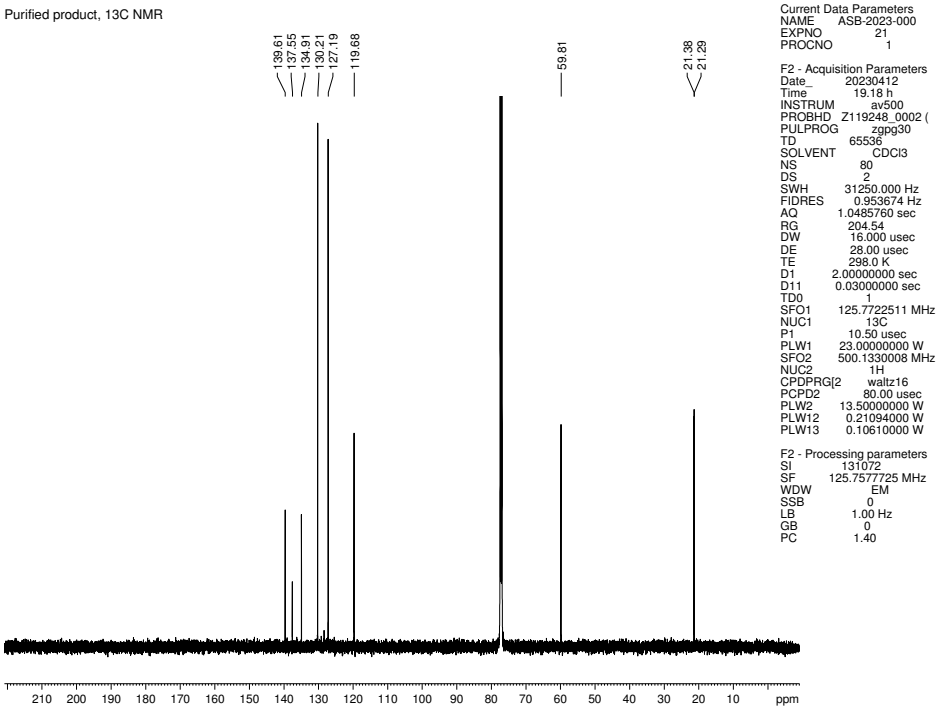


Figure 3.45. ^{13}C NMR (125 MHz, $CDCl_3$) of compound **L3.18**.

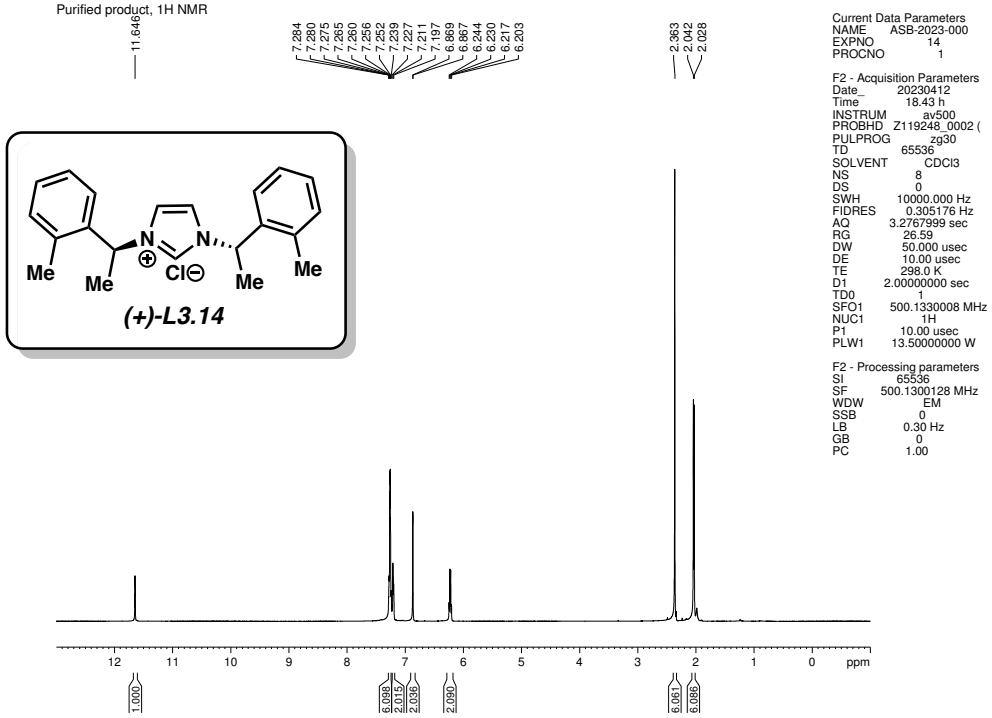


Figure 3.46. ^{1}H NMR (500 MHz, $CDCl_3$) of compound **L3.14**.

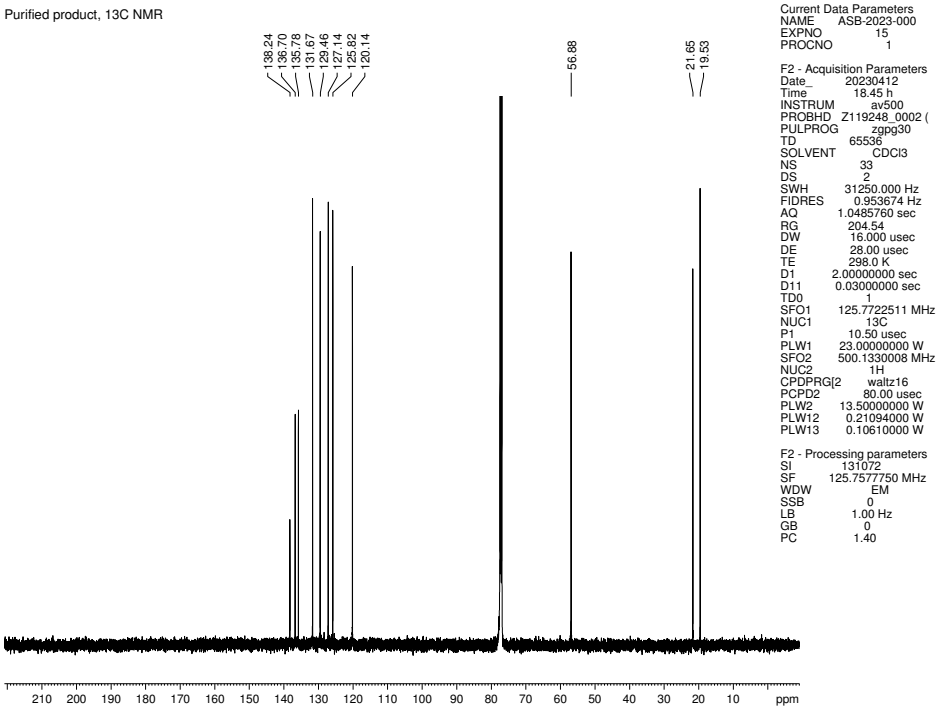


Figure 3.47. ^{13}C NMR (125 MHz, $CDCl_3$) of compound **L3.14**.

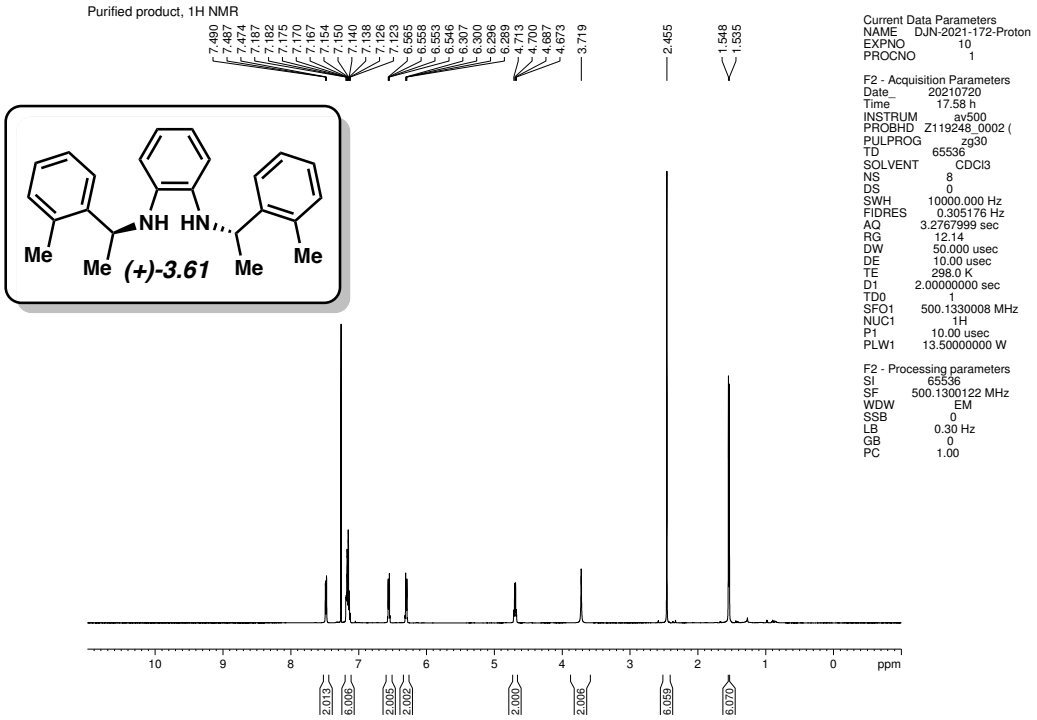


Figure 3.48. ^{1}H NMR (500 MHz, $CDCl_3$) of compound **3.61**.

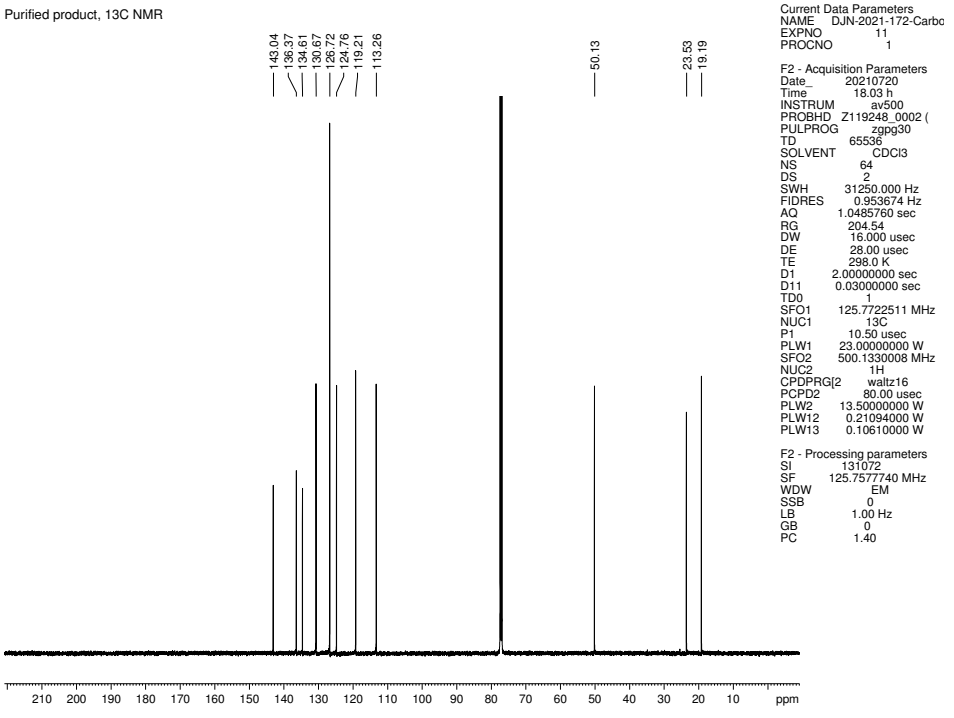


Figure 3.49. ^{13}C NMR (125 MHz, $CDCl_3$) of compound **3.61**.

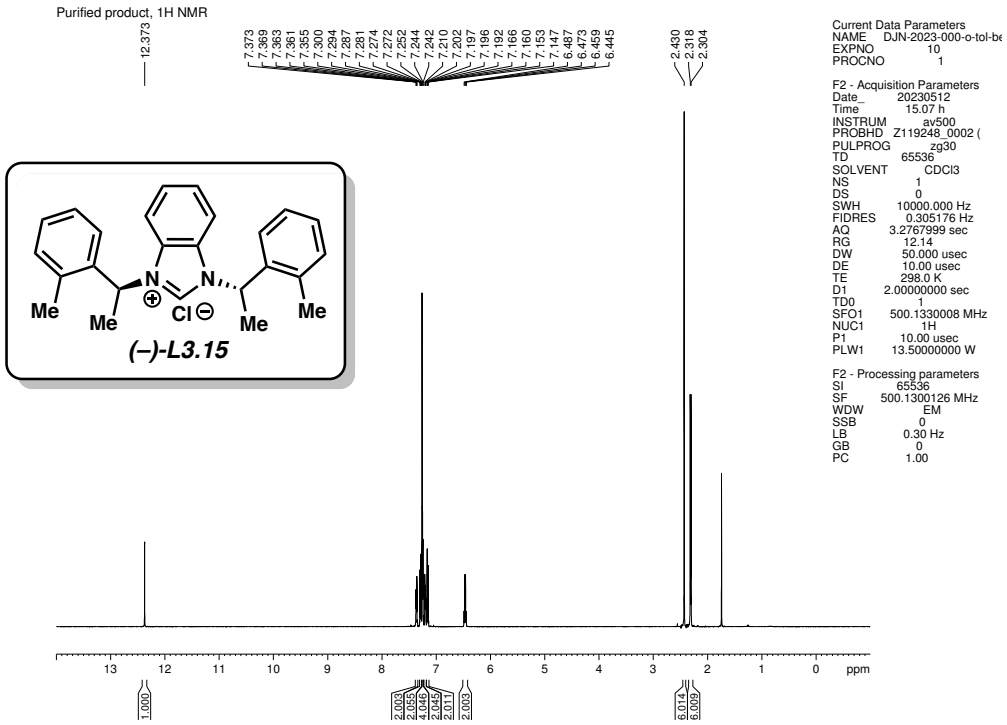


Figure 3.50. ^{1}H NMR (500 MHz, $CDCl_3$) of compound **L3.15**.

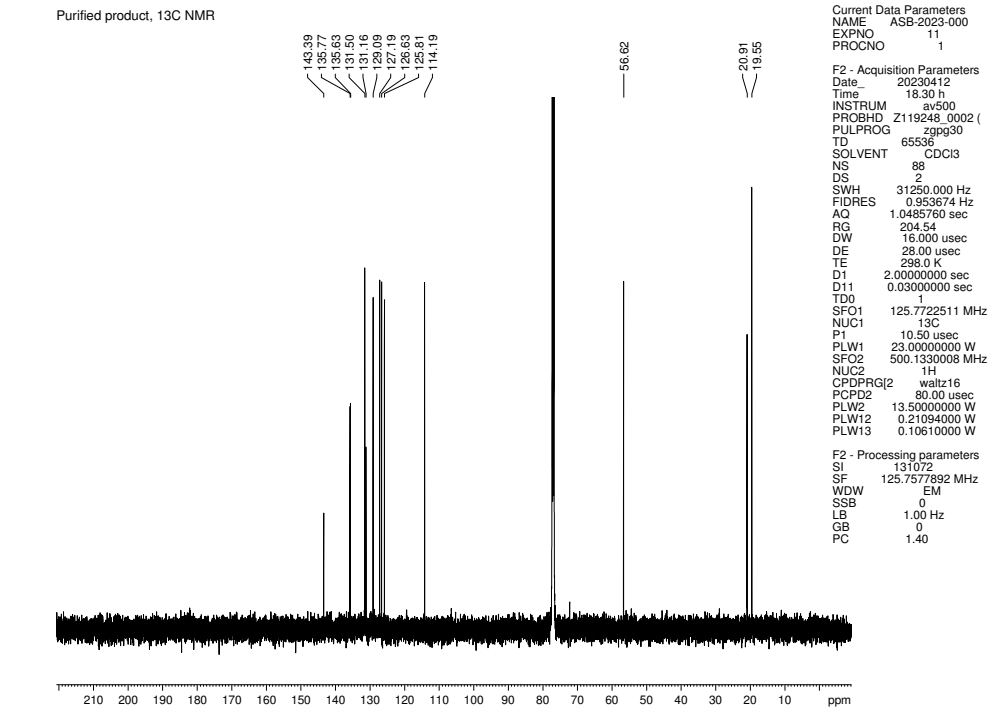


Figure 3.51. ^{13}C NMR (125 MHz, $CDCl_3$) of compound **L3.15**.

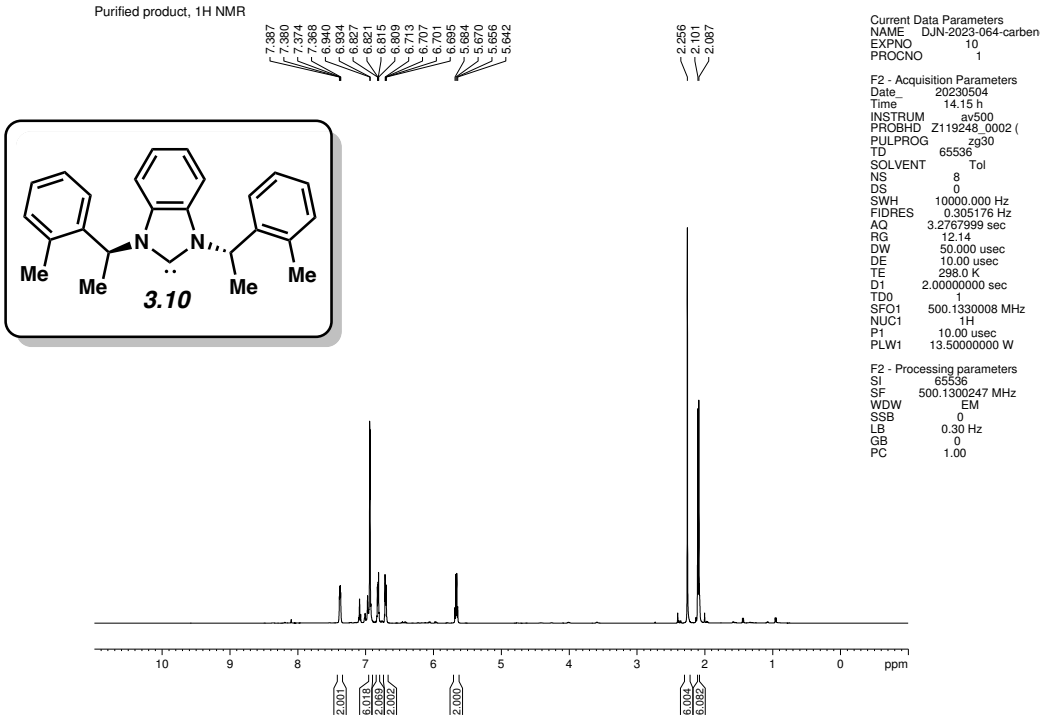


Figure 3.52. ^{1}H NMR (500 MHz, toluene-D8) of compound **3.10**.

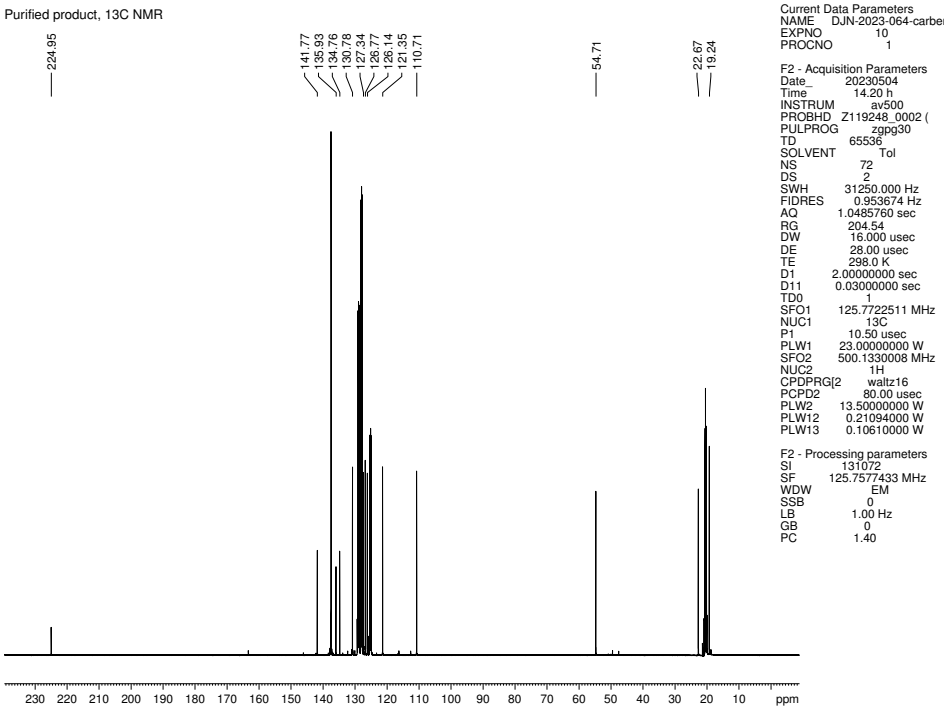


Figure 3.53. ^{13}C NMR (125 MHz, toluene-D8) of compound **3.10**.

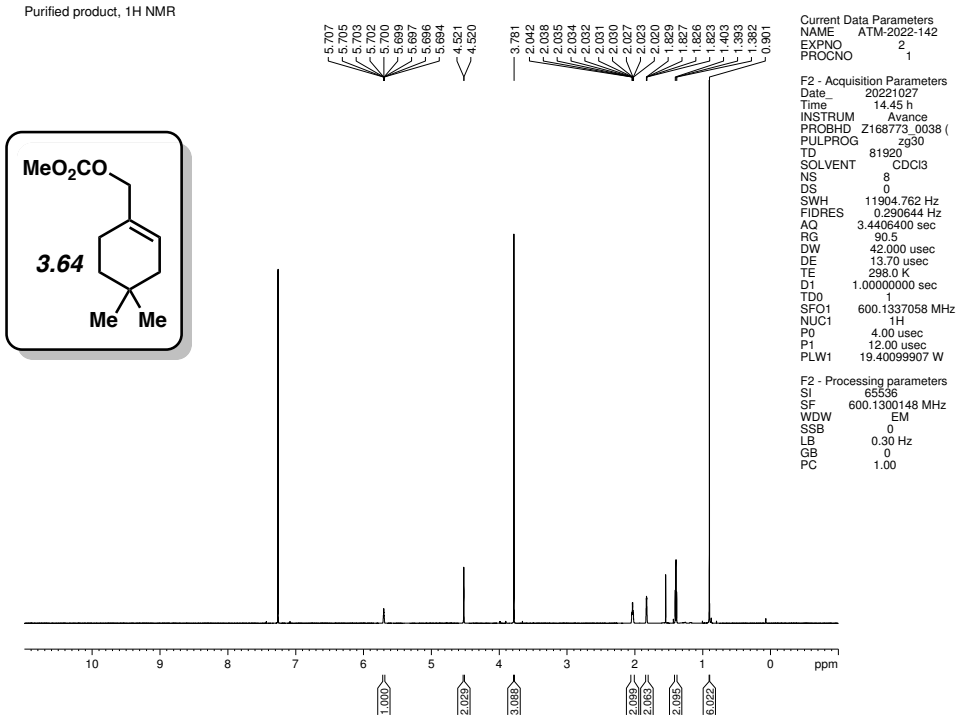


Figure 3.54. ^{1}H NMR (600 MHz, $CDCl_3$) of compound **3.64**.

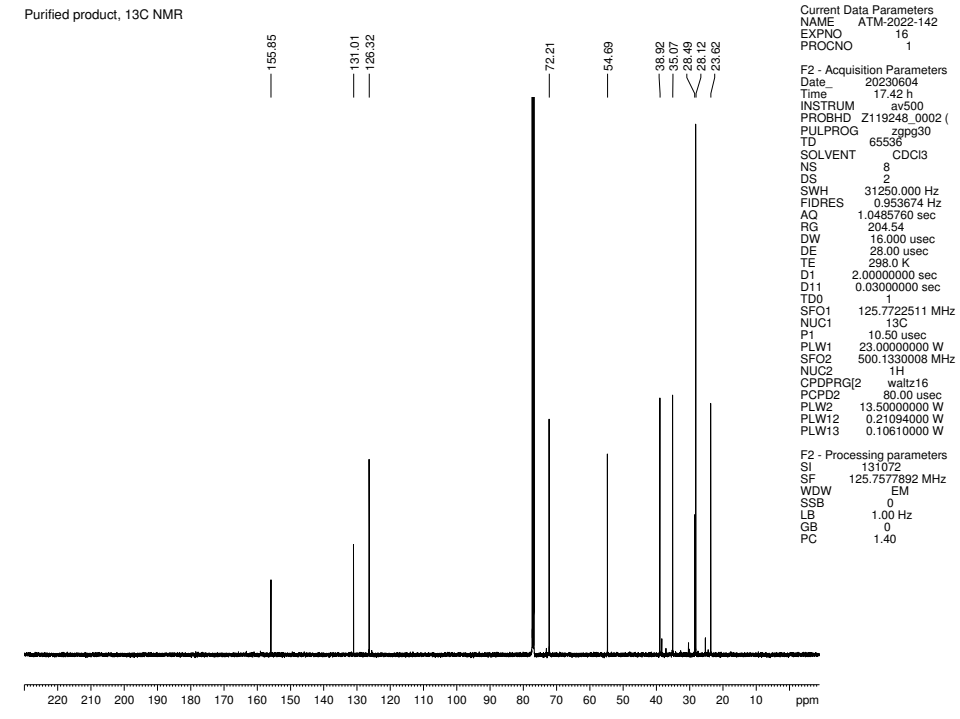


Figure 3.55. ^{13}C NMR (125 MHz, $CDCl_3$) of compound **3.64**.

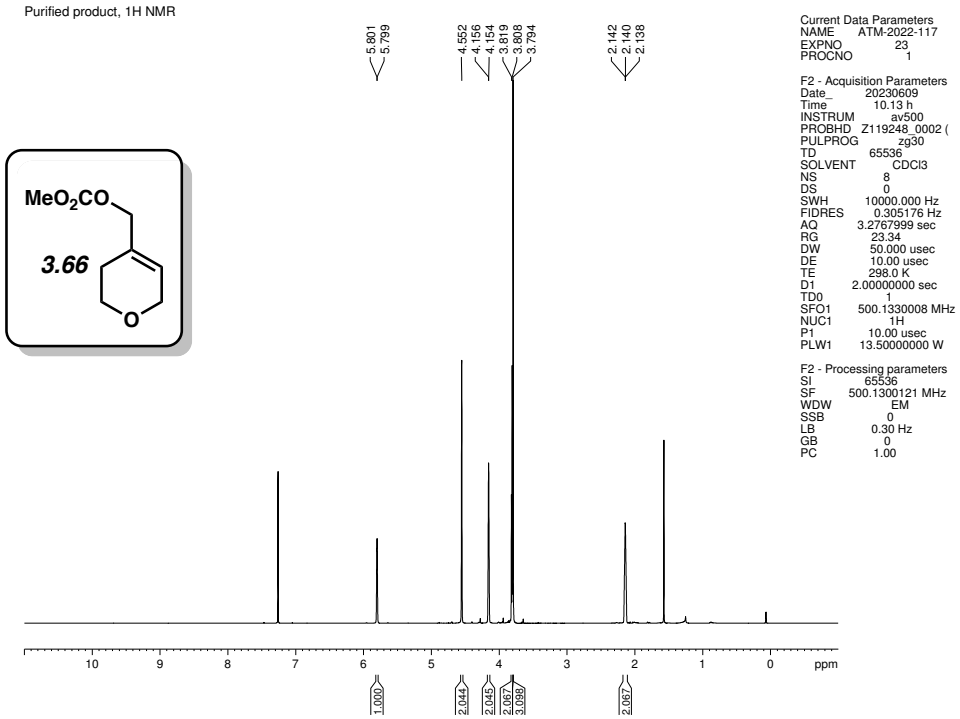


Figure 3.56. ^{1}H NMR (500 MHz, $CDCl_3$) of compound **3.66**.

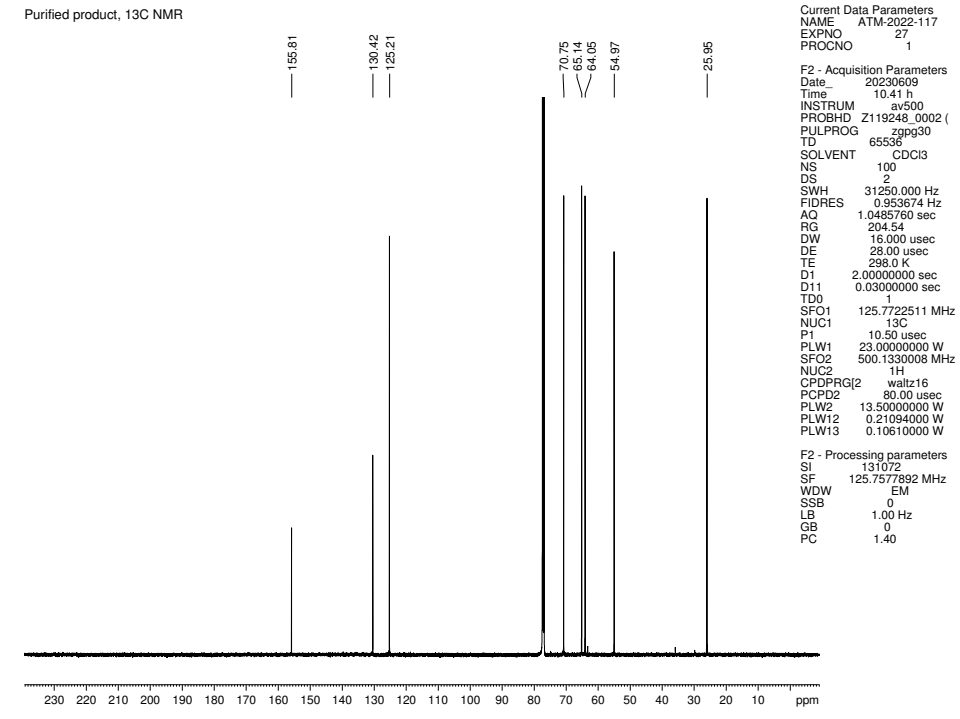


Figure 3.57. ^{13}C NMR (125 MHz, $CDCl_3$) of compound **3.66**.

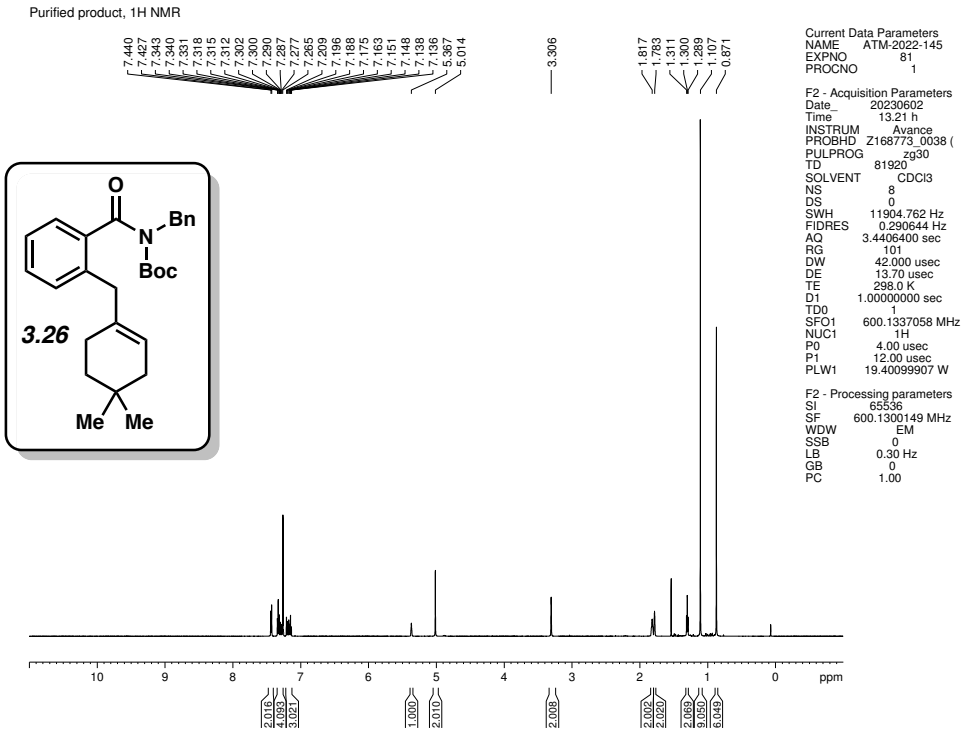


Figure 3.58. ^{1}H NMR (600 MHz, $CDCl_3$) of compound **3.26**.

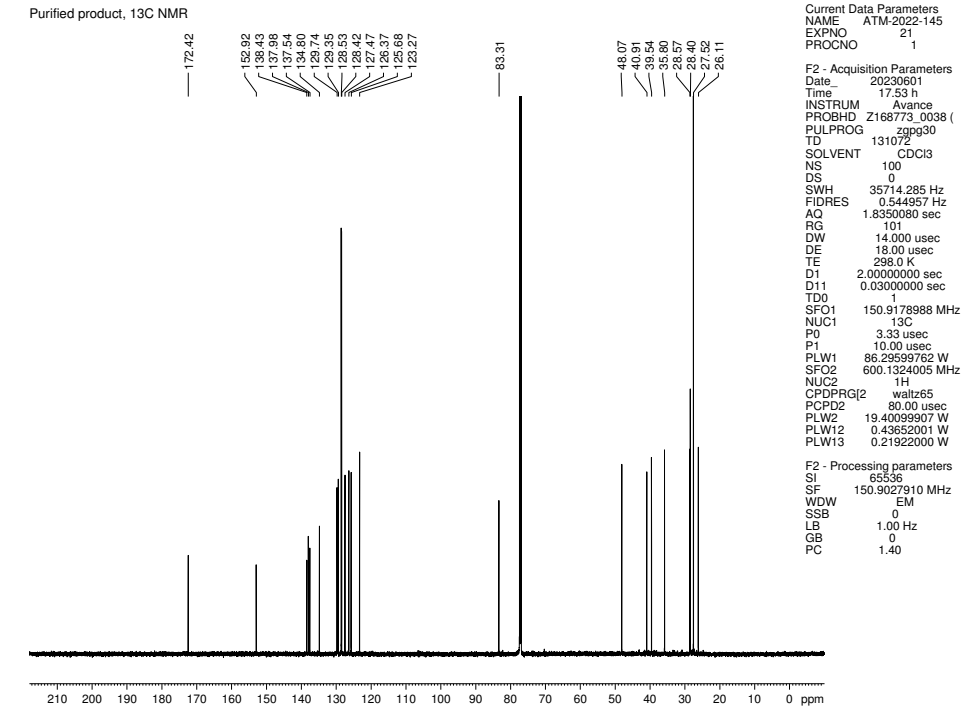


Figure 3.59. ^{13}C NMR (150 MHz, $CDCl_3$) of compound **3.26**.

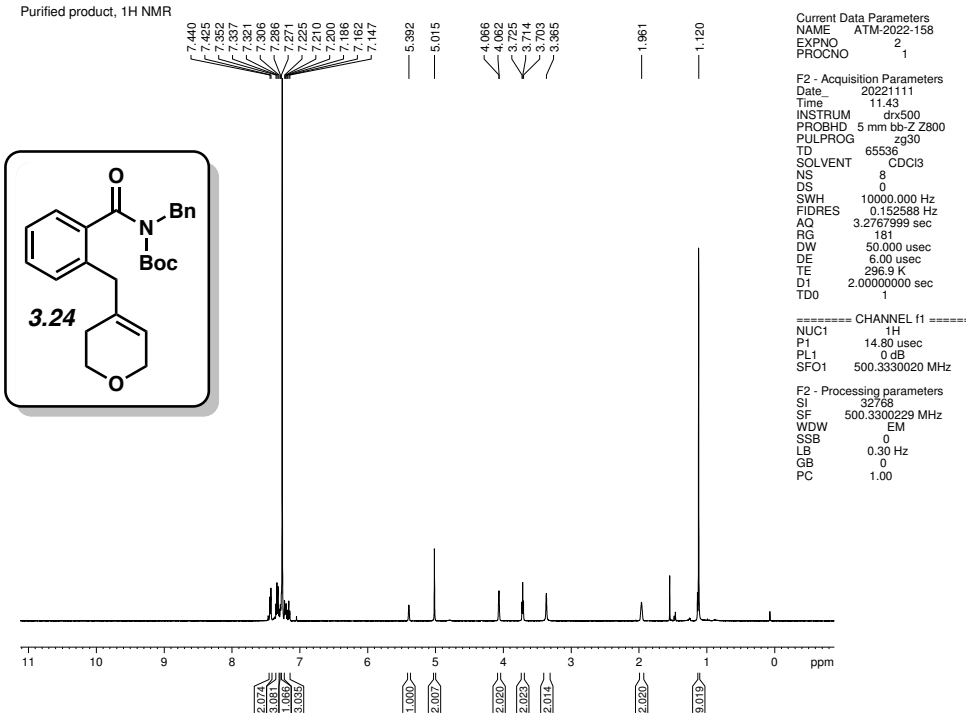


Figure 3.60. ^{1}H NMR (500 MHz, $CDCl_3$) of compound **3.24**.

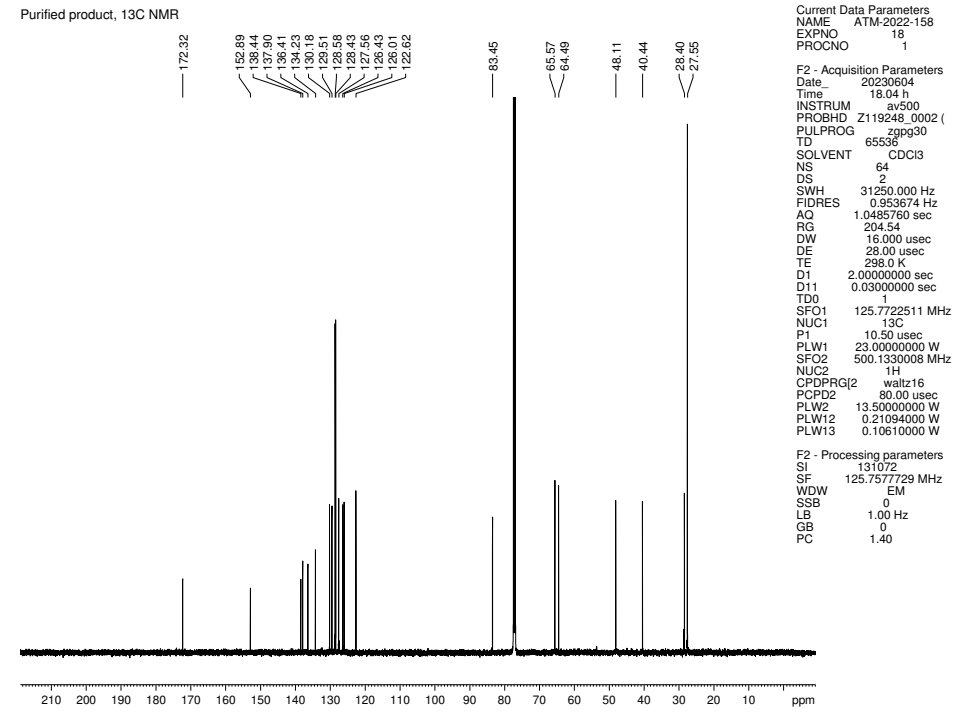


Figure 3.61. ^{13}C NMR (125 MHz, $CDCl_3$) of compound **3.24**.

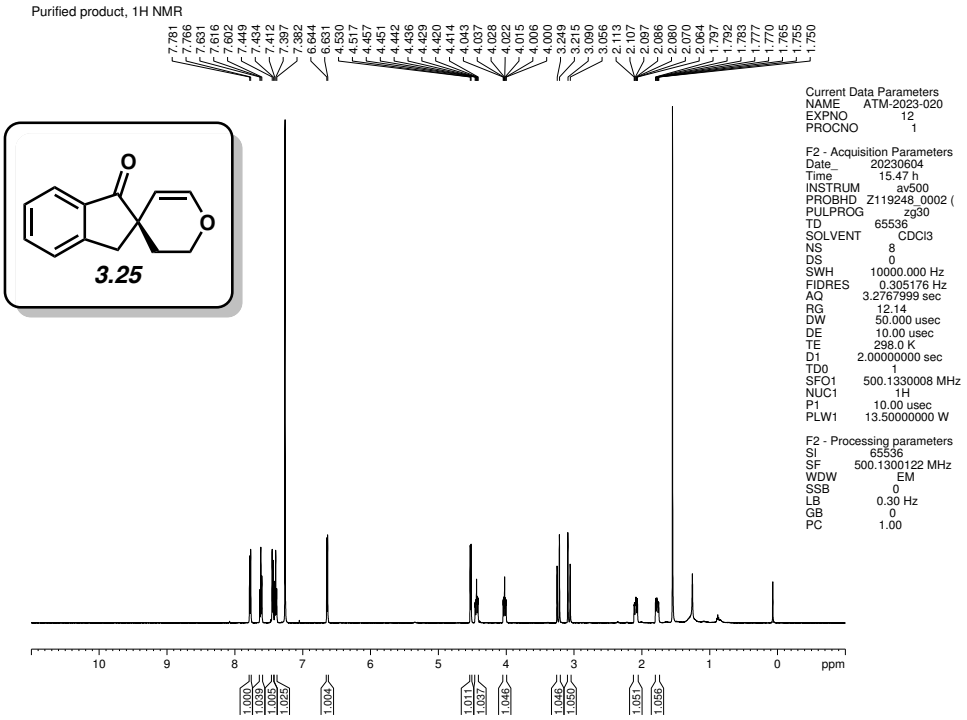


Figure 3.62. ^{1}H NMR (500 MHz, $CDCl_3$) of compound **3.25**.

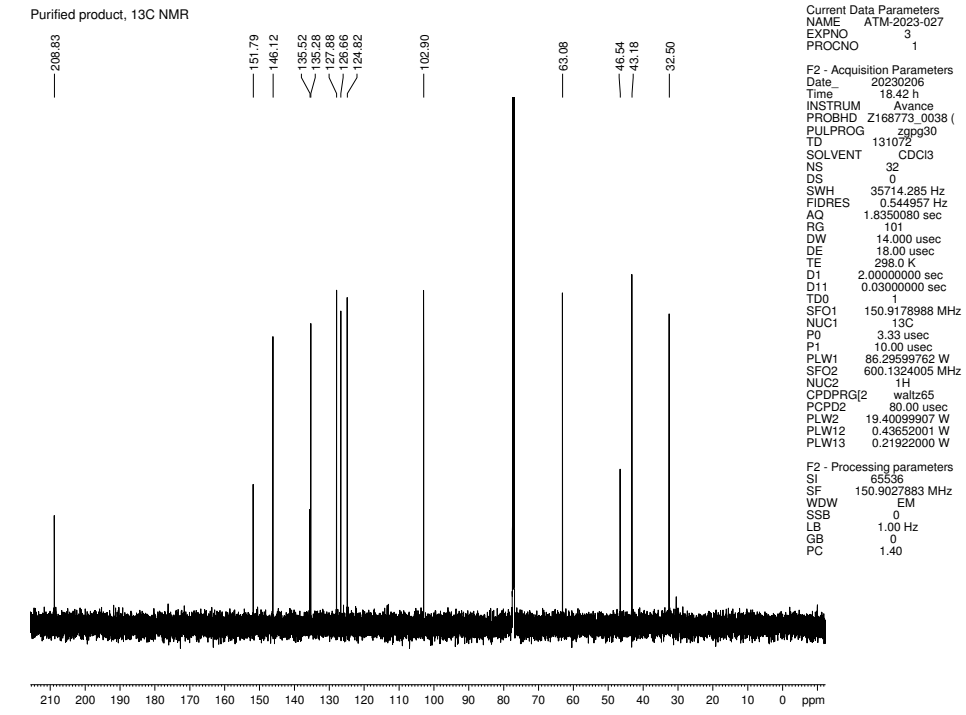


Figure 3.63. ^{13}C NMR (150 MHz, $CDCl_3$) of compound **3.25**.

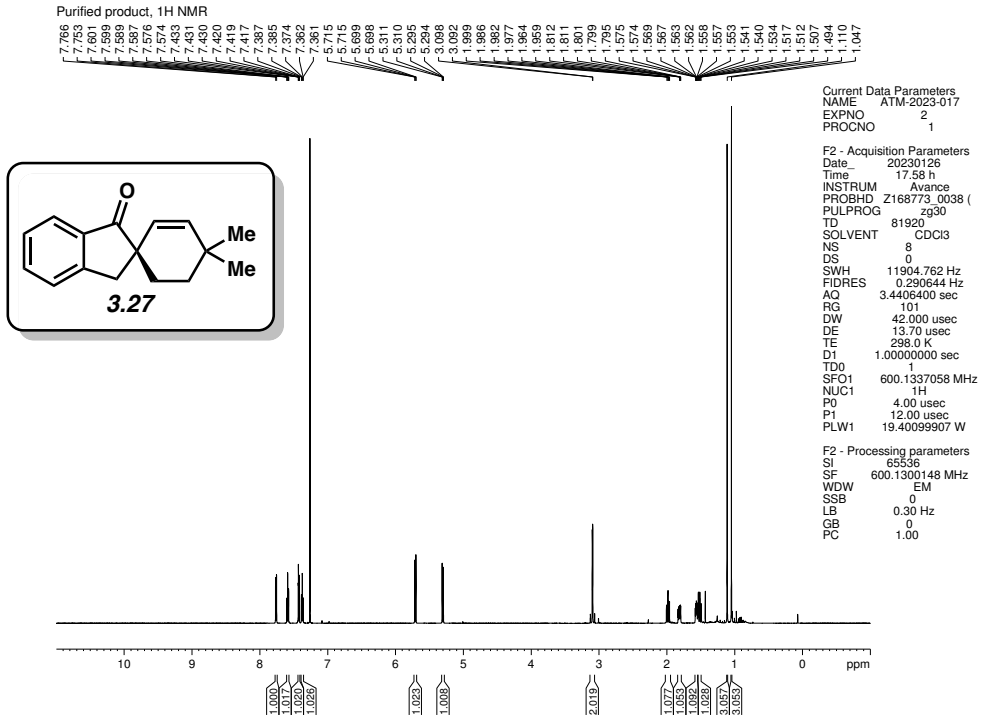


Figure 3.64. ^{1}H NMR (600 MHz, $CDCl_3$) of compound **3.27**.

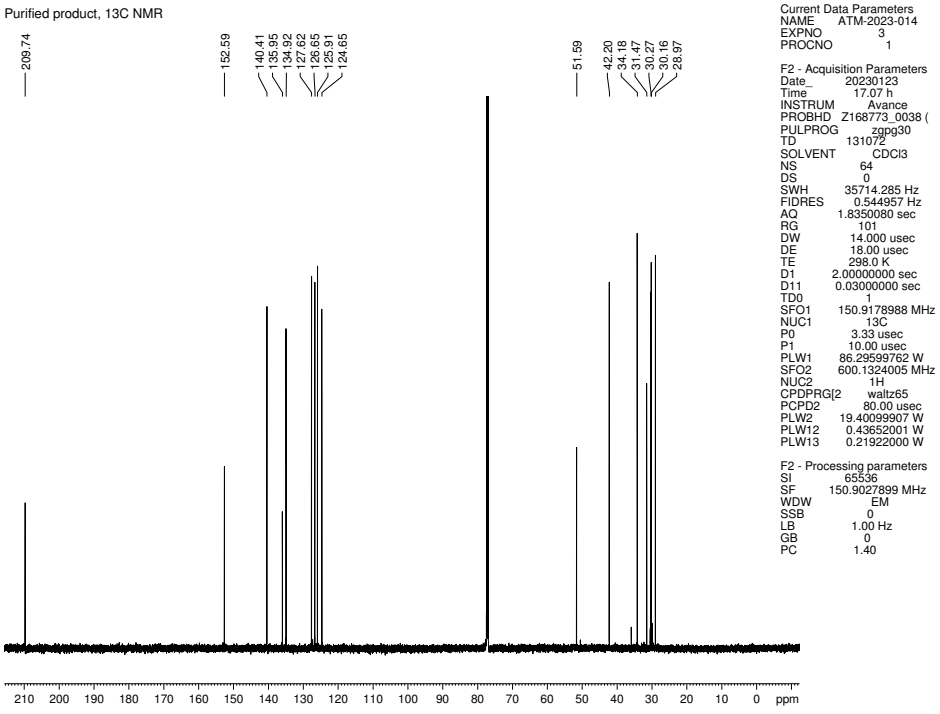


Figure 3.65. ^{13}C NMR (150 MHz, $CDCl_3$) of compound **3.27**.

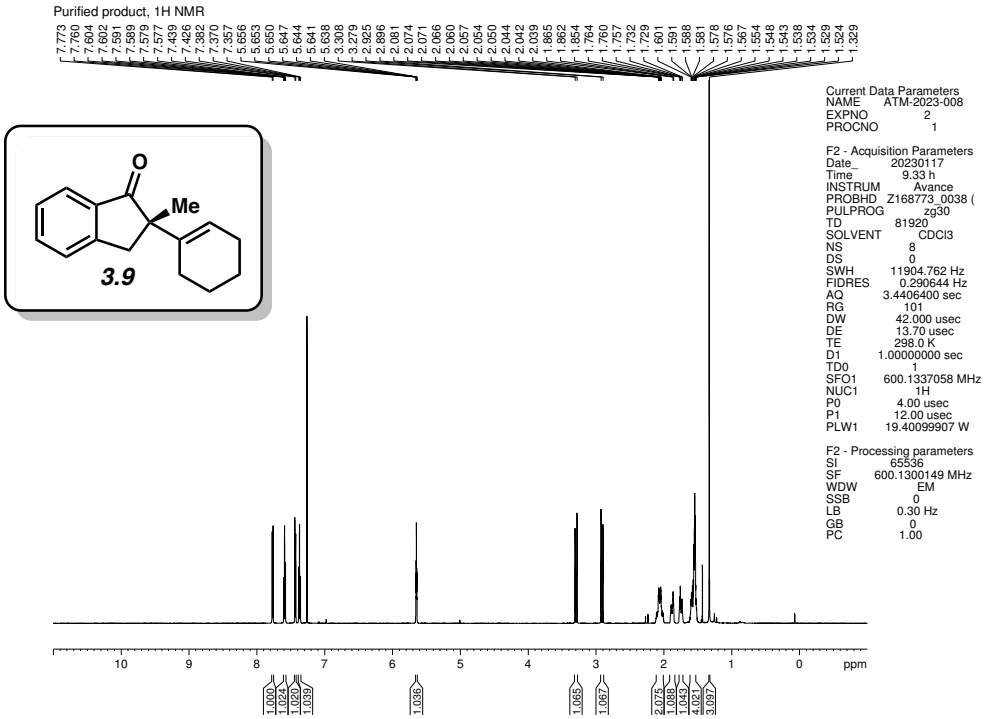


Figure 3.66. ^{1}H NMR (600 MHz, $CDCl_3$) of compound **3.9**.

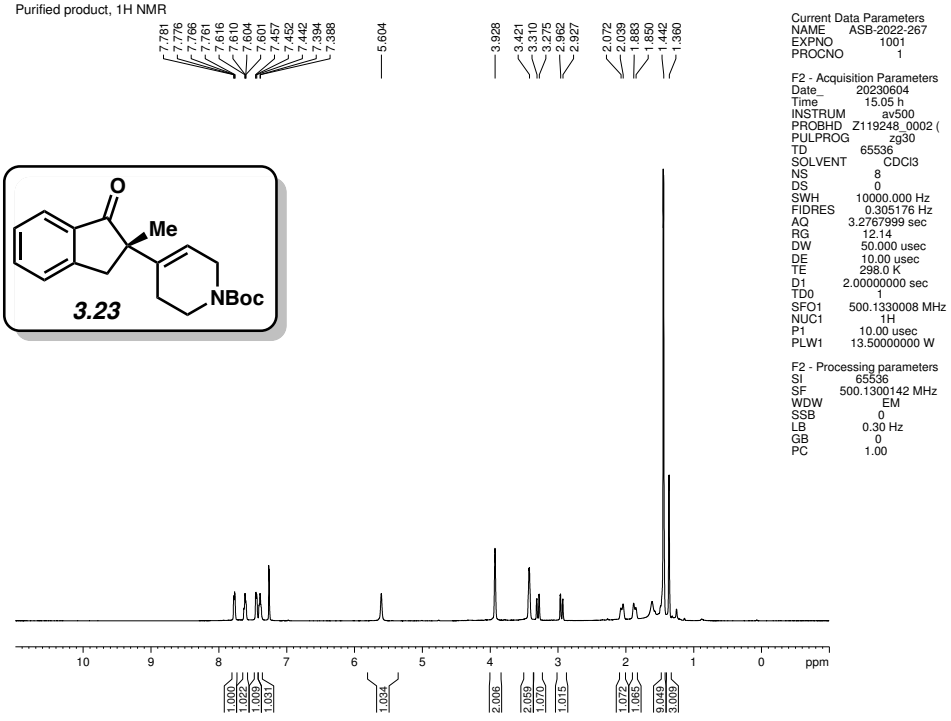


Figure 3.67. ^{1}H NMR (500 MHz, $CDCl_3$) of compound **3.23**.

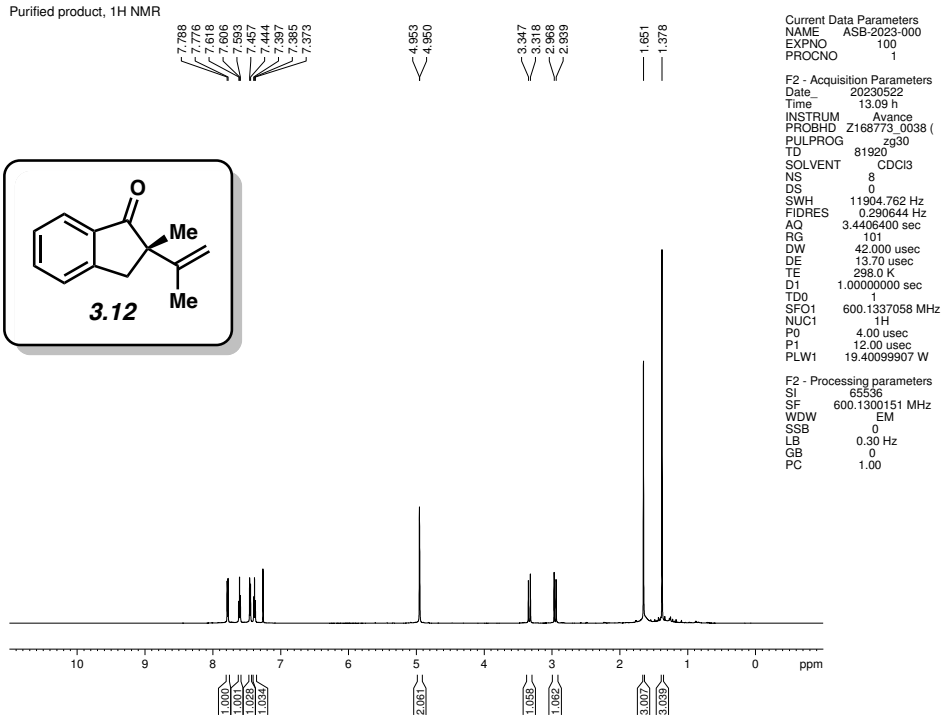


Figure 3.68. ^{1}H NMR (600 MHz, $CDCl_3$) of compound **3.12**.

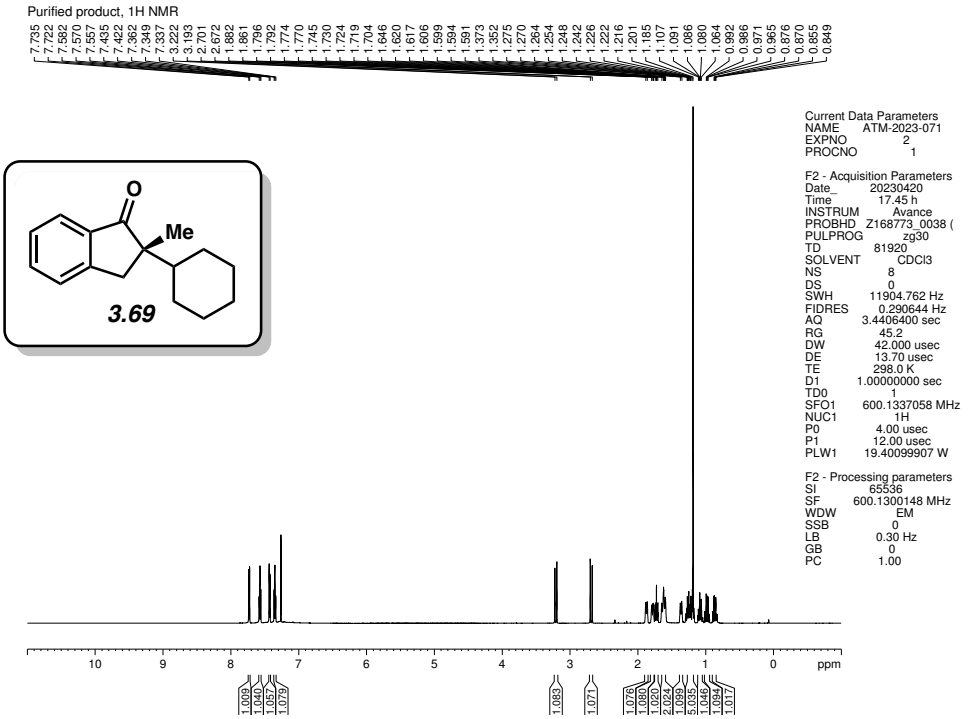


Figure 3.69. ^{1}H NMR (600 MHz, $CDCl_3$) of compound **3.69**.

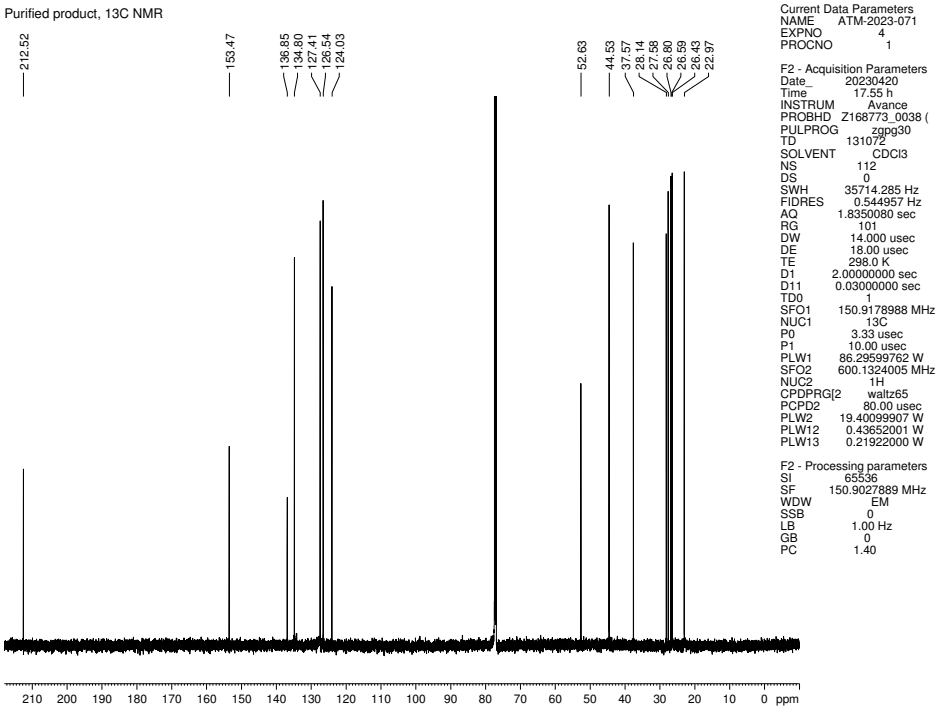


Figure 3.70. ^{13}C NMR (150 MHz, $CDCl_3$) of compound **3.69**.

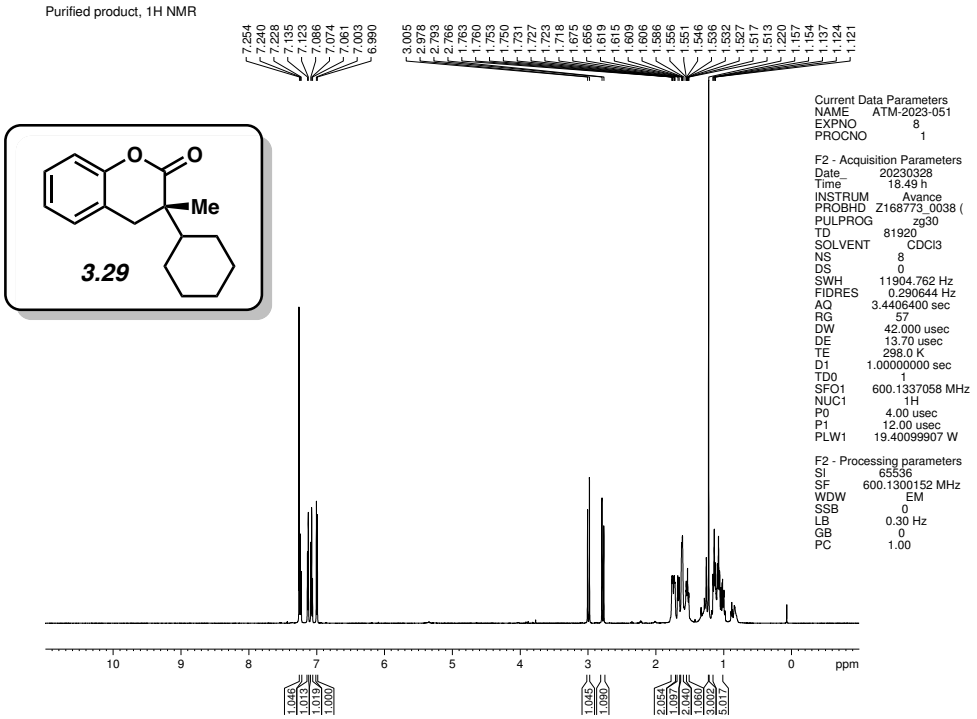


Figure 3.71. ^{1}H NMR (600 MHz, $CDCl_3$) of compound **3.29**.

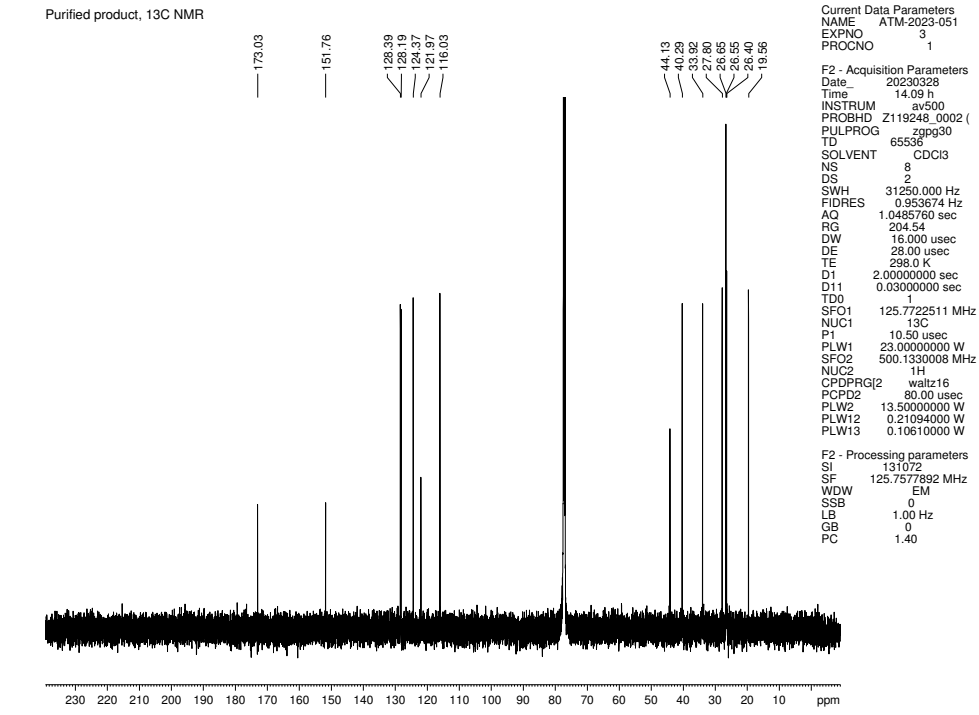


Figure 3.72. ^{13}C NMR (125 MHz, $CDCl_3$) of compound **3.29**.

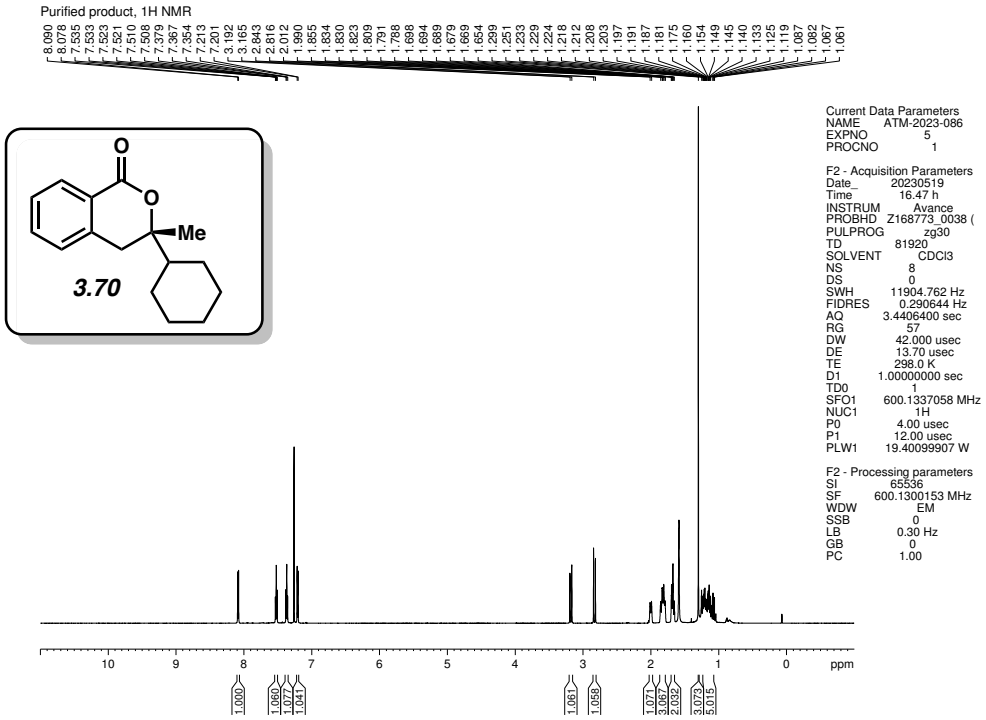


Figure 3.73. ^{1}H NMR (600 MHz, $CDCl_3$) of compound **3.70**.

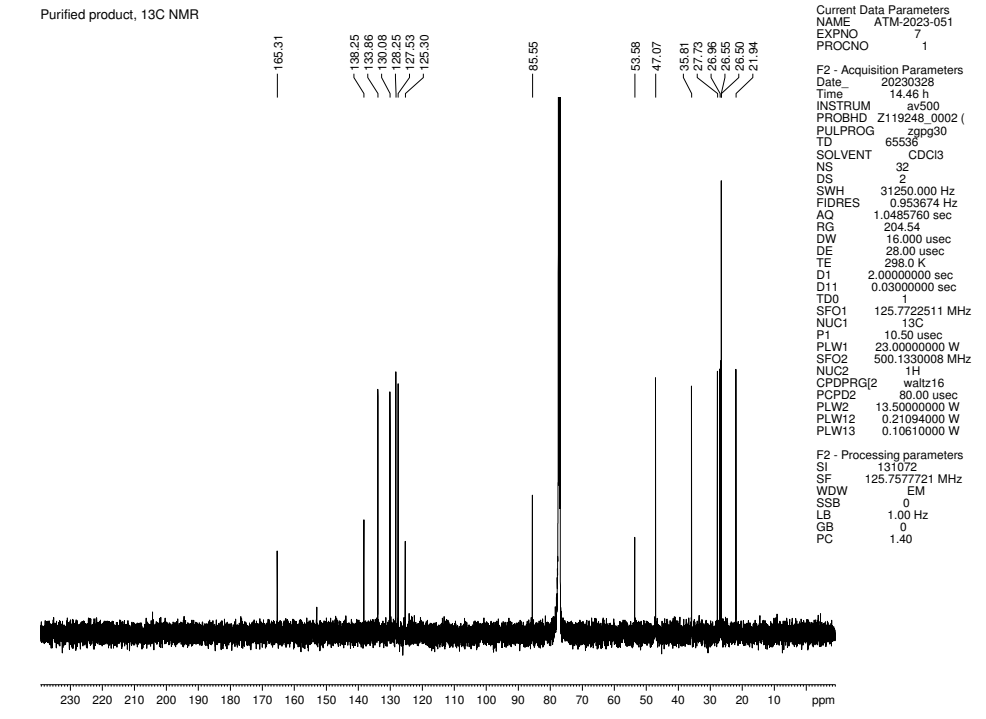


Figure 3.74. ^{13}C NMR (125 MHz, $CDCl_3$) of compound **3.70**.

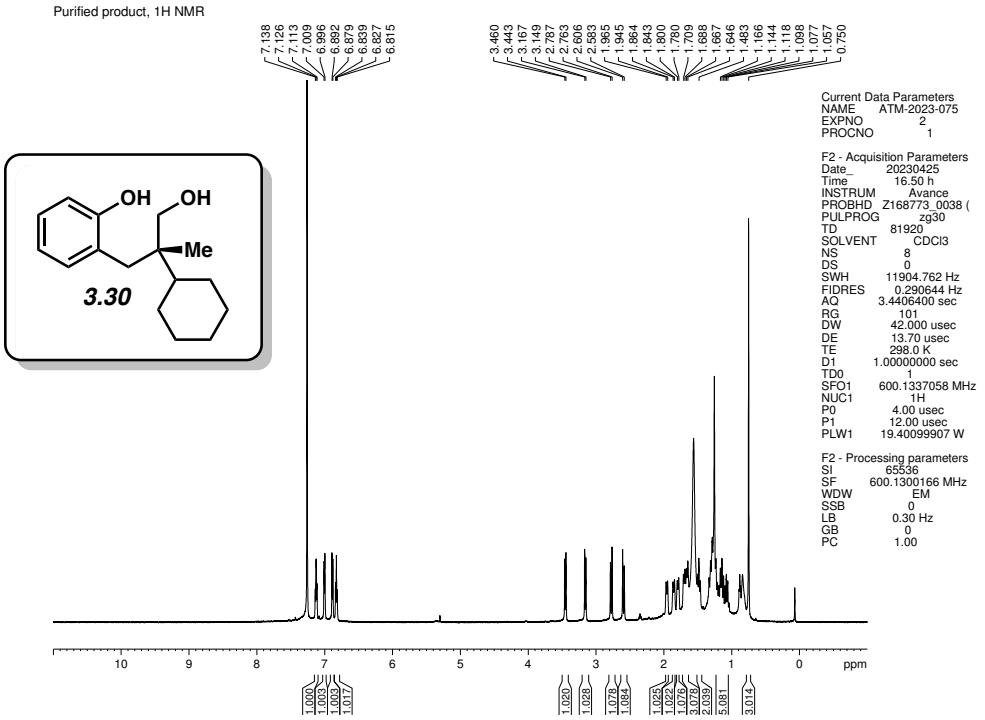


Figure 3.75. ^{1}H NMR (600 MHz, $CDCl_3$) of compound **3.30**.

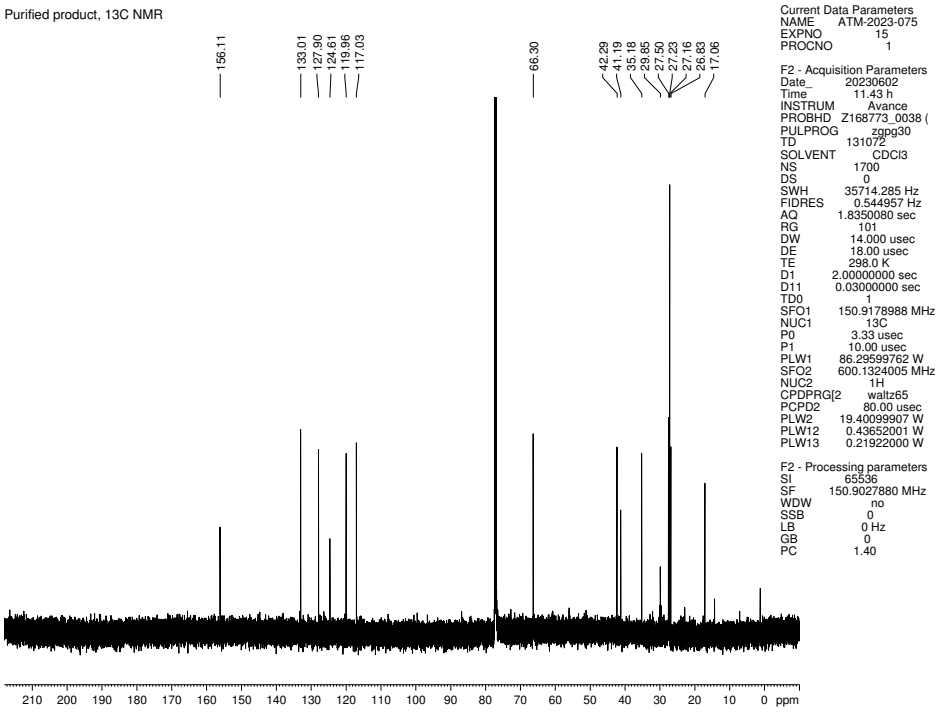


Figure 3.76. ^{13}C NMR (150 MHz, $CDCl_3$) of compound **3.30**.

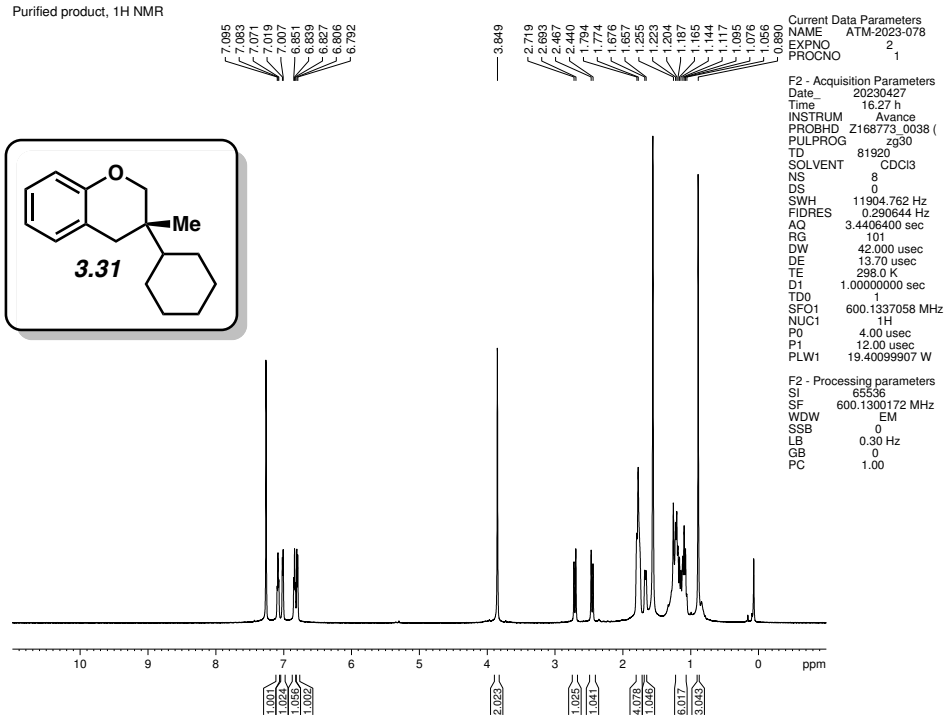


Figure 3.77. ^{1}H NMR (600 MHz, $CDCl_3$) of compound **3.31**.

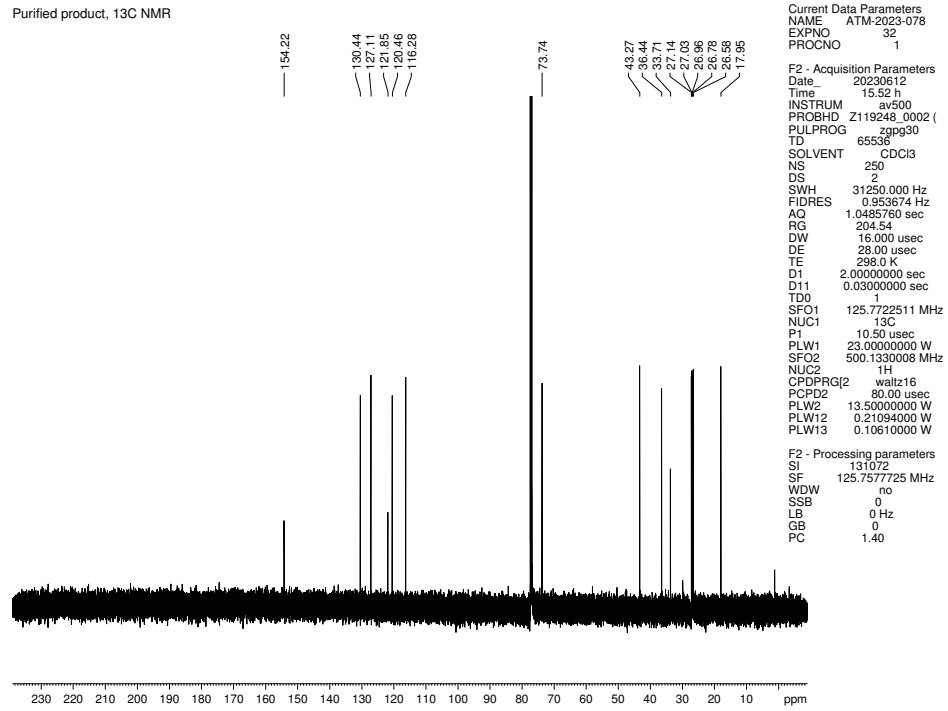


Figure 3.78. ^{13}C NMR (125 MHz, $CDCl_3$) of compound **3.31**.

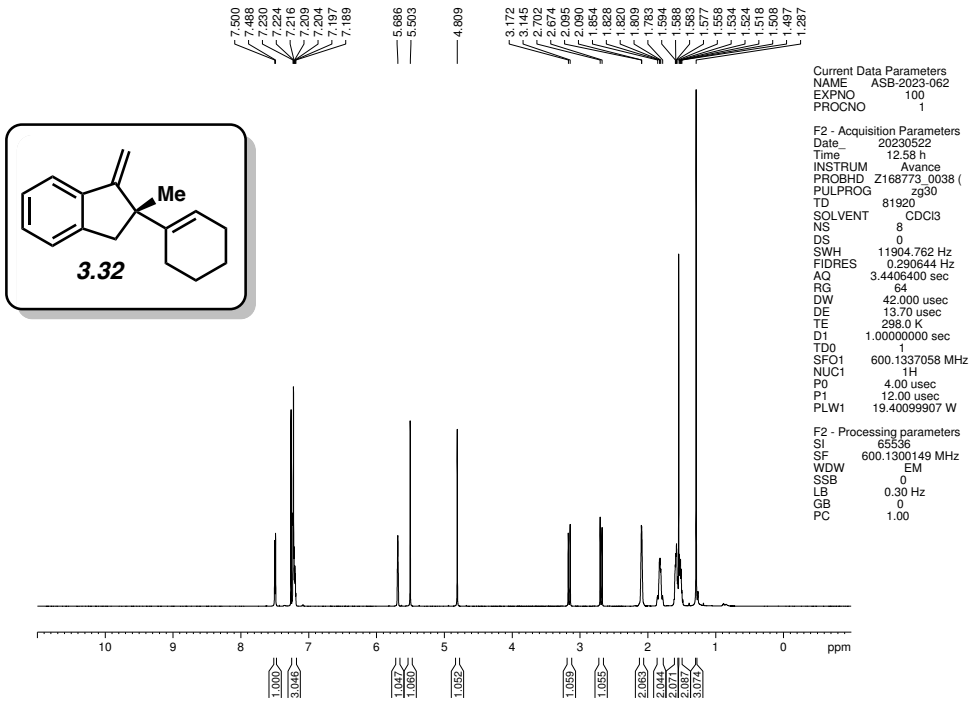


Figure 3.79. ^{1}H NMR (600 MHz, $CDCl_3$) of compound **3.32**.

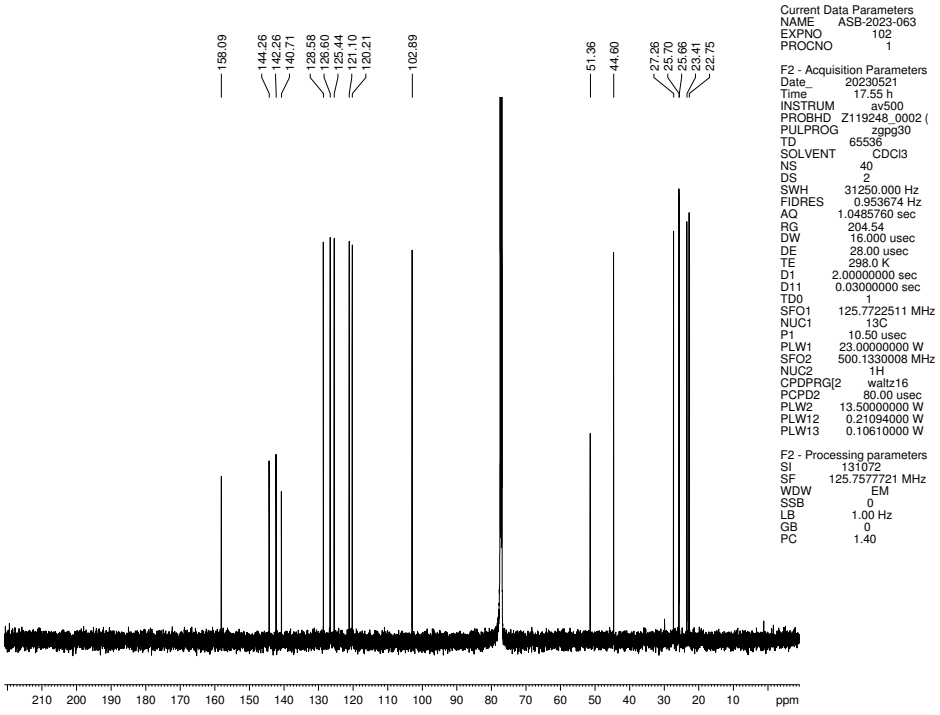


Figure 3.80. ^{13}C NMR (125 MHz, $CDCl_3$) of compound **3.32**.

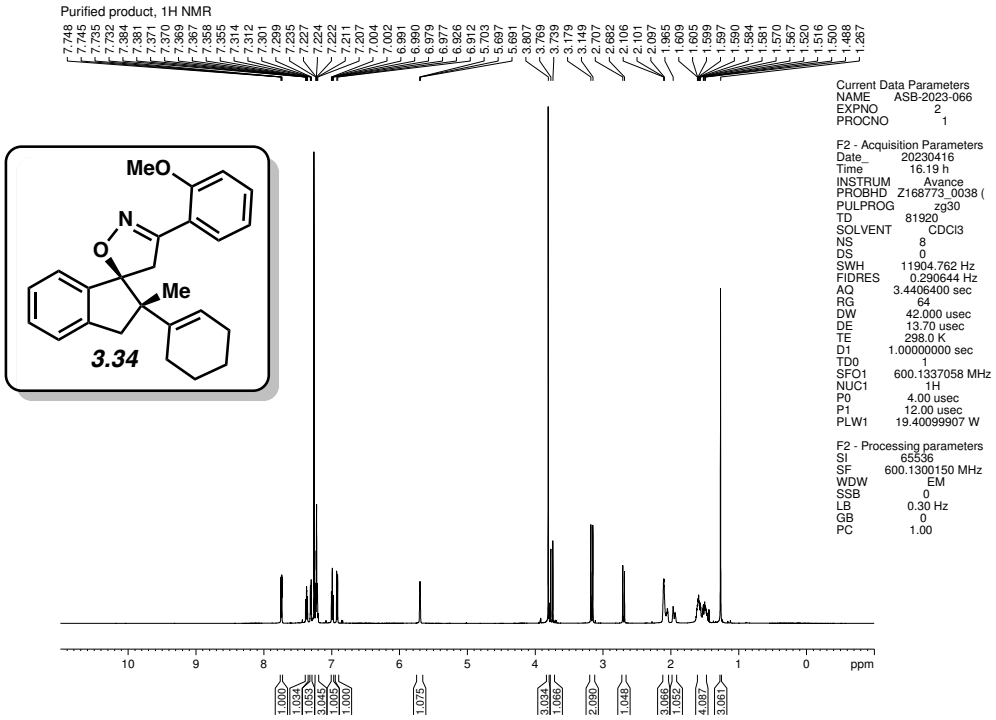


Figure 3.81. ^{1}H NMR (600 MHz, $CDCl_3$) of compound **3.34**.

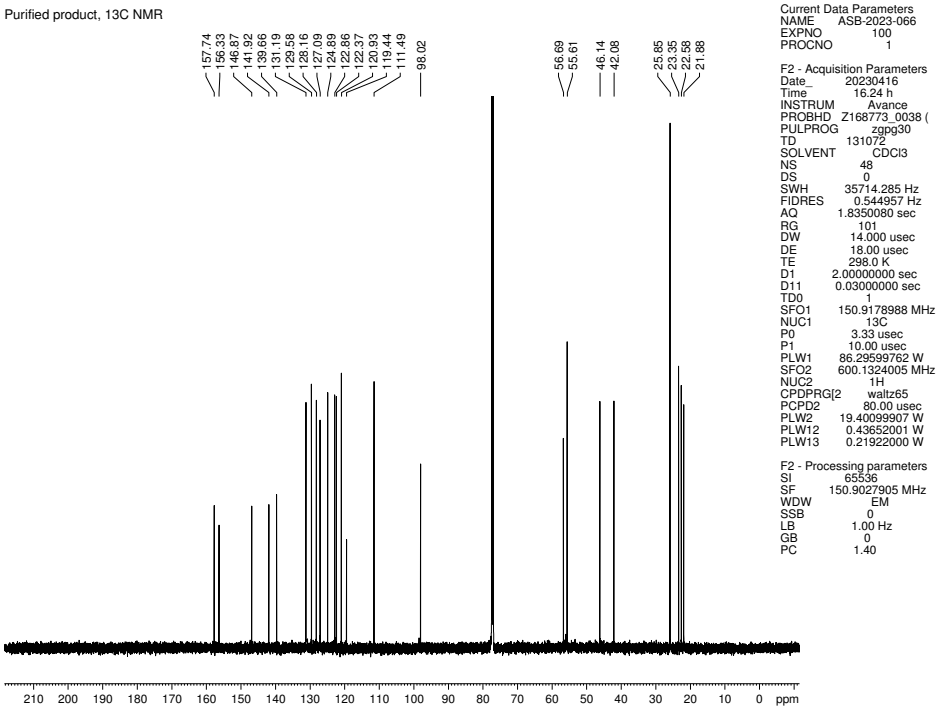


Figure 3.82. ^{13}C NMR (150 MHz, $CDCl_3$) of compound **3.34**.

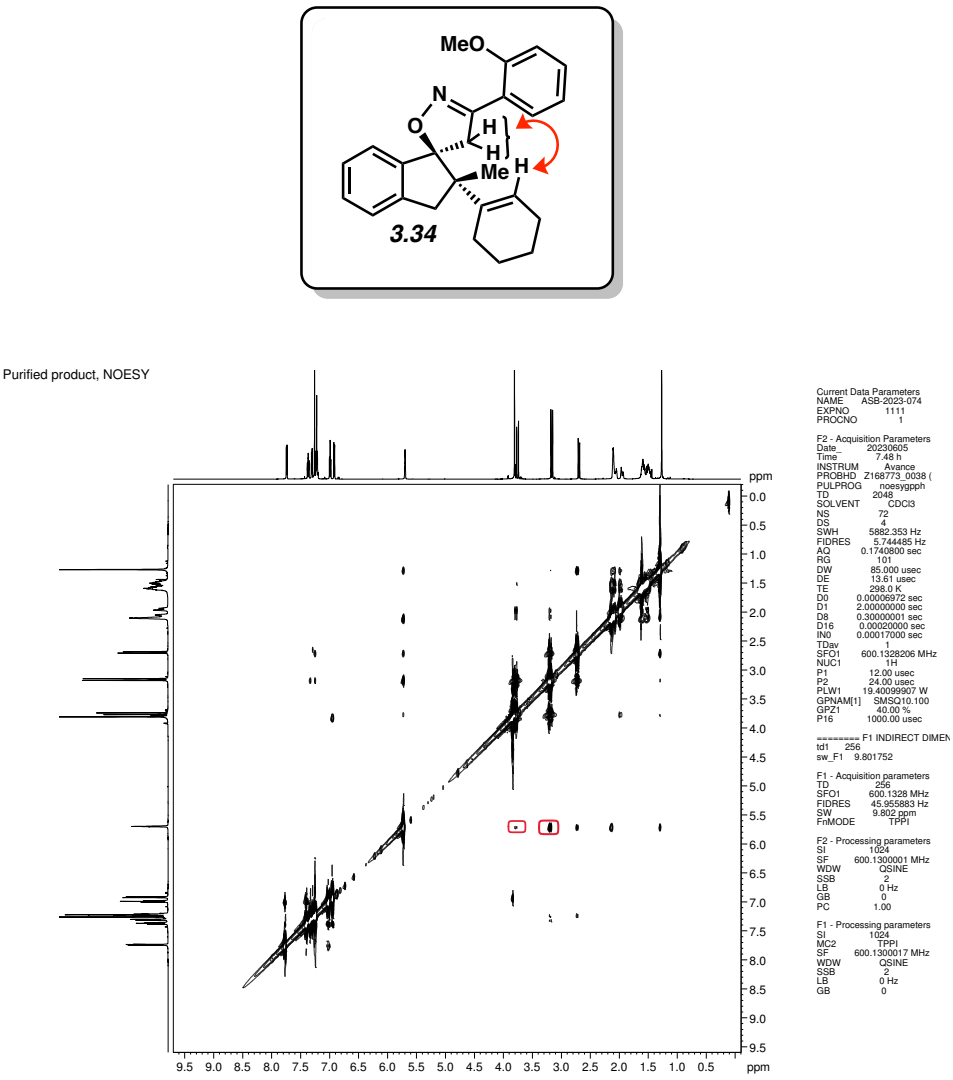


Figure 3.83. NOESY (600 MHz, $CDCl_3$) of compound **3.34**.

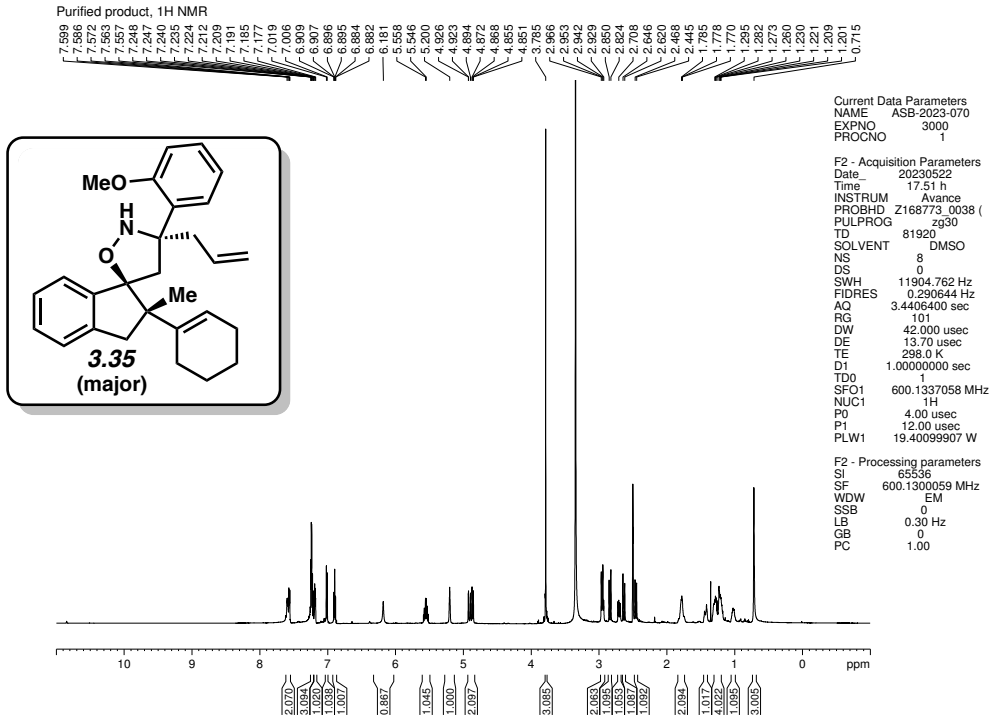


Figure 3.84. ^{1}H NMR (600 MHz, DMSO-D_6) of compound **3.35**.

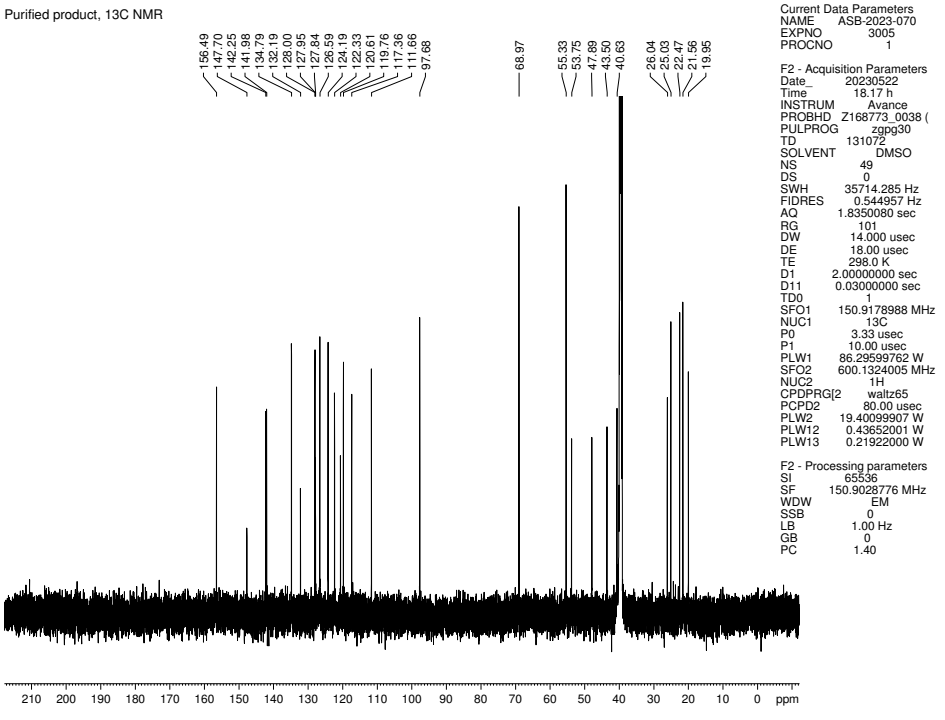


Figure 3.85. ^{13}C NMR (150 MHz, DMSO-D_6) of compound **3.35**.

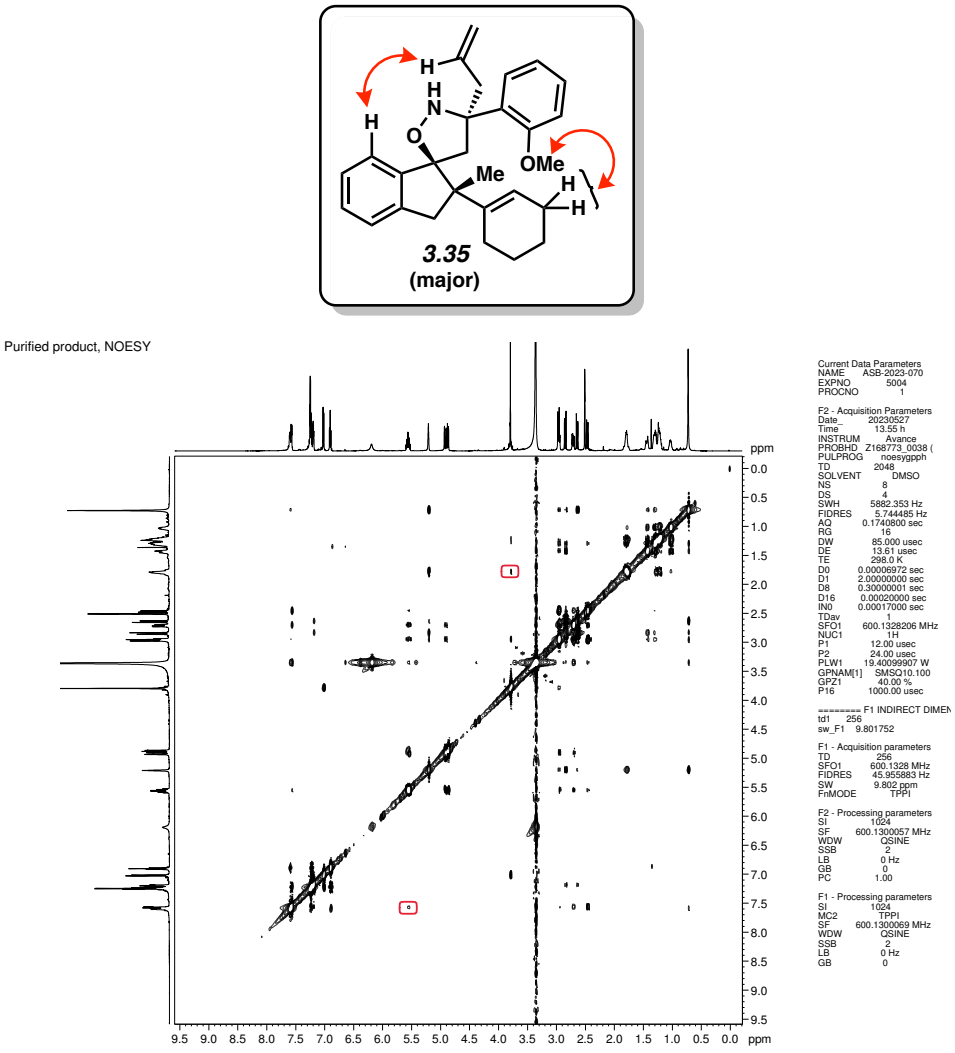


Figure 3.86. NOESY (600 MHz, DMSO-D_6) of compound **3.35**.

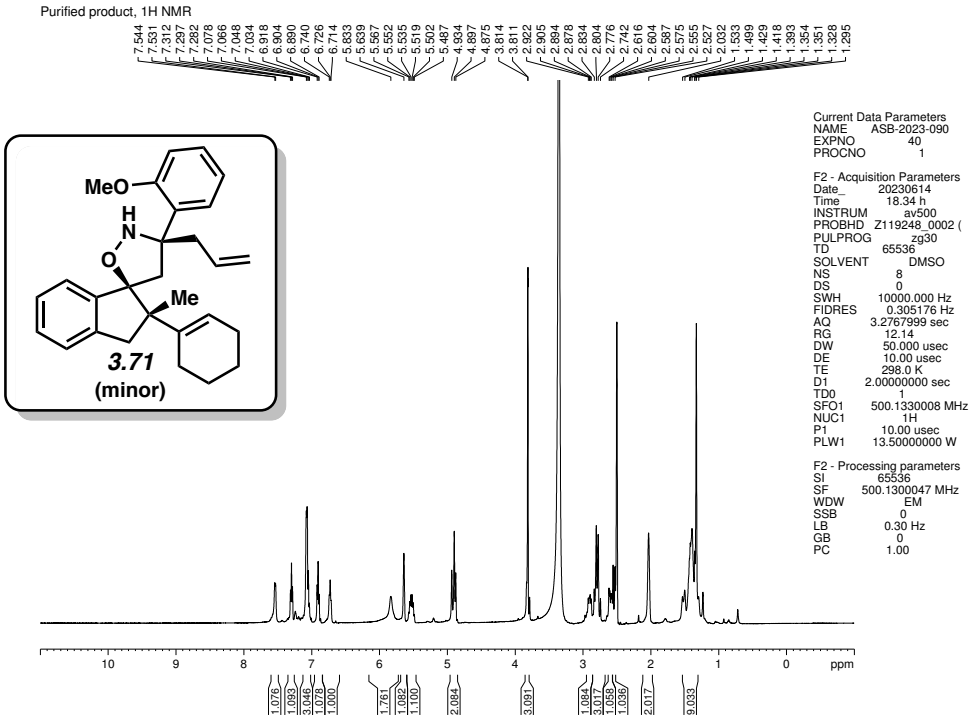


Figure 3.87. ^{1}H NMR (500 MHz, DMSO-D_6) of compound **3.71**.

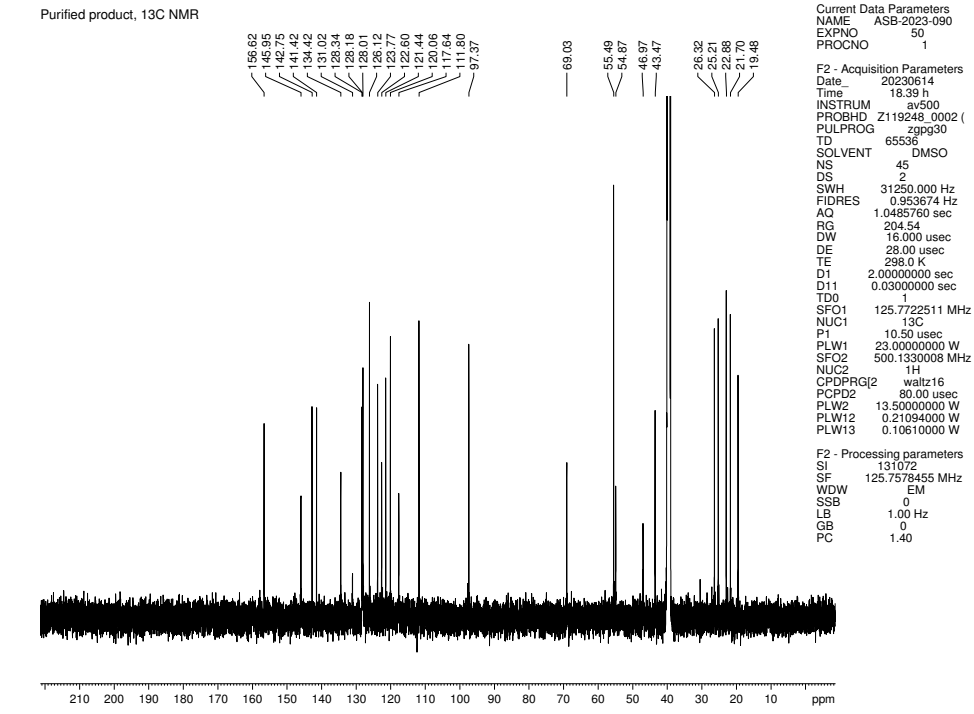


Figure 3.88. ^{13}C NMR (125 MHz, DMSO-D_6) of compound **3.71**.

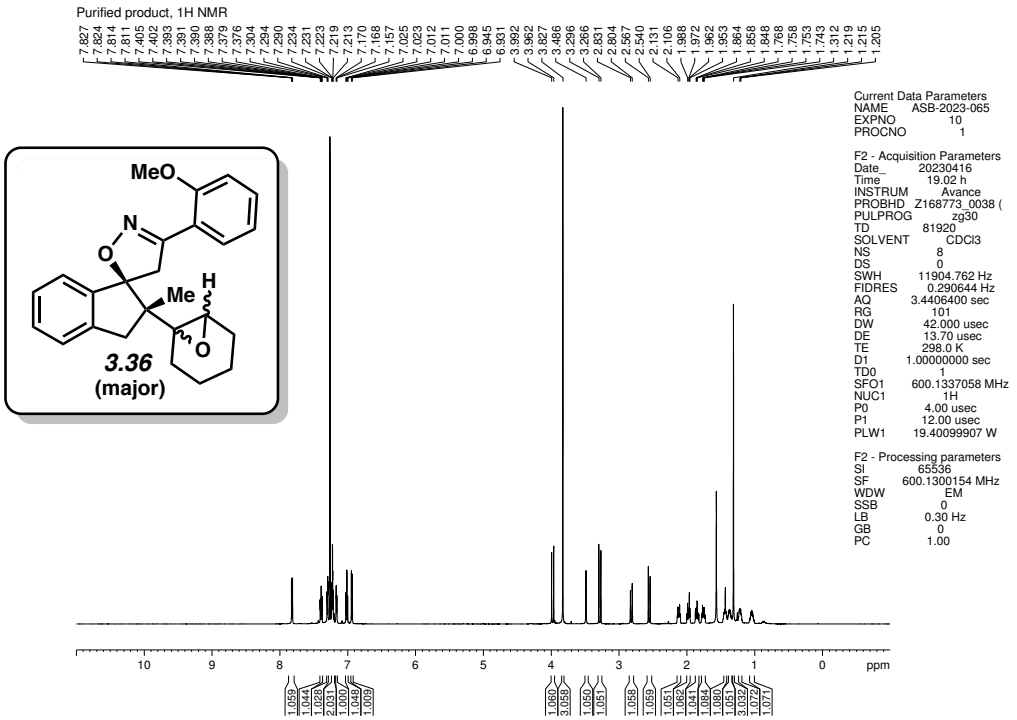


Figure 3.89. ^{1}H NMR (600 MHz, $CDCl_3$) of compound **3.36**.

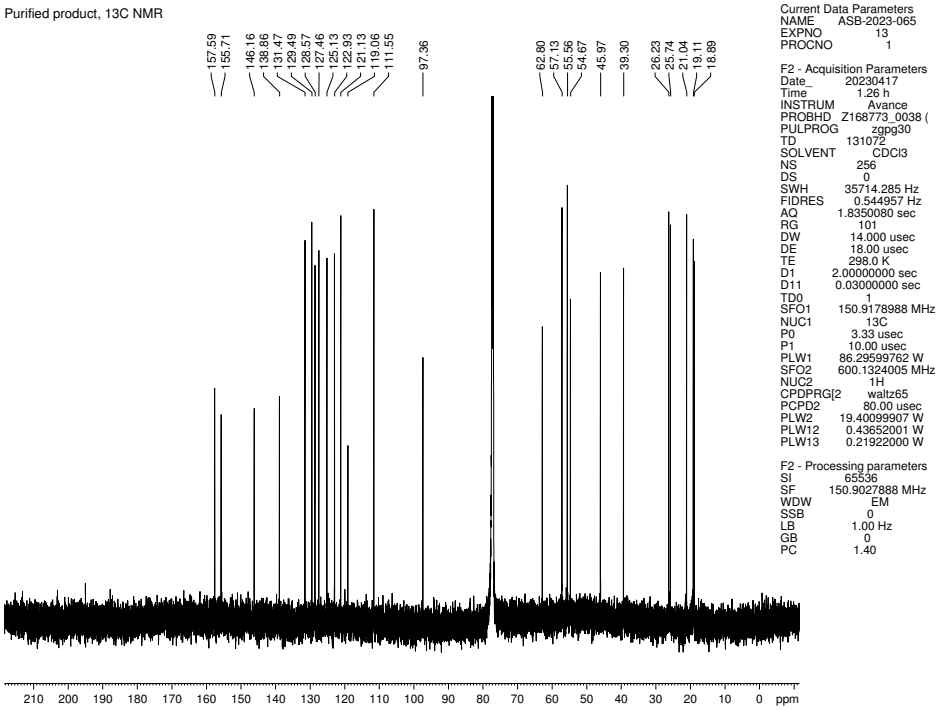


Figure 3.90. ^{13}C NMR (150 MHz, $CDCl_3$) of compound **3.36**.

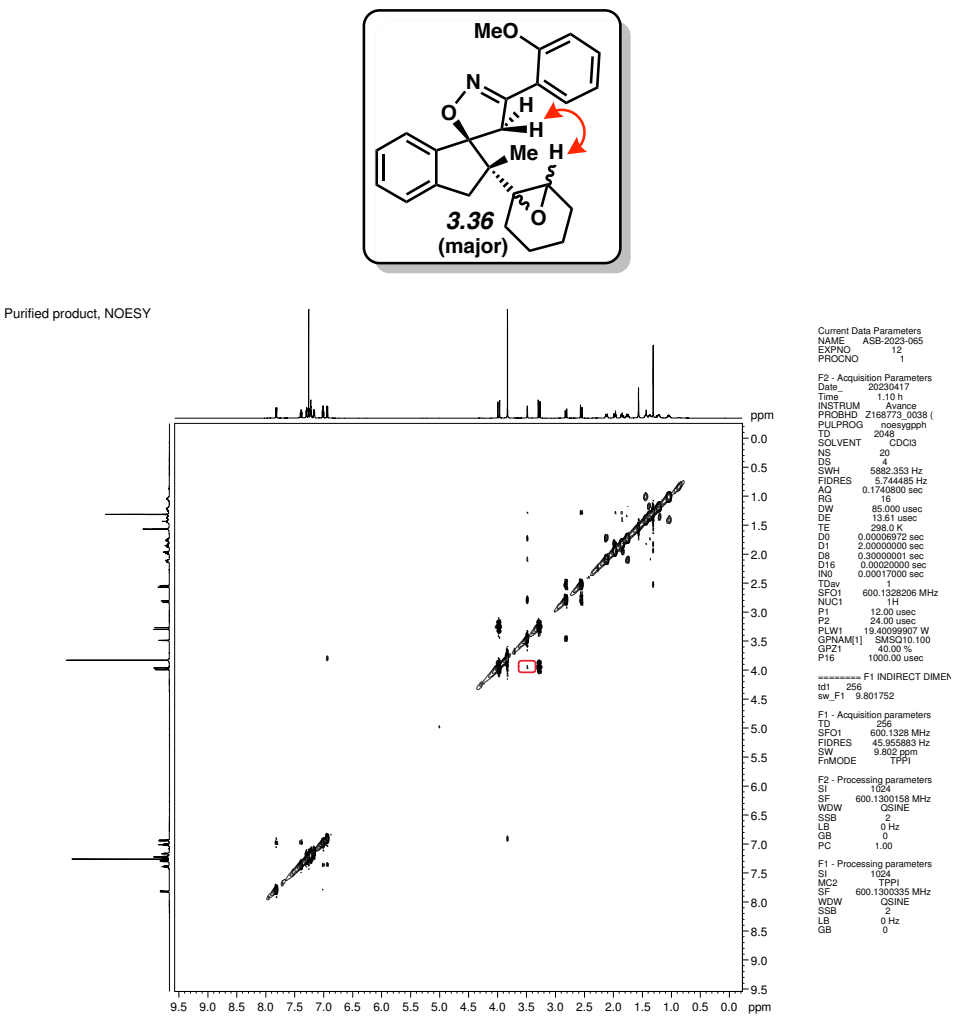


Figure 3.91. NOESY (600 MHz, $CDCl_3$) of compound **3.36**.

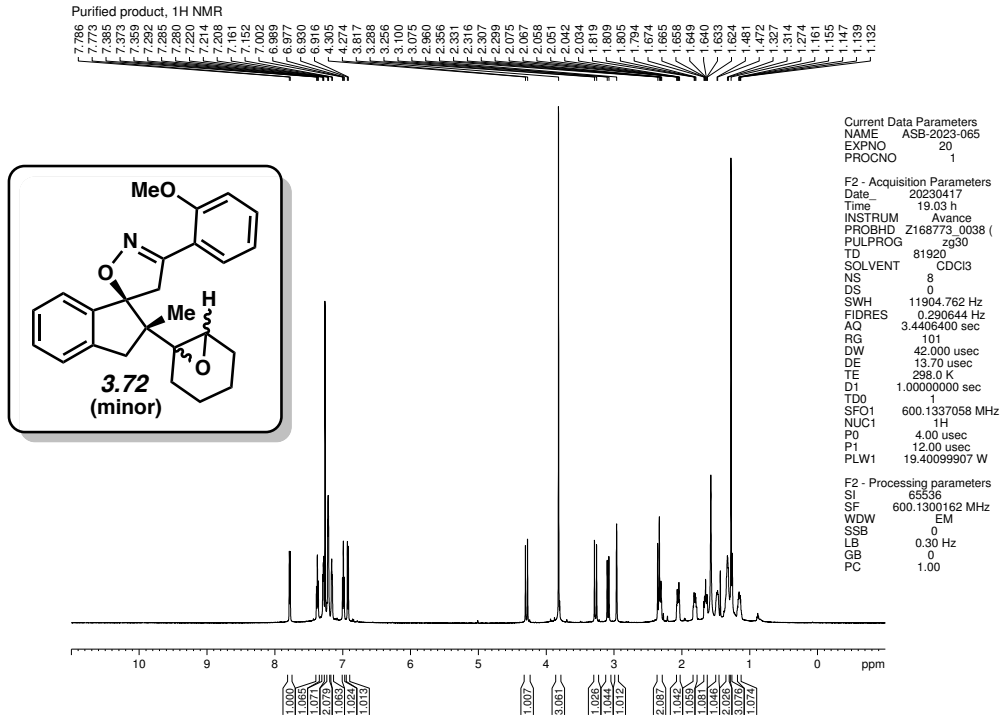


Figure 3.92. ^{1}H NMR (600 MHz, $CDCl_3$) of compound **3.72**.

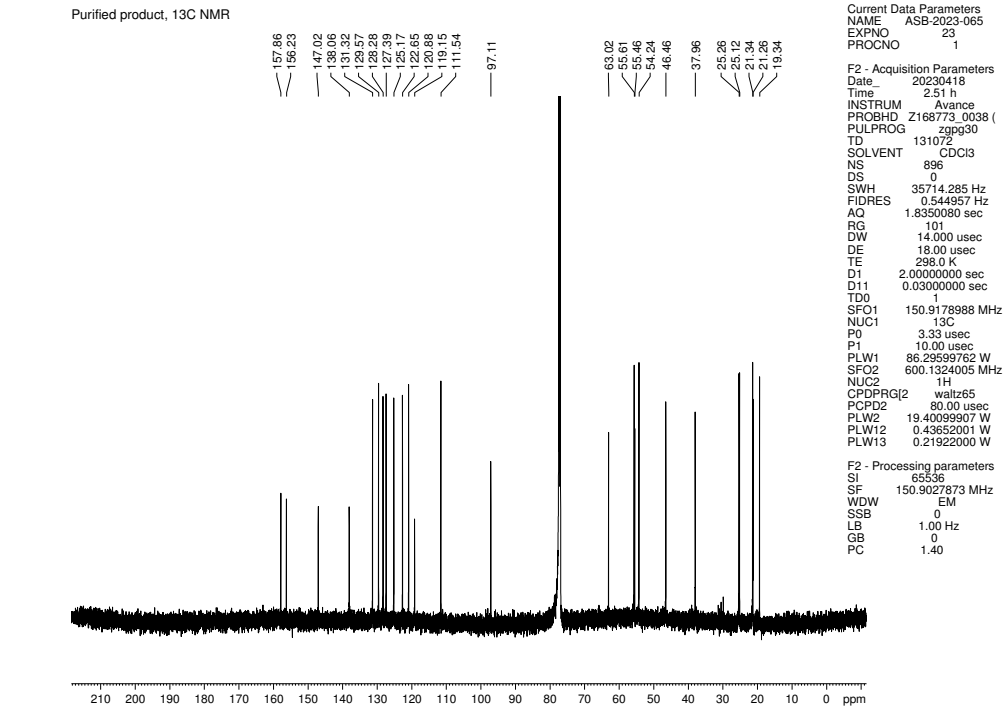


Figure 3.93. ^{13}C NMR (150 MHz, $CDCl_3$) of compound **3.72**.

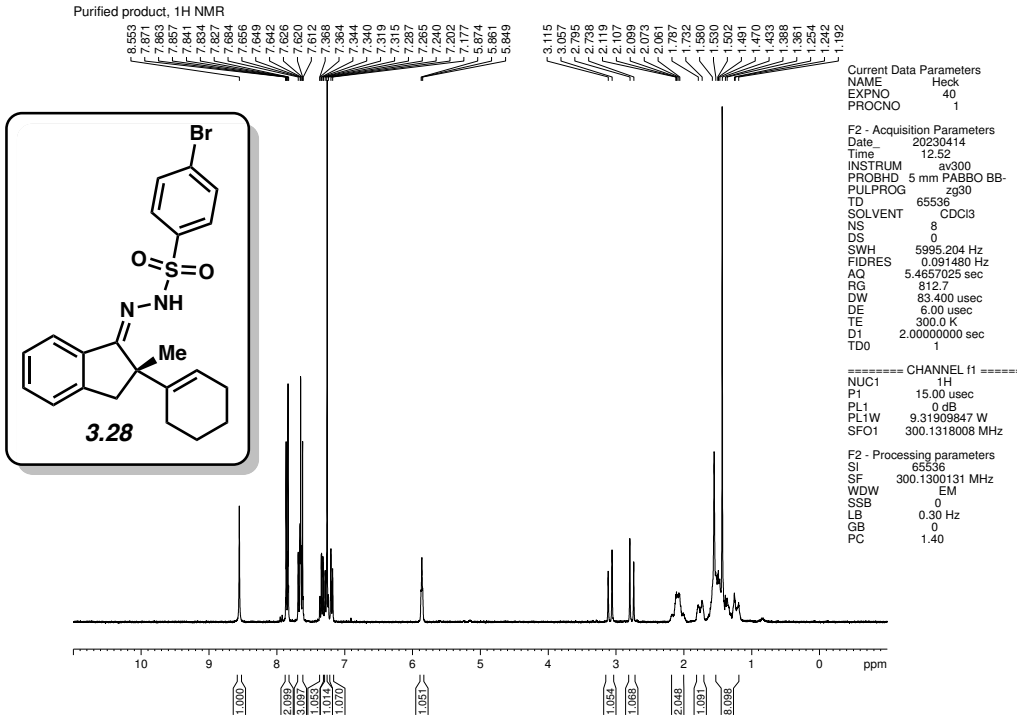


Figure 3.94. ^{1}H NMR (300 MHz, $CDCl_3$) of compound **3.28**.

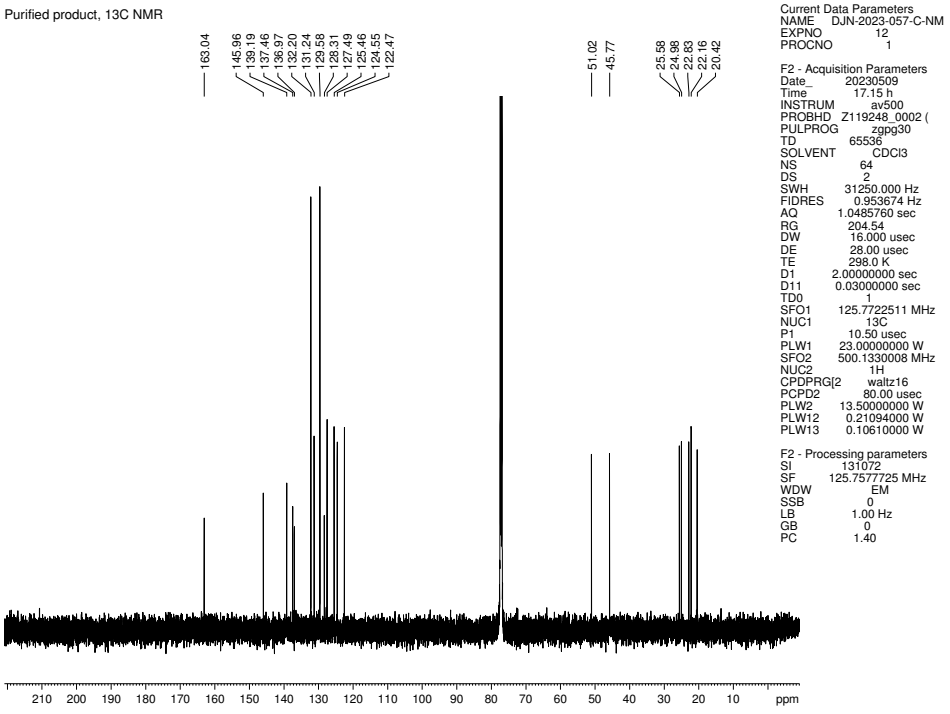


Figure 3.95. ^{13}C NMR (125 MHz, $CDCl_3$) of compound **3.28**.

3.11 Notes and References

(1) (a) C. S., Johansson; Kitching, M. O.; Colacot, T. J.; Snieckus, V. Palladium-catalyzed cross-coupling: A historical contextual perspective to the 2010 Nobel prize. *Angew. Chem., Int. Ed.* **2012**, *51*, 5062–5085. (b) Hassan, J.; Sevignon, M.; Gozzi, C.; Schulz, E.; Lemaire, M. Aryl–aryl bond formation one century after the discovery of the Ullman reaction. *Chem. Rev.* **2002**, *102*, 1359–1470. (c) Jiang, L.; Buchwald, S. L. in *Metal-Catalyzed Cross- Coupling Reactions*, 2nd ed. (Eds. A. Meijere, F. Diederich) Wiley VCH, Weinheim, 2004, pp. 699–760. (d) Corbet, J. P.; Mignani, G. Selected patented cross-coupling reaction technologies. *Chem. Rev.* **2006**, *106*, 2651–2710. (e) Negishi, E. Transition metal-catalyzed organometallic reactions that have revolutionized organic synthesis. *Bull. Chem. Soc. Jpn.* **2007**, *80*, 233–257. (f) Shen, H. C. in *Application of Transition Metal Catalysis in Drug Discovery and Development: An Industrial Perspective* (Eds. M. L. Crawley, B. M. Trost) Wiley, Hoboken, 2012; pp. 25–96. (g) Campeau, L. C.; Hazari, N. Cross-coupling and related reactions: connecting past success to the development of new reactions for the future. *Organometallics* **2019**, *38*, 3–35. (h) Suzuki, A. Cross-coupling reactions of organoboranes: An easy way to construct C–C bonds (Nobel lecture). *Angew. Chem., Int. Ed.* **2011**, *50*, 6722–6737. (i) Negishi, E. Magical power of transition metals: past, present, and future (Nobel lecture). *Angew. Chem., Int. Ed.* **2011**, *50*, 6738–6764.

(2) For select reviews on C–O, C–N and C–F bond cleaving reactions, see: (a) Boit, T. B.; Bulger, A. S.; Dander, J. E.; Garg, N. K. Activation of C–O and C–N bonds using non-precious metal catalysis. *ACS Catal.* **2020**, *10*, 12109–12126. (b) Zhang, S. Q.; Hong, X. Mechanism and selectivity control in Ni- and Pd-catalyzed cross-couplings involving carbon–oxygen bond activation. *Acc. Chem. Res.* **2021**, *54*, 2158–2171. (c) Baviskar, B. A.; Ajmire, P. V.;

Chumbhale, D. S.; Khan, M. S.; Kuchake, V. G.; Singupuram, M.; Laddha, P. R. Recent advances in nickel catalyzed Suzuki–Miyaura cross coupling reaction via C–O & C–N bond activation. *Sustainable Chemistry and Pharmacy* **2023**, *32*, 100953. (d) Tian, M.; Liu, M. The exploration of deoxygenation reactions for alcohols and derivatives using earth-abundant reagents. *Pure and Applied Chemistry* **2021**, *93*, 799–810. (e) Cornella, J.; Zarate, C.; Martin, R. Metal-catalyzed activation of ethers via C–O bond cleavage: A new strategy for molecular diversity. *Chem. Soc. Rev.* **2014**, *43*, 8081–8097. (f) Tobisu, M.; Chatani, N. Cross-couplings using aryl ethers via C–O bond activation enabled by nickel catalysts. *Acc. Chem. Res.* **2015**, *48*, 1717–1726. (g) Liu, F.; Jiang, H. J.; Zhou, Y.; Shi, Z. Direct transformation of arenols based on C–O activation. *Chin. J. Chem.* **2020**, *38*, 855–863. (h) Zhou, T.; Szostak, M. Palladium-catalyzed cross-couplings by C–O bond activation. *Catal. Sci. Technol.* **2020**, *10*, 5702–5739. (i) Qiu, Z.; Li, C. J. Transformations of less-activated phenols and phenol derivatives via C–O cleavage. *Chem. Rev.* **2020**, *120*, 10454–10515. (j) Ahrens, T.; Kohlmann, J.; Ahrens, M.; Braun, T. Functionalization of fluorinated molecules by transition-metal-mediated C–F bond activation to access fluorinated building blocks. *Chem. Rev.* **2015**, *115*, 931–972. (k) Fu, L.; Chen, Q.; Nishihara, Y. Recent advances in transition-metal-catalyzed C–C bond formation via C(sp^2)–F bond cleavage. *Chem. Rec.* **2021**, *21*, 3394–3410. (l) Becica, J.; Leitch, D. C. C–O bond activation as a strategy in palladium-catalyzed cross-coupling. *Synlett* **2021**, *32*, 641–646.

(3) For select reviews on acyl electrophiles see: (a) Buchspies, J.; Szostak, M. Recent advances in acyl Suzuki cross-coupling. *Catalysts* **2019**, *9*, 53. (b) Takise, R.; Muto, K.; Yamaguchi, J. Cross-coupling of aromatic esters and amides. *Chem. Soc. Rev.* **2017**, *46*, 5864–5888. (c) Zhou, T.; Szostak, M. Palladium-catalyzed cross-couplings by C–O bond activation. *Catal.*

Sci. Technol. **2020**, *10*, 5702–5739. (d) Gooßen, L. J.; Rodríguez, N.; Gooßen, K. Carboxylic acids as substrates in homogeneous catalysis. *Angew. Chem., Int. Ed.* **2008**, *47*, 3100–3120. (e) Dander, J. E.; Garg, N. K. Breaking amides using nickel catalysis. *ACS Catal.* **2017**, *7*, 1413–1423. f) Li, G.; Ma, S.; Szostak, M. Amide bond activation: The power of resonance. *Trends Chem.* **2020**, *2*, 914–928.

(4) For this context, "conventional" is used to refer to cross-couplings employing a nucleophile and electrophile. For select studies on asymmetric transition-metal-catalyzed reactions using thioester electrophiles, see: (a) Banchini, F.; Leroux, B.; LeGall, E.; Presset, M.; Jackowski, O.; Chemla, F.; Perez-Luna, A. Enantioselective sequential catalytic arylation-Fukayama cross-coupling of 1,1-biszincioalkane linchpins. *Chem. Eur. J.,* **2023**, *29*, e202301084. (b) Oost, R.; Misale, A.; Maulide, N. Enantioconvergent Fukayama cross-coupling of racemic benzylic organozinc reagents. *Angew. Chem., Int. Ed.* **2016**, *55*, 4587–4590. (c) Liu, M.; Wang, X.; Guo, Z.; Li, H.; Huang, W.; Xu, H.; Dai, H.-X. Pd-catalyzed asymmetric acyl-carbamoylation of an alkene to construct an α-quaternary chiral cycloketone. *Org. Lett.* **2021**, *23*, 6299–6304.

(5) For select studies on asymmetric transition-metal-catalyzed reductive or photochemical cross-coupling reactions using anhydride or acid chloride electrophiles, see: (a) Cherney, A. H.; Kadunce, N. T.; Reisman, S. E. Catalytic asymmetric reductive acyl cross-coupling: synthesis of enantioenriched acyclic α,α-disubstituted ketones. *J. Am. Chem. Soc.* **2013**, *135*, 7442–7445. (b) Ji, H.; Lin, D.; Tai, L.; Li, X.; Shi, Y.; Han, Q.; Chen, L.-A. Nickel-catalyzed enantioselective coupling of acid chlorides with α-bromobenzoates: An asymmetric acyloin synthesis. *J. Am. Chem. Soc.* **2022**, *144*, 23019–23029. c) Gandolfo, E.; Tang, X.; Roy, S. R.;

Melchiorre, P. Photochemical asymmetric nickel-catalyzed acyl cross-coupling. *Angew. Chem.* **2019**, *131*, 17010–17014.

(6) For select recent work on transition-metal-catalyzed ester C–O bond activation and cross-couplings, see: (a) Yamamoto, T.; Ishizu, J.; Kohara, T.; Komiya, S.; Yamamoto, A. Oxidative addition of aryl carboxylates to nickel(0) complexes involving cleavage of the acyl-oxygen bond. *J. Am. Chem. Soc.* **1980**, *102*, 3758–3764. (b) Amaike, K.; Muto, K.; Yamaguchi, J.; Itami, K. Decarbonylative C–H coupling of azoles and aryl esters: Unprecedented nickel catalysis and application to the synthesis of murscoride A. *J. Am. Chem. Soc.* **2012**, *134*, 13573–13576. (c) Meng, L.; Kamada, Y.; Muto, K.; Yamaguchi, J.; Itami, K. C–H alkenylation of azoles with enols and esters by nickel catalysis. *Angew. Chem., Int. Ed.* **2013**, *52*, 10048–10051. (d) Muto, K.; Yamaguchi, J.; Musaev, D. G.; Itami, K. Decarbonylative organoboron cross-coupling of esters by nickel catalysis. *Nat. Commun.* **2015**, *6*, 7508. (e) Muto, K.; Hatakeyama, R.; Itami, K.; Yamaguchi, J. Palladium-catalyzed decarbonylative cross-coupling of azinecarboxylates with arylboronic acids. *Org. Lett.* **2016**, *18*, 5106–5109. (f) Gooßen, L. J.; Paetzold, J. Pd-catalyzed decarbonylative olefination of aryl esters: Towards a waste-free Heck reaction. *Angew. Chem., Int. Ed.* **2002**, *41*, 1237–1241. (g) Gooßen, L. J.; Paetzold, J. Decarbonylative Heck olefination of enol esters: Salt-free and environmentally friendly access to vinyl arenes. *Angew. Chem., Int., Ed.* **2004**, *43*, 1095–1098. (h) Chatani, N.; Tatamidani, H.; Ie, Y.; Kakiuchi, F.; Murai, S. The ruthenium-catalyzed reductive decarbonylation of esters: Catalytic reactions involving the cleavage of acyl–oxygen bonds of esters. *J. Am. Chem. Soc.* **2001**, *123*, 4849–4850. (i) Tatamidani, H.; Yokota, K.; Kakiuchi, F.; Chatani, N. Catalytic cross-coupling reaction of esters with organoboron compounds and decarboylative reduction of esters with $HCOONH_4$: A new route

to acyl transition metal complexes through the cleavage of acyl–oxygen bonds in esters. *J. Org. Chem.* **2004**, *69*, 5615–5621. (j) Tatamidani, H.; Kakiuchi, F.; Chatani, N. A new ketone synthesis by palladium-catalyzed cross-coupling reactions of esters with organoboron compounds. *Org. Lett.* **2004**, *6*, 3597–3599. (k) LaBerge, N. A.; Love, J. A. Nickel-catalyzed decarbonylative coupling of aryl esters and arylboronic acids. *Eur. J. Org. Chem.* **2015**, *2015*, 5546–5553. (l) Ben Halima, T.; Vandavasi, J. K.; Shkoor, M.; Newman, S. G. A cross-coupling approach to amide bond formation from esters. *ACS Catal.* **2017**, *7*, 2176–2180. (m) Kruckenberg, A.; Wadepohl, H.; Gade, L. H. Bis(diisopropylphosphinomethyl)amine nickel(II) and nickel(0) complexes: Coordination chemistry, reactivity, and catalytic decarbonylative C–H arylation of benzoxazole. *Organometallics* **2013**, *32*, 5153–5170. (n) Yue, H.; Guo, L.; Liao, H.-H.; Cai, Y.; Zhu, C.; Rueping, M. Catalytic ester and amide to amine interconversion: Nickel-catalyzed decarbonylative amination of esters and amides by C–O and C–C bond activation. *Angew. Chem., Int. Ed.* **2017**, *56*, 4282–4285. (o) Yu, H.; Guo, L.; Lee, S.-C.; Liu, X.; Rueping, M. Selective reductive removal of ester and amide groups from arenes and heteroarenes through nickel-catalyzed C–O and C–N bond activation. *Angew. Chem., Int. Ed.* **2017**, *56*, 3972–3976. (p) Ben Halima, T.; Zhang, W.; Yalaoui, I.; Hong, X.; Yang, Y.; Houk, K. N.; Newman, S. G. Palladium-catalyzed Suzuki–Miyaura coupling of aryl esters. *J. Am. Chem. Soc.* **2017**, *139*, 1311–1318. (q) Hie, L.; Fine Nathel, N.; Hong, X.; Yang, Y.-F.; Houk, K. N.; Garg, N. K. Nickel-catalyzed activation of acyl C–Obonds of methyl esters. *Angew. Chem., Int. Ed.* **2016**, *55*, 2810–2814. (r) Ben Halima, T.; Masson-Makdissi, J.; Newman, S. G. Nickel-catalyzed amide bond formation from methyl esters. *Angew. Chem., Int. Ed.* **2018**, *57*, 12925–12929. (s) Zheng, Y.-L.; Newman, S. G. Methyl esters as cross-coupling electrophiles: Direct synthesis of amide bonds. *ACS Catal.* **2019**, *9*, 4426–4433. (t)

Cheung, C. W.; Ploeger, M. L.; Hu, X. Direct amidation of esters with nitroarenes. *Nat. Commun.* **2017**, *8*, 14878. (u) Banovetz, H. K.; Vickerman, K. L.; David, C. M.; Alkan, M.; Stanley, L. M. Palladium-catalyzed intermolecular alkene carboacylation via ester C–O bond activation. *Org. Lett.* **2021**, *23*, 3507–3521. (v) Zheng, Y.-L.; Xie, P.-P.; Daneshfar, O.; Houk, K. N.; Hong, X.; Newman, S. G. Direct synthesis of ketones from methyl esters by nickel-catalyzed Suzuki–Miyaura coupling. *Angew. Chem.* **2021**, *133*, 13588–13595. (w) Yang, S.; Zhou, T.; Poater, A.; Cavallo, L.; Nolan, S. P.; Szostak, M. Suzuki–Miyaura cross-coupling of esters by selective O–C(O) cleavage mediated by air- and moisture-stable [Pd(NHC)(μ-Cl)Cl]$_2$ precatalysts: Catalyst evaluation and mechanism. *Catal. Sci. Technol.* **2021**, *11*, 3189–3197.

(7) For recent articles on nickel-catalyzed reactions proceeding through amide C–N bond cleavage, see: (a) Hie, L.; Fine Nathel, N.; Shah, T. K.; Baker, E. L.; Hong, X.; Yang, Y.-F.; Liu, P.; Houk, K. N.; Garg, N. K. Conversion of amides to esters by the nickel-catalysed activation of amide C–N bonds. *Nature* **2015**, *524*, 79–83. (b) Weires, N. A.; Baker, E. L.; Garg, N. K. Nickel-catalysed Suzuki–Miyaura coupling of amides. *Nat. Chem.* **2016**, *8*, 75–79. (c) Baker, E. L.; Yamano, M. M.; Zhou, Y.; Anthony, S. M.; Garg, N. K. A two-step approach to achieve secondary amide transamidation enabled by nickel catalysis. *Nat. Commun.* **2016**, *7*, 11554. (d) Simmons, B. J.; Weires, N. A.; Dander, J. E.; Garg, N. K. Nickel-catalyzed alkylation of amide derivatives. *ACS Catal.* **2016**, *6*, 3176–3179. (e) Shi, S.; Szostak, M. Nickel-catalyzed diaryl ketone synthesis by N–C cleavage: Direct Negishi cross-coupling of primary amides by site-selective *N,N*-di-boc activation. *Org. Lett.* **2016**, *18*, 5872–5875. (f) Shi, S.; Szostak, M. Efficient synthesis of diaryl ketones by nickel-catalyzed Negishi cross-coupling of amides by carbon–nitrogen bond cleavage at room temperature accelerated by a solvent

effect. *Chem. Eur. J.* **2016**, *22*, 10420–10424. (g) Hie, L.; Baker, E. L.; Anthony, S. M.; Desrosiers, J.- N.; Senanayake, C.; Garg, N. K. Nickel-catalyzed esterification of aliphatic amides. *Angew. Chem., Int. Ed.* **2016**, *55*, 15129–15132. (h) Dey, A.; Sasmal, S.; Seth, K.; Lahiri, G. K.; Maiti, D. Nickel-catalyzed deamidative step-down reduction of amides to aromatic hydrocarbons. *ACS Catal.* **2017**, *7*, 433–437. (i) Ni, S.; Zhang, W.; Mei, H.; Han, J.; Pan, Y. Ni-catalyzed reductive cross-coupling of amides with aryl iodide electrophiles via C–N bond activation. *Org. Lett.* **2017**, *19*, 2536–2539. (j) Medina, J. M.; Moreno, J.; Racine, S.; Du, S.; Garg, N. K. Mizoroki–Heck cyclizations of amide derivatives for the introduction of quaternary centers. *Angew. Chem., Int. Ed.* **2017**, *56*, 6567–6571. (k) Li, X.; Zou, G. Acylative Suzuki coupling of amides: Acyl-nitrogen activation via synergy of independently modifiable activating groups. *Chem. Commun.* **2015**, *51*, 5089–5092. (l) Walker, J. A.; Vickerman, K. L.; Humke, J. N.; Stanley, L. M. Ni-catalyzed alkene carboacylation via amide C–N bond activation. *J. Am. Chem. Soc.* **2017**, *139*, 10228–10231. (m) Hu, J.; Wang, M.; Pu, X.; Shi, Z. Nickel-catalysed retro-hydroamidocarbonylation of aliphatic amides to olefins. *Nat. Commun.* **2017**, *8*, 14993. (n) Weires, N. A.; Caspi, D. D.; Garg, N. K. Kinetic modeling of the nickel-catalyzed esterification of amides. *ACS Catal.* **2017**, *7*, 4381–4385. (o) Shi, S.; Szostak, M. Nickel-catalyzed Negishi cross-coupling of *N*-acylsuccinimides: Stable, amide-based, twist-controlled acyl-transfer reagents via N–C activation. *Synthesis* **2017**, *49*, 3602–3608. (p) Dander, J. E.; Baker, E. L.; Garg, N. K. Nickel-catalyzed transamidation of aliphatic amide derivatives. *Chem. Sci.* **2017**, *8*, 6433–6438. (q) Huang, P.-Q.; Chen, H. Ni-catalyzed cross-coupling reactions of *N*-acylpyrrole-type amides with organoboron reagents. *Chem. Commun.* **2017**, *53*, 12584–12587. (r) Deguchi, T.; Xin, H.-L.; Morimoto, H.; Ohshima, T. Direct catalytic alcoholysis of unactivated 8-aminoquinoline amides. *ACS Catal.*

2017, *7*, 3157–3161. (s) Dander, J. E.; Giroud, M.; Racine, S.; Darzi, E. R.; Alvizo, O.; Entwistle, D.; Garg, N. K. Chemoenzymatic conversion of amides to enantioenriched alcohols in aqueous medium. *Commun. Chem.* **2019**, *2*, 82. (t) Mehta, M. M.; Boit, T. B.; Dander, J. E.; Garg, N. K. Ni-catalyzed Suzuki–Miyaura cross-coupling of aliphatic amides on the benchtop. *Org. Lett.* **2020**, *22*, 1–5. (u) Knapp, R. R.; Bulger, A. S.; Garg, N. K. Nickel-catalyzed conversion of amides to carboxylic acids. *Org. Lett.* **2020**, *22*, 2833–2837. (v) Boit, T. B.; Mehta, M. M.; Kim, J.; Baker, E. L.; Garg, N. K. Reductive arylation of amides via a nickel-catalyzed Suzuki–Miyaura-coupling and transfer-hydrogenation cascade. *Angew. Chem., Int. Ed.* **2021**, *60*, 2472–2477. (w) Buchspies, J.; Rahman, M.; Szostak, M. Transamidation of amides and amidation of esters by selective N–C(O)/O–C(O) cleavage mediated by air- and moisture-stable half-sandwich nickel(II)–NHC complexes. *Molecules* **2021**, *26*, 188.

(8) For a select example, see: Rouquet, G.; Chatani, N. Catalytic functionalization of $C(sp^2)$–H and $C(sp^3)$–H bonds by using bidentate directing groups. *Angew. Chem., Int. Ed.* **2013**, *52*, 11726–11743.

(9) (a) A. *The Amide Linkage: Structural Significance in Chemistry, Biochemistry, and Materials Science*, *Vol. 1*. (Eds.: Greenberg, A.; Breneman, C. M.; Liebman, J. F.) Wiley, Hoboken, 2003; pp. 33–43. b) Pauling, L.; Corey, R. B.; Branson, H. R. The structure of proteins; two hydrogen-bonded helical configurations of the polypeptide chain. *Proc. Natl. Acad. Sci. U. S. A.* **1951**, *37*, 205–211.

(10) For examples of traditional amide C–N bond cleavage reactions, see: (a) Nahm, S.; Weinreb, S. M. *N*-methoxy-*N*-methylamides as effective acylating agents. *Tetrahedron Lett.* **1981**, *22*,

3815–3818. (b) Balasubramaniam, S.; Aidhen, I. S. The growing synthetic utility of the Weinreb amide. *Synthesis* **2008**, *2008*, 3707–3738.

(11) For select reviews on mild amide activation strategies, see: (a) Meng, G.; Shi, S.; Szostak, M. Cross-coupling of amides by N–C bond activation. *Synlett* **2016**, *27*, 2530–2540. (b) Takise, R.; Muto, K.; Yamaguchi, J. Cross-coupling of aromatic esters and amides. *Chem. Soc. Rev.* **2017**, *46*, 5864–5888. (c) Kaiser, D.; Bauer, A.; Lemmerer, M.; Maulide, N. Amide activation: An emerging tool for chemoselective synthesis. *Chem. Soc. Rev.* **2018**, *47*, 7899–7925.

(12) This number represents a conservative estimate of the array of metal-catalyzed cross-couplings developed for amide electrophiles, demonstrated by citations of our first paper[7a] that was published in 2015.

(13) Initial attempts towards an intermolecular Mizoroki–Heck reaction proved unsuccessful, but will be the subject of future investigation.

(14) Hayashi, T.; Tang, J.; Kato, K. Palladium-catalyzed enantioselective carbonylative cyclization of aryl and alkenyl triflates with carbon monoxide. *Org. Lett.* **1999**, *1*, 1487–1489.

(15) Fan, P.; Lan, Y.; Zhang, C.; Wang, C. Nickel/photo-cocatalyzed asymmetric acyl-carbamoylation of alkenes. *J. Am. Chem. Soc.* **2020**, *142*, 2180–2186.

(16) (a) Christoffers, J.; Mann, A. Enantioselective construction of quaternary stereocenters. *Angew. Chem., Int. Ed.* **2001**, *40*, 4591–4597. (b) Li, C.; Ragab, S. S.; Liu, G.; Tang, W. Enantioselective formation of quaternary carbon stereocenters in natural product synthesis: A recent update. *Nat. Prod. Rep.* **2020**, *37*, 276–292.

(17) *N*-heterocyclic carbene ligands were of particular interest for this investigation, as opposed to other ligand classes, as they are highly electron-rich and have uniquely enabled similar non-

asymmetric catalytic amide activation reactions (for a review on NHC ligands, see Droge, T.; Glorius, F. The measure of all rings – *N*-heterocyclic carbenes. *Angew. Chem., Int. Ed.* **2010**, *49*, 6940–6952.).

(18) Ananikov, V. P. Nickel: The "spirited horse" of transition metal catalysis. *ACS Catal.* **2015**, *5*, 1964–1971.

(19) (a) Ahlin, J. S. E.; Cramer, N. Chiral *N*-heterocyclic carbene ligand enabled nickel(0)-catalyzed enantioselective three-component couplings as direct access to silylated indanols. *Org. Lett.* **2016**, *18*, 3242–3245. (b) Ahlin, J. S. E.; Donets, P. A.; Cramer, N. Nickel(0)-catalyzed enantioselective annulations of alkynes and arylenoates enabled by a chiral NHC ligand: Efficient access to cyclopentenones. *Angew. Chem., Int. Ed.* **2014**, *53*, 13229–13233.

(20) Nakanishi, M.; Katayev, D.; Besnard, C.; Kündig, E. P. Fused indolines by palladium-catalyzed asymmetric C–C coupling involving an unactivated methylene group. *Angew. Chem., Int. Ed.* **2011**, *50*, 7438–7441.

(21) Seo, H.; Hirsch-Weil, D.; Abboud, K. A.; Hong, S. Development of biisoquinoline-based chiral diaminocarbene ligands: Enantioselective S_N2' allylic alkylation catalyzed by copper-carbene complexes. *J. Org. Chem.* **2008**, *73*, 1983–1986.

(22) Hirsch-Weil, D.; Abboud, K. A.; Hong, S. Isoquinoline-based chiral monodentate *N*-heterocyclic carbenes. *Chem. Commun.* **2010**, *46*, 7525–7527.

(23) Ahlin, J. S. E.; Donets, P. A.; Cramer, N. Nickel(0)-catalyzed enantioselective annulations of alkynes and arylenoates enabled by a chiral NHC ligand: Efficient access to cyclopentenones. *Angew. Chem., Int. Ed.* **2014**, *53*, 13229–13233.

(24) A variety of other *N*-substituents were employed in the transformation, including: *N*-Ph-*N*-Boc, *N*-Ph-*N*-Ts, *N*-Ph-*N*-Ms, *N*-Bn-*N*-CO_2Et, and *N*-Me-*N*-Ph, but either led to trace amounts or no observed formation of the desired product.

(25) Although the exact impact of the additive on the mechanism is currently under investigation, alcohol additives have been shown to be enabling in nickel-catalyzed cross-couplings: see ref. 7j and Harris, M. R.; Hanna, L. E.; Greene, M. A.; Moore, C. E.; Jarvo, E. R.; Retention or inversion in stereospecific nickel-catalyzed cross-coupling of benzylic carbamates with arylboronic esters: Control of absolute stereochemistry with an achiral catalyst. *J. Am. Chem. Soc.* **2013**, *135*, 3303–3306. Amine additives have also been proposed to activate low-valent nickel species toward oxidative addition in photoredox nickel catalysis: Gizbertz, S.; Reischauer, S.; Pieber, B. Overcoming limitations in dual photoredox/nickel-catalysed C–N cross-couplings due to catalyst deactivation. *Nat. Catal.* **2020**, *3*, 611–620.

(26) The use of enantioenriched proline derivatives was also investigated; however, these attempts either resulted in low yields of the product or comparable levels of enantioselectivity.

(27) Although the turnover limiting step of the reaction has not yet been elucidated, our data from ligand optimization indicate that the β-hydride elimination step or regeneration of Ni(0) could be slow. This is supported by other proposed nickel catalysis mechanisms in the literature (see ref. 18 for more explanation on the properties of nickel as a catalyst).

(28) During our optimization campaign with the morpholine additive, we also found empirically that a 1:2 ratio of Ni(cod)$_2$: chiral ligand **3.10** was necessary to achieve the desired transformation. Although the reason for this ratio has not been unambiguously established, similar findings have been seen previously. In one study, it has been suggested based on

computations that two NHC ligands could be implicated in the catalyst resting state (see ref. 7a). Alternatively, an additional NHC ligand could be enabling for reductive elimination.

(29) Shen, H. C. Asymmetric synthesis of chiral chromans. *Tetrahedron* **2009**, *65*, 3931–3952.

(30) Jurczyk, J.; Woo, J.; Kim, S. F.; Dherange, B. D.; Sarpong, R.; Levin, M. D. Single-atom logic for heterocycle editing. *Nat. Synth.* **2022**, *1*, 352–364.

(31) Ambrosio, C.; Paradiso, V.; Costabile, C.; Bertolasi, V.; Caruso, T.; Grisi, F. Stable ruthenium olefin metathesis catalysts bearing symmetrical NHC ligands with primary and secondary *N*-alkyl groups. *Dalton Trans.* **2018**, *47*, 6615–6627.

(32) Herrmann, W. A.; Goossen, L. J.; Artus, G. R. J.; Köcher, C. Metal complexes of chiral imidazolin-2-ylidene ligands. *Organometallics* **1997**, *16*, 2472–2477.

(33) Pertschi, R.; Hatey, D.; Pale, P.; de Frémont, P.; Blanc, A. Synthesis, characterization, and catalytic activity of chiral NHC platinum(II) pyridine dihalide complexes. *Organometallics* **2020**, *39*, 804–812.

(34) Suzuki, Y.; Muramatsu, K.; Yamauchi, K.; Morie, Y.; Sato, M. Chiral *N*-heterocyclic carbenes as asymmetric acylation catalysts. *Tetrahedron* **2006**, *62*, 302–310.

(35) Xu, H.; Zhao, C.; Qian, Q.; Deng, W.; Gong, H. Nickel-catalyzed cross-coupling of unactivated alkyl halides using bis(pinacolato)diboron as reductant. *Chem. Sci.* **2013**, *4*, 4022–4029.

(36) Yu, G. J.; Yang, B.; Verkman, A. S.; Kurth, M. J. Isoxazolopyrimidines as novel ΔF508-CFTR correctors. *Synlett* **2010**, *7*, 1063–1066.

(37) Sheldrick, G. M. (1996). *SADABS*. University of Göttingen, Germany.

(38) Sheldrick, G. M. Crystal structure refinement with SHELXL. *Acta Cryst. C*, **2015**, *71*, 3–8.

CHAPTER FOUR

Strain-Promoted Reactions of 1,2,3-Cyclohexatriene and Its Derivatives

Andrew V. Kelleghan[†], Ana S. Bulger[†], Dominick C. Witkowski, and Neil K. Garg

Nature **2023**, *618*, 748–754.

4.1 Abstract

Since 1825,[1] studies of compounds with the molecular formula C_6H_6 – most notably benzene – have been the subject of rigorous scientific investigation.[2,3,4,5,6,7] Of these compounds, 1,2,3-cyclohexatriene has been largely overlooked. This strained isomer is substantially (~100 kcal/mol) higher in energy compared to benzene and, like its relatives benzyne and 1,2-cyclohexadiene, should undergo strain-promoted reactions. However, few experimental studies of 1,2,3-cyclohexatriene are known.[8,9,10,11,12] We demonstrate that 1,2,3-cyclohexatriene and its derivatives participate in a host of reaction modes including diverse cycloadditions, nucleophilic additions, and σ-bond insertions. Experimental and computational studies of an unsymmetrical derivative of 1,2,3-cyclohexatriene demonstrate the potential for highly selective reactions of strained trienes despite their high reactivity and short lifetimes. Finally, integration of 1,2,3-cyclohexatrienes into multistep synthetic sequences demonstrates their utility in rapidly assembling topologically and stereochemically complex molecules. Collectively, these efforts should fuel the further investigation of the strained C_6H_6 isomer 1,2,3-cyclohexatriene and its derivatives, as well as their strategic application in the synthesis of important compounds.

4.2 Introduction

Since Faraday's isolation of an unidentified compound of the formula C_6H_6 in 1825,[1] studies of benzene (**4.1**, Figure 4.1A) and its isomers have fueled significant advances in diverse areas including the development of resonance theory,[13,14,15] the discovery of aromaticity,[16] and the development of countless synthetic methodologies.[2] Of the hundreds of known and postulated benzene isomers, strained isomers (e.g., **4.2**–**4.4**) have a particularly rich history in organic chemistry. For example, Dewar benzene (**4.2**) and prismane (**4.4**), which often appear even in introductory textbooks, evolved from being hypothetical structures in the 19th century to intriguing synthetic targets in the 20th century.[3,4] Despite the nearly two hundred years since the original isolation of benzene, investigation of strained isomers of benzene and their derivatives continues to provide new opportunities for discovery in modern organic chemistry.[5,6,7]

One strained benzene isomer that has remained largely underexplored is 1,2,3-cyclohexatriene (**4.5**), which was not validated experimentally until 1990.[8] The three olefins in **4.5**, unlike those in benzene itself, are cumulated to give a highly strained structure. This strain, coupled with the lack of aromatic stabilization present in benzene, translates to a substantially higher free energy. The DFT-calculated free energy of **4.5** compared to benzene (**4.1**) is +101 kcal/mol (ΔG_{rel}). As such, the strong ground state destabilization of **4.5** should yield kinetically and thermodynamically favourable reactions that are difficult or not possible for benzene (Figure 4.1B). More specifically, in the case of benzene, a transformation of the type **4.1**→**4.6** would be disfavoured due to loss of aromatic stabilization, which is expected to incur an energetic penalty in the relevant transition state and comparatively destabilize the corresponding product **4.6**. In contrast, analogous reactions of 1,2,3-cyclohexatriene (**4.5**→**4.7**) should be kinetically and thermodynamically favoured due to the considerable strain release along the reaction coordinate.

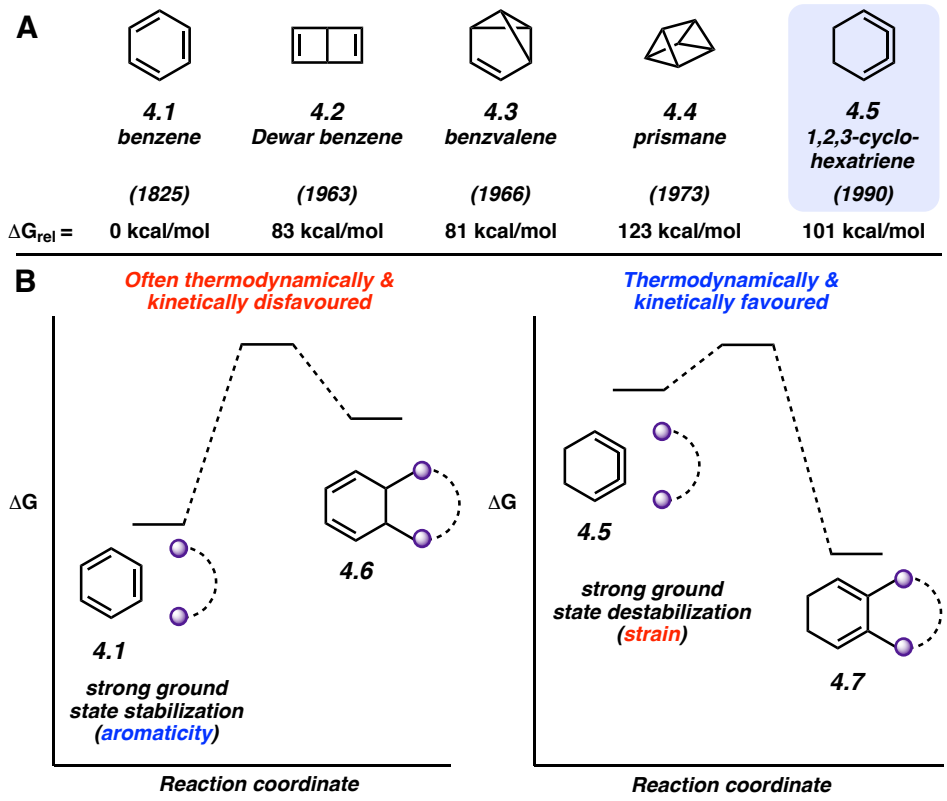


Figure 4.1. Selected strained isomers of benzene (**4.1**) and comparison of reaction coordinate diagrams. **A**) Benzene (**4.1**) and several of its strained isomers with the year each was first isolated (or generated in situ in the case of 1,2,3-cyclohexatriene (**4.5**)). Free energies at 298.15 K are reported relative to benzene (B3LYP-D3/6-311+G(d,p)). **B**) Hypothetical reaction coordinate diagrams for transformations of benzene and 1,2,3-cyclohexatriene (**4.5**).

Conceptually, strained benzene isomer **4.5** is closely related to arynes and strained cyclic alkynes (**4.8**) and strained cyclic allenes (e.g., **4.9**, Figure 4.2A). Each of these intermediates incorporates a functional group with a preferred linear geometry into a small ring. Whereas cyclic alkynes and allenes were initially mere scientific curiosities when first validated in the 1950s and 1960s,[17,18,19,20] they have since emerged as powerful tools for the construction of diverse target molecules.[21] Strained intermediates **4.11**–**4.14** highlight applications in agrochemistry,[22] materials chemistry,[23] heterocycle synthesis,[24] and natural product total synthesis, respectively.[25] Numerous studies pertaining to strained cyclic alkynes and strained cyclic allenes are available in the literature (~4,600 reports & ~160 reports, respectively, see Section 4.9.1 for details).

In sharp contrast, 1,2,3-cyclohexatrienes (e.g., **4.5**) have remained underexplored despite the fact that 1,2,3-trienes constrained to cyclic systems have intrigued chemists since the 1960s.[26,27] Only four experimental studies pertaining to **4.5** have appeared in the literature. Two Diels–Alder trapping experiments involving 1,2,3-cyclohexatriene (**4.5**) have been reported by the laboratories of Johnson[8] and Paquette,[9,10] using 1,3-diphenylisobenzofuran and cyclopentadiene, respectively. Johnson has also invoked the intermediacy of a fused bicyclic 1,2,3-cyclohexatriene during flash vacuum pyrolysis of a linear precursor.[11] Lastly, Saito and coworkers reported a [4+2] cycloaddition reaction presumed to proceed between 1,2,3-cyclohexatriene (**4.5**) and nitrones, ultimately leading to products arising from rearrangement pathways rather than the expected primary cycloadducts.[12] Substituted derivatives of 1,2,3-cyclohexatriene (**4.5**) are largely unexplored.[28] These limitations are striking given the breadth of transformations known for strained alkynes, which include (8+2), (7+2), (5+2), (4+2), (3+2), and (2+2) cycloadditions, nucleophilic trappings, ene reactions, transition metal-catalysed reactions, formal σ-bond insertions, and many others. Furthermore, the lack of study of substituted trienes is surprising given that substituted strained cyclic alkynes and allenes have been studied extensively and proven crucial for enabling synthetic applications of strained intermediates.[21]

We now report an investigation of 1,2,3-cyclohexatriene (**4.5**) and its derivatives, which we expect will fuel further research in this long-understudied area (Figure 4.2B). We describe: (a) a computational comparison of 1,2,3-cyclohexatriene (**4.5**) to its isomer benzene (**4.1**) and its close relative benzyne (**4.20**), (b) (4+2), (3+2), (2+2) and nucleophilic trapping reactions (e.g., **4.15**+**4.17**→**4.18**), (c) syntheses and trappings of new substituted cyclic 1,2,3-hexatrienes, including a geometrically-distorted silyl substituted cyclic triene that undergoes regioselective

reactions, and (d) the elaboration of cyclic triene cycloadducts by leveraging the embedded 1,3-diene to rapidly access diverse product scaffolds (e.g., **4.18**→**4.19**).

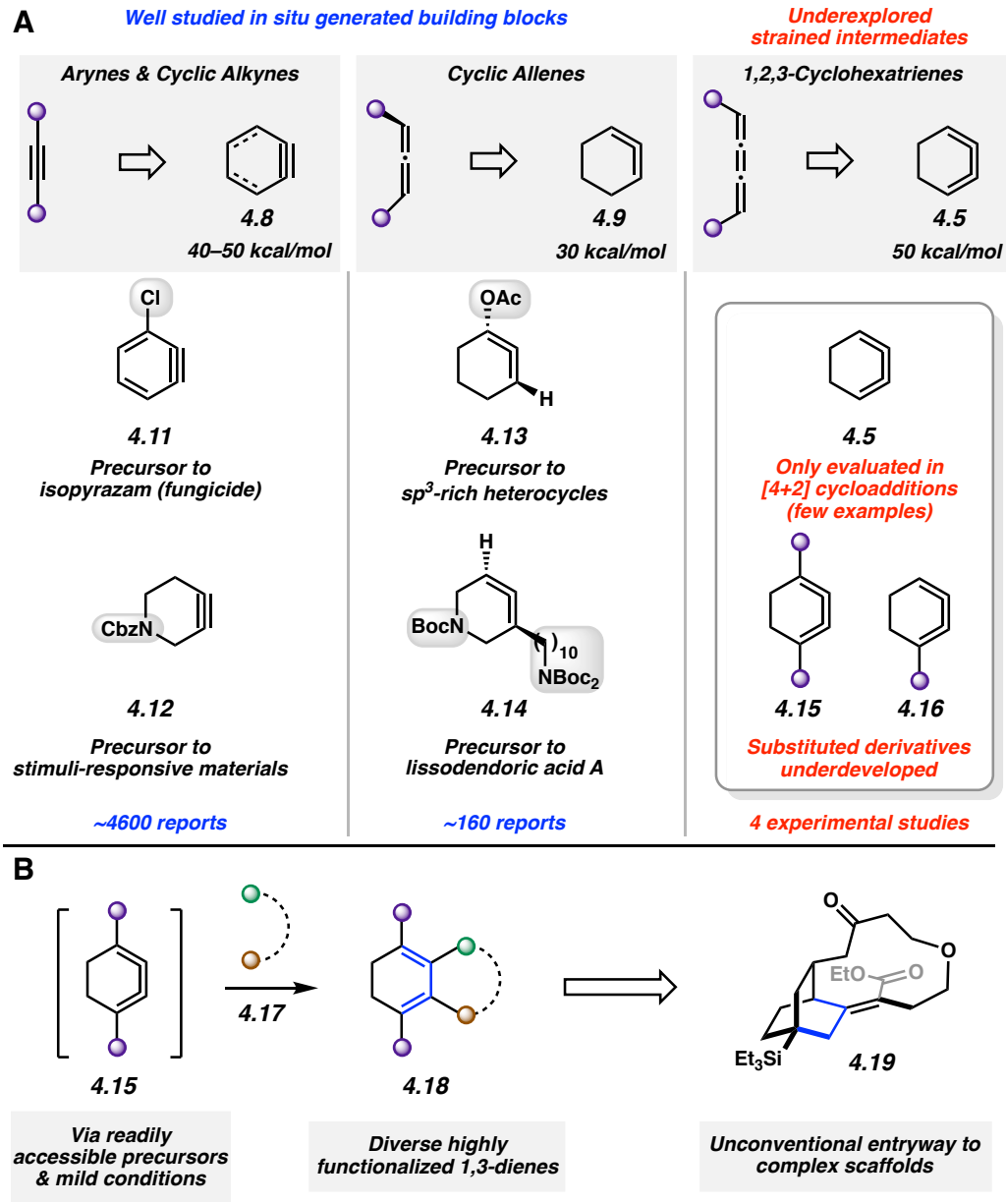


Figure 4.2. Strained cyclic intermediates and overview of current study. **A**) Representative classes of in situ generated strained intermediates with synthetically useful derivatives **4.11**–**4.14**. **B**) Overview of our current study.

4.3 Computational Structural Analysis

We performed DFT studies to directly compare the geometric and electronic structure of 1,2,3-cyclohexatriene (**4.5**) to its isomer benzene (**4.1**) and its relative benzyne (**4.20**) (Figure 4.3A). Whereas the geometry of benzene is characterized by equivalent 120° interior angles, the isomeric 1,2,3-triene **4.5** and benzyne (**4.20**) each displays a wider internal angle at the positions shown (131° and 127°, respectively) as a consequence of constraining two formally sp-hybridized carbons to a six-membered ring. This structural deformation leads to a calculated ~50 kcal/mol of strain energy for both 1,2,3-cyclohexatriene (**4.5**)[29] and benzyne (**4.20**).[30] This calculated geometry for triene **4.5** is in good agreement with earlier reports from Johnson and coworkers;[29] however, to our knowledge, the electronic structure of **4.5** has not been reported previously. We find that the HOMOs of benzene (**4.1**), its isomer 1,2,3-cyclohexatriene (**4.5**), and benzyne (**4.20**)[31] are all localized to the conjugated π-systems, but the LUMO structures differ significantly. Unlike the LUMO of benzene, the LUMO of **4.5** is largely localized to the central, in plane π-bond of the triene and is a notable 1.5 eV lower in energy. Whereas the LUMO structure and energy is very different between cyclic triene **4.5** and benzene (**4.1**), strong similarity is found by comparison to benzyne (**4.20**). This similarity suggests that triene **4.5**, unlike its well-studied isomer benzene (**4.1**), should share benzyne's strong electrophilicity and propensity to undergo cycloaddition reactions.

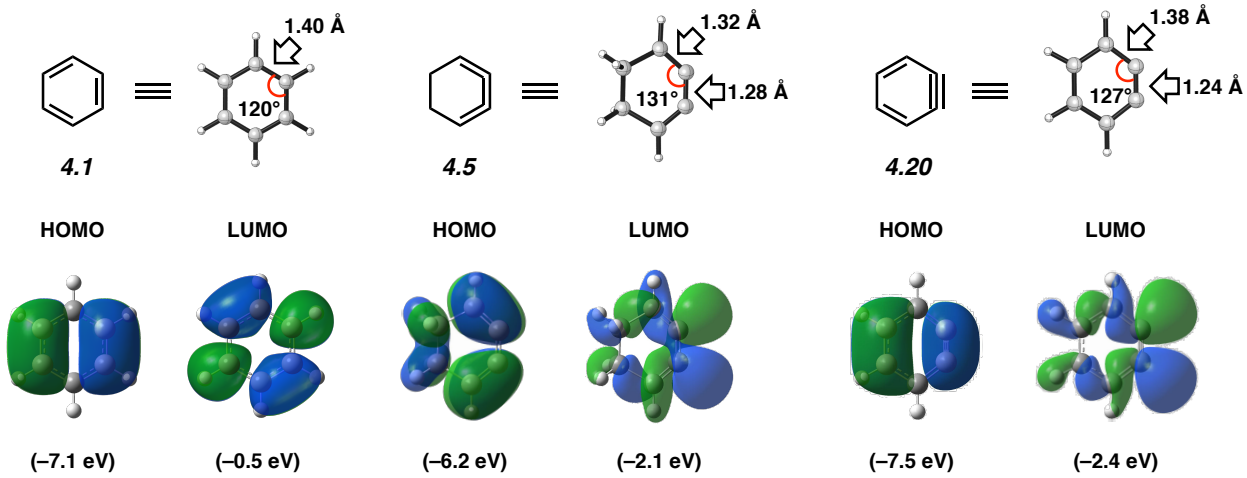
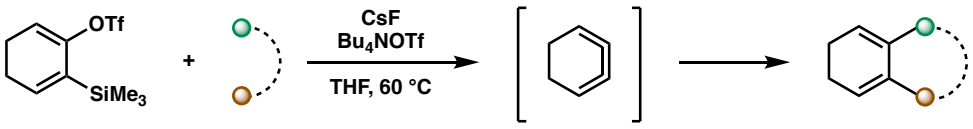


Figure 4.3A. Geometry-optimized structures and frontier molecular orbitals of benzene (**4.1**), 1,2,3-cyclohexatriene (**4.5**), and benzyne (**4.20**) (B3LYP-D3/6-311+G(d,p)).

4.4 Reactivity of 1,2,3-Cyclohexatriene (4.5)

To initiate our experimental study of 1,2,3-cyclohexatriene (**4.5**), we prepared silyl triflate **4.21**, a readily available compound known from Johnson's seminal 1990 study,[8] and performed trapping experiments (Figure 4.3B). The use of a Kobayashi silyl triflate precursor was considered ideal, as Kobayashi precursors typically require mild fluoride sources to trigger in situ formation of the desired strained intermediate.[21] After optimization (see Section 4.9.3.1 for details), we found that generation and trapping of **4.5** proceeded best using CsF as the fluoride source, tetrabutylammonium triflate as a fluoride-solubilizing agent,[32] and THF as the solvent at 60 °C. Triene **4.5** reacts smoothly with various dienes including an isobenzofuran, furans, and a pyrrole to furnish (4+2) cycloadducts **4.27**–**4.30** in good yields (entries 1–4). We also studied (3+2) cycloadditions of **4.5**, direct products of which have not been reported in the literature.[12] Gratifyingly, we found that triene **4.5** undergoes dipolar (3+2) cycloadditions with azomethine imines **4.31** and **4.32** to give cycloadducts **4.35** and **4.36**, respectively (entries 5 and 6). A formal (2+2) cycloaddition could also be achieved by employing ketene acetal **4.33** as a trap, giving cyclobutane **4.37** (entry 7). Additionally, use of phenoxide **4.34** as a nucleophile gives direct

addition product **4.38**. These results demonstrate that triene **4.5** is indeed a versatile intermediate capable of undergoing a range of trapping reactions despite having been minimally exploited in prior experimental studies.



4.21 *4.17* *4.5* *4.22*

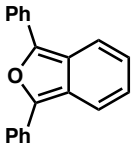
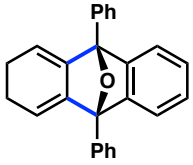
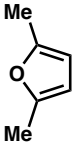
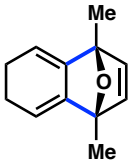
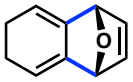
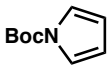
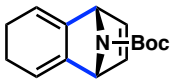
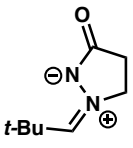
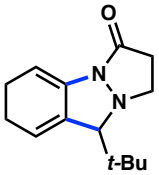
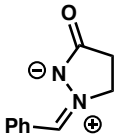
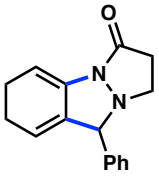
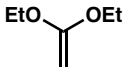
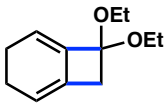
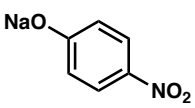
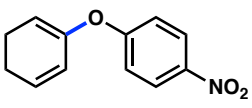
Entry	*Trapping Agent*		*Product*		*Yield*
1		*4.23*		*4.27*	65%
2		*4.24*		*4.28*	62%
3		*4.25*		*4.29*	72%
4		*4.26*		*4.30*	61%
5		*4.31*		*4.35*	59%
6		*4.32*		*4.36*	51%
7		*4.33*		*4.37*	44%
8[a]		*4.34*		*4.38*	51%

Figure 4.3B. Scope of reactions of triene **4.5**. Reaction conditions are as follows: **4.21** (1 equiv), trapping partner **4.17** (5–20 equiv), CsF (10 equiv), Bu_4NOTf (2 equiv), THF (0.1 M), 60 °C, 24 h. Yields were determined by an average of two isolation experiments. [a]Modified reaction

conditions: CsF (20 equiv), Bu_4NOTf (4 equiv), MeCN (0.1 M), 60 °C, 22 h. See Section 4.9.3.2 for details.

4.5 Reactivity of a Substituted 1,2,3-Cyclohexatriene Derivative

Substituted 1,2,3-cyclohexatrienes are largely unknown. To our knowledge, a single literature example suggestive of a substituted derivative of 1,2,3-cyclohexatriene (**4.5**) is available,[11] which required pyrolytic temperatures (600 °C) and led to unimolecular rearrangement processes of the presumed triene intermediate yielding a mixture of products. In contrast, substituted arynes, cyclic alkynes, and cyclic allenes have been investigated extensively in both fundamental and applied studies to control regioselectivity in trappings and to synthesize complex structures.[21,33,34,35] As such, we undertook the study of two new substituted 1,2,3-cyclohexatrienes (di- and mono-substituted) to validate their intermediacy and assess their synthetic potential.

To evaluate a disubstituted 1,2,3-cyclohexatriene, we prepared dimethylated silyl triflate **4.42**, the presumed precursor to **4.43**, using the sequence shown in Figure 4.4A. Known brominated vinylogous ester **4.39**[36] was first converted to the corresponding silylated vinylogous ester **4.40** via a retro-Brook rearrangement of the corresponding silyl enol ether.[37] Subsequent 1,2-addition and Stork–Danheiser transposition afforded enone **4.41**. α-Methylation followed by triflation then delivered desired silyl triflate **4.42**. This synthetic route has proven flexible and scalable, thus providing a roadmap for future studies of substituted cyclic trienes.

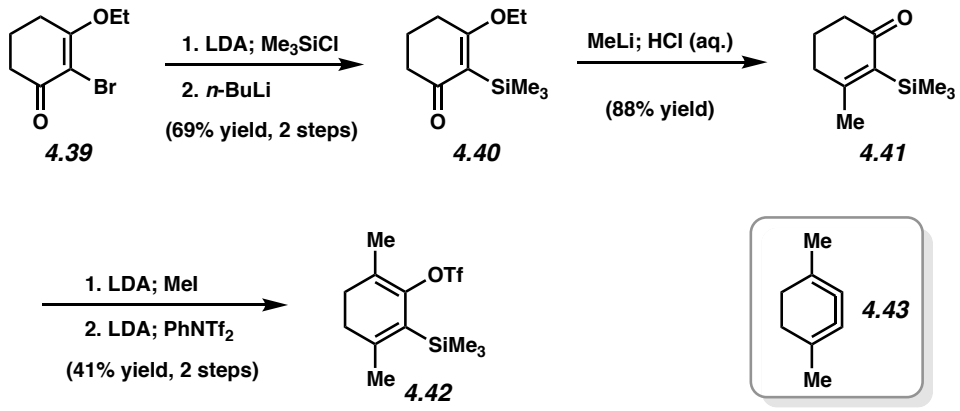
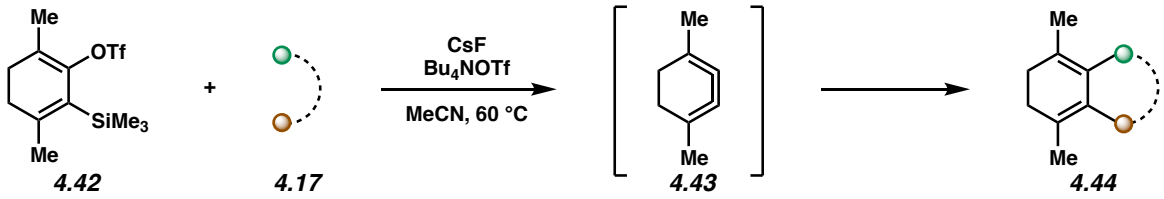
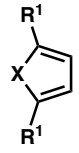
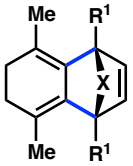
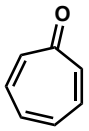
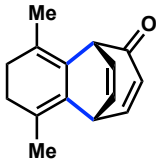
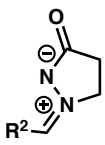
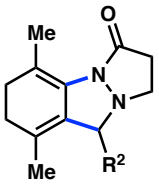
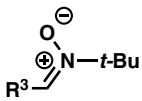
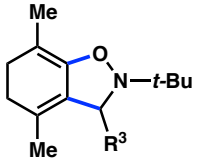
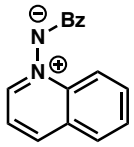
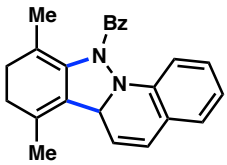
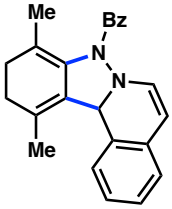


Figure 4.4A. Synthesis of silyl triflate **4.42**. See Section 4.9.3.3 for reaction details.

With silyl triflate **4.42** in hand, we studied the generation and trapping of disubstituted triene **4.43** (Figure 4.4B). Our previously optimized reaction conditions led to low conversion, but we found that switching the solvent to acetonitrile and increasing the loading of Bu_4NOTf facilitated full conversion and good yields in trappings of **4.43**. More generally, we observed that trappings of disubstituted triene **4.43** proceeded in higher yields and with broader scope compared to trappings of the parent compound, 1,2,3-cyclohexatriene (**4.5**), despite **4.43** bearing an increased steric profile. The results shown highlight the engagement of disubstituted triene **4.43** in: (a) (4+2) cycloadditions with either electron-rich or electron-deficient dienes affording **4.50**–**4.52** (entries 1–3), (b) (3+2) cycloadditions using azomethine imines (**4.31** and **4.32**), nitrones (**4.46** and **4.47**), a quinolinium imide (**4.48**), or an isoquinolinium imide (**4.49**) to generate products **4.53**–**4.58** (entries 4–9), (c) a (5+2) cycloaddition of oxidopyridinium **4.59** to give [3.2.1] bicycle **4.66** (entry 10), (d) formal (2+2) reactions using nucleophilic 2π-systems, such as ketene acetal **4.33**, enamine **4.60**, and thioketone **4.61**, to afford the corresponding cyclobutane or thietane products **4.67–4.69** (entries 11–13), and (e) nucleophilic additions using oxygen, sulfur, nitrogen, or carbon nucleophiles **4.34** and **4.62**–**4.65** to give dienes **4.70**–**4.74**, respectively (entries 14–18). Notably, in the case of carbon nucleophiles **4.64** and **4.65**, formal C–C σ-bond insertion products were

isolated, analogous to known aryne insertion reactions.[38] Collectively, these data showcase that 1,2,3-cyclic trienes may engage in a host of trappings akin to what has long been established for arynes, but largely overlooked for cyclic trienes. Additionally, a variety of structurally distinct scaffolds are accessible, including fused polycyclic compounds, bridged structures, and complex heterocycles. All of the products bear functional handles for further manipulation, particularly the 1,3-diene motif.



Entry	Trapping Agent	Product & Yield
1 2		
	X = O, R^1 = Me, ***4.24*** X = NBoc, R^1 = H, ***4.26***	***4.50***, 80% ***4.51***, 82%
3		
	4.45	***4.52***, 40%
4 5		
	R^2 = *t*-Bu, ***4.31*** R^2 = Ph, ***4.32***	***4.53***, 86% ***4.54***, 87%
6 7		
	R^3 = Ph, ***4.46*** R^3 = *t*-Bu, ***4.47***	***4.55***, 74% ***4.56***, 75%
8		
	4.48	***4.57***, 79%
9		
	4.49	***4.58***, 51%

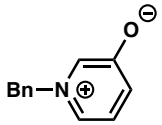
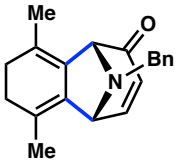
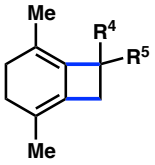
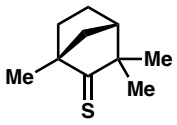
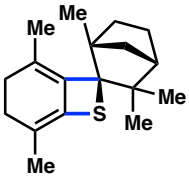
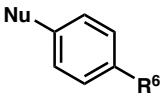
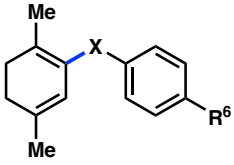
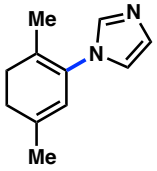
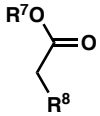
Entry	Trapping Agent	Product & Yield
10		
	4.59	***4.66***, 68%
11[a] 12[a]		
	R^4 = R^5 = OEt, ***4.33*** R^4 = $N(Boc)_2$, R^5 = CO_2Me, ***4.60***	***4.67***, 47% ***4.68***, 48%
13		
	4.61	***4.69***, 77% (2.7:1 dr)
14 15		
	Nu = NaO, R^6 = NO_2, ***4.34*** Nu = SH, R^6 = H, ***4.62***	***4.70***, 83% ***4.71***, 81%
16		
	4.63	***4.72***, 58%
17 18		
	R^7 = Et, R^8 = CN, ***4.64*** R^7 = Me, R^8 = CO_2Me, ***4.65***	***4.73***, 47% ***4.74***, 82%

Figure 4.4B. Scope of reactions of triene **4.43**. Reaction conditions are as follows: **4.42** (1 equiv), trapping partner **4.17** (5–20 equiv), CsF (20 equiv), Bu_4NOTf (4 equiv), MeCN (0.1 M), 60 °C, 24 h. Yields were determined by an average of two isolation experiments unless otherwise noted. See Section 4.9.3.4 for details. [a]Yield determined by ^1H NMR with mesitylene as external standard.

4.6 Regioselective Reactions of a Silyl-Substituted Triene

Figure 4.5 highlights studies related to **4.75**, an unsymmetrical monosubstituted 1,2,3-cyclic triene bearing a triethylsilyl substituent. Silyl substituents have previously been used to study the origins of regioselectivity in aryne trappings,[39,40,41,42] but similar insight relating to reactions of substituted 1,2,3-cyclic trienes has not been reported. The structure of **4.75** was optimized using DFT calculations (Figure 4.5A). Polarization of the C1–Si bond toward C1 leads to rehybridization of the internal, formally sp-hybridized carbons of triene **4.75** in accordance with Bent's Rule,[43,44] which states that "atomic s-character concentrates in orbitals directed toward electropositive substituents" and has been applied in previous studies of silyl-substituted arynes.[39] This rehybridization strongly distorts the ground state geometry, leading to a significantly flattened C1=C2=C3 bond angle (θ_{C2} = 146°) and a contracted C2=C3=C4 bond angle (θ_{C3} = 118°) relative to those of unsubstituted triene **4.5** ($\theta_{C2} = \theta_{C3}$ = 131°). This geometric distortion also yields a shift in the electron distribution in the substituted triene, with C2 now bearing a slight positive charge, and C3 bearing a slight negative charge consistent with the observed rehybridization. We surmised that **4.75** could undergo regioselective trapping given that analogous ground state distortion has previously led to regioselectivity in trapping reactions of silyl-substituted arynes.[39]

To test this hypothesis, we prepared triethylsilyl-substituted silyl triflate **4.76** (see Section 4.9.3.5 for details) and performed the key trapping experiments shown in Figure 4.5B. With the large enamine **4.77** as the trap, adduct **4.78** was obtained, arising from a sterically-controlled addition onto C3 of the triene, distal to the bulky triethylsilyl substituent. Conversely, with smaller phenoxide nucleophile **4.34** as the trap, a complete switch in regioselectivity was observed; and

adduct **4.79** was the sole product, arising from proximal attack at C2. We hypothesized that this contrasteric outcome could arise from reactant pre-distortion, wherein the geometric distortion in the ground state discussed above likely mirrors the geometry of the transition state leading to the observed product. Such effects have been observed extensively in aryne chemistry and have been codified by Houk et al. in the "aryne distortion model," an application of distortion/interaction activation strain (DIAS) analysis,[45] which enables the prediction of regiochemical outcomes in reactions of substituted arynes.[46,47,48,49,50] DFT studies of the phenoxide trapping were performed (using a trimethylsilyl group instead of a triethylsilyl group and omitting the Na^+ counterion) to validate the pre-distortion hypothesis (Figure 4.5C). Consistent with our experiments, addition at C2 (see **TS-4.1**) was found to be favoured over addition at C3 (see **TS-4.2)** by 3.1 kcal/mol ($\Delta\Delta G^{\ddagger}$; $\Delta\Delta E^{\ddagger}$ = 4.6 kcal/mol). To elucidate the origin of this difference, we performed DIAS analysis to decompose $\Delta\Delta E^{\ddagger}$ into two separate contributions from reactant distortion energies and interaction energies.[45] Regarding distortion, $\Delta\Delta E^{\ddagger}_{\text{distortion}}$ for nucleophile **4.34** was negligible. However, $\Delta\Delta E^{\ddagger}_{\text{distortion}}$ for triene **4.80** is 1.4 kcal/mol, indicating greater distortion of triene **4.80** in **TS-4.2** compared to **TS-4.1**. The geometry of the triene in **TS-4.1** is indeed very similar to that of ground state triene **4.80**, thus requiring minimal geometric distortion to reach **TS-4.1** geometry ($\Delta\theta_{C3}$ = –4°; $\Delta\theta_{C2}$ = 0°). Conversely, arriving at **TS-4.2** requires substantial geometric reorganization ($\Delta\theta_{C3}$ = 18°; $\Delta\theta_{C2}$ = –21°). This supports the notion that triene pre-distortion contributes to **TS-4.1** being favoured as hypothesized. DIAS analysis also indicates strong differences in interaction energies ($\Delta\Delta E^{\ddagger}_{\text{interaction}}$ = 3.2 kcal/mol.), which contribute significantly to the observed selectivity (see Section 4.9.4.4 for details). Overall, the results shown in Figure 4.5 suggest that sterics, distortion, and interaction all contribute to controlling selectivity and that substituted 1,2,3-cyclohexatrienes can be employed in regioselective reactions with potentially predictable outcomes.

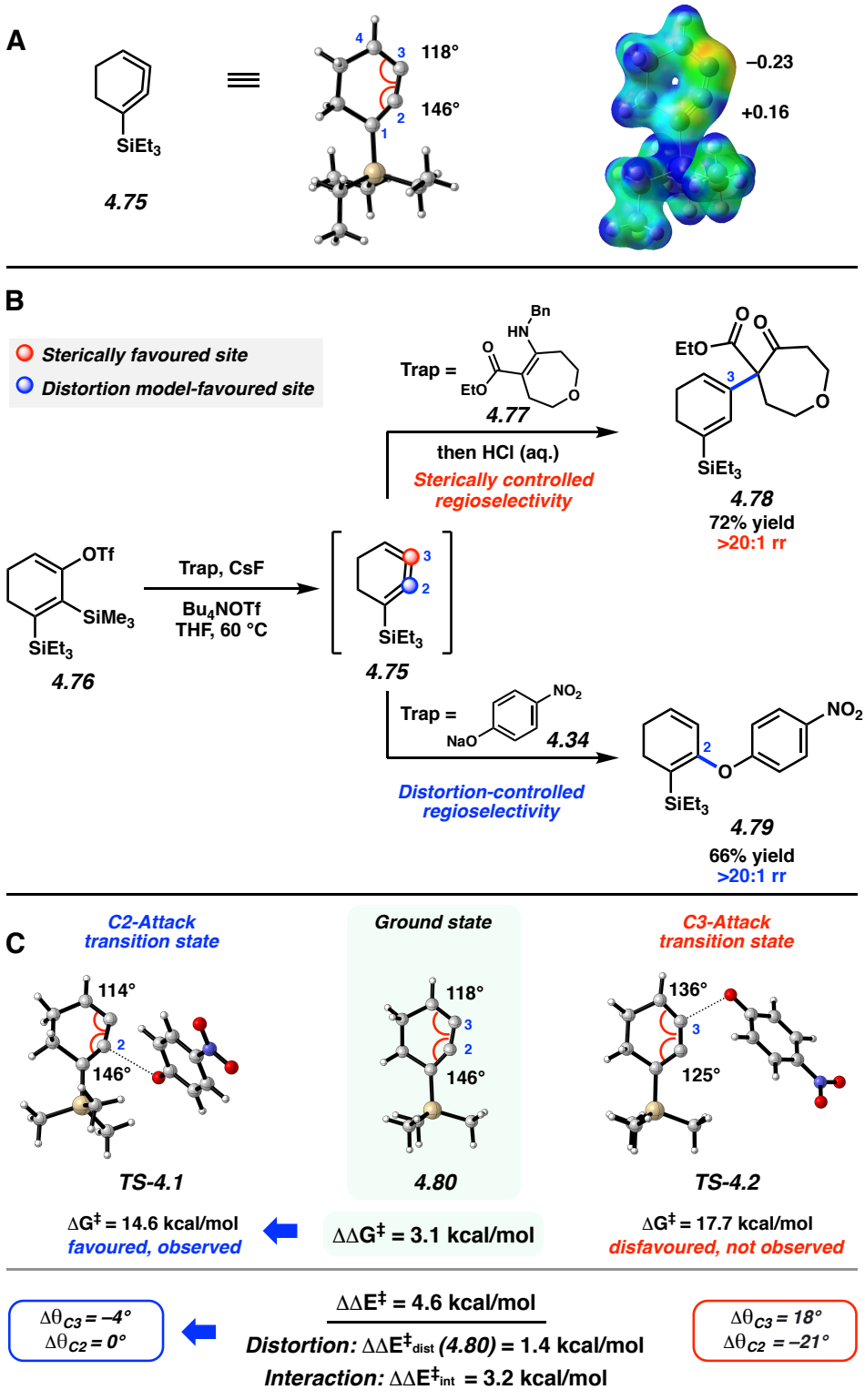


Figure 4.5. Structure and regioselective reactions of a monosubstituted cyclic triene. **A**, Geometry-optimized structure of triene **4.75** and electrostatic potential map (B3LYP-D3/6-311+G(d,p)) (NBO charges shown). **B**, Yields determined by isolation experiments. See Section 4.9.3.6 for reaction details. rr, regioisomeric ratio. **C**, Transition state analysis at 333.15 K using a trimethyl

silyl group to model the triethyl silyl group in **4.75** and omitting the Na cation of **4.34** (B3LYP-D3/6-311+G(d,p)/SMD(THF)) See Section 4.9.4.4 for details.

4.7 Leveraging Cyclic Trienes to Access Complex Scaffolds

The studies shown in Figure 4.6 highlight the previously untapped value of strained cyclic trienes for the construction of complex scaffolds. Tricyclic diene **4.35**, prepared by azomethine imine cycloaddition of triene **4.5** (see Figure 4.3B), was elaborated to four compounds with different skeletons (**4.81**–**4.84**, Figure 4.6A). Diene **4.35** underwent a Diels–Alder reaction with *N*-Ph-maleimide with high facial control guided by the *t*-Bu substituent to generate [2.2.2]-bicycle **4.81**. The diene of **4.35** can instead serve as a 2π–component in cycloaddition reactions with either a strained cyclic allene or a nitrile oxide to generate fused polycycles **4.82** and **4.83**, respectively. These transformations occur with high regioselectivity with respect to both the diene and trap and give rise to unusual heterocyclic scaffolds. Alternatively, the diene motif of **4.35** can be preserved through chemoselective reduction of the *N*–*N* bond[51] to reveal the 6/8 fused ring system of **4.84**.

The synthetic sequence shown in Figure 4.6B establishes that 1,2,3-cyclic trienes can be used to quickly assemble complex scaffolds in a highly selective manner. Silyl-substituted triene **4.75** was trapped using enantioenriched enamine **4.85**. After hydrolytic workup, diene (+)-**4.78** was obtained regioselectively in 92% ee. Subsequent allylation of (+)-**4.78** yielded diene (–)-**4.87** bearing a pendant alkene. Thermolysis of (–)-**4.87** effected a Diels–Alder (see **TS-4.3**)/retro-aldol/alkene isomerization cascade to yield (+)-**4.19** in 91% ee. (+)-**4.19** bears considerable structural complexity as exemplified by the 11-membered ring, a highly substituted [2.2.2]-bicycle, and three stereocenters. This concise, three-step elaboration of triene **4.75** to (+)-**4.19** demonstrates that, despite their high reactivity and minimal use in prior experimental studies, strained cyclic trienes can be engaged in regio- and stereoselective reactions to ultimately access complex products.

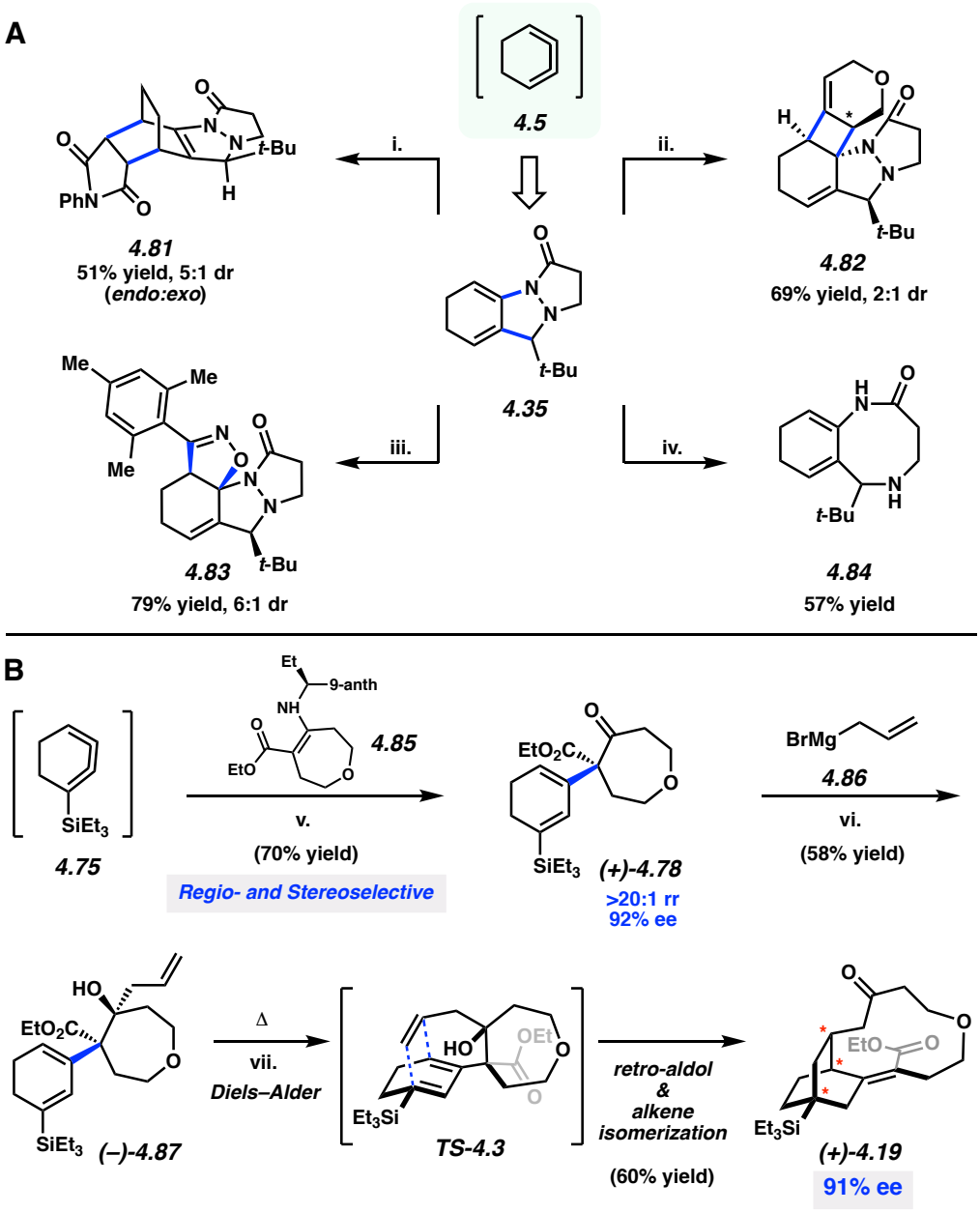


Figure 4.6. Strained 1,2,3-cyclohexatrienes in multistep synthesis. **A**, Reaction conditions are as follows: (i) *N*-Ph maleimide (2.5 equiv), benzene, 80 °C, 51% yield, 5:1 dr. (ii) oxacyclic allene precursor (1.5 equiv), CsF (5 equiv), MeCN, 23 °C, 69% yield, 2:1 dr at the stereocenter indicated by an *. (iii) mesitylene nitrile oxide (1.5 equiv), CH_2Cl_2, 0 to 40 °C, 79% yield, 6:1 dr. (iv) sodium naphthalenide (3 equiv), THF, 0 °C, 57% yield. See Section 4.9.3.7 for full reaction details. dr, diastereomeric ratio **B**, Reaction conditions are as follows: (v) enamine **4.85** (5 equiv), CsF, (10 equiv), Bu_4NOTf (2 equiv), THF, 60 °C, then HCl (1 M), 23 °C, 70% yield, >20:1 rr, 92% ee. (vi) allylMgBr (2 equiv), THF, –78 °C, 58% yield, >20:1 dr. (vii) hexadecane, 220 °C, 60% yield. See Section 4.9.3.7 for full reaction details.

4.8 Conclusion

These studies establish that the unusual benzene isomer 1,2,3-cyclohexatriene, along with its derivatives, can be harnessed in chemical synthesis. As such, these efforts should prompt the further investigation of the fundamental properties of strained cyclic 1,2,3-hexatrienes and their strategic application in the synthesis of important compounds.

4.9 Experimental Section

4.9.1 Method for Literature Searches for Strained Intermediate Studies.

The values included for the number of literature reports for various strained intermediates were obtained using keyword searching in SciFinder^n with the following keywords. For strained cyclic alkynes: "benzyne", "aryne" or "strained alkyne". For strained cyclic allenes: "1,2-cyclohexadiene", "1,2-cycloheptadiene", "1,2-cyclooctadiene" or "strained allene".

4.9.2 Materials and Methods

Unless stated otherwise, reactions were conducted in flame-dried glassware under an atmosphere of nitrogen, and commercially obtained reagents were used as received unless otherwise specified. Anhydrous solvents were either freshly distilled or passed through activated alumina columns, unless otherwise stated. Non-commercially available substrates were synthesized according to known preparations or following protocols specified in the Experimental Procedures. Prior to use in trapping experiments, acetonitrile (MeCN) and tetrahydrofuran (THF) were passed through an activated alumina column and degassed by five freeze-pump-thaw cycles. Dimethylformamide (DMF), benzonitrile (PhCN), 1,4-dioxane, 1,2-dichloroethane (DCE), 1,2-dimethoxyethane (DME), dichloromethane, benzene, and triethylamine (Et_3N) were passed through an activated alumina column prior to use. Diisopropylamine, pyridine, trimethylsilyl chloride, and triethylsilyl chloride were distilled over CaH_2 prior to use. Tetrabutylammonium iodide (Bu_4NI), tetrabutylammonium fluoride (TBAF) solution (1.0 M in THF), tris(dimethylamino)sulfonium difluorotrimethylsilicate (TASF), tetrabutylammonium trifluoromethanesulfonate (Bu_4NOTf), *n*-butyllithium (*n*-BuLi), hexadecane, methyllithium, magnesium bromide diethyl etherate, *N*-phenyl maleimide, *N*-Boc-pyrrole (**4.26**), tropone (**4.45**), thiophenol (**4.62**), imidazole (**4.63**), ethyl cyanoacetate (**4.64**), dimethyl malonate (**4.65**),

pyridinium perbromide, benzoic anhydride, Florisil® (<200 mesh, fine powder), and Brockman Grade activated basic alumina (60 mesh powder) were all purchased from Sigma-Aldrich and used as received. Cesium fluoride was obtained from Strem Chemicals, stored in a glovebox, and used as received. Methyl iodide was obtained from Thermofisher Scientific. *N*-(5-chloro-2-pyridyl)bis(trifluoromethanesulfonimide) (Comins' Reagent), 2,5-dimethylfuran (**4.24**), diphenylisobenzofuran (**4.23**), and *N*-*tert*-butyl α-phenylnitrone (**4.46**), were purchased from Combi Blocks. *N*-phenyl-bis(trifluoromethanesulfonimide) ($PhNTf_2$) was obtained from Oakwood Chemicals. Furan (**4.25**) was obtained from Acros Organics. 1,1-Diethoxyethene (**4.33**) was obtained from Fluka Chemicals. Reaction temperatures at or above 23 °C were controlled using an IKAmag temperature modulator, and unless stated otherwise, performed at room temperature (approximately 23 °C). Thin-layer chromatography (TLC) was conducted with EMD gel 60 F_{254} pre-coated plates (0.25 mm for analytical chromatography and 0.50 mm for preparative chromatography) and visualized using a combination of UV, anisaldehyde, and potassium permanganate staining techniques. Silicycle Siliaflash P60 (particle size 40–63 μm) was used for flash column chromatography unless otherwise specified. ^{1}H-NMR and 2D-NOESY spectra were recorded on Bruker spectrometers (at 400, 500, 600, and 800 MHz) and are reported relative to the residual solvent signal. Data for ^{1}H-NMR spectra are reported as follows: chemical shift (δ ppm), multiplicity, coupling constant (Hz), and integration. ^{13}C-NMR spectra were recorded on Bruker spectrometers (at 100, 125, and 150 MHz) and are reported relative to the residual solvent signal. Data for ^{13}C-NMR spectra are reported in terms of chemical shift (δ ppm) and, when necessary, multiplicity, and coupling constant (Hz). ^{19}F-NMR spectra were recorded on Bruker spectrometers (at 376 MHz) and are reported in terms of chemical shift (δ ppm), multiplicity, and integration. ^{1}H NMR yields were determined by addition of an aliquot of a stock solution of external standard,

2,5-dimethylfuran or mesitylene, in C_6D_6 to the concentrated crude reaction mixture followed by further dilution with C_6D_6 and subsequent ^1H NMR analysis. Control experiments demonstrated agreement within 2% between 2,5-dimethylfuran and mesitylene as external standards. IR spectra were recorded on a Perkin-Elmer UATR Two FT-IR spectrometer and are reported in terms of frequency absorption (cm^{-1}). DART-MS spectra were collected on a Thermo Exactive Plus MSD (Thermo Scientific) equipped with an ID-CUBE ion source and a Vapur Interface (IonSense Inc.). Both the source and MSD were controlled by Excalibur software version 3.0. The analyte was spotted onto OpenSpot sampling cards (IonSense Inc.) using $CDCl_3$ or CH_2Cl_2 as the solvent. Ionization was accomplished using UHP He plasma with no additional ionization agents. The mass calibration was carried out using Pierce LTQ Velos ESI (+) and (–) Ion calibration solutions (Thermo Fisher Scientific). Optical rotations were measured with a Rudolf Autopol III Automatic Polarimeter. Determination of enantiopurity was carried out on a JASCO SFC (supercritical fluid chromatography) using a Daicel ChiralPak AD-H column. Data for SFC chromatograms are reported in enantiomeric excess (ee). Diastereomeric ratios (dr) and regioisomeric ratios (rr) were determined by ^1H analysis of crude reaction mixtures.

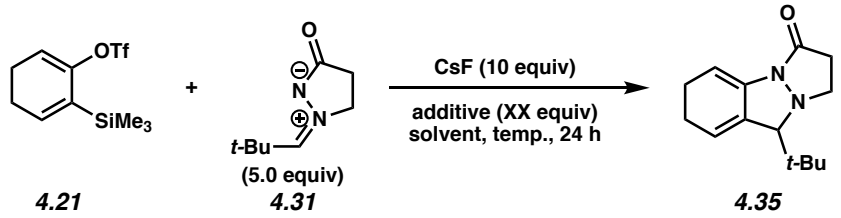
Silyl triflate **4.21**,[8] cycloadduct **4.27**,[8] azomethine imines **4.31**[52] and **4.32**,[53] phenoxide **4.34**,[54] vinylogous ester **4.39**,[55] nitrone **4.47**,[56] quinolinium imide **4.48**,[57] isoquinolinium imide **4.49**,[57] oxidopyridinium **4.59**,[58] enamine **4.60**,[59] thioketone **4.61**,[60] ketal **4.88**,[61] enamines **4.77** and **4.85**,[62] silyl triflate **4.89**,[63] nitrile oxide **4.90**,[64] are all known compounds. The ^1H NMR spectral data matched those reported in literature.

4.9.3 Experimental Procedures

4.9.3.1 Optimization of Trapping Reactions of 1,2,3-Cyclohexatriene (4.5)

Selected results from the optimization of the reaction between silyl triflate **4.21** and azomethine imine **4.31** commencing from the closest literature precedent[8] appear below. Solvent, fluoride source, and additives were varied using General Procedure 4.1, and results appear below in Table 4.1. For the use of tetrabutylammonium salts as phase transfer reagents in combination with alkali metal fluorides, see references 32 and 65.

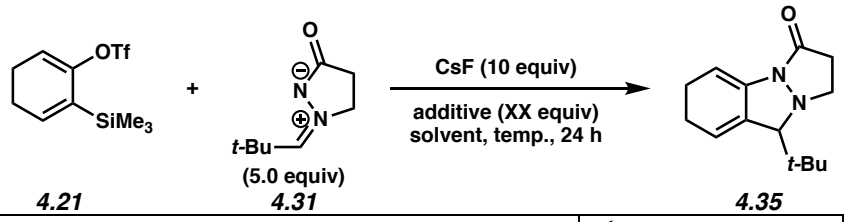
General Procedure 4.1 for the optimization of trapping reactions of triene 4.5



4.21 *4.31* *4.35*

A flame-dried 1-dram vial containing a magnetic stir bar was charged sequentially with silyl triflate **4.21** (10.0 mg, 0.03 mmol, 1.0 equiv), additive (0–2.0 equiv), azomethine imine **4.31** (25.7 mg, 0.16 mmol, 5.0 equiv), solvent (0.320 mL, 0.1 M), and CsF (48.5 mg, 0.32 mmol, 10 equiv) in a glovebox. The vial was then sealed with a Teflon-lined cap, removed from the glovebox, and stirred for 24 h at the desired reaction temperature. The mixture was then filtered over a pad of Celite, eluting with EtOAc (10 mL). The eluate was concentrated then analyzed by ^{1}H NMR using 2,5-dimethylfuran as an external standard.

Table 4.1. Selected Optimization Screening Results.



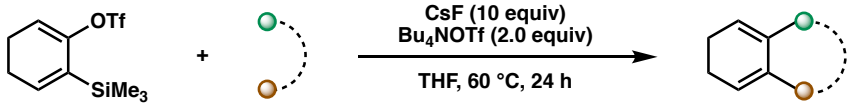
4.21 *4.31* *4.35*

Entry	Conditions	^{1}H NMR Yield[a]	Yield BRSM
1	DMSO, 23 °C	26%	26%
2	MeCN, 23 °C	2%	100%
3	Bu_4NI (1.0 equiv), MeCN, 60 °C	24%	32%
Solvent Screen			
4	Bu_4NI (1.0 equiv), DMSO, 60 °C	24%	24%
5	Bu_4NI (1.0 equiv), DMF, 60 °C	28%	28%
6	Bu_4NI (1.0 equiv), PhCN, 60 °C	19%	23%
7	Bu_4NI (1.0 equiv), Dioxane, 60 °C	14%	61%
8	Bu_4NI (1.0 equiv), DME, 60 °C	13%	25%
9	Bu_4NI (1.0 equiv), PhH, 60 °C	12%	40%
10	Bu_4NI (1.0 equiv), DCE, 60 °C	0%	N/A
11	Bu_4NI (1.0 equiv), THF, 60 °C	38%	42%
Fluoride Source Screen			
12	–CsF, +TBAF (5.0 equiv), THF, 23 °C	9%	17%
13	–CsF, +TASF (5.0 equiv), THF, 23 °C	16%	16%
14	CsF (5 equiv), Bu_4NOTf (2.0 equiv), THF, 23 °C	44%	46%
Additive Loading Screen			
15	Bu_4NOTf (1.0 equiv), THF, 60 °C	42%	76%
16	Bu_4NOTf (2.0 equiv), THF, 60 °C	54%	54%
17[b]	Bu_4NOTf (2.0 equiv), THF, 60 °C	36%[c]	40%

[a] ^{1}H NMR yield determined using 2,5-dimethylfuran as an external standard. [b] Reaction was set up according to General Procedure 4.1, but the procedure was performed entirely outside of the glovebox. [c] Yields for reactions performed outside of a glovebox under these conditions were found to vary between 36–67%. The value reported represents the low end of reaction efficiency observed in these experiments.

4.9.3.2 Scope of Trapping Reactions of 1,2,3-Cyclohexatriene (4.5)

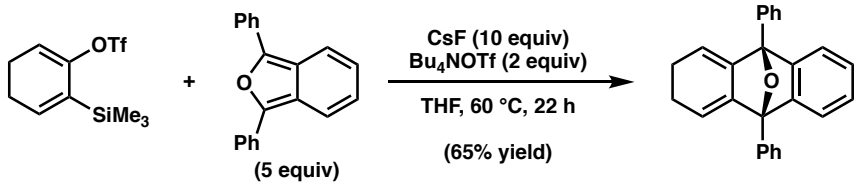
General Procedure 4.2 for the scope of trapping reactions of 1,2,3-cyclohexatriene (4.5):



4.21 *4.17* *4.22*

A flame-dried 1-dram vial containing a magnetic stir bar was charged sequentially with silyl triflate **4.21** (31.3 mg, 0.10 mmol, 1.0 equiv), Bu_4NOTf (78.3 mg, 0.20 mmol, 2.0 equiv), trapping partner **4.17** (5.0–20 equiv), THF (1.00 mL, 0.1 M), and CsF (152 mg, 1.0 mmol, 10 equiv) in a glovebox. The vial was then sealed with a Teflon-lined cap, removed from the glovebox, and stirred for 24 h at 60 °C. The mixture was then filtered over a pad of Celite, eluting with EtOAc (10 mL). The eluate was concentrated under reduced pressure then purified by chromatography to provide adducts **4.22**.

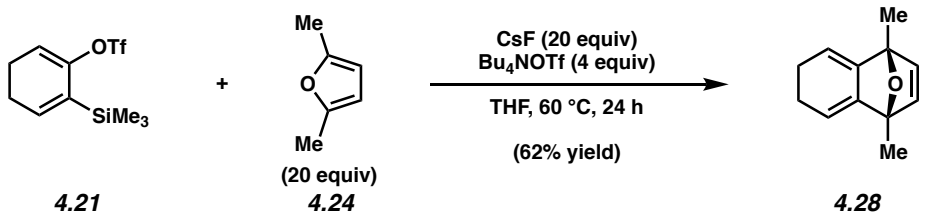
Any modification of the conditions shown in the general procedure above are specified in the following schemes. Deviations in trapping partner stoichiometry result from cursory empirical optimization. In most cases, higher loadings of trapping reagents led to higher yields, though exceptions were observed.



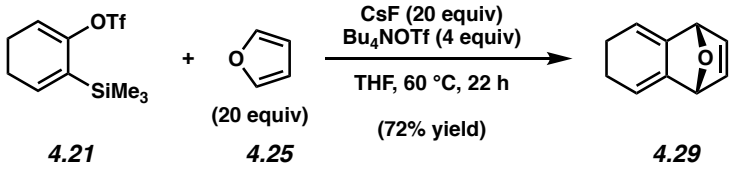
4.21 *4.23* *4.27*

Cycloadduct 4.27. Followed General Procedure 4.2. Analysis of the crude reaction mixture by ^1H NMR using 2,5-dimethylfuran as an external standard showed 71% yield. Purification by flash

chromatography on Florisil (hexanes → 40:3 hexanes:EtOAc) afforded cycloadduct **4.27** (65% yield, average of two experiments) as a pale yellow solid. **Cycloadduct 4.27**: Spectral data matched those reported in the literature.[8]

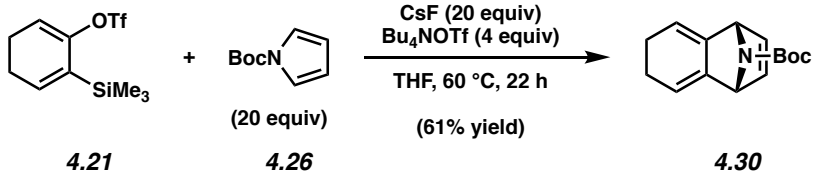


Cycloadduct 4.28. Followed a modified version of General Procedure 4.2 by altering the amount of Bu_4NOTf (157 mg, 0.4 mmol, 4.0 equiv) and CsF (304 mg, 2.0 mmol, 20 equiv). Purification by flash chromatography on Florisil (pentane → 10:1 pentane:Et_2O) afforded cycloadduct **4.28** (62% yield, average of two experiments) as a colorless oil. **Cycloadduct 4.28**: R_f 0.50 (9:1 hexanes:EtOAc); ^{1}H NMR (600 MHz, C_6D_6): δ 5.97 (s, 2H), 5.33–5.26 (m, 2H), 2.13–1.99 (m, 4H), 1.57 (s, 6H); ^{13}C NMR (150 MHz, C_6D_6): δ 141.1, 139.1, 110.6, 86.0, 22.8, 15.2; IR (film): 3058, 2930, 2877, 1381, 1145 cm^{-1}; HRMS-APCI (*m/z*) $[M + H]^+$ calcd for $C_{12}H_{15}O^+$, 175.1117; found 175.1112.



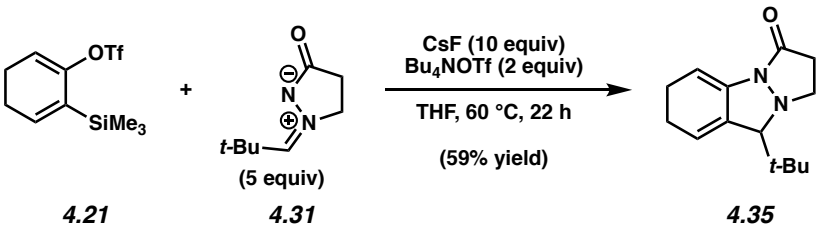
Cycloadduct 4.29. Followed a modified version of General Procedure 4.2 by altering the amount of Bu_4NOTf (157 mg, 0.4 mmol, 4.0 equiv) and CsF (304 mg, 2.0 mmol, 20 equiv). Purification by flash chromatography on Florisil (pentane → 10:1 pentane:Et_2O) afforded cycloadduct **4.29** (72% yield, average of two experiments) as a colorless oil. **Cycloadduct 4.29**: R_f 0.62 (9:1 hexanes:EtOAc); ^{1}H NMR (600 MHz, C_6D_6): δ 6.04 (s, 2H), 5.39–5.35 (m, 2H), 4.97 (s, 2H), 2.13–2.03 (m, 2H), 2.02–1.92 (m, 2H); ^{13}C NMR (150 MHz, C_6D_6): δ 135.6, 135.1, 112.8, 80.4,

23.0; IR (film): 3010, 2925, 2829, 998, 823 cm^{-1}; HRMS-APCI (m/z) $[M + H]^+$ calcd for $C_{10}H_{11}O^+$, 147.0804; found 147.0799.



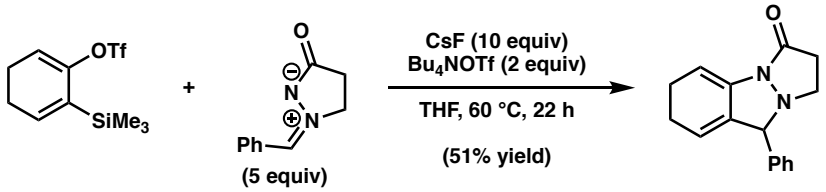
Cycloadduct 4.30. Followed a modified version of General Procedure 4.2 by altering the amount of Bu_4NOTf (157 mg, 0.4 mmol, 4.0 equiv) and CsF (304 mg, 2.0 mmol, 20 equiv). Purification by flash chromatography on Florisil (pentane → 10:1 pentane:Et_2O) afforded cycloadduct **4.30** (61% yield, average of two experiments) as a light yellow oil. **Cycloadduct 4.30**: R_f 0.38 (9:1 hexanes:EtOAc); ^1H NMR (500 MHz, CD_2Cl_2): δ 6.31 (s, 2H), 5.64 (s, 2H), 4.87 (s, 2H), 2.30–2.08 (m, 4H), 1.38 (s, 9H); ^{13}C NMR (125 MHz, CD_2Cl_2): δ 155.1, 135.1, 134.5, 114.1, 80.0, 64.3, 63.6, 27.9, 22.7; IR (film): 3037, 2929, 1704, 1337, 1251 cm^{-1}; HRMS-APCI (*m/z*) $[M + H]^+$ calcd for $C_{15}H_{20}NO_2^+$, 246.1489; found 246.1504.

*Note: **4.30** was obtained as a mixture of rotamers. These data represent empirically observed chemical shifts from the ^1H and ^{13}C-NMR spectra.*



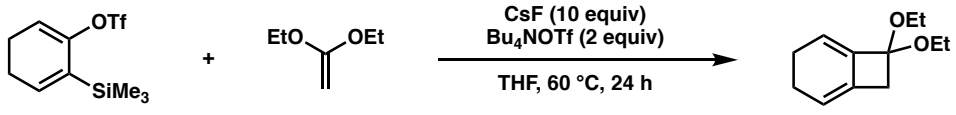
Cycloadduct 4.35. Followed General Procedure 4.2. Purification by flash chromatography on Florisil (3:1 hexanes:EtOAc) afforded **4.35** (59% yield, average of two experiments) as an off-white solid. **Cycloadduct 4.35**: Mp: 106 °C; R_f 0.21 (5:1 hexanes:EtOAc); ^1H NMR (500 MHz,

C_6D_6): δ 6.08–6.04 (m, 1H), 5.41–5.37 (m, 1H), 2.88 (t, *J* = 8.0, 1H), 2.58 (q, *J* = 2.7, 1H), 2.46 (ddd, *J* = 15.3, 13.8, 7.9, 1H), 2.16–1.91 (m, 6H), 0.86 (s, 9H); ^{13}C NMR (100 MHz, C_6D_6): δ 165.0, 136.1, 131.4, 121.4, 99.6, 76.1, 57.0, 35.7, 35.0, 26.4, 24.1, 21.2; IR (film): 2928, 2867, 1699, 1661, 1400 cm^{-1}; HRMS-APCI (*m/z*) $[M + H]^+$ calcd for $C_{14}H_{21}N_2O^+$, 233.1648; found 233.1649.



4.21 *4.32* *4.36*

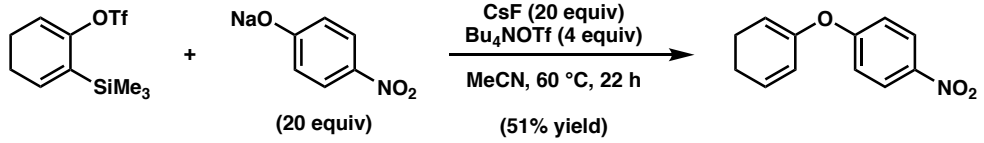
Cycloadduct 4.36. Followed General Procedure 4.2. Purification by flash chromatography on Florisil (4:1 hexanes:EtOAc → 2:1 hexanes:EtOAc) afforded **4.36** (51% yield, average of two experiments) as a white solid. **Cycloadduct 4.36**: Mp: 107–108 °C; R_f 0.20 (3:1 hexanes:EtOAc); ^{1}H NMR (500 MHz, C_6D_6): δ 7.26 (d, *J* = 7.7, 2H), 7.18 (overlapped with residual solvent peak, 2H), 7.14–7.09 (m, 1H), 6.14 (dd, *J* = 5.4, 3.1, 1H), 4.98–4.92 (m, 1H), 3.70–3.62 (m, 1H), 2.80 (t, *J* = 8.5, 1H), 2.44 (ddd, *J* = 15.8, 13.1, 8.7, 1H), 2.16–2.01 (m, 3H), 2.00–1.92 (m, 1H), 1.90–1.79 (m, 1H), 1.78–1.69 (m, 1H); ^{13}C NMR (125 MHz, C_6D_6): δ 162.8, 140.1, 137.7, 129.8, 128.8, 128.7, 128.5, 120.0, 99.9, 73.6, 52.1, 36.0, 22.1, 21.7; IR (film): 3033, 2926, 2827, 1699, 1673 cm^{-1}; HRMS-APCI (*m/z*) $[M + H]^+$ calcd for $C_{16}H_{17}N_2O^+$, 253.1335; found 253.1351.



4.21 *4.33* *4.37*

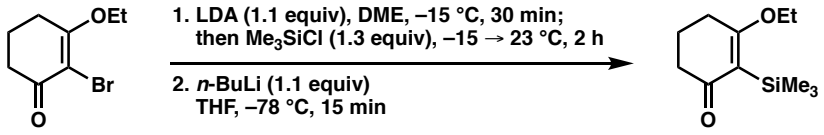
Cycloadduct 4.37. Followed General Procedure 4.2. Analysis of the crude reaction mixture by ^{1}H NMR using 2,5-dimethylfuran as an external standard showed 48% yield. Purification by preparative thin layer chromatography (10:1 hexanes:EtOAc) afforded cycloadduct **4.37** (44%

yield, average of two experiments) as a yellow oil. **Cycloadduct 4.37**: R_f 0.31 (19:1 hexanes:EtOAc); ^{1}H NMR (600 MHz, C_6D_6): δ 5.52.–5.50 (m, 1H), 5.33–5.28 (m, 1H), 3.59 (qd, *J* = 9.3, 7.1, 2H), 3.51 (qd, *J* = 9.3, 7.1, 2H), 2.99–2.95 (m, 2H), 2.08–2.04 (m, 4H), 1.15 (t, *J* = 7.1, 6H); ^{13}C NMR (150 MHz, C_6D_6): δ 143.6, 133.9, 114.3, 114.2, 105.1, 58.5, 42.8, 23.5, 23.3, 15.5; IR (film): 3046, 2975, 2824, 1251, 1055 cm^{-1}; HRMS-APCI (*m/z*) [M – OEt]$^+$ calcd for $C_{10}H_{13}O^+$, 149.0961; found 149.0957.



Adduct 4.38. Followed a modified version of General Procedure 4.2 by altering the amount of Bu_4NOTf (157 mg, 0.4 mmol, 4.0 equiv) and CsF (304 mg, 2.0 mmol, 20 equiv) and by switching the solvent to MeCN. Analysis of the crude reaction mixture by ^{1}H NMR using mesitylene as an external standard showed 50% yield. Purification by flash chromatography on Florisil (pentane → 4:1 pentane:Et_2O) afforded **4.38** (51% yield, average of two experiments) as a light yellow oil. **Adduct 4.38**: R_f 0.57 (5:1 hexanes:EtOAc); ^{1}H NMR (500 MHz, C_6D_6): δ 7.84–7.79 (m, 2H), 6.59–6.54 (m, 2H), 5.65–5.58 (m, 1H), 5.55–5.49 (m, 1H), 5.07–5.02 (m, 1H), 1.95–1.87 (m, 2H), 1.86–1.78 (m, 2H); ^{13}C NMR (125 MHz, C_6D_6): δ 161.8, 149.2, 143.0, 130.8, 125.8, 122.8, 117.0, 109.0, 22.4, 21.4; IR (film): 3080, 2933, 1589, 1512, 1241 cm^{-1}; HRMS-APCI (*m/z*) [M + H]$^+$ calcd for $C_{12}H_{12}NO_3^+$, 218.0812; found 218.0819.

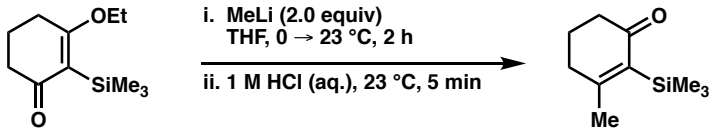
4.9.3.3 Synthesis of Silyl Triflate 4.42



4.39 (69% yield, two steps) *4.40*

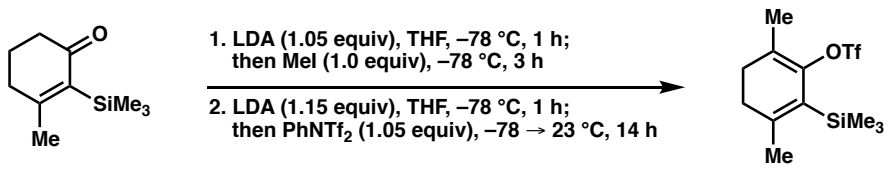
α-Silyl Vinylogous Ester 4.40. To a solution of diisopropylamine (9.15 g, 12.8 mL, 90.4 mmol, 1.2 equiv) in DME (150 mL) at –15 °C was added *n*-BuLi (2.5 M in hexanes, 33.1 mL, 1.1 equiv) dropwise over 5 min. The resulting solution was stirred at this temperature for 25 min, then vinylogous ester **4.39** (16.5 g, 75.3 mmol, 1.0 equiv) in DME (150 mL) was added dropwise via cannula over 20 min to give a bright yellow solution. Stirring was continued at this temperature for 30 min then trimethylsilyl chloride (11.9 mL, 97.9 mmol, 1.3 equiv) was added dropwise over 5 min. The cooling bath was removed, and stirring was continued for 2 h. After this time, the solvent was removed in vacuo, and the flask was evacuated and backfilled with nitrogen (3x). The heterogeneous yellow residue was suspended in pentane and filtered through Celite under a nitrogen atmosphere into a flame-dried round bottom flask (4 x 25 mL aliquots of pentane). The resulting eluate was concentrated under reduced pressure to give a yellow oil (20.8 g) which was dissolved in THF (476 mL, 0.15 M) and cooled to –78 °C. To this solution was added *n*-BuLi (2.5 M in hexanes, 31.4 mL, 1.1 equiv) dropwise over 15 min giving an orange solution. Stirring was continued for 15 min then the reaction was quenched with a mixture of saturated ammonium chloride:water (1:20; 200 mL). The mixture was diluted with Et_2O (150 mL), and the layers were separated. The aqueous layer was extracted with Et_2O (2 x 150 mL), and the organic layers were combined, dried over magnesium sulfate, filtered, and concentrated under reduced pressure. The crude residue was purified by flash chromatography (4:1 → 7:3 hexanes:EtOAc) to provide α-silyl vinylogous ester **4.40** (10.4 g, 49.0 mmol, 69% yield, two steps) as a yellow solid. **α-Silyl**

Vinylogous Ester 4.40: Mp: 46 °C; R_f 0.67 (9:1 benzene:MeCN); ^{1}H NMR (500 MHz, $CDCl_3$): δ 4.05 (q, *J* = 7.0, 2H), 2.51 (t, *J* = 6.3, 2H), 2.26 (t, *J* = 6.3, 2H), 1.95 (p, *J* = 6.3, 2H), 1.33 (t, *J* = 7.0, 3H), 0.16 (s, 9H); ^{13}C NMR (150 MHz, $CDCl_3$): δ 202.7, 182.3, 115.4, 63.4, 37.3, 26.2, 21.1, 15.0, 0.9; IR (film): 2950, 2894, 1633, 155.8, 1187 cm^{-1}; HRMS-APCI (*m/z*) $[M + H]^+$ calcd for $C_{11}H_{21}O_2Si^+$, 213.1305; found 213.1299.



4.40 **(88% yield)** ***4.41***

α-Silyl Enone 4.41. To a solution of vinylogous ester **4.40** (3.20 g, 15.0 mmol, 1.0 equiv) in THF (15 mL, 1 M) at 0 °C was added methyllithium (2.5 M in dimethoxymethane, 12.0 mL, 30.0 mmol, 2.0 equiv) dropwise over 2 min. The cooling bath was removed, and stirring was continued for 2 h. At this time, 1 M aqueous HCl (40 mL) was added carefully causing gas evolution. The biphasic mixture was stirred for 5 min then diluted with water (50 mL) and Et_2O (50 mL). The layers were separated, and the aqueous layer was extracted with Et_2O (2 x 50 mL). The organic layers were combined, dried over sodium sulfate, filtered, and concentrated. The crude residue was purified by flash chromatography (19:1 hexanes:Et_2O → 9:1 hexanes:Et_2O) to give α-silyl enone **4.41** (2.43 g, 13.3 mmol, 88% yield) as a clear colorless oil. **α-Silyl Enone 4.41**: R_f 0.78 (7:3 hexanes:EtOAc); ^{1}H NMR (400 MHz, $CDCl_3$): δ 2.34–2.23 (m, 4H), 2.02 (s, 3H), 1.95–1.85 (m, 2H), 0.21 (s, 9H); ^{13}C NMR (100 MHz, $CDCl_3$): δ 203.2, 169.5, 136.6, 37.9, 34.7, 24.8, 22.2, 1.7; IR (film): 2948, 1739, 1654, 1583, 1245 cm^{-1}; HRMS-APCI (*m/z*) [M]+H^+ calcd for $C_{10}H_{19}OSi^+$, 183.1200; found 183.1199.



4.41 (41% yield, two steps) *4.42*

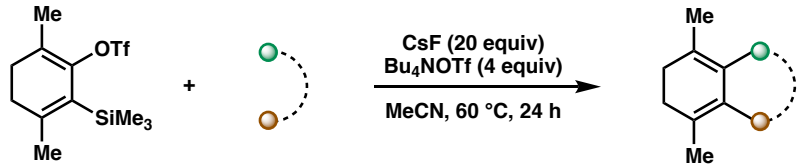
Silyl Triflate 4.42. To a solution of diisopropylamine (2.50 mL, 17.7 mmol, 1.1 equiv) in THF (25 mL) at –78 °C was added *n*-BuLi (2.4 M in hexanes, 7.05 mL, 16.9 mmol, 1.05 equiv) dropwise over 5 min. The resulting mixture was stirred for 15 min at this temperature, then the cooling bath was removed, and stirring was continued for an additional 15 min. The mixture was again cooled to –78 °C and then a solution of enone **4.41** (2.94 g, 16.1 mmol, 1.0 equiv) in THF (25 mL) was added dropwise via cannula over 8 min. The mixture was allowed to stir at –78 °C for 1 h and then iodomethane (1.00 mL, 16.1 mmol, 1.0 equiv) was added dropwise over 5 min at –78 °C. The reaction was stirred for an additional 3 h at –78 °C. At this time, the mixture was quenched with saturated ammonium chloride:water (1:20; 100 mL), diluted with Et_2O (50 mL), and the layers were separated. The aqueous layer was extracted with Et_2O (2 x 50 mL). The organic layers were combined, dried over magnesium sulfate, filtered, and concentrated to give a light yellow oil (2.98 g). The residue was dissolved in THF (14 mL) and added dropwise to a solution of LDA at –78 °C (prepared as described previously; 1.06 M in THF, 14 mL, 1.15 equiv). The resulting yellow solution was stirred at this temperature for 1 h then treated dropwise with a solution of $PhNTf_2$ (4.87 g, 13.6 mmol, 1.05 equiv) in THF (14 mL) via cannula over 4 min. The cooling bath was left in place, and the reaction was allowed to warm gradually from –78 °C to 23 °C over 14 h. After this time, the reaction was quenched with water (50 mL) and hexanes (50 mL). The layers were separated, and the aqueous layer was extracted with hexanes (2 x 50 mL). The organic layers were combined, dried over sodium sulfate, filtered, and concentrated. The residue was purified by flash chromatography on basic alumina (pentane) to give silyl triflate **4.42** (2.24 g, 6.57 mmol, 41%

yield, two steps) as a light yellow oil. Note: Discoloration of silyl triflate **4.42** was observed within 5 minutes if left exposed to air. ^{1}H NMR analysis showed no change following discoloration, but samples of **4.42** were typically stored in a glovebox to avoid air exposure. **Silyl Triflate 4.42**: R_f 0.66 (19:1 hexanes:EtOAc); ^{1}H NMR (600 MHz, $CDCl_3$): δ 2.14–2.04 (m, 4H), 2.00 (s, 3H), 1.85 (s, 3H), 0.27 (s, 9H); ^{13}C NMR (150 MHz, $CDCl_3$): δ 150.5, 145.3, 127.3, 123.3, 118.6 (q, J = 318), 30.9, 29.5, 24.0, 16.7, 1.2; ^{19}F NMR (376 MHz, $CDCl_3$): δ –73.9 (s, 3F); IR (film): 2936, 1414, 1398, 1200, 1139 cm^{-1}; HRMS-APCI (*m/z*) $[M + H]^+$ calcd for $C_{12}H_{20}F_3O_3SSi^+$, 328.0771; found 328.0762.

4.9.3.4 Scope of Trapping Reactions of Triene 4.43

Empirically, we observed that reactions of substituted trienes occurred in higher yield compared to those of the unsubstituted 1,2,3-cyclohexatriene (**4.5**). The substituents on **4.43** likely help to suppress deleterious side reactions involving the reactive 1,2,3-triene or its precursor. The nature of this beneficial effect is currently unknown and will be subject to further investigation.

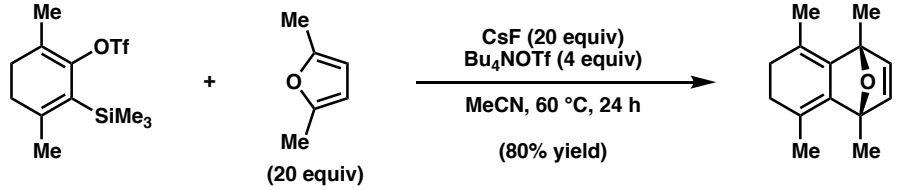
General Procedure 4.3 for the scope of trapping reactions of triene 4.43:



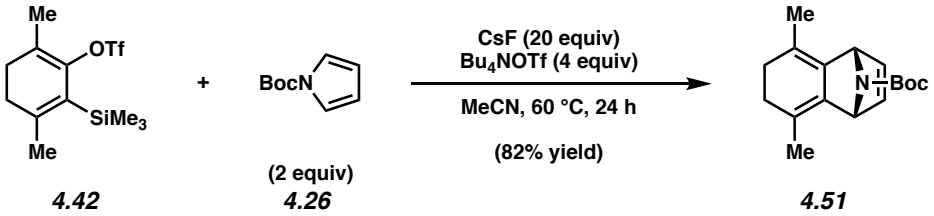
4.42 ***4.17*** ***4.44***

A flame-dried 1-dram vial containing a magnetic stir bar was charged sequentially with silyl triflate **4.42** (34.2 mg, 0.10 mmol, 1.0 equiv), Bu_4NOTf (157 mg, 0.40 mmol, 4.0 equiv), trapping partner **4.17** (2.0–20 equiv), MeCN (1.00 mL, 0.1 M), and CsF (304 mg, 2.0 mmol, 20 equiv) in a glovebox. The vial was then sealed with a Teflon-lined cap, removed from the glovebox, and stirred for 24 h at 60 °C. The mixture was then filtered over a pad of Celite, eluting with EtOAc

(10 mL). The eluate was concentrated under reduced pressure then purified by chromatography to provide adducts **4.44**.

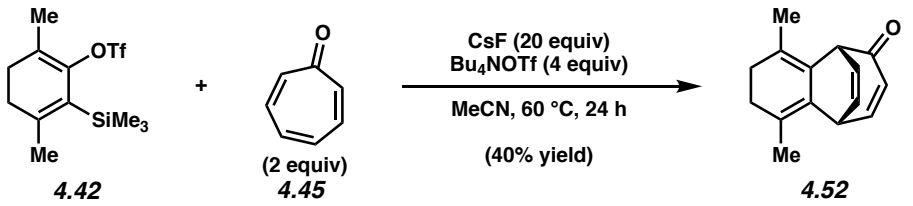


Cycloadduct 4.50. Followed General Procedure 4.3. Purification by flash chromatography on Florisil (pentane → 10:1 pentane:Et_2O) afforded cycloadduct **4.50** (80% yield, average of two experiments) as a colorless oil. **Cycloadduct 4.50**: R_f 0.23 (19:1 hexanes:EtOAc); ^{1}H NMR (600 MHz, C_6D_6): δ 6.02 (s, 2H), 2.10–2.00 (m, 2H), 1.93–1.84 (m, 2H), 1.77 (s, 6H), 1.65 (s, 6H); ^{13}C NMR (150 MHz, C_6D_6): δ 138.9, 134.1, 118.9, 86.9, 31.6, 18.9, 18.1; IR (film): 3068, 2913, 2824, 1381, 1141 cm^{-1}; HRMS-APCI (*m/z*) $[M + H]^+$ calcd for $C_{14}H_{19}O^+$, 203.1430; found 203.1422.

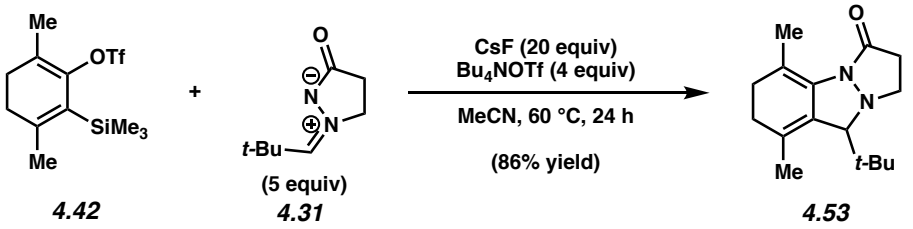


Cycloadduct 4.51. Followed General Procedure 4.3. Purification by flash chromatography on basic alumina (10:1 pentane:Et_2O → 1:1 pentane:Et_2O) afforded cycloadduct **4.51** (82% yield, average of two experiments) as a yellow oil. **Cycloadduct 4.51**: R_f 0.32 (5:1 hexanes:EtOAc); ^{1}H NMR (500 MHz, $CDCl_3$): δ 6.51–6.11 (m, 2H), 5.32–4.92 (m, 2H), 2.23–2.03 (m, 4H), 1.77 (s, 6H), 1.39 (s, 9H); ^{13}C NMR (125 MHz, $CDCl_3$): δ 155.8, 135.1, 133.7, 128.3, 127.7, 121.3, 120.8, 80.3, 62.7, 62.0, 29.5, 28.3, 19.1; IR (film): 3032, 2972, 1710, 1366, 1092 cm^{-1}; HRMS-APCI (*m/z*) $[M + H]^+$ calcd for $C_{17}H_{24}NO_2^+$, 274.1802; found 274.1794.

*Note: **4.51** was obtained as a mixture of rotamers. These data represent empirically observed chemical shifts from the ^{1}H and ^{13}C-NMR spectra.*

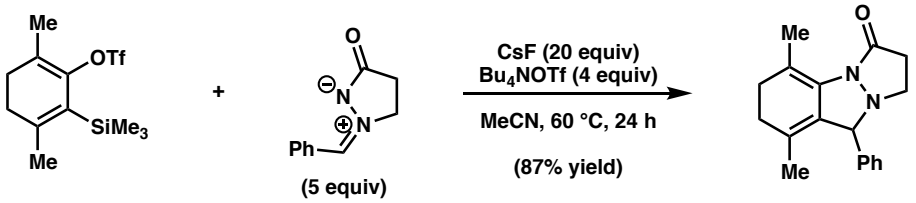


Cycloadduct 4.52. Followed General Procedure 4.3. Purification by preparative thin layer chromatography (5:1 benzene:Et_2O) afforded cycloadduct **4.52** (40% yield, average of two experiments) as a yellow oil. **Cycloadduct 4.52**: R_f 0.19 (9:1 hexanes:EtOAc); ^{1}H NMR (600 MHz, $CDCl_3$): δ 6.98 (dd, *J* = 10.9, 8.8, 1H), 6.54 (ddd, *J* = 8.3, 7.3, 1.0, 1H), 6.15 (ddd, *J* = 8.3, 7.3, 1.0, 1H), 5.65 (dd, *J* = 10.9, 1.9, 1H), 4.47–4.42 (m, 1H), 4.18 (t, *J* = 8.0, 1H), 2.27–2.17 (m, 2H), 2.16–2.01 (m, 2H), 1.85 (s, 3H), 1.82 (s, 3H); ^{13}C NMR (150 MHz, $CDCl_3$): δ 192.4, 150.5, 137.4, 131.3, 129.0, 127.4, 127.2, 124.2, 122.1, 56.9, 39.6, 31.0, 30.5, 19.3; 19.0; IR (film): 3053, 2984, 2852, 1662, 1379 cm^{-1}; H1RMS-APCI (*m/z*) $[M + H]^+$ calcd for $C_{15}H_{17}O^+$, 213.1274; found 213.1267.



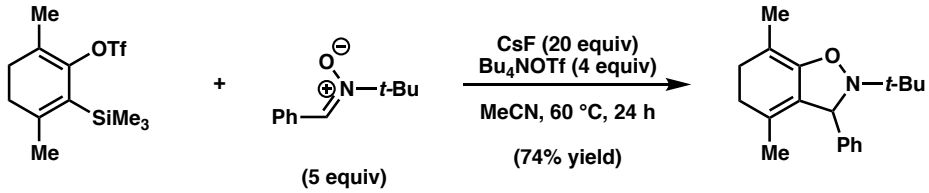
Cycloadduct 4.53. Followed General Procedure 4.3. Purification by flash chromatography on Florisil (4:1 pentane:Et_2O → 2:1 pentane:Et_2O) afforded cycloadduct **4.53** (86% yield, average of two experiments) as a white solid. **Cycloadduct 4.53**: Mp: 131–133 °C; R_f 0.28 (5:1 hexanes:EtOAc); ^{1}H NMR (500 MHz, $CDCl_3$): δ 3.58–3.52 (m, 1H), 3.05 (s, 1H), 3.02–2.87 (m, 2H), 2.45–2.38 (m, 1H), 2.28–2.14 (m, 2H), 2.06–1.98 (m, 2H), 1.97 (s, 3H), 1.74 (s, 3H), 1.54 (s,

9H); ^{13}C NMR (125 MHz, $CDCl_3$): δ 168.1, 129.1, 129.0, 128.8, 110.6, 73.8, 57.0, 38.4, 35.3, 32.0, 29.7, 26.6, 21.5, 20.2; IR (film): 2922, 2867, 1684, 1360, 1096 cm^{-1}; HRMS-APCI (*m/z*) $[M + H]^+$ calcd for $C_{16}H_{25}N_2O^+$, 261.1961; found 261.1949.



4.42 ***4.32*** ***4.54***

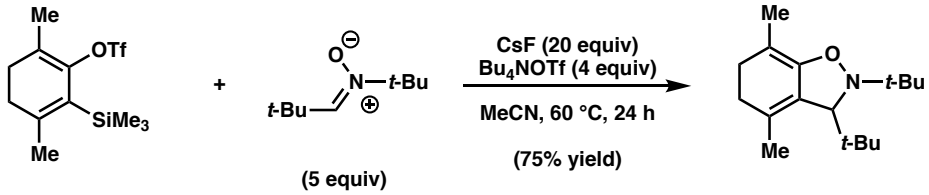
Cycloadduct 4.54. Followed General Procedure 4.3. Purification by flash chromatography on Florisil (1:1 hexanes:Et_2O → Et_2O) afforded cycloadduct **4.54** (87% yield, average of two experiments) as a white solid. **Cycloadduct 4.54**: Mp: 111 °C; R_f = 0.08 (4:1 hexanes:EtOAc); ^{1}H NMR (500 MHz, C_6D_6): δ 7.25–7.19 (m, 2H), 7.14–7.09 (m, 2H), 7.09–7.04 (m, 1H), 3.81 (br s, 1H), 2.89 (dt, *J* = 10.3, 7.5, 1 H), 2.43 (q, *J* = 9.3, 1H), 2.29 (s, 3H), 2.24–1.94 (m, 5H), 1.91–1.80 (m, 1H), 1.11 (s, 3H); ^{13}C NMR (125 MHz, C_6D_6, 14 of 16 signals observed): δ 169.0, 140.2, 132.8, 129.9, 129.1, 125.9, 113.4, 72.2, 47.9, 33.6, 30.9, 29.7, 20.7, 18.8; IR (film): 3028, 2924, 2855, 1728, 1664 cm^{-1}; HRMS-APCI (*m/z*) $[M + H]^+$ calcd for $C_{18}H_{21}N_2O^+$, 281.1648; found 281.1635.



4.42 ***4.46*** ***4.55***

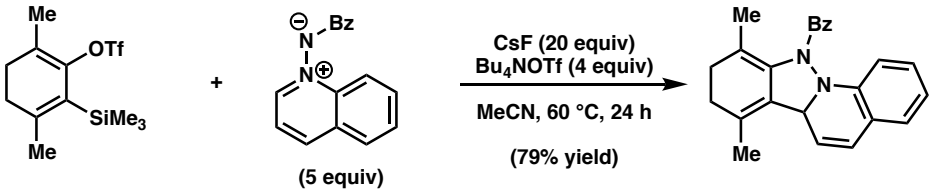
Cycloadduct 4.55. Followed General Procedure 4.3. Purification by flash chromatography on basic alumina (hexanes → 1:1 hexanes:CH_2Cl_2) afforded cycloadduct **4.55** (74% yield, average of two experiments) as a clear colorless oil. **Cycloadduct 4.55**: R_f = 0.51 (19:1 hexanes:EtOAc); ^{1}H NMR (500 MHz, CD_3CN): δ 7.34–7.28 (m, 4H), 7.27–7.21 (m, 1H), 4.99 (s, 1H), 2.35–2.02 (m, 4H), 1.68 (s, 3H), 1.64 (s, 3H), 1.11 (s, 9H); ^{13}C NMR (150 MHz, C_6D_6): δ 148.7, 143.9, 133.2,

128.7, 128.1, 127.2, 125.0, 92.4, 64.1, 61.0, 30.9, 29.0, 26.2, 19.3, 15.5; IR (film): 3036, 2971, 2920, 1479, 1390 cm^{-1}; HRMS-APCI (*m/z*) $[M + H]^+$ calcd for $C_{19}H_{26}NO^+$, 284.2009; found 284.1996.



4.42 ***4.47*** ***4.56***

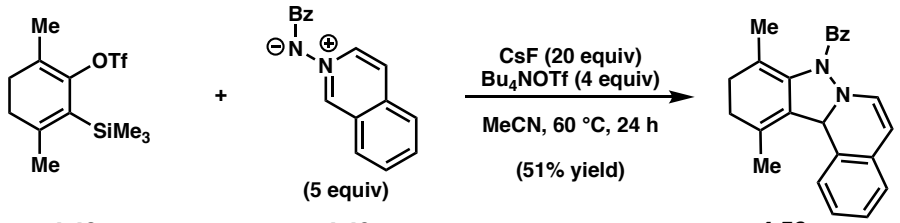
Cycloadduct 4.56. Followed General Procedure 4.3. Purification by flash chromatography on basic alumina (hexanes → 5:1 hexanes:CH_2Cl_2) afforded cycloadduct **4.56** (75% yield, average of two experiments) as a clear colorless oil. **Cycloadduct 4.56**: R_f = 0.33 (1:1 hexanes:CH_2Cl_2); ^1H NMR (500 MHz, C_6D_6): δ 3.39 (s, 1H), 2.30 (td, *J* = 16.6, 8.3, 1H), 2.02 (td, *J* = 17.2, 8.3, 1H), 1.92–1.78 (m, 2H), 1.82 (s, 3H), 1.54 (s, 3H), 1.08 (s, 9H), 1.05 (s, 9H); ^{13}C NMR (125 MHz, C_6D_6): δ 150.3, 131.4, 126.5, 90.6, 68.1, 60.6, 37.0, 31.7, 29.2, 27.3, 26.5, 21.1, 15.3; IR (film): 2973, 2916, 2868, 1700, 1363 cm^{-1}; HRMS-APCI (*m/z*) $[M + H]^+$ calcd for $C_{17}H_{30}NO^+$, 264.2322; found 264.2315.



4.42 ***4.48*** ***4.57***

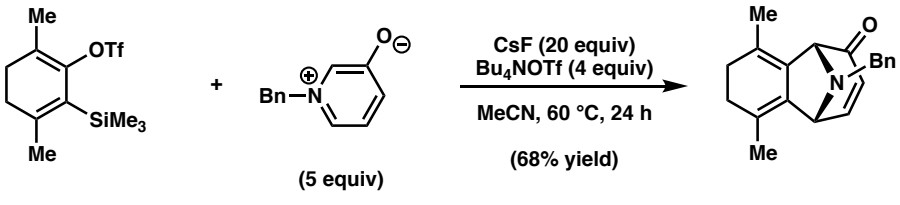
Cycloadduct 4.57. Followed General Procedure 4.3. Purification by flash chromatography on Florisil (hexanes → 9:1 hexanes:EtOAc) afforded cycloadduct **4.57** (79% yield, average of two experiments) as an off-white solid. **Cycloadduct 4.57**: Mp: 158–159 °C; R_f = 0.39 (17:3 hexanes:EtOAc); ^1H NMR (500 MHz, C_6D_6): δ 8.11 (d, *J* = 7.3, 2H), 7.35 (d, *J* = 7.9, 1H), 7.04–6.91 (m, 4H), 6.68–6.60 (m, 2H), 5.93 (d, *J* = 9.9, 1H), 5.50 (dd, *J* = 9.9, 5.6, 1H), 4.18 (br s, 1H),

2.10–1.86 (m, 2H), 2.00 (s, 3H), 1.89–1.74 (m, 1H), 1.72–1.60 (m, 1H), 1.37 (s, 3H); ^{13}C NMR (150 MHz, CD_2Cl_2): δ 171.4, 144.2, 134.6, 131.1, 130.9, 129.5, 128.6, 128.1, 127.7, 127.0, 125.09, 125.06, 123.2, 122.5, 122.2, 118.9, 115.1, 61.8, 30.6, 28.6, 19.1, 19.0; IR (film): 3070, 3034, 2910, 1663, 1482 cm^{-1}; HRMS-APCI (*m/z*) $[M + H]^+$ calcd for $C_{24}H_{23}N_2O^+$, 355.1805; found 355.1787.



4.42 ***4.49*** ***4.58***

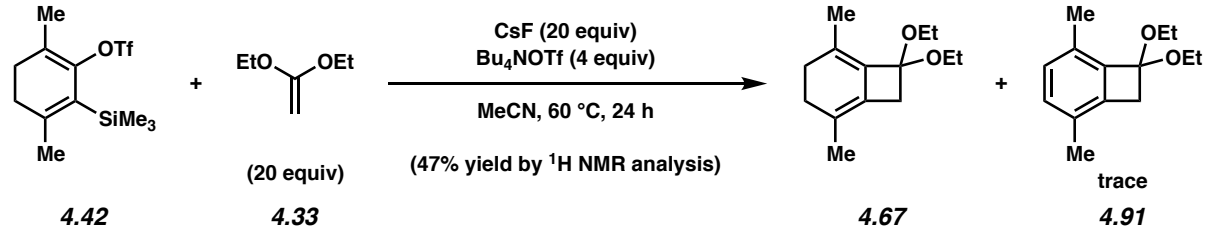
Cycloadduct 4.58. Followed General Procedure 4.3. Purification by flash chromatography on Florisil (hexanes → 18:1 hexanes:EtOAc) afforded cycloadduct **4.58** (51% yield, average of two experiments) as an off-white solid. **Cycloadduct 4.58**: Mp: 146 °C; R_f = 0.29 (9:1 hexanes:EtOAc); ^{1}H NMR (600 MHz, $CDCl_3$): δ 7.74–7.67 (m, 2H), 7.43 (tt, *J* = 7.4, 1.2, 1H), 7.40–7.34 (m, 2H), 7.19–7.13 (m, 2H), 7.04 (t, *J* = 7.5, 1H), 6.92 (d, *J* = 7.3, 1H), 6.25 (d, *J* = 7.9, 1H), 5.66 (d, *J* = 7.9, 1H), 4.68 (s, 1H), 2.51–2.40 (m, 1H), 2.36–2.14 (m, 3H), 1.83 (s, 3H), 1.34 (s, 3H); ^{13}C NMR (150 MHz, $CDCl_3$): δ 171.4, 139.4, 134.8, 131.8, 131.1, 130.7, 130.3, 129.6, 129.1, 128.8, 128.5, 127.9, 127.7, 127.3, 125.9, 124.8, 117.7, 108.4, 65.0, 31.7, 29.0, 20.0, 17.4; IR (film): 3060, 3022, 2917, 1712, 1667 cm^{-1}; HRMS-APCI (*m/z*) $[M + H]^+$ calcd for $C_{24}H_{23}N_2O^+$, 355.1805; found 355.1785.



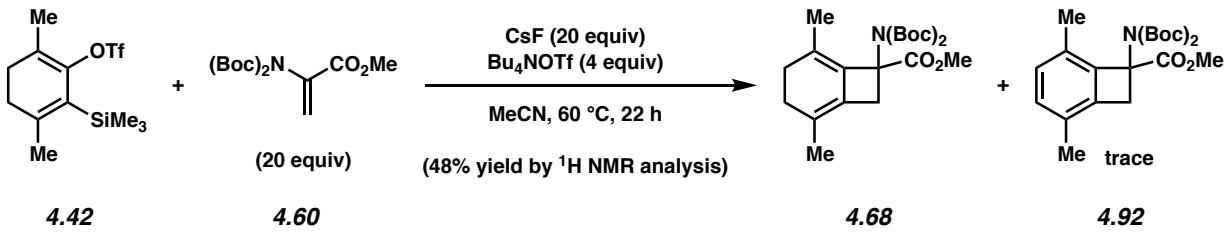
4.42 ***4.59*** ***4.66***

Cycloadduct 4.66. Followed General Procedure 4.3. Purification by flash chromatography (benzene → 9:1 benzene:Et_2O) afforded cycloadduct **4.66** (68% yield, average of two

experiments) as a light yellow oil. **Cycloadduct 4.66**: R_f = 0.42 (7:3 hexanes:EtOAc); ^{1}H NMR (600 MHz, CD_3CN): δ 7.36–7.31 (m, 2H), 7.30–7.24 (m, 3H), 7.15 (dd, *J* = 9.6, 5.8, 1H), 5.79 (dd, *J* = 9.6, 1.3, 1H), 4.16 (d, *J* = 5.8, 1H), 3.99 (s, 1H), 3.47 (d, *J* = 13.1, 1H), 3.44 (d, *J* = 13.1, 1H), 2.39–2.08 (m, 4H), 1.77 (s, 3H), 1.73 (s, 3H); ^{13}C NMR (150 MHz, CD_3CN): δ 194.5, 150.8, 139.2, 131.8, 130.1, 129.6, 129.4, 128.3, 126.6, 125.9, 125.2, 73.4, 61.6, 56.4, 30.8, 30.1, 19.9, 19.6; IR (film): 3028, 2970, 2911, 1683, 1373 cm^{-1}; HRMS-APCI (*m/z*) $[M + H]^+$ calcd for $C_{20}H_{22}NO^+$, 292.1696; found 292.1696.

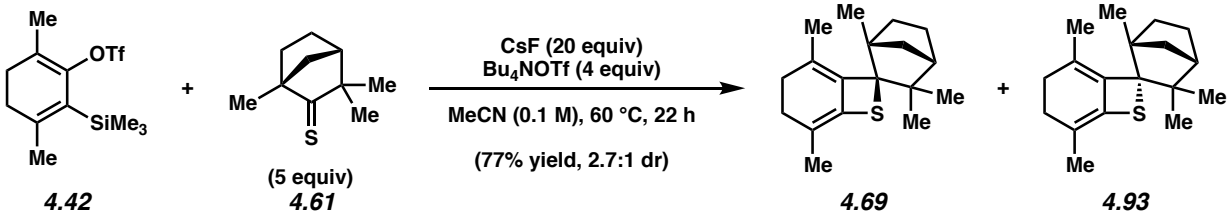


Cycloadduct 4.67. Followed General Procedure 4.3. ^{1}H NMR analysis of the reaction mixture after workup indicated 47% yield (average of two experiments) of cycloadduct **4.67** relative to a mesitylene standard. To obtain an analytical sample, the reaction mixture was then purified by preparative thin-layer chromatography (10:1 hexanes:EtOAc) to afford an inseparable mixture of **4.67** and **4.91** as a yellow oil. **Cycloadduct 4.67**: R_f 0.49 (9:1 hexanes:EtOAc); ^{1}H NMR (500 MHz, C_6D_6): δ 3.69–3.56 (m, 4H), 2.92 (s, 2H), 2.11–2.01 (m, 4H), 1.77 (s, 3H), 1.55 (s, 3H), 1.18 (t, *J* = 7.0, 6H); ^{13}C NMR (125 MHz, $CDCl_3$): δ 136.2, 126.5, 122.2, 120.3, 105.2, 58.8, 41.2, 30.9, 29.7, 19.1, 17.5, 15.5; IR (film): 2975, 2911, 1441, 1242, 1148, 1057 cm^{-1}; HRMS-APCI (*m/z*) $[M – OEt]^+$ calcd for $C_{12}H_{17}O^+$, 177.1274; found 177.1269. **Cycloadduct 4.91** was assigned by analogy of its ^{1}H NMR spectrum to known cycloadduct **4.92** (see below).



4.42 *4.60* *4.68* *4.92*

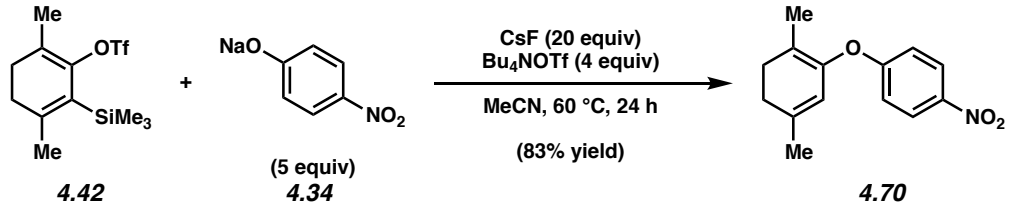
Cycloadduct 4.68 and **4.92.** Followed General Procedure 4.3. ^{1}H NMR analysis of the reaction mixture purification by flash chromatography (5:1 hexanes:EtOAc) indicated 48% yield (average of two experiments) of cycloadduct **4.68** relative to a mesitylene standard. To obtain an analytical sample, the reaction mixture was then purified by preparative thin-layer chromatography (4:1 hexanes:EtOAc) to afford an inseparable mixture of **4.68** and **4.92**[66] as a colorless oil. **Cycloadduct 4.68**: R_f 0.64 (4:1 hexanes:EtOAc); ^{1}H NMR (500 MHz, C_6D_6): δ 4.14 (d, J = 15.2, 1H), 3.46 (s, 3H), 3.17 (d, J = 15.2, 1H), 2.10–1.87 (m, 4H), 1.82 (s, 3H), 1.45 (s, 3H), 1.38 (s, 18H); ^{13}C NMR (125 MHz, C_6D_6): δ 170.4, 152.4, 132.7, 129.1, 125.6, 119.6, 82.0, 67.5, 52.1, 40.6, 31.3, 29.7, 27.8, 17.5, 16.9; IR (film): 2979, 1744, 1711, 1251, 1116 cm^{-1}; HRMS-APCI (*m/z*) $[M + H]^+$ calcd for $C_{22}H_{34}NO_6^+$, 408.2381; found 408.2395. **Cycloadduct 4.92**: Spectral data matched those reported in the literature.[8]



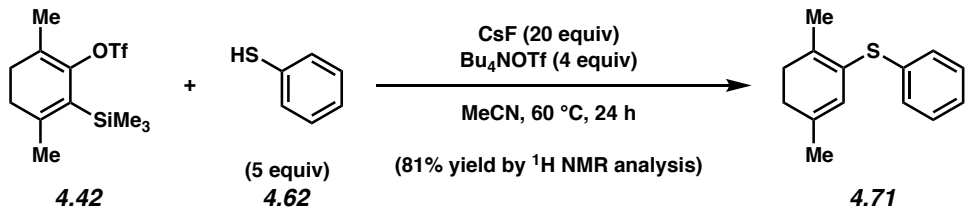
4.42 *4.61* *4.69* *4.93*

Cycloadduct 4.69 and **4.93.** Followed General Procedure 4.3. Filtration through a pad of Florisil, eluting with benzene (10 mL) followed by filtration through a second pad of Florisil, eluting with 4:1 hexanes:EtOAc (10 mL) afforded major diastereomer **4.69** and minor diastereomer **4.93** (77% combined yield, 2.7:1 dr (determined by ^{1}H NMR analysis of the crude mixture)) as a colorless oil. To obtain an analytical sample, the mixture of **4.69** and **4.93** was purified by flash

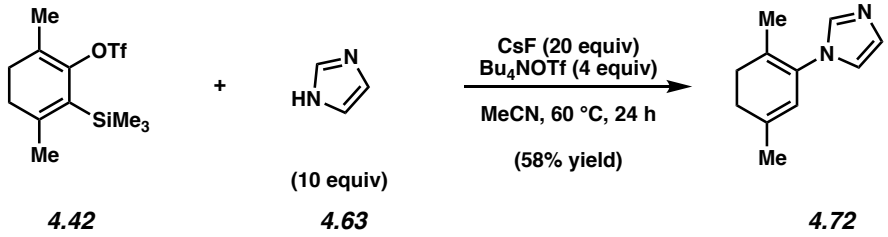
chromatography (pentane) to afford major diastereomer **4.69** as a colorless oil. **Cycloadduct 4.69** and **4.93**: R_f = 0.46 (100% hexanes); ^{1}H NMR (600 MHz, C_6D_6, major diastereomer **4.69**): δ 2.25–2.06 (m, 2H), 2.02–1.87 (m, 2H), 1.80–1.72 (m, 1H), 1.69–1.66 (m, 1H), 1.65–1.59 (m, 5H), 1.57 (s, 3H), 1.55 (s, 3H), 1.42–1.32 (m, 2H), 1.31 (s, 3H), 1.15 (s, 3H), 1.07 (d, *J* = 10.6, 1H); ^{13}C NMR (150 MHz, C_6D_6, major diastereomer **4.69**): δ 135.3, 127.0, 122.2, 112.8, 86.8, 55.2, 50.0, 45.6, 42.6, 34.4, 33.0, 32.5, 29.4, 25.5, 24.0, 21.9, 20.1, 16.6; ^{13}C NMR (125 MHz, C_6D_6, minor diastereomer **4.93**): δ 136.3, 125.8, 121.3, 112.5, 87.0, 52.6, 49.2, 45.8, 42.2, 35.0, 32.6, 29.9, 29.3, 28.3, 25.3, 20.2, 17.9, 16.7; IR (film): 2930, 2872, 1450, 1206, 1145 cm^{-1}; HRMS-APCI (*m/z*) [M + H]$^+$ calcd for $C_{18}H_{27}S^+$, 275.1828; found 275.1844. The relative stereochemistry of **4.69** and **4.93** were assigned by comparison of experimental and computed NMR chemical shift data, see Section 4.9.4.5 for details.



Adduct 4.70. Followed General Procedure 4.3. Purification by flash chromatography on Florisil (hexanes → 3:1 hexanes:Et_2O) afforded adduct **4.70** (83% yield, average of two experiments) as a yellow oil. **Adduct 4.70**: R_f 0.69 (5:1 hexanes:EtOAc); ^{1}H NMR (500 MHz, C_6D_6): δ 7.91–7.83 (m, 2H), 6.65–6.57 (m, 2H), 5.28 (s, 1H), 1.97 (t, *J* = 9.5, 2H), 1.85 (t, *J* = 9.4, 2H), 1.51 (s, 3H), 1.49 (s, 3H); ^{13}C NMR (125 MHz, C_6D_6): δ 162.5, 142.9, 142.6, 137.6, 126.0, 118.0, 116.8, 115.6, 28.8, 28.6, 22.6, 15.3; IR (film): 3039, 2926, 2824, 1513, 1340 cm^{-1}; HRMS-APCI (*m/z*) [M + H]$^+$ calcd for $C_{14}H_{16}NO_3^+$, 246.1125; found 246.1121

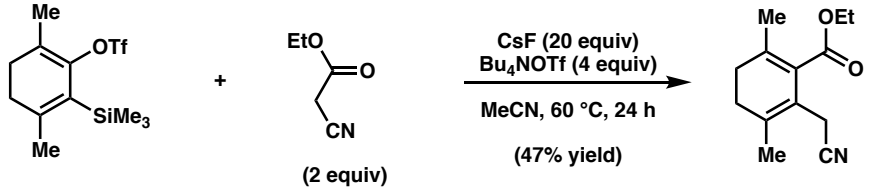


Adduct 4.71. Followed General Procedure 4.3. ^{1}H NMR analysis of the reaction mixture after workup indicated 81% yield (average of two experiments) of adduct **4.71** relative to a mesitylene standard. To obtain an analytical sample, the reaction mixture was then purified by sequential preparative thin layer chromatography (10:1 hexanes:EtOAc) and flash silica column chromatography (10:1 pentane:Et_2O) to afford adduct **4.71** as a colorless oil. **Adduct 4.71**: R_f 0.90 (10:1 hexanes:EtOAc); ^{1}H NMR (500 MHz, C_6D_6): δ 7.35–7.30 (m, 2H), 7.06–7.01 (m, 2H), 6.89 (tt, J = 7.4, 1.4, 1H), 5.80 (q, J = 1.5, 1H), 2.05 (t, J = 9.4, 2H), 1.97 (s, 3H), 1.86 (t, J = 9.4, 2H), 1.48 (s, 3H); ^{13}C NMR (150 MHz, $CDCl_3$): δ 138.7, 137.4, 134.9, 128.9, 127.6, 125.1, 123.8, 121.1, 31.4, 28.4, 22.8, 21.3; IR (film): 3058, 2922, 2822, 1477, 1025 cm^{-1}; HRMS-APCI (*m/z*) $[M + H]^+$ calcd for $C_{14}H_{17}S^+$, 217.1046; found 217.1042.



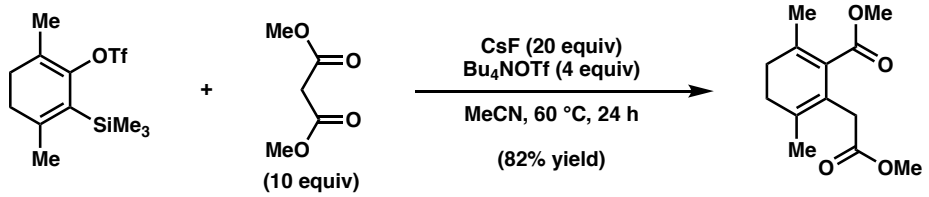
Adduct 4.72. Followed General Procedure 4.3. Purification by flash chromatography (7:3 hexanes:EtOAc → 3:7 hexanes:EtOAc) afforded adduct **4.72** (58% yield, average of two experiments) as a light yellow oil. **Adduct 4.72**: R_f = 0.25 (1:1 hexanes:EtOAc); ^{1}H NMR (600 MHz, CD_2Cl_2): δ 7.44 (s, 1H), 7.05 (s, 1H), 6.91 (s, 1H), 5.55 (q, J = 1.5, 1H), 2.35 (t, J = 9.6, 2H), 2.21 (t, J = 9.6, 2H), 1.81 (s, 3H), 1.65 (s, 3H); ^{13}C NMR (150 MHz, CD_2Cl_2): δ 136.7, 136.5,

128.1, 127.9, 125.9, 119.6, 119.3, 29.5, 27.9, 22.3, 17.5; IR (film): 3443, 3108, 2925, 2826, 1738 cm^{-1}; HRMS-APCI (*m/z*) $[M + H]^+$ calcd for $C_{11}H_{15}N_2^+$, 175.1230; found 175.1223.



4.42 ***4.64*** ***4.73***

Diene 4.73. Followed General Procedure 4.3. Purification by preparative thin layer chromatography (4:1 hexanes:acetone) afforded diene **4.73** (47% yield, average of two experiments) as a clear colorless oil. **Diene 4.73**: R_f = 0.21 (9:2:1 hexanes:CH_2Cl_2:Et_2O); ^{1}H NMR (500 MHz, $CDCl_3$): δ 4.31 (q, *J* = 7.3, 2H), 3.22 (s, 2H), 2.16 (app. s, 4H), 1.99 (s, 3H), 1.89 (s, 3H), 1.37 (t, *J* = 7.3, 3H); ^{13}C NMR (150 MHz, $CDCl_3$): δ 168.2, 140.8, 134.2, 126.4, 118.0, 117.4, 61.0, 30.1, 29.6, 21.3, 19.6, 18.0, 14.2; IR (film): 2982, 2930, 2248, 1716, 1252 cm^{-1}; HRMS-APCI (*m/z*) $[M + H]^+$ calcd for $C_{13}H_{18}NO_2^+$, 220.1332; found 220.1346.

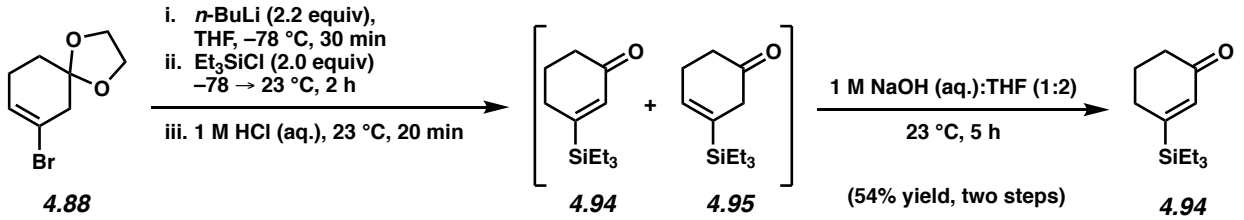


4.42 ***4.65*** ***4.74***

Diene 4.74. Followed a modified version of General Procedure 4.3 by filtering the crude reaction mixture over a basic alumina plug (5 cm) instead of Celite, eluting with EtOAc (10 mL). Purification by preparative thin layer chromatography (5:1 hexanes:EtOAc) afforded diene **4.74** (82% yield, average of two experiments) as a colorless oil. **Diene 4.74**: R_f 0.31 (5:1 hexanes:EtOAc); ^{1}H NMR (500 MHz, C_6D_6): δ 3.49 (s, 3H), 3.34 (s, 3H), 3.30 (s, 2H), 1.81 & 1.79 (app. overlapping s, 7H), 1.62 (s, 3H); ^{13}C NMR (125 MHz, C_6D_6): δ 171.4, 169.1, 137.2,

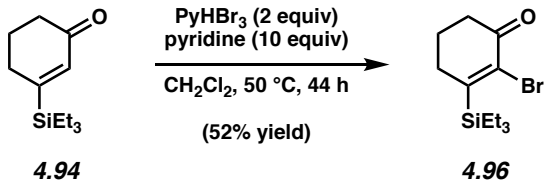
131.9, 128.8, 121.3, 51.3, 50.9, 34.9, 30.0, 29.8, 21.2, 19.7; IR (film): 2951, 2879, 1725, 1434, 1251 cm^{-1}; HRMS-APCI (*m/z*) $[M + H]^+$ calcd for $C_{13}H_{19}O_4^+$, 239.1278; found 239.1272.

4.9.3.5. Synthesis of Silyl Triflate 4.76



Enone 4.94. To a solution of bromide **4.88** (6.00 g, 27.4 mmol, 1.0 equiv) in THF (304 mL, 0.09 M) at –78 °C was added dropwise *n*-BuLi (2.4 M in hexanes, 25.1 mL, 60.3 mmol, 2.2 equiv) over 10 min to give a clear pink solution. The mixture was stirred at this temperature for 30 min, at which point it had become heterogeneous. To this solution was added triethylsilyl chloride (9.19 mL, 54.8 mmol, 2.0 equiv) dropwise over 5 min, and the resulting solution was stirred at –78 °C for 1 h. The cooling bath was then removed, and stirring was continued for an additional 1 h at 23 °C. After this time, the reaction was poured into a vigorously stirring 1 M HCl (aq.) solution (150 mL) and stirred at 23 °C for 20 min. The resulting solution was then diluted with Et_2O (100 mL), and the layers were separated. The aqueous layer was extracted with Et_2O (2 x 100 mL), and the organic layers were combined, dried over sodium sulfate, filtered, and concentrated under reduced pressure. The crude residue was purified by flash chromatography (23:2 → 9:1 EtOAc:hexanes) giving partial separation of isomers **4.94** and **4.95**. The mixed fractions were combined, concentrated, resuspended in THF (100 mL), and treated with 1 M NaOH (aq.) (50 mL). The resulting brown solution was stirred for 5 h then diluted with Et_2O (200 mL), and the layers were separated. The aqueous layer was extracted with Et_2O (2 x 200 mL), dried over sodium sulfate, filtered, and concentrated. The resulting crude oil was filtered through a silica plug eluting with 9:1 EtOAc:hexanes (300 mL), and the eluate was concentrated then combined with the pure **4.94**

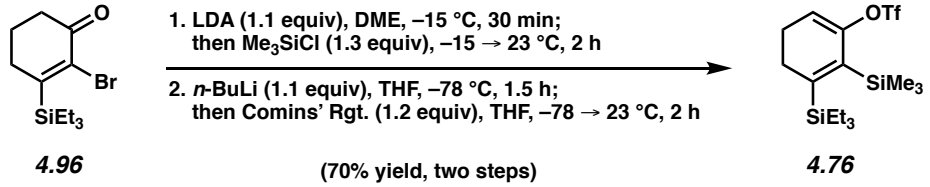
obtained from the initial column to give enone **4.94** (3.08 g, 27.4 mmol, 54% yield) as a clear colorless oil. **Enone 4.94**: R_f = 0.39 (9:2:1 hexanes:CH_2Cl_2:Et_2O); ^{1}H NMR (600 MHz, $CDCl_3$): δ 6.23 (t, *J* = 1.8, 1H), 2.43–2.38 (m, 2H), 2.33 (td, *J* = 5.6, 1.8, 2H), 1.99 (p, *J* = 6.1, 2H), 0.94 (t, *J* = 8.0, 9H), 0.67 (q, *J* = 8.0, 6H); ^{13}C NMR (150 MHz, $CDCl_3$): δ 198.5, 166.0, 137.1, 38.2, 28.6, 23.6, 7.3, 2.1; IR (film): 3072, 3036, 2954, 2876, 1671 cm^{-1}; HRMS-APCI (*m/z*) $[M + H]^+$ calcd for $C_{12}H_{23}OSi^+$, 211.1513; found 211.1507



4.94 *4.96*

Bromo enone 4.96. A round bottom flask equipped with a reflux condenser was charged with enone **4.94** (2.70 g, 12.8 mmol, 1.0 equiv), CH_2Cl_2 (128 mL, 0.10 M), and pyridine (10.4 mL, 128.3 mmol, 10.0 equiv) sequentially at 23 °C. Pyridinium perbromide (8.21 g, 25.7 mmol, 2.0 equiv) was then added rapidly in a single portion, and the reaction was heated at 50 °C with vigorous stirring for 44 h. After this time, the reaction was quenched with saturated sodium bicarbonate (50 mL), and the layers were separated. The aqueous layer was extracted with CH_2Cl_2 (2 x 50 mL), and the organic layers were combined then washed sequentially with saturated sodium thiosulfate (50 mL) and 0.5 M HCl (aq.) (50 mL). The organic layer was dried over sodium sulfate, filtered, and concentrated then purified by flash chromatography (19:1 → 9:1 petroleum ether:Et_2O) to give bromo enone **4.96** (1.91 g, 6.6 mmol, 52% yield) as a white solid. **Bromo enone 4.96**: Mp: 53 °C; R_f = 0.43 (9:2:1 hexanes:CH_2Cl_2:Et_2O); ^{1}H NMR (600 MHz, $CDCl_3$): δ 2.64–2.58 (m, 2H), 2.47 (t, *J* = 5.7, 2H), 2.04–1.98 (m, 2H), 0.97 (t, *J* = 7.5, 9H), 0.89–0.84 (m, 6H); ^{13}C NMR (150 MHz, $CDCl_3$): δ 189.9, 164.0, 132.9, 38.3, 34.0, 23.3, 7.5, 3.0; IR (film):

2954, 2875, 1739, 1691, 1549 cm^{-1}; HRMS-APCI (*m/z*) $[M + H]^+$ calcd for $C_{12}H_{22}OBrSi^+$, 289.0618; found 289.0620.

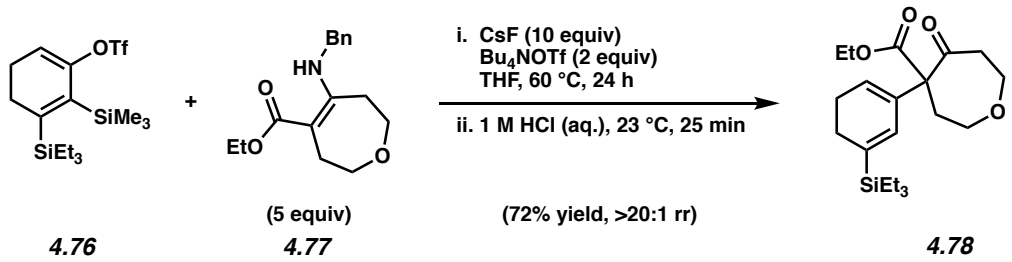


4.96 ***4.76***

Silyl triflate 4.76. To a solution of diisopropylamine (1.12 mL, 7.92 mmol, 1.2 equiv) in DME (13 mL) at –15 °C was added *n*-BuLi (2.1 M in hexanes, 3.4 mL, 7.3 mmol, 1.1 equiv) dropwise over 5 min. The resulting solution was stirred at this temperature for 25 min then treated dropwise with a solution of bromo enone **4.96** (1.91 g, 6.60 mmol, 1.0 equiv) in DME (13 mL) over 3 min. The resulting solution was stirred for 30 min then treated with trimethylsilyl chloride (1.04 mL, 8.58 mmol, 1.3 equiv) rapidly dropwise. The cooling bath was then removed, stirring of the reaction continued, and the reaction warmed to 23 °C over 2 h. After this time, the solvent was removed in vacuo, and the flask was evacuated and backfilled with nitrogen (3x). The heterogeneous yellow residue was suspended in pentane and filtered through Celite under a nitrogen atmosphere into a flame-dried round bottom flask (4 x 15 mL aliquots of pentane). The resulting eluate was concentrated under reduced pressure to give a yellow oil (2.39 g) which was dissolved in THF (44 mL, 0.15 M) and cooled to –78 °C. To this solution was added *n*-BuLi (2.4 M in hexanes, 3.03 mL, 1.1 equiv) dropwise over 12 min giving a solution which progressed from red to green to yellow over the course of addition. Stirring was continued for 1.5 h at this temperature before Comins' Reagent (3.11 g, 7.92 mmol, 1.2 equiv) in THF (13 mL) was added rapidly dropwise. The resulting pink solution was stirred at –78 °C for 15 min, then the cooling bath was removed and the reaction was stirred and gradually warmed to 23 °C over 2 h. The reaction was then quenched with water (50 mL) and diluted with hexanes (50 mL). The layers

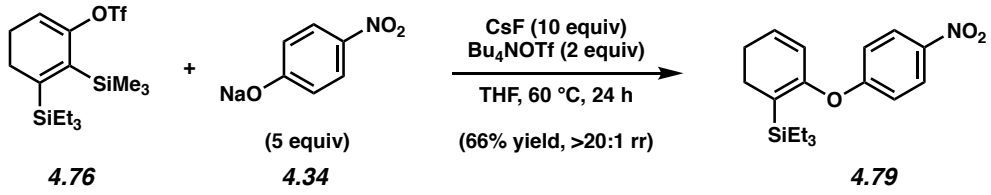
were separated, and the aqueous layer was extracted with hexanes (2 x 50 mL). The organic layers were combined, dried over magnesium sulfate, filtered, and concentrated under reduced pressure. The crude residue was purified by flash chromatography on basic alumina (petroleum ether) to provide silyl triflate **4.76** (1.94 g, 4.68 mmol, 70% yield, two steps) as a yellow oil which was stored in a glovebox. **Silyl triflate 4.76**: R_f = 0.65 (19:1 hexanes:EtOAc); ^{1}H NMR (600 MHz, C_6D_6): δ 5.64 (t, *J* = 5.4, 1H), 1.84–1.76 (m, 2H), 1.57–1.48 (m, 2H), 0.89 (t, *J* = 7.9, 9H), 0.64 (q, *J* = 7.9, 6H), 0.33 (s, 9H); ^{13}C NMR (150 MHz, C_6D_6): δ 158.5, 151.9, 144.9, 118.9 (q, *J* = 319), 114.4, 29.7, 21.6, 7.5, 4.0, 1.6; ^{19}F NMR (376 MHz, C_6D_6) –73.15 (s, 3F); IR (film): 2956, 2878, 1418, 1203, 1141 cm^{-1}; HRMS-APCI (*m/z*) [M – OTf]$^+$ calcd for $C_{15}H_{29}Si_2^+$, 265.1802; found 265.1785.

4.9.3.6 Trapping Reactions of Silyl Triene 4.75



Ketoester 4.78. Inside a glove box, a dram vial containing silyl triflate **4.76** (100.0 mg, 0.241 mmol, 1.0 equiv) was charged sequentially with enamine **4.77** (332.0 mg, 1.21 mmol, 5 equiv), Bu_4NOTf (188.9 mg, 0.482 mmol, 2.0 equiv) and THF (2.4 mL, 0.1 M). CsF (366.4 mg, 2.41 mmol, 10 equiv) was then added in a single portion, and the vial was sealed, brought out of the glovebox, and stirred at 60 °C for 24 h. After this time, the reaction was diluted with Et_2O (5 mL) and filtered through a Celite plug eluting with Et_2O (5 mL). The eluate was concentrated, and the resulting residue was resuspended in THF (3 mL) then treated with 1 M HCl (aq.) (3 mL). The mixture was stirred vigorously for 25 min, then diluted with water (5 mL) and Et_2O (5 mL). The

layers were separated, and the aqueous layer was extracted with Et_2O (2 x 5 mL). The organic layers were combined, dried over sodium sulfate, filtered, and concentrated under reduced pressure. The crude residue was purified by flash chromatography (benzene → 97:3 benzene:Et_2O) to give ketoester **4.78** (65.5 mg, 0.173 mmol, 72% yield) as a clear colorless oil. **Ketoester 4.78**: R_f = 0.55 (9:1 benzene:Et_2O); ^{1}H NMR (600 MHz, $CDCl_3$): δ 5.98 (q, *J* = 1.6, 1H), 5.66 (td, *J* = 4.5, 2.0, 1H), 4.21 (q, *J* = 7.2, 2H), 3.99 (ddd, *J* = 13.5, 7.2, 1.7, 1H), 3.89 (ddd, *J* = 12.3, 6.5, 3.6, 1H), 3.75 (ddd, *J* = 13.5, 8.3, 1.7, 1H), 3.63 (ddd, *J* = 12.3, 9.1, 2.8, 1H), 2.90 (ddd, *J* = 14.3, 9.1, 3.7, 1H), 2.71 (ddd, *J* = 14.3, 6.5, 2.8, 1H), 2.45 (ddd, *J* = 15.5, 7.2, 1.6, 1H), 2.19–1.99 (m, 5H), 1.25 (t, *J* = 7.2, 3H), 0.92 (t, *J* = 8.0, 9H), 0.59 (q, *J* = 8.0, 6H); ^{13}C NMR (150 MHz, $CDCl_3$): δ 206.5, 171.5, 138.1, 134.2, 133.3, 125.0, 68.7, 67.1, 66.8, 61.5, 46.2, 33.6, 24.5, 22.6, 14.0, 7.4, 2.5; IR (film): 2953, 2874, 1736, 1464, 1231 cm^{-1}; HRMS-APCI (*m/z*) $[M + H]^+$ calcd for $C_{21}H_{35}O_4Si^+$, 379.2299; found 379.2287.

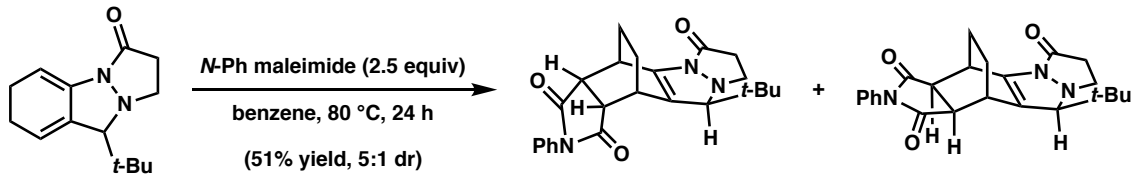


4.76 ***4.34*** ***4.79***

Adduct 4.79. Inside a glovebox, a dram vial containing phenoxide **4.34** (60.6 mg, 0.376 mmol, 5.0 equiv) was sequentially charged with CsF (114.0 mg, 0.752 mmol, 10 equiv) and Bu_4NOTf (58.9 mg, 0.150 mmol, 2.0 equiv). To this vial was then added a solution of silyl triflate **4.76** (31.2 mg, 75.2 μmol, 1.0 equiv) in THF (752 μL, 0.1 M). The vial was sealed, brought out of the glovebox, and stirred at 60 °C for 24 h. After this time, the reaction was diluted with Et_2O (5 mL) and filtered through a Celite plug eluting with Et_2O (5 mL). The eluate was concentrated, and the resulting residue was purified by flash chromatography (9:1 hexanes:CH_2Cl_2 → 4:1 hexanes:CH_2Cl_2) to afford adduct **4.79** (16.5 mg, 49.8 μmol, 66% yield) as a clear colorless oil.

Adduct 4.79: R_f = 0.44 (19:1 hexanes:EtOAc); ^{1}H NMR (600 MHz, C_6D_6): δ 7.84–7.79 (m, 2H), 6.56–6.51 (m, 2H), 5.76 (dt, *J* = 9.8, 4.4, 1H), 5.42 (dt, *J* = 9.8, 2.0, 1H), 2.11–2.05 (m, 2H), 1.85 (app. tdd, *J* = 9.4, 4.3, 1.9, 2H), 0.96 (t, *J* = 8.0, 9H), 0.62 (q, *J* = 8.0, 6H); ^{13}C NMR (150 MHz, C_6D_6): δ 161.8, 154.7, 142.8, 132.6, 126.0, 123.3, 118.4, 116.2, 25.4, 22.6, 7.8, 3.7; IR (film): 2951, 2874, 1582, 1516, 1340 cm^{-1}; HRMS-APCI (*m/z*) [M + H]$^+$ calcd for $C_{18}H_{26}SiNO_3^+$, 332.1677; found 332.1678.

4.9.3.7 Synthetic Elaboration of Triene Trapping Products



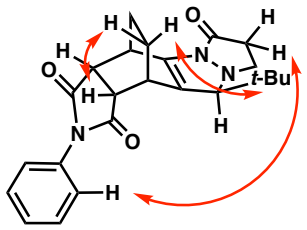
4.35 *4.81* *4.97*

4.81 and **4.97.** A 1-dram vial was charged with diene **4.35** (15.0 mg, 0.065 mmol, 1.0 equiv), *N*-phenyl maleimide (28.0 mg, 0.16 mmol, 2.5 equiv), and benzene (0.646 mL, 0.1 M). The vial was sealed with a Teflon-lined cap and stirred at 80 °C for 24 h. After this time, the reaction was cooled to 23 °C and concentrated under reduced pressure. The crude product was purified by preparative thin layer chromatography (2:1 hexanes:EtOAc) to afford a mixture of major diastereomer **4.81** and minor diastereomer **4.97** (13.3 mg, 0.033 mmol, 51% combined yield, 5:1 dr determined by ^{1}H NMR analysis of the crude reaction mixture) as a waxy-white solid. Analytical samples were obtained by preparative thin layer chromatography (1:1:1 hexanes:CH_2Cl_2:Et_2O) to provide major diastereomer **4.81** as a white crystalline solid and minor diastereomer **4.97** as a white powder. Crystals of **4.81** suitable for X-ray diffraction studies were obtained by recrystallization from Et_2O.

Cycloadduct 4.81 (major diastereomer, endo product): Mp: 188–190 °C; R_f 0.16 (1:1:1 hexanes:CH_2Cl_2:Et_2O); ^{1}H NMR (500 MHz, C_6D_6): δ 7.62–7.56 (m, 2H), 7.15–7.11 (overlapped with residual solvent peak, 2H), 6.99 (t, *J* = 7.4, 1H), 4.24–4.20 (m, 1H), 3.28 (s, 1H), 3.19–3.15

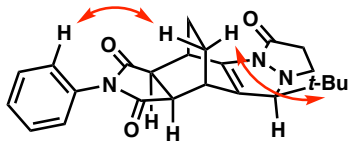
(m, 1H), 2.69 (t, J = 8.2, 1H), 2.38 (ddd, J = 15.5, 13.9, 7.8, 1H), 2.32–2.26 (m, 2H), 2.17 (ddd, J = 14.7, 8.2, 6.5, 1H), 2.01 (dd, J = 15.7, 6.4, 1H), 1.09–1.00 (m, 2H), 0.99–0.88 (m, 2H), 0.79 (s, 9H); ^{13}C NMR (125 MHz, C_6D_6, 19 of 20 signals observed): δ 176.1, 175.2, 166.2, 137.2, 132.9, 128.9, 125.7, 119.4, 82.8, 56.7, 46.6, 44.2, 35.8, 34.9, 32.8, 31.3, 26.5, 25.5, 23.0; IR (film): 2955, 2871, 1716, 1376, 1180 cm^{-1}; HRMS-APCI (*m/z*) $[M + H]^+$ calcd for $C_{24}H_{28}N_3O_3^+$, 406.2125; found 406.2126. **Cycloadduct 4.97** (minor diastereomer, exo product): Mp: 144–146 °C; R_f 0.08 (1:1:1 hexanes:CH_2Cl_2:Et_2O); ^{1}H NMR (600 MHz, $(CD_3)_2CO$): δ 7.53–7.47 (m, 2H), 7.43 (tt, J = 7.5, 1.2, 1H), 7.33–7.30 (m, 2H), 3.95 (q, J = 2.8, 1H), 3.85 (s, 1H), 3.63 (t, J = 8.2, 1H), 3.31–3.28 (m, 1H), 3.20–3.13 (m, 2H), 3.01 (ddd, J = 14.0, 8.6, 6.7, 1H), 2.91–2.84 (overlapped with H_2O peak, 1H), 2.40 (dd, J = 15.7, 6.7, 1H), 1.91–1.79 (m, 2H), 1.60–1.53 (m, 1H), 1.52–1.45 (m, 1H), 0.97 (s, 9H); ^{13}C NMR (125 MHz, $(CD_3)_2CO$): δ 177.6, 177.3, 168.3, 141.3, 133.8, 129.8, 129.3, 127.84, 127.76, 123.0, 83.3, 57.5, 47.8, 46.7, 36.5, 35.2, 34.2, 27.0, 22.5, 22.0; IR (film): 2925, 2856, 1708, 1379, 1180 cm^{-1}; HRMS-APCI (*m/z*) $[M + H]^+$ calcd for $C_{24}H_{28}N_3O_3^+$, 406.2125; found 406.2125.

The structure of **4.81** was verified by single crystal X-ray diffraction and 2D-NOESY, as the following interactions were observed:



4.81

The structure of **4.97** was verified by 2D-NOESY, as the following interactions were observed:



4.97

Crystal Structure Analysis for 4.81

Diffraction intensities were collected at 100 K on a Bruker Smart ApexII CCD diffractometer with CuKα radiation, 1.54178 Å. Absorption corrections were applied by SADABS.[67] All calculations were performed by the SHELXL-2014 packages.[68] Deposition Number 2239633 contains the supplementary crystallographic data for compound **4.81**. These data are provided free of charge by the joint Cambridge Crystallographic Data Centre and Fachinformationszentrum Karlsruhe Access Structures service www.ccdc.cam.ac.uk/structures.

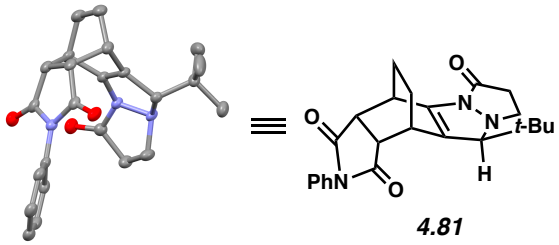
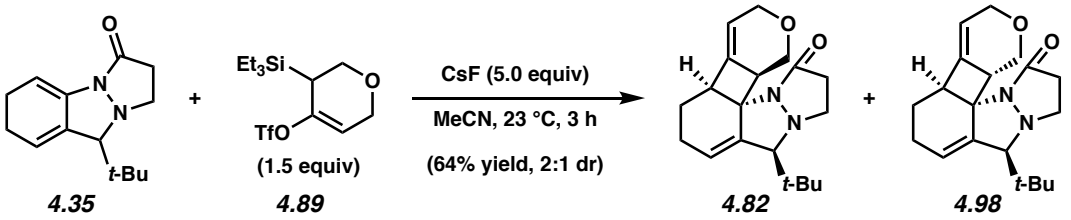


Figure 4.7. ORTEP representation of X-ray crystallographic structure **4.81**. (CCDC Registry # 2239633).

Table 4.2. Crystal data and structure refinement for compound **4.81**.

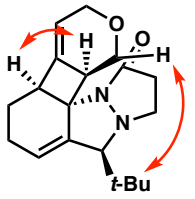
Identification code	cu_garg2301sa_a	
Empirical formula	C24 H27 N3 O3	
Formula weight	405.48	
Temperature	100(2) K	
Wavelength	1.54178 Å	
Crystal system	Monoclinic	
Space group	$P2_1/C$	
Unit cell dimensions	a = 11.7285(6) Å	a = 90°
	b = 18.1222(10) Å	b = 90.648(3)°
	c = 9.9897(6) Å	g = 90°
Volume	2123.1(2) $Å^3$	
Z	4	
Density (calculated)	1.269 Mg/m^3	
Absorption coefficient	0.679 mm^{-1}	
F(000)	864	
Crystal size	0.250 x 0.200 x 0.040 mm^3	
Theta range for data collection	3.769 to 70.042 °	
Index ranges	–12<=h<=14, –17<=k<=21, –10<=I<=11	
Reflections collected	16613	
Independent reflections	3912 [R(int) = 0.0719]	
Completeness to theta = 67.679°	99.3%	
Absorption correction	Semi-empirical from equivalents	
Max. and min. transmission	0.75 and 0.64	
Refinement method	Full-matrix least-squares on F^2	
Data / restraints / parameters	3912 / 0 / 274	
Goodness-of-fit on F^2	0.888	
Final R indices [I>2sigma(I)]	R1 = 0.0413, wR2 = 0.0864	
R indices (all data)	R1 = 0.0654, wR2 = 0.0902	
Extinction coefficient	n/a	
Largest diff. peak and hole	0.189 and –0.225 e.$Å^{-3}$	



4.82 and **4.98.** A 1-dram vial was charged with diene **4.35** (15.0 mg, 0.065 mmol, 1.0 equiv) and silyl triflate **4.89** (34.0 mg, 0.097 mmol, 1.5 equiv) and taken into a glovebox where MeCN (0.646 mL, 0.1 M) was added followed by CsF (49.3 mg, 0.097 mmol, 5.0 equiv). The vial was sealed with a Teflon-lined cap, removed from the glovebox, and stirred at 23 °C for 3 h. After this time, the reaction was filtered through a silica gel plug eluting with EtOAc (8 mL), and the eluate was concentrated under reduced pressure. The crude product was purified by preparative thin layer chromatography (2:1 hexanes:EtOAc) to afford a mixture of major diastereomer **4.82** and minor diastereomer **4.98** (12.9 mg, 0.041 mmol, 64% combined yield, 2:1 dr determined by ^{1}H NMR analysis of the crude mixture) as a white solid. Analytical samples of **4.82** and **4.98** were obtained by preparative thin layer chromatography (3:1 benzene:acetonitrile) to provide major diastereomer **4.82** as a colorless oil and minor diastereomer **4.98** as a white solid. **Cycloadduct 4.82** (major diastereomer): R_f 0.29 (3:1 benzene:MeCN); ^{1}H NMR (600 MHz, C_6D_6): δ 5.78 (br s, 1H), 5.61–5.56 (m, 1H), 4.96–4.92 (m, 1H), 4.25–4.19 (m, 1H), 4.05 (dd, *J* = 9.6, 6.3, 1H), 3.92 (dq, 16.2, 3.1, 1H), 3.85–3.79 (m, 1H), 2.97 (t, *J* = 9.7, 1H), 2.93 (t, *J* = 8.7, 1H), 2.51–2.48 (m, 1H), 2.37 (ddd, *J* = 15.8, 12.7, 8.6, 1H), 2.17 (dd, *J* = 15.8, 8.0, 1H), 2.08 (dt, *J* = 12.6, 8.5, 1H), 1.97–1.89 (m, 1H), 1.69–1.62 (m, 1H), 1.55–1.50 (m, 1H), 1.00 (tt, *J* = 13.1, 4.7, 1H), 0.76 (s, 9H); ^{13}C NMR (150 MHz, C_6D_6): δ 163.7, 141.4, 136.3, 126.9, 114.7, 79.1, 65.5, 64.3, 61.2, 54.6, 52.2, 45.5, 35.9, 34.8, 27.5, 21.7, 21.5; IR (film): 2926, 2856, 1679, 1417, 1100 cm^{-1}; HRMS-APCI (*m/z*) [M + H]$^+$ calcd for $C_{19}H_{27}N_2O_2^+$, 315.2067; found 315.2070. **Cycloadduct 4.98** (minor diastereomer): Mp: 161–163 °C; R_f 0.37 (3:1 benzene:MeCN); ^{1}H NMR (600 MHz, C_6D_6): δ 5.56–5.52 (m, 1H),

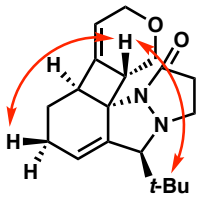
5.51 (app. br s, 1H), 5.05–4.98 (m, 1H), 4.34–4.27 (m, 1H), 4.26–4.17 (m, 2H), 3.60 (t, J = 9.6, 1H), 3.03–2.97 (m, 1H), 2.92 (t, J = 8.3, 1H), 2.55–2.51 (m, 1H), 2.37 (ddd, J = 17.8, 15.2, 8.7, 1H), 2.15–2.08 (m, 2H), 1.93–1.79 (m, 2H), 1.70 (dq, J = 13.0, 3.6, 1H), 1.25–1.17 (m, 1H), 0.76 (s, 9H); ^{13}C NMR (125 MHz, C_6D_6): δ 164.3, 145.2, 138.1, 122.9, 117.0, 78.3, 66.0, 63.9, 61.9, 55.2, 53.4, 45.0, 35.5, 34.9, 26.6, 23.8, 22.8; IR (film): 2956, 2860, 1684, 1417, 1095 cm^{-1}; HRMS-APCI (*m/z*) $[M + H]^+$ calcd for $C_{19}H_{27}N_2O_2^+$, 315.2067; found 315.2068.

The structure of **4.82** was verified by 2D-NOESY, as the following interactions were observed:

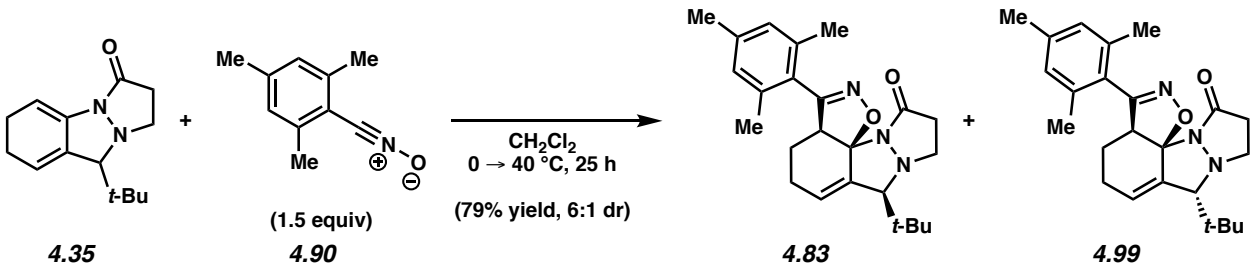


4.82

The structure of **4.98** was verified by 2D-NOESY, as the following interactions were observed:



4.98



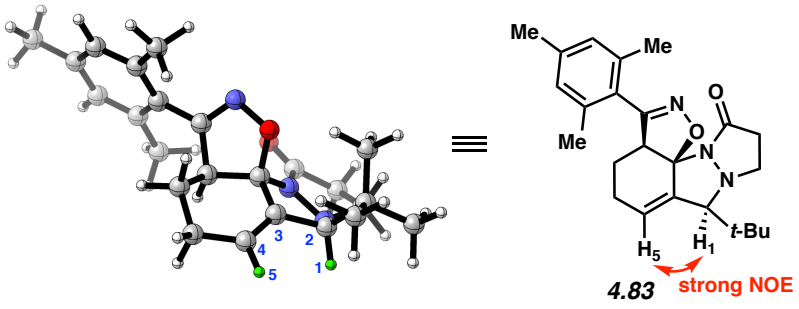
4.83 and **4.99.** A 1-dram vial was charged with nitrile oxide **4.90** (16.2 mg, 0.097 mmol, 1.5 equiv) and CH_2Cl_2 (0.646 mL, 0.1 M) and cooled to 0 °C. Diene **4.35** (15.0 mg, 0.065 mmol, 1.0 equiv) was then added in one portion, and the reaction was stirred at 0 °C for 1 h. After 1 h, the reaction was warmed to 40 °C and stirred for an additional 24 h at this temperature. After this time, the reaction was cooled to 23 °C and concentrated under reduced pressure. The crude product was purified by preparative thin layer chromatography (2:1 hexanes:EtOAc) to afford an inseparable mixture of major diastereomer **4.83** and minor diastereomer **4.99** (20.0 mg, 0.051 mmol, 79% combined yield, 6:1 dr determined by ^{1}H NMR analysis of the crude mixture) as a waxy-amorphous solid. **Cycloadducts 4.83** and **4.99**: Mp: 187–189 °C; R_f = 0.50 (2:1 hexanes:EtOAc); ^{1}H NMR (600 MHz, C_6D_6, major diastereomer **4.83**): δ 6.74 (s, 2H), 5.70 (ddd, J = 7.5, 2.9, 2.2, 1H), 5.38 (dd, J = 8.3, 2.3, 1H), 3.01 (td, J = 8.5, 1.8, 1H), 2.67–2.64 (m, 1H), 2.58 (s, 6H), 2.29 (ddd, J = 15.6, 12.4, 8.4, 1H), 2.21–2.14 (m, 1H), 2.08 (s, 3H), 2.08–2.02 (m, 1H), 1.96–1.87 (m, 1H), 1.62–1.55 (m, 1H), 1.50–1.43 (m, 1H), 1.20–1.11 (m, 1H), 1.03 (s, 9H); ^{13}C NMR (125 MHz, C_6D_6, mixture of **4.83** and **4.99**, 35 of 38 signals observed): δ 170.4, 165.1, 159.2, 157.5, 140.2, 139.8, 138.74, 138.65, 138.45, 138.42, 129.54, 129.46, 126.3, 126.1, 93.8, 91.9, 77.4, 75.4, 59.4, 54.8, 51.5, 47.1, 36.5, 35.7, 35.4, 33.6, 27.5, 27.2, 23.3, 22.6, 22.0, 21.4, 21.3, 21.2, 21.0; IR (film): 2956, 2865, 1694, 1392, 1095 cm^{-1}; HRMS-APCI (*m/z*) $[M + H]^+$ calcd for $C_{24}H_{32}N_3O_2^+$, 394.2489; found 394.2489.

The structure of **4.83** was verified by comparison of computed and observed $^4J_{HH}$ coupling constants as well as 2D-NOESY experiments. $^4J_{HH}$ coupling constants were calculated from the computationally derived H1-C2-C3-C4 dihedral angles (geometry optimized at the ωB97XD/6-31G(d) level of theory) using the modified Karplus equation in Equation 4.1. These calculated $^4J_{HH}$ coupling constants were then compared to the observed $^4J_{HH}$ coupling constants for each diastereomer (**4.83** and **4.99**), supporting **4.83** as bearing a syn relationship between the isooxazoline and *tert*-butyl substituent, and **4.99** bearing a trans relationship.

$$^4J = 1.3\cos^2(\phi) - 2.6\sin^2(\phi)$$

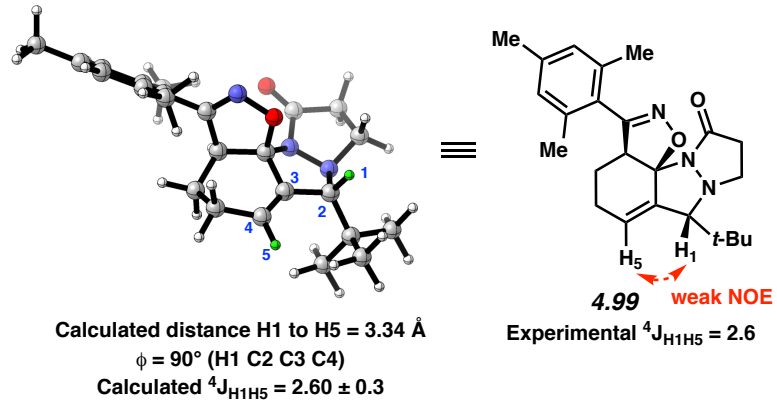
Equation 4.1. Modified Karplus equation.[69]

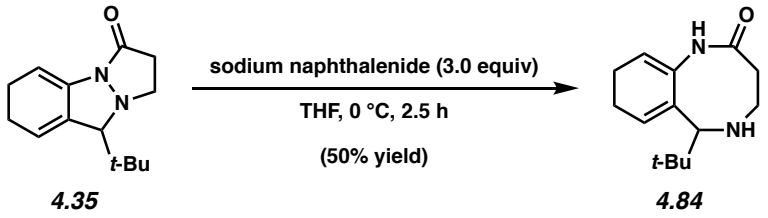
These assignments were further supported by comparison of H5–H1 NOESY signal strength to the calculated H5–H1 distances in the optimized geometries. **4.83** shows a strong H5–H1 NOE with a calculated H5–H1 distance of 2.45 Å whereas **4.99** shows a weak H5–H1 and a substantially larger H5–H1 distance of 3.34 Å.



Calculated distance H1 to H5 = 2.45 Å
ϕ = 17° (H1 C2 C3 C4)
Calculated $^4J_{H1H5}$ = 0.99 ± 0.3

Experimental $^4J_{H1H5}$ = 1.8

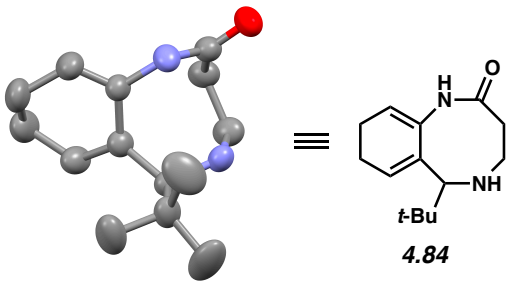




Diene 4.84. To a solution of diene **4.35** (15.0 mg, 0.065 mmol, 1.0 equiv) in THF (0.646 mL, 0.1 M) at 0 °C was added sodium naphthalenide[70] (2.0 M in THF, 97 µL, 0.194 mmol, 3.0 equiv) slowly down the side of the vial. The reaction was allowed to stir at this temperature for 2.5 h. After 2.5 h the reaction was quenched with MeOH (3.0 mL) and concentrated under reduced pressure. The crude product was purified by flash chromatography (benzene → 1:1 benzene:EtOAc → EtOAc) to afford diene **4.84** (7.6 mg, 0.032 mmol, 50% yield) as a white solid. Crystals suitable for X-ray diffraction studies were obtained by recrystallization from a mixture of CH_2Cl_2 and cyclohexane. **Diene 4.84**: Mp: 186–187 °C; R_f 0.22 (EtOAc); ^{1}H NMR (500 MHz, C_6D_6): δ 8.38 (s, 1H), 5.51–5.41 (m, 1H), 5.24–5.14 (m, 1H), 3.22–3.11 (m, 1H), 2.85 (s, 1H), 2.75–2.58 (m, 2H), 2.12 (dd, *J* = 10.4, 8.5, 1H), 1.75–1.56 (m, 5H), 0.90 (s, 9H); ^{13}C NMR (150 MHz, CD_3OD): δ 176.7, 137.5, 136.6, 131.7, 118.8, 76.2, 42.9, 36.2, 35.6, 28.3, 23.9, 22.9; IR (film): 3353, 3045, 2930, 2817, 1669 cm^{-1}; HRMS-APCI (*m/z*) $[M + H]^+$ calcd for $C_{14}H_{23}N_2O^+$, 235.1805; found 235.1800.

Crystal Structure Analysis for 4.84

Data collection and analysis were performed as detailed above for compound **4.81**. Deposition Number 2238912 contains the supplementary crystallographic data for compound **4.84**. These data are provided free of charge by the joint Cambridge Crystallographic Data Centre and Fachinformationszentrum Karlsruhe Access Structures service www.ccdc.cam.ac.uk/structures.



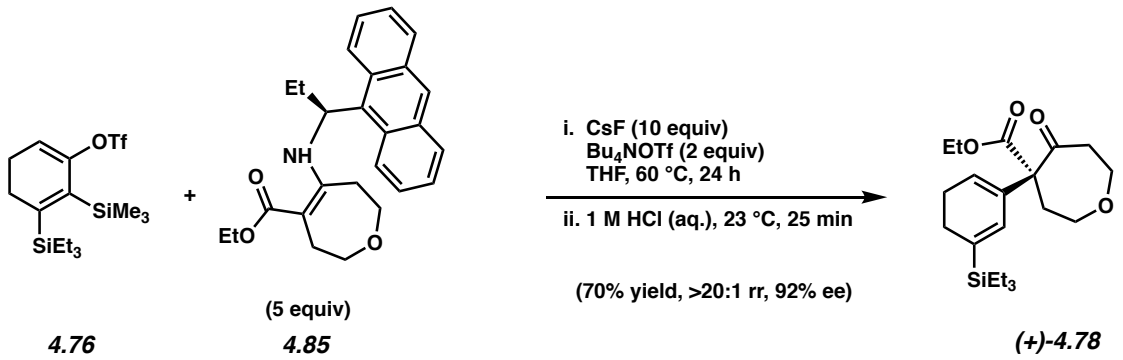
4.84

Figure 4.8. ORTEP representation of X-ray crystallographic structure **4.84**. (CCDC Registry # 2238912).

Table 4.3. Crystal data and structure refinement for compound **4.84**.

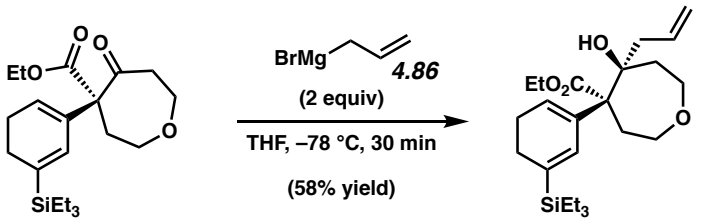
Identification code	cu_garg2207s	
Empirical formula	C14 H22 N2 O	
Formula weight	234.33	
Temperature	293(2) K	
Wavelength	1.54178 Å	
Crystal system	Triclinic	
Space group	P–1	
Unit cell dimensions	a = 7.4706(10) Å	a = 75.818(10)°
	b = 7.7662(11) Å	b = 82.253(10)°
	c = 12.6574(18) Å	g = 78.737(10)°
Volume	695.34(17) Å^3	
Z	2	
Density (calculated)	1.119 Mg/m^3	
Absorption coefficient	0.553 mm^{-1}	
F(000)	256	
Crystal size	0.30 x 0.20 x 0.06 mm^3	
Theta range for data collection	3.617 to 69.270 °	
Index ranges	–9<=h<=9, –9<=k<=7, –15<=I<=14	
Reflections collected	11182	
Independent reflections	2460 [R(int) = 0.0723]	
Completeness to theta = 67.679°	96.1%	
Absorption correction	Semi-empirical from equivalents	
Max. and min. transmission	0.75 and 0.55	
Refinement method	Full-matrix least-squares on F^2	
Data / restraints / parameters	2460 / 0 / 163	
Goodness-of-fit on F^2	1.065	

Final R indices [I>2sigma(I)]	R1 = 0.0684, wR2 = 0.1587
R indices (all data)	R1 = 0.1003, wR2 = 0.1895
Extinction coefficient	n/a
Largest diff. peak and hole	0.228 and –0.190 e.Å^{-3}



4.76 *4.85* *(+)-4.78*

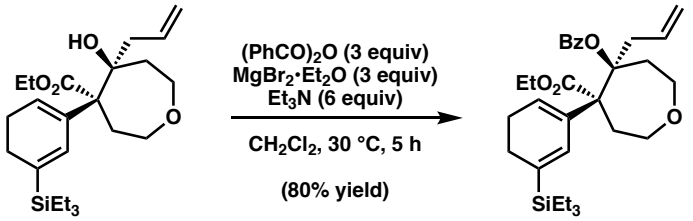
Ketoester (+)-4.78. Prepared according to the procedure above for **(±)-4.78** using silyl triflate **4.76** (50.0 mg, 0.121 mmol, 1.0 equiv) and enantioenriched enamine **4.85** (243 mg, 0.603 mmol, 5.0 equiv) to generate ketoester **(+)-4.78** (31.8 mg, 84.0 μmol, 70% yield). Absolute stereochemistry was assigned by analogy to the literature.[62] Spectral data matched those reported above for **(±)-4.78**. **Ketoester (+)-4.78**: $[\alpha]^{23.1}_{D}$ +91° (*c* = 1.00, CH_2Cl_2).



(+)-4.78 *(–)-4.87*

Alcohol (–)-4.87. To a solution of ketoester **(+)-4.78** (17.0 mg, 44.9 μmol, 1.0 equiv) in THF (449 μL, 0.10 M) at –78 °C was added dropwise a freshly prepared solution of allyl Grignard **4.86**[71] (1.0 M in Et_2O, 89.8 μL, 2.0 equiv) over 1 min. The resulting solution was stirred at this temperature for 30 min then quenched with saturated ammonium chloride (5 mL) and diluted with Et_2O (5 mL). The layers were separated, and the aqueous layer was extracted with Et_2O (2 x 5 mL). The organic layers were combined, dried over sodium sulfate, filtered, and concentrated under reduced pressure. The resulting residue was purified by preparative thin layer chromatography (plate pre-

treated by developing in 9:1 hexanes:Et_2O with 2% Et_3N, then the compound was loaded and eluted with the same solvent) to afford alcohol **(–)-4.87** (10.9 mg, 25.9 μmol, 58% yield) as a clear colorless oil. The relative stereochemistry was assigned by conversion to benzoate **4.100** (see below). **Alcohol (–)-4.87**: R_f = 0.45 (19:1 benzene:MeCN); ^{1}H NMR (600 MHz, $CDCl_3$): 6.20 (s, 1H), 5.94–5.86 (m, 1H), 5.72–5.66 (m, 1H), 5.10–5.05 (m, 1H), 5.02 (tdd, *J* = 17.0, 2.1, 1.2, 1H), 4.25 (dq, *J* = 10.8, 7.1, 1H), 4.15 (dq, *J* = 10.8, 7.1, 1H), 3.79 (td, *J* = 11.4, 5.6, 1H), 3.73 (ddd, *J* = 11.5, 7.3, 1.6, 1H), 3.70–3.62 (m, 2H), 2.99 (ddd, *J* = 14.7, 11.1, 7.3, 1H), 2.91 (dd, *J* = 14.2, 8.1, 1H), 2.30 (ddd, *J* = 14.8, 8.7, 6.5, 1H), 2.20–2.14 (m, 1H), 2.13–2.17 (m, 2H), 2.07–1.94 (m, 3H), 1.88 (ddd, *J* = 14.5, 5.5, 1.7, 1H), 1.71 (dt, *J* = 15.0, 3.0, 1H), 1.28 (t, *J* = 7.1, 3H), 0.92 (t, *J* = 8.0, 9H), 0.59 (q, *J* = 8.0, 6H); ^{13}C NMR (150 MHz, $CDCl_3$, 19 of 20 signals observed): δ 173.5, 137.6, 136.8, 135.1, 124.4, 118.1, 75.4, 66.6, 64.6, 60.4, 60.1, 44.6, 38.5, 31.8, 24.5, 22.5, 14.1, 7.4, 2.5; IR (film): 3464, 3073, 2951, 2874, 1736 cm^{-1}; HRMS-APCI (*m/z*) $[M + H]^+$ calcd for $C_{24}H_{41}O_4Si^+$, 421.2769; found 421.2766.

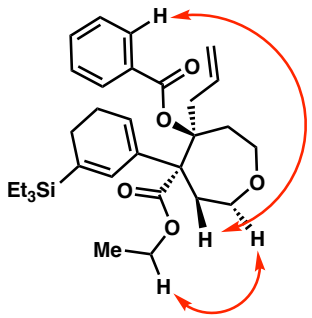


(–)-4.87 *(–)-4.100*

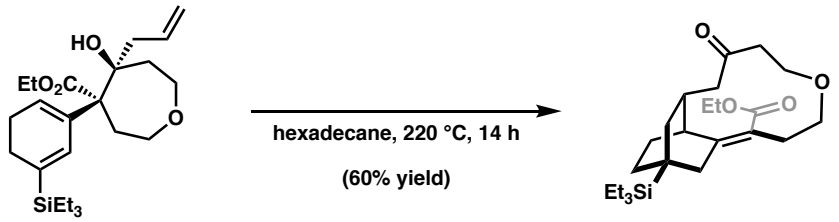
Benzoate (–)-4.100. In a glovebox, a 1-dram vial containing alcohol **(–)-4.87** (2.2 mg, 5.2 μmol, 1.0 equiv) was treated sequentially with CH_2Cl_2 (150 μL, 0.03 M), Et_3N (4.4 μL, 31 μmol, 6.0 equiv), $(PhCO)_2O$ (3.5 mg, 5.2 μmol, 3.0 equiv), and $MgBr_2$•Et_2O (4.1 mg, 16 μmol, 3.0 equiv). The vial was sealed, brought out of the glovebox, and stirred at 30 °C for 5 h. After this time, the reaction was diluted with saturated sodium bicarbonate (5 mL) and Et_2O (5 mL). The layers were separated, and the aqueous layer was extracted with Et_2O (2 x 5 mL). The organic layers were

combined, dried over sodium sulfate, filtered, and concentrated under reduced pressure. The residue was purified by preparative thin layer chromatography (9:2:1 hexanes:CH_2Cl_2:Et_2O) to give benzoate **(–)-4.100** (2.2 mg, 4.2 μmol, 80% yield) as a clear colorless oil. **Benzoate (–)-4.100**: R_f = 0.24 (97:3 benzene:Et_2O); ^{1}H NMR (400 MHz, $CDCl_3$): δ 8.03–7.94 (m, 2H), 7.57 (tt, *J* = 7.5, 1.3, 1H), 7.50–7.42 (m, 2H), 6.33–6.24 (m, 1H), 5.88–5.74 (m, 1H), 5.74–5.66 (m, 1H), 5.03–4.93 (m, 1H), 4.87 (tdd, *J* = 10.3, 2.4, 1.2, 1H), 4.29 (dq, *J* = 10.8, 7.1, 1H), 4.90–4.84 (m, 1H), 3.95 (ddd, *J* = 11.4, 9.9, 7.3, 1H), 3.79 (dt, *J* = 13.0, 3.7, 1H), 3.72 (ddd, *J* = 11.4, 8.1, 1.8, 1H), 3.49–3.39 (m, 1H), 3.22–3.17 (m, 2H), 3.12 (ddd, *J* = 14.8, 9.6, 8.2, 1H), 2.96 (ddd, *J* = 16.0, 3.0, 1.4, 1H), 2.59 (ddd, *J* = 16.0, 12.0, 3.9, 1H), 2.21–1.92 (m, 5H), 1.30 (t, *J* = 7.2, 3H), 0.82 (t, *J* = 8.0, 9H), 0.56–0.39 (m, 6H); ^{13}C NMR (100 MHz, C_6D_6): 172.9, 165.0, 136.9, 136.6, 135.2, 134.9, 132.8, 132.2, 129.4, 128.6, 126.0, 117.2, 89.8, 66.8, 65.5, 60.7, 60.3, 42.6, 36.9, 32.1, 24.1, 22.9, 14.2, 7.5, 2.6; IR (film): 3076, 2929, 2873, 1729, 1696 cm^{-1}; HRMS-APCI (*m/z*) $[M + H]^+$ calcd for $C_{31}H_{45}O_5Si^+$, 525.3031; found 525.3014. $[\alpha]^{21.6}_D$ –62° (*c* = 1.00, CH_2Cl_2).

The structure of **(–)-4.100** was verified by 2D-NOESY, as the following interactions were observed:



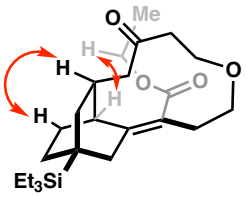
(–)-4.100



(–)-4.87 *(+)-4.19*

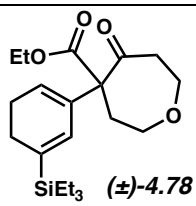
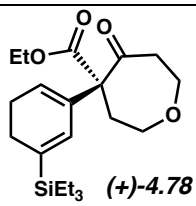
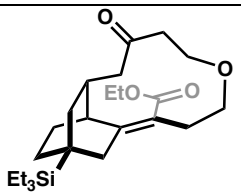
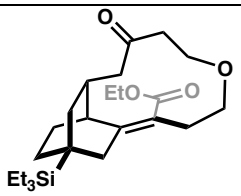
Product (+)-4.19. A flask equipped with a Teflon stopcock was charged with a solution of alcohol **(–)-4.87** (7.0 mg, 17 μmol, 1.0 equiv) in hexadecane (1.7 mL, 0.01 M). The solution was sparged vigorously with nitrogen for 15 min, then the stopcock was sealed, and the reaction was immersed in a sand bath and stirred at 220 °C for 14 h. After this time, the reaction was cooled to 23 °C then loaded onto a silica plug (5 cm) eluting first with hexanes (10 mL) to remove hexadecane then Et_2O (10 mL) to elute the remaining material. The eluate was concentrated, and the product was isolated by preparative thin layer chromatography (7:2:1 hexanes:CH_2Cl_2:Et_2O, eluted 2x) to afford product **(+)-4.19** (4.2 mg, 10 μmol, 60% yield) as a clear colorless oil. **Product (+)-4.19**: R_f = 0.33 (4:1 hexanes:acetone); ^{1}H NMR (600 MHz, $CDCl_3$): 4.23 (qd, *J* = 7.1, 2.6, 2H), 4.13 (ddd, *J* = 11.8, 9.6, 2.4, 1H), 3.97 (ddd, *J* = 10.7, 4.8, 3.2, 1H), 3.56–3.48 (m, 2H), 3.33 (ddd, *J* = 11.5, 6.1, 2.6, 1H), 2.89 (ddd, *J* = 16.5, 9.4, 2.2, 1H), 2.60–2.45 (m, 3H), 2.33–2.20 (m, 4H), 2.13–2.06 (m, 1H), 1.92 (dt, *J* = 13.7, 2.6, 1H), 1.84–1.76 (m, 1H), 1.70 (ddd, *J* = 13.4, 10.9, 2.3, 1H), 1.68–1.61 (m, 1H), 1.58–1.51 (m, 1H), 1.39–1.34 (m, 1H), 1.34 (t, *J* = 7.1, 3H), 1.02 (t, *J* = 8.0, 9H), 0.61 (q, *J* = 8.0, 6H); ^{13}C NMR (150 MHz, $CDCl_3$): δ 210.7, 169.0, 157.6, 123.8, 69.9, 67.3, 60.0, 47.9, 44.3, 36.1, 35.5, 35.1, 30.6, 29.6, 27.0, 26.7, 20.8, 14.3, 8.1, 1.4; IR (film): 2927, 2875, 1739, 1366, 1217 cm^{-1}; HRMS-APCI (*m/z*) $[M + H]^+$ calcd for $C_{24}H_{41}O_4Si^+$, 421.2769; found 421.2760. $[\alpha]^{24.4}_D$ +37° (*c* = 1.00, CH_2Cl_2).

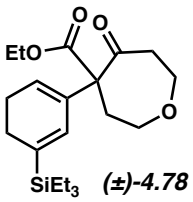
The structure of **(+)-4.19** was verified by 2D-NOESY, as the following interactions were observed:



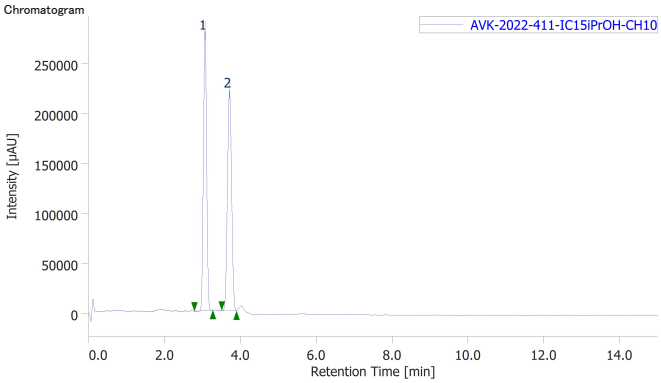
(+)-4.19

Table 4.4. SFC conditions and data.

Compound	Column	Solvent	Flow Rate	Retention Times (min)	Enantiomeric Ratio (er)
 ***(±)-4.78***	Daicel ChiralPak IC / 30 °C	15% isopropanol in CO_2	10.0 mL/min	3.07/3.71	49.6 : 50.4
 ***(+)-4.78***	Daicel ChiralPak IC / 30 °C	15% isopropanol in CO_2	10.0 mL/min	3.01/3.64	4.0 : 96.0
 ***(±)-4.19***	Daicel ChiralPak IB / 30 °C	5% isopropanol in CO_2	4.0 mL/min	5.18/6.29	49.8 : 50.2
 ***(+)-4.19***	Daicel ChiralPak IB / 30 °C	5% isopropanol in CO_2	4.0 mL/min	5.14/6.31	95.3 : 4.7



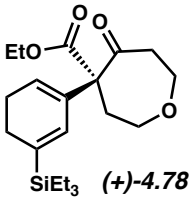
(±)-4.78



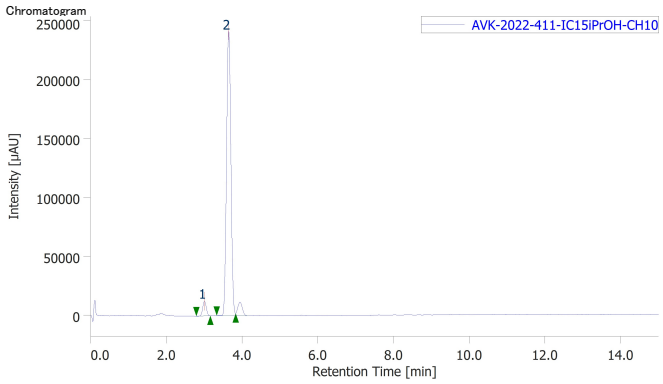
Peak Information

#	Peak Name	CH	tR [min]	Area [µV·sec]	Height [µV]	Area%	Height%	Quantity	NTP	Resolution	Symmetry Factor	Warning
1	Unknown	10	3.067	1655092	279970	49.613	55.920	N/A	6006	3.568	1.026	
2	Unknown	10	3.713	1680926	220689	50.387	44.080	N/A	5241	N/A	1.018	

Figure 4.9. SFC trace for **(±)-4.78**.



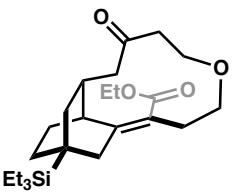
(+)-4.78



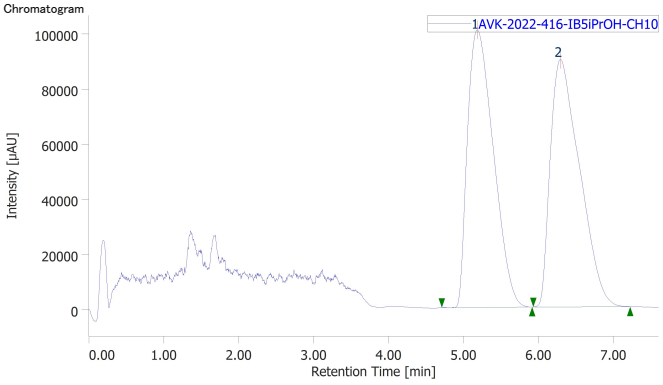
Peak Information

#	Peak Name	CH	tR [min]	Area [µV·sec]	Height [µV]	Area%	Height%	Quantity	NTP	Resolution	Symmetry Factor	Warning
1	Unknown	10	3.010	80547	12303	4.001	4.847	N/A	4634	3.256	1.018	
2	Unknown	10	3.647	1932514	241499	95.999	95.153	N/A	4593	N/A	1.047	

Figure 4.10. SFC trace for **(+)-4.78**.



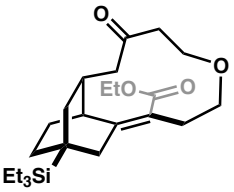
(±)-4.19



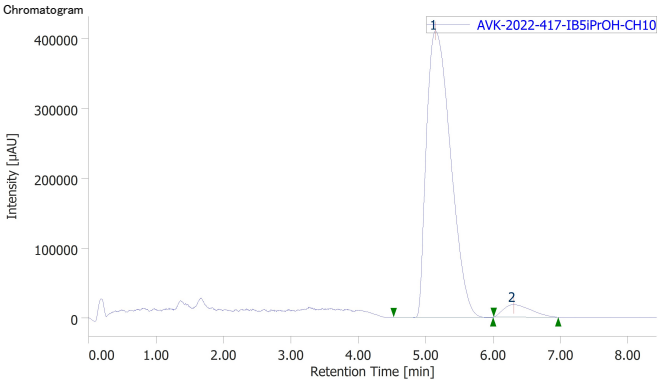
Peak Information

#	Peak Name	CH	tR [min]	Area [µV·sec]	Height [µV]	Area%	Height%	Quantity	NTP	Resolution	Symmetry Factor	Warning
1	Unknown	10	5.180	2418253	100574	49.777	52.866	N/A	967	1.563	1.545	
2	Unknown	10	6.290	2439916	89671	50.223	47.134	N/A	1103	N/A	1.687	

Figure 4.11. SFC trace for **(±)-4.19**.



(+)-4.19

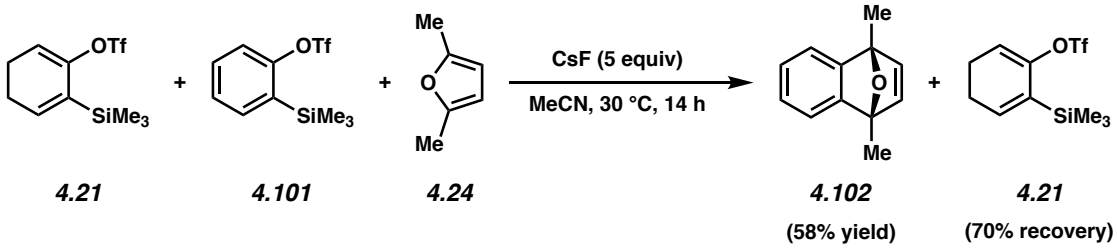


Peak Information

#	Peak Name	CH	tR [min]	Area [µV·sec]	Height [µV]	Area%	Height%	Quantity	NTP	Resolution	Symmetry Factor	Warning
1	Unknown	10	5.143	10189703	409937	95.268	95.814	N/A	900	1.576	1.560	
2	Unknown	10	6.307	506147	17911	4.732	4.186	N/A	1007	N/A	1.513	

Figure 4.12. SFC trace for **(+)-4.19**.

4.9.3.8 Competition Experiment with 1,2,3-Cyclohexatriene (4.5) and Benzyne (4.20)



4.21 *4.101* *4.24* *4.102* (58% yield) *4.21* (70% recovery)

A flame-dried 1-dram vial containing a magnetic stir bar was charged sequentially with silyl triflate **4.21** (25.0 mg, 0.08 mmol, 1.0 equiv), silyl triflate **4.101** (25.0 mg, 0.08 mmol, 1.0 equiv), and trapping partner **4.24** (8.0 mg, 0.08 mmol, 1.0 equiv), MeCN (0.810 mL, 0.1 M), and CsF (63.0 mg, 0.42 mmol, 5.0 equiv). The vial was then sealed with a Teflon-lined cap and stirred for 14 h at 30 °C. The mixture was then filtered over a pad of Celite, eluting with EtOAc (10 mL). The eluate was concentrated. Analysis of the crude reaction mixture by ^{1}H NMR using mesitylene as an external standard showed 58% yield of **4.102**, 70% recovery of **4.21**, and no formation of the cycloadduct derived from **4.21** (i.e., **4.28**). **Cycloadduct 4.102**: Spectral data matched those reported in the literature.[72]

4.9.4 Computational Section

4.9.4.1 Computational Methods

Conformational searches were performed in Spartan '20 V1.1.4[73] using Molecular Mechanics. Conformers were then optimized in Gaussian 16 A.03[74] at the B3LYP[75,76] -D3[77]/6-311+G(d,p), SMD[78](THF) level of theory. Structures for NMR calculations were optimized at the B3LYP/6-31+G(d,p) level of theory. NMR single point calculations (GIAO)[79,80,81,82,83] were performed on these geometries at the mPW1PW91[84]/6-311+G(d,p), SMD(benzene) level of theory. All geometries were verified as stationary points on the potential energy surface and characterized as transition states or minima by frequency calculations. Intrinsic reaction coordinate (IRC) calculations were performed at the same level of theory to confirm the intermediates linked by

each transition state. GoodVibes[85] (v. 3.2) with quasi-harmonic entropy[86] and enthalpy[87] treatment (frequency cut-off value: 100 cm^{-1}) was used to obtain corrected Gibbs free energies and enthalpies at either 298.15 K or 333.15 K and 1 atm. Optimized structures are presented using CYLview.[88]

4.9.4.2 Calculated Energies of Selected C_6H_6 Isomers

Table 4.5. Computed energies of selected C_6H_6 isomers at 25 °C at the B3LYP-D3/6-311+G(d,p) level of theory. All units are in Hartrees.

Structure	E	ZPE	H	T.qh-S	G(T)	qh-G(T)
Benzene (**4.1**)	-232.31633	0.10013	-232.21086	0.03281	-232.24367	-232.24368
Dewar benzene (**4.2**)	-232.18184	0.09680	-232.07952	0.03233	-232.11184	-232.11184
Benzvalene (**4.3**)	-232.18557	0.09690	-232.08340	0.03175	-232.11514	-232.11514
Prismane (**4.4**)	-232.11823	0.09635	-232.01682	0.03026	-232.04708	-232.04708
Triene **4.5**	-232.14988	0.09616	-232.04731	0.03490	-232.08221	-232.08221

4.9.4.3 Structure of 1,2,3-Cyclohexatriene (4.5)

The annotated structure of 1,2,3-cyclohexatriene (**4.5**) appears below in Figure 4.13 and was used to obtain the frontier molecular orbitals shown in Figure 4.3A. Comparison of LUMO energy with benzyne (**4.20**) suggests strong similarities in electronic structure which correlate with the similarity in reactivity reported herein. Notably, whereas the absolute magnitude of DFT-derived LUMO eigenvalues is known to deviate from experimental benchmarks,[89] the relative energies support similarity between triene **4.5** and benzyne (**4.20**).

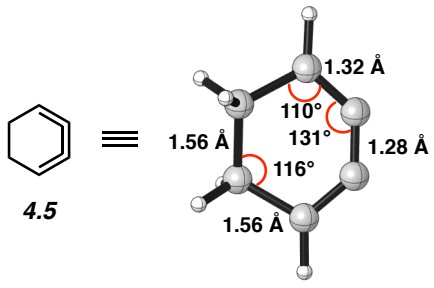


Figure 4.13. Geometry of 1,2,3-cyclohexatriene (**4.5**) at the B3LYP-D3/6-311+G(d,p) level of theory.

4.9.4.4 Transition State Analysis for Reaction of Triene 4.80 with Phenoxide 4.34

The reaction between Et_3Si-substituted triene **4.75** and phenoxide **4.34** was studied computationally using Me_3Si-substituted triene **4.80** and omitting the Na^+ cation in **4.34**. The latter approximation was motivated in part by the possibility for cation exchange with other cations in the reaction (Na^+, Bu_4N^+, and Cs^+), which convolutes the determination of the exact identity of the relevant species. Additionally, this omission circumvents potentially complex solvent-cation interactions. Analogous simplifications involving substitution of Me_3Si for Et_3Si[90] and omission of the cation[47] in computational modeling of nucleophilic additions to strained intermediates have been reported in the literature, and the resulting models demonstrate good correlation with experimentally observed outcomes.

Table 4.6. Computed energies for the reaction of triene **4.80** with phenoxide **4.34** (Na^+ omitted) at 60 °C at the B3LYP-D3/6-311+G(d,p), SMD(THF) level of theory. All units are in Hartrees.

Structure	E	ZPE	H	T.qh-S	G(T)	qh-G(T)
Triene **4.80**	-640.91356	0.19670	-640.69956	0.06186	-640.76342	-640.76142
Phenoxide **4.34**	-511.67626	0.09324	-511.57249	0.04813	-511.62142	-511.62062
TS-4.1	-1152.59402	0.29171	-1152.27476	0.08405	-1152.36413	-1152.35881
TS-4.2	-1152.58660	0.29074	-1152.26784	0.08610	-1152.36088	-1152.35393

Table 4.7. Distortion/Interaction-Activation Strain Analysis (DIAS) of the phenolate addition (**TS4.1** & **TS4.2**). All units are in kcal/mol.

	TS-4.1	**TS-4.2**
$E_{dist,triene\ \mathbf{4.80}}$	1.54	2.98
$E_{dist,triene\ \mathbf{4.34}}$	0.09	0.08
E_{int}	-4.27	-1.05

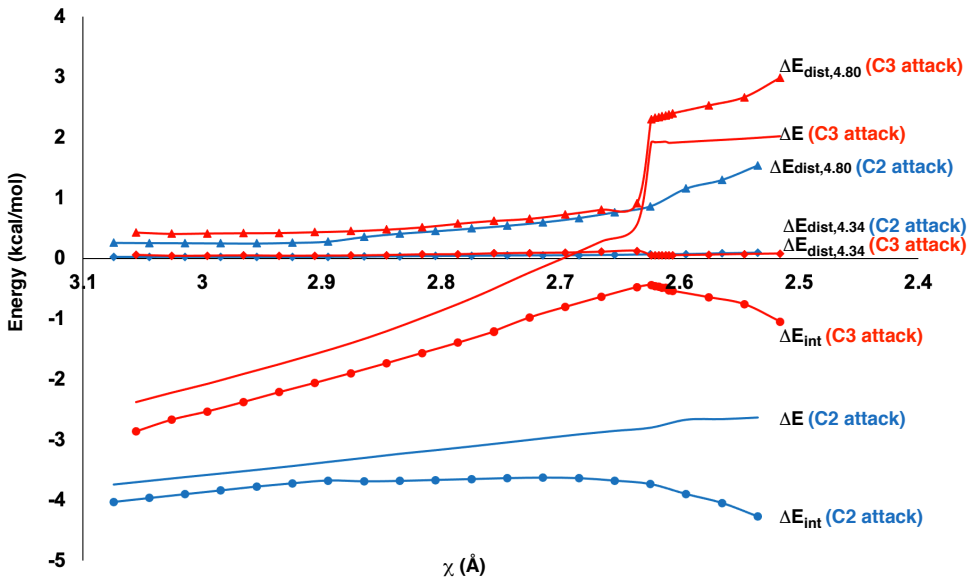


Figure 4.14. DIAS strain analysis along a relaxed scan of the forming C–O bond for attack of phenoxide **4.34** (Na^+ omitted) on triene **4.80** at C2 or C3 (B3LYP-D3/6-311+G(d,p), SMD(THF)). The x-axis corresponds to reaction progress, (i.e., the C–O bond distance for the forming bond).

DIAS analysis performed along the two competing approaches for nucleophilic attack of **4.34** onto **4.80** demonstrates that C2 attack is favoured due to both distortion and interaction effects (Figure 3.14). Whereas distortion of phenoxide **4.34** is negligible for both approaches, attack at C3 requires significant geometric distortion of triene **4.80** as bond formation advances while attack at C2 does not (as a result of the previously discussed ground state distortion). This difference is reflected in a substantially higher (1.4–1.9 kcal/mol) distortion energy for **4.80** at C–O bond lengths under 2.65 Å. C2 attack also benefits from more favourable interaction energies. Significant additional stabilization arises from attractive CH–π and C–H···O interactions between the incoming nucleophile **4.34** and the C–H groups of the $SiMe_3$ substituent, whereas the approach and transition state geometry of **TS-4.2** place the nucleophile increasingly out of reach of the $SiMe_3$ substituent as the forming C3–O bond length decreases (see Figure 4.15 below).

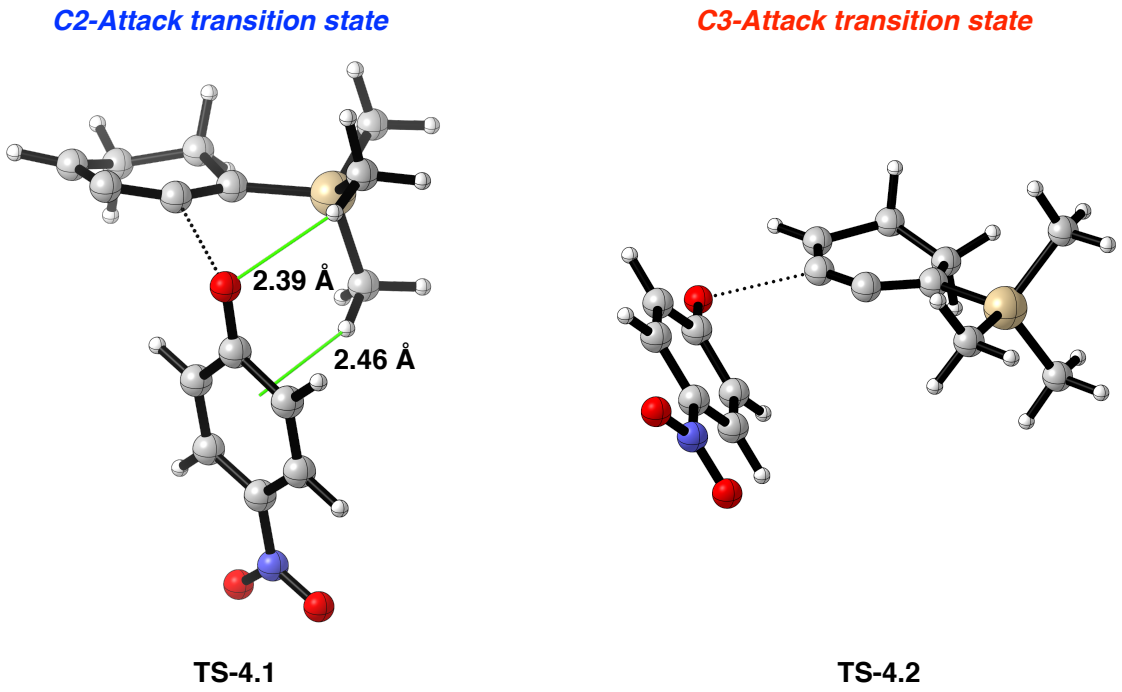


Figure 4.15. Transition state structures for the attack of **4.34** (Na^+ omitted) onto **4.80** at the B3LYP-D3/6-311+G(d,p), SMD(THF) level of theory. Stabilizing CH–π and C–H···O interactions present in **TS-4.1** are designated with green highlighting and the corresponding distances.

4.9.4.5 Relative Stereochemical Assignment of Thietanes 4.69 and 4.93

Extensive overlapping signals prevented assignment of the relative stereochemistry of thietane **4.69** using 2D-NOESY experiments, so the structural assignment was instead accomplished by comparison to computed NMR shift data (see below).

Computed NMR Shift Data

Structures used for NMR calculations were optimized at the B3LYP/6-31+G(d,p) level of theory. NMR single point calculations (GIAO) were performed on these geometries at the mPW1PW91/6-311+G(d,p), SMD(benzene) level of theory to obtain computed isotropic shielding constants (σ). Corrected chemical shifts were obtained by empirically scaling these shielding constants according to Equation 4.2 using scaling factors (m and b) from http://cheshirenmr.info which are given below.[91,92,93,94]

$$\delta = \frac{b-\sigma}{-m}$$

Equation 4.2. Empirical scaling of computed shifts.

δ = computed chemical shift relative to Me_4Si
σ = computed isotropic shielding constant
m = slope from empirical scaling data (here, –1.0286)
b = intercept from empirical scaling data (here, 185.5899)

Table 4.8. Comparison of Experimental and Computed NMR Chemical Shifts for Structure **4.69**.

	^{13}C NMR Chemical Shifts (ppm)		
Nucleus #[a]	Expt.	Computed (**4.69**)[b]	Computed (**4.93**)[b]
1	112.82	116.31	115.23
2	135.30	138.16	138.56
3	34.43	33.34	32.69
4	122.22	127.24	126.79
5	29.38	29.63	29.45
6	126.96	133.21	132.30
11	16.62	15.14	15.16
15	21.89	21.27	19.24
20	86.80	93.89	94.17
21	45.63	50.54	49.87
22	55.23	58.42	56.19
23	32.48	32.66	35.39
26	25.49	25.21	25.14
29	50.02	51.19	50.26
31	32.97	31.94	25.86
35	23.96	21.49	27.30
39	42.57	42.02	42.29
42	20.05	18.33	16.00
	CMAD[c]	2.42	2.91

[a] Nucleus labels correspond to those shown in the Figure 4.16 below Table 4.9. [b] Largest outliers are indicated in red. Note that higher than average errors are expected for the carbon atoms bearing a sulfur atom (e.g., C6 and C20) – due to heavy-atom effects. [c] CMAD = corrected mean absolute deviation and is computed as $\frac{1}{n}\sum_i^n \left|\delta_{comp} - \delta_{exp}\right|$ where δ_{comp} refers to the scaled computed chemical shifts and δ_{exp} refers to experimentally observed chemical shifts.

Table 4.9. Comparison of Experimental and Computed NMR Chemical Shifts for Structure **4.93**.

	^{13}C NMR Chemical Shifts (ppm)		
Nucleus #[a]	Expt.	Computed (**4.69**)[b]	Computed (**4.93**)[b]
1	112.48	116.31	115.23
2	136.27	138.16	138.56
3	32.57	33.34	32.69
4	121.27	127.24	126.79
5	29.31	29.63	29.45
6	125.83	133.21	132.30
11	16.71	15.14	15.16
15	20.20	21.27	19.24
20	87.00	93.89	94.17
21	45.75	50.54	49.87
22	52.60	58.42	56.19
23	35.04	32.66	35.39
26	25.25	25.21	25.14
29	49.21	51.19	50.26
31	29.85	31.94	25.86
35	28.28	21.49	27.30
39	42.17	42.02	42.29
42	17.86	18.33	16.00
	CMAD[c]	3.07	2.68

[a] Nucleus labels correspond to those shown in Figure 4.16 below. [b] Largest outliers are indicated in red. Note that higher than average errors are expected for the carbon atoms bearing a sulfur atom (CSS) – due to heavy-atom effects. [c] CMAD = corrected mean absolute deviation and is computed as $\frac{1}{n}\sum_i^n \left|\delta_{comp} - \delta_{exp}\right|$ where δ_{comp} refers to the scaled computed chemical shifts.

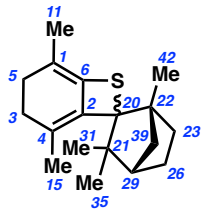


Figure 4.16. Atom numbers used in Table 4.8 and Table 4.9.

4.9.4.6 Cartesian Coordinates of Optimized Geometries

Cartesian coordinates for the optimized structures were reported in the literature.[95]

4.10 Spectra Relevant to Chapter Four:

Strain-promoted reactions of 1,2,3-cyclohexatriene and its derivatives

Andrew V. Kelleghan[†], Ana S. Bulger[†], Dominick C. Witkowski, and Neil K. Garg

Nature **2023**, *618*, 748–754.

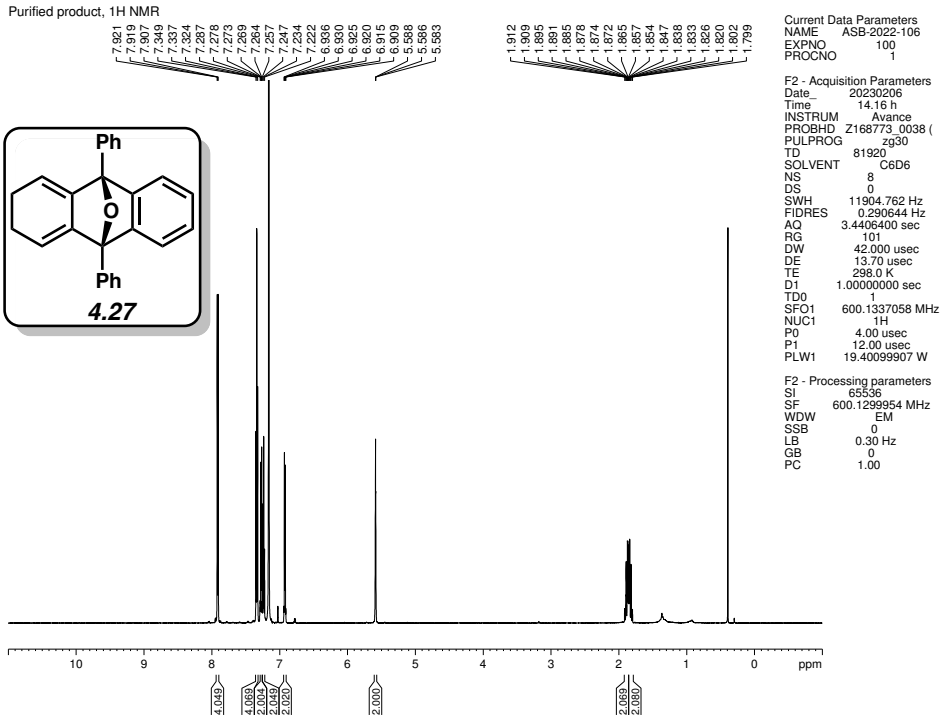


Figure 4.17. ^{1}H NMR (600 MHz, C_6D_6) of compound **4.27**.

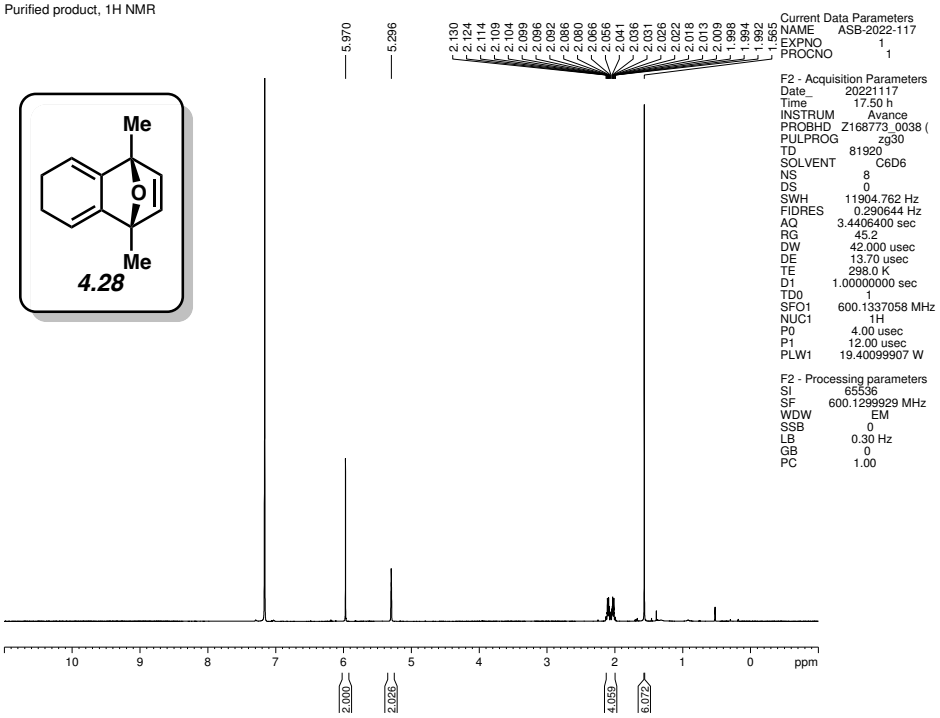


Figure 4.18. ^{1}H NMR (600 MHz, C_6D_6) of compound **4.28**.

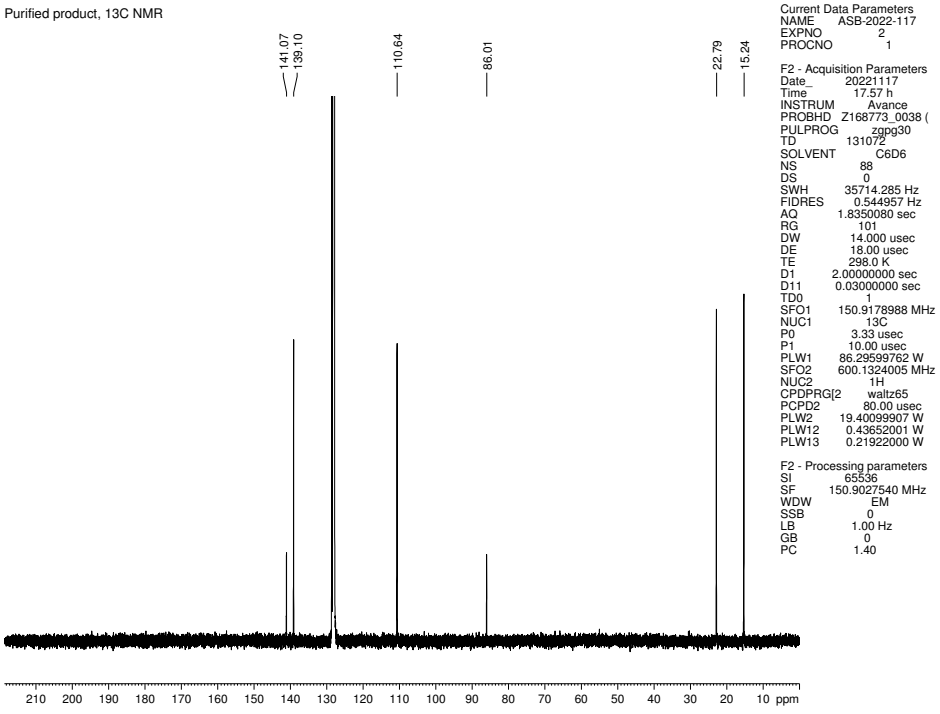


Figure 4.19. ^{13}C NMR (150 MHz, C_6D_6) of compound **4.28**.

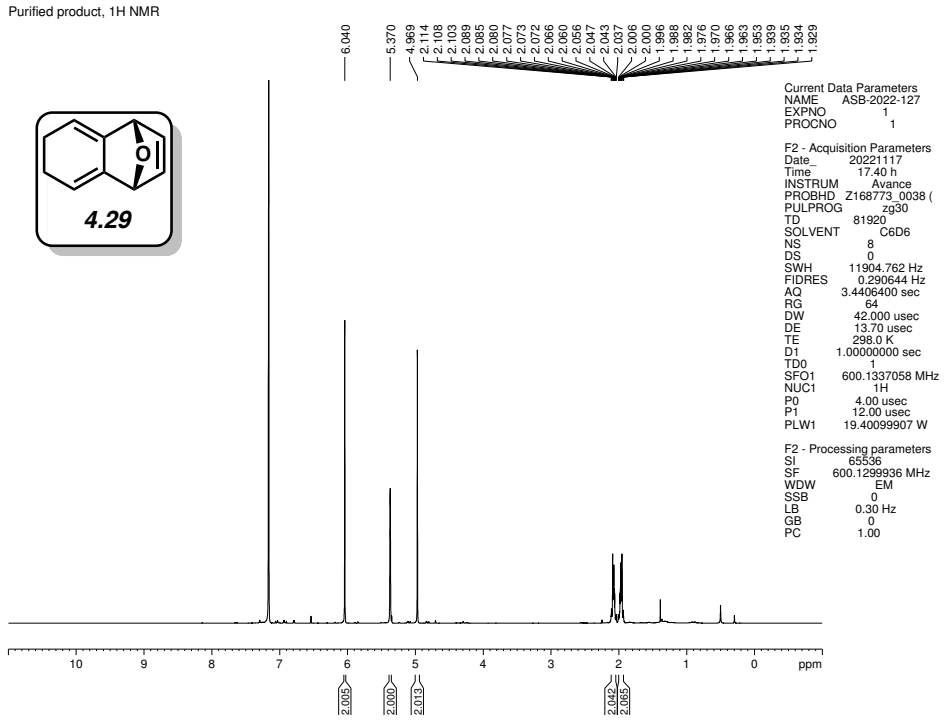


Figure 4.20. ^{1}H NMR (600 MHz, C_6D_6) of compound **4.29**.

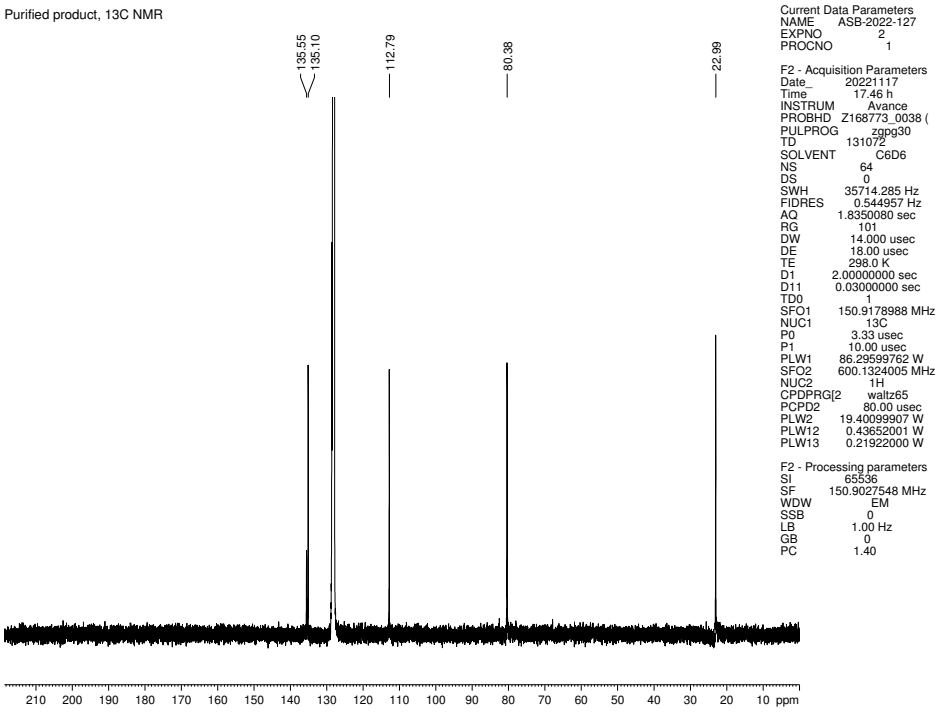


Figure 4.21. ^{13}C NMR (150 MHz, C_6D_6) of compound **4.29**.

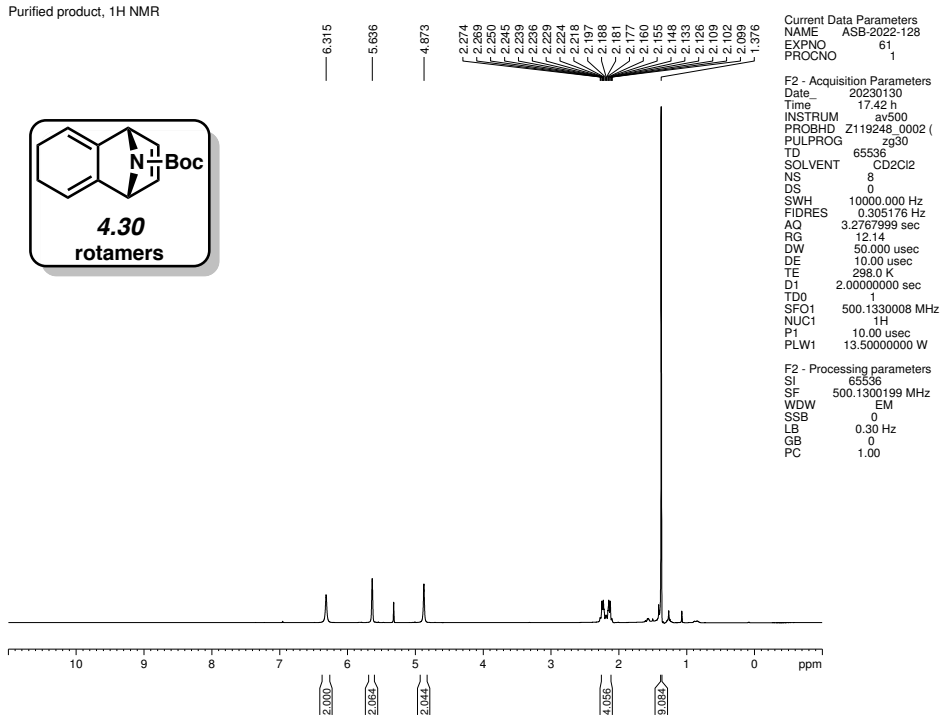


Figure 4.22. ^{1}H NMR (500 MHz, CD_2Cl_2) of compound **4.30**.

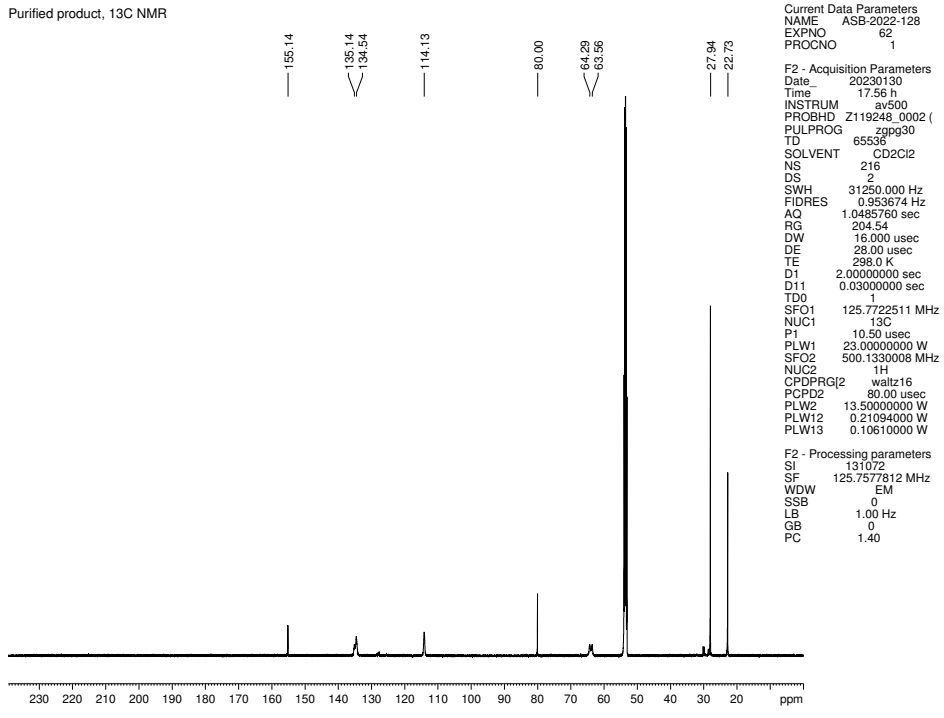


Figure 4.23. ^{13}C NMR (125 MHz, CD_2Cl_2) of compound **4.30**.

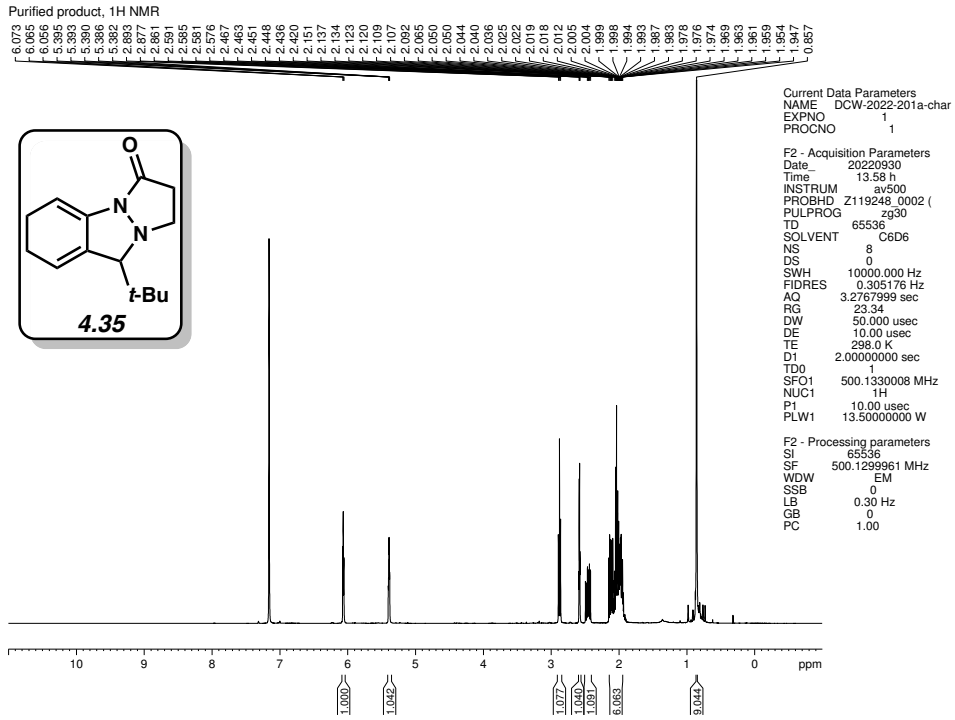


Figure 4.24. ^{1}H NMR (500 MHz, C_6D_6) of compound **4.35**.

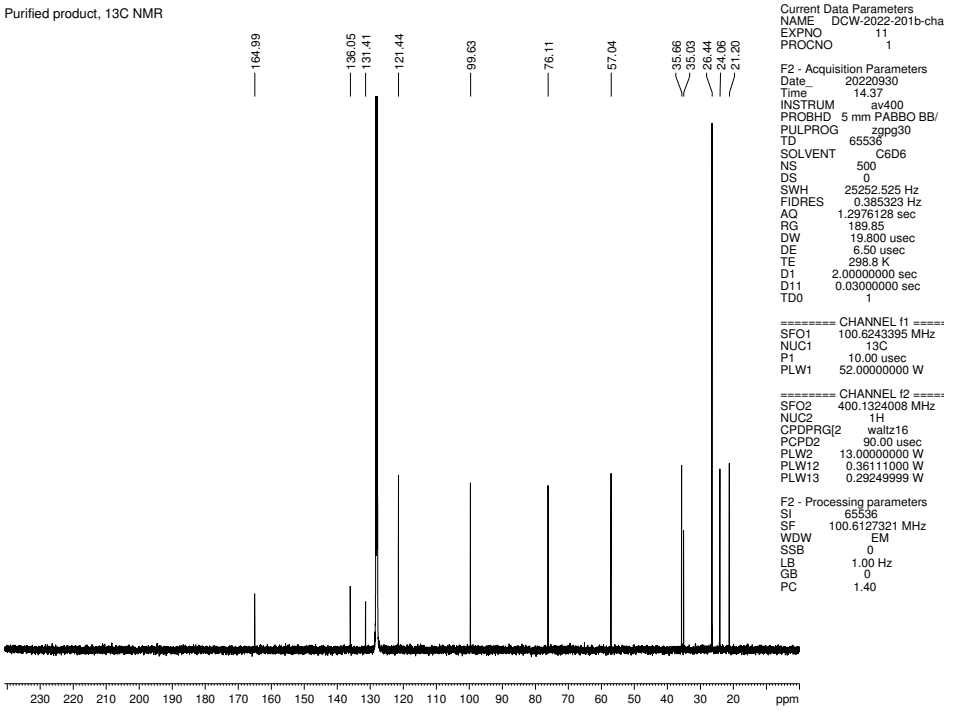


Figure 4.25. ^{13}C NMR (100 MHz, C_6D_6) of compound **4.35**.

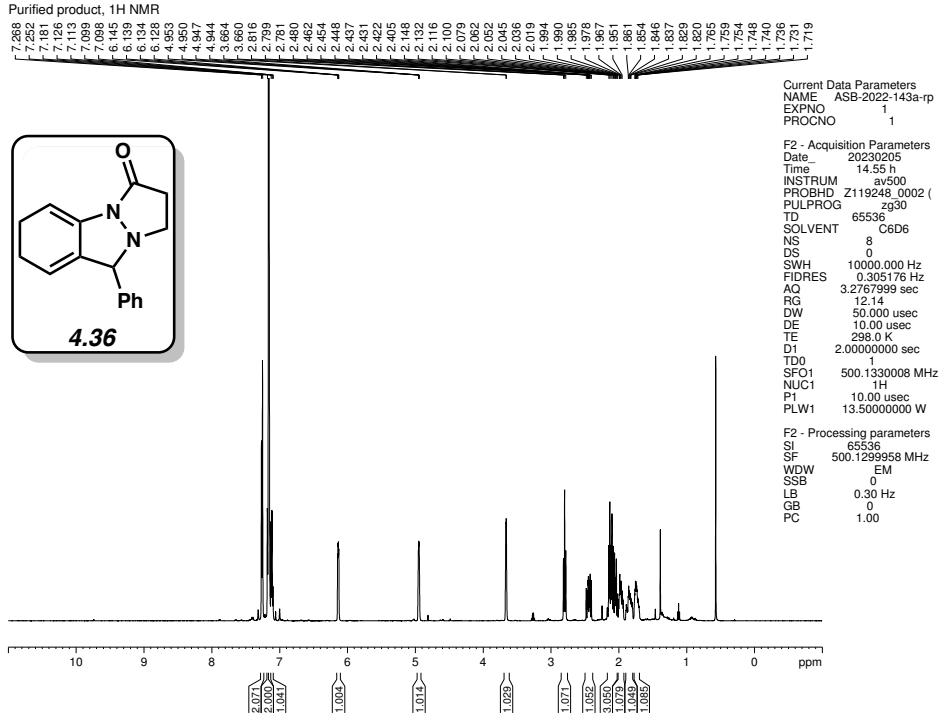


Figure 4.26. ^{1}H NMR (500 MHz, C_6D_6) of compound **4.36**.

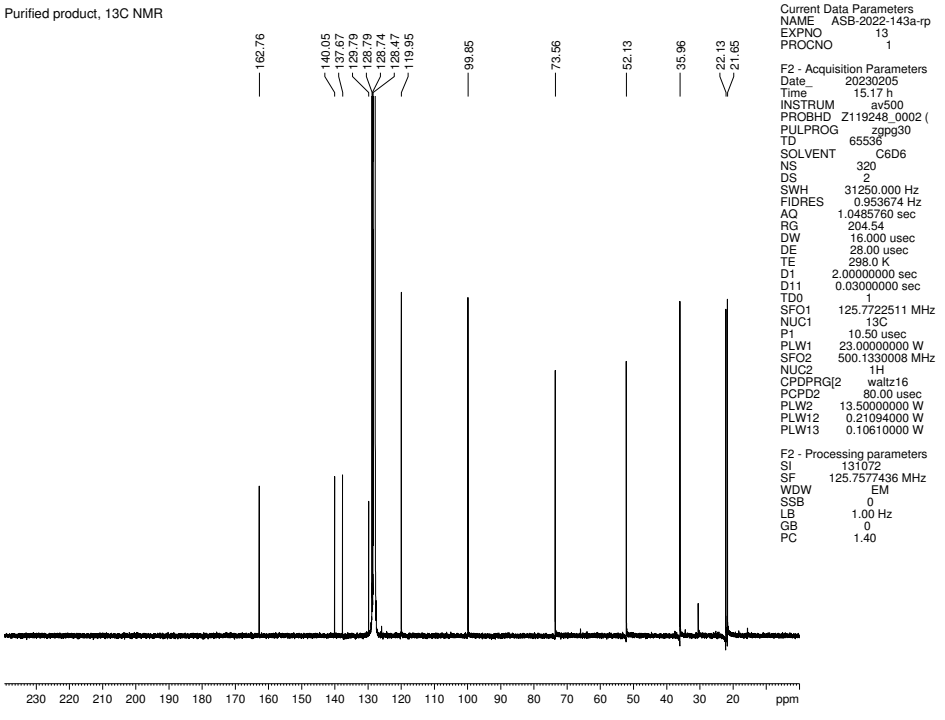


Figure 4.27. ^{13}C NMR (125 MHz, C_6D_6) of compound **4.36**.

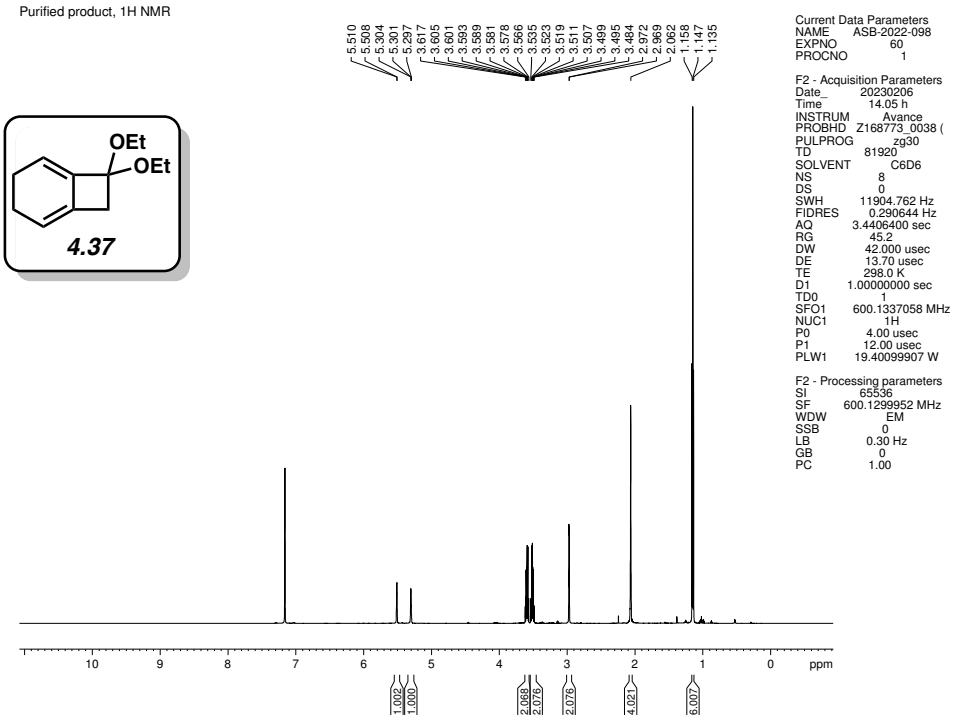


Figure 4.28. ^{1}H NMR (600 MHz, C_6D_6) of compound **4.37**.

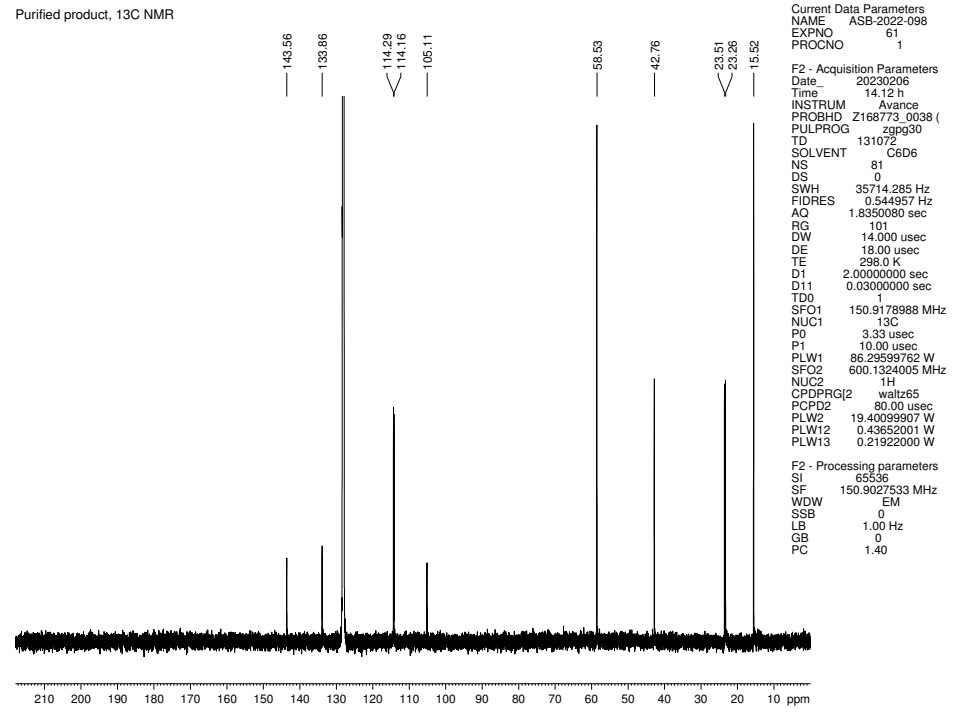


Figure 4.29. ^{13}C NMR (150 MHz, C_6D_6) of compound **4.37**.

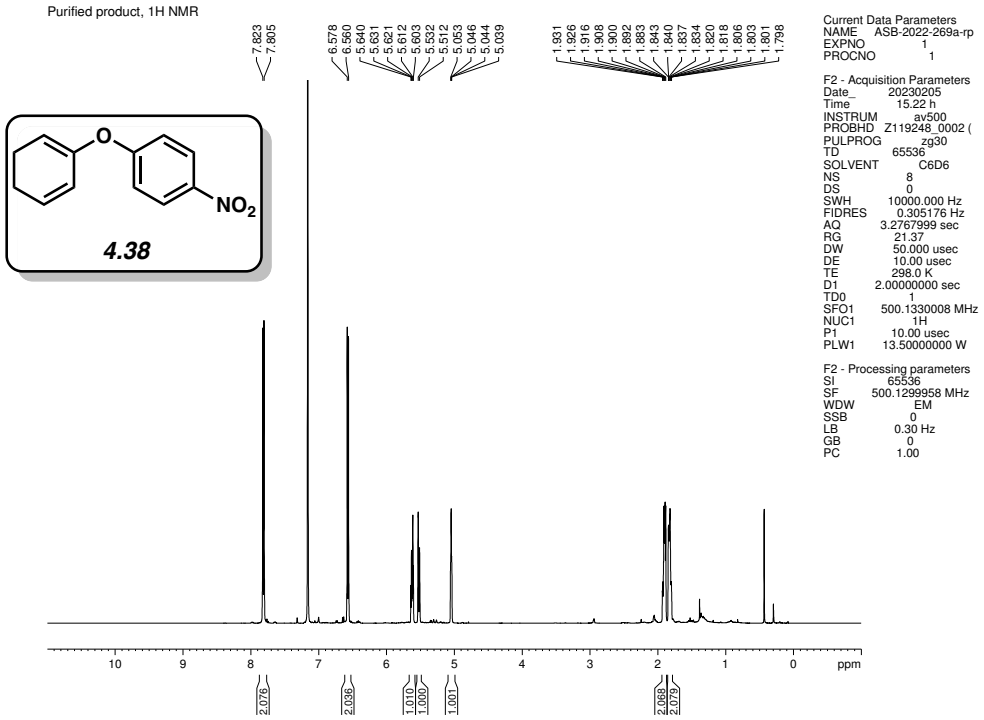


Figure 4.30. ^{1}H NMR (500 MHz, C_6D_6) of compound **4.38**.

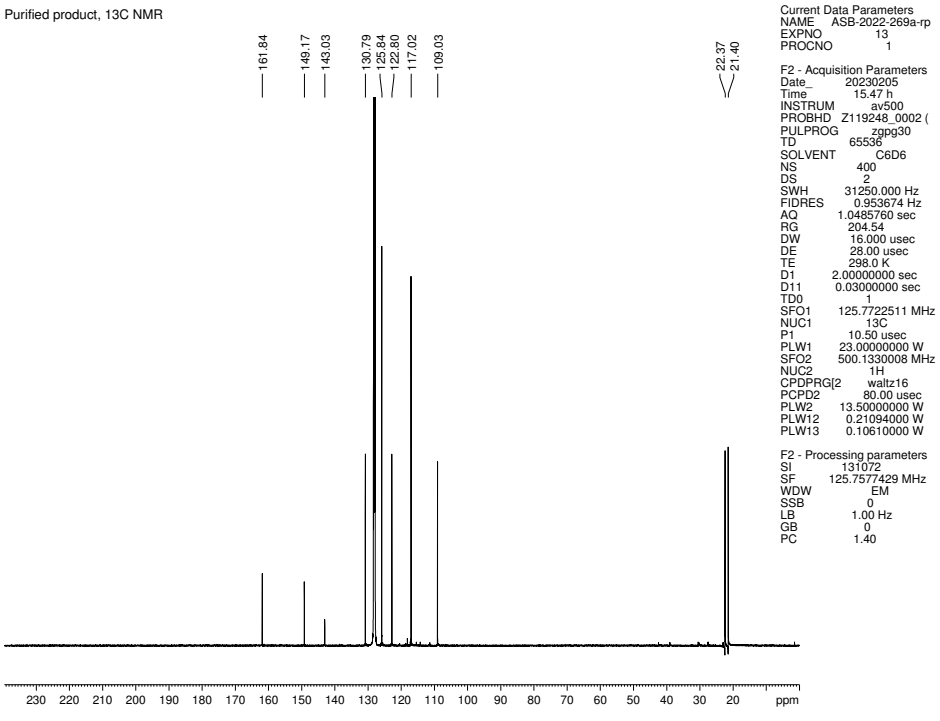


Figure 4.31. ^{13}C NMR (125 MHz, C_6D_6) of compound **4.38**.

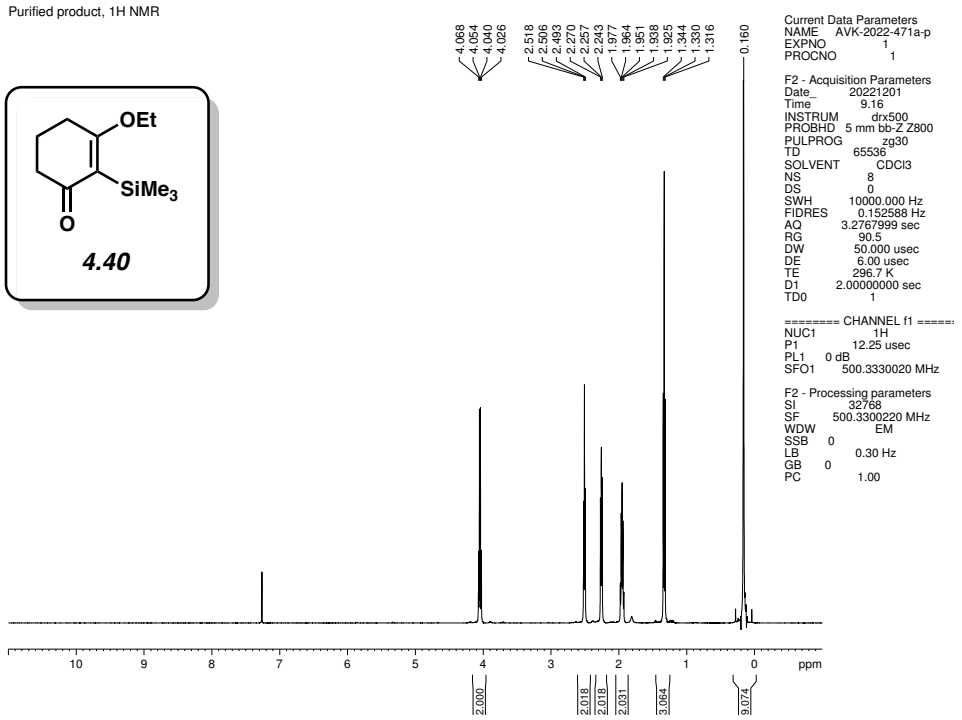


Figure 4.32. ^{1}H NMR (500 MHz, $CDCl_3$) of compound **4.40**.

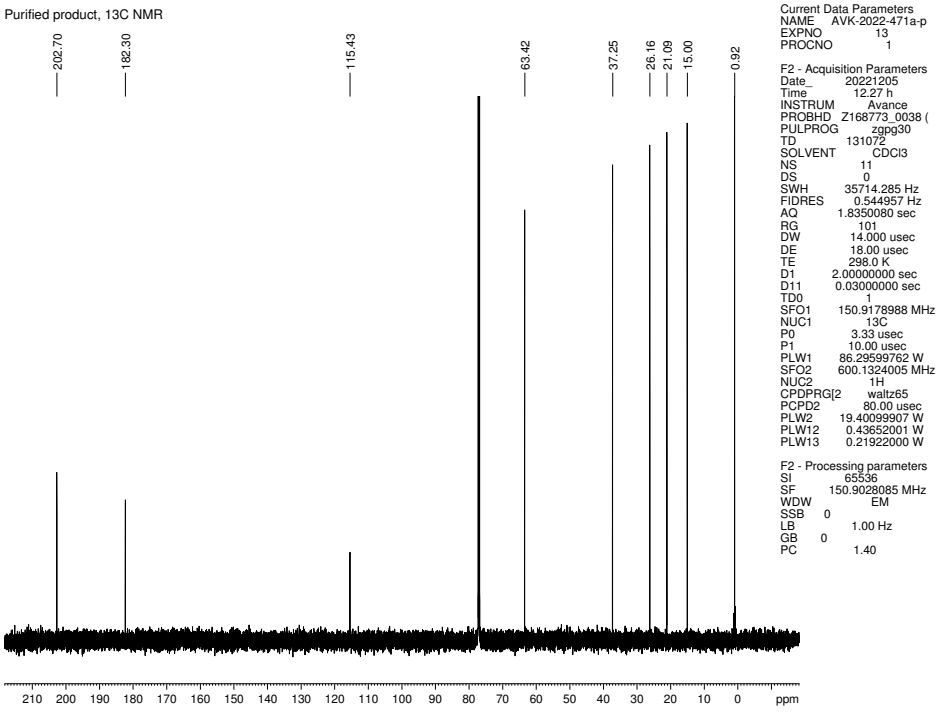


Figure 4.33. ^{13}C NMR (150 MHz, $CDCl_3$) of compound **4.40**.

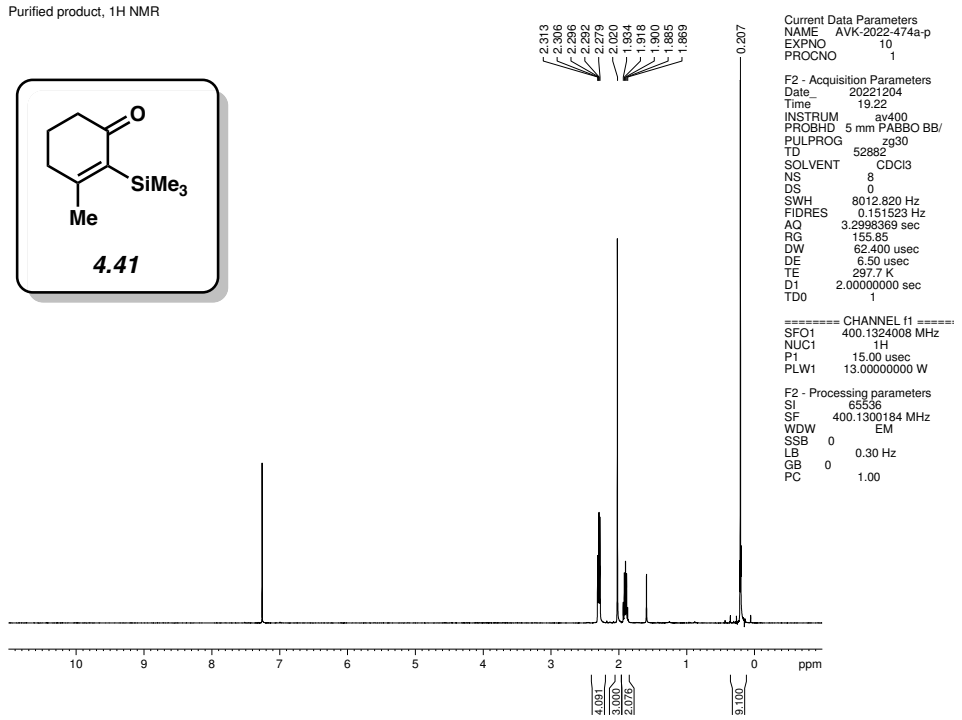


Figure 4.34. ^{1}H NMR (400 MHz, $CDCl_3$) of compound **4.41**.

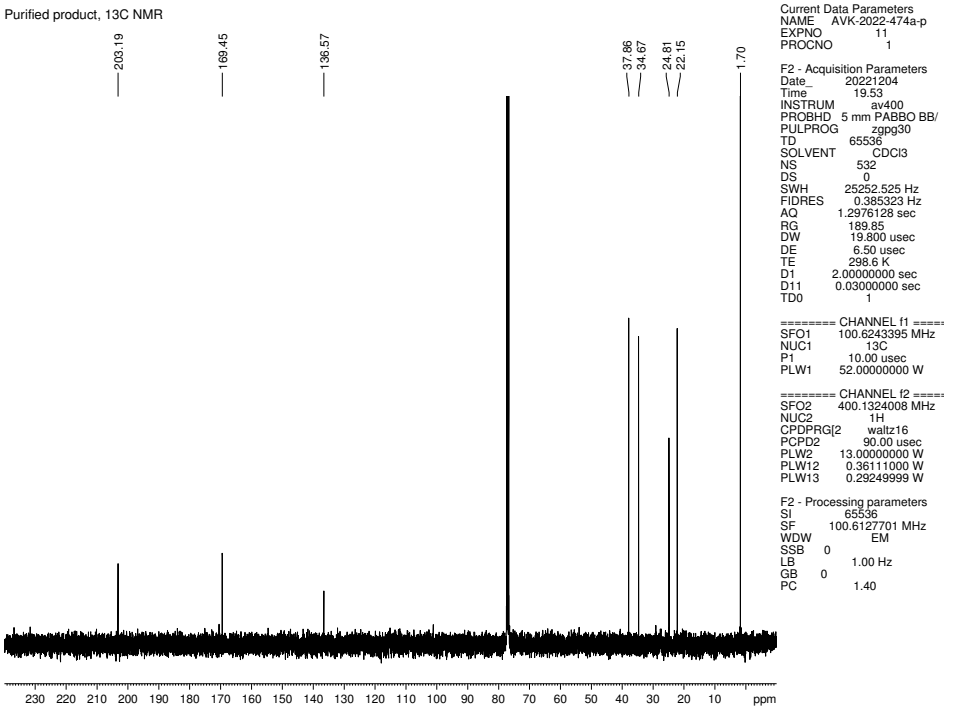


Figure 4.35. ^{13}C NMR (100 MHz, $CDCl_3$) of compound **4.41**.

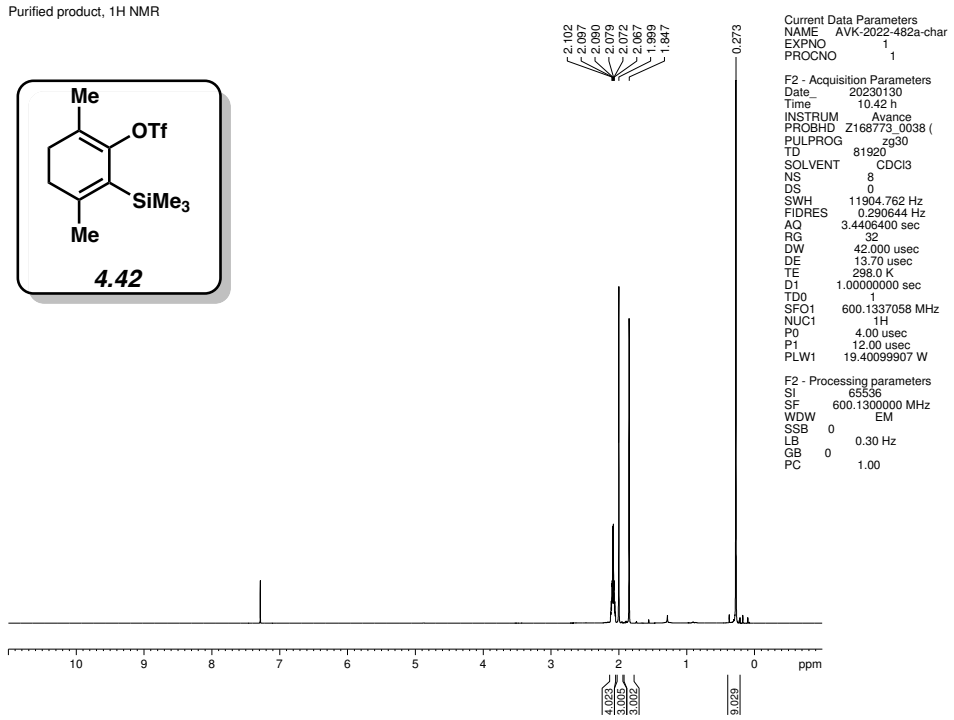


Figure 4.36. ^{1}H NMR (600 MHz, $CDCl_3$) of compound **4.42**.

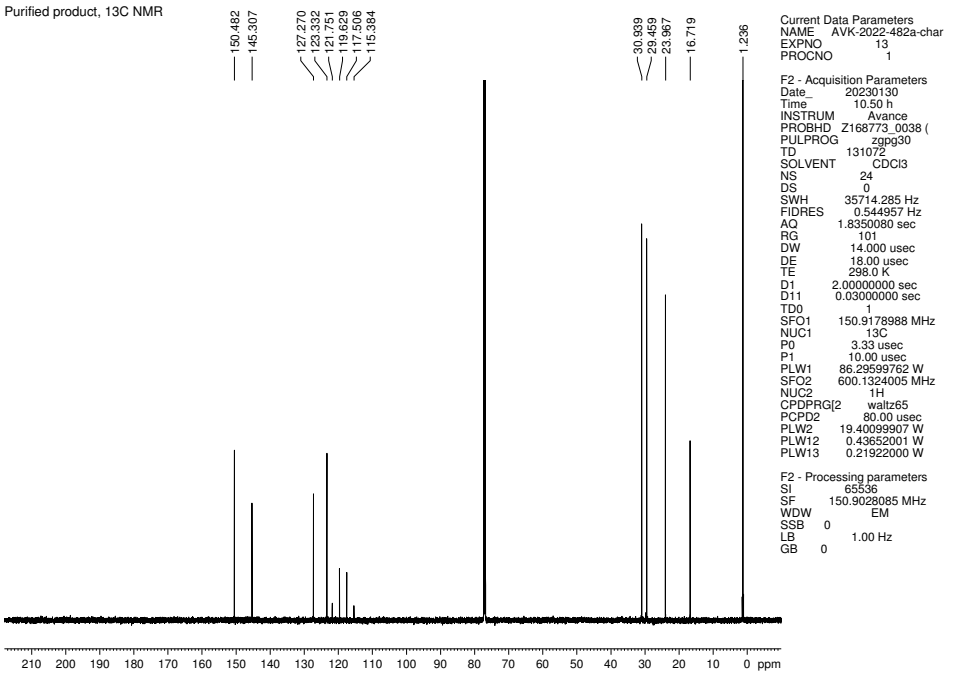


Figure 4.37. ^{13}C NMR (150 MHz, $CDCl_3$) of compound **4.42**.

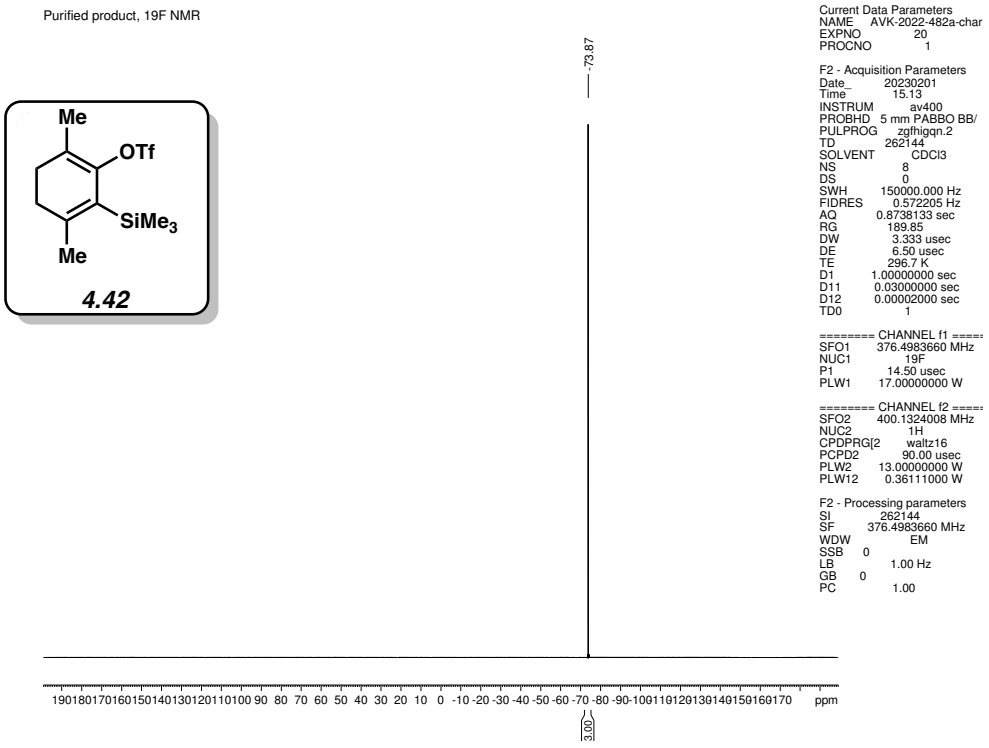


Figure 4.38. ^{19}F NMR (376 MHz, $CDCl_3$) of compound **4.42**.

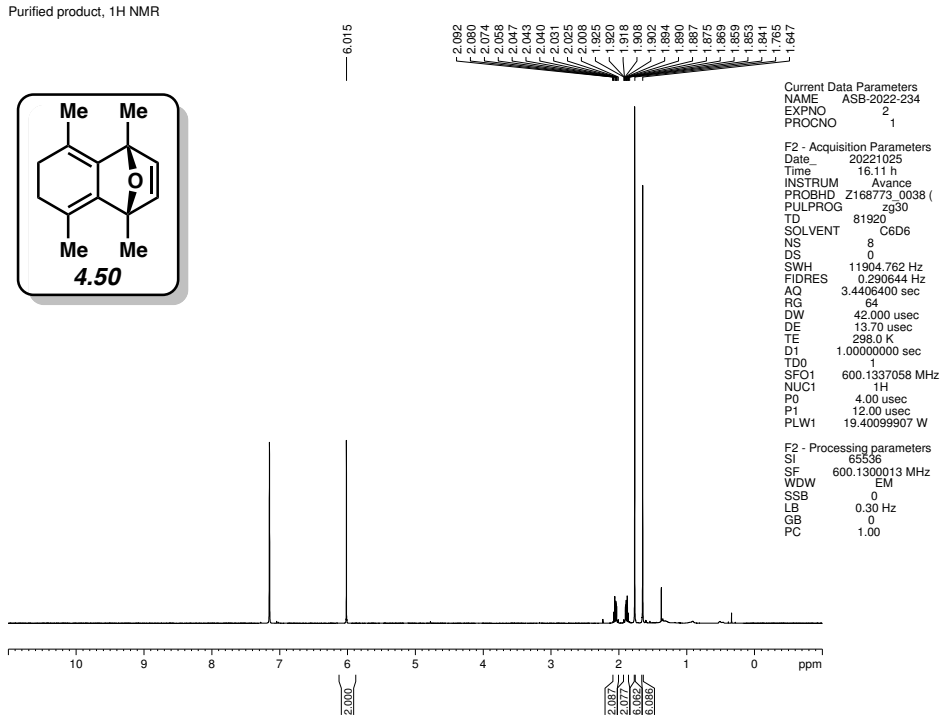


Figure 4.39. ^{1}H NMR (600 MHz, C_6D_6) of compound **4.50**.

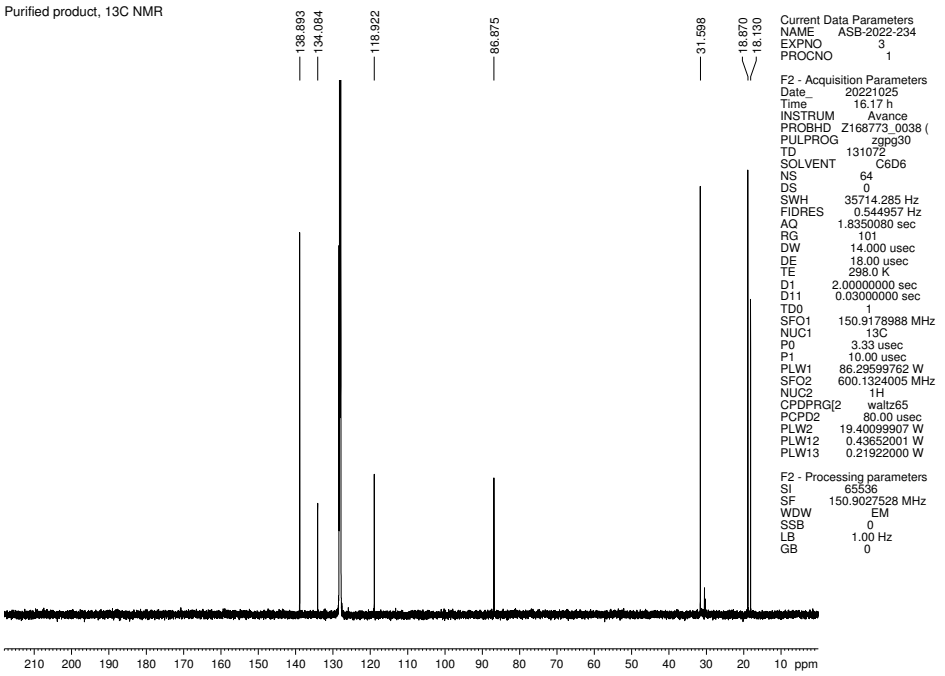


Figure 4.40. ^{13}C NMR (150 MHz, C_6D_6) of compound **4.50**.

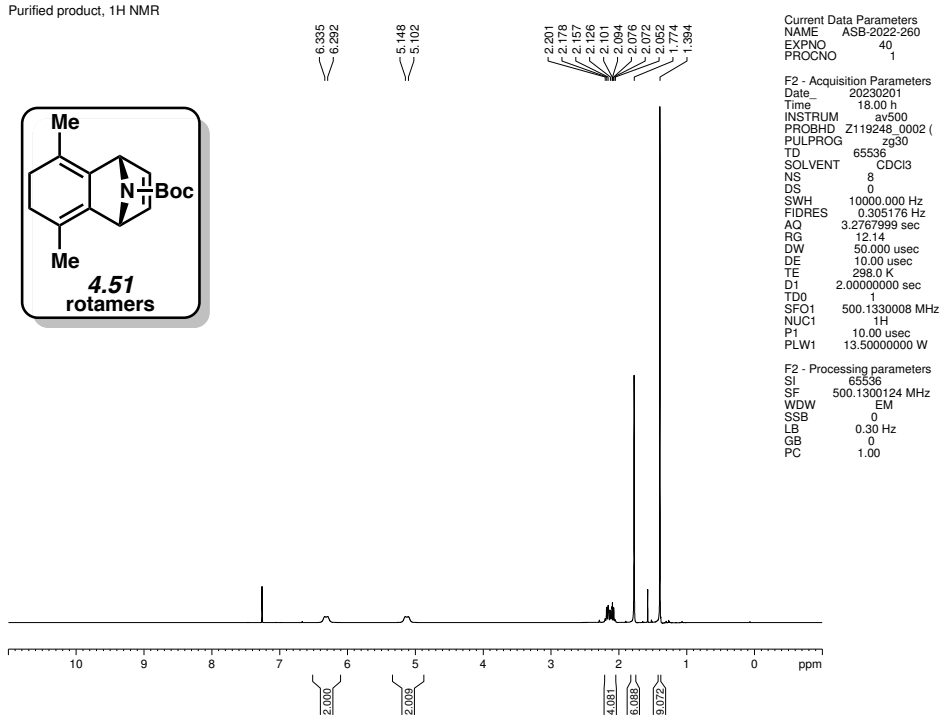


Figure 4.41. ^{1}H NMR (500 MHz, $CDCl_3$) of compound **4.51**.

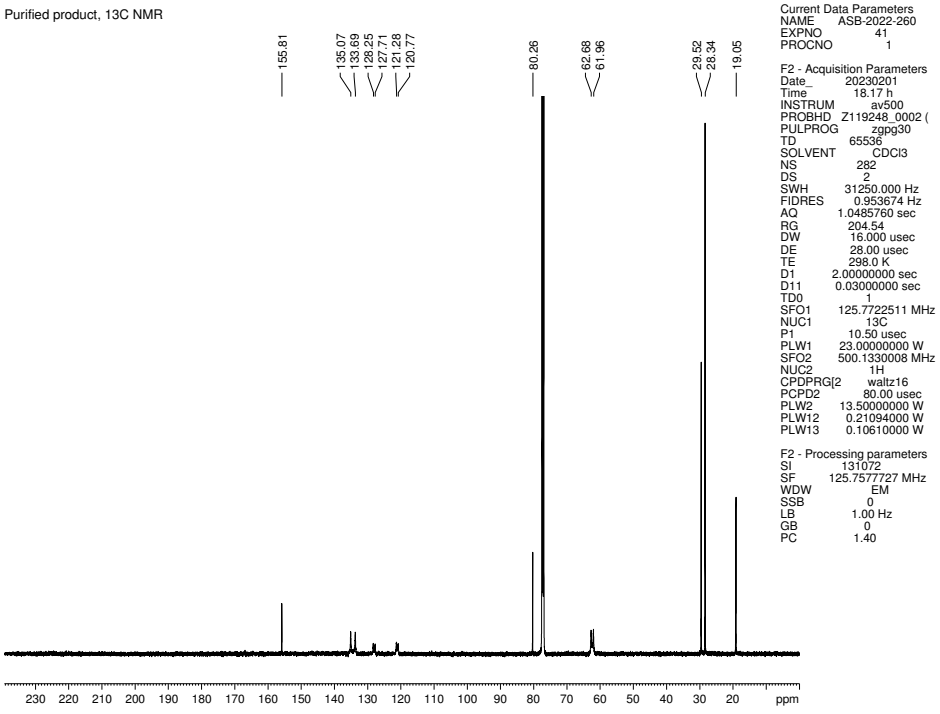


Figure 4.42. ^{13}C NMR (125 MHz, $CDCl_3$) of compound **4.51**.

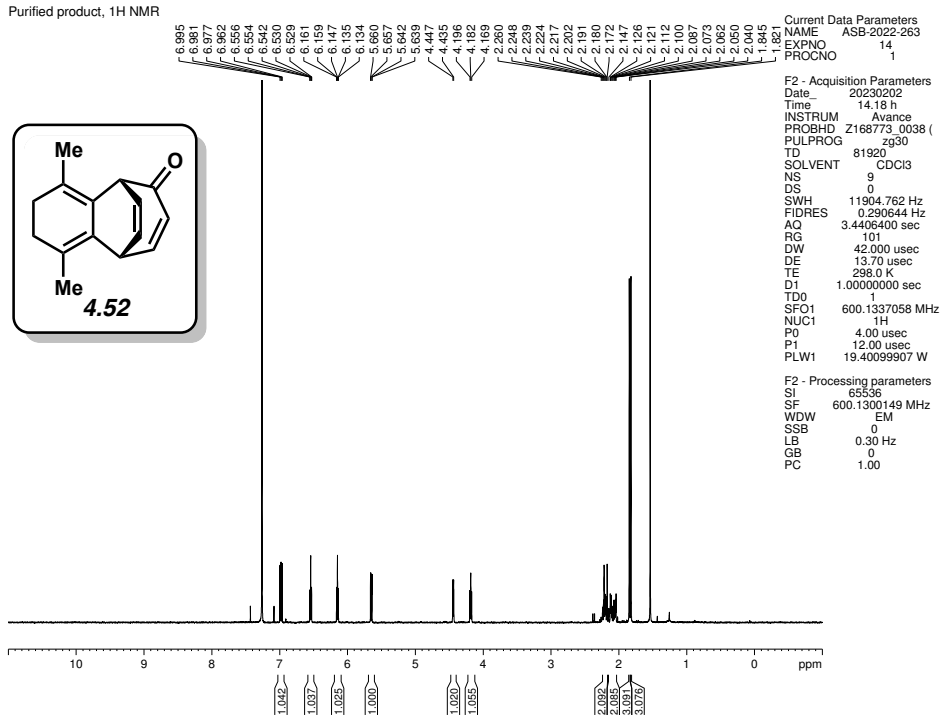


Figure 4.43. ^{1}H NMR (600 MHz, $CDCl_3$) of compound **4.52**.

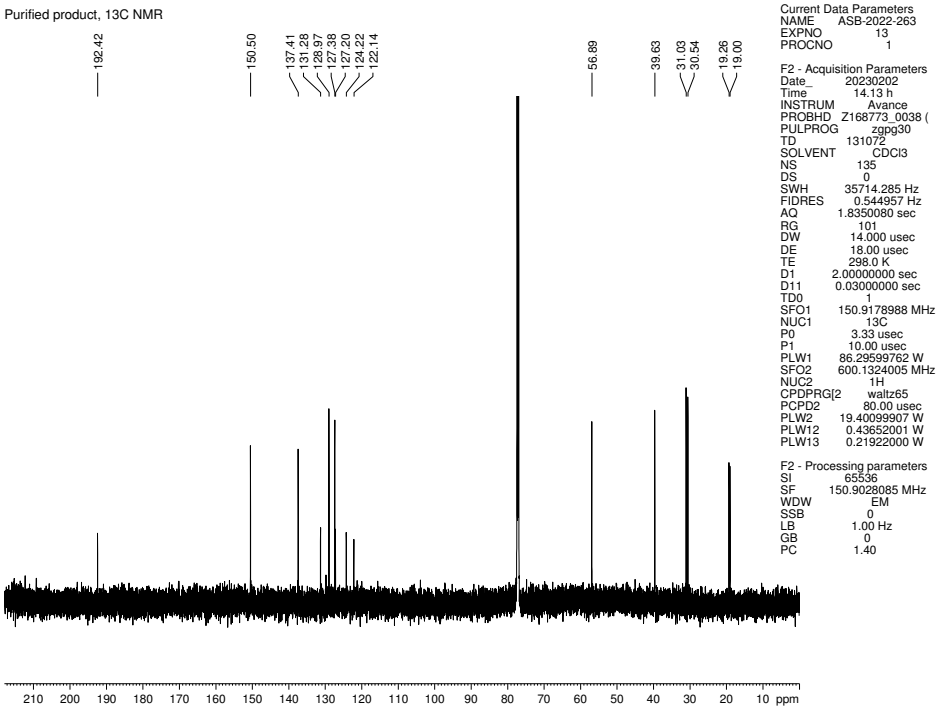


Figure 4.44. ^{13}C NMR (150 MHz, $CDCl_3$) of compound **4.52**.

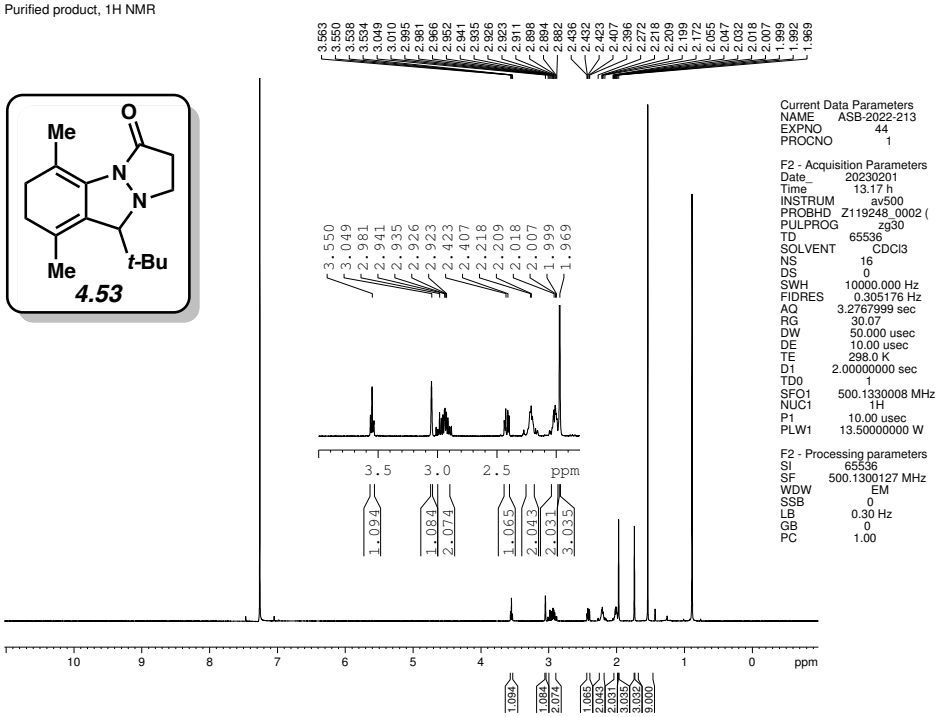


Figure 4.45. ^{1}H NMR (500 MHz, $CDCl_3$) of compound **4.53**.

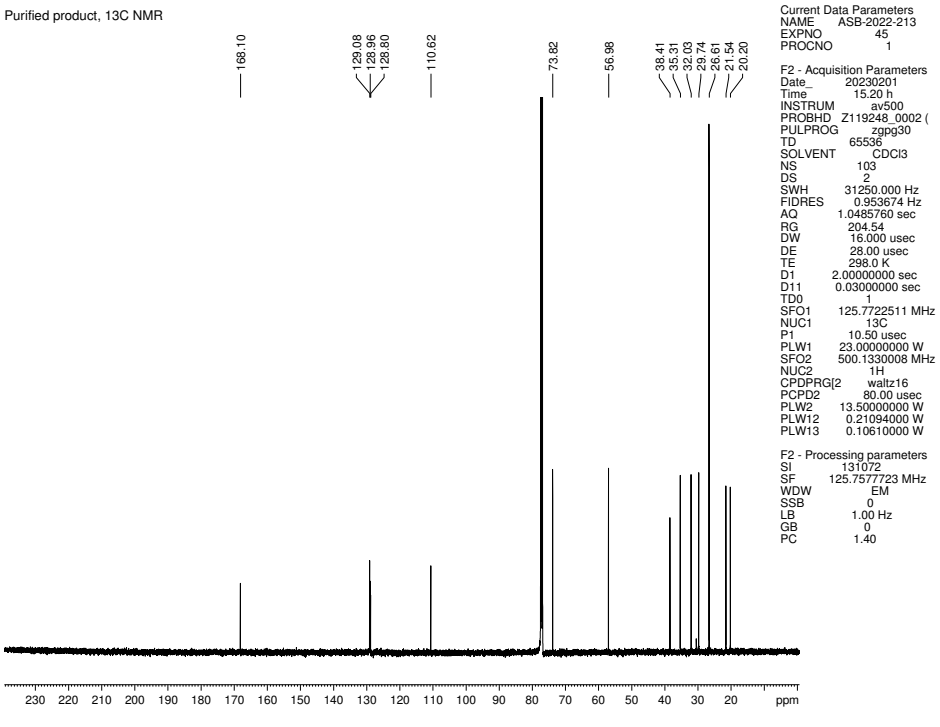


Figure 4.46. ^{13}C NMR (125 MHz, $CDCl_3$) of compound **4.53**.

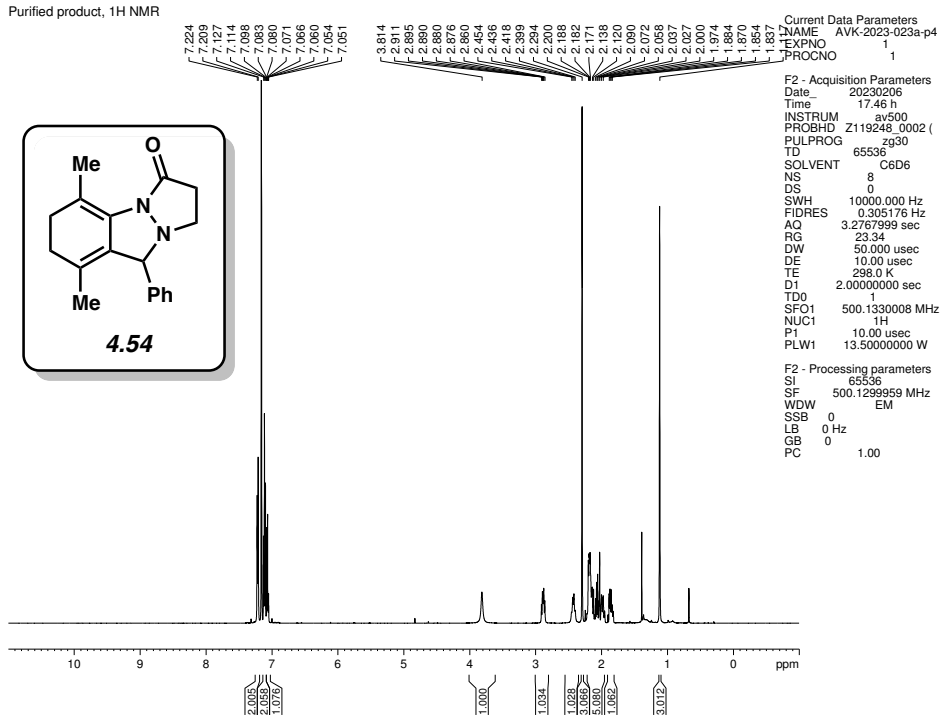


Figure 4.47. ^{1}H NMR (500 MHz, C_6D_6) of compound **4.54**.

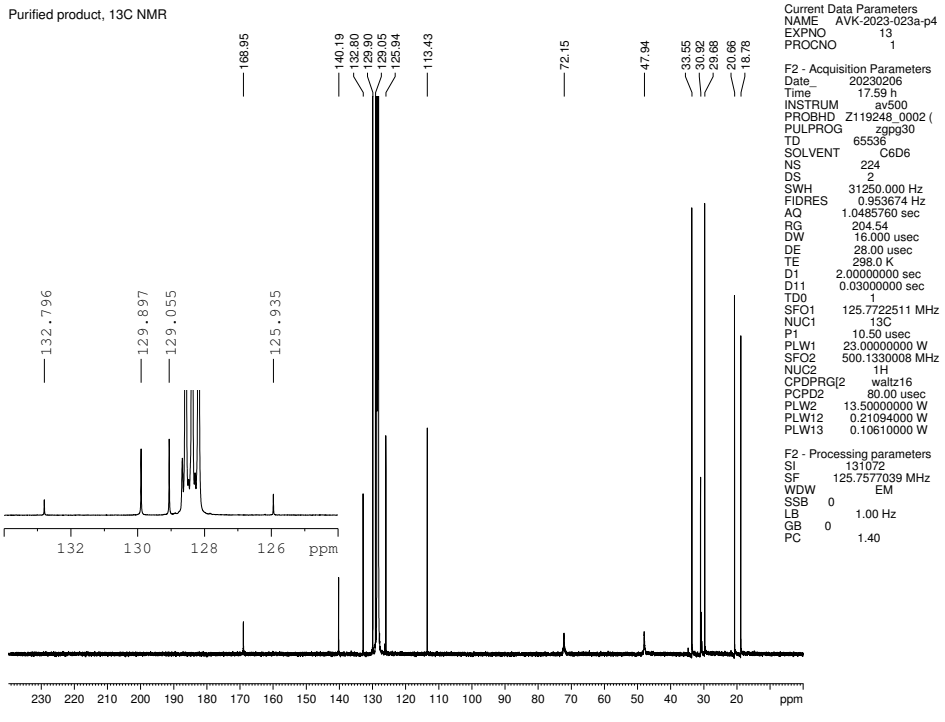


Figure 4.48. ^{13}C NMR (125 MHz, C_6D_6) of compound **4.54**.

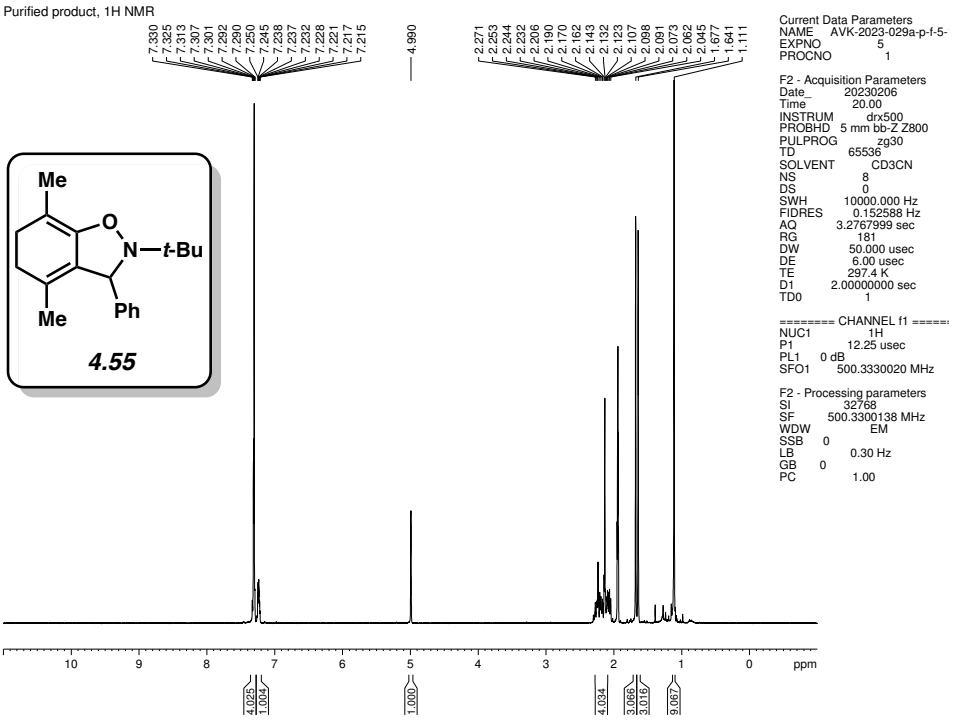


Figure 4.49. ^{1}H NMR (500 MHz, CD_3CN) of compound **4.55**.

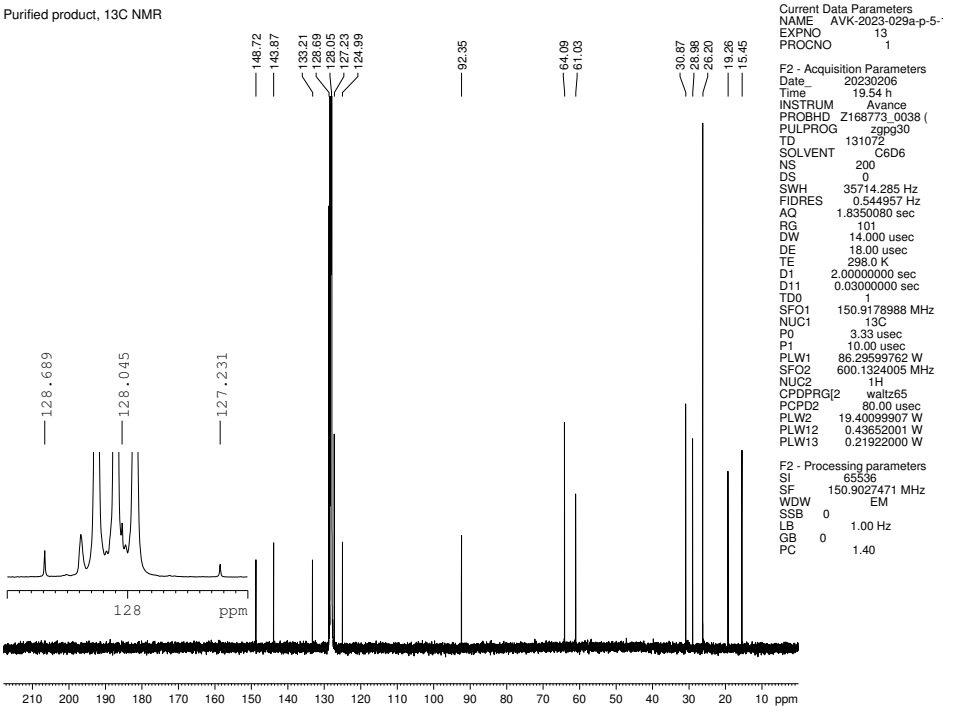


Figure 4.50. ^{13}C NMR (150 MHz, C_6D_6) of compound **4.55**.

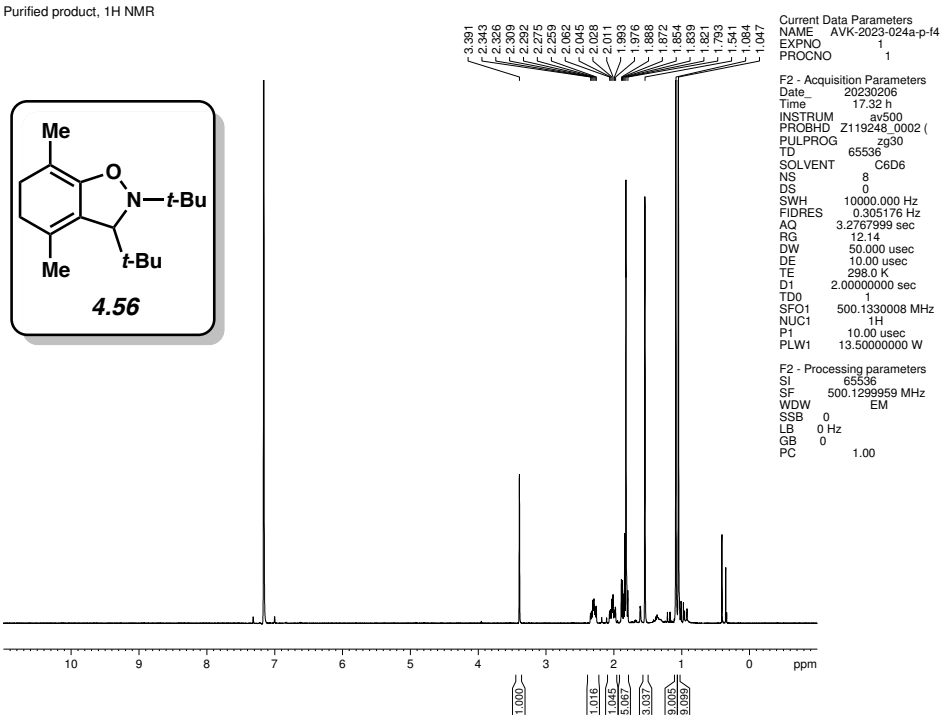


Figure 4.51. ^{13}C NMR (500 MHz, C_6D_6) of compound **4.56**.

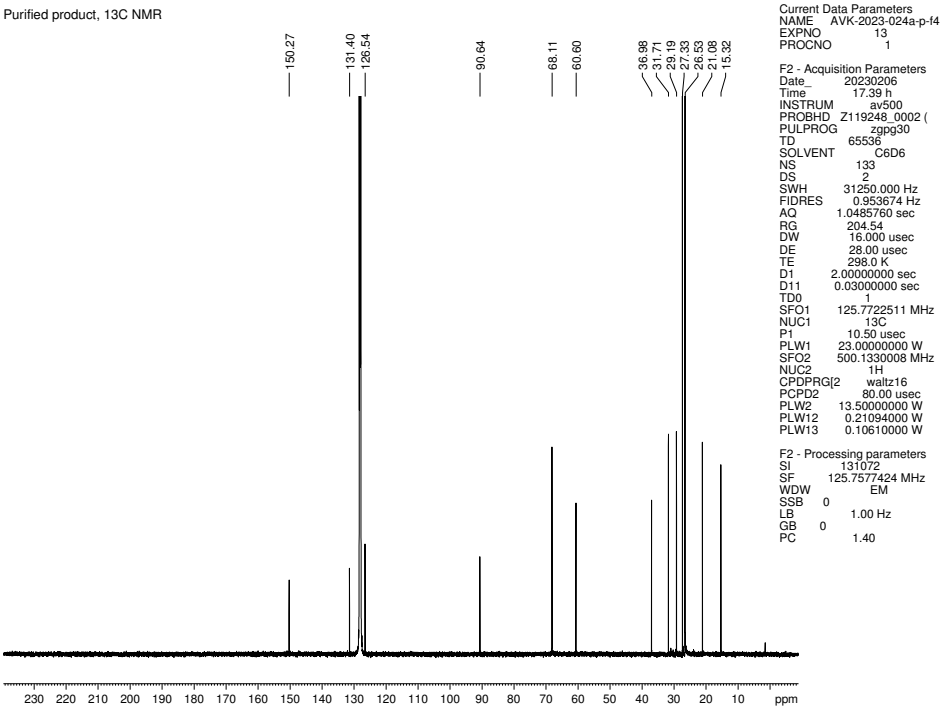


Figure 4.52. ^{13}C NMR (125 MHz, C_6D_6) of compound **4.56**.

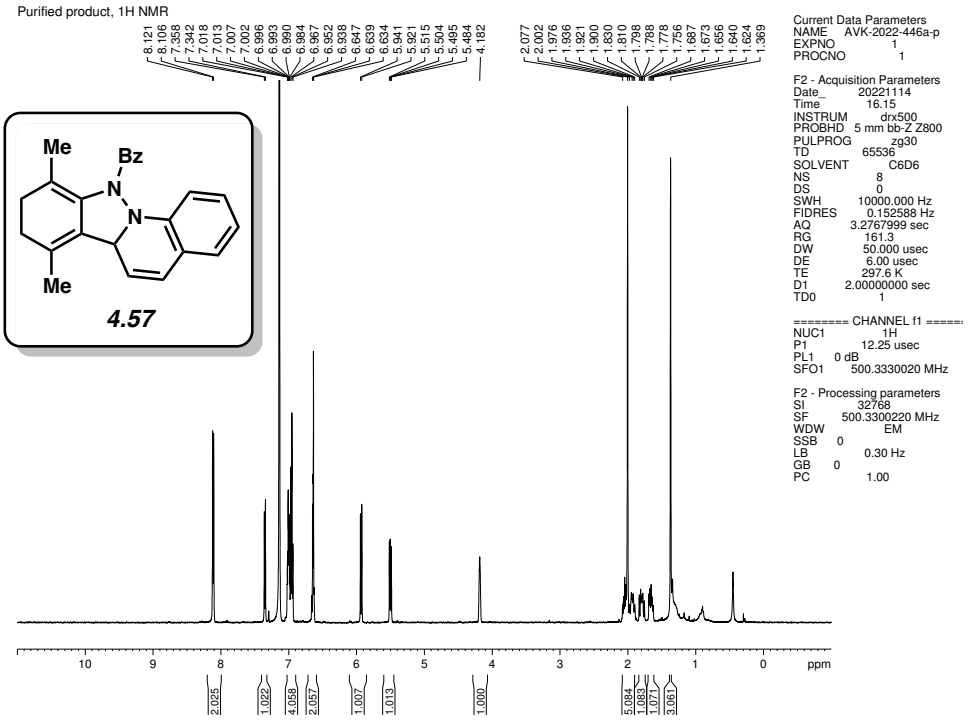


Figure 4.53. ^{1}H NMR (500 MHz, C_6D_6) of compound **4.57**.

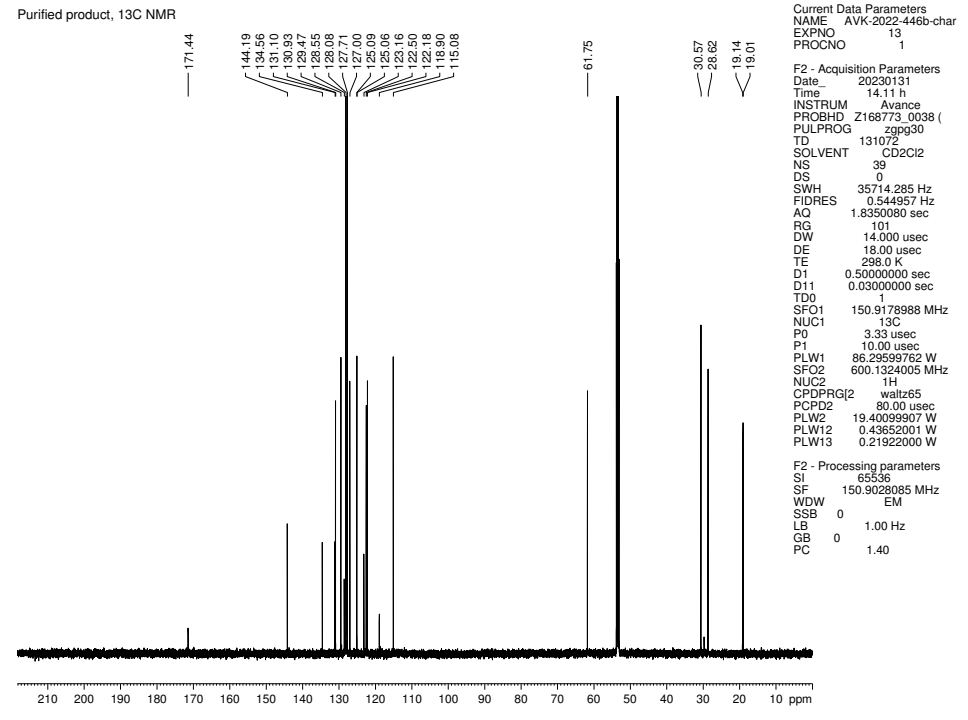


Figure 4.54. ^{13}C NMR (150 MHz, CD_2Cl_2) of compound **4.57**.

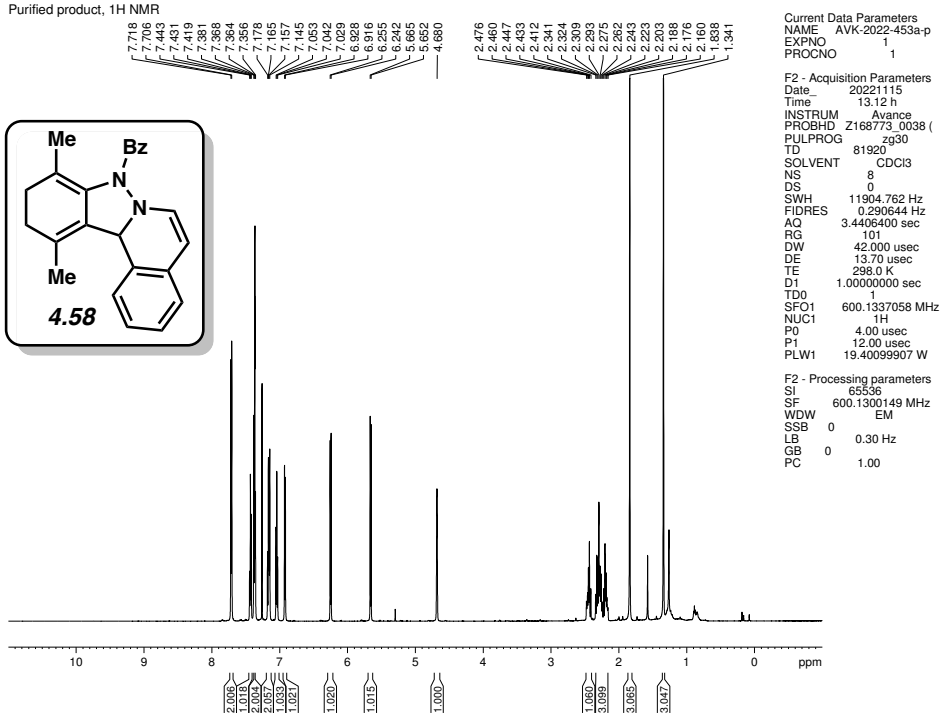


Figure 4.55. ^{1}H NMR (600 MHz, $CDCl_3$) of compound **4.58**.

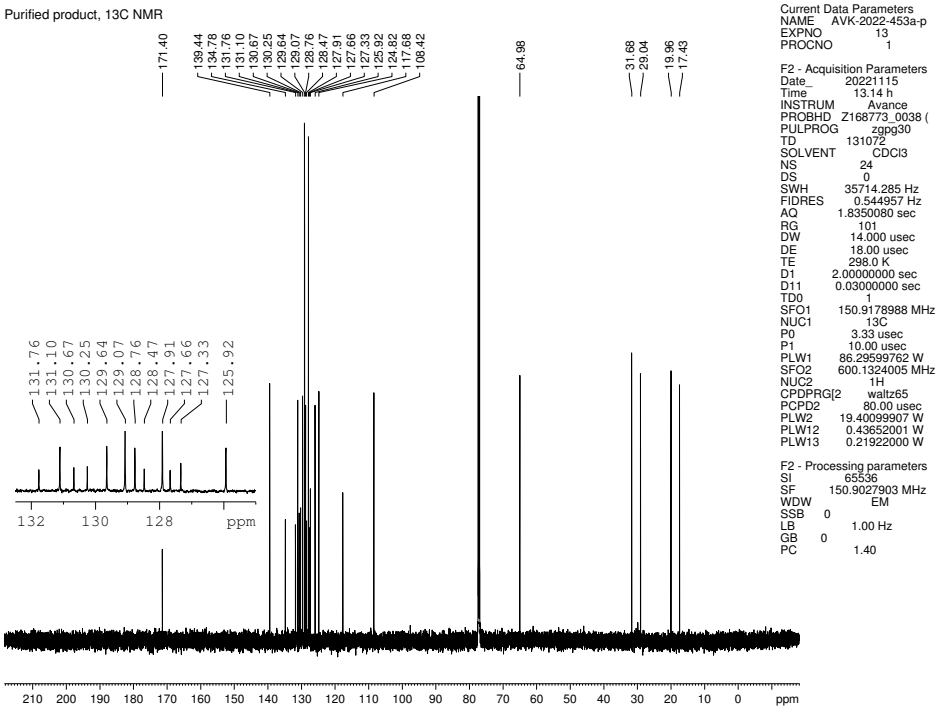


Figure 4.56. ^{13}C NMR (150 MHz, $CDCl_3$) of compound **4.58**.

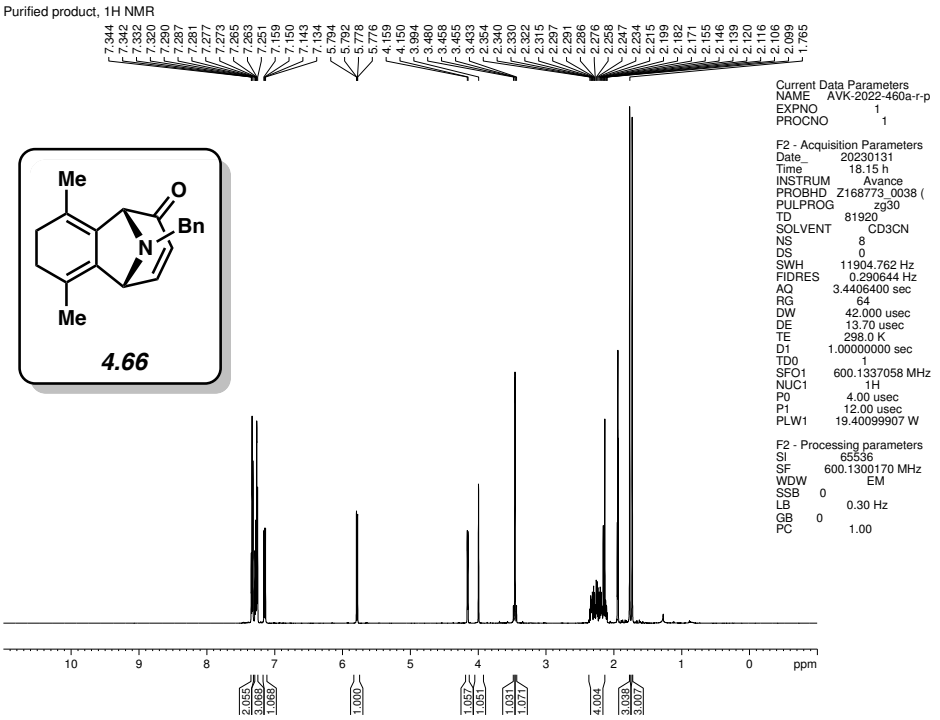


Figure 4.57. ^{1}H NMR (600 MHz, $CDCl_3$) of compound **4.66**.

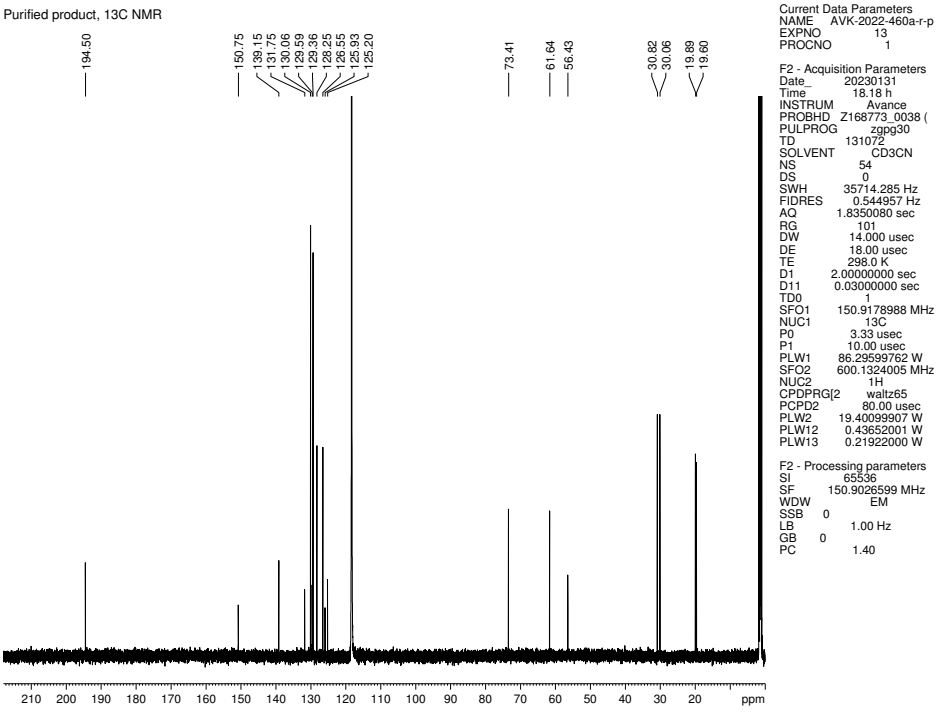


Figure 4.58. ^{13}C NMR (150 MHz, CD_3CN) of compound **4.66**.

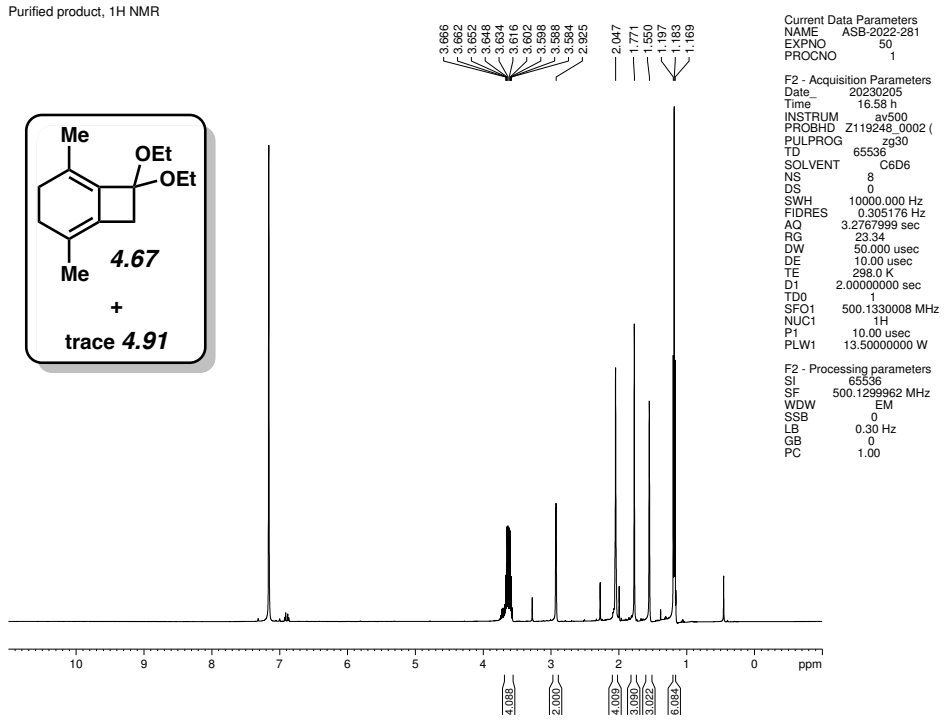


Figure 4.59. ^{1}H NMR (500 MHz, C_6D_6) of compound **4.67**.

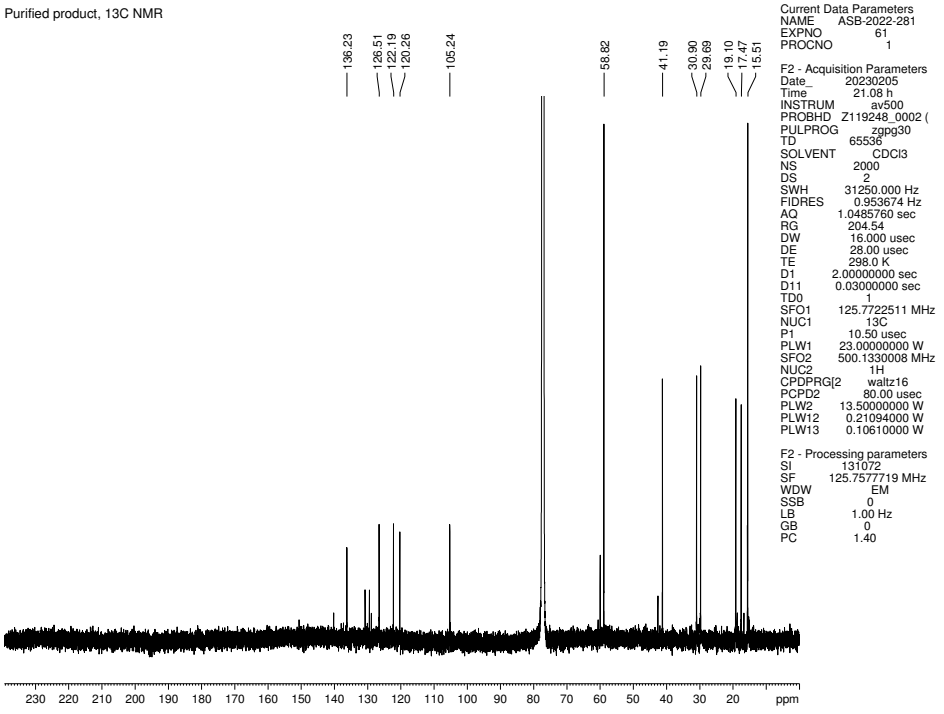


Figure 4.60. ^{13}C NMR (125 MHz, $CDCl_3$) of compound **4.67**.

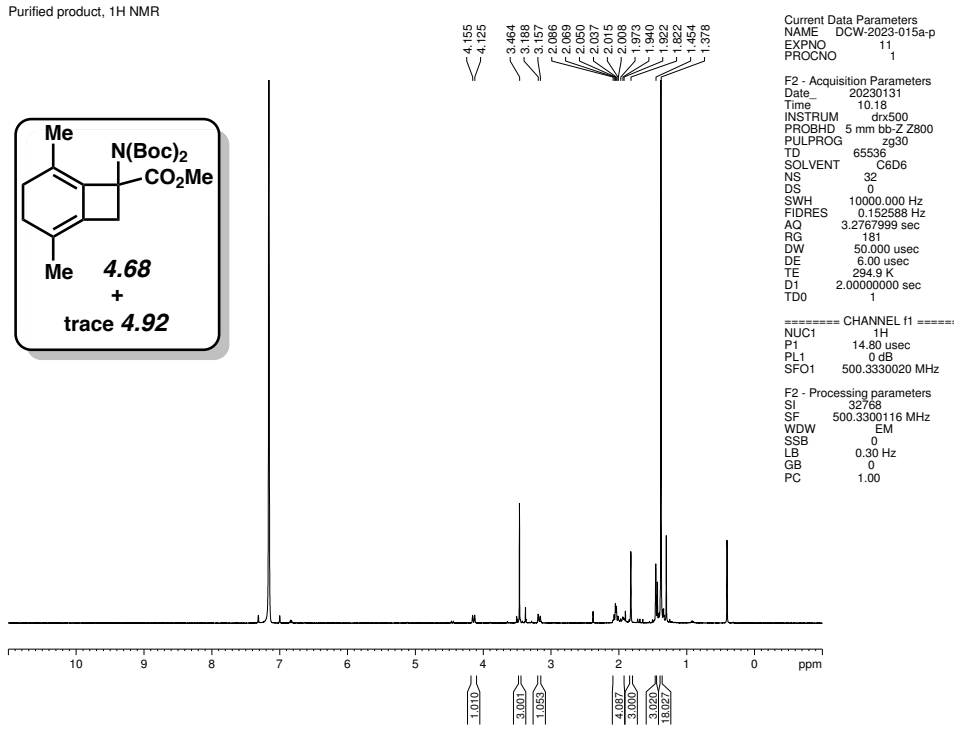


Figure 4.61. ^{1}H NMR (500 MHz, C_6D_6) of compound **4.68**.

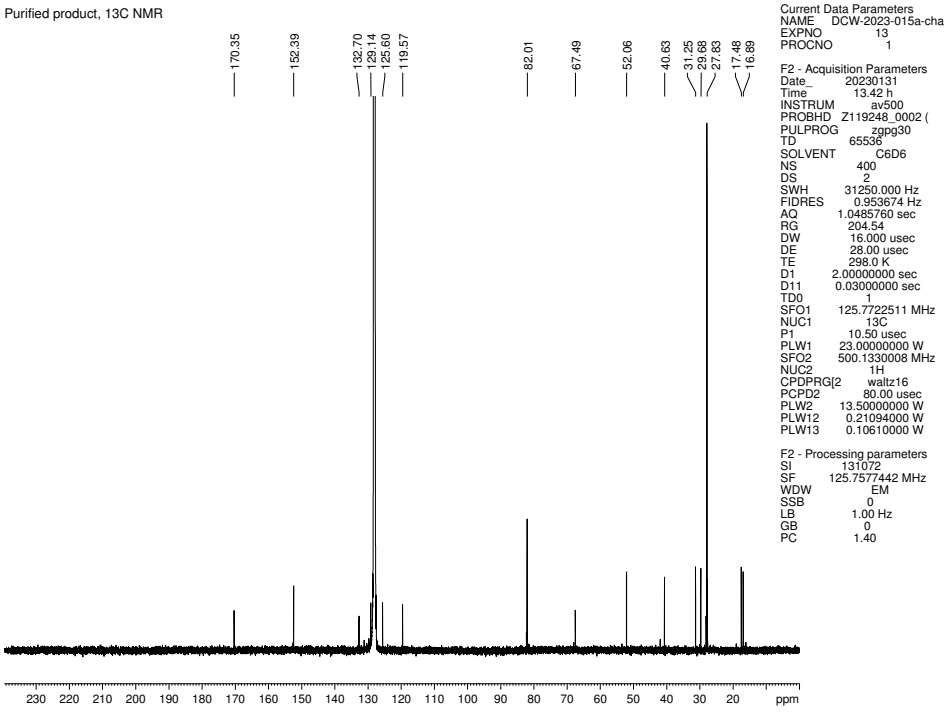


Figure 4.62. ^{13}C NMR (125 MHz, C_6D_6) of compound **4.68**.

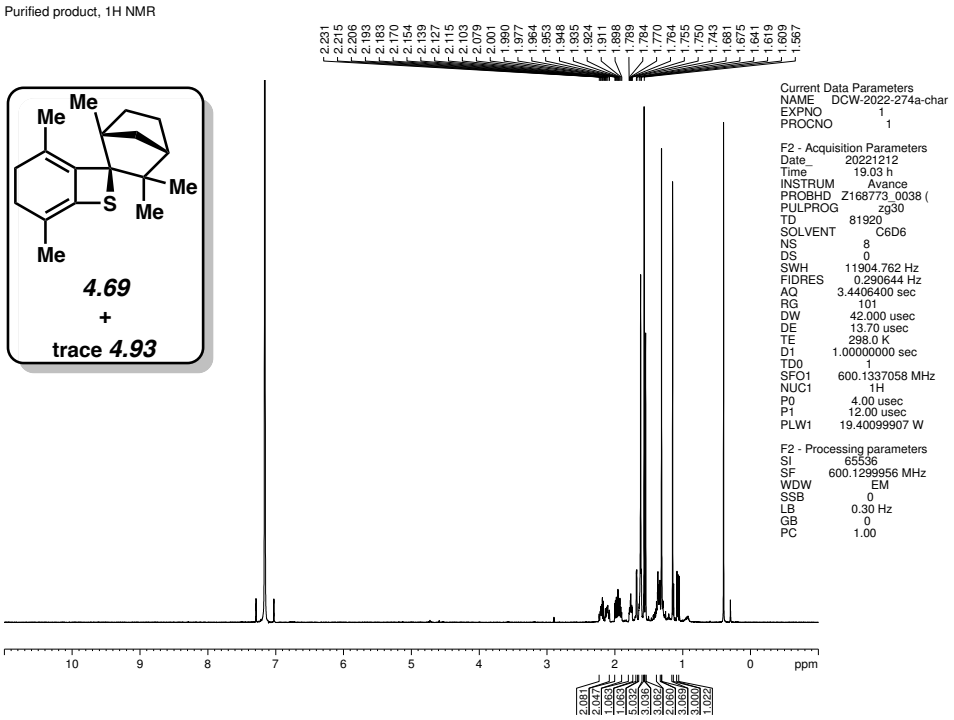


Figure 4.63. ^{1}H NMR (600 MHz, C_6D_6) of compound **4.69**.

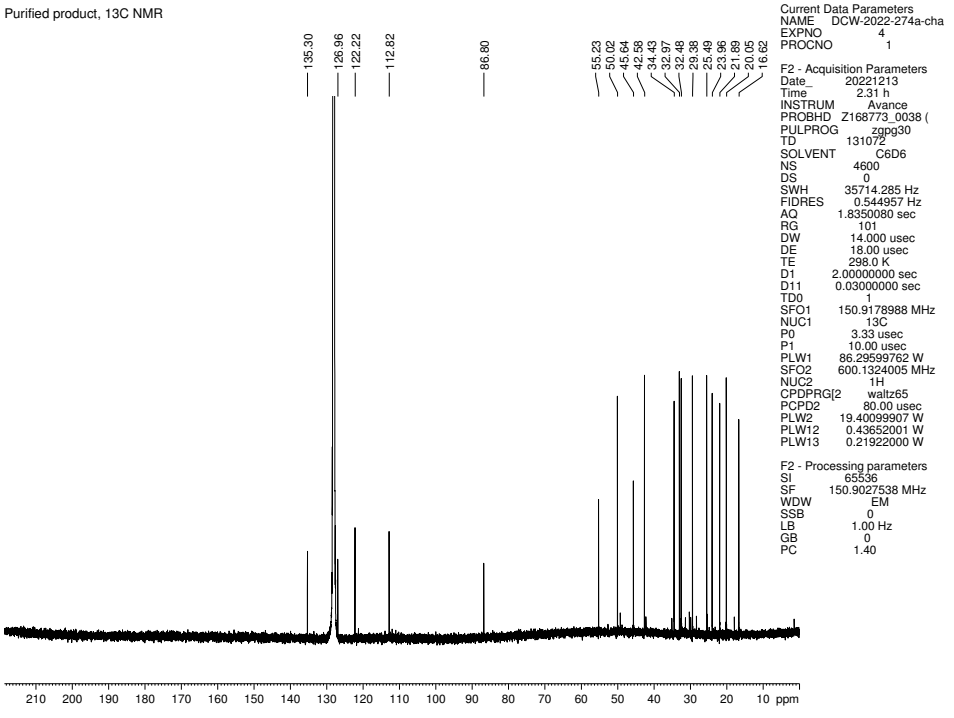


Figure 4.64. ^{13}C NMR (150 MHz, C_6D_6) of compound **4.69**.

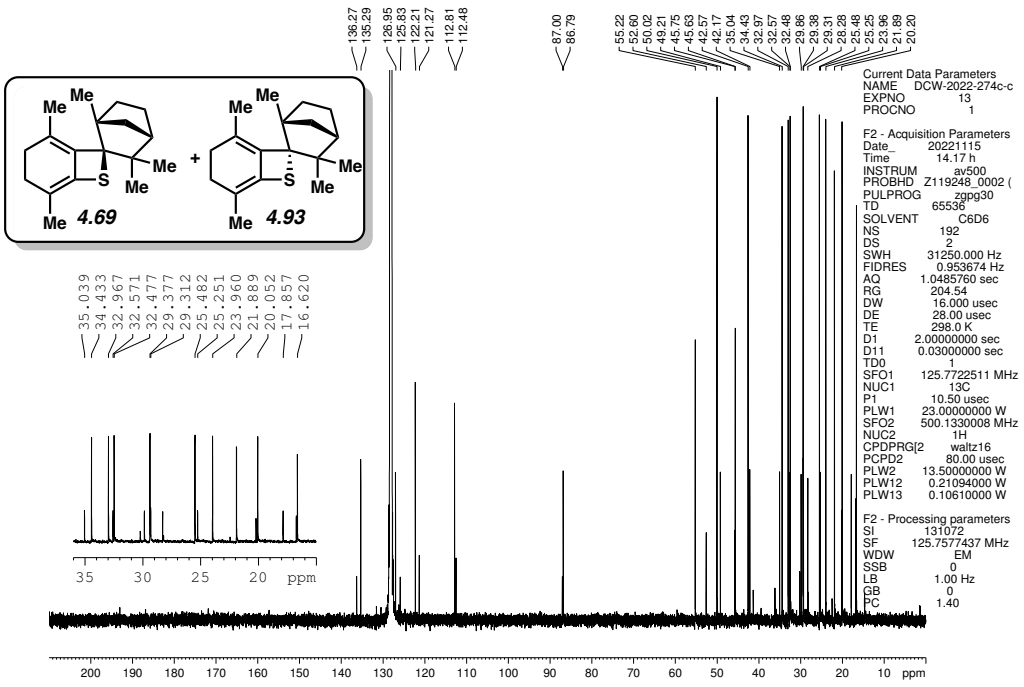


Figure 4.65. ^{13}C NMR (125 MHz, C_6D_6) of compound **4.69** and **4.93**.

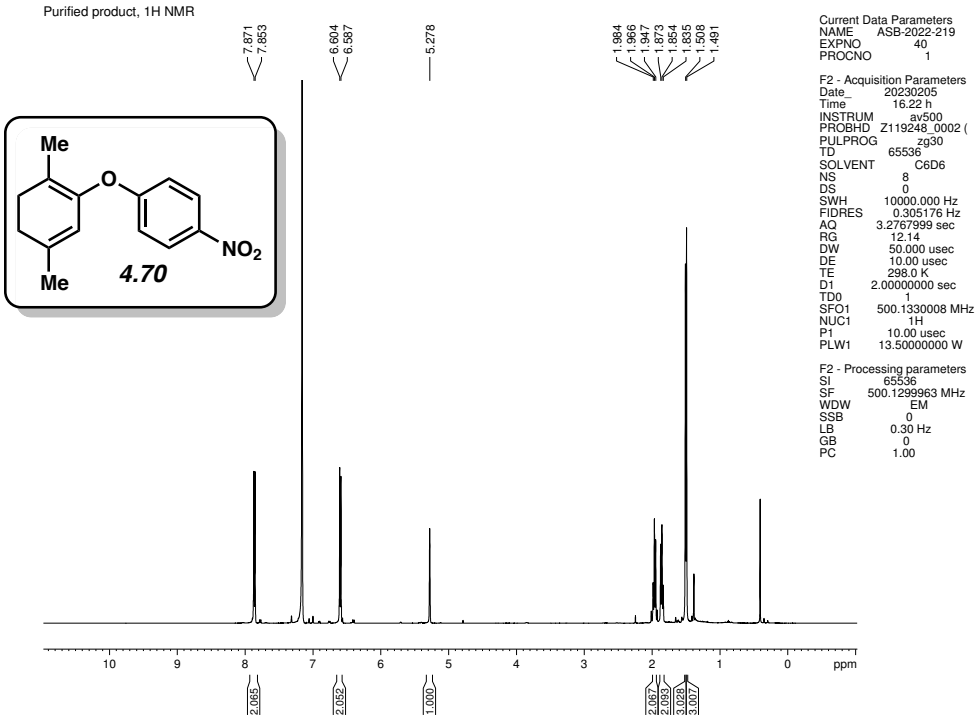


Figure 4.66. ^{1}H NMR (500 MHz, C_6D_6) of compound **4.70**.

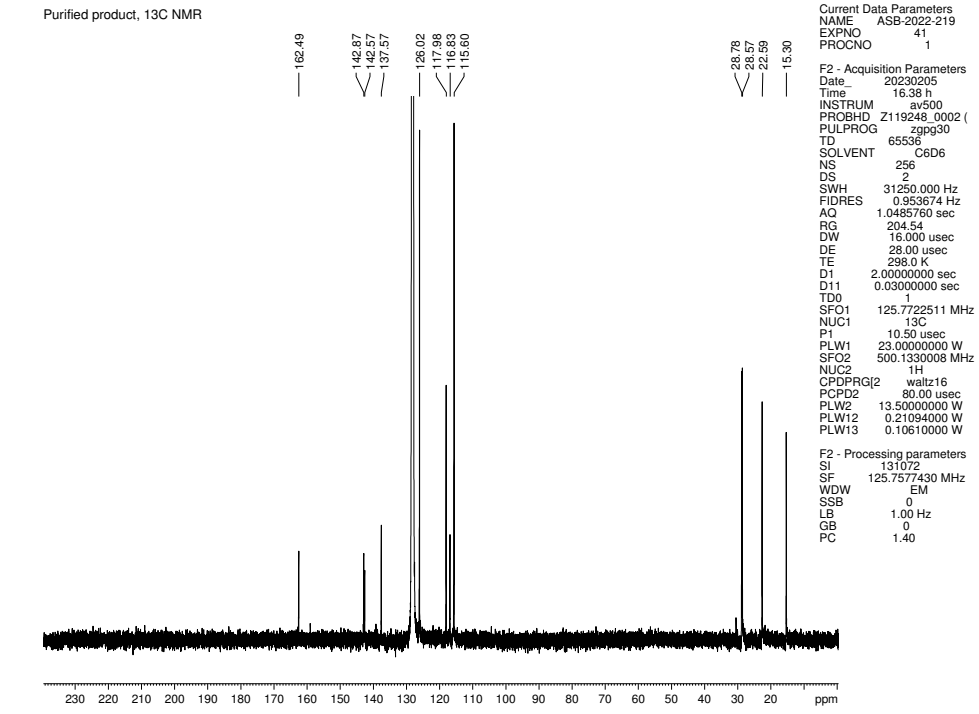


Figure 4.67. ^{13}C NMR (125 MHz, C_6D_6) of compound **4.70**.

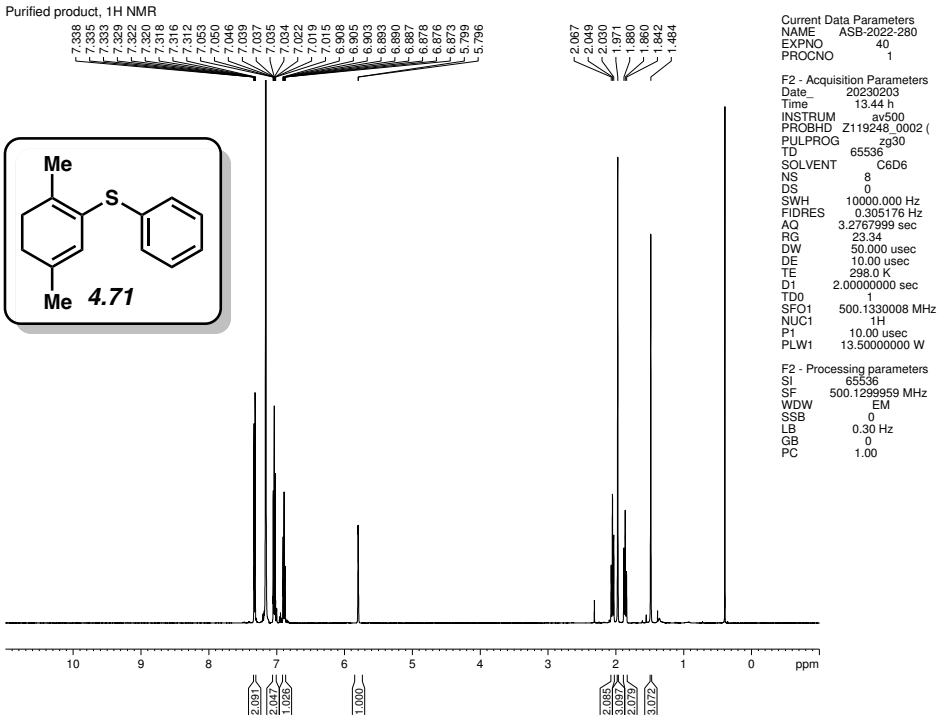


Figure 4.68. ^{1}H NMR (500 MHz, C_6D_6) of compound **4.71**.

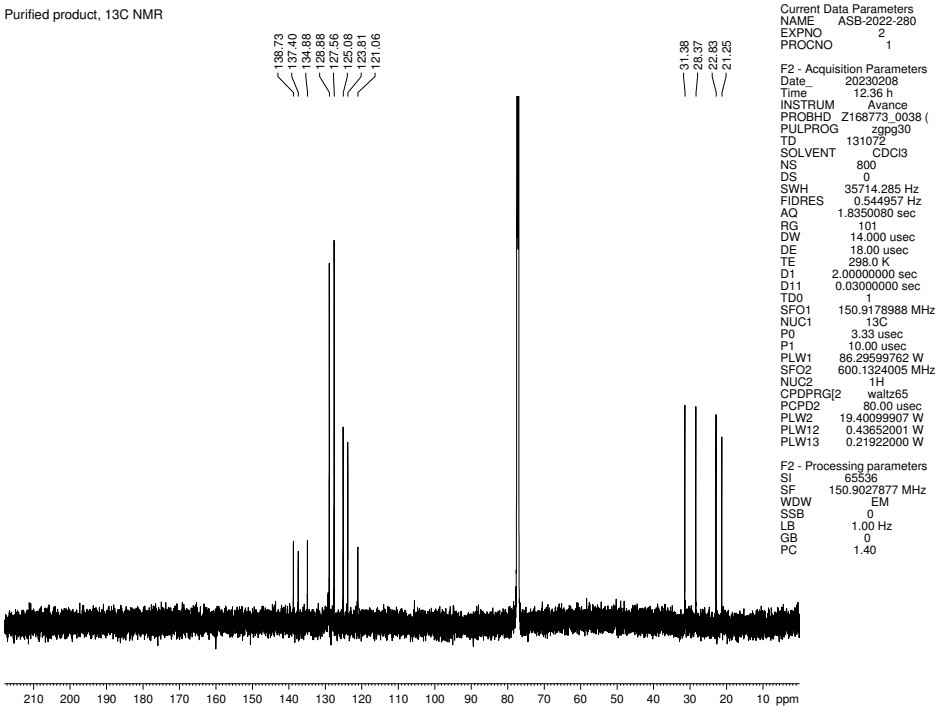


Figure 4.69. ^{13}C NMR (150 MHz, $CDCl_3$) of compound **4.71**.

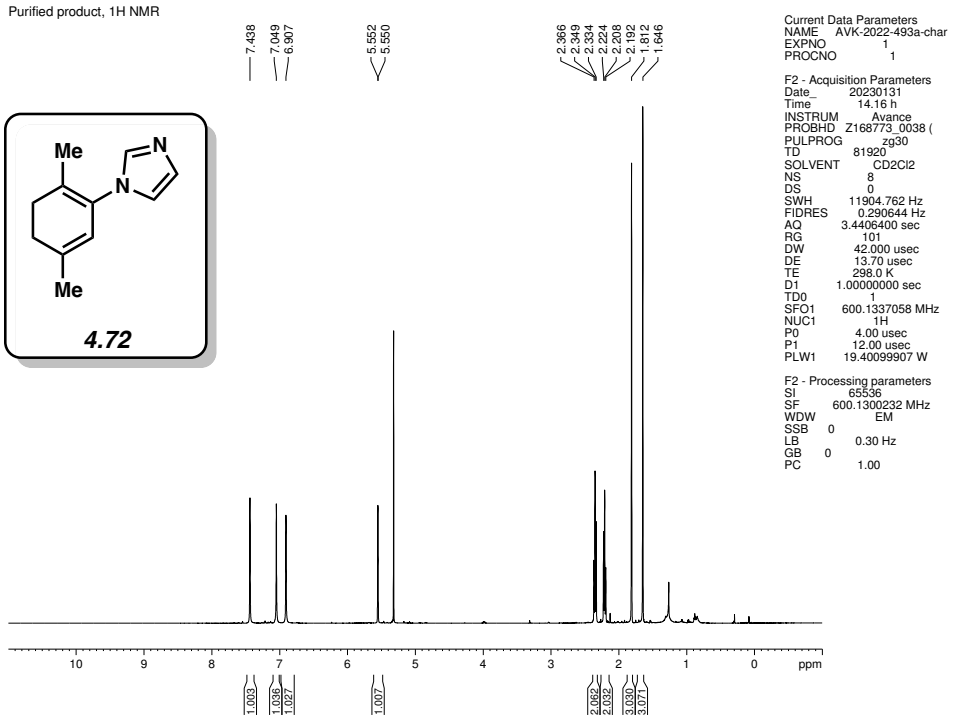


Figure 4.70. ^{1}H NMR (600 MHz, CD_2Cl_2) of compound **4.72**.

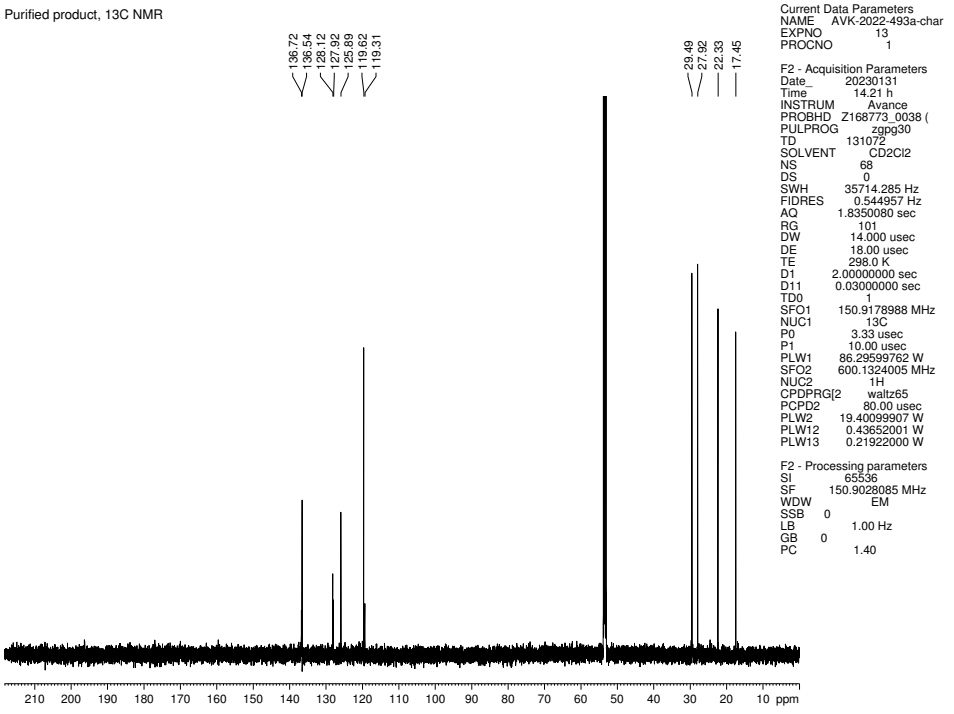


Figure 4.71. ^{13}C NMR (150 MHz, CD_2Cl_2) of compound **4.72**.

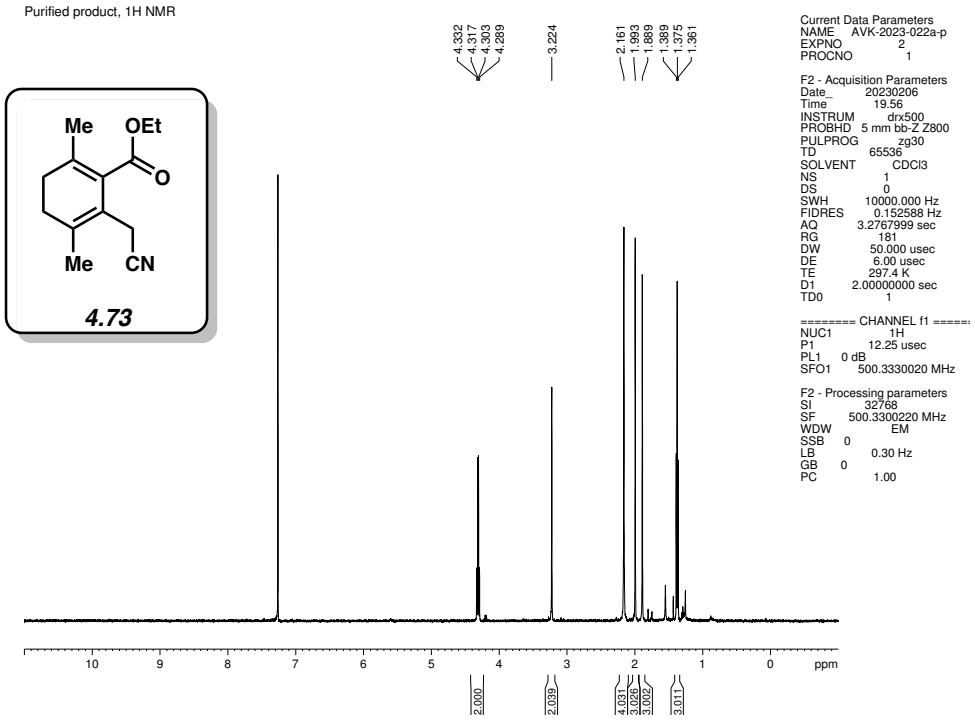


Figure 4.72. ^{1}H NMR (500 MHz, $CDCl_3$) of compound **4.73**.

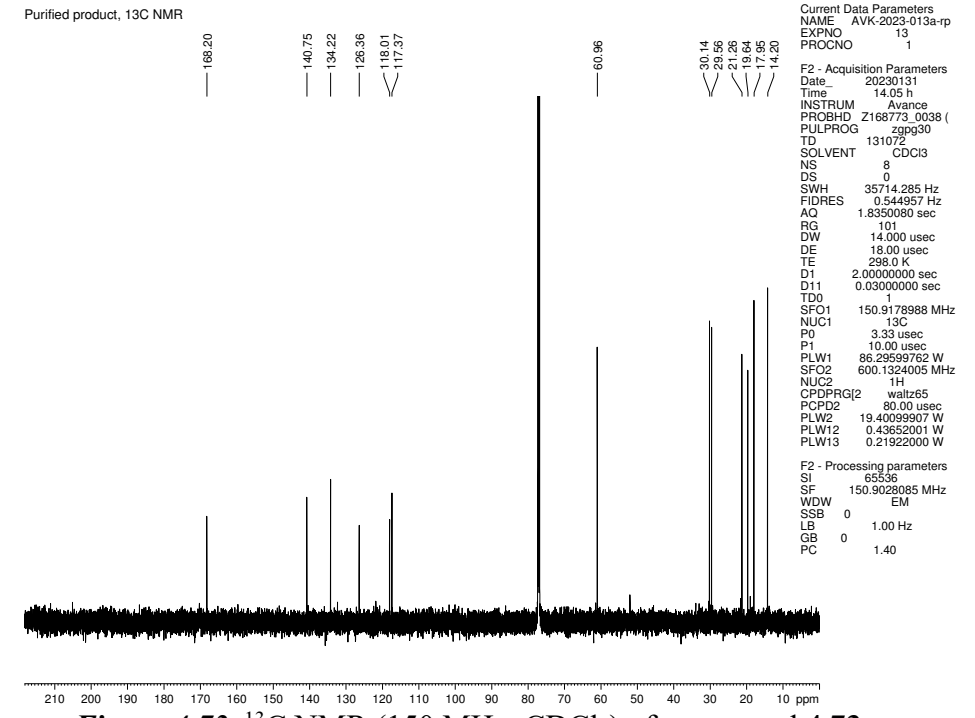


Figure 4.73. ^{13}C NMR (150 MHz, $CDCl_3$) of compound **4.73**.

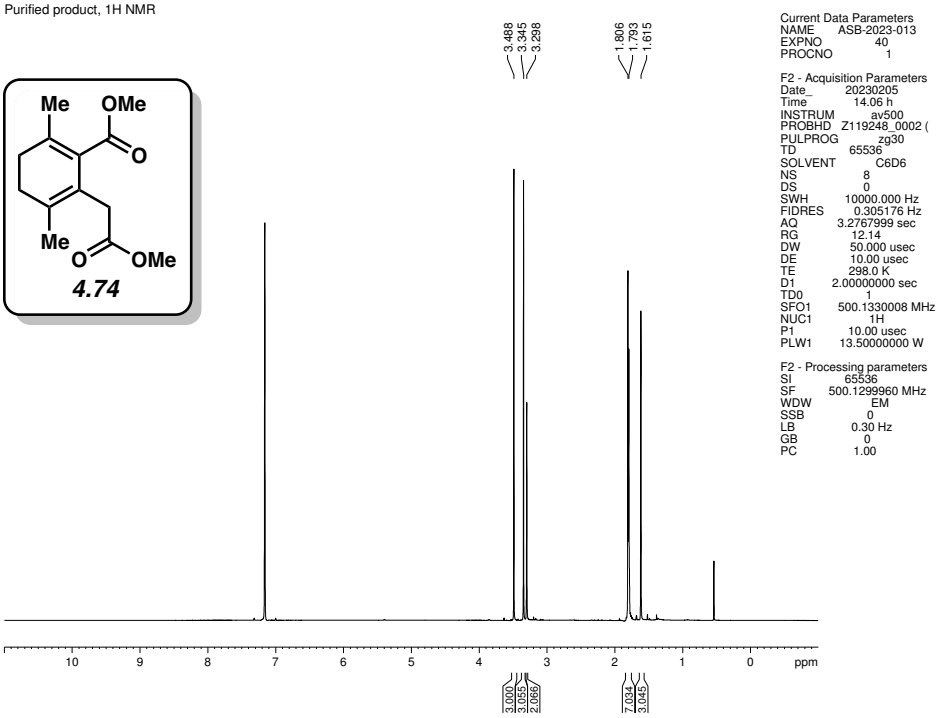


Figure 4.74. ^{1}H NMR (500 MHz, C_6D_6) of compound **4.74**.

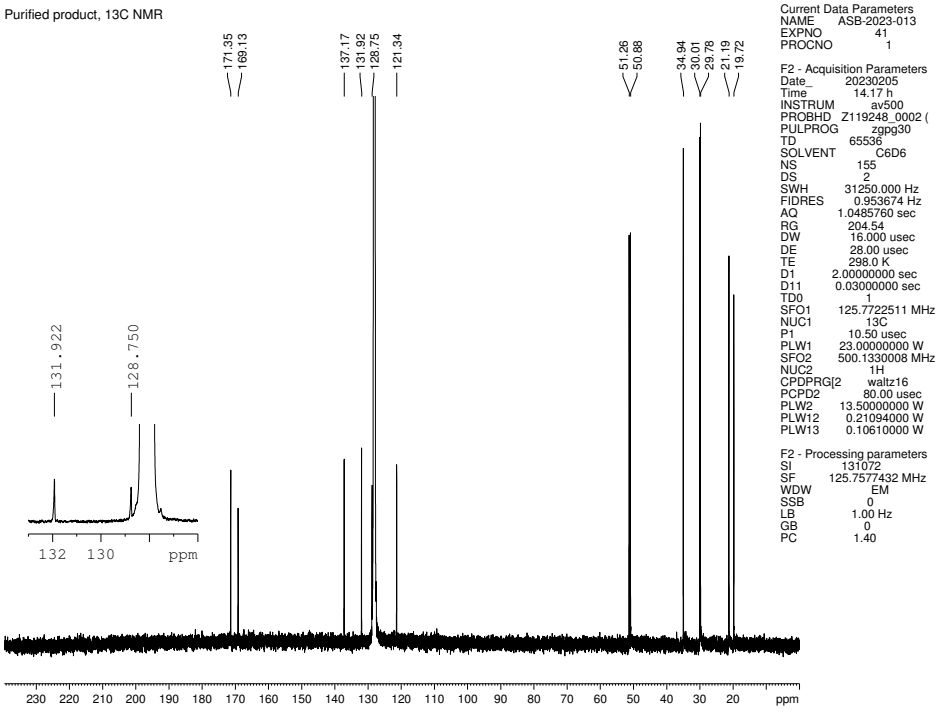


Figure 4.75. ^{13}C NMR (125 MHz, C_6D_6) of compound **4.74**.

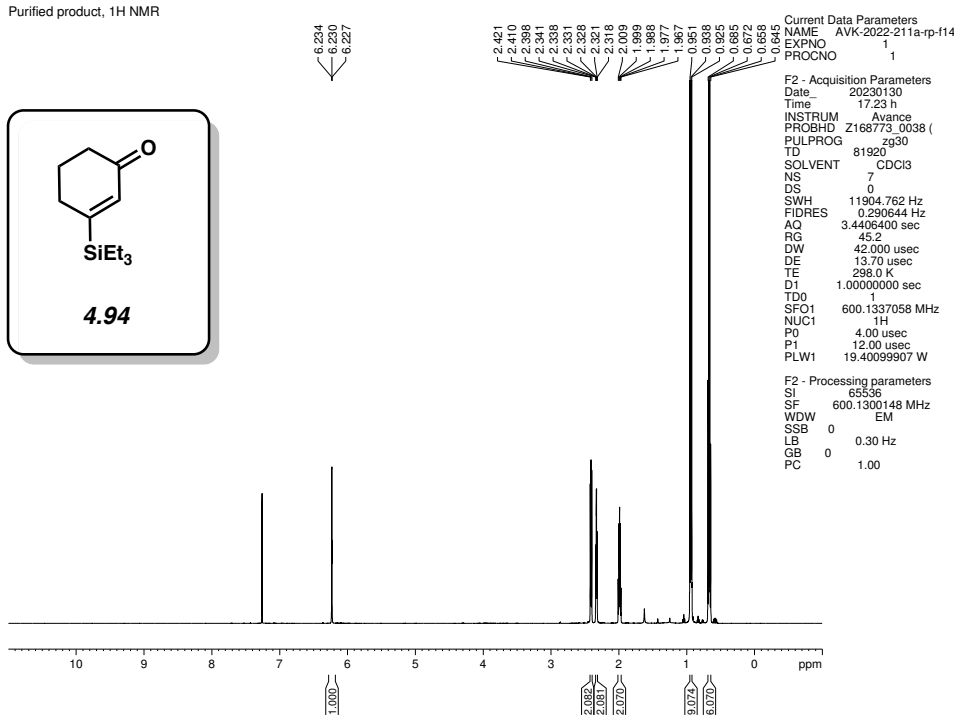


Figure 4.76. ^{1}H NMR (600 MHz, $CDCl_3$) of compound **4.94**.

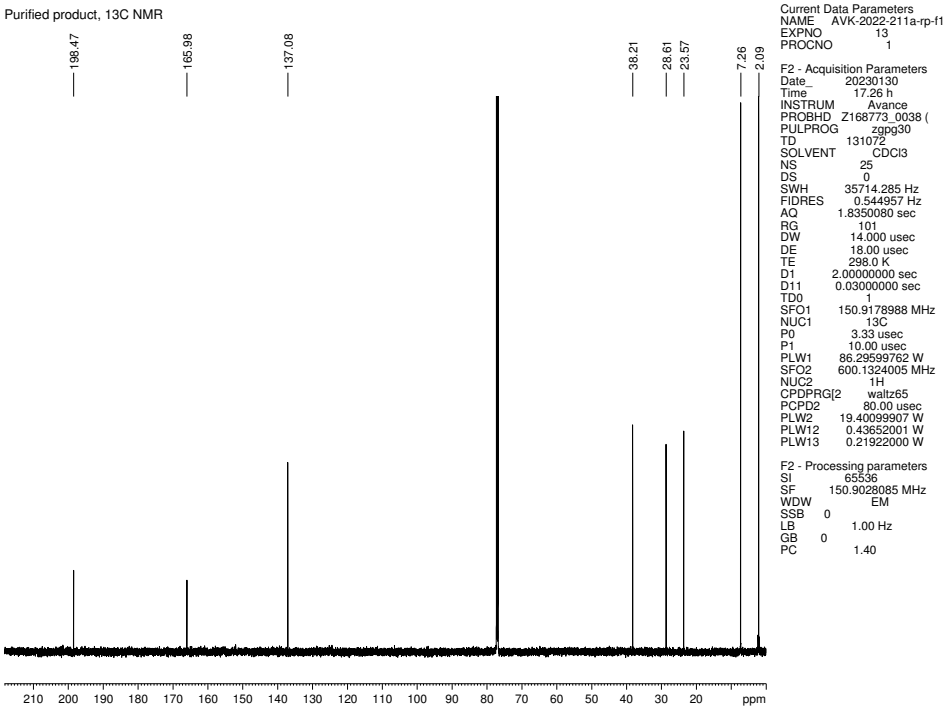


Figure 4.77. ^{13}C NMR (150 MHz, $CDCl_3$) of compound **4.94**.

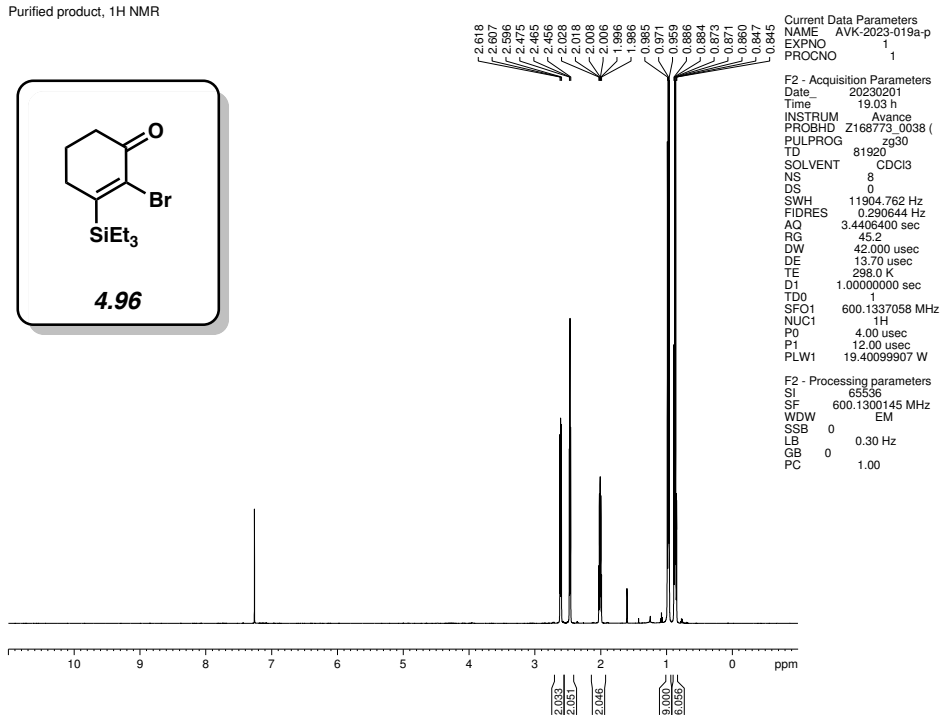


Figure 4.78. ^{1}H NMR (600 MHz, $CDCl_3$) of compound **4.96**.

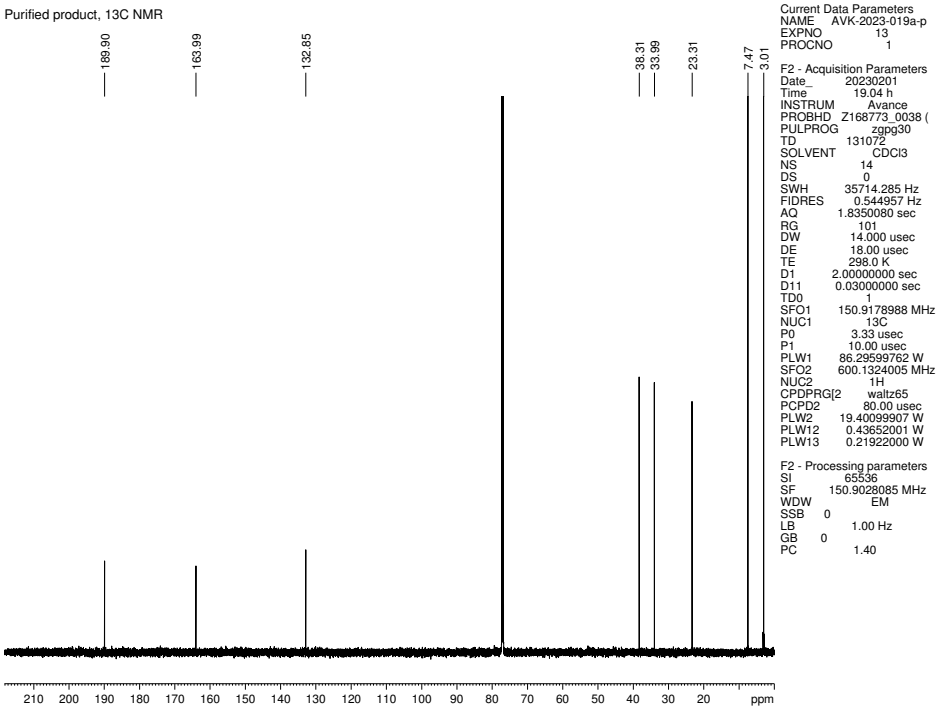


Figure 4.79. ^{13}C NMR (150 MHz, $CDCl_3$) of compound **4.96**.

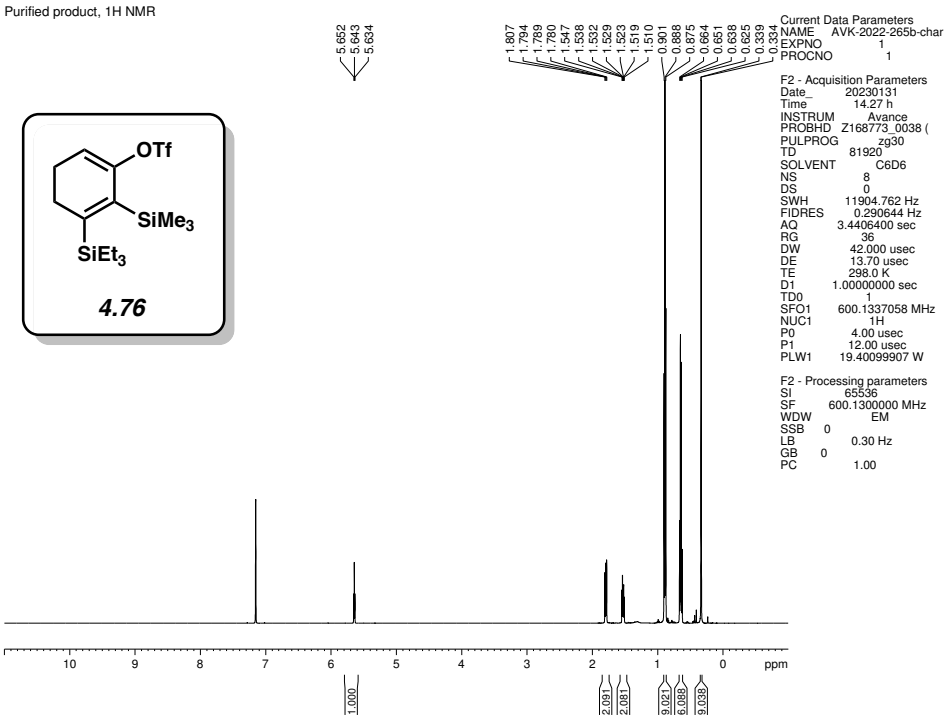


Figure 4.80. ^{1}H NMR (600 MHz, C_6D_6) of compound **4.76**.

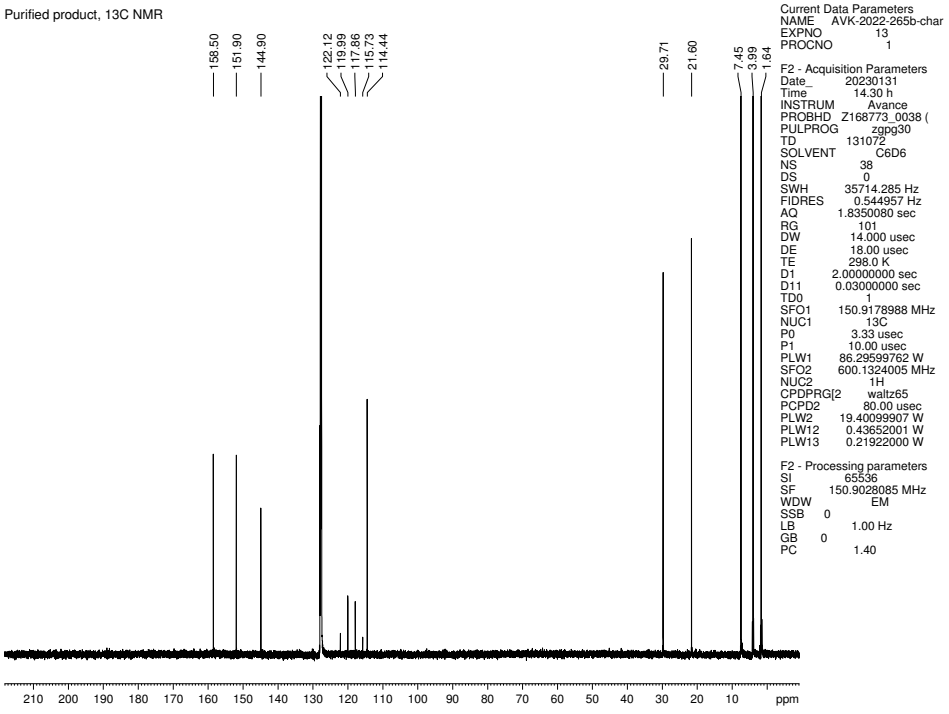


Figure 4.81. ^{13}C NMR (150 MHz, C_6D_6) of compound **4.76**.

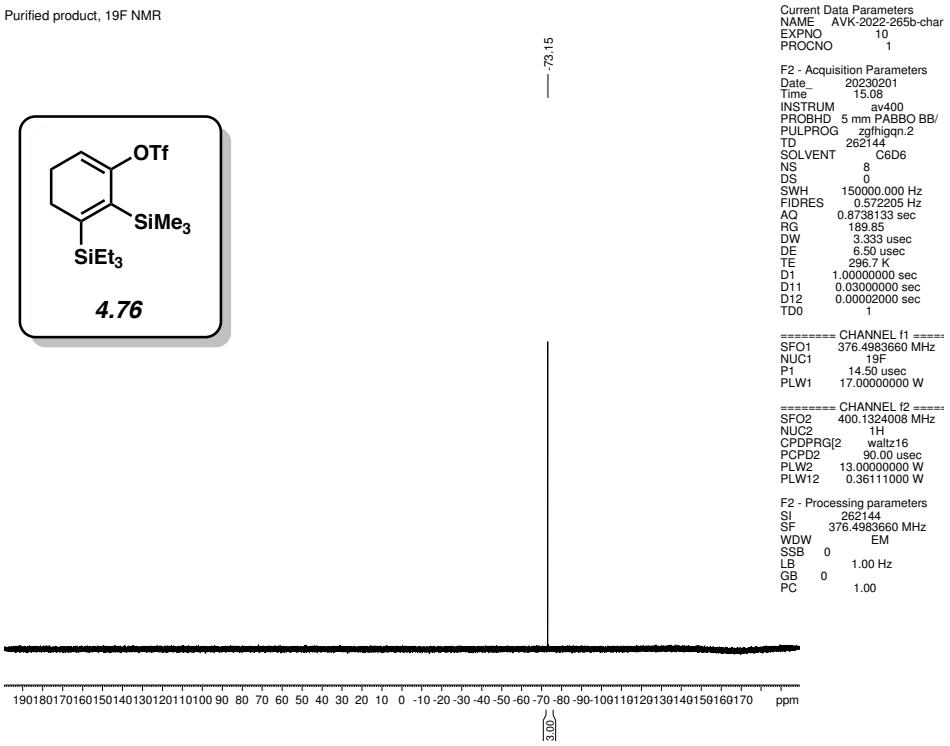


Figure 4.82. ^{19}F NMR (376 MHz, C_6D_6) of compound **4.76**.

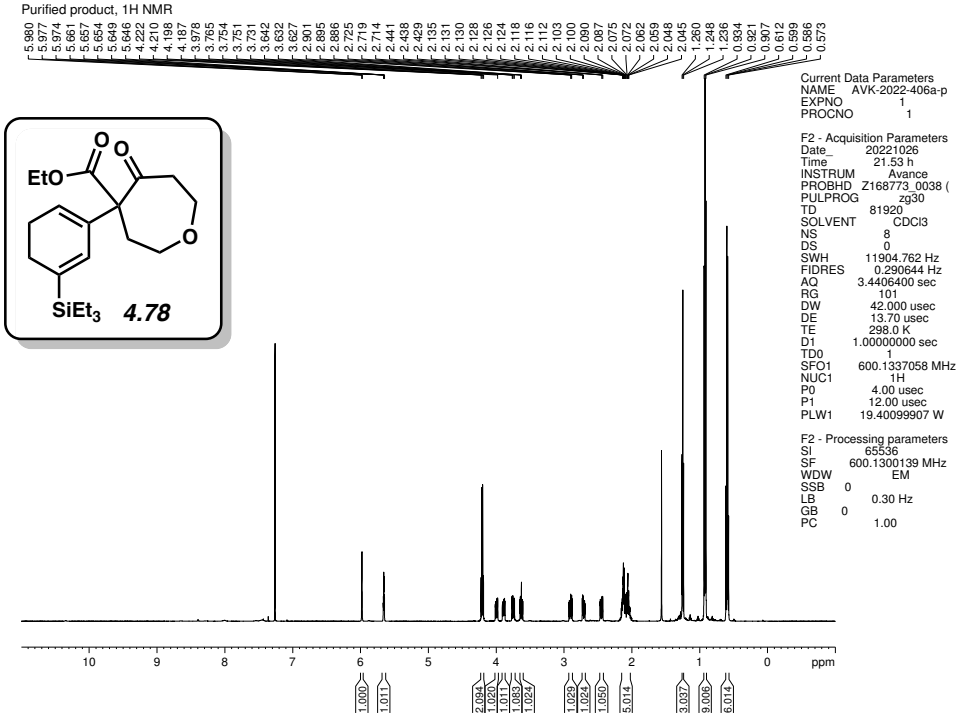


Figure 4.83. ^{1}H NMR (600 MHz, $CDCl_3$) of compound **4.78**.

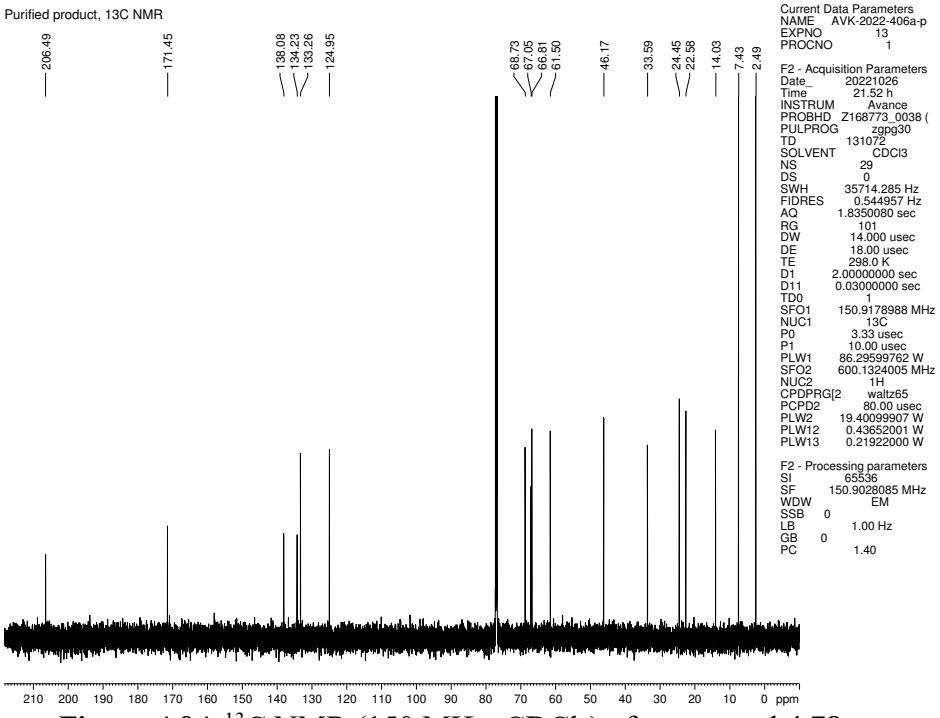


Figure 4.84. ^{13}C NMR (150 MHz, $CDCl_3$) of compound **4.78**.

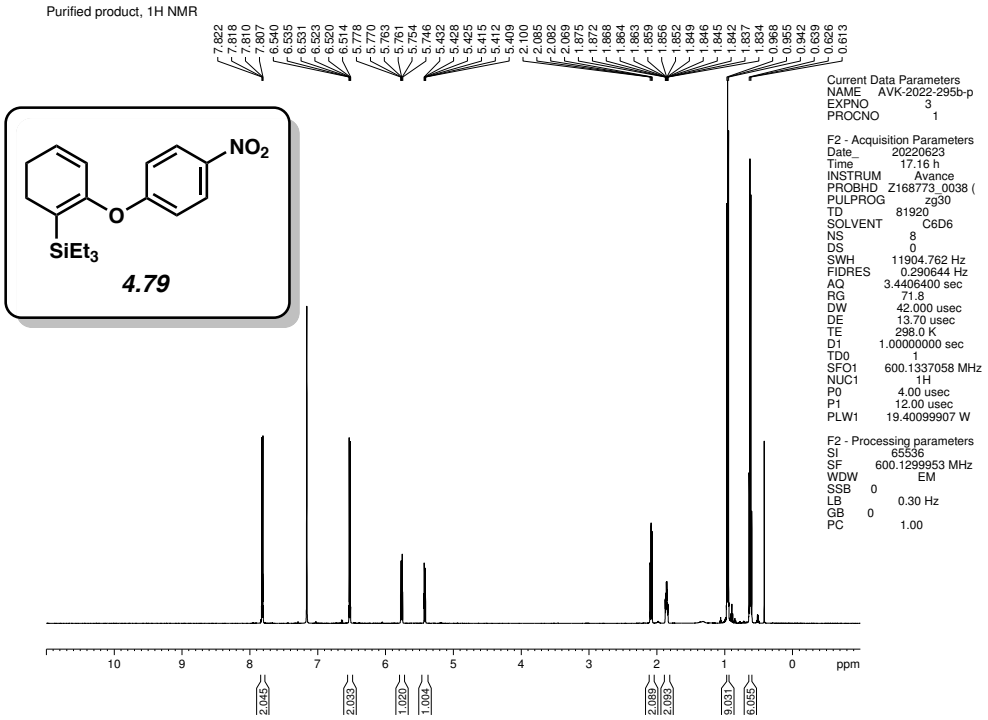


Figure 4.85. ^{1}H NMR (600 MHz, C_6D_6) of compound **4.79**.

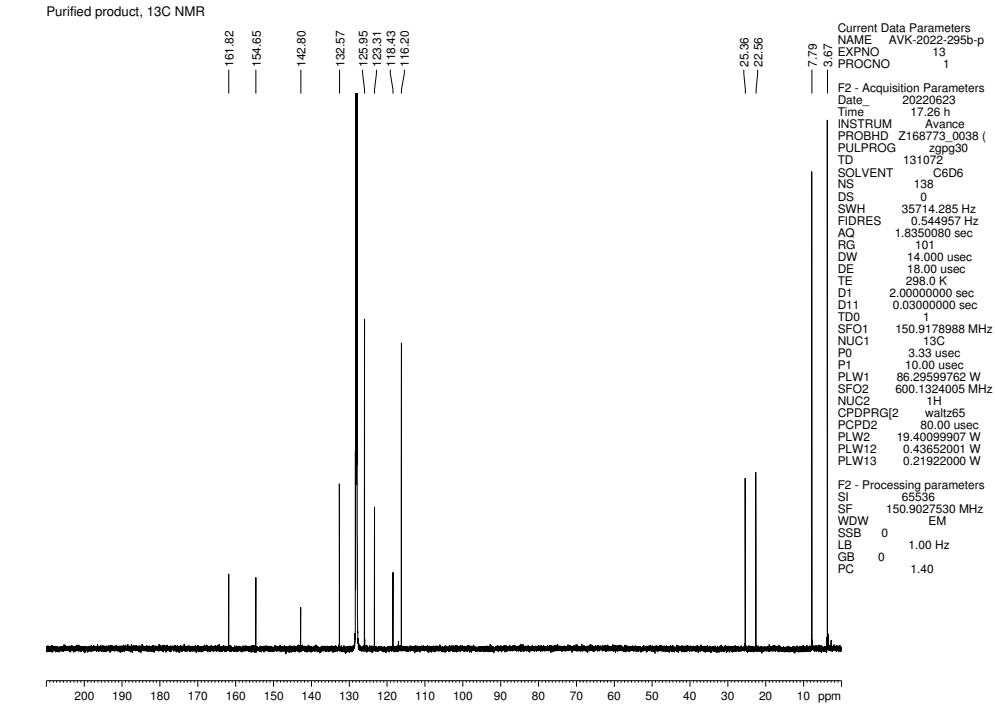


Figure 4.86. ^{13}C NMR (150 MHz, C_6D_6) of compound **4.79**.

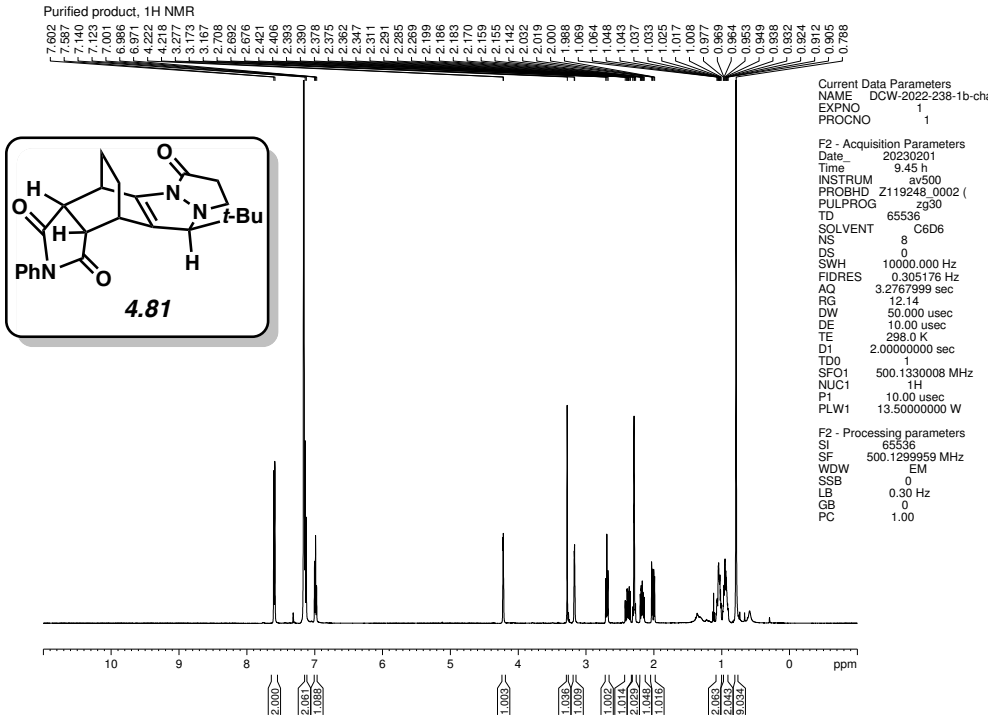


Figure 4.87. ^{1}H NMR (500 MHz, C_6D_6) of compound **4.81**.

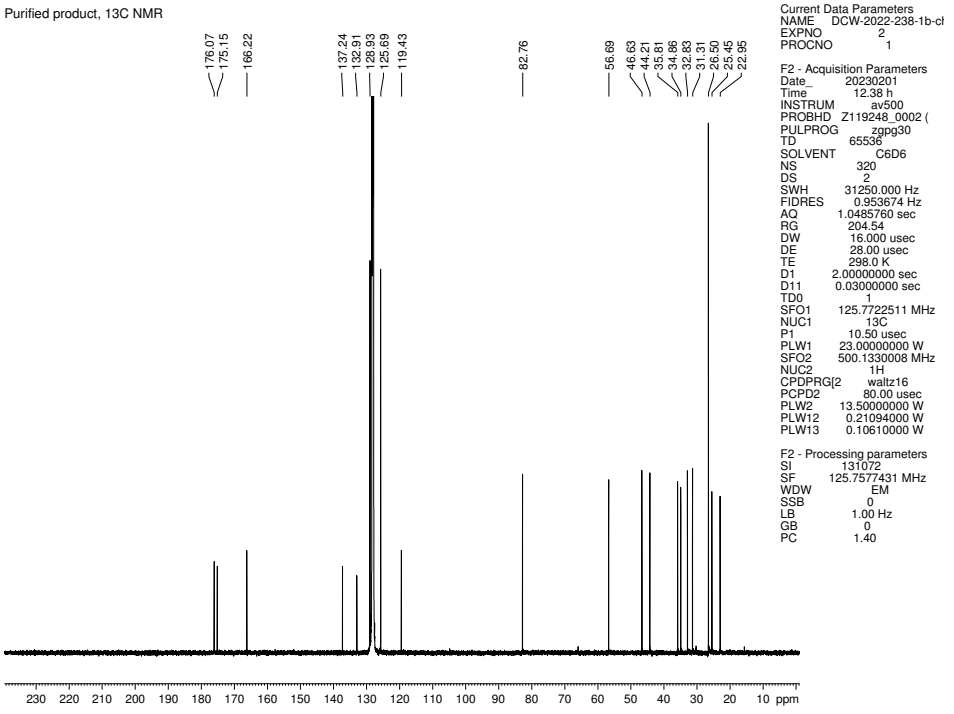


Figure 4.88. ^{13}C NMR (125 MHz, C_6D_6) of compound **4.81**

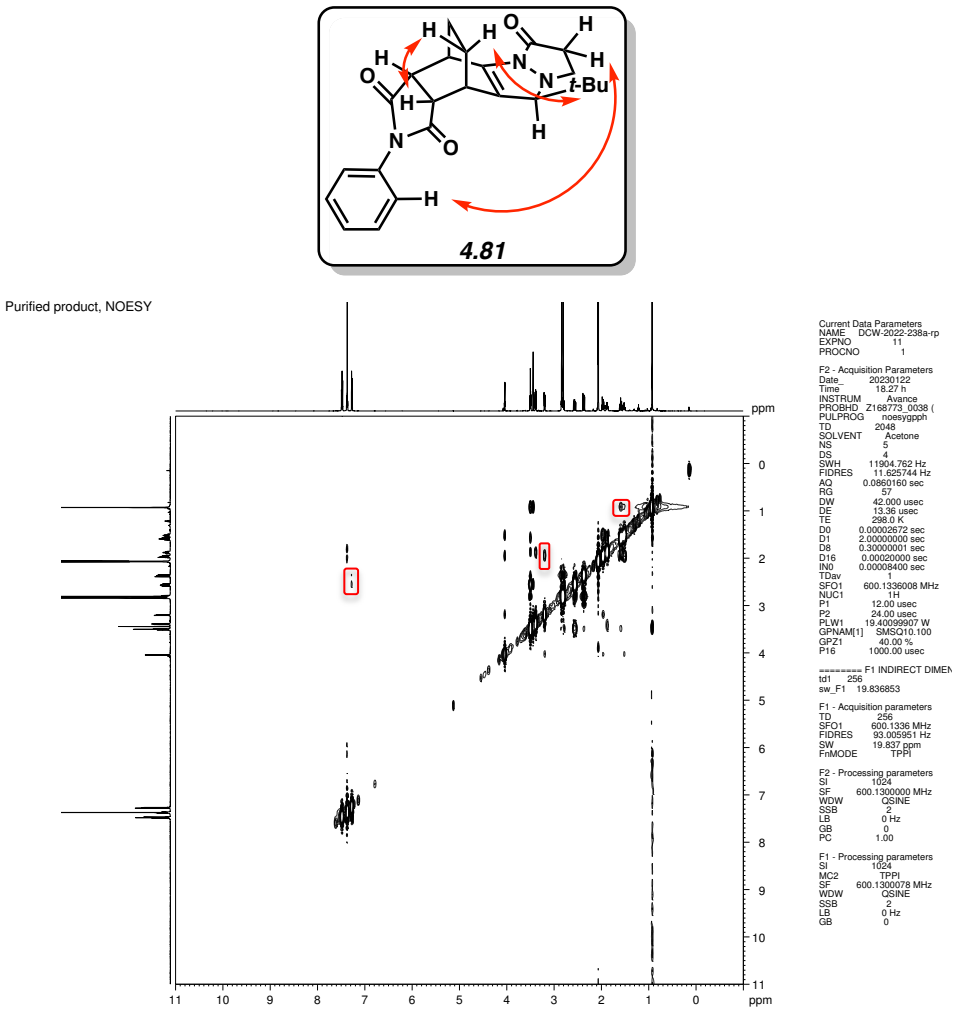


Figure 4.89. NOESY (600 MHz, acetone-d_6) of compound **4.81**.

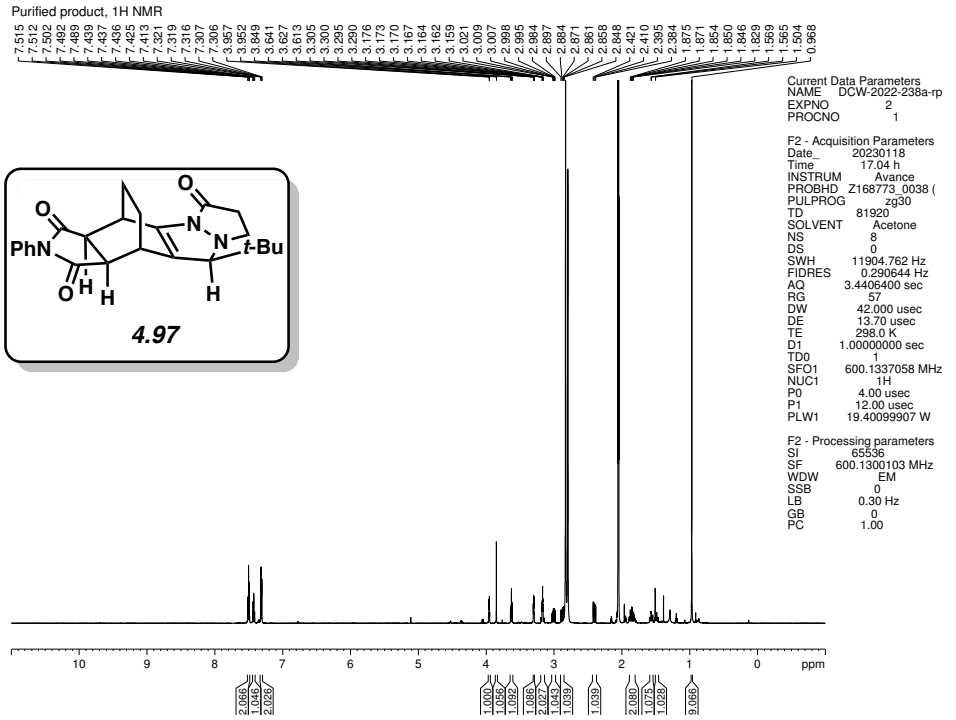


Figure 4.90. ^{1}H NMR (600 MHz, acetone-d_6) of compound **4.97**.

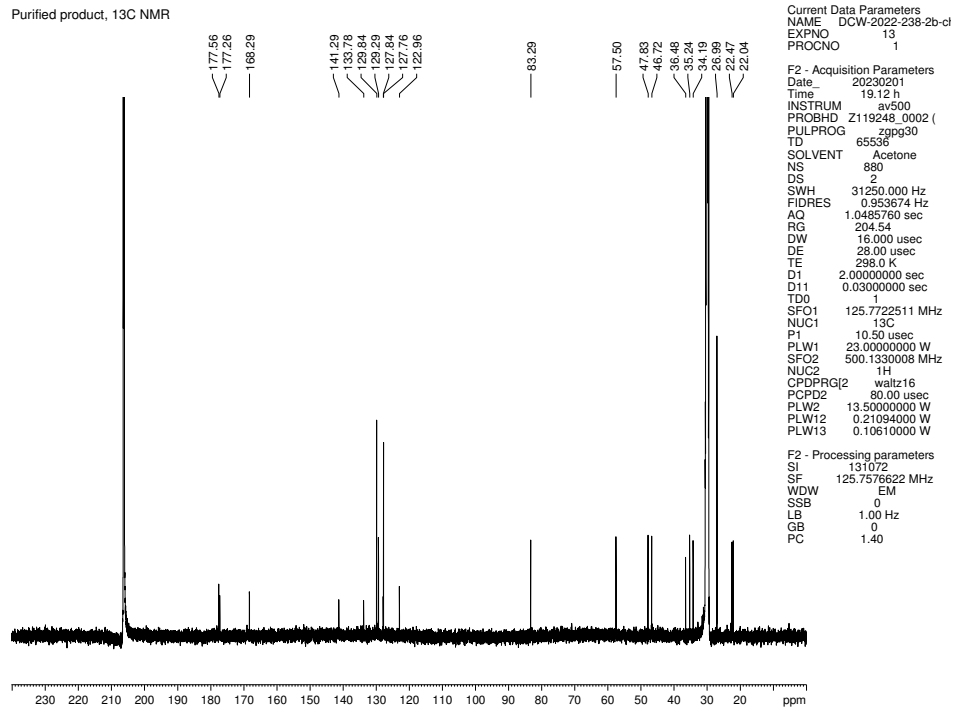
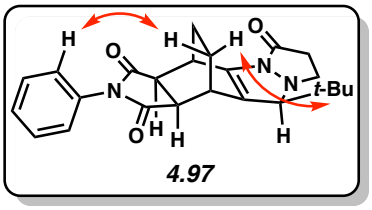


Figure 4.91. ^{13}C NMR (125 MHz, acetone-d_6) of compound **4.97**.



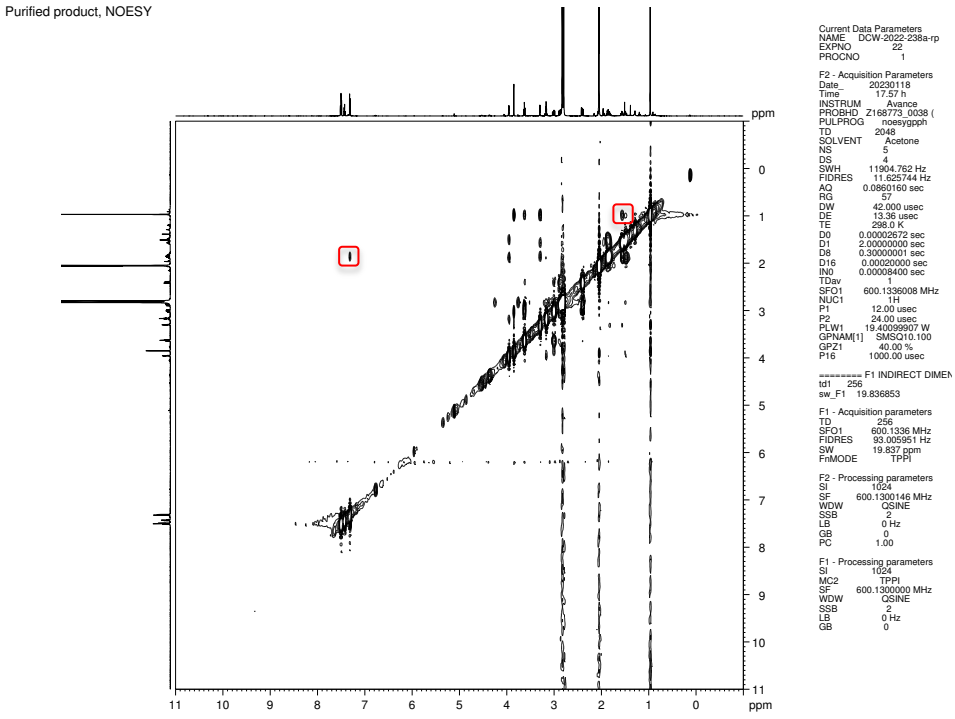


Figure 4.92. NOESY (600 MHz, acetone-d_6) of compound **4.97**.

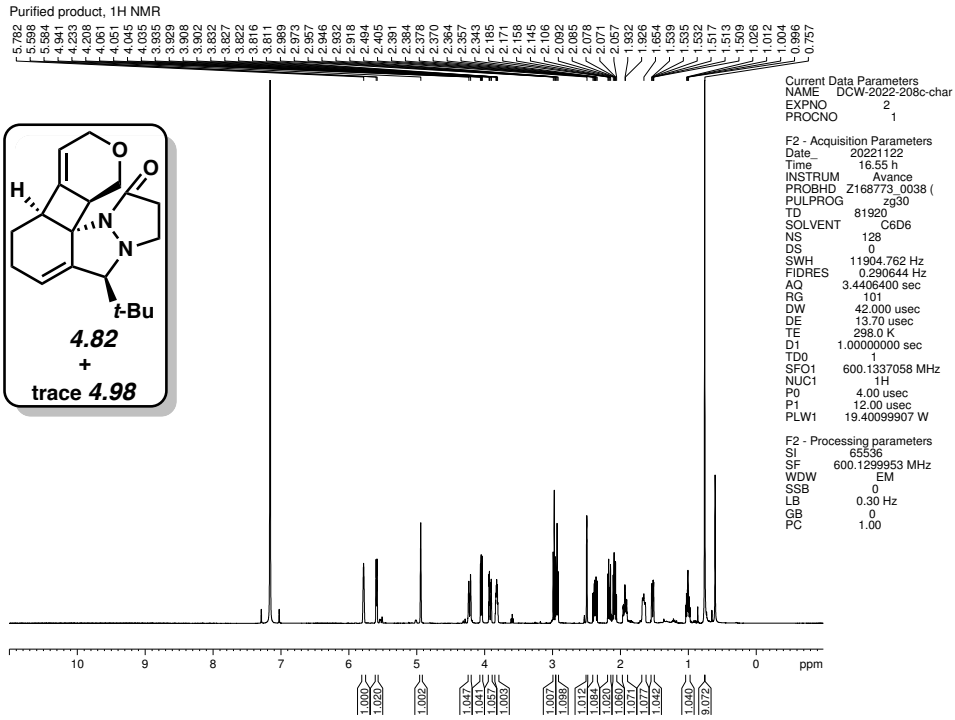


Figure 4.93. ^{1}H NMR (600 MHz, C_6D_6) of compound **4.82**.

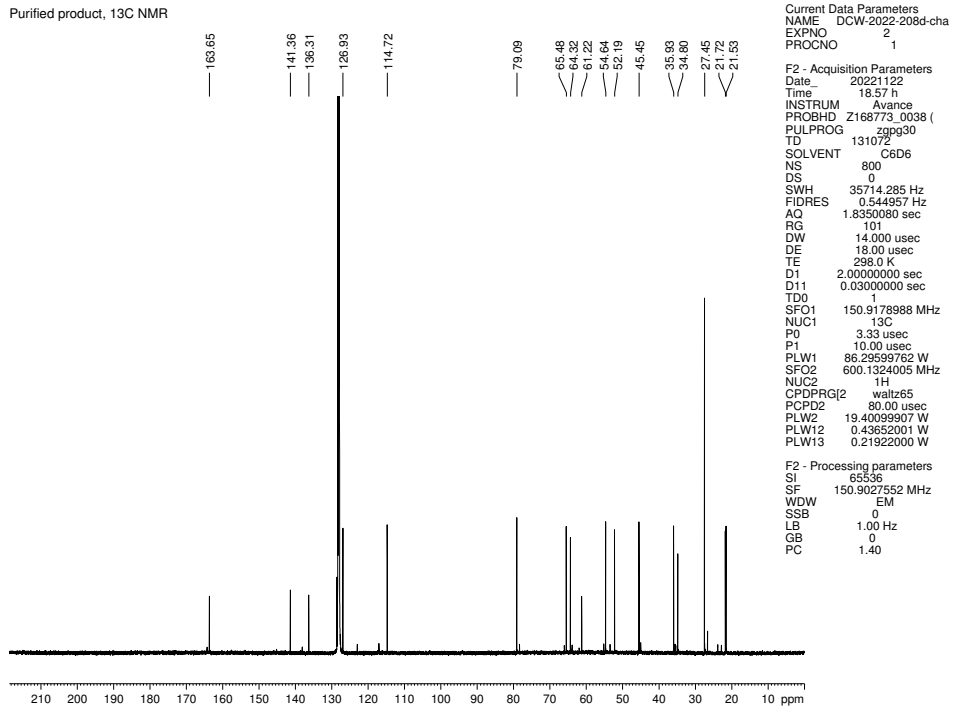


Figure 4.94. ^{13}C NMR (150 MHz, C_6D_6) of compound **4.82**.

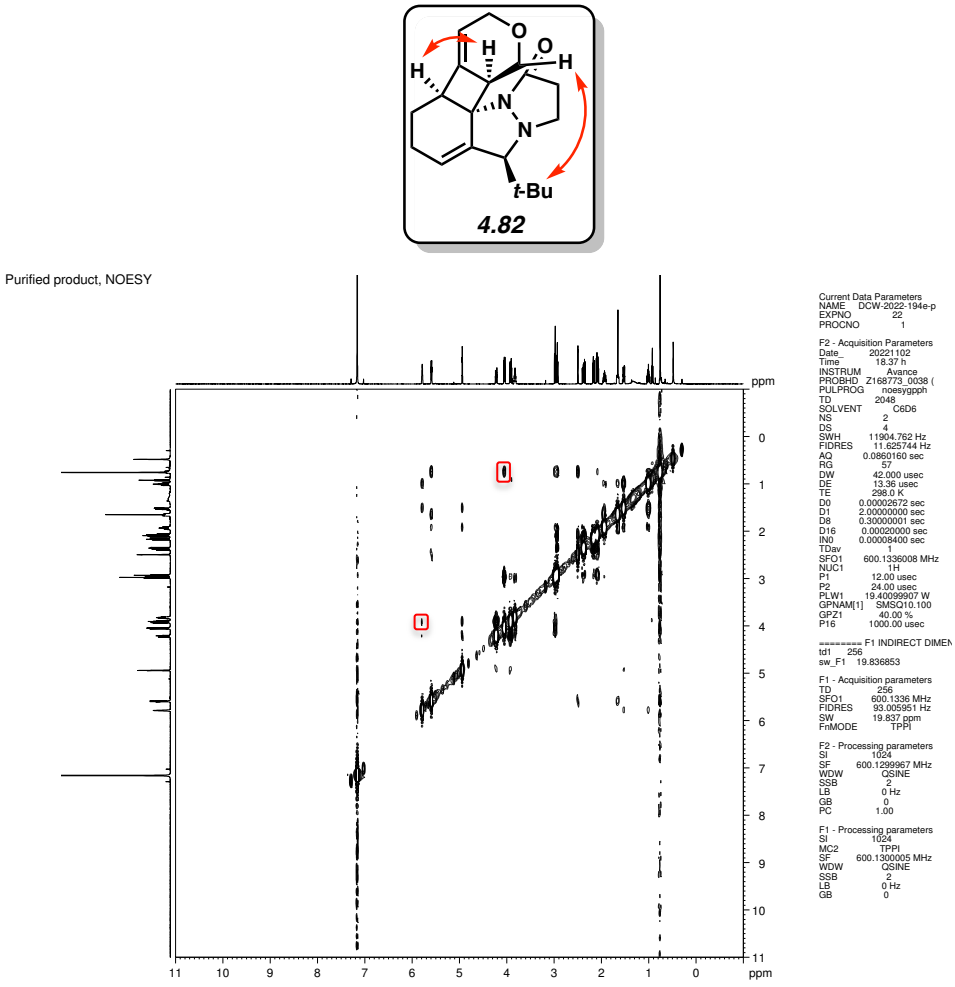


Figure 4.95. NOESY (600 MHz, C_6D_6) of compound **4.82**.

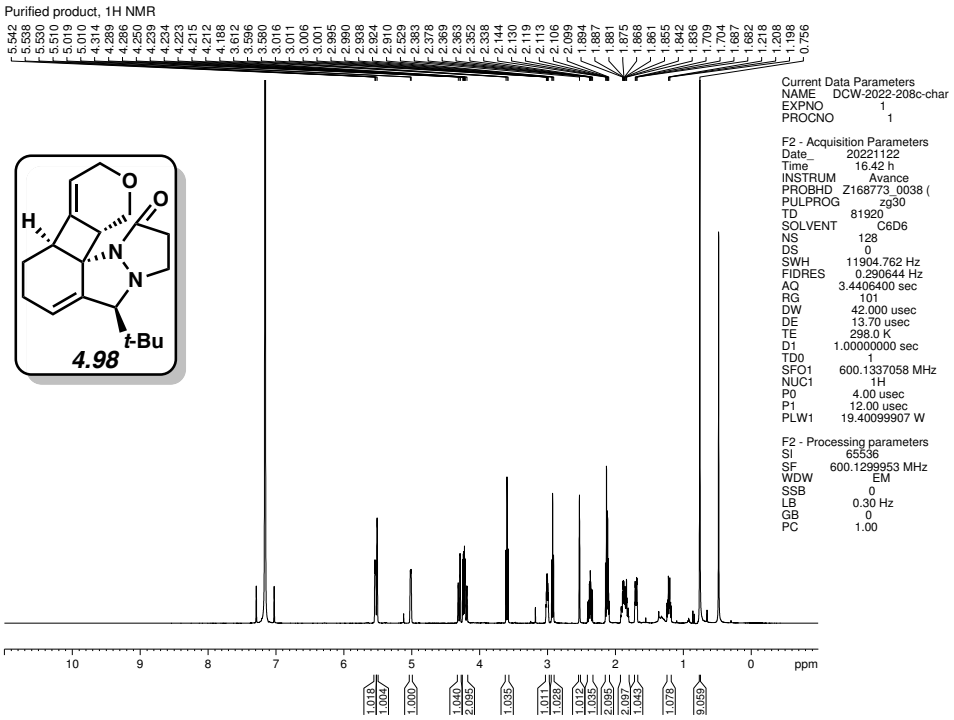


Figure 4.96. ^{1}H NMR (600 MHz, C_6D_6) of compound **4.98**.

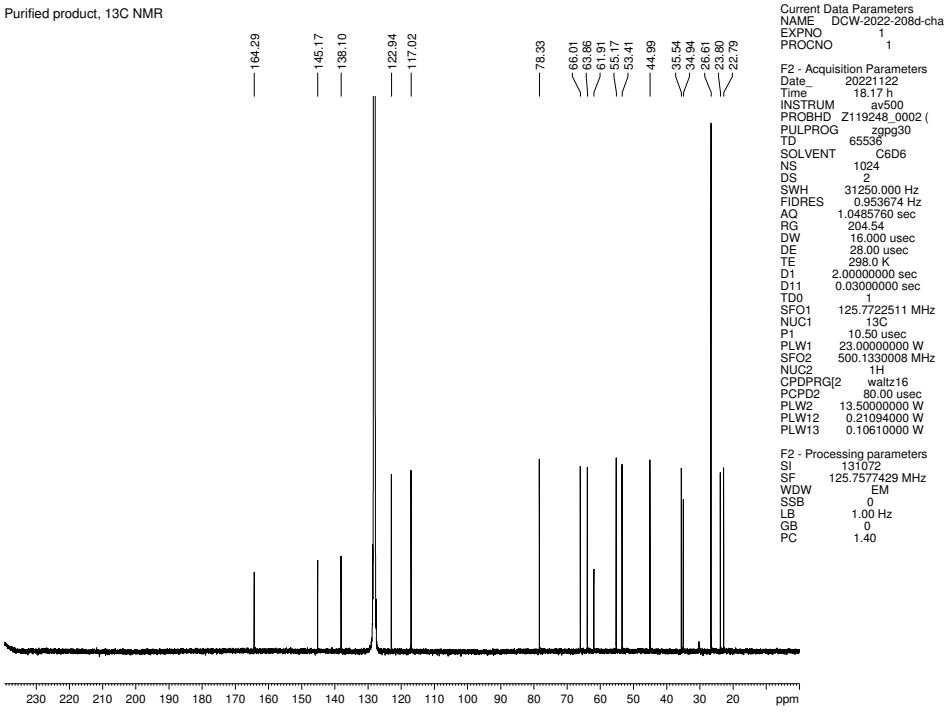


Figure 4.97. ^{13}C NMR (125 MHz, C_6D_6) of compound **4.98**.

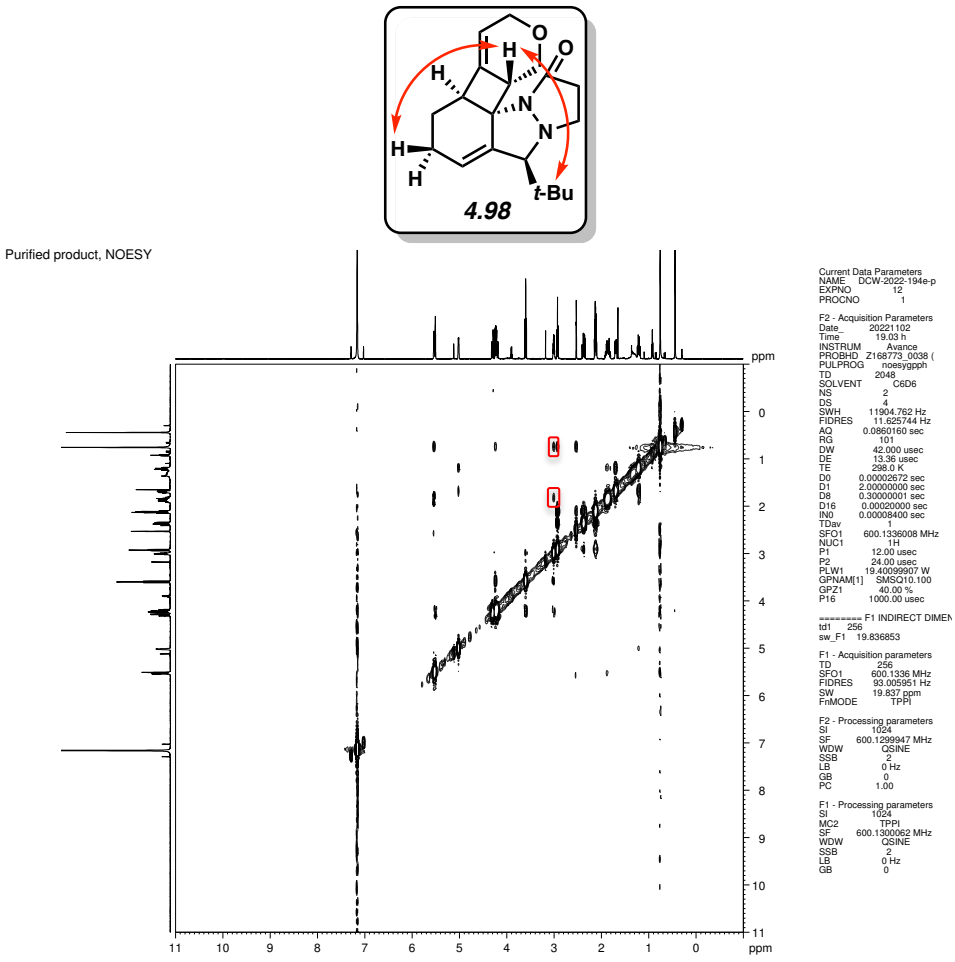


Figure 4.98. NOESY (600 MHz, C_6D_6) of compound **4.98**.

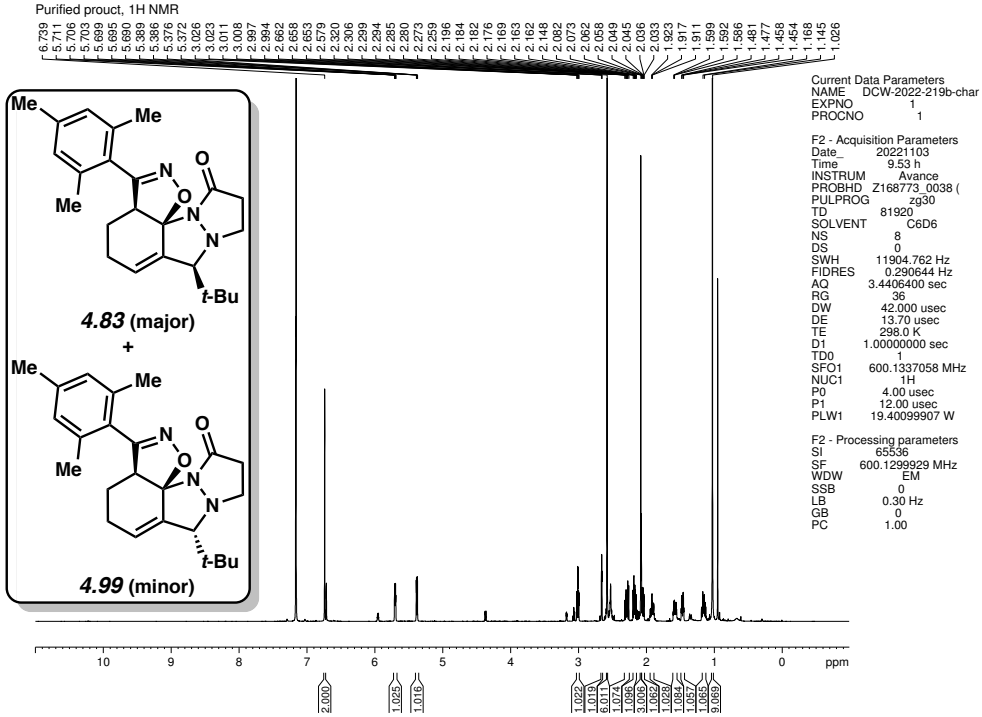


Figure 4.99. ^{1}H NMR (600 MHz, C_6D_6) of compounds **4.83** and **4.99**.

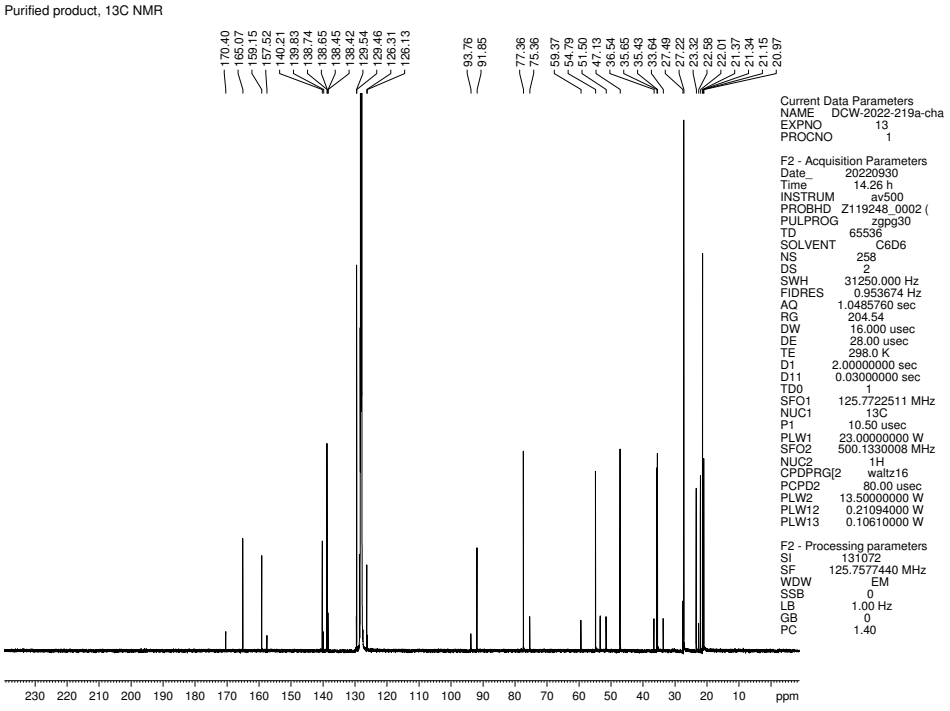
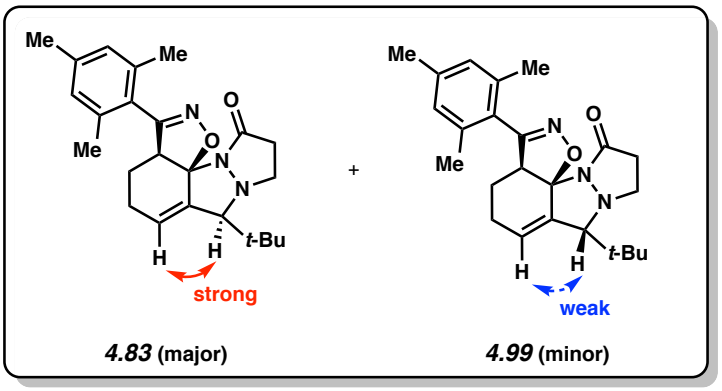


Figure 4.100. ^{13}C NMR (125 MHz, C_6D_6) of compounds **4.83** and **4.99**.



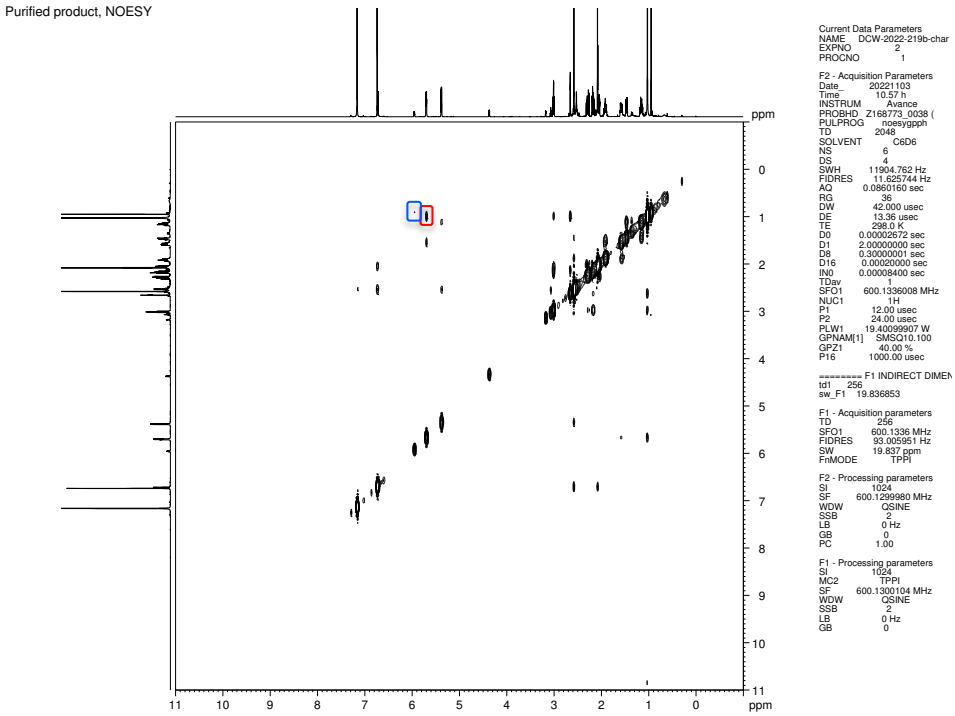


Figure 4.101. NOESY (600 MHz, C_6D_6) of compounds **4.83** and **4.99**.

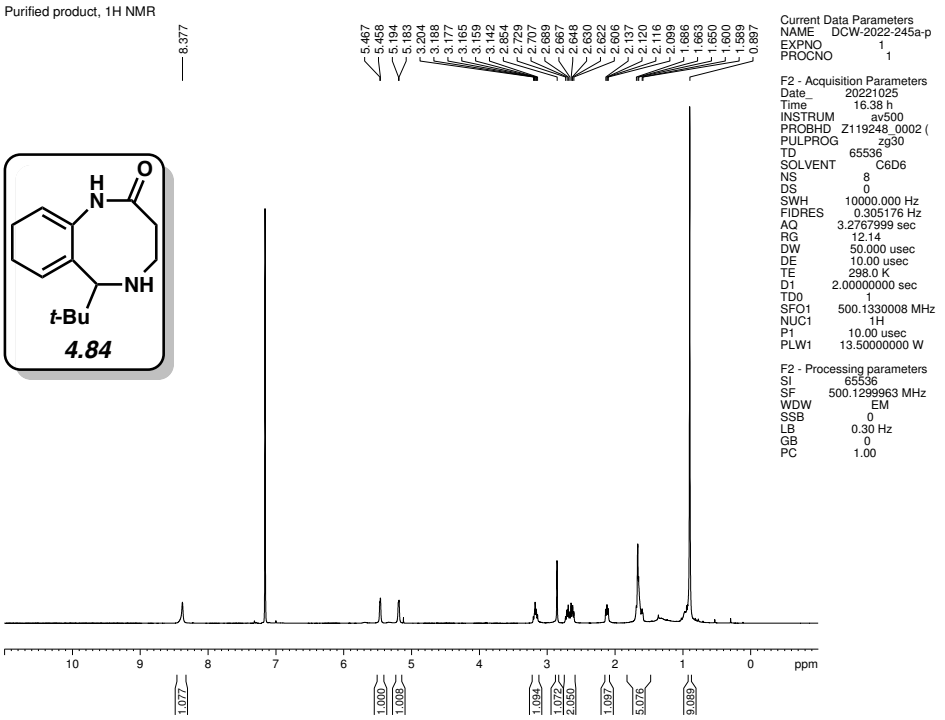


Figure 4.102. ^{1}H NMR (500 MHz, C_6D_6) of compound **4.84**.

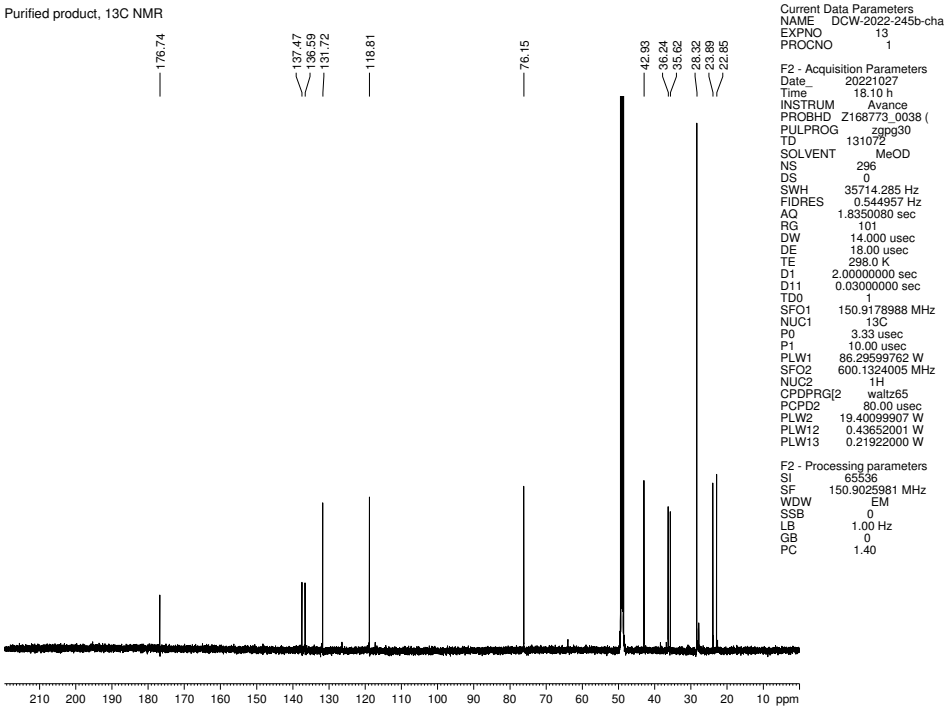


Figure 4.103. ^{13}C NMR (150 MHz, CD_3OD) of compound **4.84**.

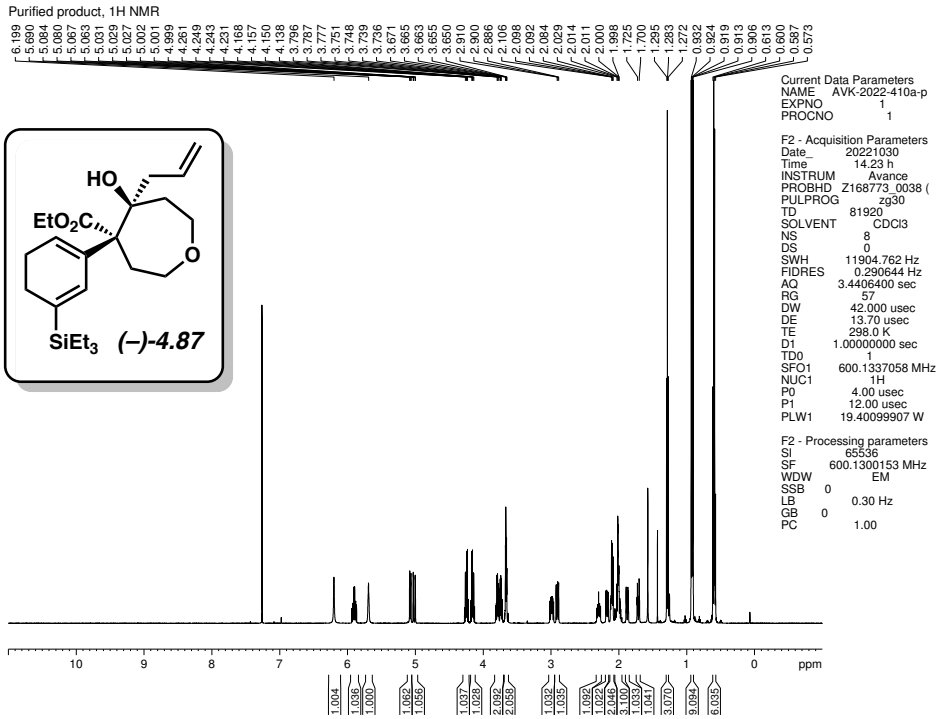


Figure 4.104. ^{1}H NMR (600 MHz, $CDCl_3$) of compound (–)-**4.87**.

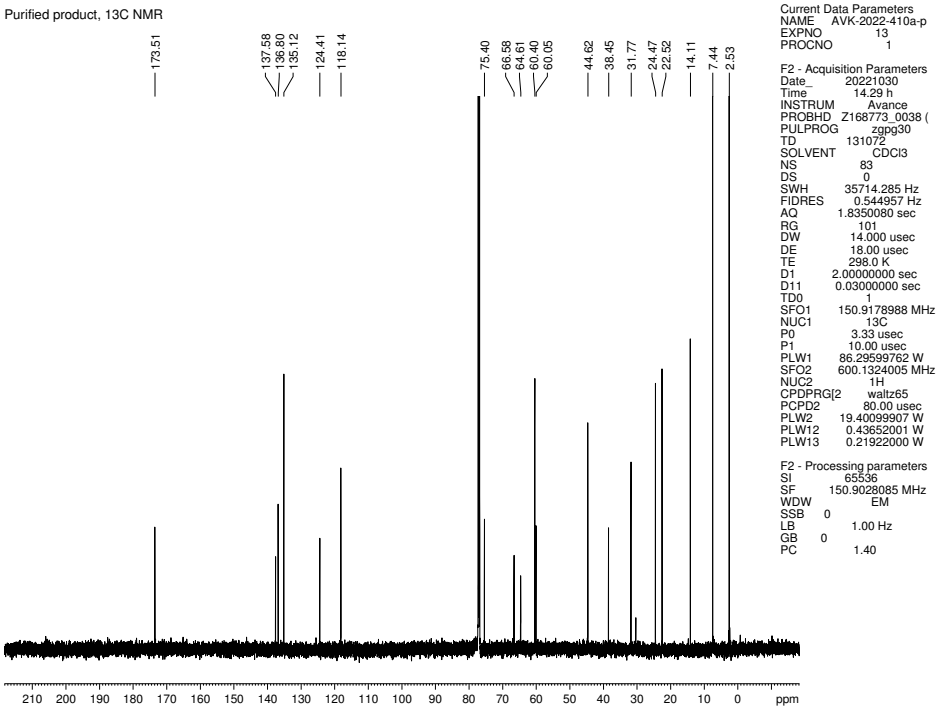


Figure 4.105. ^{13}C NMR (150 MHz, $CDCl_3$) of compound (–)-**4.87**.

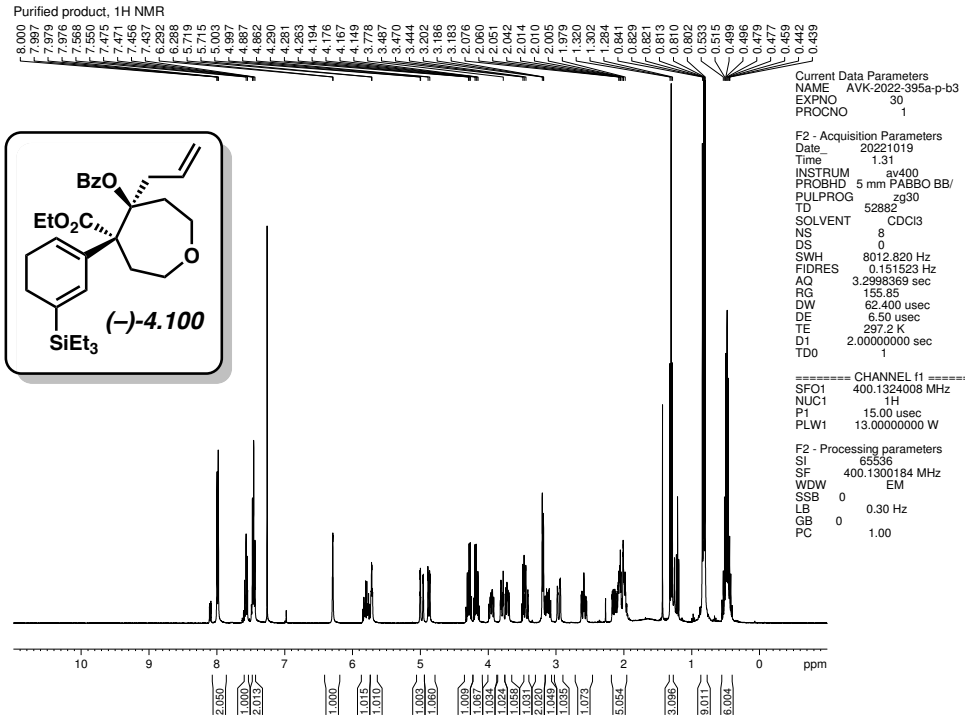


Figure 4.106. ^{1}H NMR (400 MHz, $CDCl_3$) of compound (–)-**4.100**.

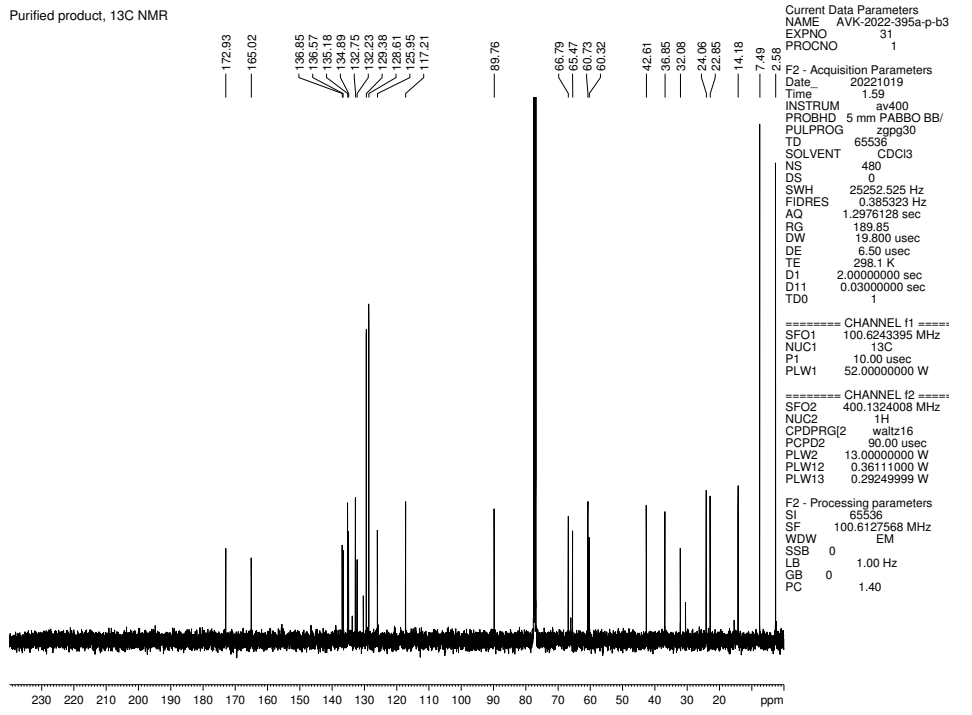


Figure 4.107. ^{13}C NMR (100 MHz, $CDCl_3$) of compound (–)-**4.100**.

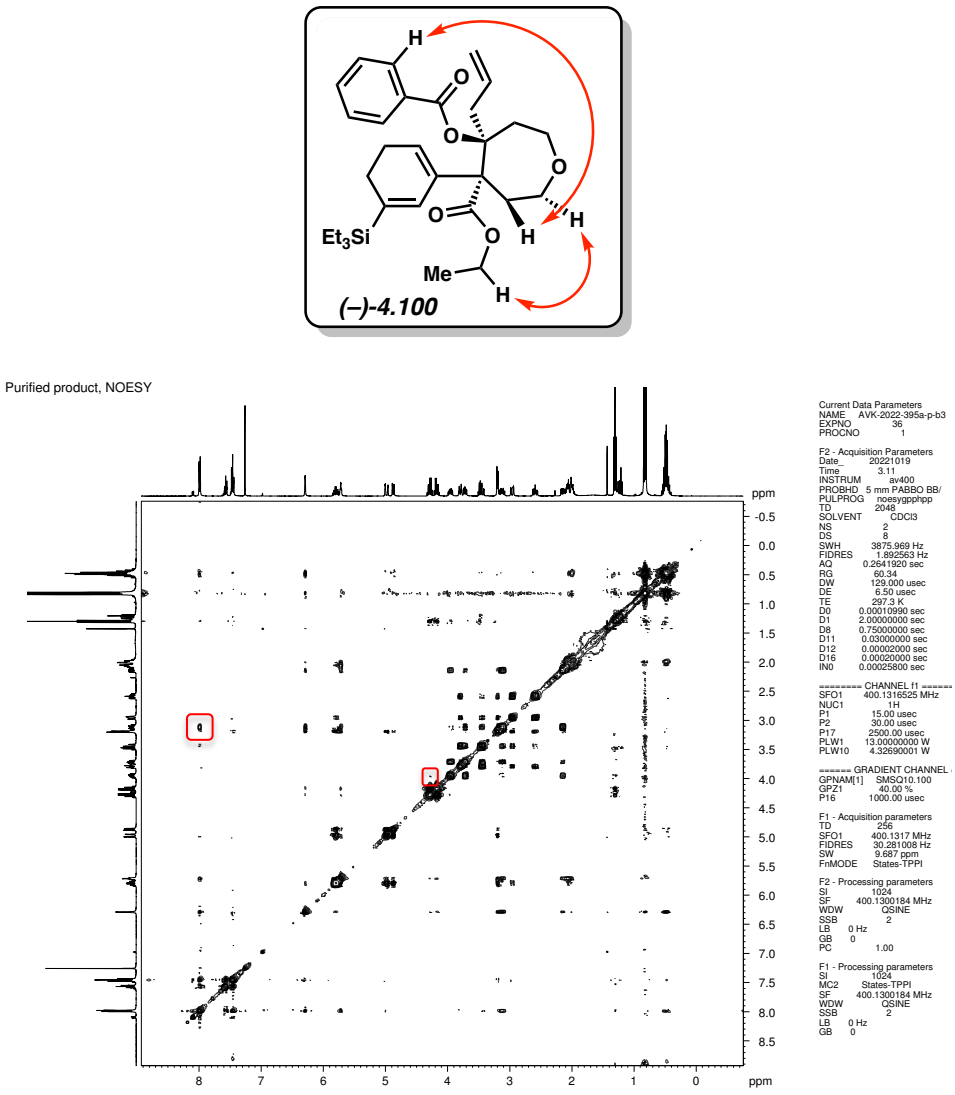


Figure 4.108. NOESY (400 MHz, $CDCl_3$) of compound (–)-**4.100**.

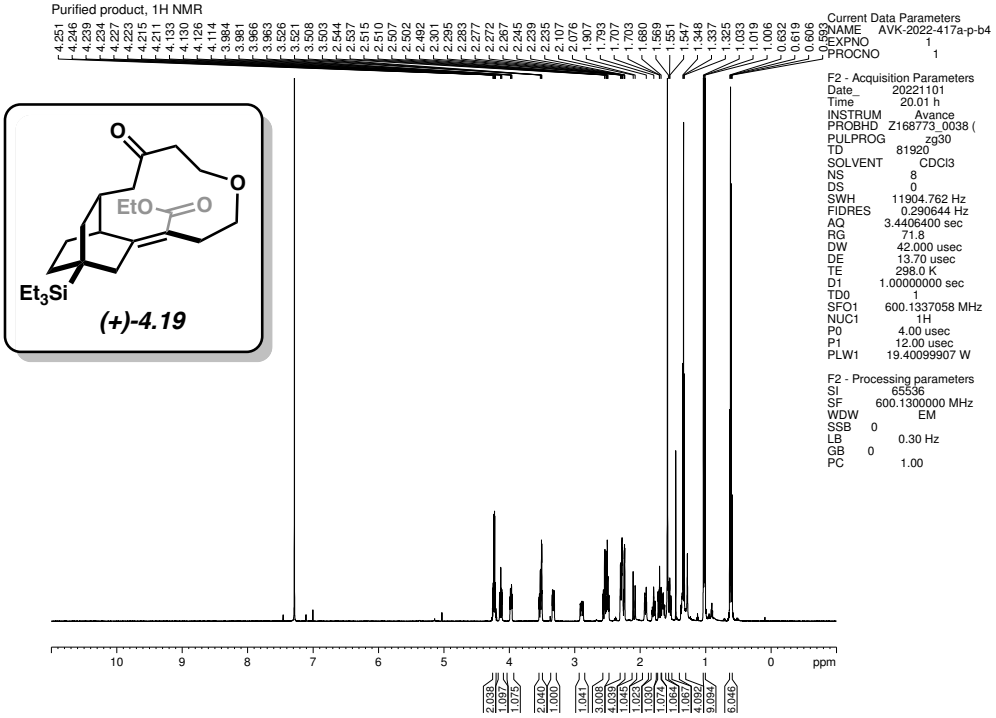


Figure 4.109. ^{1}H NMR (600 MHz, $CDCl_3$) of compound (+)-**4.19**.

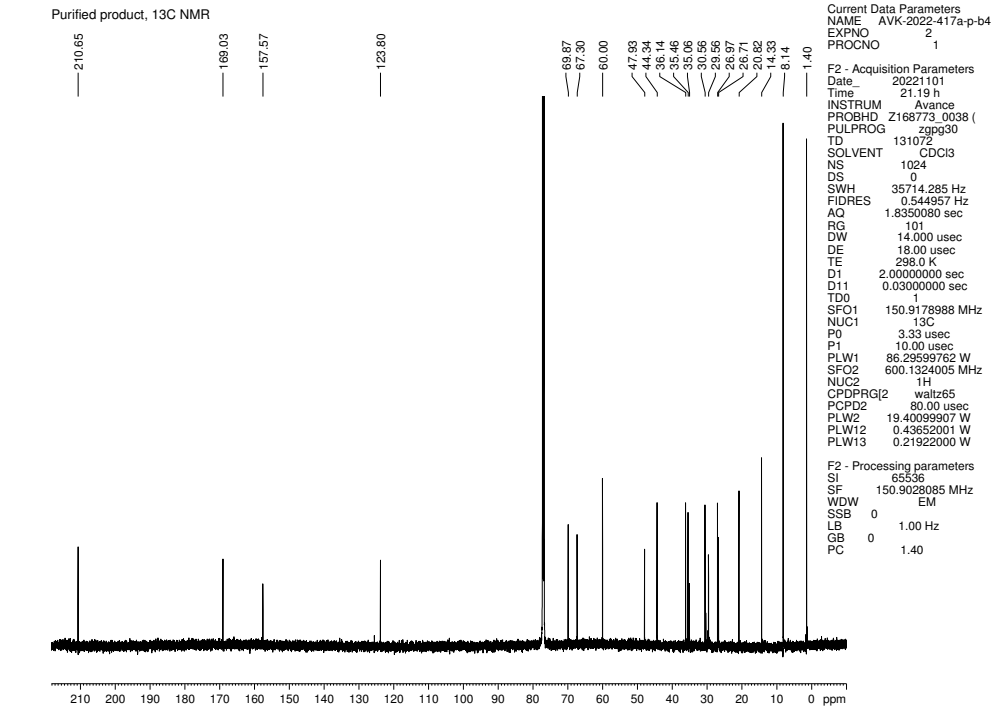


Figure 4.110. ^{13}C NMR (150 MHz, $CDCl_3$) of compound (+)-**4.19**.

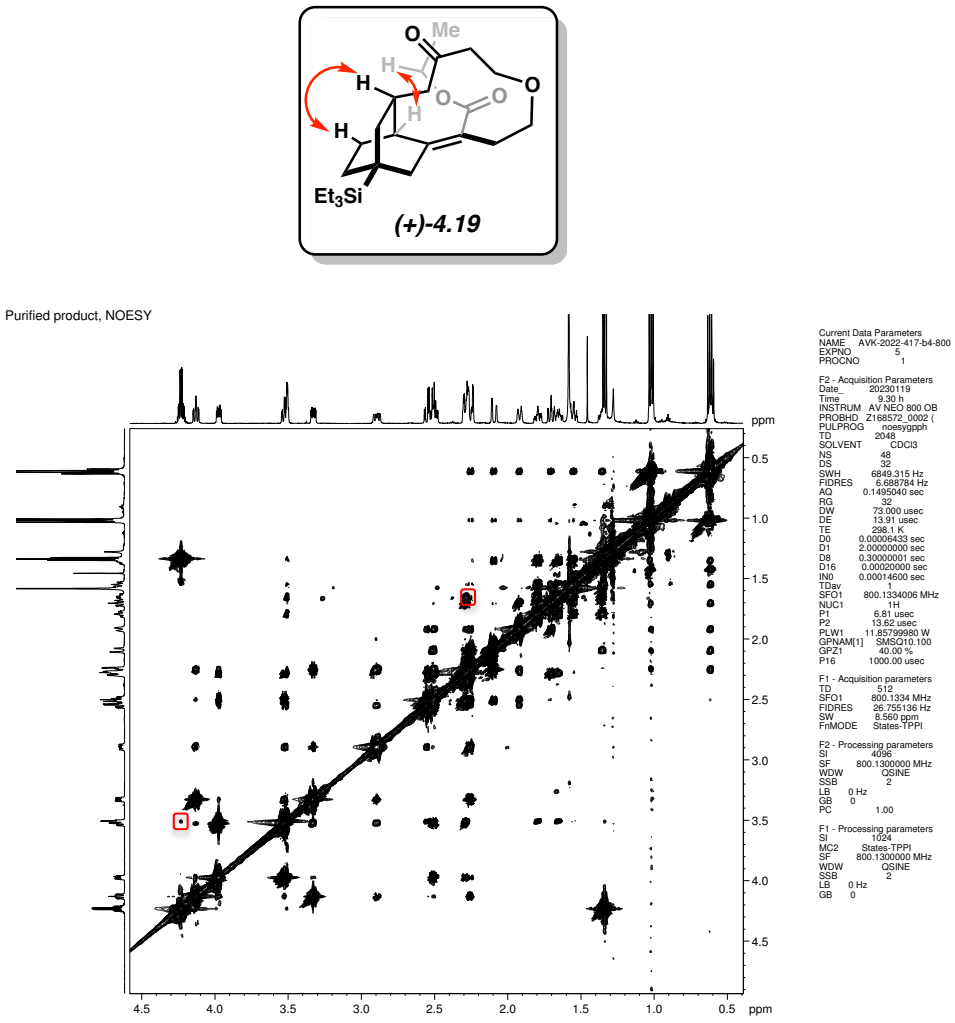


Figure 4.111. NOESY (800 MHz, $CDCl_3$) of compound (+)-**4.19**.

4.11 Notes and References

(1) Faraday, M. XX. On new compounds of carbon and hydrogen, and on certain other products obtained during the decomposition of oil by heat. *Philos. Trans. R. Soc.* **1825**, *115*, 440–466.

(2) Mortier, J. *Arene Chemistry: Reaction Mechanisms and Methods for Aromatic Compounds*. John Wiley & Sons, Inc. 2016.

(3) van Tamelen, E. E.; Pappas, S. P. Bicyclo [2.2.0]hexa-2,5-diene. *J. Am. Chem. Soc.* **1963**, *85*, 3297–3298.

(4) Katz, T. J.; Acton, N. Synthesis of prismane. *J. Am. Chem. Soc.* **1973**, *95*, 2738–2739.

(5) Huang, X.; Chen, B.-Z.; Li, P.; Ji, D.-W.; Liu, J.; Zheng, H.; Yang, S.-N.; Hu, Y.-C.; Wan, B.; Hu, X.-P.; Fu, C.; Huang, Y.; Zheng, J.; Chen, Q.-A.; Ma, S. Palladium-catalysed construction of butafulvenes. *Nat. Chem.* **2022**, *14*, 1185–1192.

(6) Preethalayam, P.; Krishnan, K. S.; Thulasi, S.; Chand, S. S.; Joseph, J.; Nair, V.; Jaroschik, F.; Radhakrishnan, K. V. Recent advances in the chemistry of pentafulvenes. *Chem. Rev.* **2017**, *117*, 3930–3989.

(7) Seo, J.; Lee, S. Y.; Bielawski, C. W. Unveiling a masked polymer of Dewar benzene reveals trans-poly(acetylene). *Macromolecules* **2019**, *52*, 2923–2931.

(8) Shakespeare, W. C.; Johnson, R. P. 1,2,3-Cyclohexatriene and cyclohexen-3-yne: Two new highly strained C6H6 isomers. *J. Am. Chem. Soc.* **1990**, *112*, 8578–8579.

(9) Hickey, E. R.; Paquette, L. A. Torsional angle decompression is not the source of facial selectivity in Diels–Alder cycloadditions involving cyclic dienes fused to bicyclic

frameworks. The case study of 1,2,3,4,6,7-hexahydro-1,4-methanonaphthalene. *Tetrahedron Lett.* **1994**, *35* 2309–2312.

(10) Hickey, E. R.; Paquette, L. A. Experimental and theoretical analysis of the effects of strain diminution on the stereoselectivity of dienophilic capture by π-facially nonequivalent homologues of isodicyclopentadiene. *J. Am. Chem. Soc.* **1995**, *117*, 163–176.

(11) Burrell, R. C.; Daoust, K. J.; Bradley, A. Z.; DiRico, K. J.; Johnson, R. P. Strained cyclic cumulene intermediates in Diels–Alder cycloadditions of enynes and diynes. *J. Am. Chem. Soc.* **1996**, *118*, 4218–4219.

(12) Sakura, M.; Ando, S.; Hattori, A.; Saito, K. Reaction of cyclohexa-1,2,3-triene with *N*,α-diphenylnitrone: Formation of seven-membered cyclic amines via piradone derivatives. *Heterocycles* **1999**, *51*, 547–556.

(13) Slater, J. C. Directed valence in polyatomic molecules. *Phys. Rev.* **1931**, *37*, 481–489.

(14) Pauling, L.; Wheland, G. W. The nature of the chemical bond. V. The quantum-mechanical calculation of the resonance energy of benzene and naphthalene and the hydrocarbon free radicals. *J. Chem. Phys.* **1933**, *1*, 362–374.

(15) L. Pauling. The theory of resonance in chemistry. *Proc. R. Soc. Lond. A* **1977**, *356*, 433–441.

(16) Garratt, P. J. *Aromaticity*. Wiley-Interscience, 1986.

(17) Roberts, J. D.; Simmons, H. E.; Carlsmith, L. A.; Vaughan, C. W. Rearrangement in the reaction of chlorobenzene-1-C14 with potassium amide. *J. Am. Chem. Soc.* **1953**, *75*, 3290–3291.

(18) Scardiglia, F.; Roberts, J. D. Evidence for cyclohexyne as an intermediate in the coupling of phenyllithium with 1-chlorocyclohexene. *Tetrahedron* **1957**, *1*, 343–344.

(19) Wittig, G.; Fritze, P. On the intermediate occurrence of 1,2-cyclohexadiene. *Angew. Chem., Int. Ed.* **1966**, *5*, 846.

(20) Moser, W. R. The reactions of *gem*-dihalocyclopropanes with organometallic reagents. Ph.D. Dissertation, Massachusetts Institute of Technology, Cambridge, MA, 1964.

(21) Shi, J.; Li, L.; Li, Y. *o*-Silylaryl triflates: A journey of Kobayashi aryne precursors. *Chem. Rev.* **2021**, *121*, 3892–4044.

(22) Schleth, F., Vettiger, T., Rommel, M. & Tobler, H. Process for the preparation of pyrazole carboxylic acid amides. International patent WO2011131544A1, 2011.

(23) Darzi, E. R.; Barber, J. S.; Garg, N. K. Cyclic alkyne approach to heteroatom-containing polycyclic aromatic hydrocarbon scaffolds. *Angew. Chem., Int. Ed.* **2019**, *58*, 9419–9424.

(24) Yamano, M. M.; Knapp, R. R.; Ngamnithiporn, A.; Ramirez, M.; Houk, K. N.; Stoltz, B. M.; Garg, N. K. Cycloadditions of oxacyclic allenes and a catalytic asymmetric entryway to enantioenriched cyclic allenes. *Angew. Chem., Int. Ed.* **2019**, *58*, 5653–5657.

(25) Ippoliti, F.; Adamsonn, N. J.; Wonilowicz, L. G.; Darzi, E. R.; Donaldson, J. S.; Garg, N. K. Total synthesis of lissodendoric acid A via stereospecific trapping of a strained cyclic allene. *Science* **2023**, *379*, 261–265.

(26) Moore, W. M.; Ozretich, T. M. Cyclic cumulenes. The synthesis and some reactions of 1,2,3-cyclodecatriene. *Tetrahedron Lett.* **1967**, *33* 3205–3207.

(27) Johnson, R. P. Strained cyclic cumulenes. *Chem. Rev.* **1989**, *89*, 1111–1124.

(28) Yin, J.; Abboud, K. A.; Jones, W. M. Synthesis of zirconocene complexes of a 1,2,3-cyclohexatriene and a cyclohexen-3-yne. *J. Am. Chem. Soc.* **1993**, *115*, 8859–8860.

(29) Daoust, K. J.; Hernandez, S. M.; Konrad, K. M.; Mackie, I. D.; Winstanley, J.; Johnson, R. P. Strain estimates for small-ring cyclic allenes and butatrienes. *J. Org. Chem.* **2006**, *71*, 5708–5714.

(30) Liebman, J. F.; Greenberg, A. A survey of strained organic molecules. *Chem. Rev.* **1976**, *76*, 311–365.

(31) Newton, M. D.; Fraenkel, H. A. The equilibrium geometry, electronic structure, and heat of formation of ortho-benzyne. *Chem. Phys. Lett.* **1973**, *18*, 244–246.

(32) Carpino, L. A.; Sau, A. C. Convenient source of 'naked' fluoride: Tetra-n-butylammonium chloride and potassium fluoride dihydrate. *J. Chem. Soc., Chem. Commun.* **1979**, 514–515.

(33) Anthony, S. M.; Wonilowicz, L. G.; McVeigh, M. S.; Garg, N. K. Leveraging fleeting strained intermediates to access complex scaffolds. *JACS Au* **2021**, *1*, 897–912.

(34) Spence, K. A.; Tena Meza, A.; Garg, N. K. Merging metals and strained intermediates. *Chem Catalysis* **2022**, *2*, 1870–1879.

(35) Wenk, H. H.; Winkler, M.; Sander, W. One century of aryne chemistry. *Angew. Chem., Int. Ed.* **2003**, *42*, 502–528.

(36) Schepens, W.; Van Haver, D.; Vandewalle, M.; Bouillon, R.; Verstuyf, A.; De Clercq, P. J. Synthesis of spiro[4.5]decane CF-ring analogues of 1α,25-dihydroxyvitamin D3. *Org. Lett.* **2006**, *8*, 4247–4250.

(37) Chari, J. V.; Ippoliti, F. M.; Garg, N. K. Concise approach to cyclohexyne and 1,2-cyclohexadiene precursors. *J. Org. Chem.* **2019**, *84*, 3652–3655.

(38) Asmadi, M.; Chikhalia, K. H. Aryne insertion into σ bonds. *Asian J. Org. Chem.* **2017**, *6*, 1331–1348.

(39) Bronner, S. M.; Mackey, J. L.; Garg, N. K. Steric effects compete with aryne distortion to control regioselectivities of nucleophilic additions to 3-silylarynes. *J. Am. Chem. Soc.* **2012**, *134*, 13966–13969.

(40) Shi, J.; Li, L.; Shan, C.; Wang, J.; Chen, Z.; Gu, R.; He, J.; Tan, M.; Lan, Y.; Li, Y. Aryne 1,2,3,5-tetrasubstitution enabled by 3-silylaryne and allyl sulfoxide via an aromatic 1,3-silyl migration. *J. Am. Chem. Soc.* **2021**, *143*, 2178–2184.

(41) Ikawa, T.; Nishiyama, T.; Shigeta, T.; Mohri, S.; Morita, S.; Takayanagi, S.-i.; Terauchi, Y.; Morikawa, Y.; Takagi, A.; Ishikawa, Y.; Fujii, S.; Kita, Y.; Akai, S. *ortho*-Selective nucleophilic addition of primary amines to silylbenzynes: synthesis of 2-silylanilines. *Angew. Chem., Int. Ed.* **2011**, *50*, 5674–5677.

(42) Matsumoto, T.; Sohma, T.; Hatazaki, S.; Suzuki, K. On the regiochemistry of cycloaddition of unsymmetrical aryne with nitrone remarkable effect of trialkylsilyl substituent. *Synlett* **1993**, *1993*, 843−846.

(43) Bent, H. A. An appraisal of valence-bond structures and hybridization in compounds of the first-row elements. *Chem. Rev.* **1961**, *61*, 275–311.

(44) Medina, J. M.; McMahon, T. C.; Jiménez-Osés, G.; Houk, K. N.; Garg, N. K. Cycloadditions of cyclohexynes and cyclopentyne. *J. Am. Chem. Soc.* **2014**, *136*, 14706–14709.

(45) Bickelhaupt, F. M.; Houk, K. N. Analyzing reaction rates with the distortion/interaction-activation strain model. *Angew. Chem., Int. Ed.* **2017**, *56*, 10070–10086.

(46) Medina, J. M.; Mackey, J. L.; Garg, N. K.; Houk, K. N. The role of aryne distortions, steric effects, and charges in regioselectivities of aryne reactions. *J. Am. Chem. Soc.* **2014**, *136*, 15798–15805.

(47) Cheong, P. H.-Y.; Paton, R. S.; Bronner, S. M.; Im, G.-Y. J.; Garg, N. K.; Houk, K. N. Indolyne and aryne distortions and nucleophilic regioselectivities. *J. Am. Chem. Soc.* **2010**, *132*, 1267–1269.

(48) Goetz, A. E.; Garg, N. K. Regioselective reactions of 3,4-pyridynes enabled by the aryne distortion model. *Nature Chem.* **2013**, *5*, 54–60.

(49) Bronner, S. M.; Goetz, A. E.; Garg, N. K. Overturning indolyne regioselectivities and synthesis of indolactam V. *J. Am. Chem. Soc.* **2011**, *133*, 3832–3835.

(50) Goetz, A. E.; Shah, T. K.; Garg, N. K. Pyridynes and indolynes as building blocks for functionalized heterocycles and natural products. *Chem. Commun.* **2015**, *51*, 34–45.

(51) Kemp, D. S.; Sidell, M. D.; Shortridge, T. J. Synthetic routes to 1,5-diazacyclooctanes via 2,6-diketo-1,5-diazabicyclo[3.3.1]octanes. *J. Org. Chem.* **1979**, *44*, 4473–4476.

(52) Shintani, R.; Hayashi, T. Palladium-catalyzed [3 + 3] cycloaddition of trimethylenemethane with azomethine imines. *J. Am. Chem. Soc.* **2006**, *128*, 6330–6331.

(53) Shintani, R.; Fu, G. C. A new copper-catalyzed [3 + 2] cycloaddition: Enantioselective coupling of terminal alkynes with azomethine imines to generate five-membered nitrogen heterocycles. *J. Am. Chem. Soc.* **2003**, *125*, 10778–10779.

(54) Arellano, L. M.; Yue, S.; Atienzar, P.; Gómez-Escalonilla, M. J.; Ortega-Higueruelo, F. J.; Fierro, J. L. G.; García, H.; Langa, F. Modulating charge carrier density and mobility in doped graphene by covalent functionalization. *Chem. Commun.* **2019**, *67*, 9999–10002.

(55) Schepens, W.; Van Haver, D.; Vandewalle, M.; Bouillon, R.; Verstuyf, A.; De Clercq, P. J. Synthesis of spiro[4.5]decane CF-ring analogues of 1α,25-dihydroxyvitamin D3. *Org. Lett.* **2006**, *8*, 4247–4250.

(56) Reeves, J. T.; Lorenc, C.; Camara, K.; Li, Z.; Lee, H.; Busacca, C. A.; Senanayake, C. H. Carbamoyl anion addition to nitrones. *J. Org. Chem*. **2014**, *79*, 5895–5902.

(57) Kumar, R.; Chaudhary, S.; Kumar, R.; Upadhyay, P.; Sahal, D.; Sharma, U. Catalyst and additive-free diastereoselective 1,3-dipolar cycloaddition of quinolinium imides with olefins, maleimides, and benzynes: Direct access to fused *N*,*N*′-heterocycles with promising activity against a drug-resistant malaria parasite. *J. Org. Chem.* **2018**, *83,* 11552–11570.

(58) Shapiro, S. L.; Weinberg, K.; Freedman, L. N-Substituted-3-oxypyridyl betaines. *J. Am. Chem. Soc.* **1959**, *81*, 5140–5145.

(59) Adams, L. A.; Aggarwal, V. K.; Bonnert, R. V.; Bressel, B.; Cox, R. J.; Shepherd, J.; de Vicente, J.; Walter, M.; Whittingham, W. G.; Winn, C. L. Diastereoselective synthesis of cyclopropane amino acids using diazo compounds generated in situ. *J. Org. Chem.* **2003**, *68*, 9433–9440.

(60) Sánchez-Arroyo, A. J.; Pardo, Z. D.; Moreno-Jiménez, F.; Herrera, A.; Martín, N.; García-Fresnadillo, D. Photochemical oxidation of thioketones by singlet molecular oxygen revisited: Insights into photoproducts, kinetics, and reaction mechanism. *J. Org. Chem.* **2015**, *80*, 10575–10584.

(61) Shih, C.; Swenton, J. S. An efficient and simple β-acylvinyl anion equivalent for cyclohexenones. *Tetrahedron Lett.* **1981**, *22*, 4217–4220.

(62) Picazo, E.; Anthony, S. M.; Giroud, M.; Simon, A.; Miller, M. A.; Houk, K. N.; Garg, N. K. Arynes and cyclic alkynes as synthetic building blocks for stereodefined quaternary centers. *J. Am. Chem. Soc.* **2018**, *140*, 7605–7610.

(63) Yamano, M. M.; Knapp, R. R.; Ngamnithiporn, A.; Ramirez, M.; Houk, K. N.; Stoltz, B. M.; Garg, N. K. Cycloadditions of oxacyclic allenes and a catalytic asymmetric entryway to enantioenriched cyclic allenes. *Angew. Chem., Int. Ed.* **2019**, *58*, 5653–5657.

(64) Altintas, O.; Glassner, M.; Rodriguez-Emmenegger, C.; Welle, A.; Trouillet, V.; Barner-Kowollik, C. Macromolecular surface design: Photopatterning of functional stable nitrile oxides. *Angew. Chem., Int. Ed.* **2015**, *54*, 5777–5783.

(65) Feng, M.; Tang, B.; Wang, N.; Xiu, H.-X.; Jiang, X. Ligand controlled regiodivergent C1 insertion on arynes for construction of phenanthridinone and acridone alkaloids. *Angew. Chem., Int. Ed.* **2015**, *54*, 14960–14964.

(66) Picard, A.; Ciblat, S.; Ramtohul, Y. K. Synthesis of α,α,-disubstituted benzocyclobutane amino acids through [2+2] annulation of benzyne and dehydroalanine. *Synlett* **2020**, *31*, 507–511.

(67) Sheldrick, G. M. (1996). *SADABS*. University of Göttingen, Germany.

(68) Sheldrick, G. M. Crystal structure refinement with SHELXL. *Acta Cryst. C*, **2015**, *71*, 3–8.

(69) Garbisch Jr., E. W. Conformations. VI. Vinyl-allylic proton spin couplings. *J. Am. Chem. Soc*. **1964**, *86,* 5561–5564.

(70) Hancock, E. N.; Kuker, E. L.; Tantillo, D. J.; Brown, M. K. Lessons in strain and stability: Enantioselective synthesis of (+)-[5]-ladderanoic acid. *Angew. Chem., Int. Ed.* **2019**, *59*, 436–441.

(71) Hauser, F. M.; Baghdanov, V. M. Regiospecific total synthesis of (±)-daunomycinone from an 11-deoxydaunomycinone precursor. *Tetrahedron* **1984**, *40*, 4719–4724.

(72) Sumida, Y.; Kato, T.; Hosoya, T. Generation of arynes via ate complexes of arylboronic esters with an *ortho*-leaving group. *Org. Lett.* **2013**, *15*, 2806–2809.

(73) Spartan'20 Wavefunction, Inc., Irvine, CA.

(74) Frisch, M. J., Trucks, G. W., Schlegel, H. B., Scuseria, G. E., Robb, M. A., Cheeseman, J. R., Scalmani, G., Barone, V., Petersson, G. A., Nakatsuji, H., Li, X., Caricato, M., Marenich, A. V., Bloino, J., Janesko, B. G., Gomperts, R.m Mennucci, B., Hratchian, H. P., Ortiz, J. V., Izmaylov, A. F., Sonnenberg, J. L., Williams-Young, D., Ding, F., Lipparini, F., Egidi, F., Goings, J., Peng, B., Petrone, A., Henderson, T., Ranasinghe, D., Zakrzewski, V. G., Gao, J., Rega, N., Zheng, G., Liang, W., Hada, M., Ehara, M., Toyota, K., Fukuda, R., Hasegawa, J., Ishida, M., Nakajima, T., Honda, Y., Kitao, O., Nakai, H., Vreven, T., Throssell, K., Montgomery, Jr., J. A., Peralta, J. E., Ogliaro, F., Bearpark, M. J., Heyd, J. J., Brothers, E. N., Kudin, K. N., Staroverov, V. N., Keith, T. A., Kobayashi, R., Normand, J., Raghavachari, K., Rendell, A. P., Burant, J. C., Iyengar, S. S., Tomasi, J., Cossi, M., Millam, J. M., Klene, M., Adamo, C., Cammi, R., Ochterski, J. W., Martin, R. L., Morokuma, K., Farkas, O., Foresman, J. B., Fox, D. J. Gaussian 16 Revision A.03 (Gaussian, Inc., 2016).

(75) Becke, A. D. Density-functional thermochemistry. III. The role of exact exchange. *J. Chem. Phys.* **1993**, *98*, 5648.

(76) Lee, C.; Yang, W.; Parr, R. G. Development of the Colle–Salvetti correlation-energy formula into a functional of the electron density. *Phys. Rev. B* **1988**, *37*, 785–789.

(77) Grimme, S.; Antony, J.; Ehrlich, S.; Krieg, H. A consistent and accurate ab initio parametrization of density functional dispersion correction (DFT-D) for the 94 Elements H-Pu. *J. Chem. Phys.* **2010**, *132*, 154104.

(78) Marenich, A. V.; Cramer, C. J.; Truhlar, D. G. Universal solvation model based on solute electron density and on a continuum model of the solvent defined by the bulk dielectric constant and atomic surface tensions. *J. Phys. Chem. B* **2009**, *113*, 6378–6396.

(79) London, F. J. Théorie quantique des courants interatomiques dans les combinaisons aromatiques. *J. Phys. Radium* **1937**, *8*, 397–409.

(80) McWeeny, R. Perturbation theory for the Fock-Dirac density matrix. *Phys. Rev.* **1974**, *124*, 1028–1034.

(81) Ditchfield, R. Self-consistent perturbation theory of diamagnetism. *Mol. Phys.* **1974**, *27*, 789–807.

(82) Wolinski, K.; Hinton, J. F.; Pulay, P. Efficient implementation of the gauge-independent atomic orbital method for NMR chemical shift calculations. *J. Am. Chem. Soc.* **1990**, *112*, 8251–8260.

(83) Cheeseman, J. R.; Trucks, G. W.; Keith, T. A.; Frisch, M. J. A comparison of models for calculating nuclear magnetic resonance shielding tensors. *J. Chem. Phys.* **1996**, *104*, 5497–5509.

(84) Adamo, C.; Barone, V. J. Exchange functionals with improved long-range behavior and adiabatic connection methods without adjustable parameters: The mPW and mPW1PW models. *J. Chem. Phys.* **2009**, *113*, 6378–6396.

(85) Luchini, G.; Alegre-Requena, J. V.; Funes-Ardoiz, I.; Paton, R. S. GoodVibes: Automated thermochemistry for heterogeneous computational chemistry data. *F1000Research* **9**, 291 (2020).

(86) Grimme, S. Supramolecular binding thermodynamics by dispersion-corrected density functional theory. *Chem. Eur. J.* **2012**, *18*, 9955–9964.

(87) Li, Y.; Gomes, J.; Sharada, S. M.; Bell, A. T.; Head-Gordon, M. Improved force-field parameters for QM/MM simulations of the energies of adsorption for molecules in zeolites and a free rotor correction to the rigid rotor harmonic oscillator model for adsorption enthalpies. *J. Phys. Chem. C* **2015**, *119*, 1840–1850.

(88) Legault, C. Y. CYLView, 1.0b; Université de Sherbrooke: Quebec, Montreal, Canada, http://www.cylview.org (2009).

(89) Zhang, G.; Musgrave, C. B. Comparison of DFT methods for molecular orbital eigenvalue calculations. *J. Phys. Chem. A* **2007**, *111*, 1554–1561.

(90) Bronner, S. M.; Mackey, J. L.; Garg, N. K. Steric effects compete with aryne distortion to control regioselectivities of nucleophilic additions to 3-silylarynes. *J. Am. Chem. Soc.* **2012**, *134*, 13966–13969.

(91) Lodewyk, M. W.; Siebert, M. R.; Tantillo, D. J. Computational prediction of 1H and 13C chemical shifts: A useful tool for natural product, mechanistic, and synthetic organic chemistry. *Chem. Rev.* **2012**, *112*, 1839–1862.

(92) Rablen, P. R.; Pearlman, S. A.; Finkbiner, J. A comparison of density functional methods for the estimation of proton chemical shifts with chemical accuracy. *J. Phys. Chem. A* **1999**, *103*, 7357–7362.

(93) Jain, R.; Bally, T.; Rablen, P. R. Calculating accurate proton chemical shifts of organic molecules with density functional methods and modest basis sets. *J. Org. Chem.* **2009**, *74*, 4017–4023.

(94) Jain, R.; Bally, T.; Rablen, P. R. Quantum-chemical simulation of 1H NMR spectra. 2.† Comparison of DFT-based procedures for computing proton–proton coupling constants in organic molecules. *J. Org. Chem.* **2011**, *76*, 4818–4830.

(95) Kelleghan, A. V.; Bulger, A. S.; Witkowski, D. C.; Garg, N. K. Strain-promoted reactions of 1,2,3-cyclohexatriene and its derivatives. *Nature* **2023**, *618*, 748–754.

CHAPTER FIVE

Evaluation of Retro-Aldol vs Retro-Carbonyl-Ene Mechanistic Pathways in a Complexity-Generating C–C Bond Fragmentation

Ana S. Bulger, Daniel W. Turner, Qingyang Zhou, K. N. Houk, and Neil K. Garg.

Org. Lett. **2024**, *26*, 3602–3606.

5.1 Abstract

We report an experimental and computational investigation of the mechanism of a cascade reaction. The reaction involves an intramolecular Diels–Alder reaction, followed by a C–C bond cleavage, to afford a complex bridged bicyclic product. As multiple reaction pathways could be envisioned for the latter step, the mechanism of the C–C bond cleavage step was investigated. Two reasonable reaction pathways were evaluated. Both computations and experiments indicate that the C–C bond cleavage step proceeds by a retro-carbonyl-ene pathway, rather than a retro-aldol pathway. This report underscores the synergy between computational and experimental studies and establishes the mechanism of an interesting complexity-generating transformation.

5.2 Introduction

Cyclic strained intermediates that bear a functional group with a preferred linear geometry have been of great interest to the synthetic community for several decades. Such compounds, such as benzyne (**5.1**), indolyne **5.2**, and strained cyclic allene **5.3** (Figure 5.1A), have seen use in a variety of applications. This includes, but is not limited to, use of strained intermediates toward the synthesis of important molecules such as bioactive compounds,[1, 2, 3, 4, 5, 6, 7] natural products,[8, 9, 10, 11, 12, 13, 14, 15,16] DNA-encoded libraries,[17] ligands,[18,19] and stimulus-responsive materials.[20] A

related class of strained intermediates comprises 1,2,3-cyclohexatrienes (**5.4**, Figure 5.1B). Such intermediates and their substituted derivatives are far less studied,[21, 22, 23, 24, 25] but have been employed in a variety of trapping experiments. Trapping reactions of **5.4** lead to functionalized dienes **5.5** that are poised to undergo further manipulation.

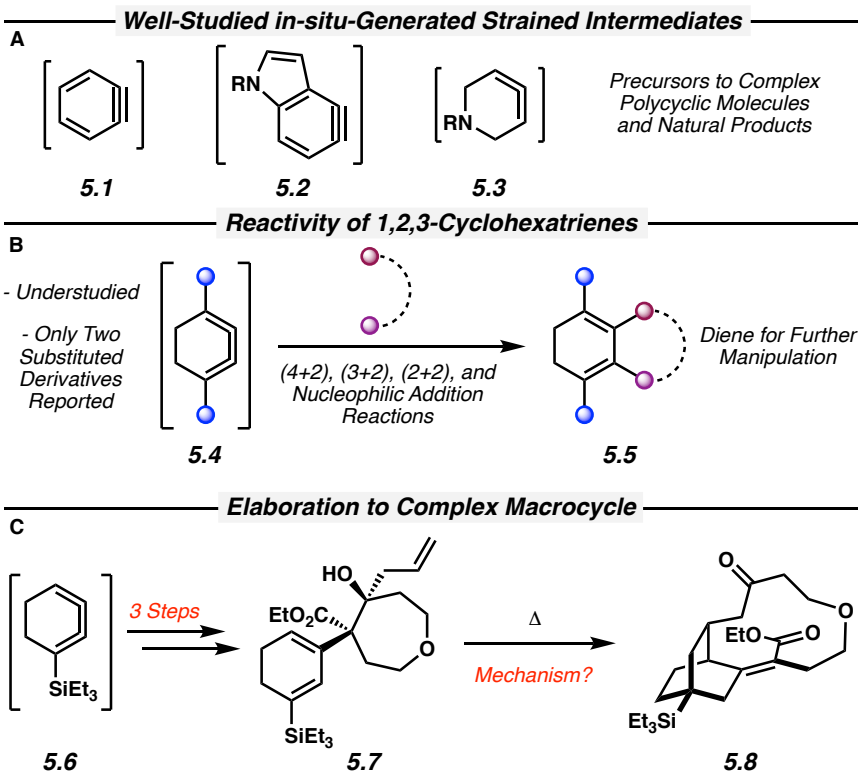


Figure 5.1. A) Prior studies of strained intermediates. B) Reactivity of 1,2,3-cyclohexatrienes. C) Elaboration of triene **5.6** to adduct **5.8**.

The present study pertains to the sequence summarized in Figure 5.1C, involving the trapping of silyl-substituted 1,2,3-cyclic triene **5.6** and further manipulations of its corresponding product.[25] To further explore the use of cumulated trienes as building blocks for complex scaffold synthesis, we accessed adduct **5.7** from intermediate **5.6** using a facile three-step sequence later detailed in Figure 5.2. Upon thermolysis of **5.7**, a Diels–Alder cycloaddition occurred with a subsequent rearrangement of the carbon skeleton to deliver macrocycle **5.8**. We describe our

computational and experimental studies to interrogate the reaction mechanism for the formation of macrocycle **5.8**.

As shown in Figure 5.2, triene precursor **5.9** and enamine **5.10** are treated with fluoride-based conditions to presumably form cumulated triene **5.6**, which, in turn, undergoes nucleophilic trapping by enamine **5.10**. Subsequent acid-promoted hydrolysis yielded adduct **5.11**. Of note, the trapping reaction occurs regioselectively, which we have previously attributed to the presence of the bulky silyl group.[25] Subsequent addition of allyl Grignard provided **5.7** via a diastereoselective 1,2-addition. In the key transformation we study herein, heating of **5.7** in hexadecane at 220 °C is presumed to facilitate Diels–Alder cycloaddition to give intermediate **5.12**. However, **5.12** was not observed or isolated; instead, macrocycle **5.8** was observed. Product **5.8** was thought to arise via an isomerization and C–C bond cleavage pathway, but the details of the likely mechanism were unknown. Two plausible pathways were deemed most viable: a retro-carbonyl-ene reaction and a retro-aldol reaction. Importantly, these two competing pathways have been the subject of both experimental and computational study for several years.[26,27,28,29] Furthermore, a better understanding of these mechanisms can inform our predictive ability and the application of such reactions,[3031] in the future construction of complex molecules, such as natural products. In this Letter, we have combined DFT calculations and experimental studies to establish the likely mechanistic pathway for the formation of macrocycle **5.8**.

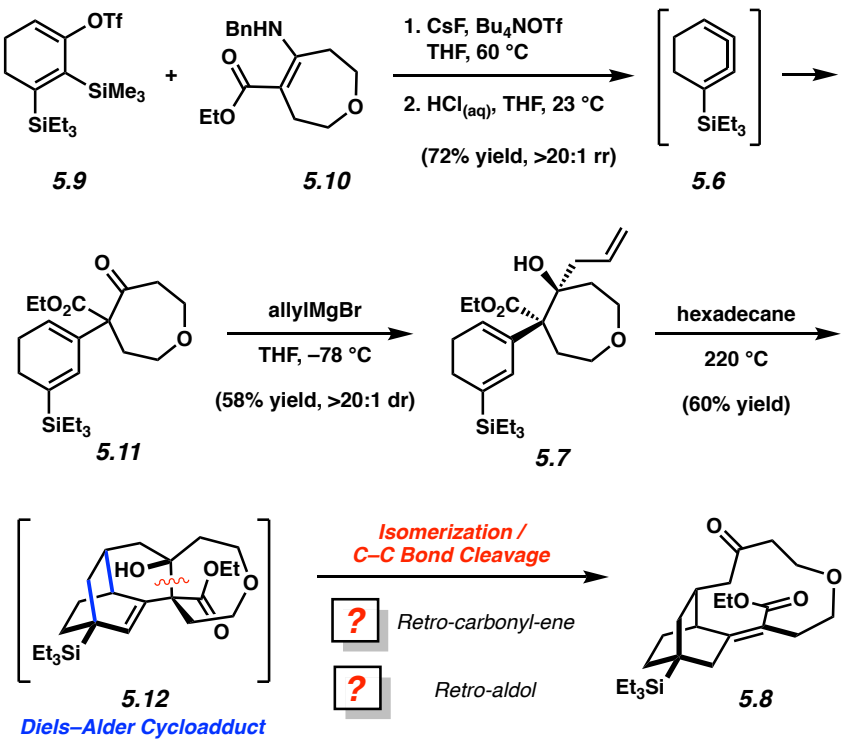


Figure 5.2. Trapping of 1,2,3-triene **5.6** and elaboration to **5.8** via retro-carbonyl-ene reaction or retro-aldol reaction.

5.3 Plausible Mechanistic Pathways

Figure 5.3 depicts the two different reaction pathways (retro-aldol and retro-carbonyl-ene reactions) that can be differentiated by tracking two key hydrogen atoms (i.e., H_A and H_B) in the conversion of Diels–Alder cycloadduct **5.12** to macrocycle **5.8**. In the retro-aldol pathway, proton transfer would allow for C–C bond cleavage (see transition structure **5.12a**[32]) and afford enol **5.13**. Subsequent protonation of the extended enol on C13 could occur without appreciable stereoselectivity, leading to formation of both **5.8a** and **5.8b**.[33] Alternatively, the concerted retro-carbonyl-ene mechanism would proceed through a completely stereoselective proton transfer through transition structure **5.12b** to give only **5.8b**. Given this rationale, we envisioned that deuterium labeling the positions at either H_A or H_B in structure **5.12** could also allow us to assess which mechanism is likely operative.

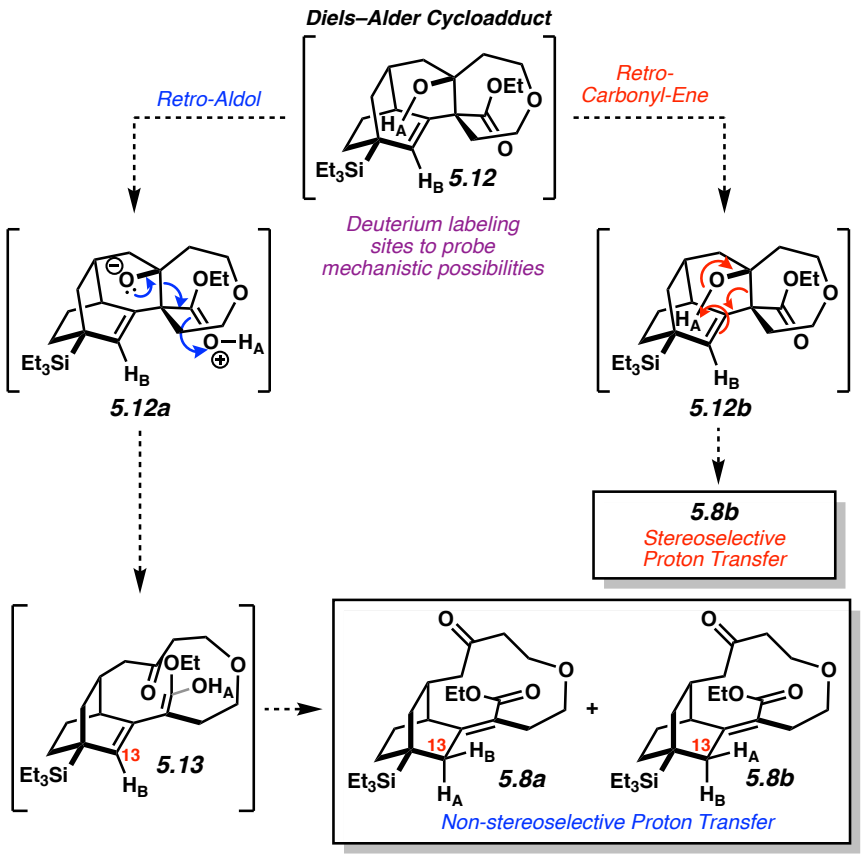


Figure 5.3. Details of plausible mechanistic pathways.

5.4 Computational Studies

Prior to performing the deuterium labeling experiments, the two potential mechanistic pathways were evaluated computationally using DFT (Figure 5.4). Calculations were performed using ωB97X-D/def2-TZVPP/SMD(nhexadecane)//ωB97X-D/def2-SVP/IEEPCM(n-hexadecane), as this functional has performed well previously in modeling the transition structures of other pericyclic reactions.[34,35] The first barrier for intramolecular Diels–Alder cycloaddition of **5.7** to give cycloadduct **5.12** was calculated to be the highest barrier of the cascade reaction at 28.7 kcal/mol (see **TS-5.1**). The Diels–Alder cycloaddition is thought to proceed through a concerted asynchronous mechanism, which is demonstrated by the different lengths of the forming C–C bonds shown in the computed structure of **TS-5.1**. The barriers for the retro-aldol and retro-carbonyl-ene mechanisms were also evaluated. The retro-carbonyl-ene pathway to give **5.8** was

calculated to proceed with an activation barrier of 22.5 kcal/mol (**TS-5.2**). Despite attempts to find a transition state structure for the retro-aldol pathway, a transition state could not be found, even under conditions using a more polar solvent (i.e., DMSO). Thus, a base catalyst is likely required for such a transformation. Inclusion of methylamine as a base gave a transition state for the retro-aldol mechanism that is predicted to be higher in energy than the retro-carbonyl-ene pathway (see section 5.7.3.2 for more details). Therefore, these computations predict that the retro-carbonyl-ene pathway is preferred over the retro-aldol alter-native reaction pathway.

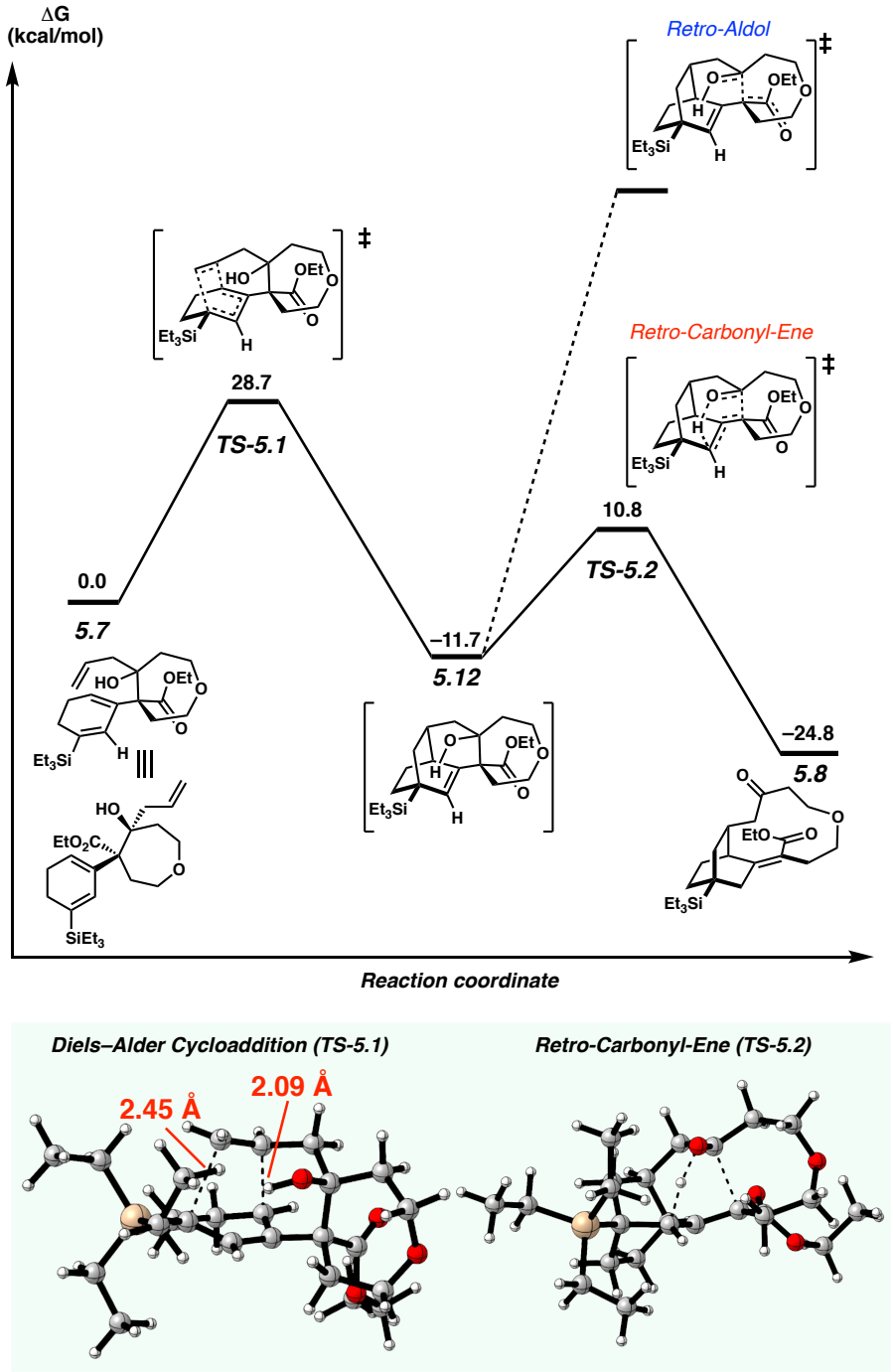


Figure 5.4. Computational study of reaction pathways predicts the retro-carbonyl-ene pathway is favorable. Energies were calculated using ωB97X-D/def2-TZVPP/SMD(*n*-hexadecane)//ωB97X-D/def2-SVP/IEFPCM(*n*-hexadecane) and are given in kcal/mol. Computed transition states **TS-5.1** and **TS-5.2** are shown.

5.5 Experimental Results

With computational results in hand, we pursued deuterium-labeling experiments as alluded to earlier. Although initial efforts aimed at labeling H_A (see **5.12**, Figure 5.3) were unsuccessful,[36] the alternative strategy of labeling H_B proved fruitful[37] (Figure 5.5). Silyl-substituted triene precursor **5.9** and labeled enamine **5.10-*d*** (93% deuterium incorporation) were carried through the synthetic sequence to furnish **5.7-*d*** (79% deuterium incorporation).[38] The first step, as previously shown in Figure 5.2, involves trapping of the 1,2,3-triene intermediate. Transition structure **5.14-*d*** suggests a plausible mechanism by which deuterium incorporation occurs in the triene trapping experiment. In the key mechanistic experiment, **5.7-*d*** was heated at 220 °C in hexadecane to provide the product **5.8-*d***. ^{1}H NMR analysis indicated that proton transfer occurred to give exclusive C13 deuteration at the pseudoaxial position (79% deuterium incorporation). This result is consistent with transition structure **5.12b** (see Figure 5.3) and the retro-carbonyl-ene mechanism, rather than the retro-aldol pathway. As such, this result is consistent with the computational results described earlier.

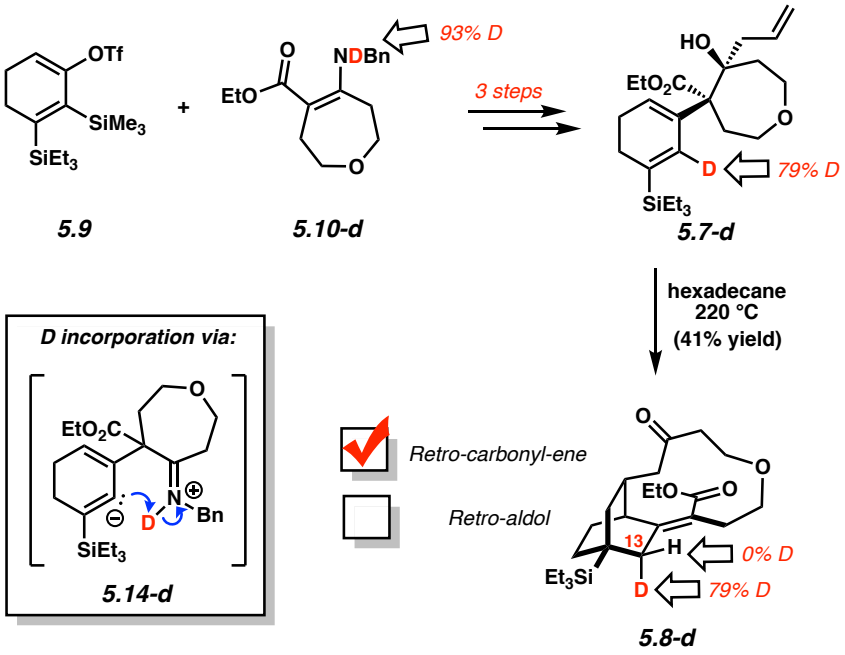


Figure 5.5 Synthesis of **5.8-*d*** and results of Diels–Alder/rearrangement cascade indicating a retro-carbonyl-ene pathway.

5.6 Conclusion

We studied the transformation of **5.7** to **5.8** through both computational and empirical methods. Calculations predicted that a retro-carbonyl-ene reaction pathway was operative, and this hypothesis was confirmed experimentally through a deuterium labeling study. This report underscores the synergy between computational and experimental studies and establishes the mechanism of this interesting complexity-generating transformation. We hope these studies may enable the further use of the retro-carbonyl-ene reaction in total synthesis and encourage the further use of computations and experiments, in tandem, to interrogate mechanistic pathways.

5.7 Experimental Section

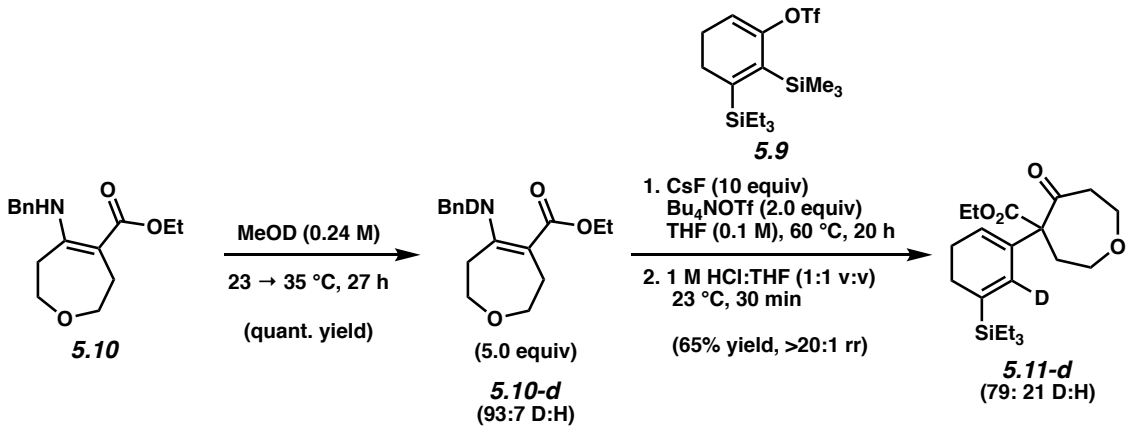
5.7.1 Materials and Methods

Unless stated otherwise, reactions were conducted in flame-dried glassware under an atmosphere of nitrogen, and commercially obtained reagents were used as received unless otherwise specified. Anhydrous solvents were either freshly distilled or passed through activated alumina columns, unless otherwise stated. Non-commercially available substrates were synthesized according to known preparations or following protocols specified in the Experimental Procedures. Prior to use in trapping experiments, tetrahydrofuran (THF) was passed through an activated alumina column and degassed by five freeze-pump-thaw cycles. Tetrabutylammonium trifluoromethanesulfonate (Bu_4NOTf) and hexadecane were purchased from Sigma-Aldrich and used as received. Cesium fluoride (CsF) was obtained from Strem Chemicals, stored in a glovebox, and used as received. MeOD was purchased from Cambridge Isotope Labs in ampules and used as received. Reaction temperatures above 23 °C were controlled using an IKAmag temperature modulator, and unless stated otherwise, performed at room temperature (approximately 23 °C). Thin-layer chromatography (TLC) was conducted with EMD gel 60 F_{254} pre-coated plates (0.25 mm for analytical chromatography and 0.50 mm for preparative chromatography) and visualized using a combination of UV, anisaldehyde, and potassium permanganate staining techniques. Silicycle Siliaflash P60 (particle size 40–63 μm) was used for flash column chromatography unless otherwise specified. ^{1}H-NMR spectra were recorded on Bruker spectrometers (at 500 and 600 MHz) and are reported relative to the residual solvent signal. Data for ^{1}H-NMR spectra are reported as follows: chemical shift (δ ppm), multiplicity, coupling constant (Hz), and integration. Data for ^{2}H NMR are reported in terms of chemical shift (77 MHz). IR spectra were recorded on a Perkin-Elmer UATR Two FT-IR spectrometer and are reported in terms of frequency absorption (cm^{-1}).

DART-MS spectra were collected on a Thermo Exactive Plus MSD (Thermo Scientific) equipped with an ID-CUBE ion source, a Vapur Interface (IonSense Inc.), and an Orbitrap mass analyzer. Both the source and MSD were controlled by Excalibur software version 3.0. The analyte was spotted onto OpenSpot sampling cards (IonSense Inc.) using $CDCl_3$ or CH_2Cl_2 as the solvent. Ionization was accomplished using UHP He plasma with no additional ionization agents. The mass calibration was carried out using Pierce LTQ Velos ESI (+) and (–) Ion calibration solutions (Thermo Fisher Scientific). Diastereomeric ratios (dr) and regioisomeric ratios (rr) were determined by ^{1}H NMR analysis of crude reaction mixtures. Enamine **5.10** and silyl triflate **5.9** are known compounds.[25] The spectral data matched those reported in the literature.

5.7.2 Experimental Procedures

5.7.2.1 Deuterium Labeling Trapping Experiment



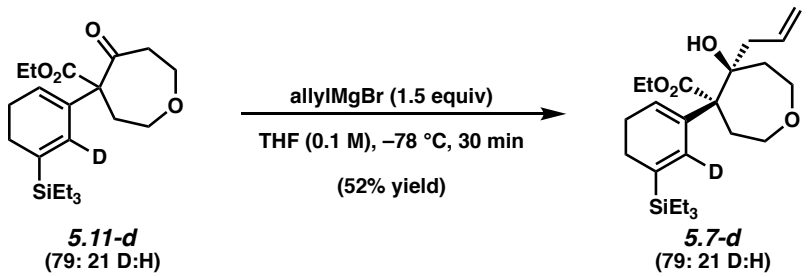
Ketoester 5.11-*d*. A suspension of enamine **5.10** (199 mg, 0.72 mmol, 1.0 equiv) in CD_3OD (3.0 mL, 0.24 M) in a flame dried 2-dram vial was allowed to stir at 23 °C for 3 h. After this time, the volatiles were removed under reduced pressure in the absence of a heating bath at 23 °C. This process of suspension, stirring, and solvent evaporation was repeated 4 more times with the stir times being 3 h, 12 h, 3 h, and 3 h, respectively. The process was repeated one final time, but with heating at 35 °C in a preheated aluminum block for 3 h (*caution*: it was found that heating for >12

h resulted in undesired deuterium incorporation at other sites on the trapping partner). This process afforded enamine **5.10-*d*** (200 mg, 0.72 mmol, quant. yield, 93% D incorporation, see section 5.8 for NMR spectra) as a white solid, which was used without further purification and brought into a glovebox for storage. R_f = 0.62 (2:1 hexanes:EtOAc); ^{1}H NMR (500 MHz, C_6D_6): δ 10.15 (s, 0.07H, site of D incorporation), 7.13–6.92 (m, 5H), 4.17 (q, *J* = 6.9, 2H), 3.78 (s, 2H), 3.71–3.59 (m, 2H), 3.39–3.25 (m, 2H), 2.96–2.82 (m, 2H), 2.34–2.17 (t, *J* = 4.2, 2H), 1.09 (t, *J* = 6.9, 3H); IR (film): 2944, 2851, 1639, 1595, 1205 cm^{-1}. Spectral data match those previously reported.[37] Deuterium incorporation was confirmed by a combination of ^{2}H NMR and HRMS. ^{2}H NMR (77 MHz, benzene) δ 10.06 (br. S, 1D); HRMS-APCI (*m/z*) $[M + H]^+$ calcd for $C_{16}H_{21}DNO_3^+$, 277.1657; found 277.1636.

Inside a glove box, a flame dried 2-dram vial containing a stir bar and silyl triflate **5.9** (60.0 mg, 0.15 mmol, 1.0 equiv) was charged sequentially with deuterated enamine **5.10-*d*** (200 mg, 0.72 mmol, 97% deuterium incorporation, 5.0 equiv), Bu_4NOTf (113 mg, 0.29 mmol, 2.0 equiv) and THF (1.45 mL, 0.1 M). CsF (220 mg, 1.45 mmol, 10 equiv) was then added in a single portion, and the vial was sealed, brought out of the glovebox, and the reaction stirred at 60 °C for 24 h. After this time, the reaction was diluted with Et_2O (5 mL) and filtered through a Celite plug eluting with Et_2O (5 mL). The eluate was concentrated, and the resulting residue was resuspended in THF (3 mL) then treated with 1 M HCl (aq.) (3 mL). The mixture was stirred vigorously for 25 min, then diluted with water (5 mL) and Et_2O (5 mL). The layers were separated, and the aqueous layer was extracted with Et_2O (2 x 5 mL). The organic layers were combined, dried over sodium sulfate, filtered, and concentrated under reduced pressure. The crude residue was purified by flash chromatography (benzene → 97:3 benzene:Et_2O) to give ketoester **5.11-*d*** (38.7 mg, 0.094 mmol, 79% deuterium incorporation, 65% yield) as a clear colorless oil. **Ketoester 5.11-*d*:** R_f = 0.55 (9:1

benzene:Et_2O); ^1H NMR (600 MHz, $CDCl_3$): δ 5.98 (q, *J* = 1.6, 0.21H, site of D incorporation), 5.68–5.62 (m, 1H), 4.21 (q, *J* = 7.2, 2H), 3.99 (ddd, *J* = 13.5, 7.2, 1.7, 1H), 3.89 (ddd, *J* = 12.3, 6.5, 3.6, 1H), 3.75 (ddd, *J* = 13.5, 8.3, 1.5 1H), 3.63 (ddd, *J* = 12.3, 9.1, 2.8, 1H), 2.90 (ddd, *J* = 14.3, 9.1, 3.7, 1H), 2.71 (ddd, *J* = 14.3, 6.5, 2.8, 1H), 2.45 (ddd, *J* = 15.5, 7.2, 1.6, 1H), 2.19–1.99 (m, 5H), 1.25 (t, *J* = 7.2, 3H), 0.92 (t, *J* = 8.0, 9H), 0.59 (q, *J* = 8.0, 6H); IR (film): 2952, 1731, 1708, 1464, 1235 cm^{-1}. Spectral data match those previously reported.[25] Deuterium incorporation was confirmed by a combination of ^2H NMR and HRMS. ^2H NMR (77 MHz, benzene) δ 6.32 (br. s, 1D); HRMS-APCI (*m/z*) $[M + H]^+$ calcd for $C_{21}H_{34}DO_4Si^+$, 380.2362; found 380.2378.

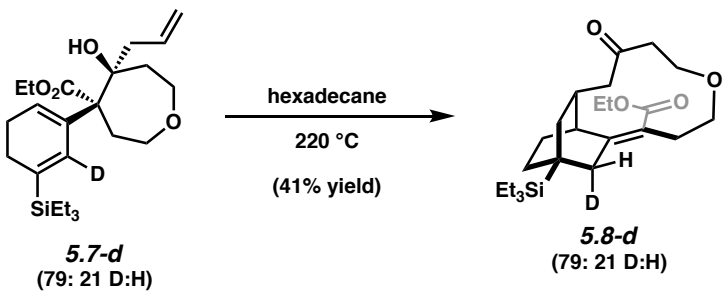
5.7.2.2 Grignard Addition



Alcohol 5.7-*d*. A solution of ketoester **5.11-*d*** (38.7 mg, 94.0 μmol, 79% deuterium incorporation, 1.0 equiv) in THF (1.02 mL, 0.1 M), in a flame dried 2-dram vial equipped with a stir bar, was cooled to –78 °C. Then, a freshly prepared solution of allyl Grignard[39] (0.2 M in Et_2O, 770 μL, 1.5 equiv) was added dropwise over 3 min. The resulting solution was stirred at –78 °C for 30 min, quenched by the addition of saturated aqueous ammonium chloride (5 mL), and diluted with Et_2O (5 mL). The layers were separated, and the aqueous layer was extracted with Et_2O (2 x 5 mL). The organic layers were combined, dried over sodium sulfate, filtered, and concentrated under reduced pressure. The resulting residue was purified by preparative thin layer chromatography (plate pre-treated by developing in 9:1 hexanes:Et_2O with 2% Et_3N, then the compound was loaded and eluted with the same solvent) to afford alcohol **5.7-*d*** (23.9 mg, 53.2 μmol, 52% yield, 79%

deuterium incorporation) as a clear colorless oil. **Alcohol 5.7-*d***: R_f = 0.45 (19:1 benzene:MeCN); ^{1}H NMR (600 MHz, $CDCl_3$): 6.20 (s, 0.21H, site of D incorporation), 5.94–5.86 (m, 1H), 5.72–5.66 (m, 1H), 5.10–5.05 (m, 1H), 5.04–4.98 (m, 1H), 4.25 (dq, *J* = 10.8, 7.1, 1H), 4.15 (dq, *J* = 10.8, 7.1, 1H), 3.82–3.71 (m, 2H), 3.70–3.62 (m, 2H), 2.99 (ddd, *J* = 14.7, 9.1, 7.3, 1H), 2.91 (dd, *J* = 14.2, 8.1, 1H), 2.30 (ddd, *J* = 14.8, 8.7, 6.5, 1H), 2.20–2.14 (m, 1H), 2.13–2.07 (m, 2H), 2.06–1.94 (m, 3H), 1.88 (ddd, *J* = 14.5, 5.5, 1.7, 1H), 1.71 (dt, *J* = 15.0, 3.0, 1H), 1.28 (t, *J* = 7.1, 3H), 0.92 (t, *J* = 8.0, 9H), 0.59 (q, *J* = 8.0, 6H); IR (film): 3542, 2874, 1730, 1207, 1108 cm^{-1}. Spectral data match those previously reported.[25] Deuterium incorporation was confirmed by a combination of ^{2}H NMR and HRMS. ^{2}H NMR (77 MHz, benzene) δ 6.61 (br. s, 1D); HRMS-APCI (*m/z*) [M + H]$^+$ calcd for $C_{24}H_{40}DO_4Si^+$, 422.2831; found 422.2851.

5.7.2.3 Formation of Compound 5.8-*d*



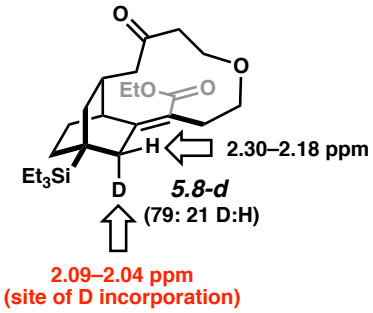
5.7-d
(79: 21 D:H)

5.8-d
(79: 21 D:H)

Product 5.8-*d*. A flame dried Schlenk flask containing a stir bar and equipped with a Teflon stopcock was charged with a solution of alcohol **5.7-*d*** (8.6 mg, 16 μmol, 1.0 equiv) in hexadecane (2.0 mL, 0.01 M). The solution was sparged vigorously with nitrogen for 15 min. The stopcock was sealed, and the reaction was immersed in a sand bath and stirred at 220 °C for 14 h, with the reaction being placed behind a blast shield. After this time, the reaction was cooled to 23 °C then loaded onto a silica plug (monster pipette, 5 cm) eluting first with hexanes (10 mL) to remove hexadecane, and then Et_2O (10 mL) to elute the remaining material. The eluate was concentrated, and the product was isolated by preparative thin layer chromatography (7:2:1

hexanes:CH_2Cl_2:Et_2O, eluted 2x) to afford product **5.8-*d*** (3.5 mg, 8.3 μmol, 41% yield, 79% deuterium incorporation) as a clear colorless oil. **Product 5.8-*d***: R_f = 0.33 (4:1 hexanes:acetone); ^{1}H NMR (600 MHz, $CDCl_3$): 4.20 (qd, *J* = 7.1, 2.6, 2H), 4.11 (ddd, *J* = 11.8, 9.6, 2.4, 1H), 3.95 (ddd, *J* = 10.7, 4.8, 3.2, 1H), 3.55–3.46 (m, 2H), 3.30 (ddd, *J* = 11.5, 6.1, 2.6, 1H), 2.87 (ddd, *J* = 16.5, 9.4, 2.2, 1H), 2.56–2.43 (m, 3H), 2.30–2.18 (m, 4H), 2.09–2.04 (m, 0.21H, site of D incorporation), 1.93–1.84 (m, 1H), 1.80–1.73 (m, 1H), 1.68 (dd, *J* = 13.4, 10.9, 1H), 1.64–1.59 (m, 1H), 1.55–1.49 (overlapped with residual solvent peak, 1H), 1.36–1.29 (m, 4H), 0.99 (t, *J* = 8.0, 9H), 0.59 (q, *J* = 8.0, 6H); IR (film): 2937, 1704, 1367, 1286, 1204 cm^{-1}. Spectral data match those previously reported.[25] Deuterium incorporation was confirmed by a combination of ^{2}H NMR and HRMS. ^{2}H NMR (77 MHz, benzene) δ 2.02 (br. s, 1D); HRMS-APCI (*m/z*) $[M + H]^+$ calcd for $C_{24}H_{40}DO_4Si^+$, 422.2831; found 422.2848.

Prior studies resulted in the given assignment of the protons distinguished below.[25] The diminished integration at 2.09–2.04 ppm is attributed to deuterium incorporation at the position indicated.



5.7.3 Computational Section

5.7.3.1 Computational Methods

All the calculations were carried out using Gaussian 16 program.[40] The geometries were optimized using ωB97X-D[41] functional with def2-SVP[42] basis set with IEEPCM solvent model[43] to describe the *n*-hexadecane or DMSO environment. Conformational search using xTB[44] and CREST[45] was conducted for all the structures except water to ensure that the conformers we

reported represented lowest energy conformations. The 10 conformers with the lowest energy, obtained from CREST, were subsequently re-optimized by DFT to determine the most stable conformer. For transition states, constraints are applied to the conformational search to preserve the TS vibration mode. Single point energies were calculated using ωB97X-D functional, def2-TZVPP basis set[42] and SMD solvent model.[46] Quasiharmonic[47] and concentration corrections to enthalpy and entropy were made using Paton's GoodVibes software[48] at 298 K, 1 atm and 1 mol/L.

5.7.3.2 Transition State Analysis for the Potential Retro-Carbonyl-Ene and Retro Aldol Mechanistic Pathways

The result indicates that the Diels-Alder transition state **TS-5.1** is concerted asynchronous, where two bonds (Bond1 and Bond2, see Figure 5.6 below) form via a single step but with unequal bond lengths at the transition state.

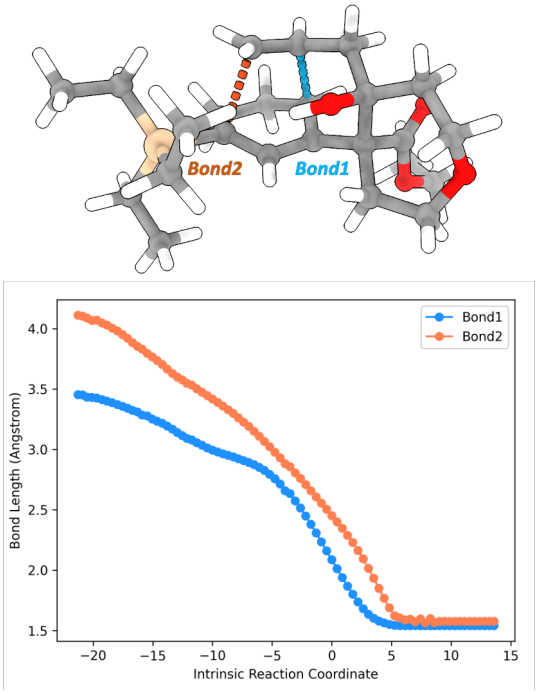


Figure 5.6. Distances of two partially formed bonds in **TS-5.1** along the IRC.

Toward the retro-aldol pathway, scanning of the increase in C–C bond length shows a dramatic energy increase during the disassociation, indicating a high barrier along this process (Figure 5.7).

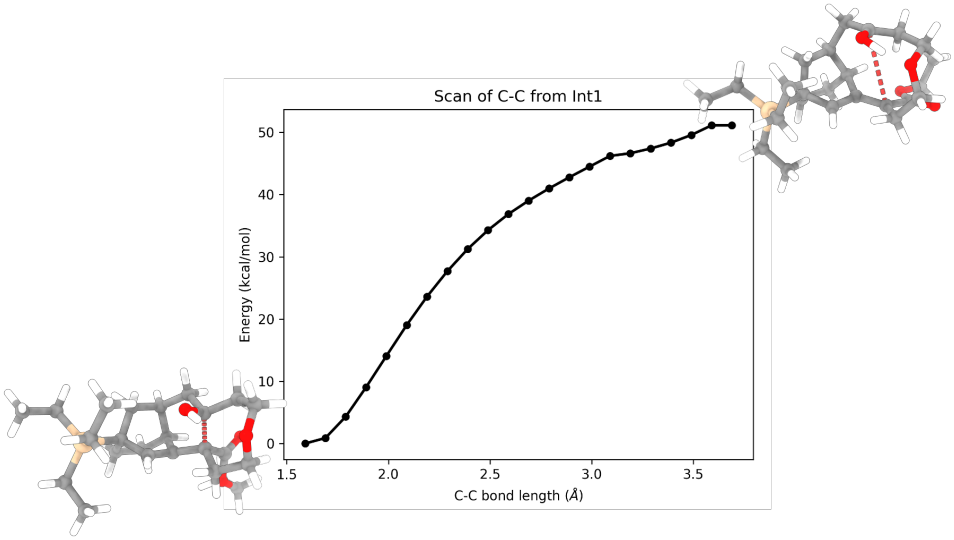


Figure 5.7. Relax scan of the C–C bond length from **5.12**, corresponding to the retro-aldol pathway.

For the retro-aldol pathway, TS optimization for the energy maximum geometries was attempted, but no saddle points could be located. It is therefore believed that the retro-aldol mechanism is disfavored and may not occur under conditions in the absence of a base. In polar DMSO solvent, with the inclusion of $MeNH_2$ as a base (Figure 5.8), transition state **TS-5.3** could be found but is still higher in energy than the transition state for the retro-carbonyl-ene (1-*O*-retro-ene) mechanism (i.e., **TS-5.2**).

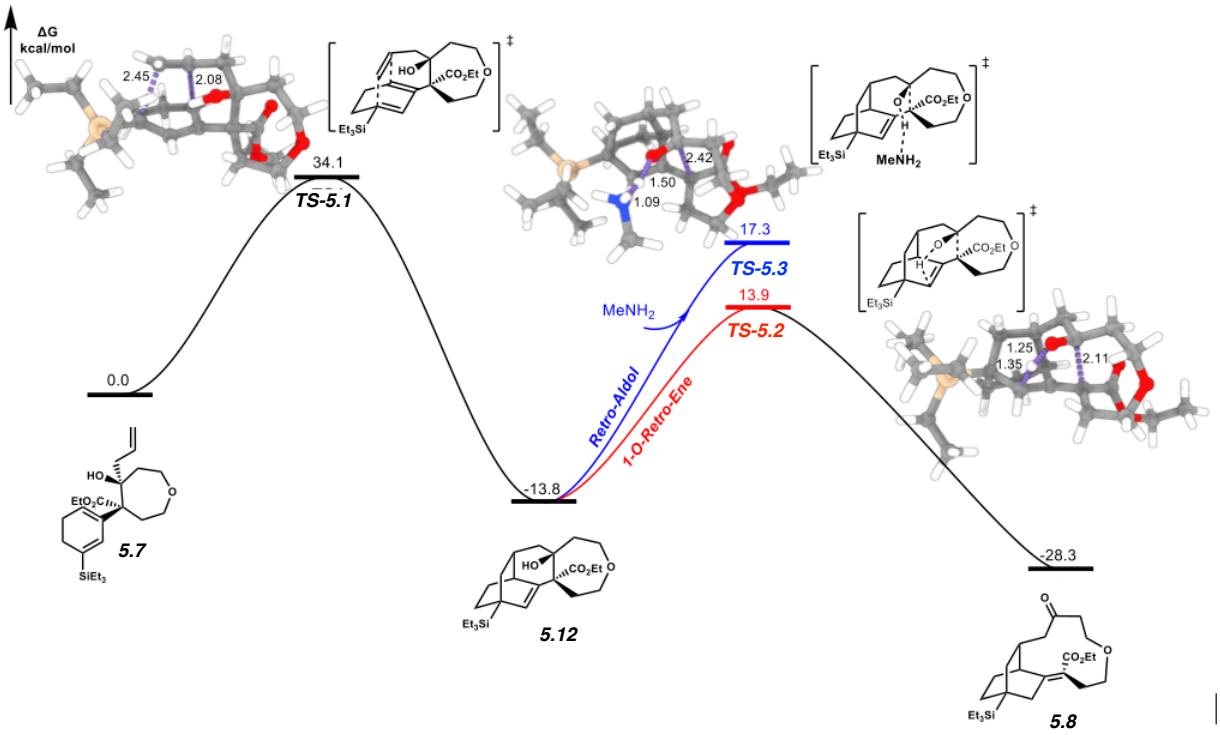


Figure 5.8. Computed energy diagram for the formation of **5.8** in DMSO. Energies were calculated by ωB97X-D/def2-TZVPP/SMD(DMSO)//ωB97X-D/def2-SVP/IEFPCM(DMSO) and are given in kcal/mol. The retro-aldol transition state **TS-5.3** can only be found in the presence of base ($MeNH_2$).

5.7.3.3 Cartesian Coordinates

Cartesian coordinates for the optimized structures were reported in the literature.[49]

5.8 Spectra Relevant to Chapter Five:

Evaluation of Retro-Aldol vs Retro-Carbonyl-Ene Mechanistic Pathways in a Complexity-Generating C–C Bond Fragmentation

Ana S. Bulger, Daniel W. Turner, Qingyang Zhou, K. N. Houk, and Neil K. Garg.

Org. Lett. **2024**, *26*, 3602–3606.

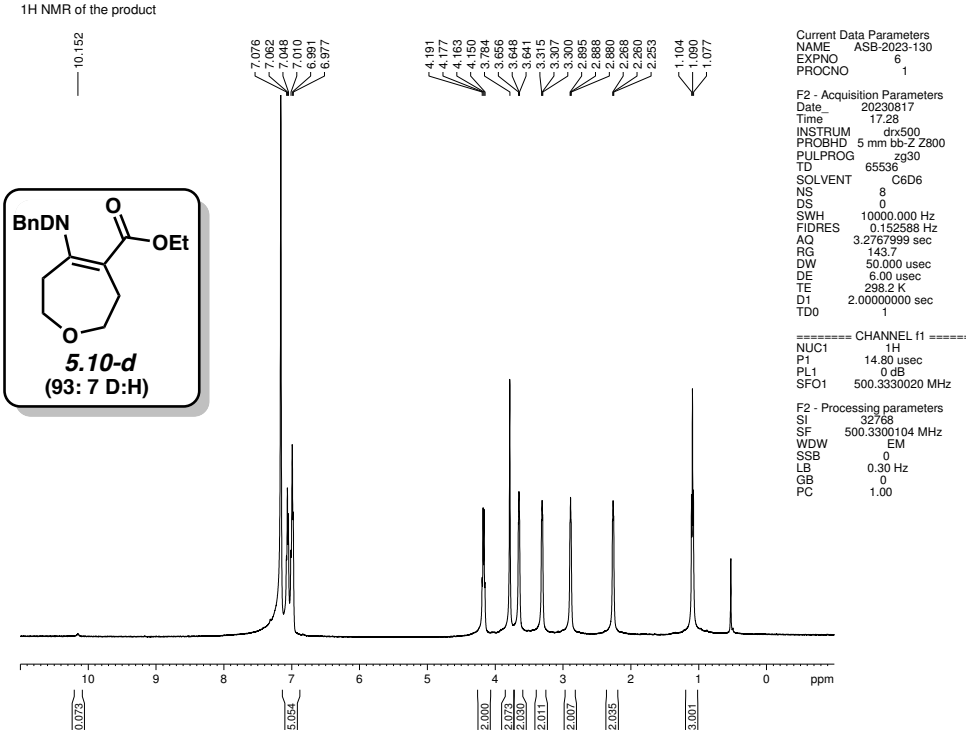


Figure 5.9. ^{1}H NMR (500 MHz, C_6D_6) of compound **5.10-*d*.**

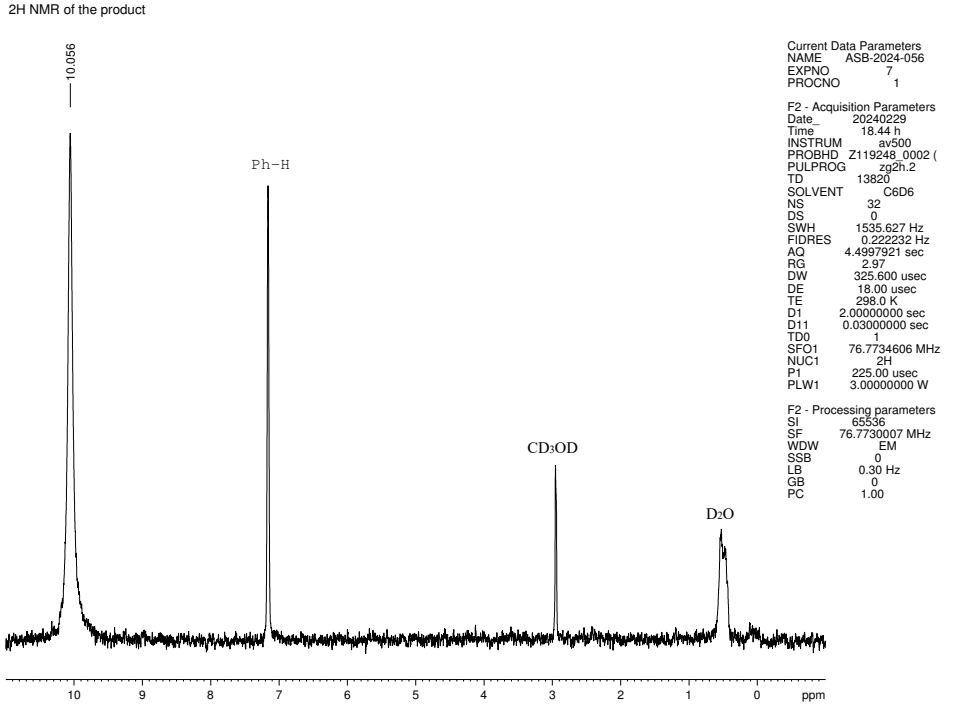


Figure 5.10. ^{2}H NMR (77 MHz, C_6H_6) of compound **5.10-*d*.**

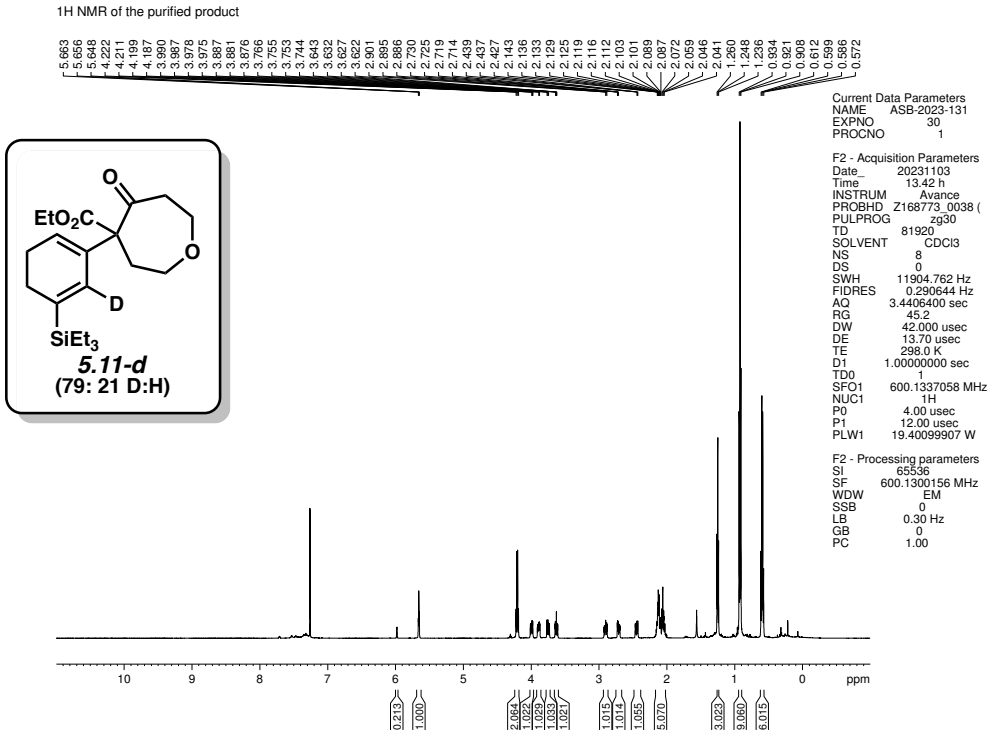


Figure 5.11. ^{1}H NMR (600 MHz, C_6D_6) of compound **5.11-*d*.**

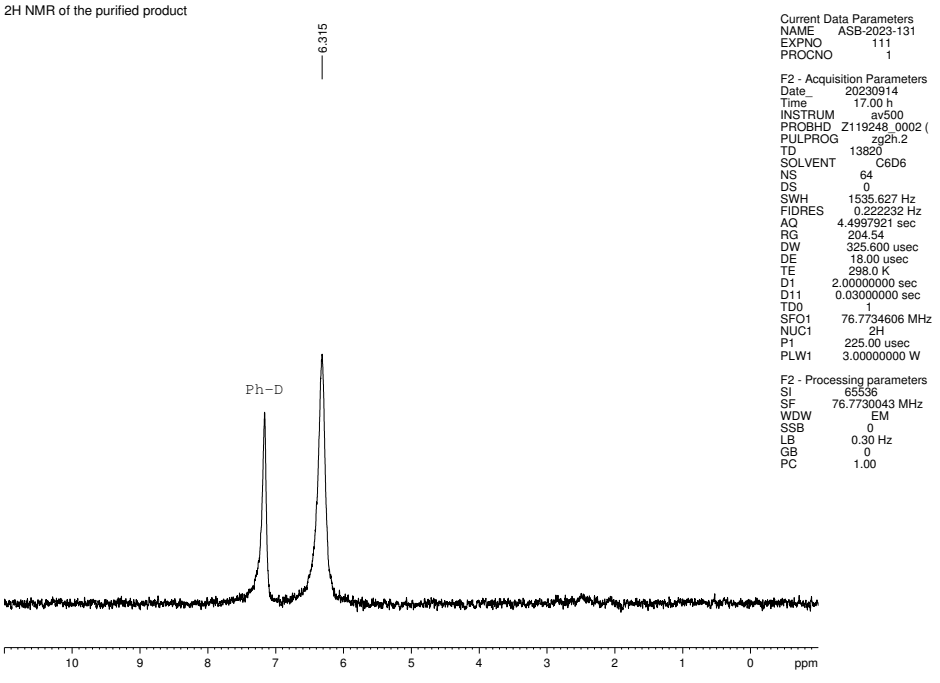


Figure 5.12. ^{2}H NMR (77 MHz, C_6H_6) of compound **5.11-*d*.**

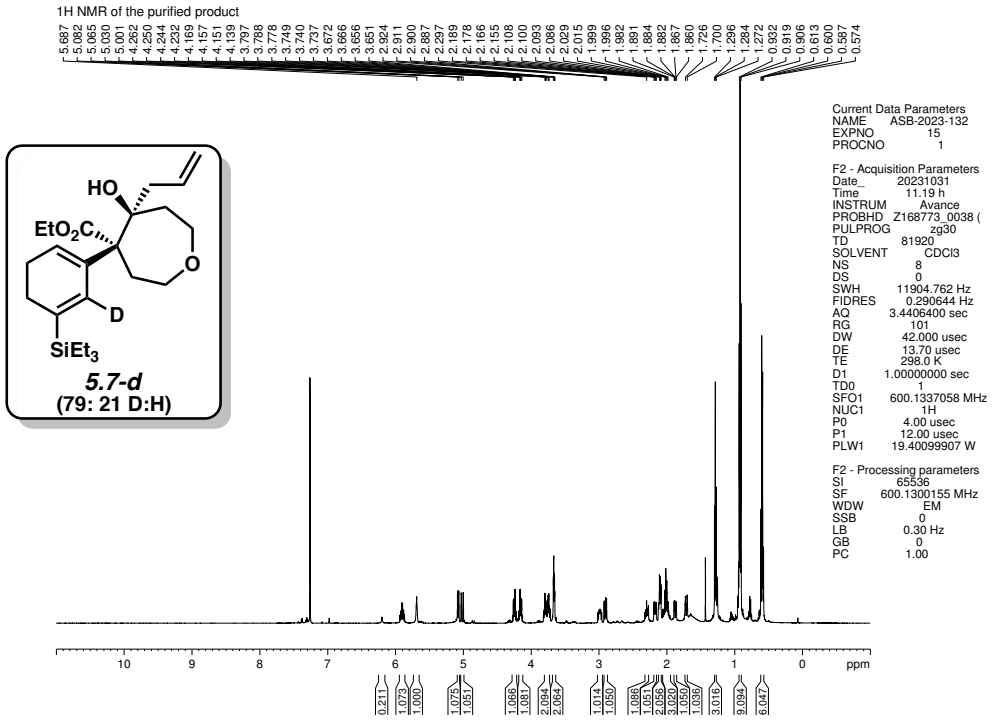


Figure 5.13. ^{1}H NMR (600 MHz, C_6D_6) of compound **5.7-*d*.**

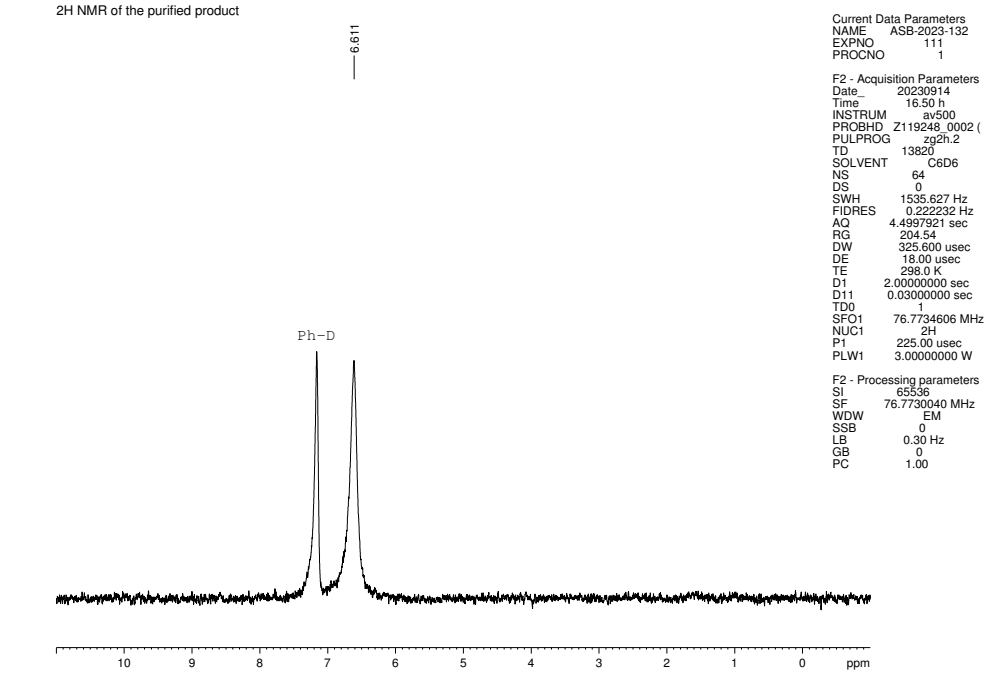


Figure 5.14. ^{2}H NMR (77 MHz, C_6H_6) of compound **5.7-*d*.**

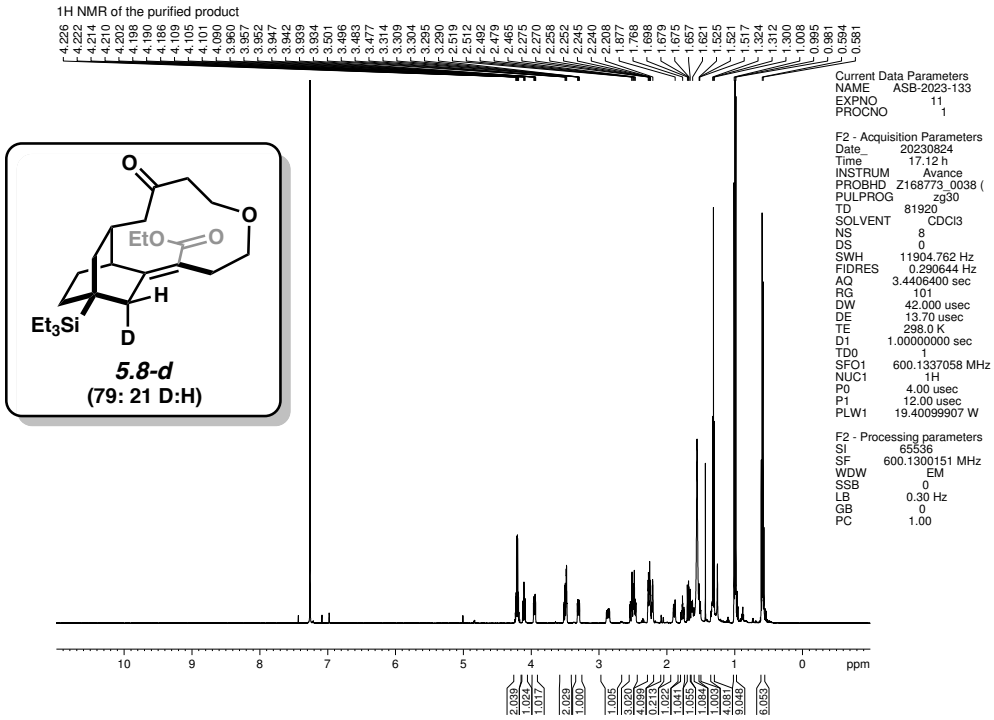


Figure 5.15. ^{1}H NMR (600 MHz, C_6D_6) of compound **5.8-*d*.**

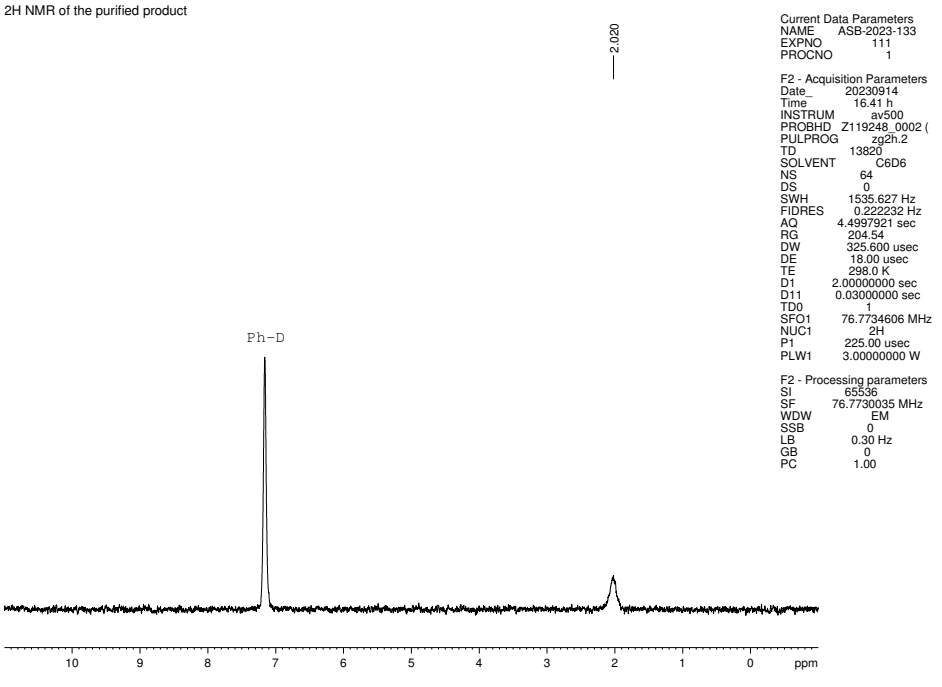


Figure 5.16. ^{2}H NMR (77 MHz, C_6H_6) of compound **5.8-*d*.**

5.9 Notes and References

(1) Carroll, F. I.; Robinson, T. P.; Brieaddy, L. E.; Atkinson, R. N.; Mascarella, S. W.; Damaj, M. I.; Martin, B. R.; Navarro, H. A. Synthesis and nicotinic acetylcholine receptor binding properties of bridged and fused ring analogues of epibatidine. *J. Med. Chem.* **2007**, *50*, 6383–6391.

(2) Kametani, T.; Kigasawa, K.; Hiragi, M.; Wagatsuma, N.; Uryu, T.; Araki, K. Syntheses of heterocyclic compounds. 509. Syntheses of analgesics. 34. Synthesis of 3-hydroxy-*N*-cyclopropylmethyl-9-azamorphinan. *J. Med. Chem.* **1973**, *16*, 301–303.

(3) Heindel, N. D.; Fives, W. P.; Lemke, T. F.; Rowe, J. E.; Snady, H. W. Synthesis, transformation, and general pharmacologic activity in 1,4-benzodiazepine-3,5-diones. *J. Med. Chem.* **1971**, *14*, 1233–1235.

(4) Bell, M. R.; Zalay, A. W.; Oesterlin, R.; Schane, P.; Potts, G. Basic ethers of 1-(*p*-hydroxyphenyl)-2-phenyl-1,2,3,4-tetrahydroquinoline and 1-(*p*-hydroxyphenyl)-2-phenyl indole antifertility agents. *J. Med. Chem.* **1970**, *13*, 664–668.

(5) Willis, P. G.; Pavlova, O. A.; Chefer, S. I.; Vaupel, D. B.; Mukhin, A. G.; Horti, A. G. Synthesis and structure-activity relationship of a novel series of aminoalkylindoles with potential of imaging the neuronal cannabinoid receptor by positron emission tomography. *J. Med. Chem.* **2005**, *48*, 5813–5822.

(6) Jacob, P., III; Shulgin, A. T. Sulfur analogues of psychotomimetic agents. Monothio analogues of mescaline and isomescaline. *J. Med. Chem.* **1981**, *24*, 1348–1353.

(7) Coe, J. W.; Brooks, P. R.; Wirtz, M. C.; Bashore, C. G.; Bianco, K. E.; Vetelino, M. G.; Arnold, E. P.; Lebel, L. A.; Fox, C. B.; Tingley, F. D., III; Schulz, D. W.; Davis, T. I.; Sands, S. B.;

Mansbach, R. S.; Rollema, H.; O'Neill, B. T. 3,5-Bicyclic aryl piperidines: A novel class of α4β2 neuronal nicotinic receptor partial agonists for smoking cessation. *Bioorg. Med. Chem. Lett.* **2005**, *15*, 4889–4897.

(8) Kou, K. G. M.; Pflueger, J. J.; Kiho, T.; Morrill, L. C.; Fisher, E. L.; Clagg, K.; Lebold, T. P.; Kisunzu, J. K.; Sarpong, R. A benzyne insertion approach to hetisine-type diterpenoid alkaloids: Synthesis of cossonidine (davisine). *J. Am. Chem. Soc.* **2018**, *140*, 8105–8109.

(9) Goetz, A. E.; Silberstein, A. L.; Corsello, M. A.; Garg, N. K. Concise enantiospecific total synthesis of tubingensin A. *J. Am. Chem. Soc.* **2014**, *136*, 3036–3039.

(10) Tadross, P. M.; Stoltz, B. M. A comprehensive history of arynes in natural product total synthesis. *Chem. Rev.* **2012**, *112*, 3550–3577.

(11) Gampe, C. M.; Carreira, E. M. Arynes and cyclohexyne in natural product synthesis. *Angew. Chem., Int. Ed.* **2012**, *51*, 3766–3778.

(12) Corsello, M. A.; Kim, J.; Garg, N. K. Total synthesis of (–)-tubingensin B enabled by the strategic use of an aryne cyclization. *Nat. Chem.* **2017**, *9*, 944–949.

(13) Gampe, C. M.; Carreira, E. M. Total syntheses of guanacastepenes N and O. *Angew. Chem., Int. Ed.* **2011**, *50*, 2962–2965.

(14) Nathel, N. F. F.; Shah, T. K.; Bronner, S. M.; Garg, N. K. Total syntheses of indolactam alkaloids (–)-indolactam V, (–)-pendolmycin, (–)-lyngbyatoxin A, and (–)-teleocidin A-2. *Chem. Sci.* **2014**, *5*, 2184–2190.

(15) Ippoliti, F. M.; Adamson, N. J.; Wonilowicz, L. G.; Nasrallah, D. J.; Darzi, E. R.; Donaldson, J. S.; Garg, N. K. Total synthesis of lissodendoric acid A via stereospecific trapping of a strained cyclic allene. *Science* **2023**, *379*, 261–265.

(16) Mehta, M. M.; Gonzalez, J. A. M.; Bachman, J. L.; Garg, N. K. Cyclic allene approach to the manzamine alkaloid keramaphidin B. *Org. Lett.* **2023**, *25*, 5553–5557.

(17) Westphal, M. V.; Hudson, L.; Mason, J. W.; Pradeilles, J. A.; Zécri, F. J.; Briner, K.; Schreiber, S. L. Water-compatible cycloadditions of oligonucleotide-conjugated strained allenes for DNA-encoded library synthesis. *J. Am. Chem. Soc.* **2020**, *142*, 7776–7782.

(18) Surry, D. S.; Buchwald, S. L. Biaryl phosphane ligands in palladium-catalyzed amination. *Angew. Chem., Int. Ed.* **2008**, *47*, 6338–6361.

(19) Mauger, C. C.; Mignani, G. A. An efficient and safe procedure for the large-scale Pd-catalyzed hydrazonation of aromatic chlorides using buchwald technology. *Org. Process Res. Dev.* **2004**, *8*, 1065–1071.

(20) Darzi, E. R.; Barber, J. S.; Garg, N. K. Cyclic alkyne approach to heteroatom-containing polycyclic aromatic hydrocarbon scaffolds. *Angew. Chem., Int. Ed.* **2019**, *58*, 9419–9424.

(21) Shakespeare, W. C.; Johnson, R. P. 1,2,3-Cyclohexatriene and cyclohexen-3-yne: Two new highly strained C_6H_6 isomers. *J. Am. Chem. Soc.* **1990**, *112*, 8578–8579.

(22) Hickey, E. R.; Paquette, L. A. Torsional angle decompression is not the source of facial selectivity in Diels–Alder cycloadditions involving cyclic dienes fused to bicyclic frameworks. The case study of 1,2,3,4,6,7-hexahydro-1,4-methanonaphthalene. *Tetrahedron Lett.* **1994**, *35*, 2309–2312.

(23) Burrell, R. C., Daoust, K. J., Bradley, A. Z., DiRico, K. J., Johnson, R. P. Strained cyclic cumulene intermediates in Diels–Alder cycloadditions of enynes and diynes. *J. Am. Chem. Soc.* **1996**, *118*, 4218–4219.

(24) Sakura, M., Ando, S., Hattori, A., Saito, K. Reaction of cyclohexa-1,2,3-triene with *N*,α-diphenylnitrone: Formation of seven-membered cyclic amines via piradone derivatives. *Heterocycles* **1999**, *51*, 547–556.

(25) Kelleghan, A. V.; Bulger, A. S.; Witkowski, D. C.; Garg, N. K. Strain-promoted reactions of 1,2,3-cyclohexatriene and its derivatives. *Nature* **2023**, *618*, 748–754.

(26) Ranganathan, S.; Kumar, R.; Maniktala, V. On the mechanism and synthetic applications of the thermal and alkaline degradation of C-18 castor oil. *Tetrahedron* **1984**, *40*, 1167–1168.

(27) Setzer, W. N. A DFT analysis of thermal decomposition reactions important to natural products. *Nat. Prod. Commun.* **2010**, *5*, 993–998.

(28) Goussougly, M.; Sirjean, B.; Glaude, P.-A.; Fournet, R. Theoretical study of the pyrolysis of β-1,4-xylan: A detailed investigation on unimolecular concerted reactions. *Phys. Chem. Chem. Phys.,* **2021**, *23*, 2605–2621.

(29) Liu, S.; Zhang, T.; Zhu, L.; Zhong, K.; Gong, J.; Yang, Z.; Bai, R.; Lan, Y. Retro-metal-ene versus retro-aldol: Mechanistic insight into Rh-catalysed formal [3+2] cycloaddition. *Chem. Commun.* **2018**, *54*, 13551–13554.

(30) Talanquer, V. Importance of understanding fundamental chemical mechanisms. *J. Chem. Educ.* **2018**, *95*, 1905–1911.

(31) Chin, Y. P.; See, N. W.; Jenkins, I. D.; Krenske, E. H. Computational discoveries of reaction mechanisms: Recent highlights and emerging challenges. *Org. Biomol. Chem.* **2022**, *20*, 2028–2042.

(32) Alternatively, C–C bond cleavage could precede proton transfer.

(33) Although a mixture could be obtained, we would expect this pathway could give a preference for the formation of **5.8a** based on kinetic protonation of **5.13** on the less hindered face of the extended enol on C13.

(34) Linder, M.; Brinck, T. On the method-dependence of transition state asynchronicity in Diels–Alder reactions. *Phys. Chem. Chem. Phys.* **2013**, *15*, 5108–5114.

(35) Goerigk, L.; Hansen, A.; Bauer, C.; Ehrlich, S.; Najibi, A.; Grimme, S. A look at the density functional theory zoo with the advanced GMTKN55 database for general main group thermochemistry, kinetics and noncovalent interactions. *Phys. Chem. Chem. Phys.* **2017**, *19*, 32184–32215.

(36) H/D exchange of the hindered tertiary alcohol was found to be challenging.

(37) Picazo, E.; Anthony, S. M.; Giroud, M.; Simon, A.; Miller, M. A.; Houk, K. N.; Garg, N. K. Arynes and cyclic alkynes as synthetic building blocks for stereodefined quaternary centers. *J. Am. Chem. Soc.* **2018**, *140*, 7605–7610.

(38) Deuterium incorporation was determined by ^{1}H NMR analysis. Relative integration of the signal corresponding to the labeled atom informed the extent of hydrogen retention and deuterium incorporation. Deuterium presence was confirmed by ^{2}H NMR analysis and HRMS.

(39) Hauser, F. M.; Baghdanov, V. M. Regiospecific total synthesis of (±)-daunomycinone from an 11-deoxydaunomycinone precursor. *Tetrahedron* **1984**, *40*, 4719–4724.

(40) Frisch, M. J.; Trucks, G. W.; Schlegel, H. B.; Scuseria, G. E.; Robb, M. A.; Cheeseman, J. R.; Scalmani, G.; Barone, V.; Petersson, G. A.; Nakatsuji, H.; Li, X.; Caricato, M.; Marenich, A. V.; Bloino, J.; Janesko, B. G.; Gomperts, R.; Mennucci, B.; Hratchian, H. P.; Ortiz, J. V.; Izmaylov, A. F.; Sonnenberg, J. L.; Williams; Ding, F.; Lipparini, F.;

Egidi, F.; Goings, J.; Peng, B.; Petrone, A.; Henderson, T.; Ranasinghe, D.; Zakrzewski, V. G.; Gao, J.; Rega, N.; Zheng, G.; Liang, W.; Hada, M.; Ehara, M.; Toyota, K.; Fukuda, R.; Hasegawa, J.; Ishida, M.; Nakajima, T.; Honda, Y.; Kitao, O.; Nakai, H.; Vreven, T.; Throssell, K.; Montgomery Jr., J. A.; Peralta, J. E.; Ogliaro, F.; Bearpark, M. J.; Heyd, J. J.; Brothers, E. N.; Kudin, K. N.; Staroverov, V. N.; Keith, T. A.; Kobayashi, R.; Normand, J.; Raghavachari, K.; Rendell, A. P.; Burant, J. C.; Iyengar, S. S.; Tomasi, J.; Cossi, M.; Millam, J. M.; Klene, M.; Adamo, C.; Cammi, R.; Ochterski, J. W.; Martin, R. L.; Morokuma, K.; Farkas, O.; Foresman, J. B.; Fox, D. J. *Gaussian 16 Rev. C.01*, Wallingford, CT, 2016.

(41) Chai, J.-D.; Head-Gordon, M. Long-range corrected hybrid density functionals with damped atom–atom dispersion corrections. *Phys. Chem. Chem. Phys.* **2008**, *10*, 6615– 6620.

(42) Weigend, F.; Ahlrichs, R., Balanced basis sets of split valence, triple zeta valence and quadruple zeta valence quality for H to Rn: Design and assessment of accuracy. *Phys. Chem. Chem. Phys.* **2005**, *7*, 3297–3305.

(43) Scalmani, G.; Frisch, M. J., Continuous surface charge polarizable continuum models of solvation. I. General formalism. *Chem*. *Phys*. **2010**, *132*, 114110.

(44) Bannwarth, C.; Ehlert, S.; Grimme, S., GFN2-xTB—An accurate and broadly parametrized self-consistent tight-binding quantum chemical method with multipole electrostatics and density-dependent dispersion contributions. *J. Chem. Theory Comput.* **2019**, *15*, 1652–1671.

(45) Pracht, P.; Bohle, F.; Grimme, S., Automated exploration of the low-energy chemical space with fast quantum chemical methods. *Phys. Chem. Chem. Phys.* **2020**, *22*, 7169–7192.

(46) Marenich, A. V.; Cramer, C. J.; Truhlar, D. G., Universal solvation model based on solute electron density and on a continuum model of the solvent defined by the bulk dielectric

constant and atomic surface tensions. *J. Phys. Chem. B.* **2009**, *113*, 6378–6396.

(47) Grimme, S., Supramolecular binding thermodynamics by dispersion-corrected density functional theory. *Chem. Eur. J.* **2012**, *18*, 9955–9964.

(48) Luchini, G.; Alegre-Requena, J.; Funes-Ardoiz, I.; Paton, R., GoodVibes: automated thermochemistry for heterogeneous computational chemistry data [version 1; peer review: 2 approved with reservations]. *F1000research.* **2020**, *9,* 291.

(49) Bulger, A. S.; Turner, D. W.; Zhou, Q.; Houk, K. N.; Garg, N. K. Evaluation of retro-aldol vs retro-carbonyl-ene mechanistic pathways in a complexity-generating C–C bond fragmentation. *Org. Lett*. **2024**, *26*, 3602–3606.

CHAPTER SIX

Generation and Trapping of an Azacyclic 1,2,3-Hexatriene

6.1 Abstract

Interest in strained cyclic intermediates such as strained cyclic alkynes and strained cyclic allenes has led to an expansion of their study and usage within the past several decades. Despite this interest, closely-related cyclic 1,2,3-trienes are much less explored. Moreover, the heterocyclic variants of cyclic 1,2,3-trienes are unknown, which further motivates this study, as the discovery of analogous heterocyclic arynes and allenes has been essential for the adoption of strained cyclic intermediates in complex molecule synthesis. In this manuscript, we detail an approach toward an azacyclic 1,2,3-triene and demonstrate its generation and trapping in the context of (4+2) cycloadditions. We also outline an ambitious future plan for the usage of these strained cyclic intermediates. The successful implementation of these proposed studies should establish a previously unexplored class of strained intermediates as a versatile building block for multistep synthesis.

6.2 Introduction

Strained cyclic intermediates that bear a functional group geometrically distorted from a preferred linear geometry have been of great interest to the synthetic community for the last several decades (e.g., Figure 6.1A, **6.1**–**6.4**).[1] Strained cyclic alkynes and cyclic allenes have seen usage in myriad settings, including the synthesis of bioactive molecules[2] and natural products,[3,4] materials chemistry,[5] and more. Moreover, their heterocyclic variants have also been disclosed and used widely. Interestingly, although hundreds of reports exist for the study and usage of strained

cyclic alkynes and allenes, their relatives, the cyclic cumulated trienes (e.g., **6.5** and **6.6**, Figure 6.1B) are relatively underexplored. Only recently, our lab and others have disclosed studies of carbocyclic trienes **6.5**[6] and **6.6**[7] which have been shown to be highly reactive trapping partners in cycloadditions.

In contrast to their alkyne and allene counterparts, the investigation of strained heterocyclic cumulated trienes (i.e., **6.7**, **6.8**, and **6.9**, Figure 6.1B) remains an unexplored frontier in strained intermediate chemistry. The development of chemistry to generate and trap such intermediates could provide a new entryway into accessing a variety of functionalized azacycles, which are important motifs in drugs and natural products.[8] Additionally, the presence of a heteroatom adjacent to the cumulated triene introduces asymmetry to the geometry and internal angles of the functional group, which could be leveraged to achieve regioselective reactions based on analogy to results seen for related strained intermediates.[9] Thus, we have been particularly interested in uncovering the potential intermediates such as **6.7**–**6.9**. We were especially interested in the study of **6.9**, as the pyridone is considered a privileged motif in several medicines and natural products.[10]

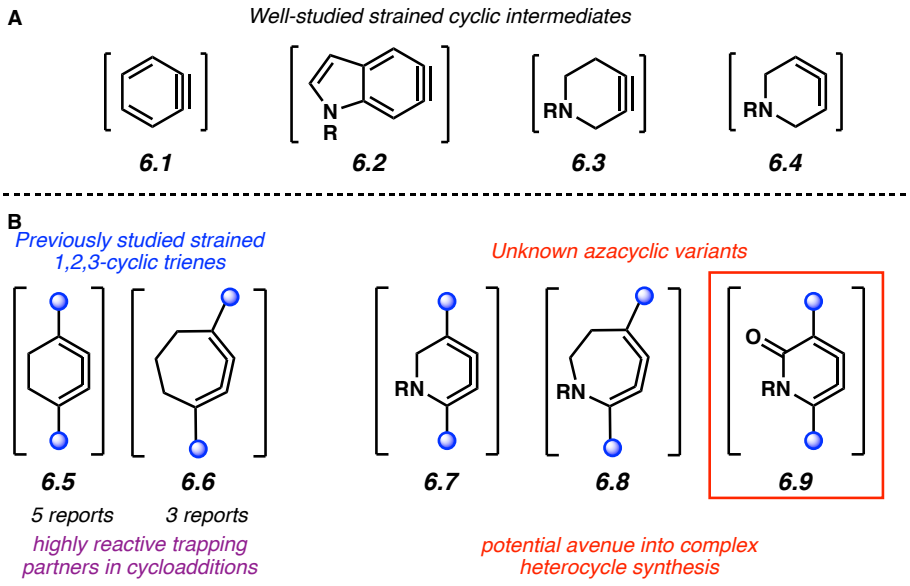


Figure 6.1. Overview of strained intermediates. A) Examples of strained cyclic alkynes and allenes that have been explored. B) Previously studied cyclic 1,2,3-trienes. C) Unexplored azacyclic trienes of interest.

6.3 Synthesis of Azacyclic Triene Precursor

In order to gain access to azacyclic trienes **6.9**, we devised a route to the Kobayashi-type silyl nonaflate precursor **6.14** (Figure 6.2). We assumed **6.14** could be used to generate the unsubstituted variant of **6.9** *in situ* using a fluoride-mediated elimination, as has been used to accomplish the trapping of a variety of other strained intermediates.[1a] Beginning from commercially available pyridine **6.10**, deprotonation and silylation can be used to form **6.11**[11] on decagram scale. Subsequently, **6.11** can undergo lithium-halogen exchange, borylation, and oxidation[12] in the same pot on multigram scale to provide pyridyl alcohol **6.12**. Nonaflation[13] gives the pyridyl silyl nonaflate **6.13** in 69% yield. Finally, treatment of **6.13** with trimethylsilyl iodide formed in situ,[14] followed by methylation,[15] provides the desired azacyclic triene precursor **6.14** in 46% yield over two steps. Notably, we envision this route could also be adaptable to other substituted azacyclic triene precursors.

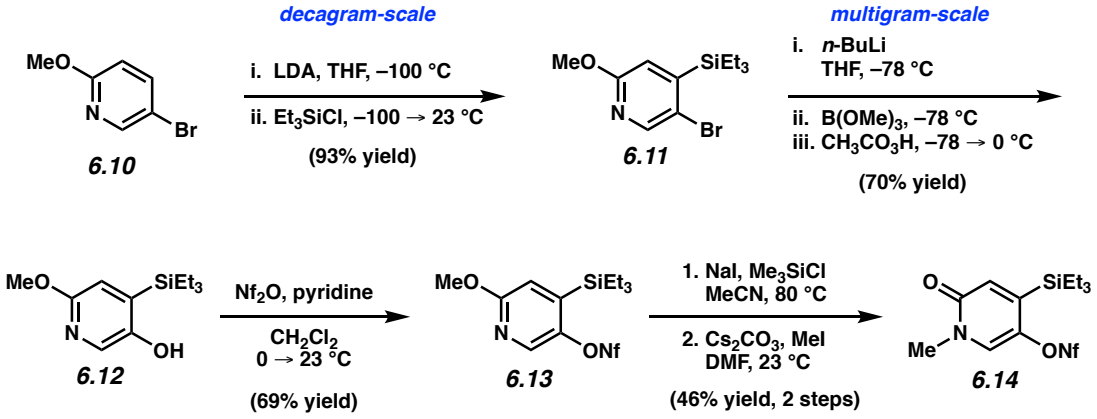


Figure 6.2. Route to azacyclic triene precursor **6.14**.

6.4 Key Validation of Azacyclic Triene

Following the synthesis of azacyclic triene precursor **6.14**, current efforts are focused on evaluating the reactivity of the in situ-generated triene in cycloaddition reactions. Prior optimization revealed that the silyl nonaflate reacted most efficiently under conditions using KF and 18-crown-6 in THF at 60 °C. Under these conditions, it is assumed that the fluoride present in solution effects a 1,2-elimination of the silyl triflate, thus generating the azacyclic triene. Experiments until this point have focused on understanding the reactivity of the azacyclic triene with symmetric (4+2) trapping partners such as those shown in Figure 6.3. Two key scope examples are shown here, where the azacyclic triene can be generated and trapped with either **6.16** or **6.17** to provide adducts **6.15** or **6.18**, respectively, in synthetically useful yields. Current studies are aimed at further evaluating the scope, especially with respect to unsymmetric (4+2) cycloaddition trapping partners, in (3+2) and (2+2) cycloadditions, and nucleophilic trapping reactions.

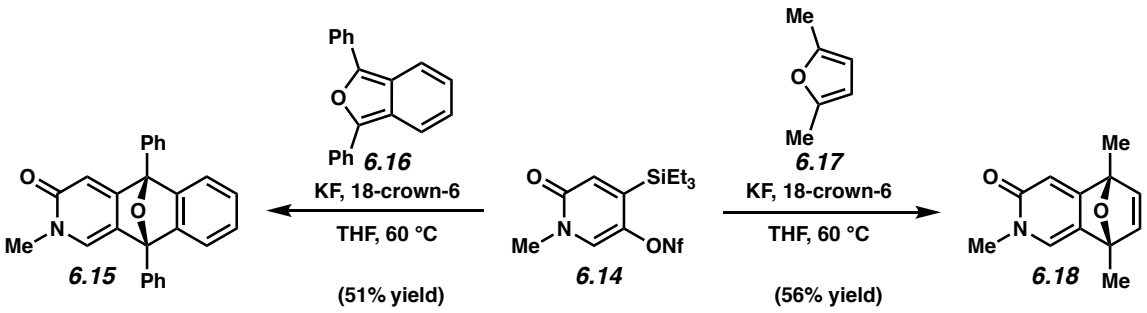


Figure 6.3. (4+2) Cycloadditions using azacyclic triene precursor **6.14**.

6.5 Future Directions

Plans for future studies are shown in Figure 6.4. As mentioned, efforts will be made to understand how the azacyclic triene behaves in other modes of reactivity, including in (4+2), (3+2), and (2+2) cycloadditions (Figure 6.4A). Alternatively, the study of symmetrically substituted

azacyclic triene precursors, such as **6.23**, should demonstrate whether more sterically hindered azacyclic trienes can be generated and trapped from the corresponding precursors. Additionally, the reactivities of ring-fused azacyclic trienes such as **6.24** and **6.25** are of interest. These scope studies are expected to provide a better understanding of how these strained intermediates react and to allow for the synthesis of a diverse set of heterocyclic products.

In addition to the scope of reactivity for these azacyclic trienes, their ability to participate in regioselective reactions, specifically in nucleophilic addition reactions will also be assessed using experiments in tandem with computational predictions. In the ground state, it has been found that the unsubstituted azacyclic triene structure **6.22** contains a triene with significant geometric distortion seen by the differing angles at either end of the central bond of the triene (Figure 6.4B). Specifically, when evaluated computationally, the internal angles of the **6.22** are widened between C1=C2=C3 at an angle of 139°, whereas between C2=C3=C4 proximal to the nitrogen, the angle is relatively contracted at 115°. Importantly, in related strained systems,[9] including the mono-substituted carbocyclic 1,2,3-hexatriene,[6e] it has been found that the site with the larger internal angle is preferred for nucleophilic addition. This has been related to minimized geometric reorganization that occurs at the transition state of the nucleophilic addition reaction, where the internal angle between the C=C=C bond distorted most toward linearity (180°) is closer in structure to the transition state structure. Therefore, in the parent azacyclic triene **6.22**, it is predicted that the carbon in red may preferentially undergo attack by nucleophiles. However, we are also interested in evaluating the effects of substituents on these regioselective nucleophilic additions, as in other related systems, sterically bulky substituents have shown to also influence reactivity.[9] For example, with addition of a phenyl group adjacent to the carbon highlighted in red (i.e., **6.26**), the ground state structure of the azacyclic triene is still predicted to have a wider internal angle at

that position. However, the phenyl group is sterically bulky, which could greatly influence how the reactants in the nucleophilic addition are able to come together in the transition state and could disfavor addition at the carbon in red. Understanding the effects of geometric distortion and substitution on regioselectivity trends will be very helpful for the adoption of these strained intermediates in complex molecule synthesis.

We are also interested in investigating the use of azacyclic trienes **6.9** for multistep synthesis. One avenue that could demonstrate their potential utility toward this application would be in examining their ability to undergo intramolecular trappings. A proposed scheme is shown in Figure 6.4C, where pyridone **6.27**, which has been accessed, could be elaborated to **6.28**. Azacyclic triene precursor **6.28** could then be used under the fluoride-mediated conditions to effect an intramolecular trapping reaction, which would give rise to the polyheterocyclic product **6.29**. Demonstration of successful azacyclic triene reactivity in this setting could allow for an understanding of whether these strained intermediates could be useful in future synthetic applications, such as in an intramolecular trapping toward a complex natural product. It could also reveal what factors are important (e.g., tether length, necessary orbital overlap, etc.) for intramolecular trappings to be accomplished.

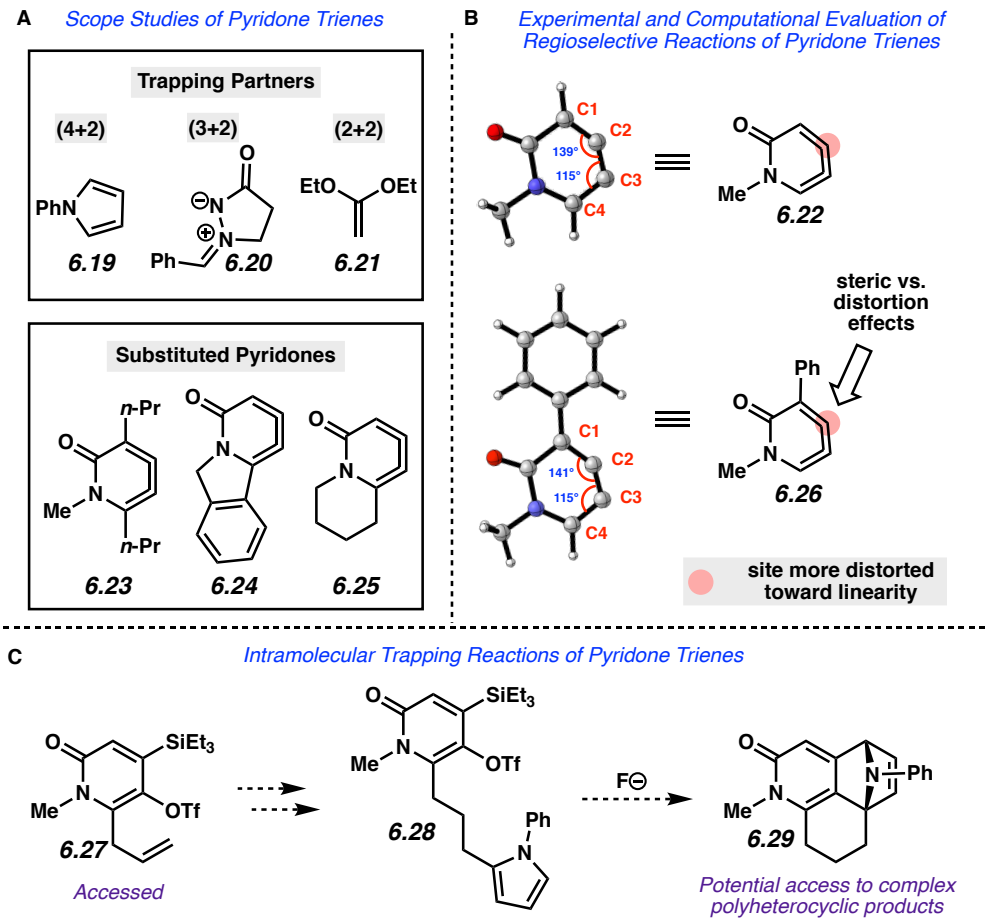


Figure 6.4. Outline for future studies including: A) Scope studies with respect to trapping partners and substituted azacyclic trienes, B) Computational predictions on potential regioselective nucleophilic addition reactions of azacyclic trienes **6.22** and **6.26**,[16] and C) Complex molecule synthesis through intramolecular trappings.

6.6 Conclusion

We have detailed the first generation and trapping of azacyclic 1,2,3-trienes. Our study includes a scalable route to the azacyclic triene precursor, the silyl nonaflate, as well as the established proof-of-concept studies that demonstrate generating and trapping of the desired azacyclic 1,2,3-trienes in (4+2) cycloadditions. Current efforts are underway to investigate the scope of reactivity with respect to unsymmetric traps in cycloaddition and nucleophilic addition reactions. Computational studies suggest that the azacyclic triene contains structural similarities to other substituted or heterocyclic strained alkynes that been shown to undergo highly

regioselective reactions. Understanding the factors that control regioselectivity for the azacyclic trienes is of great interest for their use in synthetic planning. Additionally, the reactivity of substituted and ring-fused pyridone azacyclic trienes presents an opportunity for future study. Finally, future efforts will examine the use of these intermediates in intramolecular trappings to demonstrate their potential utility and impact in complex heterocycle synthesis.

6.7 Experimental Section

6.7.1 Materials and Methods

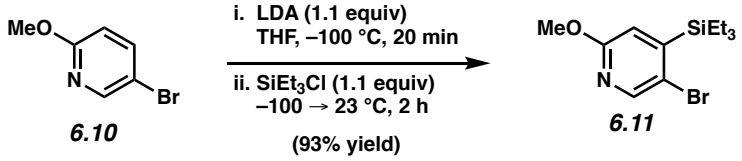
Unless stated otherwise, reactions were conducted in flame-dried glassware under an atmosphere of nitrogen, and commercially obtained reagents were used as received unless otherwise specified. Anhydrous solvents were either freshly distilled or passed through activated alumina columns, unless otherwise stated. Prior to use in trapping experiments tetrahydrofuran (THF) was passed through an activated alumina column and degassed by five freeze-pump-thaw cycles. Dimethylformamide (DMF), acetonitrile (MeCN), and CH_2Cl_2 were passed through an activated alumina column prior to use. Diisopropylamine, pyridine, trimethylsilyl chloride, and triethylsilyl chloride were distilled over CaH_2 prior to use. Potassium fluoride (stored in a glovebox), *n*-butyllithium (*n*-BuLi), nonafluorobutanesulfonic anhydride (Nf_2O), peracetic acid (39 wt. % in acetic acid), 2,5-dimethylfuran (**6.17**) and Florisil (<200 mesh, fine powder) were all purchased from Sigma-Aldrich and used as received. Cesium carbonate was obtained from Strem Chemicals and used as received. Methyl iodide and trimethyl borate were obtained from Thermofisher Scientific and used as received. 5-Bromo-2-methoxy pyridine (**6.10**) and diphenylisobenzofuran (**6.16**) were purchased from Combi Blocks and **6.16** was purified on silica prior to use (hexanes). 18-Crown-6 was purchased from Chem Impex International, azeotroped with benzene, and stored in a glovebox prior to use. Sodium iodide was purchased from Oakwood chemicals and used as received. Reaction temperatures at or above 23 °C were controlled using an IKAmag temperature modulator, and unless stated otherwise, performed at room temperature (approximately 23 °C). Thin-layer chromatography (TLC) was conducted with EMD gel 60 F254 pre-coated plates (0.25 mm) and visualized using a combination of UV, anisaldehyde, potassium permanganate, and Dragendorff's reagent staining techniques. Silicycle Siliaflash P60 (particle size 40–63 μm) was

used for flash column chromatography unless otherwise specified. ^{1}H-NMR spectra were recorded on Bruker spectrometers (at 500 and 600 MHz) and are reported relative to the residual solvent signal. Data for ^{1}H-NMR spectra are reported as follows: chemical shift (δ ppm), multiplicity, coupling constant (Hz), and integration. ^{13}C-NMR spectra were recorded on Bruker spectrometers (at 125 and 150 MHz) and are reported relative to the residual solvent signal. Data for ^{13}C-NMR spectra are reported in terms of chemical shift (δ ppm) and, when necessary, multiplicity, and coupling constant (Hz). ^{19}F-NMR spectra were recorded on Bruker spectrometers (at 565 MHz) and are reported in terms of chemical shift (δ ppm), multiplicity, and integration. IR spectra were recorded on a Perkin-Elmer UATR Two FT-IR spectrometer and are reported in terms of frequency absorption (cm^{-1}). DART-MS spectra were collected on a Thermo Exactive Plus MSD (Thermo Scientific) equipped with an ID-CUBE ion source and a Vapur Interface (IonSense Inc.). Both the source and MSD were controlled by Excalibur software version 3.0. The analyte was spotted onto OpenSpot sampling cards (IonSense Inc.) using $CDCl_3$ or CH_2Cl_2 as the solvent. Ionization was accomplished using UHP He plasma with no additional ionization agents. The mass calibration was carried out using Pierce LTQ Velos ESI (+) and (–) Ion calibration solutions (Thermo Fisher Scientific). ESI-TOF measurements were carried out in positive ionization mode on a Waters LCT-Premier XE Time of Flight Instrument controlled by MassLynx 4.1 software (Waters Corporation, Milford MA). The instrument was equipped with the Multi Mode Ionization source operated in the electrospray mode. A solution of Leucine Enkephalin (Sigma Chemical, L9133) was used in the Lock-Spray to obtain accurate mass measurements. Samples were infused using direct loop injection on a Waters Acquity UPLC system. GC-MS measurements were carried out using an Agilent Model 7693 Autosampler, 7890B Gas Chromatograph, and 7250 Q-TOF Mass Selective Detector in the Electron Ionization mode. Sample injection was carried out in split mode with inlet

temperature set to 280 °C. Separation was carried out on an Agilent HP5-MS column with dimensions 30m x 250 μm x 0.25 μm. Ultra High Purity Grade He (Airgas) was used as carrier gas with the flow set to 1.1 mL/min in constant flow mode. The initial oven temperature was set to 70 °C for 1 min followed by a 20 °C/min ramp to a final temperature of 300 °C which was maintained for 4 min. A 3.0 min solvent delay was used. EI energy was set to 70 eV. The MSD was set to scan the 50–500 m/z range. Data collection and analysis were performed using Mass Hunter Acquisition and Qualitative Analysis software (Agilent). Silyl bromide **6.11**[11] is a known compound. The ^{1}H NMR spectral data matched those reported in literature.

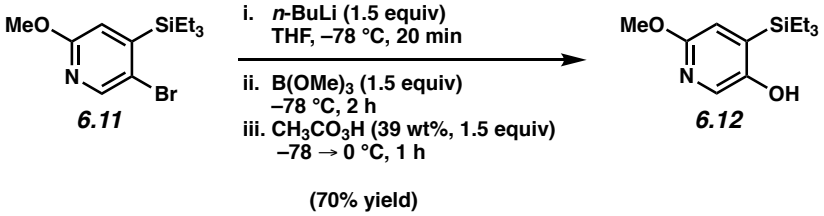
6.7.2 Experimental Procedures

6.7.2.1 Synthesis of azacyclic triene precursor 6.14.



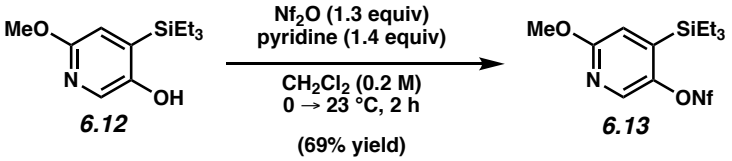
Silyl Bromide 6.11. To a solution of diisopropylamine (6.3 g, 8.8 mL, 62.4 mmol, 1.15 equiv) in THF (130 mL) at –100 °C under nitrogen atmosphere was added *n*-BuLi (2.3 M in hexanes, 25.9 mL, 59.7 mmol, 1.10 equiv) dropwise over 5 min. The cooling bath was removed and the resulting solution was stirred for 30 min. The mixture was again cooled to –100 °C and stirring was continued for 10 min. A solution of pyridine **6.10** (10.2 g, 54.2 mmol, 1.0 equiv) in THF (51 mL) was added slowly dropwise via cannula over 30 min. The mixture was allowed to stir at 100 °C for 20 minutes at and then triethylsilyl chloride (9.0 g, 10.0 mL, 59.7 mmol, 1.10 equiv) was added dropwise over 5 min at 100 °C. The cooling bath was removed and stirring was continued for 2 h while the reaction warmed to 23 °C. After this time, the mixture was quenched with deionized water (20 mL), diluted with deionized water (50 mL) and Et_2O (50 mL), and the layers were separated. The aqueous layer was extracted Et_2O (2 x 50 mL). The combined organic layers were

combined, washed with brine (50 mL), dried over sodium sulfate, filtered, and concentrated under reduced pressure to give a dark orange oil. The crude residue was purified by flash chromatography (100% hexanes → 55% Et_2O in hexanes) to provide silyl bromide **6.11** (15.2 g, 54.2 mmol, 93% yield) as a light-yellow oil. **Silyl Bromide 6.11**: R_f 0.65 (1:1 hexanes:benzene); ^1H NMR (500 MHz, $CDCl_3$): δ 8.18 (s, 1H), 6.77 (s, 1H), 3.90 (s, 3H), 0.97–0.91 (m, 15H). Spectral data match those previously reported.[11]



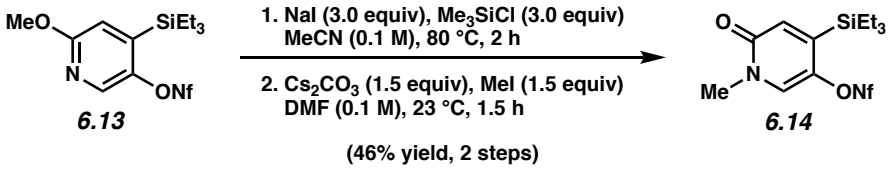
Silyl alcohol 6.12. To a solution of silyl bromide **6.11** (2.9 g, 9.6 mmol, 1.0 equiv) in THF (96 mL, 0.10 M) at –78 °C was added *n*-BuLi (2.3 M in hexanes, 6.3 mL, 14 mmol, 1.5 equiv) dropwise over 5 min. The resulting solution was stirred at this temperature for 20 min, then trimethyl borate (1.5 g, 1.6 mL, 14 mmol, 1.5 equiv) was added dropwise over 5 min. Stirring was continued at this temperature for 2 h then peracetic acid (2.8 g of a 39 wt% solution in glacial acetic acid, 2.5 mL, 14 mmol, 1.5 equiv) was added dropwise over 2 min. The reaction was then allowed to warm to 0 °C and stirred was continued for 1 h. At this time, the mixture was quenched at 0 °C with saturated aqueous sodium hydrogensulfite (30 mL), which was added dropwise over 1 minute, and the resulting mixture was allowed to warm to 23 °C and stirred for 10 min. The mixture was then diluted further with deionized water (50 mL) and CH_2Cl_2 (50 mL) and the layers were separated. The aqueous layer was extracted CH_2Cl_2 (2 x 50 mL). The organic layers were combined, dried over sodium sulfate, filtered, and concentrated under reduced pressure. The crude residue was purified by flash chromatography (100% hexanes → 100% Et_2O) to provide silyl alcohol **6.12** (1.6 g, 9.6 mmol, 70% yield) as a beige solid. **Silyl alcohol 6.12:** Mp: 76–77 °C; R_f 0.37 (3:1

hexanes:EtOAc); ^{1}H NMR (600 MHz, C_6D_6): δ 7.29 (s, 1 H), 6.94 (s, 1 H), 4.29 (s, 1H), 3.86 (s, 3H), 0.98–0.93 (m, 9 H), 0.87–0.80 (m, 6 H); ^{13}C NMR (150 MHz, C_6D_6): δ 159.1, 152.1, 137.6, 131.4, 117.7, 53.3, 7.6, 3.3; IR (film): 3111, 2954, 1377, 1210, 724 cm^{-1}; HRMS-APCI (*m/z*) [M + H]$^+$ calcd for $C_{12}H_{22}NO_2Si^+$, 240.1414; found 240.1414.



Pyridyl silyl nonaflate 6.13. To a solution of silyl alcohol **6.12** (1.0 g, 4.2 mmol, 1.0 equiv) in CH_2Cl_2 (21 mL, 0.20 M) were added sequentially pyridine (460 mg, 0.47 mL, 5.9 mmol, 1.4 equiv) and Nf_2O (3.2 g, 1.7 mL, 5.4 mmol, 1.3 equiv) at 0 °C. After stirring at this temperature for 1 h, the reaction was warmed to 23 °C and stirred for an additional 1 h. After this time, the reaction was quenched with deionized water (15 mL) and diluted with CH_2Cl_2 (20 mL). The layers were then poured into a separatory funnel containing a mixture of saturated sodium bicarbonate (40 mL) and deionized water (20 mL). The organic and aqueous layers were separated and the aqueous layer was extracted CH_2Cl_2 (2 x 20 mL). The combined organic layers were dried over sodium sulfate, filtered, and concentrated under reduced pressure. The crude residue was purified by flash chromatography (100% hexanes → 25% CH_2Cl_2 in hexanes) to provide pyridyl silyl nonaflate **6.13** (1.5 g, 4.2 mmol, 69% yield) as a yellow oil. **Pyridyl silyl nonaflate 6.13**: R_f 0.78 (3:1 hexanes:EtOAc); ^{1}H NMR (600 MHz, $CDCl_3$): δ 8.13 (s, 1 H), 6.82 (s, 1 H), 3.94 (s, 3H), 0.98–0.93 (m, 9 H), 0.93–0.86 (m, 6 H); ^{13}C NMR (125 MHz, $CDCl_3$): δ 162.2, 147.1, 143.8, 138.0 (t, J = 3.6), 120.8–105.5 (m), 118.4, 54.0, 7.1, 2.8; ^{19}F NMR (565 MHz, $CDCl_3$): δ –80.6 (t, J = 9.8, 3 F), –109.4 (t, J = 9.8, 2 F), –120.7–(–121.1) (m, 2F), –125.7–(–125.9) (m, 2F); IR (film): 2960,

1348, 1238, 1143, 1032 cm^{-1}; HRMS-ESI (*m/z*) $[M + H]^+$ calcd for $C_{16}H_{21}F_9NO_4SSi^+$, 522.0817; found 522.0833.

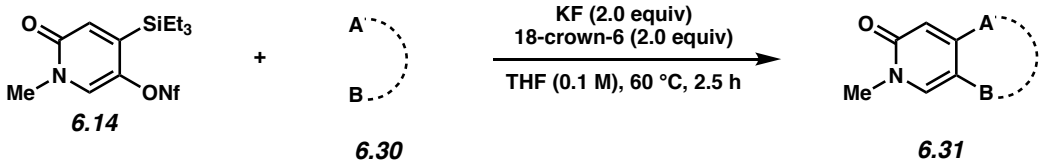


Triene precursor 6.14. To a solution of pyridyl silyl nonaflate **6.13** (1.9 g, 3.6 mmol, 1.0 equiv) in MeCN (36 mL, 0.10 M) were added sequentially NaI (1.6 g, 11 mmol, 3.0 equiv) in a single portion and trimethylsilyl chloride (1.2 g, 1.4 mL, 11 mmol, 3.0 equiv) at 23 °C. The reaction flask was then fitted with an air condenser and heated to 80 °C in an oil bath. After stirring at this temperature for 2 h, the reaction was cooled to 23 °C and poured into a separatory funnel containing a 5% wt solution of aqueous disodium thiosulfate (50 mL). The mixture was then diluted with EtOAc (50 mL), and the layers were separated. The aqueous layer was extracted with EtOAc (3 x 50 mL). The organic layers were combined, dried over sodium sulfate, filtered, and concentrated under reduced pressure to provide a light-yellow solid (1.8 g) which was dissolved in DMF (36 mL, 0.1 M). To this solution were added sequentially Cs_2CO_3 (1.8 g, 5.4 mmol, 1.5 equiv) and MeI (770 mg, 340 mL, 5.4 mmol, 1.5 equiv) at 23 °C. The mixture was stirred at this temperature for 1.5 h. The reaction was the quenched with deionized water (20 mL). The biphasic mixture was then poured into a separatory funnel containing deionized water (500 mL) and EtOAc (200 mL) and the layers were separated. The aqueous layer was extracted with EtOAc (3 x 100 mL). The organic layers were combined, washed with deionized water (3 x 100 mL), dried over sodium sulfate, filtered, and concentrated under reduced pressure. The crude residue was purified by flash chromatography (100% hexanes → 75% EtOAc in hexanes) to provide triene precursor **6.14** (0.93 g, 3.6 mmol, 46% yield, two steps) as an amber oil. **Triene precursor 6.14**: R_f 0.58 (1:1 hexanes:EtOAc); ^1H NMR (600 MHz, $CDCl_3$): δ 7.34 (s, 1 H), 6.67 (s, 1 H), 3.54 (s, 3H),

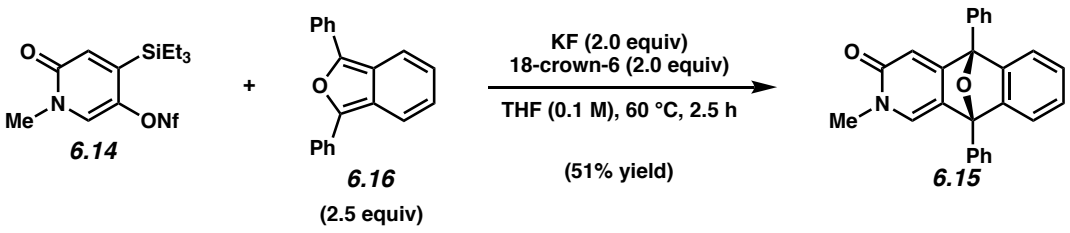
0.97–0.92 (m, 9 H), 0.88–0.82 (m, 6 H); ^{13}C NMR (150 MHz, C_6D_6): δ 160.5, 147.0, 137.1, 129.6, 129.1, 120.3–106.3 (m), 38.2, 7.2, 2.8; ^{19}F NMR (565 MHz, $CDCl_3$): δ –80.6 (t, *J* = 9.7, 3 F), –109.6 (t, *J* = 13.6, 2 F), –120.7–(–120.9) (m, 2 F), –125.5–(–125.8) (m, 2 F); IR (film): 2958, 1666, 1600, 1421, 1199 cm^{-1}; HRMS-ESI (*m/z*) [M + H]$^+$ calcd for $C_{16}H_{21}F_9NO_4SSi^+$, 522.0817; found 522.0840.

6.7.2.2 Azacyclic 1,2,3-triene trapping experiments.

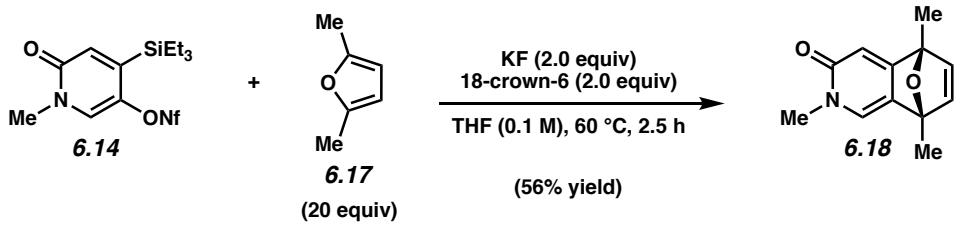
General procedure 6.1 for the scope of trapping reactions using azacyclic triene precursor 6.14:



A flame-dried 1-dram vial containing a magnetic stir bar was charged sequentially with silyl triflate **6.14** (55.2 mg, 0.11 mmol, 1.0 equiv), trapping partner **6.30** (2.5–20 equiv), THF (1.06 mL, 0.1 M), KF (12.3 mg, 0.21 mmol, 2.0 equiv), and 18-crown-6 (56.0 mg, 0.21 mmol, 2.0 equiv) in a glovebox. The vial was then sealed with a Teflon-lined cap, removed from the glovebox, sealed further with electrical tape, and stirred for 2.5 h at 60 °C. The reaction vessel was allowed to cool to 23 °C. The mixture was then filtered over a pad of Celite, eluting with acetone (15 mL). The eluate was concentrated under reduced pressure then purified by chromatography to provide adducts **6.31**.



Cycloadduct 6.15. Followed general procedure 6.1. Purification by flash chromatography on Florisil (benzene to elute excess trapping partner, then 25% EtOAc in hexanes → 50% EtOAc in hexanes) afforded cycloadduct **6.15** (51% yield, average of two experiments) as a beige solid. **Cycloadduct 6.15**: Mp: **6.15** turned brown and appeared to decompose at 118 °C; R_f 0.17 (1:1 hexanes:EtOAc); ^{1}H NMR (500 MHz, $CDCl_3$): δ 7.87–7.80 (m, 4H), 7.63–7.54 (m, 4H), 7.54–7.47 (m, 2H), 7.43–7.38 (m, 1H), 7.36–7.32 (m, 1H), 7.21–7.14 (m, 2H), 7.13 (d, J = 0.4, 1H), 6.59 (s, 1H), 3.39 (s, 3H); ^{13}C NMR (125 MHz, $CDCl_3$): δ 162.4, 160.7, 148.8, 146.8, 134.2, 133.4, 129.2, 129.03, 128.96, 128.89, 127.4, 127.01, 126.96, 126.7, 126.3, 121.3, 119.9, 112.2, 89.8, 88.7, 37.8 (21 of 22 signals observed); IR (film): 3065, 2918, 1679, 1618, 990 cm^{-1}; HRMS-ESI (m/z) [M + H]+ calcd for $C_{26}H_{20}NO_2^+$, 378.1494; found 378.1511.



Cycloadduct 6.18. Followed general procedure 6.1. Purification by flash chromatography on silica (10% acetone in hexanes → 80% acetone in hexanes) afforded cycloadduct **6.18** (56% yield, average of two experiments) as a yellow oil. **Cycloadduct 6.18**: R_f 0.22 (EtOAc); ^{1}H NMR (500 MHz, $CDCl_3$): δ 6.91 (s, 1H), 6.60 (d, J = 5.4, 1H), 6.51 (d, J = 5.4, 1H), 6.36 (s, 1H), 3.41 (s, 3H), 1.80 (s, 3H), 1.77 (s, 1H); ^{13}C NMR (125 MHz, $CDCl_3$): δ 163.1, 162.6, 145.2, 142.2, 128.0, 126.3, 110.7, 87.7, 86.7, 37.5, 15.3, 14.8; IR (film): 2933, 1680, 1607, 1424, 1140 cm^{-1} ; HRMS-APCI (m/z) [M + H]+ calcd for $C_{12}H_{14}NO_2^+$, 204.1019; found 204.1019.

6.8 Spectra Relevant to Chapter Six:

Generation and Trapping of an Azacyclic 1,2,3-Hexatriene

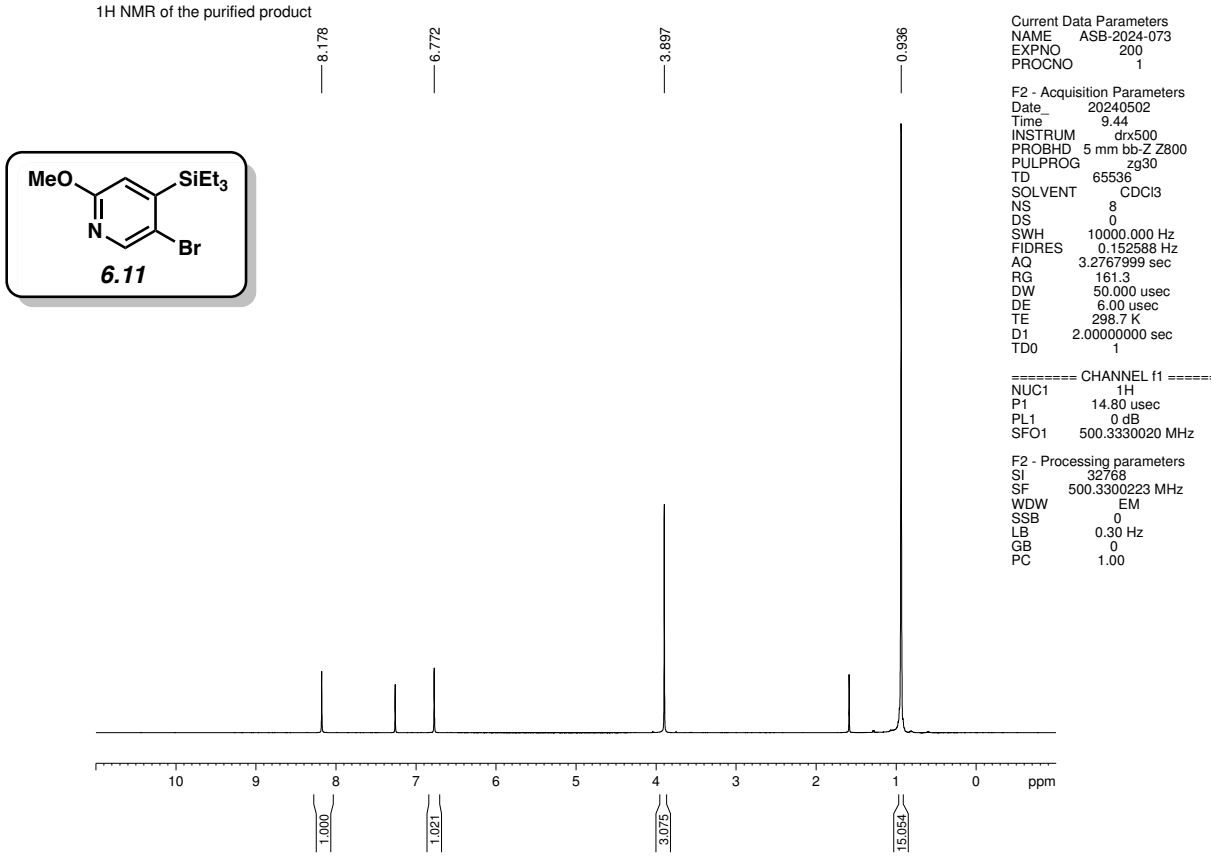


Figure 6.5. ^{1}H NMR (500 MHz, $CDCl_3$) of compound **6.11**.

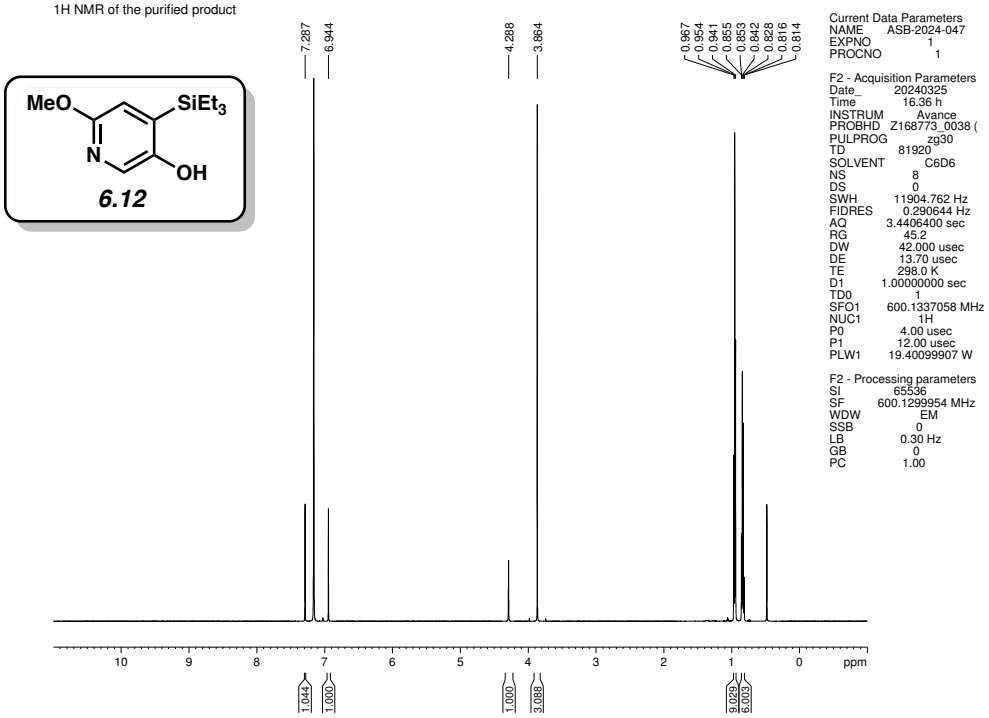


Figure 6.6. ^{1}H NMR (600 MHz, C_6D_6) of compound **6.12**.

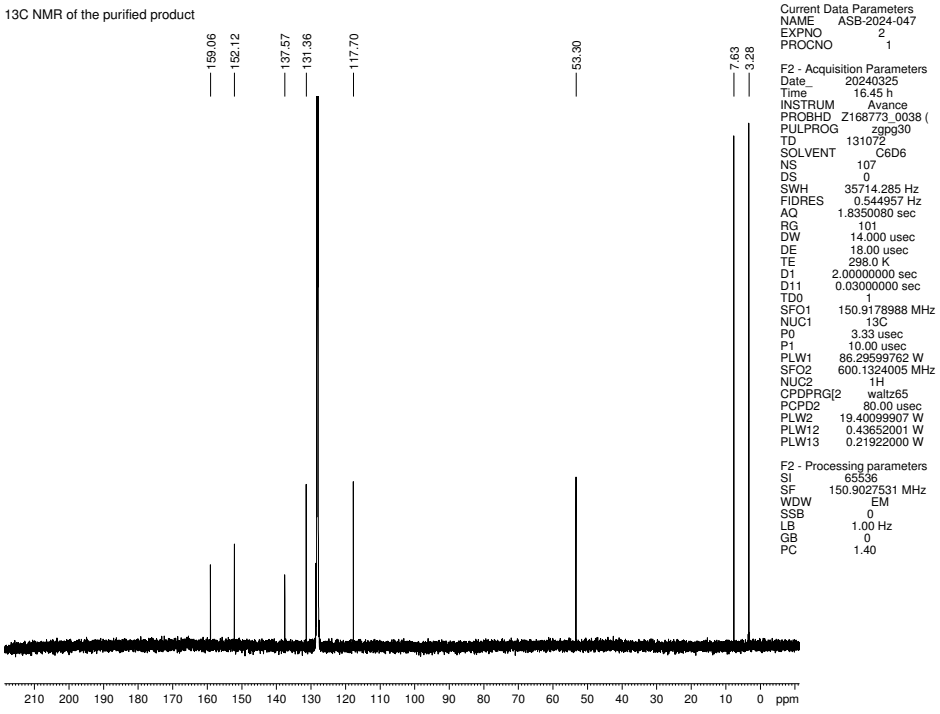


Figure 6.7. ^{13}C NMR (150 MHz, C_6D_6) of compound **6.12**.

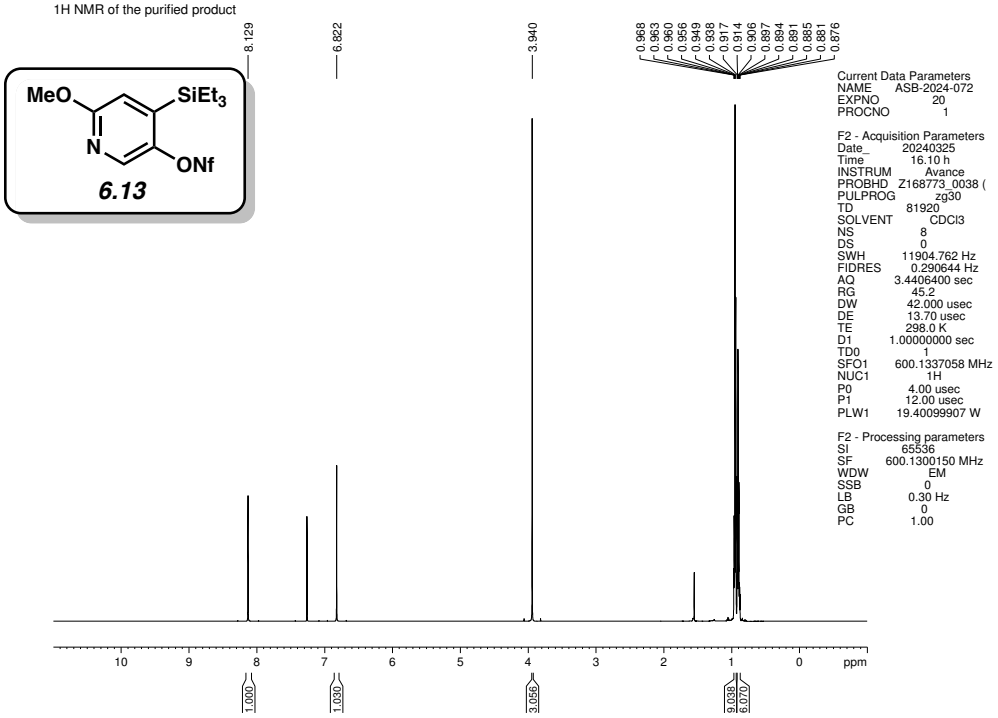


Figure 6.8. ^{1}H NMR (600 MHz, $CDCl_3$) of compound **6.13**.

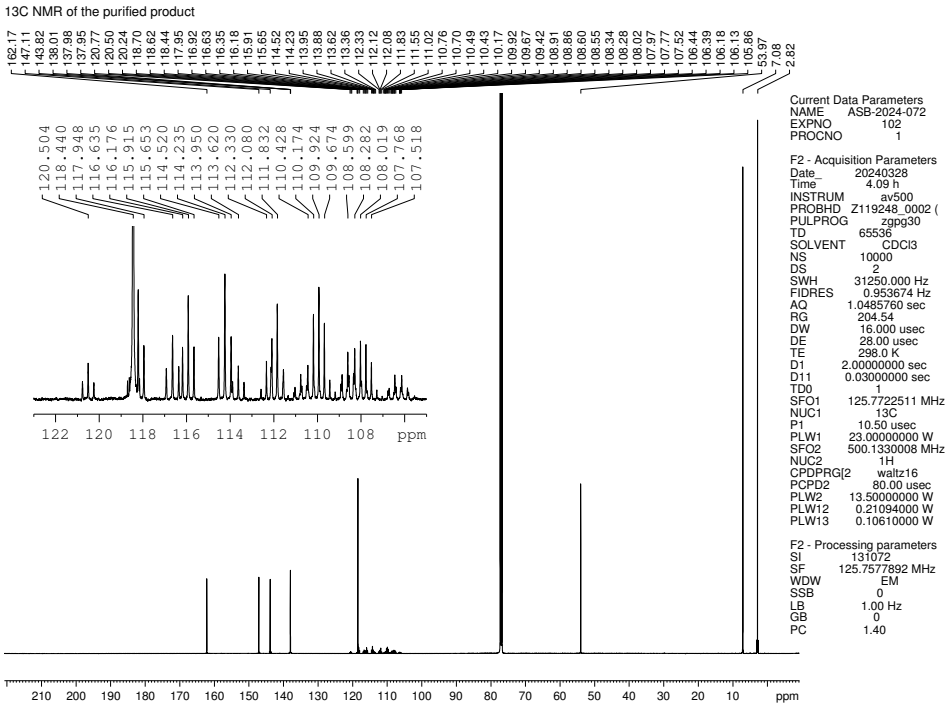


Figure 6.9. ^{13}C NMR (125 MHz, $CDCl_3$) of compound **6.13**.

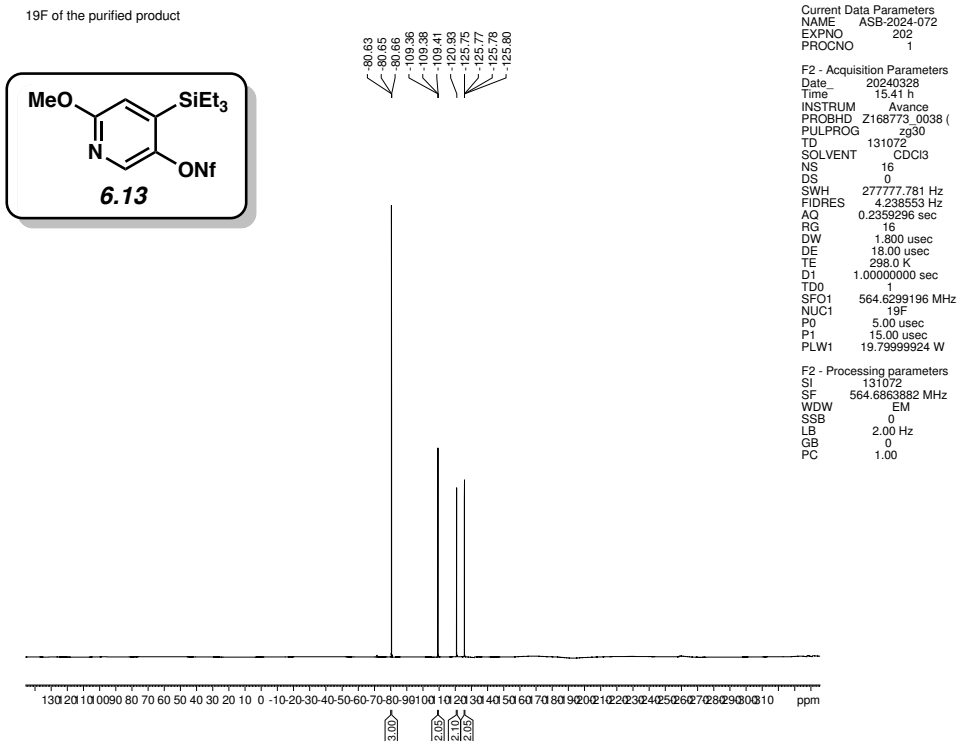


Figure 6.10. ^{19}F NMR (565 MHz, $CDCl_3$) of compound **6.13**.

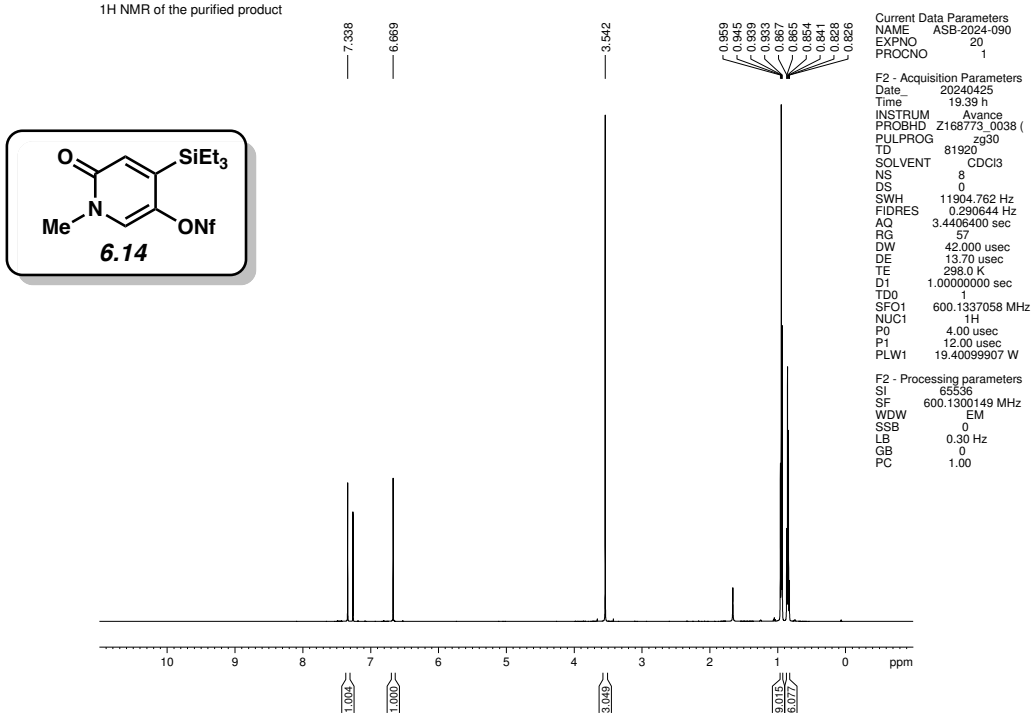


Figure 6.11. ^{1}H NMR (600 MHz, $CDCl_3$) of compound **6.14**.

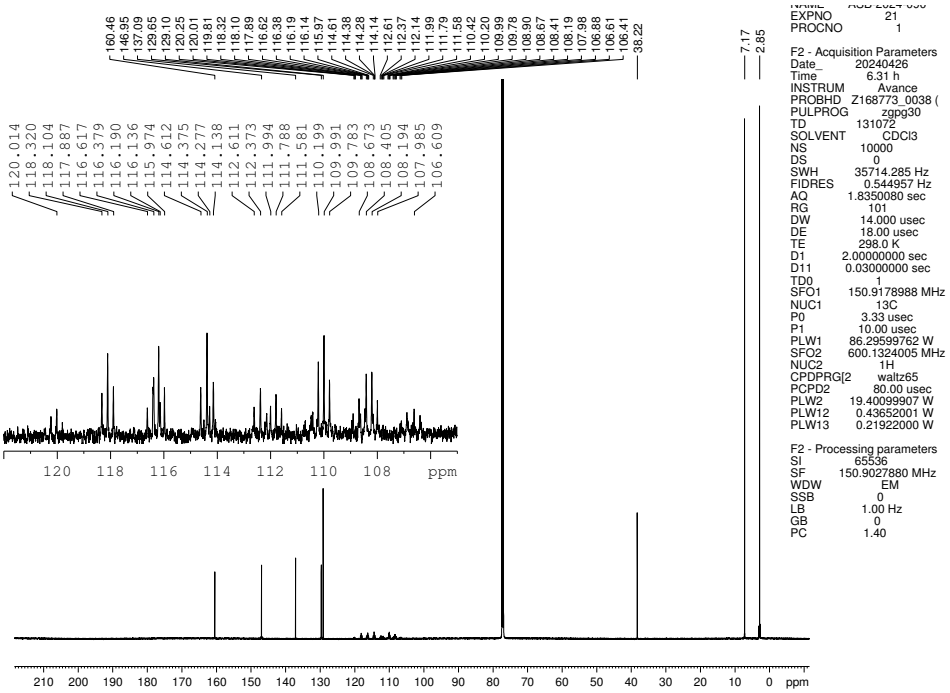


Figure 6.12. ^{13}C NMR (150 MHz, $CDCl_3$) of compound **6.14**.

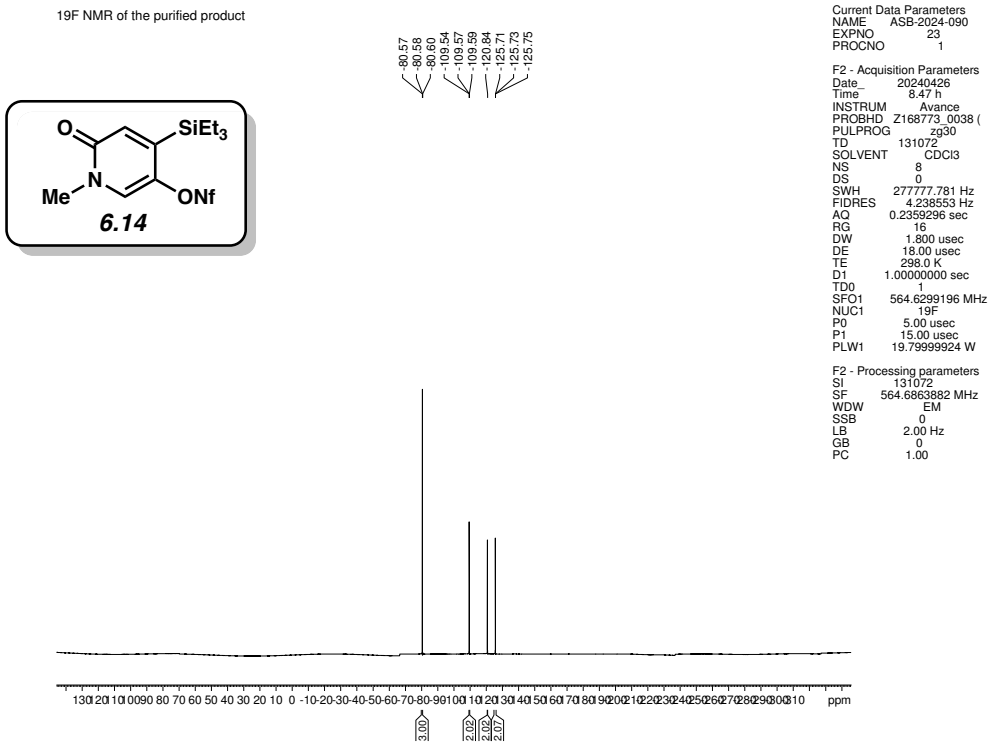


Figure 6.13. ^{19}F NMR (565 MHz, $CDCl_3$) of compound **6.14**.

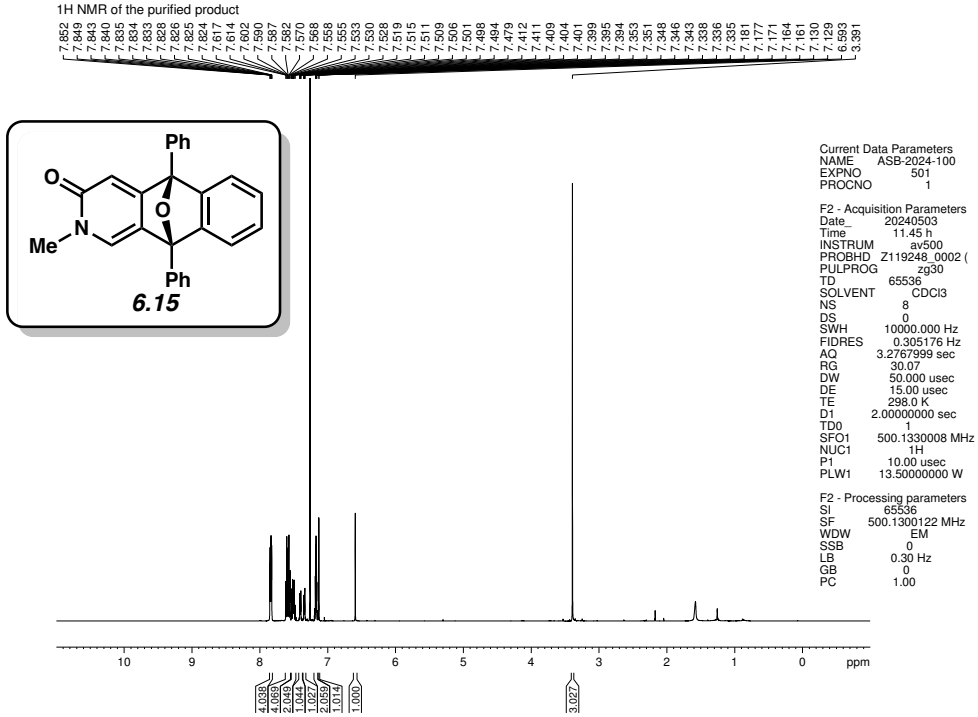


Figure 6.14. ^{1}H NMR (500 MHz, $CDCl_3$) of compound **6.15**.

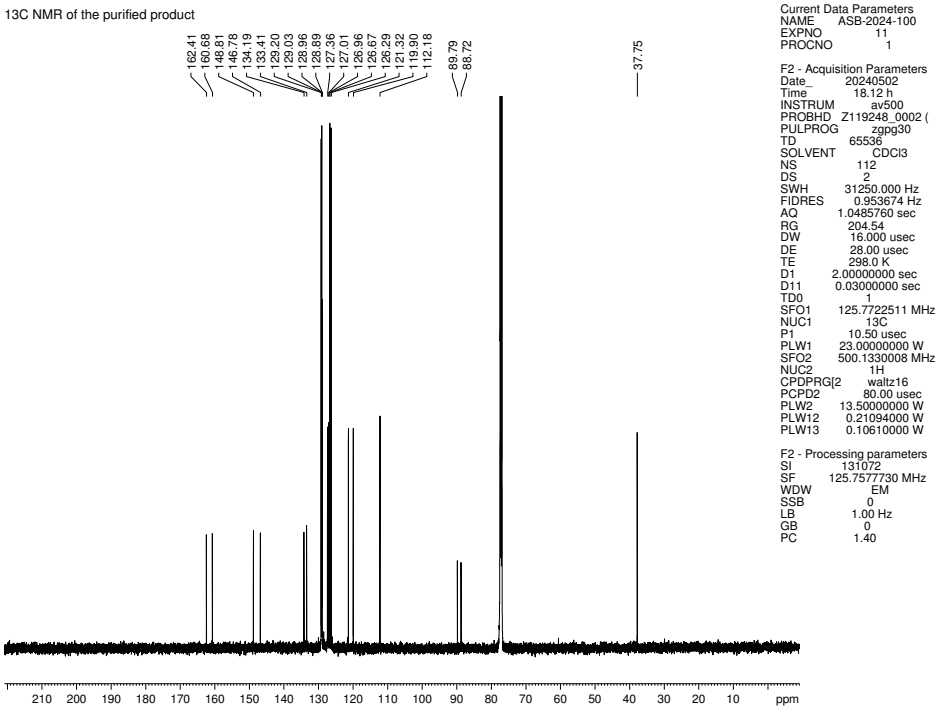


Figure 6.15. ^{13}C NMR (125 MHz, $CDCl_3$) of compound **6.15**.

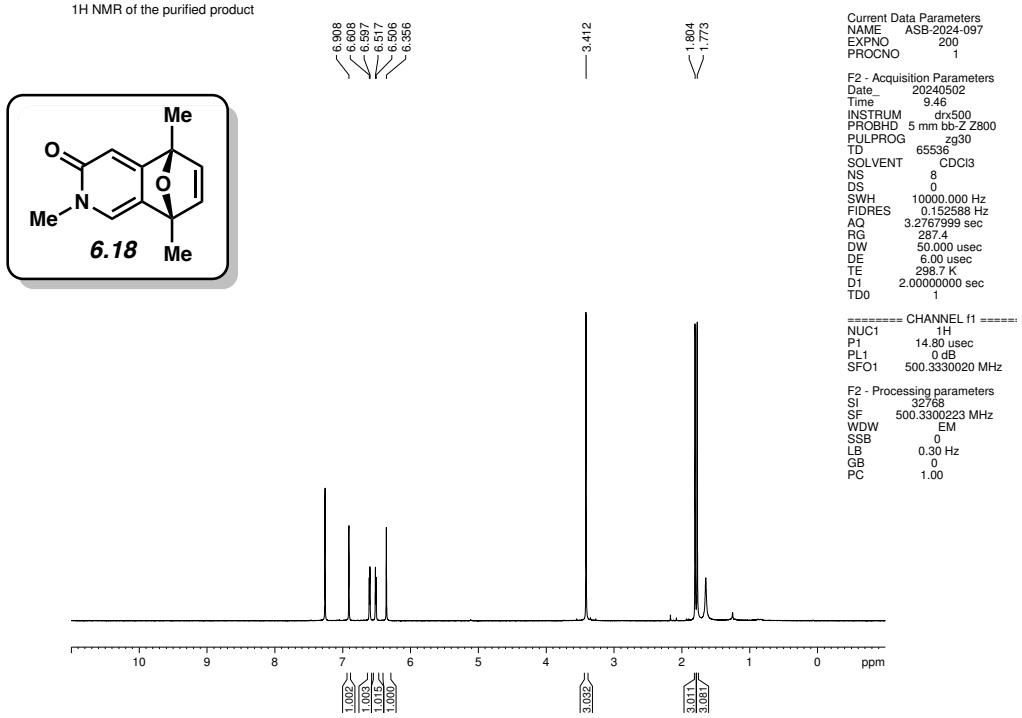


Figure 6.16. ^{1}H NMR (500 MHz, $CDCl_3$) of compound **6.18**.

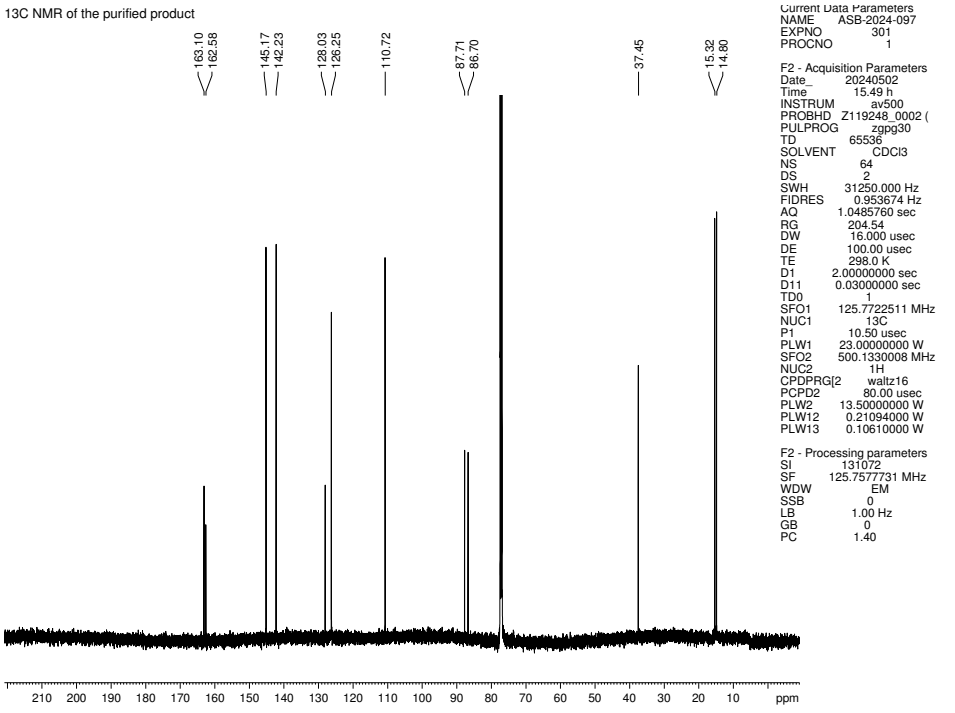


Figure 6.17. ^{13}C NMR (125 MHz, $CDCl_3$) of compound **6.18**.

6.9 Notes and References

(1) For select reviews on strained intermediates, see (a) Shi, S.; Li, L.; Li, Y. *o*-Silylaryl triflates: A journey of Kobayashi aryne precursors. *Chem. Rev.* **2021**, *121*, 3892–4044. (b) Spence, K. A.; Tena Meza, A.; Garg, N. K. Merging metals and strained intermediates. *Chem Catalysis* **2022**, *2*, 1870–1879. (c) Goetz, A. E.; Shah, T. K.; Garg, N. K. Pyridynes and indolynes as building blocks for functionalized heterocycles and natural products. *Chem. Commun.* **2015**, *51*, 34–45. (d) Anthony, S. M.; Wonilowicz, L. G.; McVeigh, M. S.; Garg, N. K. Leveraging fleeting strained intermediates to access complex scaffolds. *JACS Au* **2021**, *1*, 897–912.

(2) (a) Carroll, F. I.; Robinson, T. P.; Brieaddy, L. E.; Atkinson, R. N.; Mascarella, S. W.; Damaj, M. I.; Martin, B. R.; Navarro, H. A. Synthesis and nicotinic acetylcholine receptor binding properties of bridged and fused ring analogues of epibatidine. *J. Med. Chem.* **2007**, *50*, 6383−6391. (b) Kametani, T.; Kigasawa, K.; Hiragi, M.; Wagatsuma, N.; Uryu, T.; Araki, K. Syntheses of heterocyclic compounds. 509. syntheses of analgesics. 34. synthesis of 3-hydroxy-*N*-cyclopropylmethyl-9-azamorphinan. *J. Med. Chem.* **1973**, *16*, 301−303. (c) Heindel, N. D.; Fives, W. P.; Lemke, T. F.; Rowe, J. E.; Snady, H. W. Synthesis, transformation, and general pharmacologic activity in 1,4-benzodiazepine-3,5-diones. *J. Med. Chem.* **1971**, *14*, 1233−1235. (d) Bell, M. R.; Zalay, A. W.; Oesterlin, R.; Schane, P.; Potts, G. Basic ethers of 1-(p-hydroxyphenyl)-2-phenyl-1,2,3,4-tetrahydroquinoline and 1-(p-hydroxyphenyl)-2-phenyl indole antifertility agents. *J. Med. Chem*. **1970**, *13*, 664−668. (e) Willis, P. G.; Pavlova, O. A.; Chefer, S. I.; Vaupel, D. B.; Mukhin, A. G.; Horti, A. G. Synthesis and structure-activity relationship of a novel series of aminoalkylindoles with potential of imaging the neuronal cannabinoid receptor by positron emission tomography. *J.*

Med. Chem. **2005**, *48*, 5813−5822. (f) Jacob, P., III; Shulgin, A. T. Sulfur analogues of psychotomimetic agents. Monothio analogues of mescaline and isomescaline. *J. Med. Chem*. **1981**, *24*, 1348−1353. (g) Coe, J. W.; Brooks, P. R.; Wirtz, M. C.; Bashore, C. G.; Bianco, K. E.; Vetelino, M. G.; Arnold, E. P.; Lebel, L. A.; Fox, C. B.; Tingley, F. D., III; Schulz, D. W.; Davis, T. I.; Sands, S. B.; Mansbach, R. S.; Rollema, H.; O'Neill, B. T. 3,5-Bicyclic aryl piperidines: A novel class of α4β2 neuronal nicotinic receptor partial agonists for smoking cessation. *Bioorg. Med. Chem. Lett.* **2005**, *15*, 4889−4897.

(3) For select examples, see: (a) Kou, K. G. M.; Pflueger, J. J.; Kiho, T.; Morrill, L. C.; Fisher, E. L.; Clagg, K.; Lebold, T. P.; Kisunzu, J. K.; Sarpong, R. A Benzyne insertion approach to Hetisine-type diterpenoid alkaloids: Synthesis of cossonidine (davisine). *J. Am. Chem. Soc.* **2018**, *140*, 8105−8109. (b) Goetz, A. E.; Silberstein, A. L.; Corsello, M. A.; Garg, N. K. Concise enantiospecific total synthesis of tubingensin A. *J. Am. Chem. Soc.* **2014**, *136*, 3036−3039. (c) Neog, K.; Borah, A.; Gogoi, P. Palladium(II)-catalyzed C−H bond activation/C−C and C−O bond formation reaction cascade: Direct synthesis of coumestans. *J. Org. Chem.* **2016**, *81*, 11971−11977. (d) Neumeyer, M.; Kopp, J.; Brückner, R. Controlling the substitution pattern of hexasubstituted naphthalenes by aryne/siloxyfuran Diels−Alder additions: Regio and stereocontrolled synthesis of arizonin C1 analogs. *Eur. J. Org. Chem.* **2017**, *2017*, 2883−2915. (e) Corsello, M. A.; Kim, J.; Garg, N. K. Total synthesis of (−)-tubingensin B enabled by the strategic use of an aryne cyclization. *Nat. Chem.* **2017**, *9*, 944−949. (f) Gampe, C. M.; Carreira, E. M. Total syntheses of guanacastepenes N and O. *Angew. Chem., Int. Ed.* **2011**, *50*, 2962−2965. (g) Nathel, N. F. F.; Shah, T. K.; Bronner, S. M.; Garg, N. K. Total syntheses of indolactam alkaloids (−)-indolactam V, (−)-pendolmycin,

(−)-lyngbyatoxin A, and (−)-teleocidin A-2. *Chem. Sci.* **2014**, *5*, 2184−2190. (h) Ippoliti, F. M.; Adamson, N. J.; Wonilowicz, L. G.; Nasrallah, D. J.; Darzi, E. R.; Donaldson, J. S.; Garg, N. K. Total synthesis of lissodendoric acid A via stereospecific trapping of a strained cyclic allene. *Science* **2023**, *379*, 261–265. (i) Mehta, M. M.; Gonzalez, J. A. M.; Bachman, J. L.; Garg, N. K. Cyclic allene approach to the manzamine alkaloid keramaphidin B. *Org. Lett.* **2023**, *25*, 5553–5557.

(4) For reviews on this topic, see: (a) Tadross, P. M.; Stoltz, B. M. A Comprehensive History of Arynes in Natural Product Total Synthesis. *Chem. Rev.* **2012**, *112*, 3550−3577. (b) Gampe, C. M.; Carreira, E. M. Arynes and Cyclohexyne in Natural Product Synthesis. *Angew. Chem., Int. Ed.* **2012**, *51*, 3766−3778.

(5) For select examples, see: (a) Darzi, E. R.; Barber, J. S.; Garg, N. K. Cyclic alkyne approach to heteroatom-containing polycyclic aromatic hydrocarbon scaffolds. *Angew. Chem., Int. Ed.* **2019**, *58*, 9419–9424. (b) Darzi, E. R.; Stanfield, D. A.; McDermott, L.; Kelleghan, A. V.; Schwartz, B. J.; Garg, N. K. Facile synthesis of 2-aza-9,10-diphenylanthracene and the effect of precise nitrogen atom incorporation on OLED emitters performance. *Mater. Adv.* **2023**, *4*, 3351–3355. (c) Spence, K. A; Chari, J. V.; Di Niro, M.; Susick, R. B.; Ukwitegetse, N.; Djurovich, P. I.; Thompson, M. E.; Garg, N. K. π-Extension of heterocycles via a Pd-catalyzed heterocyclic aryne annulation: π-extended donors for TADF emitters. *Chem. Sci.* **2022**, *13*, 5884–5892. (d) Ramirez, M.; Darzi, E. R.; Donaldson J.; Houk, K. N.; Garg, N. K. Cycloaddition cascades of strained alkynes and oxadiazinones. *Angew. Chem., Int. Ed.* **2021**, *60*, 18201–18208. (e) Chari, J. V.; Spence, K. A.; Susick, R. B.; Garg, N. K. A platform for on-the-complex annulation reactions with transient aryne intermediates. *Nat. Commun.* **2021**,

12, 3706–3715. (f) Lin, J. B.; Shah, T. K.; Goetz, A. E.; Garg, N. K.; Houk, K. N. Conjugated trimeric scaffolds accessible from indolyne cyclotrimerizations: Synthesis, structures, and electronic properties. *J. Am. Chem. Soc.* **2017**, *139*, 10447–10455. (g) Medina, J. M.; Ko, J. H.; Maynard, H. D.; Garg, N. K. Expanding the ROMP toolbox: Synthesis of air-stable benzonorbornadiene polymers by aryne chemistry. *Macromolecules* **2017**, *50*, 580–586.

(6) For studies pertaining to the six-membered carbocyclic 1,2,3-trienes, see: (a) Shakespeare, W. C.; Johnson, R. P. 1,2,3-Cyclohexatriene and cyclohexen-3-yne: Two new highly strained C_6H_6 isomers. *J. Am. Chem. Soc.* **1990**, *112*, 8578–8579. (b) Hickey, E. R.; Paquette, L. A. Torsional angle decompression is not the source of facial selectivity in Diels–Alder cycloadditions involving cyclic dienes fused to bicyclic frameworks. The case study of 1,2,3,4,6,7-hexahydro-1,4-methanonaphthalene. *Tetrahedron Lett.* **1994**, *35*, 2309–2312. (c) Hickey, E. R.; Paquette, L. A. Experimental and theoretical analysis of the effects of strain diminution on the stereoselectivity of dienophilic capture by π-facially nonequivalent homologs of isodicyclopentadiene. *J. Am. Chem. Soc.* **1995**, *117*, 163–176. (d) Sakura, M.; Ando, S.; Hattori, A.; Saito, K. Reaction of cyclohexa-1,2,3-triene with *N*,α-diphenylnitrone: Formation of seven-membered cyclic amines via piradone derivatives. *Heterocycles* **1999**, *51*, 547–556. (e) Kelleghan, A. V.; Bulger, A. S.; Witkowski, D. C.; Garg, N. K. Strain-promoted reactions of 1,2,3-cyclohexatriene and its derivatives. *Nature* **2023**, *618*, 748–754. (f) Matsuoka, S.; Jung, S.; Miyakawa, K.; Chuda, Y.; Sugimoto, R.; Hamura, T. Didehydroisobenzofuran: A new reactive intermediate for construction of isoacenofuran. *Chem. Eur. J.* **2018**, *24*, 18886–18889. (g) Schulz, F.; García, F.; Kaiser, K.; Pérez, D.;

Guitián, E.; Gross, L.; Peña, D. Exploring a route to cyclic acenes by on-surface synthesis. *Angew. Chem., Int. Ed.* **2019**, *58*, 9038–9042.

(7) For studies pertaining to the seven-membered 1,2,3-carbocyclic trienes, see: (a) Zoch, H.-G.; Szeimies, G.; Romer, R.; Schmitt, R. 1,2,3-Cycloheptatriene by isomerization of tricyclo[4.1.0.0]-hept-1(7)-ene. *Angew. Chem., Int. Ed.* **1981**, *20*, 877–878. (b) Zoch, H.-G.; Szeimies, G.; Romer, R.; Germain, G.; Declrercq, J.-P. Zur thermischen isomerisierung des tricyclo[4.1.0.0]hept-1(7)-ens: Buildung und abfangreaktionen von 1,2,3-cycloheptatrien. *Chem. Ber.* **1983**, *116*, 2285–2310. (c) Hashmi, S.; Polborn, K.; Szeimies, G. Nickel(0)-katalysierte dimerisierung von 1,2,3-cycloheptatrien: Cyclobuta[1,2:3,4]dicycloheptatetraen, ein [4[radialen-derivative. *Chem. Ber.* **1989**, *122*, 2399–2401.

(8) For reviews on this topic, see: (a) Vitaku, E.; Smith, D. T.; Njardarson, J. T. Analysis of the structural diversity, substitution patterns, and frequency of nitrogen heterocycles among U.S. FDA approved pharmaceuticals. *J. Med. Chem.* **2014**, *57*, 10257–10274. (b) Lamberth, C. Heterocyclic chemistry in crop protection. *Pest Manag. Sci.* **2013**, *69*, 1106–114. (c) Joule, J. A. in Advances in Heterocyclic Chemistry (eds. Scriven, E. F. V. & Ramsden, C. A.) Vol. 119, 81–106 (Elsevier, 2016).

(9) For select studies, see: (a) Medina, J. M.; Mackey, J. L.; Garg, N. K.; Houk, K. N. The role of aryne distortions, steric effects, and charges on regioselectivities in aryne reactions. *J. Am. Chem. Soc.* **2014**, *136*, 15798–15805. (b) Goetz, A. E.; Garg, N. K. Regioselective reactions of 3,4-pyridynes enabled by the aryne distortion model. *Nat. Chem.* **2013**, *5*, 54–60. (c) Bronner, S. M.; Mackey, J. L.; Houk, K. N.; Garg, N. K. Steric effects compete with aryne distortion to control regioselectivities of nucleophilic additions to 3-silylarynes. *J. Am. Chem.*

Soc. **2012**, *134*, 13966–13969. (d) Cheong, P. H.-Y.; Paton, R. S.; Bronner, S. M.; Im, G.-Y.; Garg, N. K.; Houk, K. N. Indolyne and aryne distortions and nucleophilic regioselectivities. *J. Am. Chem. Soc.* **2010**, *132*, 1267–1269.

(10) Yadav, N.; Sangwan, S.; Kumar, R.; Chauhan, S.; Duhan, A.; Singh, A.; Arya, R. K. Comprehensive overview of progress in functionalization of 2-pyridone and 2,4-dihydroxy pryidine: key constituents of vital natural products. *ChemistrySelect* **2021**, *6*, 11792–11821.

(11) Ikawa, T.; Urata, H.; Fukumoto, Y.; Sumii, Y.; Nishiyama, T.; Akai, S. Concise synthesis of multisubstituted isoquinolines from pyridines by regioselective Diels–Alder reactions of 2-silyl-3,4-pyridynes. *Chem. Eur. J.* **2014**, *20*, 16228–16232.

(12) Van de Poël, H.; Guillaumet, G.; Viaud-Massaurd, M. C. Synthesis of melatonin analogues derived from furo[2,3-b]- and [2,3-c]pyridines by use of a palladium-copper catalyst system. Heterocycles **2002**, *57*, 55–71.

(13) Nibin Joy, M.; Bodke, Y. D.; Abdul Khader, K. K.; Syed Ali Padusha, M.; Sajith, A. M.; Muralidharan, A. A rapid and modified approach for C-7 amination and amidation of 4-methyl-7-nonafluorobutylsulfonyloxy coumarins under microwave irradation. *RSC Adv.* **2014**, *4*, 19766–19777.

(14) Voelkel, M. H. H.; Engelgage, E.; Kondratiuk M.; Huber, S. M. Evaluation of 6-halogenated 2-pyridone moieties as halogen bond donors. *Eur. J. Org. Chem.* **2022**, e202200211.

(15) Maity, S.; Das, D.; Sarkar, S.; Samanta, R. Direct Pd(II)-catalyzed site-selective C5-arylation of 2-pyridone using aryl iodides. *Org. Lett.* **2018**, *20*, 5167–5171.

(16) Calculations performed at the B3LYP/6-311+G(d,p)//B3LYP/6-31G(d) level of theory. Computational details will be published at a later date.